The Enhanced Binary Single Machine Equivalent Method for Transient Stability Limit Searching

Hui-Min Tan

A thesis submitted to

The School of Electrical & Electronic Engineering

Faculty of Engineering, Computer and Mathematical Sciences

The University of Adelaide

In partial fulfilment of the requirements

For the degree of

Doctor of Philosophy

31st January 2016

Table of Contents

Abstract

This thesis proposes the novel Enhanced Binary Single-Machine Equivalent Method (EBSIME) to provide a fast, robust and systematic approach to search for the transient stability limits (TSLs) of multi-machine power systems. The algorithm is an extension of the SIME method [1] and provides an approach to estimate a transient stability margin for a given scenario – where the system operating conditions and a contingency are specified. The margins estimated for a pair of different scenarios is used to predict and accelerate an iterative search for the TSLs. The search bisects the search bounds whenever the limit prediction using the transient stability margins cannot be applied, thereby ensuring search convergence. Unlike alternative hybrid-direct TSL searching methods the EBSIME algorithm is general and does not require any model simplification, or heuristic tuning for application to the specific power system under investigation.

The EBSIME algorithm is designed to be implemented as a peripheral add-on to the standard time domain simulation (TDS) and load-flow software; and does not require access to, or modification of, the primary transient stability analysis software. As some important applications of EBSIME are perceived within the Australian power industry the algorithm has been implemented using PSS®E. In this thesis the algorithm is applied to locate the TSLs on the IEEE simplified 14-generator model of the South-East Australian power system. The results indicate that the EBSIME algorithm can locate the TSL up to 30% faster than a plain binary search, and at worst a few simulation seconds longer than a plain binary search.

Statement of Originality

I certify that this work contains no material which has been accepted for the award of any other degree or diploma in any university or other tertiary institution to Hui-Min Tan and, to the best of my knowledge and belief, contains no material previously published or written by another person, except where due reference has been made in the text.

In addition, I certify that no part of this work will, in the future, be used as a submission in my name for any other degree or diploma in any university or other tertiary institution without the prior approval of the University of Adelaide and where applicable, any partner institution responsible for the joint award of the degree.

I give consent to this copy of my thesis when deposited in the University Library, being made available for loan and photocopying, subject to the provisions of the Copyright Act 1968.

I give permission for the digital version of my thesis to be made available on the web, via the University's digital research repository, the Library catalogue, the Australasian Digital Theses Program (ADTP) and also through web search engines, unless permission has been granted by the University to restrict access for a period of time.

Signed: ——————————————

Name: Hui-Min Tan

Date: 19 January 2016

Acknowledgements

I wish to express my gratitude to the following people and organizations who have supported me through the writing of the thesis:

The University of Adelaide, South Australia, who provided me with funding, resources and the research support to pursue the Ph.D.,

Dr Rastko Zivanovic, my principle supervisor, for his technical and financial research support to assist with the completion of my candidature.

Mr David Vowles, my co-supervisor and mentor, who has volunteered countless hours in discussions on the conception, design, implementation of the EBSIME algorithm and software. I am very grateful for the time and effort that David has generously volunteered into proof-reading, in detail, my various publications, and the thesis in its entirety.

The staff of the University of Liège, Belgium, who provided me with access to the programming code for the SIME algorithm for TSL searching, enabling me to benchmark it against the novel EBSIME algorithm that is proposed in the thesis.

My colleagues at the University of Adelaide, and Powerlink Queensland, who encouraged me to persist, and who were enthusiastic to provide me with technical assistance and advice;

Last but not least, to my mum, dad and siblings who have been extremely patient and supportive of my Ph.D. endeavours in every way from the beginning to the end.

List of Acronyms

ABS	Accelerated Binary Search
AEMC	Australian Energy Market Commission
AEMO	Australian Energy Market Operator
APBS	Accelerated Parallel Binary Search
AU14GEN	The 14-generator South-East Australian power system model
AVR	Automatic Voltage Regulator
BCU	Boundary of Stability Controlling Unstable Equilibrium Point
CCT	Critical Fault Clearing Time
CM	Critical machine(s)
CT	Fault Clearing Time
COI	Centre of Inertia
CUEP	Controlling Unstable Equilibrium Point
DAD	Differential-Algebraic-Discrete (equations model)
DAE	Differential-Algebraic-Equation
DEEAC	Direct Extended Equal Area Criterion
deg	Degrees
DM	Dynamical Method
DSA	Dynamic Security Analysis
EAC	Equal Area Criterion
EBSIME	The Enhanced Binary Single Machine Equivalent Method
EEAC	Static Extended Equal Area Criterion
ESC	Early Simulation Stopping Criteria
EP	Equilibrium point
EPRI	The Electric Power Research Institute
FS	Forward-Swing
FSL	Forward-Swing (transient stability) Limit
G1	Generator 1
G2	Generator 2
GUI	Graphical User Interface
IEEE	The Institute of Electrical and Electronic Engineers
KE	Kinetic energy
LB	Lower Search Bound
MBASE	Machine Base Power
MG	Machine Groups; (two) Groups of Machines
MOD	Mode of Disturbance
MOI	Mode of Instability
MS	Multi-swing
MSL	Multi-Swing Limit - the transient stability limit
MW	Megawatt
NEM	National Electricity Market
NER	National Electricity Rules
NR	The Newton-Raphson method

NSW	New South Wales, Australia
OMIB	One Machine Infinite Bus power system
ODE	Ordinary Differential Equation
PBS	Parallel Binary Search
PEBS	Potential Energy Boundary Surface
PE	Potential energy
PSS®E	Power System Simulator for Engineering
PT	Power Transfer
PTL	Power Transfer Limit
pu	Per unit
QLD	Queensland, Australia
rad	Radians
SA	South Australia
SBASE	System Base Power
SEEAC	Static EEAC (the same meaning as EEAC)
SEP	Stable Equilibrium Point
SIME	Single Machine Equivalent
sim-s	Simulation seconds
SPM	Structure Preserving Model
SPEF	Structure Preserving Energy Function
SV	Transient Stability Search Variable
SVC	Static Var Compensator
TD	Time Domain
TDS	Time Domain Simulation
TEF	Transient Energy Function
TEM	Transient Stability Energy Margin
TSA	Transient Stability Assessment
TSIM	Time taken to assess transient stability in Simulation Seconds
TSL	Transient Stability Limit (also referred to as the MSL)
TSM	Transient Stability Margin
TSIM	Time in Simulation Seconds
UEP	Unstable Equilibrium Point
ULTC	Under-Load Transformer Tap Changers
UB	Upper Search Boundary
VIC	Victoria, Australia
VSL	Voltage Stability Limit

Glossary

A_{acc}	Acceleration area for the equation area criterion	[pu-rad]
A_{dec}	Deceleration area for the equation area criterion	[pu-rad]
A_{0ij}	Amplitude of the dominant pole for a stable post-fault voltage response	
A_{1ij}	Amplitude of the DC component for a post-fault voltage response	
B	SVC susceptance	[pu]
d_{q0}	The direct-quadrature-zero transformation to represent the rotor, and three-phase stator, quantities in terms of a two-axis rotating reference frame	
θ, δ	Generator rotor angle	[deg or rad]
δ_0	OMIB rotor angle when system operation is in the steady state	[deg or rad]
δ_{clr}	OMIB rotor angle at the instant an applied fault is cleared	[deg or rad]
δ_{limit}	The OMIB rotor angle threshold for forward-swing stability	[deg or rad]
δ_{max}	Maximum OMIB rotor angle, at the instant when a perturbed system returns to synchronism on the forward-swing	[deg or rad]
$\delta_{SIMEmax}$	A tuned parameter used by the SIME method to check that a diagnosis of the transient stability is correct	[deg or rad]
$\tilde{\theta}$	A vector of machine rotor angles at a given post-fault operating point	[deg or rad]
$\tilde{\theta}_s$	A vector of machine angles at the post-fault stable equilibrium point	[deg or rad]
$\tilde{\theta}_{si}$	The machine angles of a generator at the post-fault stable equilibrium point	[deg or rad]
$\hat{\theta}^{UEP}$	Vector of system machine angles at the unstable equilibrium point (i.e. the operating point where the system is marginally unstable)	[deg or rad]

$\hat{\theta}^{S2}$	Vector of machine angles at the post-fault stable equilibrium point	[deg or rad]
$\hat{\theta}^{cl}$	Vector of machine angles at the point of fault clearance	[deg or rad]
$\hat{\theta}^{S1}$	Vector of machine angles at the pre-fault stable equilibrium point	[deg or rad]
ε_k	The transient energy function margin	
H	The machine inertia coefficient	
k	The iteration number of the current search scenario	
M	Matrix of 2 x Machine Inertia Constants	
M	Twice the machine inertia coefficient	
mmf	Magneto-motive force	
N	The number of machine groups that are considered in the SIME method for TSA at each time-step of a TDS	
n_{tol}	Margin tolerance, used by the SIME limit prediction search	[pu-rad]
ω	Generator rotor speed	[rad/s]
ω_{limit}	The OMIB rotor speed when the OMIB rotor angle = δ_{limit}	[rad/s]
ω_{0ij}	Angular frequency of the dominant pole for a stable post-fault voltage response	[rad]
P_a	Generator acceleration power	[pu]
P_e	Generator electrical power output	[pu]
P_m	Mechanical input power to a generator shaft	[pu]
$\mathbf{P_e}$	Vector of machine electrical power outputs	[pu]
$\mathbf{P_m}$	Vector of machine mechanical power inputs	[pu]
P_a^T	A vector of acceleration power of all the machines in a power system	[pu]
P_a-δ_{OMIB}	The OMIB acceleration power versus angle characteristic	[pu-rad]

$^{(s)}$	Standard international (SI) units	
σ_{0ij}	Damping constant of the dominant pole for a post-fault voltage response	
σ_{1ij}	Damping constant of the dominant pole for a stable post-fault voltage response	
t	Time	[s]
$\mathbf{T}$	Time Vector	[s]
t_f	The instant when a fault is applied to a power system	[s]
t_r	The instant when a perturbed system returns to synchronous operation on the forward-swing	[s]
t_u	The instant in time when a generators in a power system lose synchronism	[s]
t_{obs}	The time instant at which an unstable TDS is halted	[s]
V_{cl}	The system energy at the instant of fault clearance for the energy function	
V_{cr}	The change in potential energy between the operating points described by $\hat{\theta}^{UEP}$ and $\hat{\theta}^{S2}$	
$V_{\text{correction}}$	Residual kinetic energy correction factor	
$V_{KE\cdot corr}$	The corrected kinetic energy	

Maximum simulation time	Typically the maximum prescribed simulation time is 10s to 20s
Limit prediction search phase	The phase of the EBSIME search where the SIME limit prediction steps are performed to determine the TSL. Also referred to as the “forward-swing search phase”.

Chapter 1 Thesis Introduction

This chapter introduces the concept of the reliability and security of electrical power systems. It gives an overview of the different classifications of power system stability and the criteria used in their assessment. The state-of-the-art developments in dynamic security analysis applications to monitor power system stability are also reviewed. The requirements for the next phase of development for dynamic security analysis on the Australian power system are highlighted. The chapter concludes by summarizing the original contribution of this work, and outlining the thesis structure.

1.1. Power System Reliability and Security

Due to the deregulation of the electrical power industry and the increasing demand for electricity, modern electrical power systems have evolved into large complex systems interconnecting many items of plant that generate, transmit and distribute electricity over vast geographical areas. In the wake of open access transmission and energy trading, the electricity markets are continually seeking to minimize costs by maximizing the available transmission capacity of the grid and to operate it closer to the maximum secure limit.

Modern network utilities are expected to facilitate power transfers that are very different to those for which they were originally designed. With the growing use of distributed and renewable energy generation, such as wind and solar power, system generation and network loads are becoming more dynamic and increasingly difficult to predict and control. Aging utilities and increased regional interconnections have also increased the possible sources of system disturbances. In this environment the reliable and secure operation of modern power systems is a challenging task.

Power system *reliability* describes the ability of a power system to provide satisfactory electrical service over an extended period of time. Power system *security* refers to the degree of risk in the ability of a power system to survive a defined set of potential disturbances without interrupting customer service [2]. The reliable operation of a power system requires that it must be designed with *security* as a primary consideration. The grid must be monitored and controlled to ensure there are sufficient *security* margins at all times [3]. Maintaining system *security* is a critical function. An insecure system is exposed to severe and potentially catastrophic system failures which can result in widespread and cascading blackouts. Such events have enormous economic costs and may even lead to loss of life. The importance of system security is especially emphasized by the significant number of large-scale blackouts that have occurred around the world in the past decade or so [2].

Power system *security* depends on the system operating condition as well as the probability of contingencies [2]. Security assessment can be classified into Static Security Assessment (SSA) and Dynamic Security Assessment (DSA). SSA is concerned with preemptively determining if, following a physical disturbance, system plant, equipment and lines are operating within their respective current limits, and that system voltages are within their prescribed limits. DSA is concerned with determining whether the components of an interconnected power system can remain connected for each contingency in a set of critical disturbances. The novel contribution of this thesis is concerned with DSA. The state-of-the-art developments and tools employed in DSA are reviewed in section 1.4.

1.2. Power System Stability

Power system stability analysis is an integral part of system security and reliability assessment. Power system stability is a time-varying attribute that is concerned with the ability of a system to return to a stable operating state following a physical disturbance [2]. There are three types of stability, as shown in Figure 1-1: rotor angle stability, frequency stability and voltage stability. These can be divided into sub-categories based on the size of the disturbance, the time span of interest, and the devices and processes that must be considered in the stability assessment [2].

Power system stability is a single problem that must be broken down into smaller components so that the whole problem can be completely understood [2]. Traditionally DSA has focused on transient stability assessment. However, in recent years the concept of DSA has expanded to optionally include voltage, small-signal, and frequency stability [2, 3]. Assessment of all forms of stability is essential for the secure operation of the power system. This thesis focuses on one form – namely transient stability.

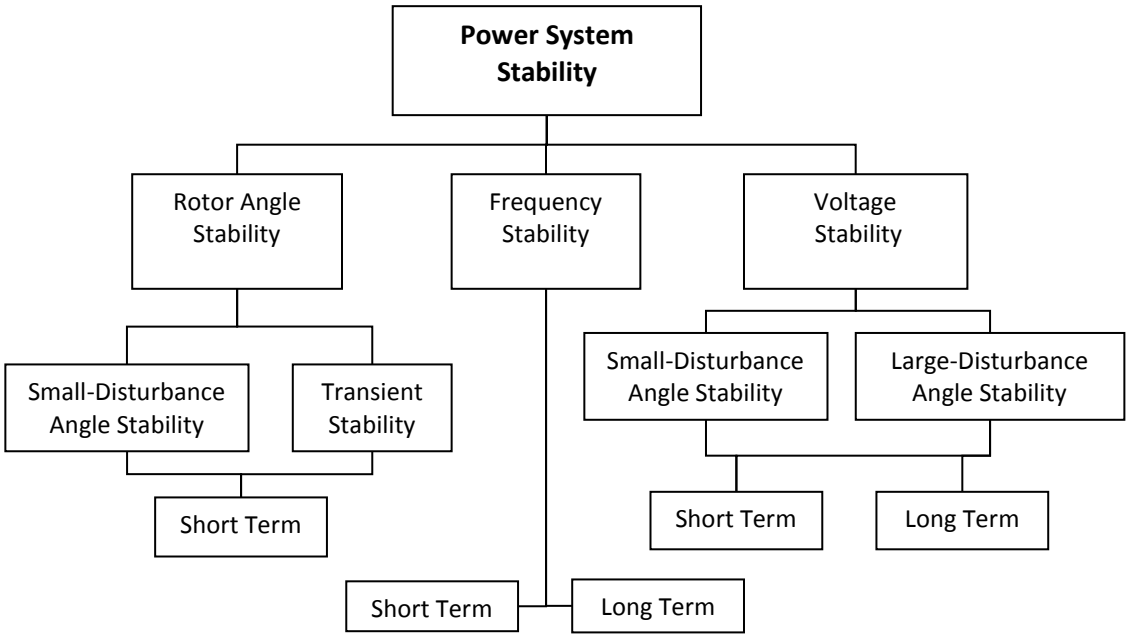

Figure 1-1. Classifications of power system stability, adapted from [2]

1.2.1. Rotor Angle Stability

Rotor angle stability refers to the ability of the synchronous machines of an interconnected power system to remain in synchronism after being subjected to a disturbance. It depends on the ability to maintain/restore equilibrium between the

electro-magnetic torque and the mechanical torque of each synchronous machine in the system. Instability that may result occurs in the form of increasing angular swings of some generators leading to their loss of synchronism with other generators [2]. The time frames associated with these phenomena are in the order of ten seconds or so.

Rotor angle stability involves the study of the electromechanical oscillations inherent in power systems - how the power outputs of synchronous machines vary with respect to the machine rotor angles - according to Newton's laws of rotational motion. When the system is in a state of equilibrium the input mechanical torque and output electromagnetic torque of each generator is equal. When the system is disturbed the machines will either accelerate or decelerate. If one generator runs faster than another, the rotor angle of the faster machine will advance with respect to the slower one.

The restoring torque of a synchronous machine due to the change in rotor angle is resolved into two parts: the synchronizing component – which is in phase with, and therefore opposes, rotor angle deviation; and the damping component – which is in phase with, and opposes, the speed deviation. Insufficient synchronizing torque will cause an aperiodic or non-oscillatory form of instability. Insufficient damping torque usually causes oscillatory instability [2]. Rotor angle stability is further classified into two subcategories: small-signal stability and transient stability.

1.2.1.1. *Small-Signal Angle Stability*

Small-signal rotor-angle stability is concerned with the ability of the power system to maintain synchronism under small disturbances, such as the incremental changes in the system load, or a line switching operation. The disturbances are considered to be sufficiently small that linearization of system equations is permissible for purposes of analysis. Small-signal instability is usually associated with insufficient damping of electro-mechanical oscillations [2, 4].

Small-signal rotor-angle instability may be caused by local or inter-area oscillations. Local plant mode oscillations are usually associated with the rotor angle oscillations of a single power plant against the rest of the system or oscillations between a small group of closely connected generators. Inter-area oscillations typically involve large groups of generators in one area swinging against the generators in another area via a relatively weak interconnection. If the system is small-signal unstable the oscillations may grow to the point where machines loose synchronism with each other. This may cause transmission line and generator protection to trip, imposing further stress on the system.

1.2.1.2. *Transient Stability*

Transient stability, or large disturbance rotor angle stability, is concerned with the ability of the synchronous machines in an interconnected power system to remain in-step (i.e. synchronized) with one another following a large disturbance. Large disturbances, such as a lightning strike on a transmission line, or a short circuit fault that causes the loss of a large generator or power transformer, may require structural changes to the network to clear the fault [2]. The resulting system response involves large excursions of generator rotor angle, which are governed by the non-linear relationship between the generator output power and angle. Transient instability is usually caused by insufficient synchronizing torque. Although instability often occurs during the forward-swing, in large power systems the interaction of local modes and slow inter-area swing modes, or the non-linear effects of local plant, may cause instability after the forward-swing [2].

Although a scenario may be classified as transiently stable, it may be voltage unstable due to the large fluctuations in voltage that tend to accompany severe disturbances. Thus, when the transient stability of a power system is assessed, voltage stability should also be considered.

1.2.2. Voltage Stability

Voltage stability refers to the ability of a power system to maintain steady voltages at all buses in the system after being subjected to a disturbance from a given initial operating condition. It depends on the ability to maintain/restore equilibrium between load demand and load supply from the power system – and in particular the balancing of the demand and supply of reactive power [2]. Automated dynamic reactive reserves, such as synchronous condensers, generators and static var compensators (SVCs), are used to regulate system voltages.

Excess reactive power causes voltage levels to rise. Sustained high voltages may occur when a power system operates under light-load conditions and there are insufficient reserves of inductive reactive power. Extremely high voltages can damage expensive power system equipment. Insufficient reserves of capacitive reactive power in the network will cause voltage levels to drop. Low voltages may be caused by factors such as high power transfer over long distances, transmission line and reactive equipment outages or motor stalling [5]. Low voltage is typically accompanied by large currents, thus heavily loaded plant are at increased risk of thermal damage. Low voltages reduce the amount of power drawn by constant load sources, such as heating elements.

The supply of reactive power to loads can be severely compromised due to, for example, the loss of transmission lines following a disturbance resulting in increased losses of reactive power in the remaining transmission network. Voltage instability results in unacceptable voltage levels in at least part of the system and in the worst case can lead to voltage collapse of the entire system. If there is inadequate available reactive power in the network a proportion of system load may need to be shed to avoid voltage collapse [5]. During voltage collapse the capacitive reactive reserves of a power system will be exhausted.

The relevant time frame for voltage stability varies from a few seconds to tens of minutes [2]. Short-term voltage instability can be revealed through the tools used for transient stability analysis.

1.2.3. Frequency Stability

Frequency stability refers to the ability of a power system to maintain steady frequency following a severe system upset resulting in a significant imbalance between generation and load. It depends on the ability to maintain/ restore equilibrium between system generation and load, with minimum unintentional loss of load [2]. Frequency instability generally causes large fluctuations in system power flows, voltages, and other variables which may trigger control and protections system processes that are not conventionally modelled in transient stability or voltage stability studies. Sustained frequency swings may lead to the tripping of generating units or loads, and further cascading outages.

Governors are designed to adjust the mechanical power input to the generator to control the shaft speed of individual generators, thereby stabilizing the system frequency; although they maintain a balance between load and generation rather than maintaining a specific speed [5]. In Australia the Automatic Generation Control (AGC) system is used to regulate the system frequency to its nominal value (50Hz). The governors stabilize the system frequency following a large disturbance such as the loss of a generator, and the AGC returns the system to the scheduled frequency [5]. To prevent widespread blackouts in the event, say, of cascading generator outages, under-frequency load-shedding schemes are employed as a back-up to governor controls.

Frequency instability typically occurs due to insufficient generation reserve, inadequate equipment responses, or poor use of control and protection equipment. It may be a short-term phenomenon or a long-term phenomenon ranging from several seconds to tens of seconds or several minutes [2].

1.3. Stability Performance Criteria

For each classification of power system stability there are operation and planning guidelines to ensure the stable operation of a power system. There are similarities in the power system stability assessment criteria around the world. This section provides examples of stability performance criteria from the Australian National Electricity Rules (NER), which are specified by the Australian Energy Market Commission (AEMC) [6].

1.3.1. Rotor Angle Stability Performance Criteria

For a specified operating condition and disturbance, rotor angle stability requires that the machines in a power system are able to remain in synchronism, and that there is adequate damping of any power system oscillations. The ability of a power system to maintain synchronism is determined by observing the time-varying responses of the machine rotor angles either from simulations or measured real-time data of the post-disturbance system. If the rotor angles of any two machines continuously diverge then it is concluded the system is transiently unstable. For practical reasons in transient stability simulation studies the system is typically deemed to be unstable if the difference in rotor angles between machine pairs exceeds a threshold value.

Although the machines in the system may remain synchronized following a disturbance, the damping of the associated oscillations must also be adequate. According to the NER oscillations must have a halving time of 5 seconds or less. In other jurisdictions damping performance is based on damping ratios [6].

1.3.2. Voltage Stability Performance Criteria

The NER require that stable voltage control must be maintained under normal steady-state operating conditions, and following a credible contingency. Under normal conditions the system bus voltage may vary between 90% and 110% of the nominal bus voltage.

In the event of a contingency at the point where a generating system connects to the larger network, the NER allow fluctuations outside of the normal voltage as follows*:*

- 80% to 90% of the normal voltage for a period of up to 10s, and
- 70% to 80% of the rated voltage for a period of up to 2s.

The instantaneous system voltages are allowed to rise to a maximum overvoltage of 130% of the normal voltage for a period of up to 0.06s. If the instantaneous voltage at

any node is within 110% and 130% of the rated voltage, then it may be sustained for the maximum time shown in Figure 1-2.

Except as a consequence of a contingency, if any of the above rules are violated, or if the voltage level at any system node falls below 70% or rises above 130% of the nominal voltage, then voltage performance is classified as inadequate.

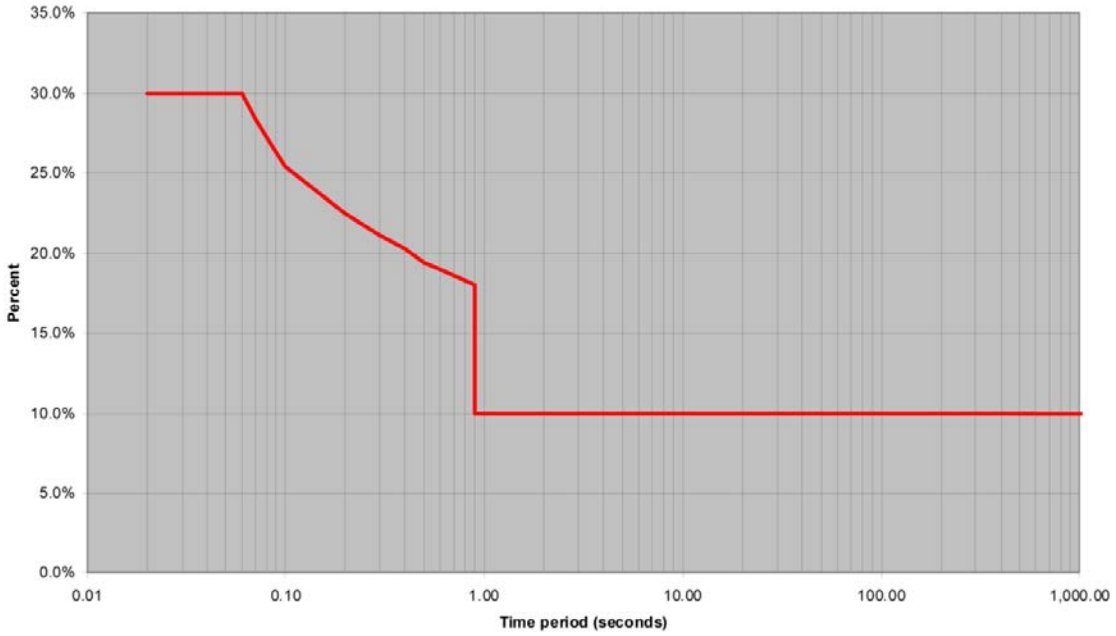

Figure 1-2. The allowable time period for which generation over-voltages may be sustained following a credible contingency [6].

1.3.3. Frequency Performance Criteria

In the Australian power system the scheduled system frequency is 50Hz. To ensure frequency can be stabilized in the event that it falls in the range between 47Hz to 49Hz a number of interruptible loads are made available for under-frequency load shedding.

The NER define a set of frequency performance criteria which govern the operation of system generators in response to a frequency disturbance. There are four frequency band classifications shown in Figure 1-3. In the *normal operating frequency band* (A), all online generators must be capable of continuous uninterrupted operation. The system may operate in the *normal operational frequency tolerance* band (B) for a maximum *recovery time* of 10 minutes; and in the *extreme frequency tolerance band* (C) for a maximum *stabilization time* of 2 minutes before returning to band A or B. If the operating frequency exceeds the *extreme frequency tolerance band* it is allowed to deviate as far as the extreme frequency excursion tolerance limits (bands D) for the

transient limit time, 9s. If the operating frequency exceeds the e*xtreme frequency excursion tolerance limits*, or the system operates outside of the normal operating frequency band for longer than the allowable duration then the system frequency performance is inadequate. The minimum performance criteria require that all online generators are able to remain in operation for the defined periods within each frequency band (A to D).

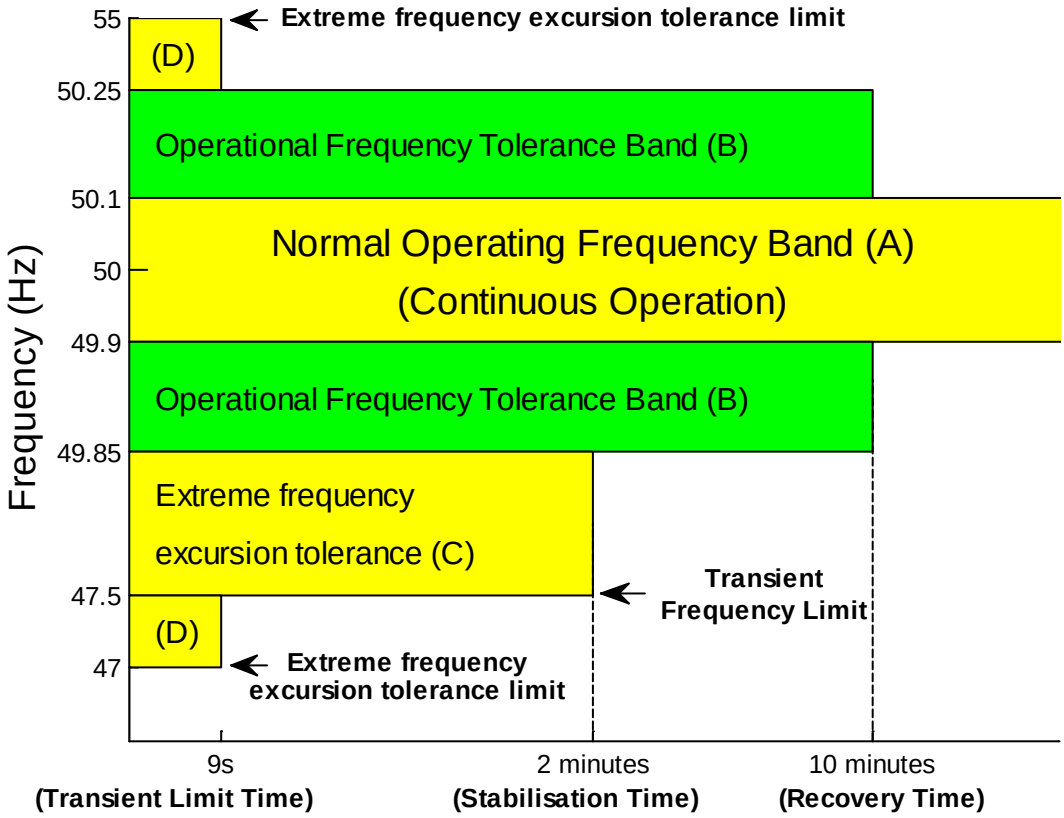

Figure 1-3. Summary of the minimum access frequency stability criteria for the Mainland Australian power system (adapted from [6]).

1.4. Dynamic Security Assessment

This section provides a review of the state-of-the-art techniques and tools for off- and on-line DSA that have been reported in literature. It outlines the implementation of DSA techniques in the context of the Australian power system, and their limitations.

1.4.1. Offline Dynamic Security Assessment

Detailed models and specific analytical tools are required to investigate the physical phenomena associated with each aspect of power system stability. Each stability classification must be assessed individually. The complexity of stability analysis

increases for large interconnected power systems due to the vast amounts of data, significant computing times, and technically demanding assessments that are required to interpret results. As such, system operators have traditionally relied on the results of off-line operational planning studies, based on near-term forecasted conditions, to guide them through day-to-day operations [3].

For the more complex parts of security assessment, it is necessary to calculate system operating limits in advance for the forecast operating states. However, the calculated system limits are not constant, and vary according to the factors such as the system loading, network bus voltages and network topology. To account for this uncertainty constraints can be modeled in the form of limit equations, as a function of independent measurable quantities such as generation, inertia and load. However, the predicted constraints are usually conservative. Worse, the limit equations may in some cases be optimistic, which may lead to undetected insecure operation [3]. To avoid some of the short comings of limit equations, online dynamic security assessment that takes into account the actual current operating state of the system can be deployed as a very useful complement.

1.4.2. Online Dynamic Security Assessment

Online DSA is currently operational, or being implemented, in a number of networks worldwide [7]. Online DSA uses SCADA and synchronized phasor measurement units (PMUs) to collate a real-time snapshot of the system state at regular time intervals, as depicted in Figure 1-4. It addresses the transient stability problem, as the real-time snapshot is used to evaluate the ability of the system, under current operating conditions, to return to stable operation for a set of defined and credible contingencies. Time-domain simulations (TDS) are used to determine if the system machines can remain in synchronism with one another in response to each contingency [8]. If a scenario is identified as transiently unstable then corrective operator intervention must be taken, otherwise the next credible contingency is considered.

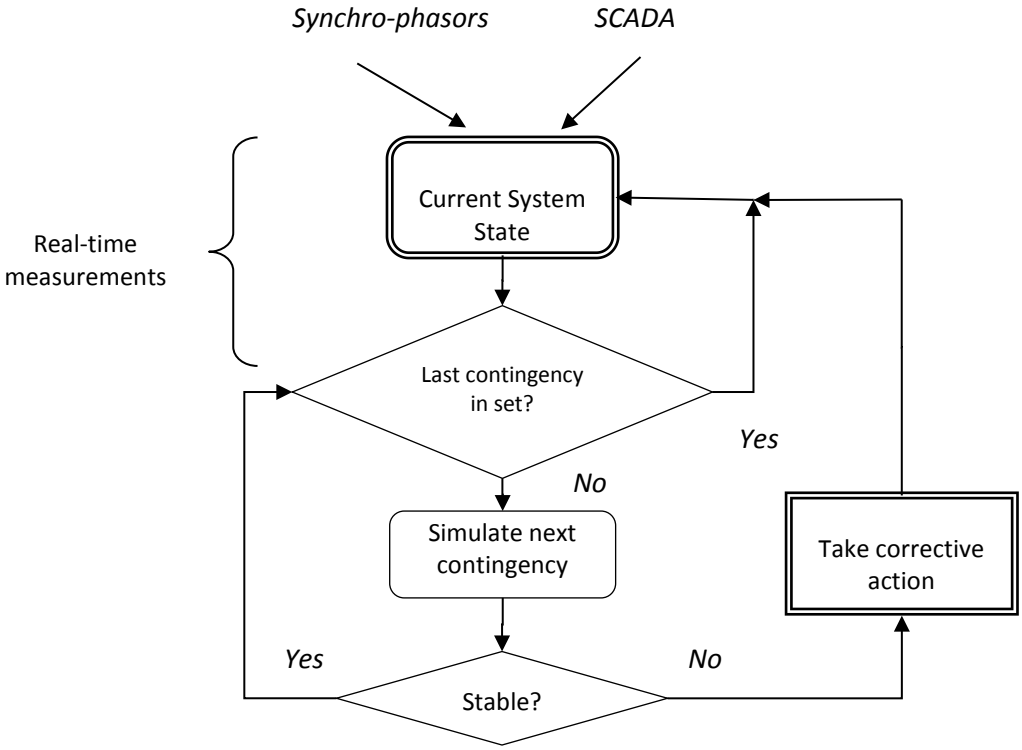

Figure 1-4: The Dynamic Security Assessment cycle

For each contingency a system operator will want to know 1) how far the system is from the secure operating limit in terms of controllable parameters, 2) if the system operation is secure how it can be manoeuvred to operate closer to the limit, and 3) if the system operation is insecure how may it be driven back to a secure operating point. This information cannot be directly inferred from TDS. However, transient stability margins (TSM) can assist the operator to determine appropriate responses.

The DSA cycle time must be short enough to allow for operators to take the necessary corrective actions to ensure that adequate security is maintained. TDS methods for transient stability analysis are recognized to produce the most accurate results. However, the speed of TDS in DSA applications is a limitation, particularly for large power systems. If faster approaches to an accurate stability assessment can be implemented then larger sets of credible contingencies could be assessed, which would improve the reliability of the DSA.

On-going research has produced a wide variety of stability and limit assessment methods for online DSA, which vary in computational complexity. Direct methods, such as the energy function methods for transient stability analysis, use a combination of system approximations and quantities that can be measured directly from the grid. They offer the advantage of fast calculations, and can provide information that is

complementary to TDS methods applied to detailed system models. However, they usually use reduced network models, and have difficulty representing discontinuities. Hybrid DSA methods combine and extend the benefits of the TDS and direct methods. Some of these techniques have been implemented or are under-development at online DSA sites around the world [3]. A review of the state-of-the-art transient stability analysis techniques is in Chapter 2.

Stability limit assessment methods which are based on TDS, or approximate methods that may potentially be applied to online DSA, have also been developed. Chapter 3 provides a review of the most recent techniques that have been proposed for locating transient stability limits.

1.4.3. Dynamic Security Assessment in the Australian Power System

The South-East Australian interconnected power system stretches approximately 5000 km along the Australian coastline, encompassing the states of Queensland, New South Wales, Victoria, South Australia and Tasmania. The large inter-regional power transfers and the narrow transmission corridors [9] cause it to be particularly susceptible to transient instability. The critical points on the South-East (SE) Australian power system tend to be at the inter-regional boundaries.

The Australian Energy Market Operator (AEMO) has utilized online DSA since 2001 to assess the transient security of the SE Australian power system [8, 9]. Real-time snapshots of the system operation are collated at regular 30 minute intervals. To comply with the rules of the National Electricity Market (NEM) the DSA is required to return results within a 10-15 minute time-frame [10].

In the online DSA, transient stability assessment is performed using fixed-step time-domain simulations calculated with PSS®E [11], the widely employed simulation engine in the Australian power industry. Studies to determine the transient stability limits (TSL) of the system, such as the maximum allowable power transfer over an interconnection, are performed offline due to the computationally intensive calculations that are involved. Application of TDS in DSA is problematic because the computation is slow, for large systems, which may cause the TDS algorithm to be unfeasibly slow. Direct methods that require the utilization of reduced equivalent network models are generally considered to be unreliable. This is due to the important role of control systems in enhancing transient-stability limits of the grid. These control systems and their associated limits cannot, in general, be adequately represented in the direct methods. SVCs are critical to the transient performance of the NEM system.

Presently AEMO's online DSA does not have tools to estimate the distance of the current system operating point to the transient stability limits in terms of controllable system parameters. Control decisions are determined off-line using trial and error methods that involve the computationally intensive repetition of many similar transient stability studies and a significant engineering task of assessing the results. Tools that systematically and efficiently assess the sensitivity of transient stability limits to the factors which influence them are needed [9, 10]. This could help power system operators to accurately determine transfer limits, and to identify strategies to maximize the transfer capability of the system.

A rigorous and consistent approach to transient stability sensitivity analysis would enable the transient performance of power systems to be understood and assessed with more accuracy and insight. This information can potentially be used to operate existing electrical transmission infrastructure closer to the stability limits, thereby extending transfer capability, with the same reliability to which we are accustomed. It may be possible to use TSMs to identify automatic control strategies to enhance system transient performance. This could have significant economic and environmental impacts by delaying investments in new infrastructure, effectively saving many millions of dollars.

1.5. Original Contribution of the Thesis

The thesis provides a methodology to assist with the next stage of development for online DSA on the Australian power system. It introduces the novel Enhanced Binary-Single Machine infinite bus Equivalent (EBSIME) algorithm that provides a fast, robust and systematic approach to searching for transient stability limits of multi-machine power systems. The algorithm does not require any model simplification and provides an approach to estimating the transient stability margins. The margins are used to linearly predict and thereby accelerate the search for transient stability limits. The margins provide information that can potentially be applied for online or offline transient stability sensitivity analysis.

The EBSIME algorithm adapts concepts from the SIME method for transient stability analysis and limit searching [1]. It enhances the robustness of the basic SIME algorithm for limit searching by bisecting the search bounds whenever the limit prediction using the SIME transient stability margins cannot be applied, ensuring search convergence. Unlike the SIME algorithm it is independent of the system network model and does not require heuristic tuning. Nevertheless to preserve the advantages of SIME such tuning is desirable over time as experience with the user's own network increases.

The EBSIME algorithm can be implemented and integrated with standard TDS and load-flow software. The algorithm is peripheral to the TDS software and does not require access to, or modification of, the TDS source code. As some important applications for the EBSIME software are perceived within the Australian power industry the algorithm has been implemented as an add-on to PSS®E.

The thesis describes the novel design and implementation of the EBSIME software. It uses a modular software architecture to facilitate alternative search methods for research and comparison purposes. The implemented algorithm is applied to assess the transient stability margins and limits for a range of contingencies on the IEEE simplified 14-generator model of the South-East Australian power system (AU14GEN) [12]. The thesis provides an original and rigorous critique about the application and suitability of the EBSIME algorithm for transient stability limit searching on the Australian power system.

1.6. Thesis Structure

The thesis structure is shown in Figure 1-5. The first 3 chapters review literature in the field. The remainder of the thesis comprises 3 parts. The first part, comprising chapters 4 and 5, demonstrates how the SIME response for a multi-machine power system is derived without resorting to any model reductions or simplification - a view that has not yet been considered in SIME-related literature. The characteristics of the SIME margins and early stop criteria are examined, and the two machine model is used to explore the sensitivity of the transient stability limits to parameter variations in the system, and to the SIME transient stability margins. Insights drawn from the physical behaviour of the two machine network can potentially apply to larger power systems.

The second part, comprising Chapters 6 to 8, describes the design and implementation the EBSIME algorithm. The algorithm is integrated into the PSS®E [11] software, the power system analysis software used by the Australian power industry. The algorithm is implemented as a PSS®E user-defined model such that direct access or modification of the original PSS®E source code is not required.

The last part, comprising Chapters 9 and 10, investigates the transient stability of the AU14GEN system. It demonstrates the fast, robust and reliable performance of the EBSIME algorithm when it is applied to search for critical clearing times (CCTs) and power transfer limits (PTLs) for transient faults applied on the major interconnectors. The investigations identify operating conditions that yield unexpected or anomalous relationships between the CCT and interconnector power transfer, where the EBSIME algorithm reverts to a plain binary search. This reversion is due to the failure of the basic SIME algorithm to converge to a limit. The anomalies that cause the basic SIME algorithm to fail are explored. It is emphasized that the EBSIME algorithm does in fact find the limit in these cases, because following the failure of the basic SIME algorithm the EBSIME reverts to a binary search. Finally, the thesis is concluded in Chapter 11.

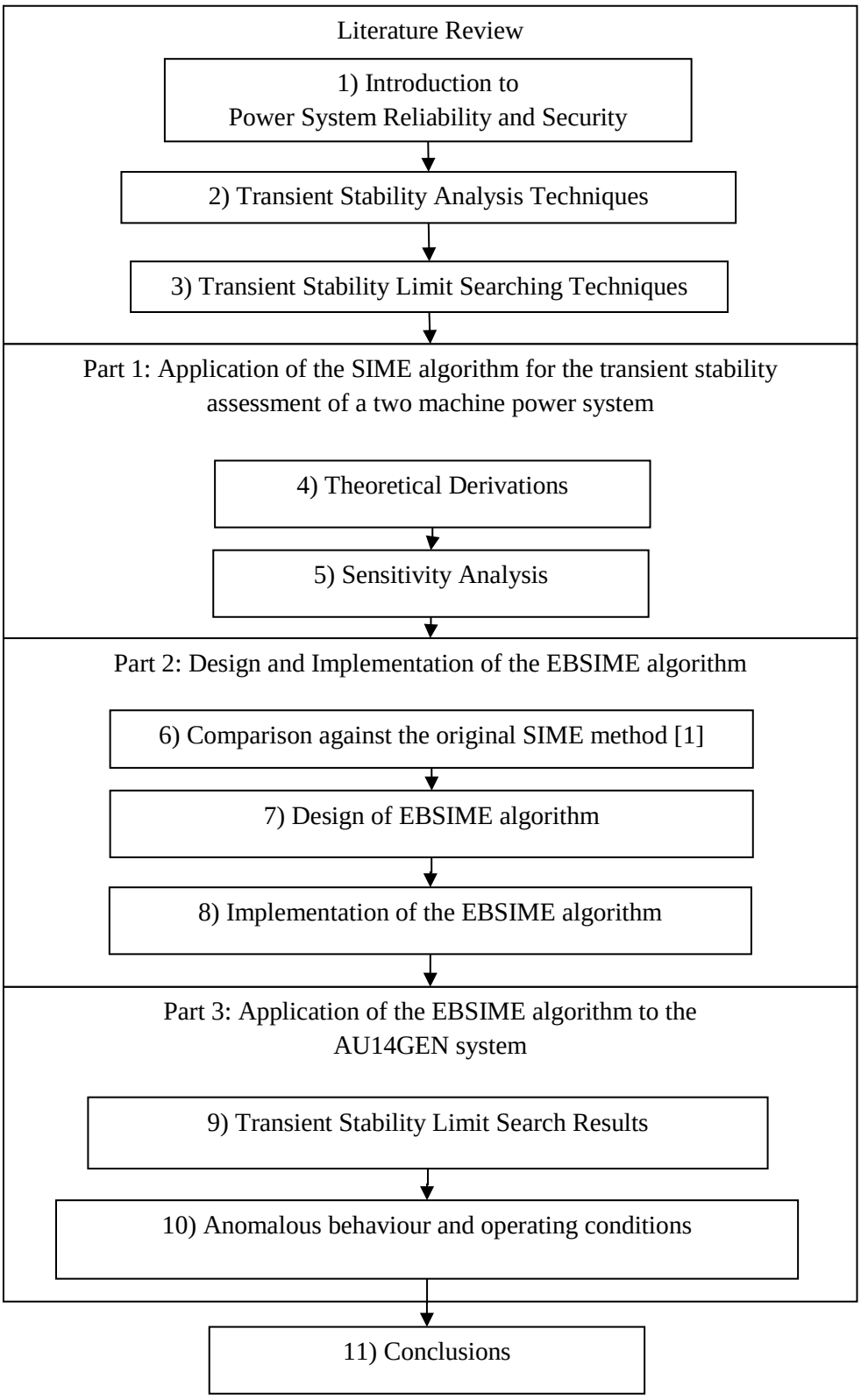

Figure 1-5. Thesis structure

Chapter 2 Transient Stability Analysis

This chapter introduces the concept of transient stability analysis (TSA) and discusses the research and development leading to the state-of-the-art innovations in the field. In section 2.1 the theory for transient stability studies is introduced. Section 2.2 provides an overview of time-domain simulation (TDS) - the conventional tool for assessing transient stability. While some utilities use TDS for online dynamic security assessment (DSA), TDS is computationally complex and requires long processing times, in addition to the time and expertise required to assess results.

Direct methods use simplified modelling assumptions to perform fast TSA, and to estimate transient stability margins (TSMs). There are two branches of direct methods: the Equal Area Criterion (EAC) and the Transient Energy Function (TEF) methods. Sections 2.3 and 2.4 describe the core concepts of these methods respectively. Section 2.5 reviews how they have been applied for the direct TSA of multi-machine power systems.

Traditionally direct methods have not been applied due to the restricted modelling capabilities. Thus hybrid-direct methods such as the SIME method for TSA have emerged. They combine the flexible modeling capabilities and accuracy of TDS with the time-saving and margin estimation techniques of the direct methods [3]. Section 2.6 reviews of the state-of-the-art hybrid-direct methods. Section 2.7 highlights the research gaps that are addressed by the novel Enhanced Binary-SIME (EBSIME) algorithm presented in the thesis.

2.1. Mathematical Model for a Synchronous Machine

Transient stability is concerned with the ability of synchronous machines in an interconnected power system to maintain synchronism with one another following a severe disturbance. Transient stability depends on the ability of each generator in a power system to maintain equilibrium between its output electromagnetic torque, and input mechanical torque. In transient stability studies non-linear differential-algebraic equations that describe the dynamic behaviour of equipment - such as generators, the transmission network, loads, SVCs and their controls - are used to assess whether or not a power system is secure. In the following sections a mathematical model that is used to describe the dynamic behaviour of the synchronous machines is presented.

2.1.1. Base Quantities

In the following analyses the base value of power is:

$$MBASE\ MVA = MBASE \times 10^6\ VA \tag{2.1}$$

the base value of speed is $\omega_0 = 2\pi f_0$ (2.2)

the base value of time is 1 second; and the base value of angle is 1 radian.

2.1.2. Deriving the Generator Swing Equations from Newton's Second Law

The generator swing equations describe the motion of the synchronous machine rotor. They are derived from first principles according to Newton's second law for rotational motion:

$$J_m^{(s)} \frac{d\omega_m^{(s)}}{dt} = T_m^{(s)} - T_e^{(s)} \tag{2.3}$$

where

$J_m^{(s)}$ = Combined moment of inertia of the generator and turbine in $\left(N \cdot m \cdot s^2\right)$

$T_m^{(s)}$ = Mechanical torque in $\left(N \cdot m\right)$

$T_e^{(s)}$ = Electrical torque in $\left(N \cdot m\right)$

$\omega_m^{(s)}$ = Rotor mechanical angular velocity in $\left[{}^{rad}/_{s}\right]$

t = Time in seconds

(s) indicates SI units

$\delta_m^{(s)}$ is the mechanical angular position of the generator rotor with respect to a synchronous reference frame.

The mechanical rotor speed is:

$$\frac{d\delta_m^{(s)}}{dt} = \omega_m^{(s)} - \omega_{0m} \tag{2.4}$$

The moment of inertia is assumed to have been adjusted to refer to the generator synchronous speed of $\omega_{0m} = \frac{2\pi f_0}{N_p}$ measured in $\left[{}^{rad}/_{s}\right]$, where N_p is the number of pole pairs.

The relationship between the electrical and mechanical rotor angles and speeds is:

$$\delta^{(s)} = N_p \delta_{mp} \tag{2.5}$$

$$\omega^{(s)} = N_p \omega_m^{(s)} \tag{2.6}$$

where

$\delta^{(s)}$ = Rotor electrical angle in radians

δ_{mp} = Rotor mechanical angle in radians

$\omega^{(s)}$ = Rotor electrical angular velocity in $\left[{}^{rad}/_{s}\right]$.

Multiplying both sides of equation (2.3) by $\omega_m^{(s)}$:

$$J_m^{(s)} \omega_m^{(s)} \frac{d\omega_m^{(s)}}{dt} = T_m^{(s)} \omega_m^{(s)} - T_e^{(s)} \omega_m^{(s)} \tag{2.7}$$

$$J_m^{(s)} \omega_m^{(s)} \frac{d\omega_m^{(s)}}{dt} = P_m^{(s)} - P_e^{(s)} \tag{2.8}$$

Define: $$\omega^{(p)} = \frac{\omega_m^{(s)}}{\omega_{0m}} \quad [\text{p.u.}] \tag{2.9}$$

where $^{(p)}$ indicates a per unit quantity. Substituting $\omega_m^{(s)} = \omega^{(p)} \omega_{0m}$ in to (2.4) gives

$$\frac{d\delta^{(s)}}{dt} = \frac{d\delta^{(p)}}{dt} = \left(\omega^{(p)} - 1\right)\omega_{0m} \tag{2.10}$$

and equation (2.8) becomes:

$$J_m \omega_{0m}^2 \omega^{(p)} \frac{d\omega^{(p)}}{dt} = P_m^{(s)} - P_e^{(s)} \tag{2.11}.$$

Then dividing (2.11) by the MVA base of the generator gives:

$$\frac{\left(J_m^{(s)} \omega_{0m}^2\right)\omega^{(p)} \frac{d\omega^{(p)}}{dt}}{MBASE \times 10^6} = \frac{P_m^{(s)} - P_e^{(s)}}{MBASE \times 10^6} = P_m^{(p)} - P_e^{(p)} \tag{2.12}.$$

Define: $$H^{(p)} = \frac{1}{2} \frac{J_m^{(s)} \omega_{0m}^2}{MBASE \times 10^6} \left[\frac{Joules}{Joules / s}\right] \tag{2.13}$$

as the machine inertia constant of the generator. $H^{(p)}$ represents the kinetic energy stored in the rotor at synchronous speed, in per unit (pu) of the machine MVA base. This leads to the swing equation in per-unit form:

$$2H^{(p)}\omega^{(p)}\frac{d\omega^{(p)}}{dt} = P_m^{(p)} - P_e^{(p)} \tag{2.14}.$$

In realistic power systems the deviation in rotor speed from synchronous speed is usually small. It is common to assume that $\omega^{(p)} \approx 1$; thus equation (2.14) becomes:

$$2H^{(p)}\frac{d\omega^{(p)}}{dt} = P_m^{(p)} - P_e^{(p)} \tag{2.15}.$$

2.1.3. The Centre of Inertia Assessment Criteria

For TSA it is convenient to describe the dynamic behaviour of a power system by expressing the rotor angle of individual generators with respect to an inertial centre. The centre of inertia (COI) rotor angle, also known as centre of angle (COA), is defined as:

$$\delta_{COI}(t) \triangleq \frac{1}{H_T}\sum_{i=1}^{n} H_i\delta_i(t) \tag{2.16}$$

where H_T is the sum of the inertia constants of the n online generators in the system. Note that all inertia constants are converted to a common base, usually the system MVA base. The derivative of (2.16) yields the following definition for the COI slip speed $\Delta\omega_{COI}$ [13]:

$$\frac{d\left(\delta_{COI}\right)}{dt} = \Delta\omega_{COI}\omega_0 \tag{2.17},$$

where ω_0 is synchronous speed in electrical rad/s and:

$$\Delta\omega_{COI} = \left(\tfrac{1}{H_T}\sum H_i\omega_i^{(p)} - 1\right) \tag{2.18}.$$

The motion of the rotor angle of an individual system generator, with respect to the COI, is defined as [13]:

$$\theta_i = \delta_i - \delta_{COI} \tag{2.19}.$$

The generator speed with respect to the COI is [13]:

$$\omega_i = \frac{\dot{\theta}_i}{\omega_0} = \left(\frac{\dot{\delta}_i}{\omega_0} - \Delta\omega_{COI}\right) pu \tag{2.20}.$$

Equations (2.19) and (2.20) can be used to assess the transient stability of a power system with respect to the COI reference frame. In an assessment using TDS, a scenario is classified as stable if the angle and speed responses for all generators converge towards the COI during the investigated timeframe. Conversely, a scenario is classified

as unstable if the angle and speed responses, of at least one significant generator, diverge from the COI before the end of the simulation period (see section 1.3.1).

2.2. The Time Domain Simulation (TDS)

Time domain simulations (TDS), also referred to as dynamic simulations, are the widely accepted tool for assessing transient stability. TDS have extensive modelling capabilities. They are able to accurately simulate the time-evolving responses of all variables in a multi-machine power system. In TDS an investigated power system is modelled by a set of non-linear differential and algebraic equations (DAEs). A fundamental-frequency positive-phase-sequence admittance representation of the transmission network is employed. This representation of the network is valid for transients within the bandwidth of interest in rotor-angle dynamics of around 0-10 Hz. The differential equations describe the dynamic characteristics of the system, such as the motion of the system generator angles and speeds, the electromagnetic behaviour of generators, flexible AC transmission system (FACTS) devices, HVDC links, the transient behaviour of loads, control systems fitted to generators and other plant, special protection systems and special stability controls [14]. Step-by-step numerical integration is used to solve the DAEs over the time-frame of interest.

2.2.1. Numerical Integration Techniques for Time Domain Simulations

TDS are able to provide results for very detailed and accurate system models. However, calculations are complex and computationally demanding, especially for modern systems with large networks that require complex models. Traditionally a TDS uses the trapezoidal integration method to calculate, step-by-step, a time-varying solution. Fixed-size time-steps are used, however they must be smaller than the smallest time-constant in the dynamic system model to avoid numerical instability. For larger power systems, the numerical conditions are stiffer. These issues can be mitigated to some degree by employing an A-stable integration method such as the trapezoidal method or more advanced variable step-size algorithms. This contributes to the significant computational burden of the TDS [15, 16].

For real-time DSA accelerated numerical integration procedures that do not compromise solution accuracy are desirable. The mixed Adams-Bashforth-Moulton Backwards Differential Formula method (ABM-BDF) uses a variable time-step and variable-order-algorithm. It is currently used to solve TDS for online DSA of the Brazilian power system. In [16] Jardim claims that ABM-BDF is able to accelerate the TDS assessment

speed by a factor of ten, while maintaining a high level of numerical stability. Jalili-Marandi propose a very different concept where the TDS is performed using parallel processing with NVIDIA's CUDA graphics acceleration card [17, 18]. Using a fully detailed model of the IEEE 39-bus test system they demonstrate that this TDS with CUDA can be processed up to 340 times faster than the conventional TDS with PSS®E.

However, the TDS numerical integration methods are ultimately determined by the power system software that is used by a system operator. In Australia PSS®E is the widely used tool in the power industry. It provides facilities to solve TDS using the Modified Euler's methods with a fixed step-size.

2.2.2. Limitations of the Time Domain Simulation

Computation speed is a critical factor for TSA, as well as the time required by engineers to assess the results. While the TDS can provide a stable or unstable diagnosis, it does not provide information about how far a system operating condition is from the transient stability limits. Typical measures of transient stability, such as the critical clearing time (CCT) of a fault, provide some indication of the degree of power system stability following a disturbance. However, they do not provide further insight into how system parameters - such as interconnector transfer levels, generator outputs or system load - should be regulated to ensure adequate system security. Knowledge of the sensitivity of operating limits to controllable system parameters reduces the dependence on trial and error analysis and augments the experience of the system operator.

2.3. The Equal Area Criterion (EAC)

The equal area criterion is a classical method of transient stability analysis that is based on the assessment of a lossless One Machine Infinite Bus power system (OMIB) model, as in Figure 2-1. The OMIB is representative of a single generator delivering power, P_e, to a large system. A classical second order model is used to represent the generator and the large system is represented by an infinite bus - an ideal voltage source that maintains constant magnitude, phase and frequency.

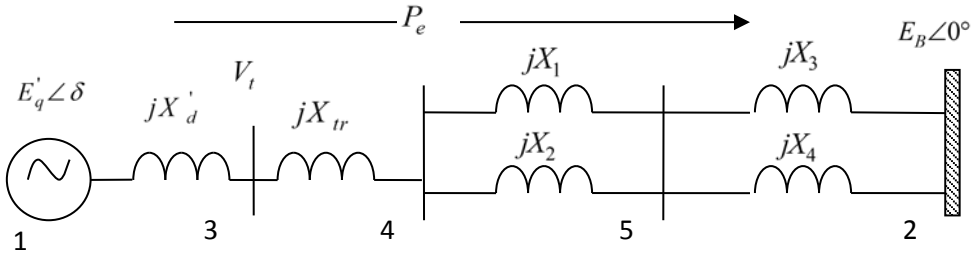

Figure 2-1. A lossless one machine infinite bus power system (OMIB)

In Figure 2-1:
E_B is the constant voltage of the infinite bus,
X_i for i =1, 4 are the transfer reactances of the transmission line segments,
V_t is the generator terminal voltage,
$X_d^{'}$ is the generator transient reactance,
X_{tr} is the equivalent transformer reactance, and
$E_q^{'}$ is the internal generator voltage.

In transient stability studies the rotor dynamics for the classical generator are described by the velocity and acceleration equations respectively:

$$\frac{d\delta}{dt} = \omega_0 (\omega - 1) \tag{2.21}$$

$$2H\omega \frac{d\omega}{dt} = P_m - P_e \tag{2.22}$$

where H is the machine inertia constant,
ω is the per-unit angular velocity of the rotor,
δ is the rotor angle (in radians),
P_m is the per-unit mechanical power supplied by the prime mover (minus mechanical losses), and
P_e is the per-unit electrical power output from the generator.

Following a transient disturbance the network topology changes as the result of the application of the fault and then the network switching operations required to clear it. Thus three network states – initial steady-state, fault and post-fault – are identified for the total network admittance, $\hat{Y}_{12}$. For the lossless OMIB system in Figure 2-1, where the machine is connected to node 1 and the infinite bus is connected to node 2, the generator power output is [19]:

$$P_e = B_{12} E_q^{'} E_B \sin\delta \tag{2.23}$$

where the series susceptance B_{12}, between nodes (1) and (2), depends on the network state.

The EAC is used to determine whether or not the OMIB system will remain stable following a disturbance, without solving the system state equations. Stability is established by using the OMIB power-angle curve, in Figure 2-2, to determine if the kinetic energy absorbed by the generator rotor during the fault can be transferred to the system after fault clearance, thus enabling the rotor to return to synchronous speed [13, 20].

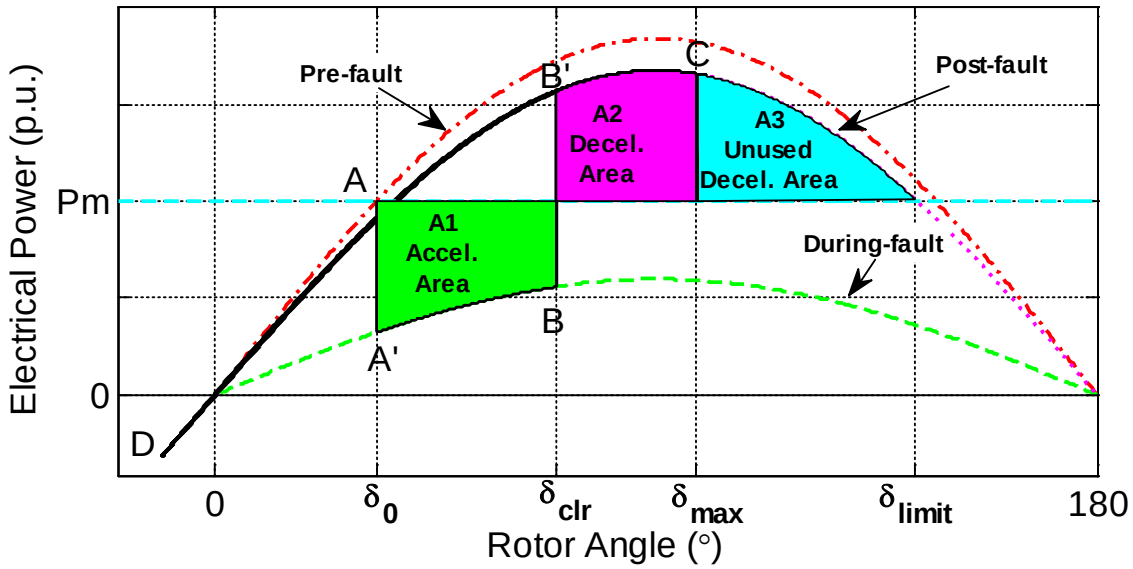

Figure 2-2. The OMIB electrical power versus rotor angle characteristic demonstrating the equal area criterion for a stable scenario.

In Figure 2-2 the system begins in a state of equilibrium at point A. After the fault is applied (A→A') the net torque becomes positive. This causes the rotor to accelerate and the rotor angle increases (A'→B) until the fault is cleared at $\delta = \delta_{clr}$ (B→B'). After fault clearance the net torque is negative. This causes the rotor to decelerate, although since the generator is running above synchronous speed the rotor angle will continue to increase on the trajectory (B'→C). At the maximum angle δ_{max} the rotor returns to synchronous speed, then the rotor angle begins to decrease on the trajectory (C→B'→D). The system is stable on the forward-swing.

The rotor continues to decelerate below synchronous speed. When P_e decreases below P_m the rotor accelerates again. The system follows the trajectory C→B'→D, and reaching synchronous speed and the minimum angle at point D. The system is stable on the back-swing. Then, the rotor angle and speed rise as the rotor is still accelerating. Since the system is undamped, the rotor angle and electrical power oscillate between points C and D and the system remains synchronized.

It can be shown that when the machine returns to synchronous speed (point C) that the deceleration area A2 is equal to the acceleration area A1. By the EAC if this is possible then the system is forward-swing stable. Otherwise if the total deceleration area (A2) is less than the acceleration area (A1) the generator will lose synchronism with the rest of the system [13] as shown in Figure 2-3. Stability requires that $P_e(\delta_{max}) \geq P_m$ or equivalently $\delta_{max} \leq \delta_{limit}$, where δ_{limit} is the OMIB rotor angle limit.

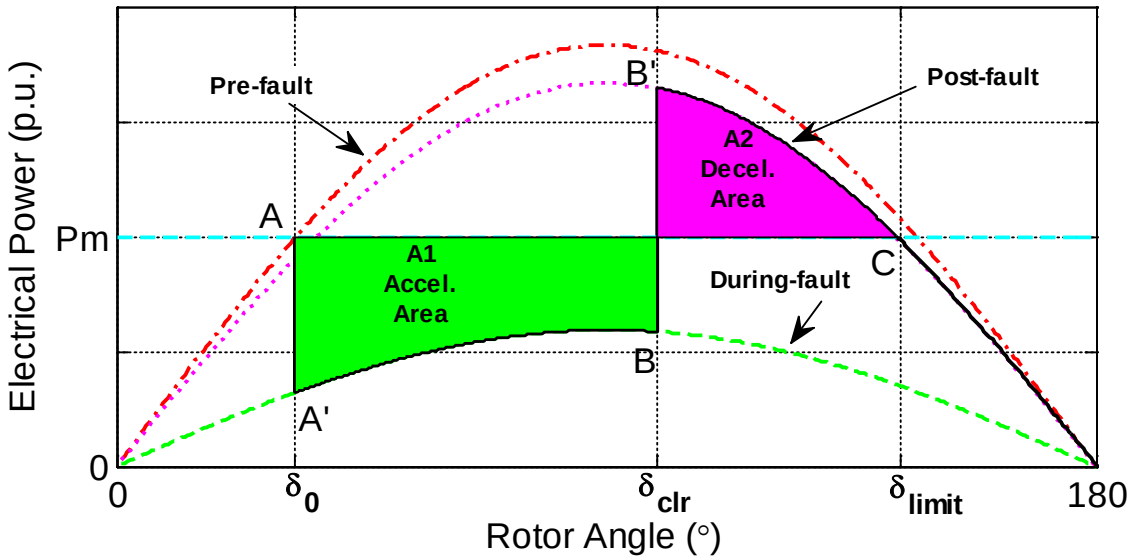

Figure 2-3. The OMIB electrical power versus rotor angle characteristic demonstrating the equal area criterion for an unstable scenario.

2.3.1. Margin Criteria for the Equal Area Criterion

The EAC uses the acceleration and deceleration areas formed by the power-angle curve to quantify the distance of a system from the forward-swing transient stability limit (TSL). For stable scenarios the margin is defined as the unused deceleration area (A3) where:

$$\eta = -\int_{\delta\max}^{\delta\text{limit}} P_a d\delta = A3 \tag{2.24}$$

where $P_a = P_m - P_e$. For unstable scenarios the margin is defined as the amount by which the acceleration area exceeds the available deceleration area:

$$\eta = -\left(A_{acc} - A_{dec}\right) = \int_{\delta 0}^{\delta\text{limit}} P_a d\delta < 0 \tag{2.25}$$

where δ_0 is the OMIB rotor angle in the steady state prior to the fault application, and A_{acc} and A_{dec} are the acceleration area (A1) and deceleration area (A2) as per Figure 2-3.

This interpretation of the unstable margin differs from the kinetic energy-based approaches presented by Kundur, Pavella et al, and Sauer in [1, 13, 21] which assume that equation (2.25) is equal to:

$$\eta_{KE} = -\frac{1}{2} M \omega_{\text{limit}}^2 \tag{2.26}$$

Here M is the OMIB inertia coefficient [1, 21] and ω_{limit} is the OMIB generator speed when $\delta = \delta_{limit}$. However, an analysis of equations (2.25) and (2.26), for a lossless system, reveals the following relationship:

$$\eta = \int_{\delta 0}^{\delta \text{limit}} P_a d\delta = \frac{1}{2\omega_0} M \omega_{\text{limit}}^2 = \frac{\eta_{KE}}{\omega_0} \tag{2.27}$$

where ω_0 is defined in (2.2).

It is important to note that equation (2.26) does not represent the kinetic energy or the change in kinetic energy of the rotor. This is discussed in detail in Appendix A.

2.3.2. Early Stop Criteria (ESC) for the Equal Area Criterion

In [1] Pavella et al propose that early stopping criteria (ESC) for the early detection of both forward-swing stability and instability can be derived from the EAC. The two criteria are explained as follows:

Criteria 1: For a forward-swing stable scenario, stability is anticipated at time t_r when the OMIB rotor velocity $\omega(t_r) = 0$ and the OMIB accelerating power is negative $P_a(t_r) = P_m(t_r) - P_e(t_r) < 0$. The criteria assumes that $\omega(t) > 0$ for $t_f < t < t_r$, where t_f is the time when the fault is applied. A caveat of the forward-swing stability criteria is that the system is not necessarily stable because it may become transiently unstable on an ensuing power swing.

Criteria 2: Instability can first be determined at time t_u when the OMIB acceleration power $P_a(t_u) = 0$, $\frac{dPa}{dt}\Big|_{t=tu} > 0$ and $\omega(t) > 0 \text{ for } t_f < t < t_u$, where t_u is the time when the system loses synchronism. Pavella et al also claim that the unstable ESC can be extended to identify multi-swing instability [1].

Figure 2-4 demonstrates the application of the ESC for a stable scenario, and an unstable scenario. Other examples of the ESC are shown in Appendix A.

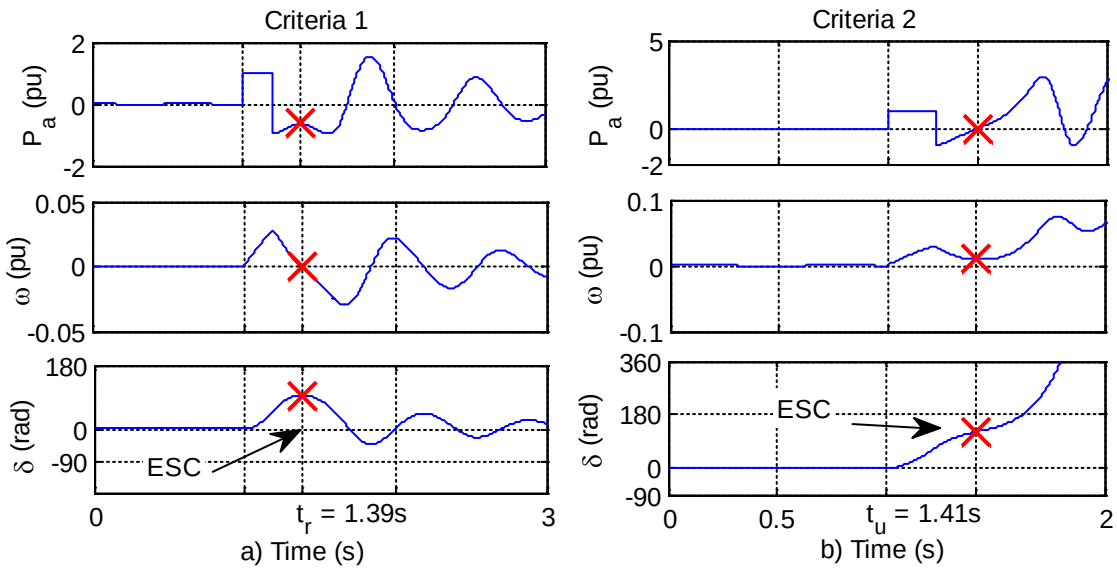

Figure 2-4. The acceleration power (P_a), speed(ω) and angle (δ) of the OMIB system, demonstrating the ESC stop criterion for a) a forward-swing stable, and b) a forward-swing unstable scenario.

2.3.3. Multi-Swing Instability

The ESC provides a fast method to assess transient stability or instability on the forward-swing of the OMIB response of a power system. The forward-swing refers to the portion of the OMIB power-angle curve where the angle increases in response to an applied fault. The forward-swing begins when the fault is applied. The forward-swing ends when the system returns to synchronous speed (forward-swing stable - i.e. from point A to C in Figure 2-2). If the OMIB angle exceeds δ_{limit} before the end of the forward-swing happens then the system operation is constrained by forward-swing instability.

In some circumstances the system operation may return to synchronism at the end of the forward swing, but become unstable on a subsequent swing. In this situation the system operation is constrained by multi-swing instability. This is demonstrated in the OMIB response of a multi-swing unstable shown in Figure 2-5. The system is classified by the ESC as forward-swing stable at t = 1.8s, but it later becomes unstable on a the subsequent-swing at t = 2.6s.

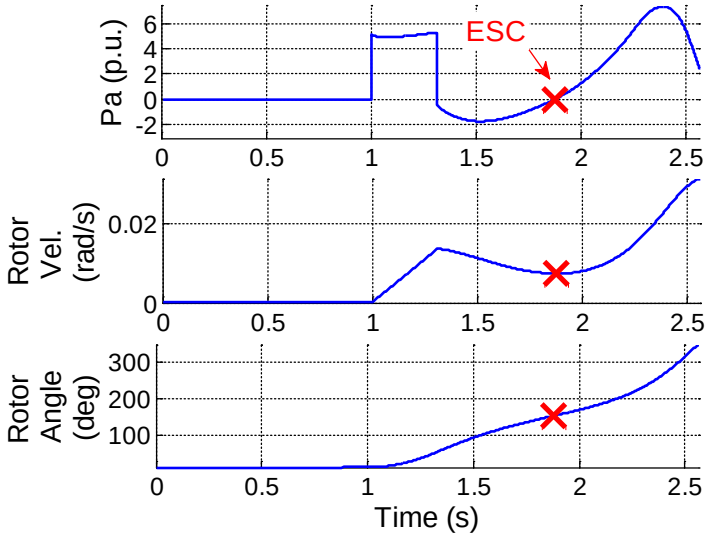

Figure 2-5 OMIB response demonstrating a multi-swing scenario

2.3.4. Limitations of the EAC

The pure EAC is used to perform fast transient stability assessment using the angle, speed and power response from a single generator response the OMIB system. It is limited to classical second-order machine modelling to represent the dynamic generator response and assumes the system is lossless. The transient stability assessment that is based on the EAC is constrained to a fast diagnosis of forward-swing transient (in)stability, and not multi-swing (in)stability.

The EAC can be applied for fast and accurate transient stability analysis of multi-machine power systems by using TDS to calculate the fully detailed system response. The machines responses, calculated using the TDS, can be linearly combined to derive a single machine response that represents the dynamic behaviour of all system machines. Fast forward-swing TSA can be performed by applying the ESC to the single machine response that has been calculated using the TDS. Furthermore, multi-swing transient instability can be reliably assessed using the TDS.

2.4. The Transient Energy Function Method (TEF)

The transient energy function (TEF), derived from Lyapunov's method, is a direct approach to TSA that has been extensively researched in the literature [21]. It can be used to determine whether or not a multi-machine power system will remain forward-swing stable, by evaluating a TEF that models the dynamic behaviour of the post-fault system. Transient stability energy margins (TEM) can be estimated from the TEF.

Presently TEF methods have significant limitations because of their restricted modelling capabilities. The TEF concept is limited to the analysis of forward-swing instability. It does not extend to scenarios that are susceptible to multi-swing instability – which is a real concern on the Australian power system [103-106].

2.4.1. Modelling a Power System with the Classical Transient Energy Function

The TEF technique considers the behaviour of a power system in the fault and post-fault time-frames, and assumes a lossless system. To formulate a TEF, or Lyapunov function, the algebraic nodal network equations for a power system must be reduced to a form where only the internal generator buses are represented. An example of this procedure is described in section 4.2. The dynamic behaviour of the system is represented by applying the reduced network equations to the synchronous generator equation (2.15). Rearranging equation (2.15) for each system machine [21] the individual machine energy function for the *i*th machine is defined as:

$$V_i(\theta_i, \omega_i) = \frac{1}{2} M_i \omega_i^2 - \int_{\theta si}^{\theta i} P_{ai}(\theta_i) d\theta_i, \qquad for\ i = 1, m \tag{2.28}$$

where

m is the total number of online machines when the system is in the post-fault state,

$M_i = 2H_i$, where H_i is the machine inertia of the ith machine,

θ_i and ω_i are the rotor angle and speed of the ith machine relative to the COI in the post-fault network – as described in (2.19) and (2.20),

θ_{si} is the post-fault rotor angle that the ith generator converges to if the scenario is forward-swing stable– also called the stable equilibrium point (SEP), and

$P_{ai}(\theta_i)$ is the acceleration power of the ith machine as a function of rotor angle.

The TEF to represent the entire system is calculated by summing together the individual machine energy functions. This yields [21]:

$$V(\theta, \omega) = \frac{1}{2} \sum_{i=1}^{m} M_i \omega_i^2 - \sum_{i=1}^{m} \int_{\theta si}^{\theta i} P_{ai}(\theta_i) d\theta_i \tag{2.29},$$

which is interpreted as the sum of the system kinetic energy accumulated during the fault and the potential energy of the post-fault system. The system kinetic energy is defined as[1]:

$$V_{KE} = \frac{1}{2} \sum_{i=1}^{m} M_i \omega_i^2 \tag{2.30}$$

[1] This is the same as equation (2.26). As discussed in section 2.3.1 and Appendix A this equation does not describe kinetic energy.

and the post-fault system potential energy is defined as:

$$V_{PE} = -\sum_{i=1}^{m} \int_{\theta si}^{\theta i} P_{ai}\left(\theta_i\right) d\theta_i \tag{2.31}.$$

To qualify as a valid energy function equation (2.29) must be positive-definite such that $V\left(\theta,\omega\right) > 0$ and $\dot{V}\left(\theta,\omega\right) < 0$.

For the OMIB system in Figure 2-1 the energy function is [21]:

$$V(\theta,\omega) = \frac{1}{2} M \omega^2 - \int_{\theta s}^{\theta} P_m - P_{e\max} \sin\theta d\theta \tag{2.32}.$$

where $P_{e\max} = B_{12} E_q^{'} E_B$ for the post-fault network, as described in (2.23). Then:

$$V_{PE}(\theta) = -P_m\left(\theta - \theta_s\right) - P_{e\max}\left(\cos\theta - \cos\theta_s\right) \tag{2.33},$$

where equation (2.33) is also the deceleration area A2 in Figure 2-2.

From equation (2.33) the gradient function for the OMIB system is derived:

$$-\frac{\partial V_{PE}}{\partial \theta} = P_m - P_{e\max} \sin\theta \tag{2.34}.$$

The gradient function is significant as it is used by the Boundary Controlling UEP (BCU) method for TSA, as discussed in section 2.5.6.

For a multi-machine power system there are many possible TEFs that cover different ranges of operating conditions and contingencies [22]. To satisfy the positive-definite criteria all generators are represented as classical machines, the network is lossless and network loads are represented as constant impedances, therefore the network transfer conductance is ignored. Reactive power demand and voltage variations at the load buses, flux decay and exciter controls are neglected. Furthermore, information on the transient behaviour of different system equipment in the system and their positions are lost when network-reduction is applied to formulate the TEF. User-discretion is required to select the TEF that encompasses the largest possible set of stable operating conditions over the desired range of operating conditions for the best approximation of system behaviour [9, 21, 23-27].

2.4.2. The Potential Energy Boundary Surface (PEBS) Method

The PEBS method postulates that under transient conditions power system operation can be likened to a ball rolling on a bowl-shaped potential energy surface [13, 28]. Prior to a fault, the system rests at its pre-fault SEP where the system has minimum potential energy. The SEP is surrounded by a set of unstable equilibrium points (UEP). In a transient unstable scenario the system operation will converge towards one of the UEPs.

The stability boundary that connects all the UEPs is known as the PEBS. It is calculated based on the post-fault system network.

When a fault is applied to the system, there is an imbalance of system energy which makes the system gain both kinetic and potential energy. This causes the system energy trajectory to move up the potential energy surface. When the fault is cleared the trajectory continues up the surface as the kinetic energy gained during the fault is converted into potential energy. If all the accrued kinetic energy can be converted into potential energy before the energy trajectory reaches the PEBS, then the system is classified as forward-swing stable. If the system is forward-swing stable then the trajectory will return to the post-fault SEP. Otherwise if the system is unstable the trajectory will cross the PEBS before all of the kinetic energy can be expended.

The PEBS is demonstrated on the OMIB system in Figure 2-6 where equations (2.32) and (2.33) are plotted. Equation (2.32) is plotted for a stable scenario.

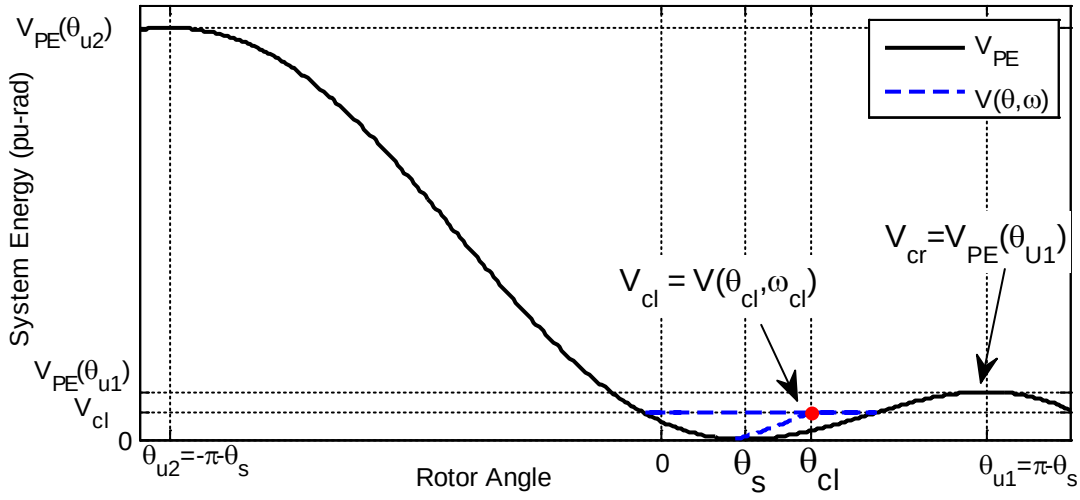

Figure 2-6 Overlay of the Potential Energy Curve and the TEF for the OMIB system for a stable scenario.

The post-fault SEP is given by the solution of [21]:

$$P_m - P_{e\max} \sin\theta_s = 0 \tag{2.35}$$

where

$$\theta_s = \sin^{-1}\left(\frac{P_m}{P_{e\max}}\right) \tag{2.36}.$$

The SEP at θ_s is bounded by two UEPs at $\theta_{u1} = \pi - \theta_s$ and $\theta_{u2} = -\pi - \theta_s$, which correspond to saddle points on V_{PE} in Figure 2-6. In this example the two UEPS form

the PEBS. When the fault is applied, the system absorbs kinetic energy causing the machine angle and system energy to increase. As the system is lossless the post-fault value of $V(\theta,\omega)$ is a constant value that is determined when the fault is cleared at $V_{cl} = V\left(\theta_{cl}, \omega_{cl}\right)$. If $V_{cl} > V_{PE}\left(\theta_{U1}\right)$ when the rotor angle is increasing then the system is unstable on the forward swing, otherwise it is stable. If $V_{cl} > V_{PE}\left(\theta_{U2}\right)$ and the rotor angle is decreasing due to deceleration then the system is also unstable.

For a marginally unstable case when the energy trajectory crosses the PEBS, the cross-over point (i.e. θ_{U1}) is called the "exit point". The exit point is analogous to the network operating condition at the maximum allowable rotor angle, δ_{limit} , from the EAC in section 2.3. Foaud and Stanton explain that the critical energy of a system is calculated by [29]:

$$V_{cr} = V\left(\hat{\theta}_{UEP}\right) - V\left(\hat{\theta}_{S}\right) \tag{2.37}$$

where $\hat{\theta}_{UEP}$ and $\hat{\theta}_{S}$ respectively represent the vector of machine angles at the UEP closest to the exit point and at the post-fault SEP. It is assumed that the system machines are able to return to synchronism at the exit point such that the kinetic energy at $\hat{\theta}_{UEP}$ and $\hat{\theta}_{S}$ is zero. V_{cr} dictates how much transient kinetic energy can be absorbed by the post-fault system before forward-swing instability occurs.

Forward-swing stability is assessed by comparing V_{cr} against the instantaneous system energy when the fault is cleared [29]:

$$V_{cl} = V\left(\hat{\theta}_{cl}\right) - V\left(\hat{\theta}_{S1}\right) \tag{2.38}$$

where $\hat{\theta}_{cl}$ and $\hat{\theta}_{S1}$ are respectively the vector of machine angles at the point of fault clearance, and at the pre-fault SEP of the system. The system will maintain forward-swing stability if:

$$V_{cl} < V_{cr} \tag{2.39}$$

otherwise it will lose synchronism [21].

2.4.3. The Corrected Kinetic and Potential Energy

For a marginally unstable scenario, equations (2.37) and (2.38) assume that the kinetic energy modeled by a TEF should reduce to zero when the energy trajectory reaches the PEBS. However, Fouad and Stanton find that the system kinetic energy at the PEBS is predominantly a non-zero value [29]. They postulate that the residual kinetic energy at the PEBS does not contribute to the desynchronizing forces in the system, and it is due

to V_{cr} and V_{cl} being calculated from two different reference points[2]. From equations (2.37) V_{cr} is calculated with respect to the post-fault network, and from equation (2.38) V_{cl} is calculated with respect to the pre-fault steady-state network. Foaud and Stanton [29] define the residual kinetic energy:

$$V_{KEcorr} = V\left(\hat{\theta}_S\right) - V\left(\hat{\theta}_{SS}\right) \tag{2.40}$$

where $\hat{\theta}_{SS}$ represents the vector of machine angles at the pre-fault SEP.

This correction factor must be added to equation (2.37) to ensure V_{cr} and V_{cl} are calculated in the same reference frame. The kinetic and potential energies in equations (2.30) and (2.31) also must be adjusted by the correction factor [28, 30, 31]. In this way the TEF can represent conservation of energy for a lossless system.

Vaheedi et al [32] propose a method to calculate the corrected kinetic and potential energies for a multi-machine power system. Fang et al [31] postulate the notion of a corrected TEF, which is the sum of the corrected kinetic energy and the correct potential energy. The corrected TEF influences V_{cr} and the transient energy margins (TEM), described in section 2.4.6, that are calculated for the system.

2.4.4. The Mode of Disturbance (MOD)

The method for calculating the corrected kinetic and potential energies [32] is based on the assumption that the loss of synchronism of a power system is caused by a subset of machines that accelerate away from the rest of the system such that it separates into two aggregate groups of machines. In TEF literature the pattern by which the machines lose synchronism and separate is referred to as the mode of disturbance (MOD)[3]. According to Rahimi and Xue et al [33, 34] there is a unique MOD associated with each UEP that enables the fastest possible TSA, and yields the smallest possible margin for a given scenario. The MOD is dependent on the system topology, type and location of the fault, and also on system loading conditions [33]. The concept of the MOD, and the assumption that an unstable system separates into two coherent subsets of machines, are also embraced by the direct-EAC methods.

2.4.5. The Controlling Unstable Equilibrium Point

The UEP used to assess forward-swing stability that is closest to the system trajectory of a disturbed system is called the controlling *UEP* (CUEP) [29]. The trajectory, and

[2] This is different to the problem of the interpretation of the unstable margin mentioned in sections 2.3.1 and 2.4.1.

[3] In some publications it is called the mode of separation, or the mode of instability, but for consistency in this document it is referred as the MOD.

therefore the CUEP, depend on the initial system operating conditions, and the type and location of an applied disturbance. In the scenario shown in Figure 2-6 the CUEP is at $V(\theta_{U1})$. The CUEP and its associated MOD are important as they are required to calculate the corrected kinetic and potential system energies, and V_{cr}.

In this thesis the term scenario describes the combination of an initial operating condition, applied disturbance, and the fault clearance scheme. For a given scenario, there is one critical trajectory that can pass through the CUEP [29]. It corresponds to the scenario that is marginally forward-swing unstable. Locating the CUEP of a scenario is a computationally intensive and multi-dimensional optimization problem, especially for large multi-machine power systems. The CUEP can be determined from the critical trajectory, but this involves a repetitive numerical integration procedure to locate the corresponding marginally unstable scenario that the direct methods aim to avoid [29].

2.4.6. The Transient Energy Margin (TEM)

The TEM is:

$$\varepsilon_k = V_{cr} - V_{cl} \tag{2.41}$$

where $\varepsilon_k > 0$ for forward-swing stable scenarios and $\varepsilon_k < 0$ for forward-swing unstable scenarios [35]. For the stable scenario, ε_k represents the additional potential energy that remains to be converted into kinetic energy before the energy trajectory crosses the PEBS. For the unstable scenario ε_k represents the total kinetic energy that cannot be absorbed by the post-fault system before the trajectory reaches the PEBS.

2.4.7. Transient Energy Function Stop Criteria

Forward-swing instability can be diagnosed as soon as a system trajectory crosses the PEBS. At the PEBS crossing the system behaviour is described by the dot product:

$$P_a^T\left(\tilde{\theta}\right)\cdot\left(\tilde{\theta}-\tilde{\theta}_s\right)=0 \tag{2.42}$$

where

P_a^T is the vector of the acceleration power for all online systems machines at the instant the system trajectory crosses the PEBS,

$\tilde{\theta}$ is a vector of the machine rotor angles at an arbitrary post-fault operating point, and

$\tilde{\theta}_s$ is a vector of the machine angles at the post-fault SEP.

The PEBS crossing can be determined by solving equation (2.42) at every time-step. If the polarity of equation (2.42) changes during fault application or after fault clearance

then the *trajectory* has crossed the PEBS and the scenario is unstable [21]. The instant at which instability is detected is t_{PEBS} .

For early determination of forward-swing stability, the following dot product is monitored: $$\tilde{\omega} \cdot \left(\tilde{\theta} - \tilde{\theta}_s \right) \tag{2.43}$$

where $\tilde{\omega}$ is the vector of machine speeds.

After fault clearance, if equation (2.43) changes sign before the unstable TEF early stop criteria is satisfied, then the system is forward-swing stable. This instant at which stability is detected is t_{stable} . The change in sign reflects the first instant when the system returns to synchronous speed after the forward-swing. At this point the kinetic energy of the system trajectory is at a minimum. Equations (2.42) and (2.43) are analogous to the EAC stop criteria reviewed in section 2.3.2. However, the detection of forward swing stability does not preclude the possibility of back-swing or multi-swing instability.

2.5. Direct Methods for Transient Stability Analysis

The pure-direct methods for transient stability analysis apply either the EAC or TEF to perform transient stability analysis on a multi-machine power system. The motivation behind the pure-direct methods is that fast TSA can be performed by assessing a time-invariant function that approximates the post-fault dynamic behaviour of a multi-machine system. In the direct TEF methods the time invariant function is the TEF. In the direct-EAC methods it is a function that approximates an equivalent OMIB representation of the post-fault system. Then, the only additional information that is needed is the system condition at the instant after fault clearance. This can be obtained by running a TDS until the instant when the fault is cleared [33].

The pure-EAC and pure-TEF methods share a number of common features:

- Representation of system machines and loads is restricted to classical models
- Loss of synchronism is attributed to a system splitting into two aggregate groups of machines [1, 34]. This is a physical interpretation of the MOD, described in section 2.4.4, and
- The MOD is used to formulate the time-invariant function for the post-fault network.

The disadvantages of the direct methods are:

- The time invariant function of the post-fault system response must be tuned to the investigated network. Furthermore the function is unable to accurately model the system response under stressed operating conditions and when inter-area mode stability issues are present [28]
- The procedures to search for the MOD require tuning, based on prior knowledge of the system behaviour
- The correct MOD must be used otherwise the TSA, and calculated margins, may be too conservative, or potentially incorrect [34, 36]
- Limited modelling capability; ie. direct methods are unable to capture limits on machine excitation which can significantly affect transient performance.

The features that distinguish the direct methods from one another are:

- How the time-invariant function is formulated
- The approach taken to calculate or approximate the MOD, and
- How the TSMs are calculated.

In literature, two principal direct-EAC methods have been developed: the static extended EAC [1, 34], and the Generalized EAC [33]. These approaches are concerned with applying the EAC to the OMIB approximation of a full power system. In [37-39] Haque postulates a different approach where the EAC is applied to assess the behaviour of a single machine that is considered most responsible for loss of synchronism in a multi-machine system. These methods are reviewed in sections 2.5.1 to 2.5.3.

In the Extended Equal Area Criterion (EEAC) and methods derived from it, the MOD is described with respect to an aggregate group of machines that pull away from the rest of the network, thus causing loss of synchronism. The divergent group of machines is called the ‘critical cluster’ or ‘critical machines’ (CM).

The MOD, the PEBS and the Boundary Controlling UEP (BCU) methods are the three kinds of direct-energy based approaches that have been reported in TEF literature for transient stability analysis. The defining aspect that sets each of these methods apart is how the CUEP is identified. Once located V_{cr} can be estimated and the transient stability of the system can be directly assessed. These methods are reviewed in sections 2.5.4 to 2.5.6.

The main disadvantage of the direct-energy methods are the model simplifications that are assumed since they are based on the *classical energy function model*. To overcome the limitations of the classical TEF, structure preserving models (SPM) and their associated energy functions (SPEFs) were developed. However when applied to assess

transient stability with the direct-energy methods the SPMs and SPEFs exhibit some of the same limitations. The developed SPMs, SPEFs and their integration with the direct-TEF methods is reviewed in section 2.5.7.

2.5.1. The Generalized Equal Area Criterion (GEAC)

In the GEAC the dynamic OMIB response of a multi-machine system is represented by the time-varying equation:

$$M_{OMIB}\frac{d^2\psi}{dt^2} = P - P_{\max}\sin(\psi - \nu) \tag{2.44}$$

$$M_{OMIB} = \frac{M_A M_B}{M_A + M_B} \tag{2.45}$$

$$\psi = \delta_A - \delta_B \tag{2.46}$$

where

M_A and M_B are the total machine inertias of the generators in machine groups A and B, respectively, as defined by the MOD (see section 2.4.4), and $M_A \le M_B$,

M_{OMIB} is the equivalent machine inertia of the OMIB system,

δ_A and δ_B are the COI angles of the two machine groups,

ψ is the aggregate angle difference between the two machine groups,

P and P_{max} are the DC offset and the maximum amplitude of the OMIB electrical power respectively, and

ν is the angle offset of ψ.

Calculation of P, P_{max} and ν require a network reduction so that the system admittance-matrix (**Y**) describes the network at the internal generator nodes only. P, P_{max} and ν are time varying values, dependent on the system machine angles. It is assumed that P, P_{max} and ν oscillate periodically about a steady-state value. Thus, the GEAC formulates a time-invariant version of equation (2.44), where the average values of P, P_{max} and ν are used as constant parameters. The EAC is applied to the time invariant equation (2.44), and used to derive analytical equations for the acceleration and deceleration areas. For a given *scenario*, where the fault clearing time is specified, fast TSA can be performed without using TDS.

Rahimi proposes the following stability index (SI), similar to the EAC margin equations (2.24) and (2.25):

$$SI = \frac{A_{dec} - A_{acc}}{\min(A_{dec}, A_{acc})} \tag{2.47}.$$

A limitation of the GEAC is that for each considered *scenario* a repetitive search to select the MOD must be performed. A good initial guess for the MOD, based on

knowledge from extensive offline studies, must be provided as the speed and accuracy of the search depends on the initial guess.

2.5.2. The Extended Equal Area Criterion

The Extended Equal Area Criterion (EEAC) uses equation (2.44) to represent the dynamic OMIB equivalent behaviour of the post-fault system [40]. The EEAC uses a fourth order Taylor series approximation to estimate the time-varying OMIB rotor angle response. The approximation is used to formulate the OMIB power-angle characteristic for use with the EAC.

The EEAC uses the margin equations of the EAC in section 2.3.1. As an additional measure of transient stability it provides an analytical expression for the CCT. This equation is based on the approximated OMIB rotor angle. Xue et al propose an approach for extending the EAC margins and stop criteria to assess scenarios constrained by back-swing instability [34].

The EEAC method is based on the view that transient instability is caused by the separation of the power system into two groups of coherent machines. It defines the critical group of machines (CM) as the cluster of machines that yield the largest COI angle at the end of the forward-swing of an unstable scenario. The term CM is synonymous with the MOD. A thorough and repetitive search is required to select the CM, where an operator must provide a good initial guess of the CM. The desired CM yields the lowest CCT. However the EEAC is constrained to assess forward-swing instability. Furthermore, the CM search is very slow for a bad initial guess, or if there are equal numbers of CMs and non-CMs.

2.5.3. The Severely Disturbed Machine (SDM) Method

The SDM method [38, 39] uses the assumption that the transient stability of a multi-machine system can be assessed by applying the EAC to a single machine. The SDM is considered to be the machine that is most responsible for loss of synchronism in the network. It is determined by assessing the post-fault acceleration power of individual machines and identifying the first machine that exceeds a selected threshold. The post-fault dynamic response of the SDM is approximated with a time-invariant equation. While this method avoids calculating the MOD, the acceleration power threshold must be tuned to identify the correct SDM. Furthermore, it does not consider the responses of other machines that may significantly influence system stability [39].

2.5.4. The Mode of Disturbance Method

The MOD method, also called as the lowest energy UEP method [21], presents a direct-energy approach for TSA that requires identification of the MOD corresponding to the CUEP of a given scenario. The desired MOD will yield the lowest value of the normalised critical system energy [41]

$$\Delta V_{PE \cdot n} = \frac{V_{cr}}{V_{KE \cdot corr}} \tag{2.48}$$

where $V_{KE \cdot corr}$ is the corrected kinetic energy.

The lowest value of $\Delta V_{PE \cdot n}$ and its CUEP can be used for TSA of the investigated scenario. Early versions of the method require an analyst to suggest several MODs that may yield the CUEP [42], which requires prior experience of the system behaviour. Analysis is also limited to small systems that operate under moderate load.

Vittal, et al. propose a scheme to auto-generate the correct MOD and CUEP for large stressed power systems [41]. The potential MODs are determined at the instant immediately after fault clearance by ranking online system machines in descending order of accelerating power and $V_{KE \cdot corr}$. The desired MOD is one of the top-ranking MODs that yields the lowest $\Delta V_{PE.n}$. However, the automated MOD search is a computationally intensive multi-dimensional optimization problem [43]. Under stressed operating conditions the search may fail to converge, or converge to the wrong CUEP. This makes the automated MOD method unacceptable for online DSA applications [28].

2.5.5. The PEBS Method

The PEBS method, also known as the sustained fault method, or Kyoto approach, [44] [45] avoids the difficult problem of calculating the MOD by directly approximating the CUEP and the critical system energy, V_{cr}. The CUEP is estimated by simulating the system TEF in the fault-state until it crosses the PEBS at the operating point θ^*. The TEF stop criteria from equation (2.42) is used to identify the PEBS crossing and halt the simulation. θ^* is approximated to be the CUEP. V_{cr} is calculated from the estimated PEBS crossing point and used for fast TSA and calculating TEMs.

The PEBS method is based on the assumption that the energy *trajectory* of a marginally stable scenario will pass close to the PEBS at an operating point that is also very close to the CUEP [21]. However Mansour and Maria et al report that the *trajectory* of a marginally stable scenario may vary greatly from the *trajectory* of the sustained fault

particularly under stressed operating conditions [28, 43]. Another limitation is that the sustained fault method assumes that the PEBS is flat near to the CUEP. This assumption is false when inter-machine oscillations and inter-area mode instability issues are present [28].

2.5.6. The Boundary Controlling UEP (BCU) Method

The BCU method, or Exit method, was introduced to address the short-comings of the PEBS method [46]. An artificial reduced dimension model of the system must be formulated for which a TEF exists [47]. TSA is performed by determining the CUEP of the reduced-state model and then relating it back to the original system model. The reduced model is described by the gradient function that describes the system dynamics in the post-fault state [46]:

$$\dot{\theta} = -\left(\frac{\partial V_{PE}(\theta)}{\partial \theta}\right) = f(\theta)\ \dot{\theta} = -\frac{\partial V_{PE}(\theta)}{\partial \theta} = f(\theta) \tag{2.49}.$$

The BCU method is based on the observation that as a system energy trajectory approaches the CUEP the gradient function $\dot{\theta}$ will tend towards zero. At the CUEP the gradient function is [48]:

$$\dot{\theta} = f(\theta) = 0 \tag{2.50}.$$

The CUEP can be determined from the load-flow solution that satisfies (2.50). The BCU method uses the PEBS method to locate the PEBS exit point. The PEBS exit point is used as an initial guess to solve for the exit point which is at the minimum of $\dot{\theta}$. The minimum exit point is then used as an initial guess to solve for the operating point that satisfies equation (2.50).

It is reported that the iterative Newton-Raphson method (NR) is commonly used to solve equation (2.50) [48, 49]. However, NR exhibits a complicated fractal nature that may cause an alternative UEP to be mistaken for the CUEP. The *exit point* must lie within the fractal that corresponds to the CUEP [48]. To increase the likelihood of correctly identifying the CUEP Liu and Thorp propose the Dynamical Method (DM). The DM locates the CUEP by applying a spectral decomposition to the Jacobian matrix of the gradient function [49]. Although the DM is more reliable for locating the correct CUEP, it is less computationally efficient than NR [48]. Luna-Lopez et al assert that the DM may be integrated into the BCU method as a back-up solver for NR, but cannot replace it.

Treinen et al propose the Shadowing Technique as an alternative to NR. It avoids calculation of the exit point altogether [50]. A sequence of points that progressively converge towards the CUEP are identified, and the last point in the sequence is used as the initial guess for equation (2.50). Equation (2.50) is solved via the Runge-Kutta method. While the Shadowing Technique appears to improve the BCU method it is constrained to specific operating conditions. Ultimately the BCU method is based on the assessment of the classical TEF which has many modeling restrictions.

2.5.7. Structure Preserving Models and Energy Functions

To compensate for the modelling constraints of the classical TEF Bergen and Hill proposed the concept of structure preserving models (SPM) and their associated energy functions (SPEFs) [51]. SPMs enable a TEF to represent a power system in greater detail. The additional details enable a more accurate, less conservative TSA if the assessment method is correctly tuned to the SPEF [52]. Formulating a SPEF does not require network reduction of the corresponding SPM. This avoids the problems associated with network-reduction procedures such as decreased solution efficiency, and, for very large networks, failure to calculate a reduced network solution [52].

Bergen and Hill initially proposed a SPM that allows loads to be represented as frequency-dependent powers, but with overly conservative voltage independent loads. Building on this concept Narasimhamurthi and Musavi proposed a SPEF that uses less onerous voltage dependent real-power loads [53].

Van Cutsem and Ribbens-Pavella extended Bergen and Hills' work by proposing a SPEF that generalizes the representation of several types of load. Hiskens et al developed SPMs and SPEFs that allow modelling of non-linear loads [52]. SPEFs that consider the flux decay of the generator field windings [54], or that represent phase shifting transformers [55], static series synchronous compensator [56], and unified power flow controllers [57] have also been developed. With the present state of knowledge, the use of the direct methods are constrained to the assumptions of a lossless system and classical generator modelling [51, 58].

To address this, Hiskens, Hill and Mareels proposed a generalized SPM that allows the network behaviour to be described in full detail with a set of differential-algebraic equations (DAEs) [52, 59]. However, to formulate the SPEF the SPM must be lossless so that it can translate to a set of equivalent ODEs, and the ODEs are for a reduced range of operating conditions. Chiang and Zou et al proposed a generalized SPM that avoids conversion of the DAEs into an equivalent set of ODEs by directly relating the

DAE to the PEBS [27, 60]. However it uses the BCU method which must be tailored to the generalized SPM [27, 60]. Ultimately TEFs and the concepts of the PEBS and CUEP, are much less understood for large complex systems with detailed models [21, 28, 43].

2.6. Hybrid Direct Methods For Transient Stability Assessment

The fast TSA and margin estimation capabilities of the pure-direct methods described above in section 2.5 are desirable for online DSA applications. However the required modelling restrictions and simplifications are unacceptable except for screening purposes. The hybrid-direct methods for TSA aim to overcome this by combining techniques derived from the direct methods with TDS assessment. In the hybrid-direct methods TDS are used to calculate the full system response of scenarios before the fault, during the fault, and after it is cleared. The early stopping criteria (ESC) of the direct techniques are used to stop a simulation as soon as possible. There are two categories of hybrid-direct methods: the hybrid-EAC described in sections 2.6.1 and 2.6.2.

The hybrid-direct methods require some form of model reduction for TSA or otherwise the assessment method is tailored to suit the characteristics of the investigated system. In general, all hybrid-direct methods for TSA must be tuned to the investigated power system. Depending on the quality of this tuning, these methods are prone to failure. This lack of robustness is addressed by the EBSIME algorithm.

2.6.1. Hybrid–Direct EAC Methods

2.6.1.1. The Single Machine Equivalent Method (SIME)

The Single Machine Equivalent Method (SIME) is the most promising hybrid-EAC method that has emerged. It utilizes the fast TSA and margin estimation methods of the EAC, without requiring *any* model reductions or simplifications. For this reason the SIME method is the basis for the novel EBSIME algorithm that is proposed in this thesis. Furthermore it can reveal multi-swing as well as forward-swing instability, a feature that is important in Australia where multi-swing instability is a real concern [103-106].

The Single Machine Infinite bus Equivalent method (SIME) derives an equivalent time-varying OMIB response from the TDS of a multi-machine power system [1]. Since no model reductions are required to formulate the time-varying OMIB response the SIME

method has the ability to accurately analyze arbitrarily complex power system models, and to reveal forward-swing and multi-swing stability limits. The method applies the EAC to the OMIB response to enable fast assessment of transient stability and estimation of TSMs.

Pavella et al [1] discuss how the SIME approach has evolved from the EEAC into its current form. Like its predecessors, SIME assumes that transient instability is caused by the machines in a system irrevocably separating into two coherent groups. The defining feature of the method is its simultaneous formation of the OMIB system response during calculation of a TDS, and its identification of the CMs that are required to formulate the OMIB. At every time step during the post-fault period, $t(n)$, the SIME method performs the following steps:

1) The machine angles are arranged into descending order $\delta_i > \delta_{i+1},\ i = 1,....,N-1$; where δ_i is associated with machine $m(i)$; where N is the number of online machines connected to the network.

2) The difference between adjacent machine-angles is $\Delta\delta_i = \delta_i - \delta_{i+1} \geq 0$; identify the indices $j_k,\ k = 1,...,K$ of the K largest values in $\Delta\delta_i$, where K is a user selected value.

3) For each $CM(k)$ *where* $k = 1,...,K$
the machines in one group are:

$$G1 = \{m(1),...m(j_k)\} \tag{2.51}$$

and in the other group:

$$G_2 = \{m(j_k + 1),...m(N)\} \tag{2.52}.$$

4) Calculate the equivalent OMIB values of rotor angle, speed, and acceleration power at the current and previous simulation steps, t(n) and t(n-1) respectively. The equations used to formulate the SIME response are well-known and described in Appendix B.

5) Apply the EAC ESC criteria 2 (see section 2.3.2) to the OMIB response at t(n-1) and t(n) to test for forward-swing or multi-swing transient instability.

5a) If the ESC indicates instability and the OMIB angle at $t(n)$ is greater than $\delta_{\min}$ then instability is diagnosed and the simulation halted. $CM(k)$ is applied to the TDS to form the time-varying SIME response for the scenario.

5b) If instability is not detected then steps 1 to 4 are repeated at the next simulation-step. If the simulation continues until the end of the integration period and instability remains undetected, then the scenario is deemed to be stable. However, CMs cannot be identified from a stable scenario.

An example of the above procedure is demonstrated in Chapter 6. The SIME method applies the EAC equations (2.24), (2.25) and (2.26) to the SIME response to calculate the forward-swing TSMs. The authors propose an adaptation of these equations to estimate multi-swing stability margins.

Pavella et al claim [1] that the SIME algorithm enables the fastest possible detection of both forward- and multi-swing instability and that the EAC ESC may be extended to assess multi-swing stability. However the algorithm fails to provide a system-independent solution since parameters K and $\delta_{\min}$ must be tuned to ensure that the selected CMs, stability diagnoses, and the OMIB are correct.

2.6.1.1.1 Applications of the SIME Method

The SIME algorithm can be integrated with standard TDS software without requiring alterations to the TDS source code. The Filtering, Ranking and Assessment (FILTRA) [1, 61] tool employs the SIME TSA and forward-swing margin for contingency screening and ranking. Via FILTRA the tuned SIME algorithm has been implemented in a number of programs and applied off-line to investigate detailed models of the Brazilian and Hydro-Quebec extra high voltage (EHV) systems [1, 61].

Ruiz-Vega and Pavella describe an automatic TSA and control method (TSC) for real-time DSA that integrates an iterative limit prediction procedure with an optimal power flow (OPF) algorithm [1, 62]. Using the unstable forward-swing SIME margins the OPF calculates how generators should be rescheduled to minimize cost and maximise power transfer in the event of a credible contingency. The TSC is improved in the SIME-based Open Loop Emergency Control (OLEC) method, which additionally takes known generator tripping schemes into consideration.

The Open Market Access and Security Assessment System (OMASES) project provides a collection of online DSA tools [1]. The TSC and FILTRA tools have been implemented for OMASES using the dynamic simulation software EUROSTAG® [63]. Through the OMASES project [1, 64, 65] SIME tools have been operated on- and off-line at test-facilities in the Italian and Greek Power Systems [64, 65]. However Bihain and Van Cutsem et al comment that transient instability is rarely of concern on these systems [64, 66].

In [67, 68] the SIME algorithm is implemented with PSS®E for forward-swing contingency screening on the South Korean Electric Power Cooperation (KEPCO) system. The KEPCO approach proposes an index for each machine that quantifies the time-varying angular variation of all system machines from the post-fault COA. The CMs are identified using the proposed index instead of the absolute machine angle. Lee et al [67, 68] claim that the index enables faster determination of CMs and forward-swing stability for stable and unstable scenarios. However, the KEPCO SIME algorithm still requires heuristic tuning to the investigated system.

Mariotto et al [69] apply the SIME algorithm to calculate TSMs for power systems that have a high penetration of wind power. Finally Bhat et al [23] describe an implementation of the SIME algorithm using the GUIDE and SIMULINK tools of MATLAB®, a popular software used by many universities. This implementation is an educational resource for power engineering students to learn about TSA.

2.6.1.2. *The Single Machine Equal Area Criterion (SMEAC)*

Wu proposes the single machine equal area criterion (SMEAC) for multi-machine power systems [70]. It resembles Haque's direct SDM method described in section 2.5.3. The SMEAC is based on the observation that when transient instability occurs one machine loses synchronism first. This machine is also called the critical machine (CM). The TDS of the CM is used to identify if a system remains forward-swing stable, or not [70, 71].

To identify the CM a group of potential CMs are first selected. The potential CMs are the generators whose rotor angle and kinetic energies exceed a specified threshold. The EAC ESC is applied to the potential CMs to assess forward-swing stability at every simulation step. If a machine in the group of potential CMs satisfies the criteria for forward-swing stability, the TDS is halted. The generator that experiences the largest angle deviation during the TDS is the CM. If a potential CM satisfies the unstable ESC first, then it is the CM and the TDS is stopped due to detection of forward-swing instability. The weakness of the SMEAC is that it ignores the dynamic responses of all other machines except for the CM. The rotor angle or kinetic energy threshold values must be tuned to the investigated network to avoid incorrectly classifying the stability of a scenario.

2.6.2. The Hybrid-Direct TEF Methods

2.6.2.1. *The Hybrid Transient Energy Margin (TEM) Method*

The Hybrid TEM method combines the direct TEF techniques and TDS, for fast TSA, to estimate forward-swing margins [28]. It is an improvement of the PEBS method. The Hybrid TEM method calculates system energy trajectories directly from the TDS of a fully detailed system model. Unstable scenarios are rapidly assessed by applying the TEF stop criteria described in section 2.4.7. The unstable TEM is directly calculated from an unstable trajectory. However for stable scenarios, to perform fast TSA and calculate the associated TEMs, the PEBS crossing must be known. To identify the PEBS the post-fault SEP must be estimated from a reduced model of the post-fault system.

For stable scenarios the Hybrid TEM method presumes that the post-fault trajectory will encounter several local peaks before descending back to the post-fault SEP. Whenever a local peak energy trajectory is encountered during the TDS an imaginary ray is projected between the peak and the post-fault SEP. If the ray intersects the PEBS then a local TEM is estimated. The estimated TEMs are used to gauge the end of the forward-swing, it occurs when the TEM exceeds a user-specified threshold. The desired margin is the smallest TEM that was calculated during the simulation.

The Hybrid TEM method has a number of problems:

- For very stable cases it may potentially perform many iterations on the ray search or miss the PEBS crossing altogether [43],
- It assumes that the PEBS is relatively flat; but when inter-area oscillations are present this is not the case. For TSA close to the limit, irregularities in the PEBS will cause solution inaccuracies,
- The MOD is required for correct calculation of the TEMs. It is identified by using the pure-direct MOD method (see section 2.5.4),
- Formulating the simplified system model is not trivial. The reduced model may significantly differ from the full model introducing further inaccuracies into the TSA.

2.6.2.2. *The BCU-Guided Time-Domain Method*

The BCU-guided time-domain method is a hybrid version of the pure-direct BCU method. The BCU-guided time-domain method calculates system energy trajectories from the TDS of a full-scale power system model. For correct calculation of the TEMs the CUEP must first be determined from a reduced model [46, 47, 72].

The BCU-guided time domain method has been developed for online DSA by the Tokyo Electric Power Company (TEPCO-BCU) [73] where it is applied for forward-swing contingency screening. The severity of credible contingencies is ranked using TEMs or CCTs. The TEMs are also used to determine preventive control solutions against insecure and critical contingencies, and for off-line planning. A separate Hybrid-BCU method has also been developed by the Electrical Power Research Institute (EPRI) and the Northern States Power Company [74] for contingency screening, and power transfer limit searching.

Like the Hybrid method, the BCU-guided time-domain method is disadvantaged by the need to formulate a simplified system model that complements the full-scale system model. Furthermore identification of the MOD, to correctly calculate the TEMs, requires heuristic tuning.

2.7. Chapter Conclusion

This chapter provides an introduction to the theory for the TSA of multi-machine power systems. TDS is the conventional approach as it has comprehensive modeling capabilities and, due to the rigorous numerical integration procedure, it is able to provide reliable and accurate results. While some utilities use TDS for the online DSA, TDS are computationally complex and require long processing times, in addition to the time and expertise required to interpret the results. Furthermore, TDS do not indicate how far a given stable scenario is from TSLs in terms of controllable parameters.

The pure-direct EAC and TEF methods present a variety of different approaches to accelerate TSA, and to estimate the diagnosis of transient (in)stability. However, the direct methods can only be applied to reduced power system models. When more complicated models are used, the method is tailored to the investigated model.

The hybrid-direct methods combine the margin estimation and fast TSA of the direct methods with the versatility and accuracy of the TDS. The SIME method shows the greatest potential for online DSA in the Australian context, since it does not require any simplification of the power system model. Furthermore it can reveal multi-swing as well as forward-swing instability, a feature that is important in Australia where multi-swing instability is a real concern [103-106]. The hybrid-TEF methods require the use of a reduced system model to perform fast TSA. A short-coming of all the hybrid-direct methods, including SIME, is that they must be heuristically tuned to the investigated system model. The tuning may also be dependent on the initial operating condition and the contingency being studied.

The novel contribution of this thesis is the EBSIME algorithm to search for transient stability limits. It uses aspects of the SIME method to perform accelerated TSA, to calculate TSMs for limit-prediction, and to generate sensitivity data as a by-product. The EBSIME algorithm improves upon the SIME method by removing the need for heuristic tuning, and significantly improving the robustness of the solution.

Chapter 3 Transient Stability Limit (TSL) Searching

Chapter 3 introduces the concept of transient stability limits (TSL) and the importance of identifying them. The conventional approaches to TSL searching that are commonly used in industry are reviewed, as well the state-of-the-art solutions that are proposed or implemented in the online environment on realistic power systems.

3.1. Introduction to Transient Stability Limit (TSL) Searching

The secure operation of many power systems is constrained due to transient instability [75]. For example, the power transfer of an interconnection between two areas may be limited under certain operating conditions due to transient instability and not the current carrying capacity of the transmission lines. The aim of the TSL search is to find an operating condition that is marginally stable in the event of a specified contingency. However, the task is not straightforward as TSLs are dependent on the initial operating state of the system and the nature of the investigated disturbance.

As discussed in Chapters 1 and 2, a TSL search tool with the following qualities is desirable:

- enable fast and reliable identification of multi-swing TSLs;
- easily integrated into the online dynamic security assessment (DSA) environment;
- automated without human intervention
- provide quantifiable measures of the distance of investigated scenarios from the TSL by the use of meaningful transient stability margins (TSM).

With these characteristics in mind, this chapter reviews the TSL search methods, ranging from the conventional to the state-of-the-art, that have been reported in literature.

3.2. Types of Transient Stability Limit

The TSL for a given scenario is usually defined in terms of the power transfer limit (PTL) over an interconnection, or the critical clearing time (CCT) for the studied disturbance. The transient stability search variable (SV) is the only parameter that varies during a search. In a CCT search the SV is the fault clearing time (CT); in a PTL search the SV is the interconnector power transfer (PT) in a specified direction.

When performing a CCT search the CT is the only parameter that needs to be adjusted during the search traversal. In contrast, for a PTL search, there are a many methods that can be used to adjust the power transfer, such as load or generation dispatch on either side of the interconnector. Multiple operating parameters may need to be adjusted to achieve the desired change in power transfer. The network load-flow must be adjusted and solved at each power transfer level (i.e. at each scenario in the search), introducing the risk of load-flow convergence failure.

3.2.1. Summary of the Transient Stability Limit Searching Methods

Table 3-1 summarizes the key features of the reviewed TSL search methods. Aside from the second kick method, all investigated transient stability assessment (TSA) techniques are based on *n-1* contingencies, where a single piece of equipment in the post-fault network is switched out-of-service to clear the fault. The direct approaches for TSL searching are not reviewed as they are unsuitable for application to realistic power systems due to their limited modelling capabilities [21, 22]. Table 3-1 summarizes the advantages (A) and disadvantages (D) of each method.

TABLE 3-1. MAIN FEATURES OF THE REVIEWED TRANSIENT STABILITY LIMIT SEARCHING METHODS

Search Method	Key Features	Section
Linear Search	The search is performed in ascending or descending order with fixed size SV steps between scenarios (A) Time-Domain Simulation (TDS) based method (D) Does not provide TSM information (D) Slow if the starting point is distant from the limit.	3.3.1
Plain Binary Search	The search is traversed using bisection of the upper and lower search bounds between scenarios (A) TDS based method (A) Faster than the linear search (D) Does not provide TSM information	3.3.2
Parallel Binary Search	A parallel processing version of the plain binary search (A) TDS based method (A) Faster than the plain binary search (D) Additional parallel processors are required	3.3.3
Signal Energy Limit Estimation Method	Signal energies are calculated from the dynamic voltage or the machine rotor angle responses at selected buses. The TSL can be estimated from three stable or unstable scenarios, based on the assumption that the signal energy has an exponential relationship to power transfer. (A) TDS-based method (A) Signal energies provide multi-swing TSM information (D) Stable and unstable margins are incomparable. (D) Verification of the TSL requires a tuned threshold value.	3.4
Trajectory Sensitivity Analysis	Generates a set of trajectory sensitivities that describe how the dynamic response of a fully-detailed power system changes for small changes from the nominal scenario. Trajectory sensitivities can be used to accelerate the search for the forward-swing TSLs. (A) Sensitivities are calculated simultaneas the nominal TDS (A) The system is represented as a hybrid differential-algebraic-discrete (DAD) model which allows representation of both continuous and discrete behaviour (D) Search convergence depends on the initial conditions at the start of the search. (D) The TSL search does not use the hybrid DAD model, and therefore cannot be applied to systems with discrete switching behaviour.	3.5
SIME Method	A hybrid EAC method that uses linear prediction of the SIME margins and SIME early stop criterion (ESC) to accelerate the TSL search. (A) Identifies multi-swing limits using TSMs. (D) Employs a heuristic approach to the TSL search. (D) Must be tuned to the investigated system.	3.6.1
The Modified Boundary Controlling Unstable Equilibrium Point (BCU)-guided Time-Domain	A hybrid transient energy function (TEF) method that enables an accelerated forward-swing PTL search by modifying the hybrid BCU-guided Time-Domain method. (A)Applies TEF stop criteria to assess forward-swing stability (D)TEF stability margins do not have a meaningful interpretation (D) The search algorithm is dependent on system tuning and heuristic decisions (D) Full-scale power system models must be simplified	3.6.2

3.3. Time-Domain Simulation Methods for TSL Searching

This section describes the TDS based methods for TSL searching that are used in the power industry or reported in literature. A common disadvantage of TDS methods is that they are unable to indicate how far a scenario is from the TSL in terms of controllable parameters. Reliance on TDS tends to make the TSL search too slow for real-time application.

3.3.1. The Linear Search

The linear search is a common TDS-based approach used by practising power system engineers to identify the TSL. The search requires an operator to define upper and lower search bounds, and a fixed search step-size, to iteratively increment, or decrement, the SV. The step size is also the search tolerance. It must be confirmed that the system is stable at the lower bound and unstable at the upper bound, such that the TSL exists in between these bounds. If not the search bounds and/or system operating state must be redefined. The upper bound must be increased if the system is stable at the upper search bound; or a new operating condition and contingency must be selected if the lower bound is unstable. The linear search is iterative and may proceed from either the upper or lower bound.

Figure 3-1 shows the traversal of a descending linear CCT search with a step-size of 50ms. It commences at the upper bound (k=1, CT=500ms) where a TDS is used to assess the stability of the corresponding scenario. As required the upper bound is unstable, the CT for the next step (k=2) is determined by reducing the CT by 50ms. The transient stability of the next scenario (k=2) is assessed by running the corresponding TDS. If the scenario is stable, the limit is found. Otherwise the SV of the current scenario becomes the new upper bound. The next search step is determined by reducing the current SV by 50ms. This procedure continues iteratively until a stable scenario is identified. The first encountered stable scenario is the TSL.

While the linear search provides very reliable off-line assessment, to achieve a fine tolerance a small step size is required and it will potentially require a large number of iterations to converge to the limit; for a coarser step-size it will yield a more conservative result. If a scenario is stable then the TDS must be run for the entire simulation period, (i.e. 10s or 20s). In contrast transient instability is diagnosed when the system machine angles diverge, before the full simulation period is complete. The greater the network stress, the sooner transient instability will be apparent. Therefore it

is advantageous to commence the linear search at the unstable upper bound as more unstable scenarios will be assessed, and therefore total search time will be faster.

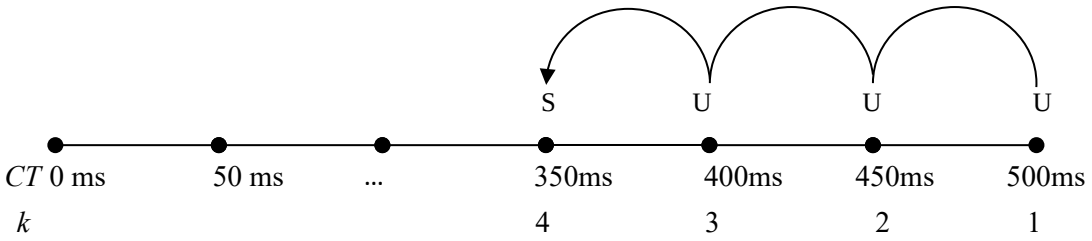

Figure 3-1. A descending linear search for the CCT. S indicates 'stable', and U indicates 'unstable' cases. The indices, k, indicate the search iteration number. The CCT is between 350ms and 400ms.

3.3.2. The Binary Search

The binary-search TSL search can be easily implemented using conventional TDS tools. In practice it is commonly used off-line to determine the TSLs on fully detailed multi-machine system models [8]. The binary search requires the specification of a selected upper and lower search bound, and the search tolerance. Figure 3-2 shows an example of a binary-search for the CCT.

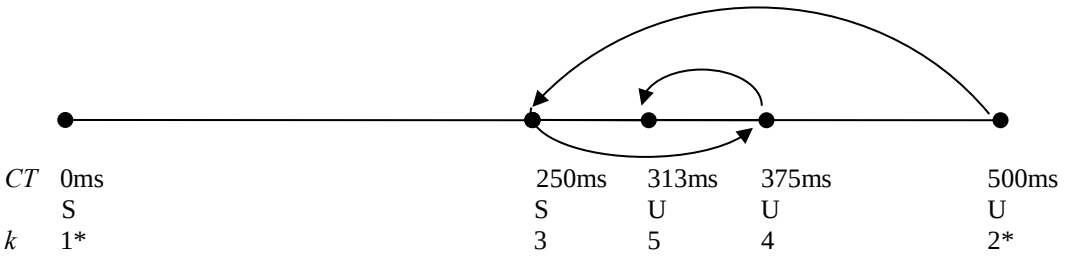

Figure 3-2. An example of the binary-search iteration procedure. S indicates 'stable', and U indicates 'unstable' cases. The k indices indicate the search iteration number. '' indicates test simulations to confirm the initially chosen lower and upper bounds are stable and unstable respectively.*

The search bounds that are initially selected are 0ms and 500ms. Studies are conducted to confirm that the system is stable at the lower bound and unstable at the upper bound. If this is not the case the bounds and/or operating scenarios must be reassessed. The CCT exists between the specified bounds. The binary-search proceeds iteratively. TDS are used to determine the stability of the system for the SV that is at the midpoint of the current set of search bounds. If the current test point is stable then the SV becomes the new lower bound and the current upper bound is retained for the next iteration of the search. Conversely if the current test point is unstable the SV becomes the new upper bound and the current lower bound is retained. This process continues until the difference between the search bounds drops below the search tolerance. The TSL is the

final lower bound. The binary search provides an accurate assessment of the TSLs and a reliable classification of multi-swing stability or instability.

3.3.3. Parallel Binary Search (PBS)

Marceau et al describe the concept of the iterative parallel binary search (PBS) for the TSLs [76], where multiple scenarios are simultaneously assessed at each iteration using parallel processing. The input parameters to the PBS are the upper and lower search bounds, the search tolerance, and the number of available processors, *q*, which can be used to simultaneously run TDS for the search. At each iteration *q* different TDS scenarios are simultaneously executed. The *q* SVs are equidistant from one another and from the search bounds. The size of this interval is the distance between the current search bounds divided by *q+1*.

At the end of each iteration the stable case with the highest SV, and the unstable case with the lowest SV are identified. If the distance between the two SVs is smaller than the search tolerance, the TSL is found and is the value of the SV of the stable case. Otherwise the SVs of the two cases become the new lower and upper bounds and the search continues until the tolerance is reached.

Figure 3-3 demonstrates a PBS for the CCT with an initial search range between 0 and 500ms, search tolerance of 5ms, and four available processors. At the third iteration the CCT of 312ms is identified. The integration period of each iteration is the length of a single stable TDS, thus the entire search takes the equivalent time span of three stable TDS. An equivalent plain binary search would require 8 iterations of varying length.

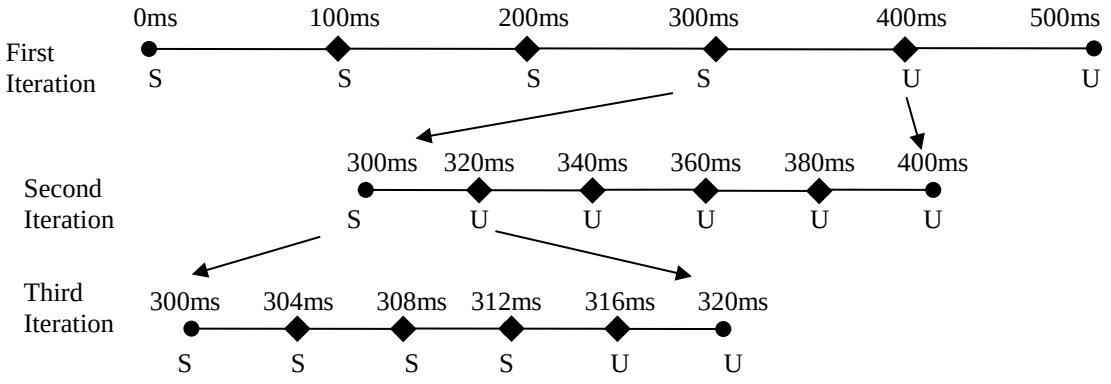

Figure 3-3. A Parallel Binary Search for the CCT using 4 processors, for search tolerance of 5 ms, and the solution is obtained at the end of the third iteration. The initial search bounds of 0 and 500ms are confirmed to be respectively stable and unstable during the initialization phase.

3.4. The Signal Energy Method

The signal energy limit estimation technique, introduced by Marceau et al [76-78], provides a TDS-based strategy to accelerate the search for TSLs and long-term voltage stability limits (VSL). All scenarios are assessed by TDS. For a given TDS, Marceau et al define the *actual* system signal energy from the root-mean-square (RMS) voltage responses at selected network buses. Marceau, Carlson and Jin et al present various approaches to estimate the relationship between the system signal energy and power transfer (PT) [79] to determine the transfer limit.

The estimation is based on the concept that the post-fault response to a transient disturbance can be estimated by an impulse response. A linear model to approximate the relationship between system signal energy and PT is formed by mapping the impulse response from the time-domain to the frequency-domain.

For stable scenarios the signal energies rise asymptotically towards the PTL as the PT increases [77]. For unstable scenarios the signal energies rise asymptotically towards the PTL as PT decreases. This is demonstrated in Figure 3-4. Marceau et al claim that the actual signal energies calculated from the TDS of three stable scenarios can be used together with an approximation model to accurately estimate both TSL and VSLs, where the power transfer of at least one of the scenarios must be within 5% of the limit [76, 77]. Yet, the requirement for a 5% tolerance is fine and implies that a good estimate of the limit must already be available.

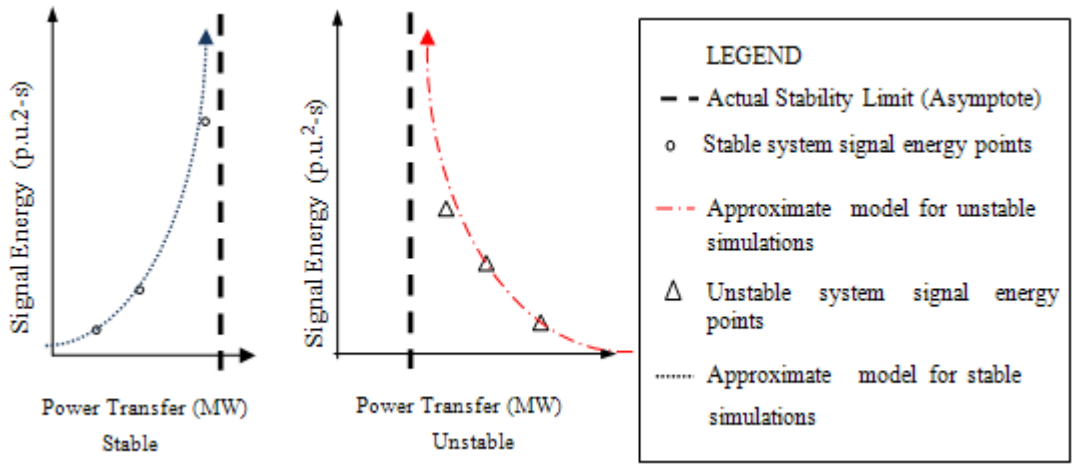

Figure 3-4. The relationship between the signal-energy and PT for a) stable and b) unstable scenarios is asymptotic; signal-energies tend towards ∞ as they approach the limit.

3.4.1. Signal Energy Limit Estimation

In this approach a transient disturbance is likened to an impulse signal applied to the network, therefore the post-fault network behaviour is represented by a voltage impulse response. Marceau et al define the *actual* signal energy of a transiently stable scenario:

$$E_{ij}(P_i) = \int_{t_0}^{t} r_{ij}\left(t, P_i\right)^2 dt \tag{3.1}$$

where t and t_0 are the start and end times of the post-fault TDS simulation period, and $r_{ij}(t, PT)$ is the deviation of the TDS per unit voltage signal $v_{ij}(t, PT)$ from the post-fault steady-state voltage $V_{ij}(PT)$:

$$r_{ij}(t, PT) = v_{ij}(t, PT) - V_{ij}(PT) \tag{3.2}.$$

The voltage signal is monitored at bus *j*, for a contingency applied at bus *i*, at the pre-fault PT level. $V_{ij}(PT)$ is obtained from the load-flow solution of the post-fault network. For stable scenarios the time-varying impulse response that is used to estimate the relationship between the post-fault signal energies and PT is [76]:

$$r_{ij}\left(t, PT\right) = A_{0i}\, j e^{-\sigma_{0ij} t} \sin\left(\omega_{oij} t\right) + A_{1ij} e^{-\sigma_{1ij} t} \tag{3.3}$$

where A_{0ij}, σ_{0ij} and ω_{0ij} are the amplitude, damping and angular frequency associated with the dominant pole of the impulse response $h(t)$, and

A_{1ij} and σ_{1ij} are the amplitude and damping associated with the non-oscillatory part of the signal. The network transfer function, in the frequency domain, can be obtained by applying the Fourier transform to equation (3.3):

$$H\left(\omega\right) = \int_{-\infty}^{\infty} h\left(t\right) e^{-j\omega t} dt \tag{3.4}$$

where ω is the driving frequency.

A realistic network may have thousands of poles (modes) and zeros represented in the complex plane, where the imaginary ($j\omega$) axis represents the network oscillation frequency and the real axis represents signal damping (σ). Stability theory requires that for a system to be stable, all poles must be on the left hand side of the $j\omega$ axis in the complex plane where damping is negative ($\sigma < 0$). Changing a parameter such as the generation dispatch, will cause a number of poles in $H(\omega)$ to move towards the $j\omega$ axis. The poles closest to the $j\omega$ axis tend to dominate the behaviour of the impulse response, and are therefore the *dominant poles*. A system response featuring damped oscillatory behaviour is represented by at least two complex conjugate poles. The

transfer function for a fault applied at node i, and monitored from node j can be approximated as:

$$H_{ij}^{'}(\omega)=\frac{K_i^{'}}{\left(j\omega-p_{ij}\right)\left(j\omega-p_{ij}^{*}\right)} \tag{3.5}$$

where the dominant pair of complex conjugate poles are:

$$p_{ij}=\sigma_{ij}+j\omega_{ij} \text{ and } p_{ij}^{*}=\sigma_{ij}-j\omega_{ij} \text{ and } \sigma_{ij}<0,\ \omega_{ij}>0 \tag{3.6}.$$

$K_i^{'}$ is the scaling factor by which the amplitude of the voltage impulse, caused by the fault, is reduced from the impulse function. This approximate model is demonstrated in the Figure 3-5, where X indicates the dominant pole pairs. The model's limitation to a single pair of dominant poles can be misleading on systems that exhibits strong multi-modal behaviour that have several dominant poles.

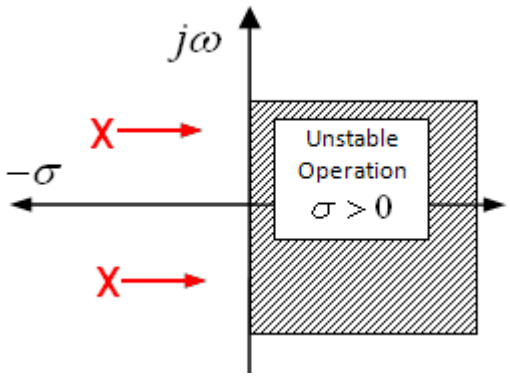

Figure 3-5 The approximate transfer function in the complex plane, features a single dominant pole pair which approach the jω axis as PT is increased.

Rayleigh's energy theorem states that the signal energy can be calculated by:

$$E_i=\int_{-\infty}^{\infty}h_i(t)^2dt=\int_{-\infty}^{\infty}\left|H_i(\omega)\right|^2d\omega \tag{3.7}$$

where

$$\left|H_i(\omega)\right|^2=H_i(\omega)H_i^{*}(\omega) \tag{3.8}.$$

Applying Rayleigh's theorem to (3.5) yields:

$$H_i(\omega)H_i^{*}(\omega)=\frac{\left|K_i\right|^2}{(\omega+jp_i)(\omega-jp_i)\left(\omega+jp_i^{*}\right)\left(\omega-jp_i^{*}\right)} \tag{3.9}.$$

Cauchy's integral formula states that if a function $f(z)$ is analytic in a simply connected domain D – such as a circle or ellipse- then for any point z_0 in D and any simple closed path, C, that encloses z_0:

$$\oint_C\frac{f(z_0)}{z-z_0}dz=j2\pi f(z_0) \tag{3.10}.$$

Applying Cauchy's integral formula to equation (3.7), where C encloses the poles $-jp_i$ and $-jp_i^*$ and is in the anti-clockwise direction in the positive halve of the complex plane yields [80]

$$E_{ij}\left(\sigma_{ij}\right)=\frac{-\pi\left|K_i\right|^2}{2\sigma_{ij}\left(\sigma_{ij}^2+\omega_{ij}^2\right)} \tag{3.11}.$$

In (3.11) the signal energy is solely a function of damping and is always positive since $\sigma_{ij}<0$ for stability. Increasing PT causes a larger post-fault voltage swing and decreased damping. Assuming there is a linear relationship between damping and PT, the damping is approximated by the first-order polynomial:

$$\sigma_{ij}=k_{ij}(P_i-L_i) \tag{3.12}$$

where L_i is the value of the power transfer, P_i, when the dominant poles cross the $j\omega$ axis. Substituting (3.12) into (3.11) yields:

$$E_{ij}(P_i)=\frac{-C_{1ij}}{(P_i-L_i)\left[(P_i-L_i)^2+C_{3ij}\right]} \tag{3.13}$$

where $$C_{1ij}=\frac{\pi\left|K_i\right|^2}{2k_{ij}^3} \text{ and } C_{3ij}=\frac{\omega_{ij}^2}{k_{ij}^2} \tag{3.14}.$$

As the system approaches instability $\sigma_i\to 0$, this implies $\left(P_i-L_i\right)\to 0$. Close to instability the further approximation is made:

$$E_{ij}(P_i)\approx\frac{-C_{1ij}}{\left(P_i-L_i\right)C_{3ij}}\cong\frac{-C_{0ij}}{\left(P_i-L_i\right)} \tag{3.15}$$

where $$C_{0ij}=\frac{C_{1ij}}{C_{3ij}} \tag{3.16}.$$

L_i is estimated by substituting the actual signal energies from two stable simulations for different values of P_i into (3.15) [78]. A third TDS is used to verify that the system is stable at L_i. Rewriting (3.15) where $P_i'=P_i/L_i$ yields:

$$E_{ij}(P_i')=\frac{C_{0ij}}{L_i}\left(\frac{1}{1-P_i'}\right)=\frac{C_{0ij}}{L_i}E'(P_i') \tag{3.17}.$$

The slope of the signal energy between the two stable scenarios is:

$$m=\left|\frac{\Delta E'\left(P_i'\right)}{\Delta P_i'}\right| \tag{3.18}.$$

A larger slope yields a more accurate solution [78]. A satisfactory estimation is obtained when $m\geq K$, where K is a system-dependent parameter that must be tuned over a large variety of credible contingencies and signal monitoring locations.

The automated signal energy limit estimation method only uses stable scenarios, therefore the signal energy equations for the unstable scenario are not discussed in detail. The *actual* signal energy for an unstable scenario is similar to equation (3.1). However, the unstable signal energy only considers the parts of the voltage response that exceed a tuned threshold. For the unstable scenario the approximation model for $E_{ij}(P_i')$ is different from equation (3.17). It requires three scenarios to estimate the PTL as long as at least one scenario is within 5% of the limit [77]. This seems to imply prior knowledge of the limit.

3.4.2. Alternative Definitions of the Signal Energy

The accuracy of the signal energy limit estimation method is influenced by the location, *j*, of the monitored signal. On radial power systems the best monitoring location is close to the transmission corridor of interest. In meshed systems the best location is close to the region(s) where power is injected. At monitoring locations close to voltage-support equipment, the signal energy curves have been observed to rise to an asymptote beyond the limit, resulting in an optimistic solution. For locations far from the voltage support equipment, the signal energy tends rise to an asymptote that falls short of the limit, causing a conservative estimate [78].

To reduce dependence on the signal monitoring location Marceau et al suggest that the average signal energy of the voltage responses at all extra-high and ultra-high voltage buses should be considered. They define the average signal energy [76, 78] as

$$E_{i\,av}(PT) = \frac{1}{N}\sum_{j=1}^{N} E_{ij}(PT) = \frac{C_{1i}}{(L_i - PT)} \tag{3.19}$$

where N is the number of monitored locations, and

$$C_{1i} = \frac{1}{N}\sum_{j=1}^{N} C_{0ij} \tag{3.20}.$$

Equation (3.19) is used for limit estimation when the optimal monitoring location is unknown. Marceau et al find that the asymptote of the average signal energy curve still deviates from the transfer limit for radial or longitudinal networks. In these situations they use the *corridor signal energy,* of equation (3.19) which is applied to all generator, voltage-support and load stations along the target interconnection.

Jin et al address the same issue by proposing the envelope method which uses an alternate definition for signal energy. They define the signal energy for stable scenarios by using the post-fault rotor angle responses of the system machines, instead of bus voltages [81]. This yields an asymptotic relationship between signal energy and PT. For this approximation model the signal energies for the online machines are:

$$\delta_{ij}(t, P_i)\Big|_T = A_{ij} \exp(\sigma_{ij} t) \tag{3.21}$$

where A_{ij} and σ_{ij} are constants, the latter being the damping constant for the dominant pole of the angle response. The signal energy is then calculated by:

$$E_{ij}(P_i) = \int_{t0}^{t} \delta_{ij}(t, P_i)^2 dt \tag{3.22}.$$

The limit estimation is performed from a pair of stable scenarios, using a weighted combination of equations (3.22) and (3.17). Jin et al claim that this improves the limit estimation due to the closer fit between the rotor angle signal energy and the weighted approximation model. However, the possibility of strong multi-modal behaviour in the approximation model is still ignored.

3.4.3. Automated Signal-Energy Limit Estimation Methods

Marceau et al [76] propose the accelerated binary search (ABS), which enables fast limit calculation by combining the signal-energy limit estimation with a linear search, and a binary search. The binary search used in the ABS is different from the method described in section 3.3.2. Instead it commences with an ascending linear search. When the first unstable scenario is encountered the search continues by iterative bisection of the upper and lower search bounds - determined from the unstable scenario and the last encountered stable scenario respectively. The ABS requires the specification of a lower search bound, a linear search interval, a user-tuned slope tolerance, K_{tol} and a search tolerance. It commences with the above described search initialization to locate the first two stable scenarios. Then:

1. The signal energy of the two-stable simulations with the highest transfer are calculated using equations (3.1) and (3.2).
2. L_i is estimated from equation (3.17)
3. The slope between the signal energies of the two scenarios, m, is calculated by equation (3.18).
4. If $m \geq K_{tol}$ then the limit is found, and the search ends.
5. If m is too far below K_{tol} (i.e. $m << K_{tol}$), L_i is ignored and the next stable scenario is determined by continuing the binary search. Determining what is considered “too far” requires tuning on the investigated system.
6. The search ends if the distance between the search bounds is below the search tolerance.
7. Otherwise if $m < K_{tol}$ then a linear step or bisection is used to determine the next stable scenario, and steps 1 to 5 are applied in the next iteration.

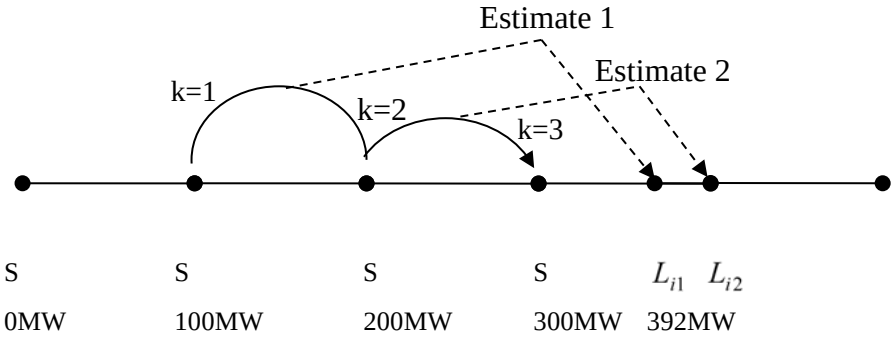

Figure 3-6. Example of the Accelerated Binary Search (ABS) traversal

While the ABS accelerates the plain binary search for the PTL, it relies on the user-specified parameter, K_{tol}, and tuning of the approximation model – both are factors that vary with the system operating conditions. Marceau et al propose the accelerated parallel binary search (APBS), an automated TSL search that combines the PBS, discussed in section 3.3.3, with the signal-energy limit estimation method [76]. At every iteration the signal energies and slope, *m*, for the two stable scenarios with the highest PTs are simultaneously calculated. At each iteration, step 4 of the ABS method is applied APBS to test for convergence to the TSL.

Marceau et al report [76, 78] that the ABS search is almost twice as fast as the binary search. On the test system used by Marceau the APBS is 3.3 times faster than the binary search and 2.2 faster than the ABS. Jin et al propose that the ABS and APBS can be further accelerated by applying the envelope method (see section 3.4.2). However, ultimately the success of the APBS is dependent on the user-tuned value, K_{tol}, and the accuracy of the limit approximation model.

The signal energy limit estimation methods provide an accelerated approach to identifying the TSLs and VSLs by using a linear model that approximates the relationship between signal energy and PT. There are concerns that this TSL search method lacks robustness when applied to large realistic power systems since:

- Multi-modal behaviour is not considered since the linear approximation only considers a single dominant complex pole pair,
- Tuning is required to determine the best locations to measure the signal energy. This influences the accuracy of the limit approximation model; and
- the search algorithm requires tuning of the parameter K_{tol} to determine when the limit is identified.

3.5. Trajectory Sensitivity Analysis

Trajectory sensitivity analysis provides an approach to efficiently computing trajectory sensitivities, a set of time-responses that describe how the dynamic behaviour of a fully-detailed power system will change from a base-case time response due to minor variations from the initial operating conditions. The trajectory sensitivities are calculated concurrently with the *nominal system trajectory*, which is the base-case TDS. Once computed, they can be used to directly approximate the change from the nominal trajectory for small changes in initial operating conditions and parameters [82, 83]. Hiskens et al propose a method that uses trajectory sensitivity analysis to search for TSLs. Trajectory sensitivities have also been proposed for applications such as load modelling and parameter estimation [84].

3.5.1. The Hybrid Differential Algebraic Discrete (DAD) Model

The hybrid differential-algebraic-discrete (DAD) model proposed by Hiskens et al is based on the observation that the dynamic behaviour of electrical power systems are characterized by a combination of continuous and discrete operating states, and discrete switching events. Between switching events the system behaviour is described by a set of differential-algebraic equations (DAE). In trajectory sensitivity analysis only the post-fault operating condition is modelled. Each set of DAEs represents the continuous dynamic behaviour between discrete events such as step changes, impulse switching, or other discontinuous triggers, allowing a power system to be represented in full-modelling detail.

The dynamic model of the power system must be rewritten into the form of the hybrid DAD model where, in the time interval between two events, the system is described by the DAEs:

$$\dot{x} = \underline{f}\left(\underline{x}, y\right) \tag{3.23}$$

$$0 = g\left(\underline{x}, y\right) \tag{3.24}$$

and

$$\underline{x} = \begin{bmatrix} x \\ z \\ \lambda \end{bmatrix} \text{ and } \underline{f} = \begin{bmatrix} f \\ 0 \\ 0 \end{bmatrix} \tag{3.25}.$$

where x are continuous dynamic state variables - such as rotor angle and speed;
y are the algebraic state variables - such as network voltages and angles;
z are discrete state variables such as transformer tap positions or relay states; and
λ are other parameters such as fault clearing time or load.

The nominal system flow corresponding to a set of DAEs is defined as:

$$\phi\left(\underline{x}_0, t\right) = \begin{bmatrix} \phi_{\underline{x}}\left(\underline{x}_0, t\right) \\ \phi_{\underline{y}}\left(\underline{x}_0, t\right) \end{bmatrix} = \begin{bmatrix} \underline{x}(t) \\ y(t) \end{bmatrix} \qquad (3.26)$$

where $\underline{x}_0$ is the initial condition of the entire set of parameters [82] for the nominal scenario.

3.5.2. Formulation of the Trajectory Sensitivities

The deviation from the nominal system trajectory, for small changes to the initial conditions, is described by [82]

$$\Delta\phi(\underline{x}_0, t) = \begin{bmatrix} \Delta\underline{x}(t) \\ \Delta\underline{y}(t) \end{bmatrix} = \begin{bmatrix} \underline{x}_{\underline{x}0}(t) \\ y_{\underline{x}0}(t) \end{bmatrix} \Delta\underline{x}_0 \qquad (3.27)$$

where by the Taylor series expansion, from (3.26), can be expressed as:

$$\Delta\underline{x}(t) = \frac{\partial\phi_{\underline{x}}(\underline{x}_0, t)}{\partial\underline{x}_0}\Delta\underline{x}_0 + \text{higher order terms} \qquad (3.28).$$

Neglecting the higher order terms, and from (3.27)

$$\Delta\underline{x}(t) \approx \frac{\partial\underline{x}(t)}{\partial\underline{x}_0}\Delta\underline{x}_0 \equiv x_{\underline{x}0}(t)\Delta\underline{x}_0 \qquad (3.29)$$

and similarly $$\Delta y(t) \approx \frac{\partial y(t)}{\partial\underline{x}_0}\Delta\underline{x}_0 \equiv y_{\underline{x}0}(t)\Delta\underline{x}_0 \qquad (3.30),$$

The trajectory sensitivities are $x_{\underline{x}0}(t)$ and $y_{\underline{x}0}(t)$. Once they are computed, the sensitivity of the system trajectory, ϕ, to small changes in the initial conditions can be determined using (3.27).

Omitting the higher order terms increases the approximation error in (3.27) [82-89]. The error can be reduced if the precise timing of the discrete events is known a-priori [88], however the information may not be available. For operating conditions close to the stability limit the accuracy of (3.27) deteriorates since the omitted higher order terms become more significant. Hiskens et al propose that the accuracy of (3.27) under stressed operating conditions can be improved by estimating a first-order moving hyper-plane from the nominal trajectory equation (3.26) and the uncorrected solution of (3.27). The approach has been demonstrated on a simple OMIB system [89].

3.5.3. Calculating the Trajectory Sensitivities

Trajectory sensitivity analysis uses numerical integration to compute the trajectory sensitivities concurrently with the nominal trajectory. The sensitivities, $x_{\underline{x}0}(t)$ and

$y_{\underline{x}0}(t)$, at each time step are calculated simultaneously with each time-step of the nominal TDS. There are at least $n \times p \times l$ additional differential equations to solve, where *n* is the number of state variables, *l* is the number of switching events, and *p* is the number of system parameters (λ). For large power systems, the number of additional equations can quickly become computationally prohibitive, particularly with increased network size and modelling detail.

Hiskens et al demonstrate that the trajectory sensitivities can be calculated simultaneously with the TDS, by using the trapezoidal numerical integration method [82]. First, applying the trapezoidal method to equations (3.23) to (3.25), for a given time step, the values of $\underline{x}$ and y are approximated using:

$$\underline{x}^{k+1} = \underline{x}^{k} + \frac{\Delta t}{2}\left[\underline{f}\left(\underline{x}^{k}, y^{k}\right) + \underline{f}\left(\underline{x}^{k+1}, \underline{y}^{k+1}\right)\right] \tag{3.31}$$

$$0 = g\left(\underline{x}^{k+1}, y^{k+1}\right) \tag{3.32}$$

where *k* corresponds to the time instant t_k ; and

k+1 corresponds to the time instant t_{k+1} ; and

$\Delta t = t_{k+1} - t_k$.

To solve for $\underline{x}^{k+1}$ and y^{k+1} equations (3.31) and (3.32) are rearranged:

$$F\left(\underline{x}^{k+1}, y^{k+1}\right) = \begin{bmatrix} \frac{\Delta t}{2}\underline{f}\left(\underline{x}^{k+1}, y^{k+1}\right) - \underline{x}^{k+1} + \frac{\Delta t}{2}\underline{f}\left(\underline{x}^{k}, y^{k}\right) + \underline{x}^{k} \\ g\left(\underline{x}^{k+1}, y^{k+1}\right) \end{bmatrix} = 0 \tag{3.33}.$$

Equation (3.33) has the form $F(X) = 0$, and so it is solved iteratively by applying Newton's iterative technique:

$$\mathrm{X}_{i+1} = \mathrm{X}_i - F_{\mathrm{X}}\left(\mathrm{X}_i\right)^{-1} F\left(\mathrm{X}_i\right) \tag{3.34}$$

where *i* is the iteration index of the equation solver - not related to the time index k; and F_{X} is the Jacobian of (3.33), with respect to X :

$$F_{\mathrm{X}} = \begin{bmatrix} \frac{\Delta t}{2}\underline{f}_{\underline{x}} - I & \frac{\Delta t}{2}\underline{f}_{y} \\ g_{\underline{x}} & g_{y} \end{bmatrix} \tag{3.35}.$$

$\underline{x}^{k+1}$ and y^{k+1} are obtained when equation (3.34) converges.

Note that differentiation of equations (3.23) and (3.24) with respect to $\underline{x}_0$ yields:

$$\dot{\underline{x}}_{\underline{x}0} = \underline{f}_{\underline{x}}(t)\underline{x}_{\underline{x}0} + \underline{f}_{y}(t)y_{\underline{x}0} \tag{3.36}$$

$$0 = g_{\underline{x}}(t)\underline{x}_{\underline{x}0} + g_{y}(t)y_{\underline{x}0} \tag{3.37}$$

where $\underline{f}_{\underline{x}}, \underline{f}_y, g_{\underline{x}}$ and g_y are calculated from the nominal TDS. Using trapezoidal integration, (3.36) and (3.37) are approximated by:

$$\underline{x}_{\underline{x}0}^{k+1} = \underline{x}_{\underline{x}0}^{k} + \frac{\Delta t}{2}\left[\underline{f}_{\underline{x}}^{k} \underline{x}_{\underline{x}0}^{k} + \underline{f}_y^{k} y_{\underline{x}0}^{k} + \underline{f}_{\underline{x}}^{k+1} \underline{x}_{\underline{x}0}^{k+1} + \underline{f}_y^{k+1} y_{\underline{x}0}^{k+1} \right] \tag{3.38}$$

$$0 = g_{\underline{x}}^{k+1} \underline{x}_{\underline{x}0}^{k+1} + g_y^{k+1} y_{\underline{x}0}^{k+1} \tag{3.39}.$$

$\underline{x}_{\underline{x}0}^{k+1}$ and $y_{\underline{x}0}^{k+1}$ are solved from the following rearrangement of equations (3.38) and (3.39):

$$\begin{bmatrix} \frac{\Delta t}{2} \underline{f}_{\underline{x}}^{k+1} - I & \frac{\Delta t}{2} \underline{f}_y^{k+1} \\ g_{\underline{x}}^{k+1} & g_y^{k+1} \end{bmatrix} \begin{bmatrix} \underline{x}_{\underline{x}0}^{k+1} \\ y_{\underline{x}0}^{k+1} \end{bmatrix} = \begin{bmatrix} -\frac{\Delta t}{2}\left(\underline{f}_{\underline{x}}^{k} \underline{x}_{\underline{x}0}^{k} + \underline{f}_y^{k} y_{\underline{x}0}^{k} \right) - \underline{x}_{\underline{x}0}^{k} \\ 0 \end{bmatrix} \tag{3.40}.$$

As the matrix on the left hand side of (3.40) is exactly the same as the Jacobian in equation (3.35) , the factors of this matrix are calculated as a by-product of calculating $\underline{x}^{k+1}$ and y^{k+1}. Then the trajectory sensitivities $\underline{x}_{\underline{x}0}^{k+1}$ and $y_{\underline{x}0}^{k+1}$ are calculated from (3.40).

3.5.4. TSL Searching With Trajectory Sensitivity Analysis

Hiskens et al propose an algorithm that uses trajectory sensitivity analysis to identify the values of selected system parameters that cause marginally stable behaviour [84]. However, it represents the post-fault network using a continuous DAE model, and therefore discrete switching behaviour are not considered. The inputs to the search algorithm are an initial value for the search variable, the search tolerance and a weighted quadratic cost function that represents how close the system operating state is to the forward-swing stable and unstable equilibrium points (SEPs and UEPs). When the cost function is at a minimum, near zero, then the system is close to a UEP.

An iterative Gauss-Newton method, guided by the trajectory sensitivities for the parameter of interest, is applied to locate the minimum of the cost function where the minimum cost yields the forward-swing TSL. The search ends when the minimum value of the cost function falls below the search tolerance. This implies that user-tuning is required to decide an acceptable tolerance for the cost. Local minima may cause failure to converge. In this situation the search must be re-initialized at an adjusted starting point. Hiskens et al acknowledge that the algorithm performance depends on the initial value of the search variable, and that it requires further investigation [84]. Furthermore the search is constrained to locating the forward-swing stability limit. Thus, the approach will need to be augmented with another search method if system operation is constrained by multi-swing instability.

Fang et al propose a method that combines a hybrid TEF approach with trajectory sensitivities to perform a fast search for CCTs and output power limits for individual generators [90]. Again, the search is constrained to power systems that feature continuous behaviour as the nominal scenario and sensitivities are modelled by a single set of DAEs. The trajectory sensitivity of the corrected kinetic energy (CKE) to variation in the CT is computed and used to accelerate the search for the CCT. The trajectory sensitivity with the lowest minimum corresponds to the CCT. Again the search is constrained to locating the forward-swing stability limit.

Trajectory sensitivity analysis provides a fast approach to forecasting variations in the dynamic power system response, for small changes in initial operating conditions from a nominal operating condition. The system can be represented with full-modeling detail using the hybrid DAD model, and the trajectory sensitivities can be simultaneously calculated at the same time as the nominal TDS. However, the additional computations can quickly become computationally expensive for large power systems, and particularly as modeling detail is increased.

The proposed limit searching algorithms that use trajectory sensitivities, to guide and accelerate the search for the TSL, do not use the hybrid DAD model. Therefore realistic power systems cannot be represented in full modeling detail, as discrete switching events and behaviour are not considered. Furthermore, the proposed TSL searching methods are designed to search for the forward-swing TSL, which may potentially be multi-swing unstable.

3.6. Hybrid-Direct Methods for TSL Searching

This section reviews hybrid-direct methods for fast TSL searching. Each described approach is based on a corresponding hybrid-direct TSA technique described in section 2.6. The common features between each of the mentioned hybrid-direct TSL searches are that they apply early stop criteria (ESC), and use limits predicted from computed TSMs to accelerate the search. An advantage of the hybrid-direct methods for TSL searching is that they are peripheral to TDS software and therefore have the potential to be integrated with commonly used commercial transient stability packages without requiring access to, or modification of, the TDS source code. However, a common drawback is the need to employ heuristic measures and system-tuned parameters to ensure that the search converges to the correct solution.

3.6.1. The SIME method for TSL Searching

Pavella et al propose an approach for using the Single Machine Equivalent Method (SIME) TSA algorithm to rapidly locate forward- and multi-swing TSLs. It is able to represent realistic power system models without simplification and uses SIME ESC, and linear prediction with the SIME margins, to accelerate the search. Pavella et al report that the SIME algorithm has been implemented for TSL searching with the TDS tools included in a number of commercial software packages [1].

The SIME TSL search is composed of an initialization stage, and an iterative search phase. For each iteration in the search a TDS is run and the SIME ESC is applied to assess the transient stability of the corresponding scenario. Forward-swing or multi-swing instability can be detected by the unstable SIME ESC criteria. A scenario is classified as multi-swing stable if the TDS runs for a full simulation period without satisfying the unstable ESC.

3.6.1.1. *Initialization of the SIME Limit Search*

The inputs to the SIME TSL search are an upper and lower search bound, the step size for the initial linear search phase and the search tolerance. A descending linear search (see section 3.3.1), whose characteristics are defined by the input search parameters is used to locate an unstable scenario that has a defined SIME margin.

If a suitable scenario cannot be located then the search bounds or step size must be adjusted, and the search must be restarted. When the first suitable unstable scenario is identified, the corresponding SV becomes the new upper bound. Another linear step is taken to obtain the next search step, and the iterative search phase begins.

3.6.1.2. *Iterative Phase of the SIME limit Search*

The steps taken in the iterative part of the SIME TSL search vary depending on whether the scenario of the current iteration is stable or unstable. The main differences lie in the formulation of the SIME margins.

Current scenario stable

1a) The current SV becomes the new lower search bound.
1b) The OMIB response is formed using the critical machines (CM) defined by the most recent unstable scenario.

1c) The OMIB response is used to attempt to estimate the SIME margin.

1ci) If the attempt is successful then the estimated stable margin exists it is paired with the last unstable margin to interpolate for the TSL. This interpolated limit is also the next search step.

1c.ii) Otherwise heuristic measures are taken to select the next search step.

Current scenario is unstable

2) The TDS of the current scenario is unstable and the current SV becomes the new upper search bound. Then, the following questions are answered:

2a.i) Are the CMs of the last unstable scenario and the current unstable scenario the same?

2a.ii) Do the two unstable scenarios become unstable on the same swing?

2a.iii) Is an unstable margin defined for the current unstable scenario?

2b) If the answers to the questions are yes then linear prediction with the margins of the two unstable scenarios are used to estimate the limit for the next search step by linear extrapolation.

2c) Otherwise a heuristic approach is used to determine the next value of the SV. In this situation the algorithm does not indicate the next step in the search. To break this deadlock heuristic procedures have been devised to allow the practical application of the method.

The search continues iteratively until the distance between the upper and lower bound fall below the search tolerance, where the multi-swing stability limit is the lower search bound.

Pavella et al indicate that when search settings are correctly tuned, a search for the multi-swing limit can be accurately performed within a few predominantly stable simulations. However, they also note that the algorithm efficiency is strongly influenced by the step size of the initial linear search. Since the SIME TSL search revolves around the use of the SIME algorithm, it inherits the same disadvantages as the SIME algorithm described in section 2.6.1.1. The success of the SIME TSL search is hindered by (i) the SIME algorithm's dependence of system tuning, and (ii) the requirement to use heuristic measures to select the next value of the search variable when attempts to determine a stability margin fail.

3.6.2. Modified BCU-guided Time-Domain Method for TSL Searching

Ejebe et al propose two TSL search approaches using a modified version of the Boundary-Controlling Unstable Equilibrium Point (BCU)-Guided Time-Domain (TD)

method (see section 2.6.2.2) [74]. Both search algorithms have been implemented as part of the North American EPRI online DSA software for calculating forward-swing power flow limits. They apply the TEF stop criteria for forward-swing (in)stability, to produce a fast TSL search. The original BCU-Guided TD method is modified using a set of alternative stability margins:

$$\eta_{stable} = {}^{1}\!/_{t_{stable}} \text{ and } \eta_{unstable} = {}^{-1}\!/_{t_{PEBS}} \tag{3.41}$$

where t_{stable} and t_{PEBS} are the respective instances in time when forward-swing stability and instability are detected.

The first version Ejebe et al present is based on a fusion of the binary search and the modified Hybrid BCU method. In this approach all TSA is performed using the modified Hybrid BCU-guided method. This includes application of the TEF stop criteria for early identification of forward-swing stability or instability to accelerate the search. The stability margins, η, from equation (3.41), are computed for each traversed scenario. The search begins with a binary-search to identify the first forward-swing stable scenario. When it is found η and the PTs corresponding to the scenario and the unstable scenarios of the upper search bounds are used to linearly interpolate for the forward-swing PTL (where η=0). This yields the SV of the next search scenario.

The iterative part of the search proceeds as follows:

1) The search begins with a TDS assessment of the SV scenario using the Hybrid BCU-guided TD method.
2) If the SV is stable, and η that is smaller than the user-specified threshold, then it is the PTL.
3) Otherwise, if the SV is i) stable with a forward-swing margin above the threshold or ii) an unstable scenario, the SV will become the new lower or upper search bound, respectively. The next SV is determined by linear interpolation using the updated lower and upper PT search bounds, and the corresponding η at those transfer levels. Steps 1 to 3 are iteratively traversed until the PTL is found.

The second version of the modified Hybrid BCU-guided TD method for the TSL search is based on the observation that $\eta_{unstable}$ and PT have an exponential relationship that can be represented by:

$$\eta_{unstable} = a\exp(b \cdot PT) + c \;\; \eta = a\exp(b \cdot PT) + c \tag{3.42}$$

where *a*, *b* and *c* are unknown constants for a given operating condition. A weighted least square fitting technique is used to identify the values for *a*, *b* and *c* over a range of

critical contingencies. Ejebe et al claim that this can be done using at least three forward-swing unstable scenarios. The PTL can be identified by substituting $\eta=0$ into equation (3.42).

While the modified BCU-guided methods provide a fast approach to TSL limit searching they are constrained to forward-swing TSA, and both approaches must be calibrated to suit the investigated system. Furthermore, as described in section 2.6.2.2, a simplified version of the investigated power system must be provided to use the BCU-guided TD method for TSA.

3.7. Chapter Conclusion

This chapter reviews several approaches to TSL searching, ranging from methods used by system operators in industry, to the innovative techniques developed at the forefront of TSL research. An objective of this thesis is to develop a methodology that can be readily integrated into the online DSA environment, to perform a fast, accurate and robust search for TSLs and provide TSM information based on the search traversal.

While the TDS-based approaches discussed in section 3.3 provide a reliable assessment of transient stability, generally they are also too slow for online applications. The exception is the PBS method where the search speed is dependent on the number of available processors. For fast determination of TSLs the signal energy, trajectory sensitivity analysis and the modified BCU-guided methods each employ some form of model simplification or approximation to locate the limit. The SIME method for TSL searching do not require any model simplification. A common problem of the alternative TSL search methods, reviewed in sections 3.4 to 3.6, is that the search success depends on the correct selection of various threshold or model parameters. These parameters are system dependent and must be based on many off-line studies.

The signal energy and SIME methods are the only techniques that provide TSM definitions with a meaningful interpretation. In the signal energy method the stable and unstable margins cannot be used together for control or limit prediction purposes. As for the SIME method, margins from different scenarios can collectively provide meaningful information, if they are calculated from the same MOD and power-swing. However, in the SIME approach to the TSL search these factors are likely to vary between search scenarios.

The EBSIME search method, presented in the following chapters, combines concepts from the binary-search and the SIME method to provide an accelerated and robust approach to TSL searching. The algorithm does not require any modelling simplifications, and can be integrated with standard TDS software as an add-on. If the iterative SIME part of the search fails to converge to the limit, then bi-section steps are taken to guide the search towards the correct TSL. An important characteristic of the EBSIME algorithm is that it does not need to be tuned to a power system model for the correct identification of the TSLs.

Chapter 4 Transient Stability Assessment of a Two Machine Power System

This chapter performs the SIME calculations for a longitudinal 9-bus two machine system. The two machine system was chosen because it is possible to perform the mathematical to demonstrate how the equivalent one machine infinite bus (OMIB) response is obtained without applying any model simplifications to a fully detailed power system.

The generator rotor equations of motion - the “swing equations” - are discussed and related to the dynamic behaviour of some stable and unstable scenarios on the two machine system. The investigations consider the transient response of the system when a three-phase fault is applied near to the sending-end. The SIME transformation is applied to the generator dynamic equations. The relationship between the OMIB responses and the multi-machine system is explained. The SIME early stop criteria (ESC) and the SIME margins are demonstrated on the investigated scenarios. All simulations are performed with PSS®E.

The outcomes of this chapter are:

1. A derivation:
    a) that shows how the SIME algorithm does not require any simplification of the fully detailed power system model; and
    b) that relates the dynamic behaviour of the two-machine system equations to the OMIB equations used in the SIME analysis.
2. Application of the SIME ESC and estimation of SIME stability margins over range of stable and unstable example scenarios;
3. An analysis of how an SVC connected to the mid-point of the transmission line on the two-machine system influences the transient stability. These observations may potentially be applied to larger power systems where transient stability is a concern.

4.1. Derivation of the Two Machine Power System Model

The two machine power system is a modified version of the IEEE 11 bus 4-machine 2-area system [13, 91] with a static var compensator (SVC) included. The 4 machine system with the SVC connected is described in Appendix C. The derivation of the parameters of the two machine system are described in Appendix D. The single line diagram for the two machine power system is shown in Figure 4-1.

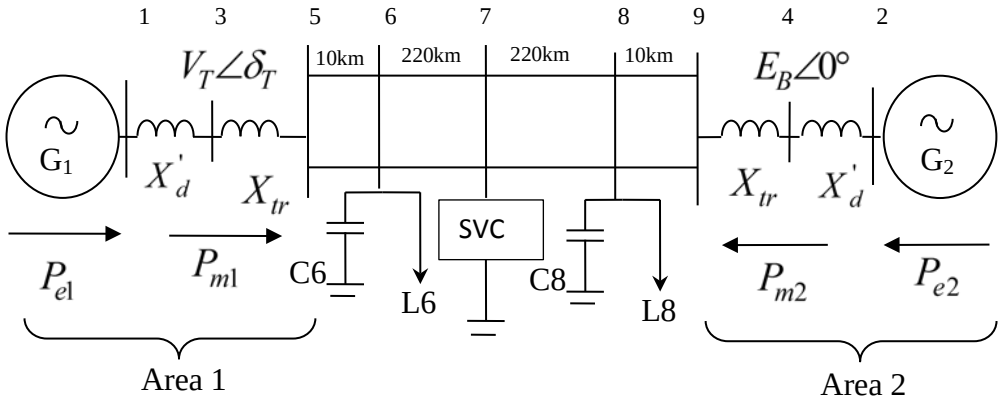

Figure 4-1. The 9-bus two machine power system

In the two machine power system the generators, G1 and G2, are represented by the second order generator model where the field flux linkages are assumed to be constant (see section 5.3.1 of [13]). Thus AVRs are not represented. Furthermore governors are not represented. The two machine system is derived from the test system by merging the two generators in area 1, and merging the two generators in area 2. Merging the generators requires the calculation of an equivalent generator inertia constant given by:

$$H_{equivalent} = \frac{1}{SBASE}\sum_{i\in N} H_i \cdot MBASE_i \qquad (4.1),$$

where i is the generator number and N is the set of generators in a given area. An equivalent transient reactance, X'_d, is calculated as the parallel combination of the transient reactances of the merged generators. The equivalent generator transformer reactances, X_{tr}, are similarly calculated. The shorter parts of the interconnector are modelled by a pair of 10km transmission lines in parallel. The 440km double circuit transmission line between buses 6 and 8 is sectioned at the mid-point, bus 7, to which the SVC is connected. The SVC is modelled so as to keep the voltage at the SVC bus constant.

The generator terminals are located at buses 3 and 4. Buses 1 and 2 are the points behind the transient reactance of the equivalent generators. Node 4 is the slack bus. All lines are lossless.

4.1.1. Parameters of the Base-Line Operating Condition

Under the steady-state base-line system operating conditions 100MW is transferred from area 1 to 2. The power transfer is achieved by adjusting the proportion of the power absorbed by loads P_{L6} and P_{L8}. The network parameter values for the two machine system under these conditions is summarized in Table 4-1.

TABLE 4-1. NETWORK VALUES FOR THE STEADY-STATE BASE-LINE SYSTEM OPERATION

Parameter	Value	Units	Description
f_0	**60**	**Hz**	**System frequency**
SBASE	**100**	**MVA**	**System base**
MBASE	**1800**	**MVA**	**G1 & G2 base power rating**
X'_d	**0.15**	**p.u. on MBASE**	**Transient reactance behind the terminals of G1 & G2**
X_{tr}	**0.075**	**p.u. on SBASE**	**Transformer impedance**
X_{10km}	**0.01**	**p.u. on SBASE**	**Per circuit reactance of the 10km lines**
X_{220km}	**0.22**	**p.u. on SBASE**	**Per circuit reactance of the 220km lines**
b_{10km}	**0.01**	**p.u. on SBASE**	**Per circuit line charging susceptance of the 10km lines**
b_{220km}	**0.22**	**p.u. on SBASE**	**Per circuit line charging susceptance of the 220km lines**
P_L	**27.34**	**p.u. on SBASE**	**Total system load (active power)**
P_{L6}	**12.67**	**p.u. on SBASE**	**Real load at node 6**
P_{L8}	**14.67**	**p.u. on SBASE**	**Real load at node 8**
Q_{L6}	**-1**	**p.u. on SBASE**	**Reactive load at node 6**
Q_{L8}	**-1**	**p.u. on SBASE**	**Reactive load at node 8**
Q_{C6}	**2**	**p.u. on SBASE**	**Shunt capacitance at node 6**
Q_{C8}	**3.5**	**p.u. on SBASE**	**Shunt capacitance at node 8**
H_1	**6.5**	**p.u. on MBASE**	**Machine inertia of G1**
H_2	**6.175**	**p.u. on MBASE**	**Machine inertia of G2**
H_{EQ}	**3.17**	**p.u. on MBASE**	**H_{EQ} is the equivalent OMIB inertia of the system**
V_R	**20**	**kV**	**Generator rated voltage**
V_S	**1**	**p.u. on 230kV base**	**Setpoint voltage of the SVC when connected**
V_T	$1\angle\delta_T$	**p.u. on 20 kV base**	**Terminal 3 voltage**
E_B	$1\angle 0°$	**p.u. on 230kV base**	**Slack bus voltage**
Where δ_T is the voltage angle at the terminal of G1.			

4.2. Derivation of Network Equations for the Two Machine System

Some of the fundamental concepts of the SIME method are described in detail in this section, with particular attention to how the OMIB responses of a multi-machine system are derived without simplifying the power system model. Formulating the OMIB response of the two machine system is analogous to calculating the OMIB response for a multi-machine system after the two composite machines groups have been selected.

In this section the steps to calculate the OMIB responses for the two machine system are isolated and examined. The equations for the generator electrical power, P_{e1} and P_{e2}, are formulated using nodal equations for the system network. Later the analysis focuses on how the system responses are transformed into a single OMIB electrical power response.

4.2.1. Representing the Two Machine System Network

The two machine system can be represented by the nodal network equations - partitioned to separate the buses connected to current sources ($\mathbf{I_G}$) from the buses connected to passive nodes:

$$\begin{bmatrix} \mathbf{Y_{GG}} & \mathbf{Y_{GN}} \\ \mathbf{Y_{NG}} & \mathbf{Y_{NN}} \end{bmatrix} \begin{bmatrix} \mathbf{V_G} \\ \mathbf{V_N} \end{bmatrix} = \begin{bmatrix} \mathbf{I_G} \\ 0 \end{bmatrix} \tag{4.2}$$

Here, for a system with a total of n nodes, and n_G nodes to which current sources (i.e. generators, SVC) are connected,
$\mathbf{V_G}$ is the vector of n_G voltages at buses that are connected to current sources,
$\mathbf{V_N}$ is the vector of $n - n_G$ voltages at the remaining passive buses, and
$\mathrm{I_G}$ is the vector of n_G injected currents.

From (4.2) the following relationships can be deduced:

$$\mathbf{V_N} = -\left(\mathbf{Y_{NN}}\right)^{-1} \mathbf{Y_{NG}} \mathbf{V_G} \tag{4.3}$$

$$\mathbf{I_G} = \left(\mathbf{Y_{GG}} - \mathbf{Y_{GN}} \left(\mathbf{Y_{NN}}\right)^{-1} \mathbf{Y_{NG}}\right) \mathbf{V_G} \tag{4.4}$$

$$\mathbf{I_G} = \hat{\mathbf{Y}}_{\mathbf{GG}} \mathbf{V_G} \tag{4.5}$$

where $$\hat{\mathbf{Y}}_{\mathbf{GG}} = \left(\mathbf{Y_{GG}} - \mathbf{Y_{GN}} \left(\mathbf{Y_{NN}}\right)^{-1} \mathbf{Y_{NG}}\right) \tag{4.6}.$$

The electrical power output of the ith current source (e.g. generator or SVC) is then:

$$P_{ei} = \mathrm{Re}\left[V_{Gi} I_{Gi}^{*}\right] \qquad i = 1, 2, \ldots, n_G \tag{4.7}$$

In the event of a fault the network topology changes as a result of the application of the fault and the switching operations required to clear it. Thus, three network states are identified where different nodal admittances apply: $\hat{\mathbf{Y}}_{\mathbf{GGpre}}$, $\hat{\mathbf{Y}}_{\mathbf{GG\,fault}}$ and $\hat{\mathbf{Y}}_{\mathbf{GG\,post}}$.

4.2.2. Steady-State Network Solution When the SVC is Disconnected

Equations (4.2) to (4.7) can be applied to determine the formula for the electrical power output from G1 and G2, as a function of the generator transmission angle:

$$\delta_{12} = \delta_1 - \delta_2 \tag{4.8}.$$

It is desirable to examine the relationship between the generator power and the transmission angle as this provides some insight into the transient stability of the system for a given operating condition.

Without SVC compensation the two machine power system can be represented as an equivalent two port system, where the ports are situated at nodes 1 and 2, behind the transient reactances of the generators. Then using equation (4.6) the nodal network equation to describe the system is:

$$\begin{bmatrix} I_1 \\ I_2 \end{bmatrix} = \begin{bmatrix} Y_{11} & Y_{12} \\ Y_{21} & Y_{22} \end{bmatrix} \begin{bmatrix} E'_{q1} \\ E'_{q2} \end{bmatrix} \tag{4.9}$$

where, respectively, $\mathbf{I_1}$ and $\mathbf{I_2}$ are the currents injected by G1 & G2; and $\mathbf{E'_{q1}}$ and $\mathbf{E'_{q2}}$ are the internal voltages behind the transient reactance of G1 & G2.

By equation (4.7) the electrical power from behind the transient reactance of G1 is:

$$P_{e1} = G_{11} E'^{2}_{q1} + G_{12} E'_{q1} E'_{q2} \cos\delta_{12} + B_{12} E'_{q1} E'_{q2} \sin\delta_{12} \tag{4.10}$$

where $\delta_{12} = \delta_1 - \delta_2$ and δ_1 and δ_2 are the rotor angle of G1 and G2 respectively.

Similarly, the output electrical power from behind the transient reactance of G2 is:

$$P_{e2} = G_{22} E'^{2}_{q2} + G_{12} E'_{q1} E'_{q2} \cos\delta_{12} - B_{12} E'_{q1} E'_{q2} \sin\delta_{12} \tag{4.11}.$$

From equations (4.10) and (4.11) it is apparent that before the electrical power can be calculated the magnitude of the voltages, E'_{q1} and E'_{q2}, must be determined. This procedure is described in section 4.2.2.1. In the steady-state the generators are in a state of equilibrium, thus:

$$P_{e1} = P_{m1} \text{ and } P_{e2} = P_{m2} \tag{4.12}.$$

Since the two machine power system is lossless P_{e1} is the same as the power transmitted at the generator terminal (bus 3). Similarly P_{e2} is the same as the power transmitted to the system at bus 4.

4.2.2.1. *Determining Generator Voltage When the SVC is Offline*

In the base-line case $\mathbf{E_B}$ and the initial values of $|V_T|$ and P_{m1} are as specified in Table 4-2. $\mathbf{E'_{q1}}$, $\mathbf{E'_{q2}}$, P_{e1} and δ_{12} are unknowns that must be determined. First δ_T must be determined. This is done by considering the network between buses 3 and 4.

Using equation (4.2) to model the reduced network the generator terminals (buses 3 and 4) can be treated as current sources. From equation (4.5) the equivalent 2 port matrix is:

$$\begin{bmatrix} \mathbf{I_T} \\ \mathbf{I_B} \end{bmatrix} = \begin{bmatrix} \mathbf{Y_{TT}} & \mathbf{Y_{TB}} \\ \mathbf{Y_{TB}} & \mathbf{Y_{BB}} \end{bmatrix} \begin{bmatrix} \mathbf{V_T} \\ \mathbf{E_B} \end{bmatrix} \tag{4.13}$$

where $\mathbf{I_T}$ and $\mathbf{I_B}$ are the injected current sources at buses 3 & 4 respectively;

$\mathbf{V_T}$ and $\mathbf{E_B}$ are the voltages at buses 3 & 4 respectively. Applying equation (4.13) to (4.7), for the reduced system the electrical power at the generator terminals are:

$$P_{m1} = P_{e1} = P_{e3} = G_{TT}V_T^2 + G_{TB}V_T E_B \cos\delta_T + B_{TB}V_T E_B \sin\delta_T \tag{4.14}$$

$$P_{m2} = P_{e2} = P_{e4} = G_{BB}E_B^2 + G_{TB}V_T E_B \cos(-\delta_T) + B_{TB}V_T E_B \sin(-\delta_T) \tag{4.15}$$

where $\delta_{TB} = \delta_T$ is the unknown voltage transmission angle between buses 3 and 4; B_{TB} is the imaginary part of Y_{TB}; G_{TB} is the real component of Y_{TB}, and similarly for G_{TT} and G_{BB}. Equations (4.14) and (4.15) can be solved to obtain δ_T using a non-linear equation solution algorithm such as the Newton-Raphson method. For the two machine system a closed-form solution for δ_T is also possible. It is as explained in section 4.2.2.2.

The currents $\mathbf{I_T}$ and $\mathbf{I_B}$ are calculated by equation (4.13) and can be applied with Kirchoff's current law at the G1 terminal to obtain:

$$\begin{aligned} \mathbf{I_T} &= \frac{\mathbf{E'_{q1}} - \mathbf{V_T}}{jX'_d} \\ &= \frac{E'_{q1}\cos\delta_1 + jE'_{q1}\sin\delta_1 - (V_T\cos\delta_T + jV_T\sin\delta_T)}{jX'_d} \end{aligned} \tag{4.16}.$$

Similarly, at the terminal of G2:

$$\mathbf{I_B} = \frac{E_{q2}^{'}\cos\delta_2 + jE_{q2}^{'}\sin\delta_2 - E_B}{jX_d^{'}} \tag{4.17}$$

By equating the real and imaginary parts of (4.16):

$$\delta_1 = \arctan\left(\frac{\mathrm{Re}(\mathbf{I_T})X_d^{'} + V_T\sin\delta_T}{\mathrm{Im}(\mathbf{I_T})X_d^{'} - V_T\cos\delta_T}\right) \tag{4.18}$$

and

$$E_{q1}^{'} = \frac{\mathrm{Re}(\mathbf{I_T})X_d^{'} + V_T\sin\delta_T}{\sin\delta_1} \tag{4.19}$$

Similarly from (4.17):

$$\delta_2 = arc\tan\left(\frac{\mathrm{Re}(\mathbf{I_B})X_d^{'}}{E_B - \mathrm{Im}(\mathbf{I_B})X_d^{'}}\right) \tag{4.20}$$

and

$$E_{q2}^{'} = \frac{\mathrm{Re}(\mathbf{I_B})X_d^{'}}{\sin\delta_2} \tag{4.21}$$

4.2.2.2. *Closed Form Solution for Two Machine System When the SVC is Offline*

The equations (4.14) and (4.15) have the following general form:

$$0 = a + b\sin\theta + c\cos\theta \tag{4.22}$$

A closed form solution of (4.22) is now derived which is then used to solve (4.14) and (4.15). The following trigonometric identities can be used:

$$\sin 2\theta = \frac{2\tan\theta}{1+\tan^2\theta} \qquad and \qquad \cos 2\theta = \frac{1-\tan^2\theta}{1+\tan^2\theta} \tag{4.23}$$

Substituting them into equation (4.22) the following relation is obtained:

$$0 = a + b\frac{2\tan\frac{\theta}{2}}{1+\tan^2\frac{\theta}{2}} + c\frac{1-\tan^2\frac{\theta}{2}}{1+\tan^2\frac{\theta}{2}} \tag{4.24}$$

Setting

$$\beta = \frac{\theta}{2} \tag{4.25},$$

(4.24) becomes:

$$0 = a + b\frac{2\tan\beta}{1+\tan^2\beta} + c\frac{1-\tan^2\beta}{1+\tan^2\beta} \tag{4.26}$$

By multiplying both sides of the equation (4.26) by $1+\tan^2\beta$ we obtain:

$$0 = a(1+\tan^2\beta)+b\left(2\tan\beta\right)+c\left(1-\tan^2\beta\right) \quad (4.27)$$

$$= \left(a-c\right)\tan^2\beta+2b\tan\beta+\left(a+c\right) \quad (4.28)$$

Setting $x=\tan\beta$ (4.29)

(4.28) can be written in the general form

$$Ax^2+Bx+C=0 \quad (4.30).$$

Where $A=a-c,\qquad B=2b$ and $C=a+c$ (4.31).

Solving equation (4.30) for *x* the closed form solution is obtained:

$$x=\frac{-B\pm\sqrt{B^2-4AC}}{2A}=\frac{-b\pm\sqrt{b^2-a^2+c^2}}{a-c} \quad (4.32).$$

The angles β and θ are obtained from equations (4.25) and (4.29). For a real solution to exist $B^2\geq 4AC$. Equation (4.14) can be rewritten in the form:

$$G_{TT}V_T^2-P_{m1}+B_{TB}V_TE_B\sin\delta_T+G_{TB}V_TE_B\cos\delta_T=0 \quad (4.33)$$

thus:

$$A=G_{TT}V_T^2-P_{m1}$$
$$B=B_{TB}V_TE_B \quad (4.34).$$
$$C=G_{TB}V_TE_B$$

δ_T is determined by applying (4.34) to equations (4.25), (4.29) and (4.32). This approach can also be applied to determine the SVC voltage angle when the SVC is online.

4.2.2.3. *Steady State Base-Line Operating Conditions when SVC is Offline*

δ_T is computed as described in section 4.2.2.2, and then used to compute δ_1, E'_{q1}, δ_2 and E'_{q2} according to equations (4.18) to (4.21). The base-line operation occurs when $\delta_{12}=13.33°$ where $P_{e1}=P_{m1}$ and $P_{e2}=P_{m2}$. The generator parameter values at this operating point are summarized in Table 4-2.

TABLE 4-2. GENERATOR PARAMETER VALUES FOR THE STEADY-STATE BASE-LINE OPERATION WHEN THE SVC IS OFFLINE

Variable	Steady-State Value	Unit
$E_{q1}^{'}$	1.040	Per unit (p.u)
$E_{q2}^{'}$	1.019	p.u.
$V_7 = V_{SVC}$	1.053	p.u.
δ_1	26.8	degrees
δ_2	13.47	degrees
$\delta_{12} = \delta_1 - \delta_2$	13.33	degrees
$\delta_7 = \delta_{SVC}$	-3.83	degrees
P_{m1}	14.0	Per unit on SBASE
P_{m2}	14.24	Per unit on SBASE
$E_{q1}^{'}$, $E_{q2}^{'}$, P_{m1} and P_{m2} are fixed quantities.		

4.2.3. Steady-State Network Solution When the SVC is Online

When the SVC is connected to the system the voltage at the midpoint of the transmission line is maintained at the set-point voltage $\mathbf{V_S}$, as per Table 4-1. When SVC compensation is included the network can be represented by an equivalent three port admittance matrix, as per equation (4.3). In this matrix ports 1 and 2, are located at nodes 1 and 2 behind the generator transient reactances, and port 3 is at the SVC node. The reduced nodal network equation for the compensated system is derived according to (4.3) to (4.6):

$$\begin{bmatrix} \mathbf{I_1} \\ \mathbf{I_2} \\ \mathbf{I_S} \end{bmatrix} = \begin{bmatrix} \mathbf{Y_{11}} & \mathbf{Y_{12}} & \mathbf{Y_{1S}} \\ \mathbf{Y_{21}} & \mathbf{Y_{22}} & \mathbf{Y_{2S}} \\ \mathbf{Y_{1S}} & \mathbf{Y_{2S}} & \mathbf{Y_{SS}} \end{bmatrix} \begin{bmatrix} \mathbf{E_{q1}^{'}} \\ \mathbf{E_{q2}^{'}} \\ \mathbf{V_S} \end{bmatrix} \tag{4.35}$$

Here, the values of the network admittance matrix should correspond to the original uncompensated system. i.e. the SVC susceptance is not included in the network admittance matrix.

By applying equation (4.35) the electrical power output from G1 and G2 are:

$$\begin{aligned} P_{e1} \;=\; & G_{11}E_{q1}^{'2} + E_{q1}^{'}E_{q2}^{'}G_{12}\cos\delta_{12} + E_{q1}^{'}E_{q2}^{'}B_{12}\sin\delta_{12} \\ & + E_{q1}^{'}V_S G_{1S}\cos\delta_{1S} + E_{q1}^{'}V_S B_{1S}\sin\delta_{1S} \end{aligned} \tag{4.36}$$

and

$$\begin{aligned} P_{e2} &= G_{22}E_{q2}^{'2} + E_{q1}^{'}E_{q2}^{'}G_{12}\cos\delta_{12} - E_{q1}^{'}E_{q2}^{'}B_{12}\sin\delta_{12} \\ &\quad + E_{q2}^{'}V_S G_{2S}\cos\delta_{2S} + E_{q2}^{'}V_S B_{2S}\sin\delta_{2S} \end{aligned} \quad (4.37),$$

where δ_{12} is the transmission angle between ports 1 and 2 $\left(\delta_{12} = \delta_1 - \delta_2\right)$, δ_{2S} is the transmission angle between port 2 and port 3 ($\delta_{2S} = \delta_2 - \delta_S$), and similarly for δ_{1S}. δ_{1S} can be represented as a function of the generator transmission angle such that:

$$\delta_{1S} = \delta_{12} + \delta_{2S} \quad (4.38).$$

The quantities B_{ij} and G_{ij} are the susceptances and conductances that are obtained from the 3-port admittance matrix of equation (4.35). It should be noted that since there is no direct connection between ports 1 and 2 the quantities B_{12} and G_{12} are both zero. Thus equations (4.36) and (4.37) simplify to:

$$P_{e1} = G_{11}E_{q1}^{'2} + E_{q1}^{'}V_S G_{1S}\cos\delta_{1S} + E_{q1}^{'}V_S B_{1S}\sin\delta_{1S} \quad (4.39)$$

and

$$P_{e2} = G_{22}E_{q2}^{'2} + E_{q2}^{'}V_S G_{2S}\cos\delta_{2S} + E_{q2}^{'}V_S B_{2S}\sin\delta_{2S} \quad (4.40).$$

At the SVC node the injected current is:

$$\mathbf{I_S = Y_{1S}E_{q1}^{'} + Y_{2S}E_{q2}^{'} + Y_{SS}V_S} \quad (4.41).$$

The SVC can only inject reactive power into the system:

$$P_S = 0 \quad (4.42)$$

and therefore by equations (4.41) and (4.7), and recognizing (4.38) the active power injected from the SVC port to the rest of the system is:

$$\begin{aligned} P_S &= 0 \\ &= G_{SS}V_S^2 \\ &\quad + E_{q1}^{'}V_S G_{1S}\cos\left(\delta_{12} + \delta_{2S}\right) - E_{q1}^{'}V_S B_{1S}\sin\left(\delta_{12} + \delta_{2S}\right) \\ &\quad + E_{q2}^{'}V_S G_{2S}\cos\delta_{2S} - E_{q2}^{'}V_S B_{2S}\sin\delta_{2S} \end{aligned} \quad (4.43).$$

4.2.3.1. *Determining the Generator Voltages for the Two Machine System When the SVC is Online*

An iterative sequence of calculations is required to determine the steady-state value of generator voltages $E_{q1}^{'}$ and $E_{q2}^{'}$ and the SVC susceptance B_S to satisfy the user-specified values V_T, E_B, δ_T and V_S. The procedure used to calculate these values is

shown in the Figure 4-2. It begins by initializing the estimated SVC susceptance, B_S, to zero and extracting the SVC susceptance:

$$Y_{SS} = -B_{SS} \tag{4.44}$$

from the equivalent 3-port admittance matrix of the uncompensated system (step A in Figure 4-2). After initialization E'_{q1} and E'_{q2} are calculated from the equivalent 2-port system representation using the method in section 4.2.2.1 (step B). The voltage at the SVC node can be calculated by solving the network nodal equations for the full admittance matrix (4.2), and using the calculated values of E'_{q1} and E'_{q2}. Then ΔV_S, the error between the SVC set-point voltage and the calculated SVC bus voltage, is determined (step C).

If ΔV_S is less than the specified tolerance, $V_{tol} = 0.001pu$, the desired value for B_S is found (step D) and the iteration is stopped. Otherwise, a new estimate of B_S:

$$B_{Snew} = B_S + \Delta B_S \tag{4.45}$$

must be calculated. The perturbation ΔB_S from its current value is related to the associated perturbation in SVC voltage and current by:

$$I_S + \Delta I_S = \left(B_S + \Delta B_S\right)\left(V_S + \Delta V_S\right) \tag{4.46}.$$

Assuming $\Delta B_S \Delta V_S$ is negligible:

$$\Delta I_S = V_S \Delta B_S + B_S \Delta V_S \tag{4.47}$$

$$\Delta B_S = \frac{\Delta I_S - B_S \Delta V_S}{V_S} \tag{4.48}.$$

From (4.35) $$\Delta I_S = Y_{1S}\Delta E'_{q1} + Y_{2S}\Delta E'_{q2} + Y_{SS}\Delta V_S \tag{4.49}$$

It is assumed: $$\Delta E'_{q1} = 0 \text{ and } \Delta E'_{q2} = 0 \tag{4.50}$$

thus $$\Delta I_S = -B_{SS}\Delta V_S \tag{4.51}.$$

At step E equations (4.51) is substituted into (4.48), to calculate ΔB_S. This result is applied to equation (4.45) to calculate B_{Snew} - the next estimate for B_S. If B_{Snew} exceeds the SVC limits it is set to the limiting value, B_{Slimit} (step F), and the network admittance matrix is updated to reflect the new estimate for B_S (step G). Steps B to G are processed iteratively until V_{tol} is reached, or the SVC reserve capacity is reached. If the latter occurs (step H), then a solution to satisfy the base-line conditions cannot be determined. Otherwise, the desired solution is the last estimate of the complete system admittance matrix.

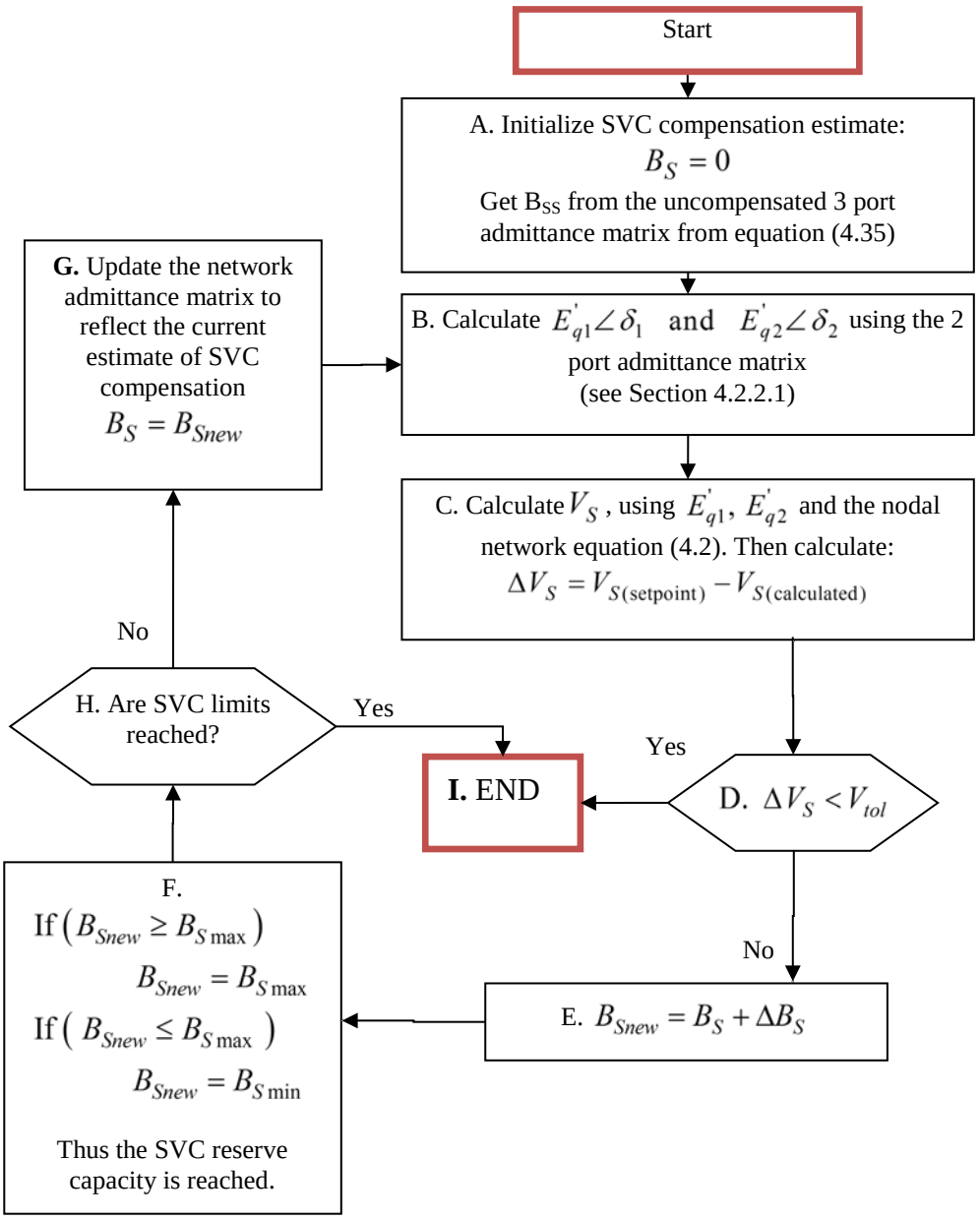

Figure 4-2. Iterative sequence of steps for calculating E'_{q1} and E'_{q2} when the SVC is online

4.2.3.2. *Closed Form Solution for the Two Machine System When the SVC is Online*

When the SVC is connected to the two machine network, the system behaviour is constrained by equation (4.43). Equation (4.43) can be rewritten as:

$$\begin{aligned} P_S &= 0 \\ &= G_{SS}V_S^2 \\ &+\cos\delta_{2S}\left(E'_{q1}|V_S|G_{1S}\cos\delta_{12} - E'_{q1}|V_S|B_{1S}\sin\delta_{12} + E'_{q2}|V_S|G_{2S}\right) \\ &+\sin\delta_{2S}\left(-E'_{q1}|V_S|G_{1S}\sin\delta_{12} - E'_{q1}|V_S|B_{1S}\cos\delta_{12} - E'_{q2}|V_S|G_{2S}\right) \end{aligned} \quad (4.52).$$

Equation (4.52) has the same form as equation (4.22) in section 4.2.2.2. Thus, for specified values of E'_{q1}, E'_{q2}, V_S and δ_{12} a closed form solution for δ_{2S}, based on equation (4.30), is determined, where:

$$\begin{aligned} a &= G_{SS}V_S{}^2 \\ b &= -E'_{q1}|V_S|G_{1S}\sin\delta_{12} - E'_{q1}|V_S|B_{1S}\cos\delta_{12} - E'_{q2}|V_S|B_{2S} \\ c &= E'_{q1}|V_S|G_{1S}\cos\delta_{12} - E'_{q1}|V_S|B_{1S}\sin\delta_{12} + E'_{q2}|V_S|G_{2S} \end{aligned} \quad (4.53)$$

and

$$x = \tan\frac{\delta_{2S}}{2} \quad (4.54).$$

4.2.3.3. *Extreme Behaviour when the SVC is Connected*

The steady-state generator parameters for the base-line system operation are summarized in Table 4-3. By solving equations (4.30) and (4.53) the following solutions for *x* are found by applying equations (4.53) and (4.54) to (4.31) and (4.32). From equation (4.32) a solution for δ_{12} only exists when:

$$b^2 + c^2 - a^2 \geq 0 \quad (4.55)$$

The boundaries for this region are defined by:

$$b^2 + c^2 - a^2 \geq 0 \quad (4.56)$$

Applying (4.53) to (4.56) yields:

$$\begin{aligned} 0 \quad = \quad & 2E'_{q1}E'_{q2}|V_S|^2\left(G_{1S}B_{2S} - G_{2S}B_{1S}\right)\sin\delta_{12} \\ & +2E'_{q1}E'_{q2}|V_S|^2\left(B_{1S}B_{2S} - G_{1S}G_{2S}\right)\cos\delta_{12} \\ & +\left(E'_{q1}|V_S|\right)^2\left(G_{1S}^2 + B_{1S}^2\right) + \left(E'_{q2}|V_S|\right)^2\left(G_{2S}^2 + B_{2S}^2\right) - \left(G_{SS}V_S^2\right)^2 \end{aligned} \quad (4.57).$$

As equation (4.57) is like (4.22) the procedure in section 4.2.2.2 can also be applied to solve (4.57). The two solutions provided by equation (4.32) are the boundary values $\delta_{12} = 167°$ and $\delta_{12} = 186.5°$. Therefore, a solution does not exist between these boundary values.

TABLE 4-3. THE GENERATOR PARAMETER VALUES FOR THE BASE-LINE SYSTEM WHEN THE SVC IS CONNECTED UNDER STEADY-STATE CONDITIONS

Variable	Steady-State Value	Unit
E'_{q1}	**1.048**	**Per unit**
E'_{q2}	**1.024**	**Per unit**
V_S	**1**	**Per unit**
δ_1	**29.8**	**degrees**
δ_2	**13.08**	**degrees**
δ_{12}	**16.71**	**degrees**
δ_S	**-2.23**	**degrees**
P_{m1}	**14.0**	**Per unit**
P_{m2}	**13.91**	**Per unit**
B_{SVC}	**-80.8**	**MVar**
E'_{q1}, E'_{q2}, V_S, P_{m1} and P_{m2} are fixed quantities.		

4.2.4. Final Comments About the Two Machine Power System Model

Sections 4.2.1 to 4.2.3 introduce the two machine system model and its power transfer characteristics. They highlight the network equations used to model electrical power as a function of transmission angle, and also the system constraints and procedures that are used to calculate the steady-state network solution. The base-line solutions of the two machine system, when the SVC is off-line or on-line, are an important reference point for the next section which explores how the responses of the two generators are combined to form an equivalent response, without further simplifying the system model. This transformation is used in the SIME technique and the Enhanced Binary-SIME (EBSIME) algorithm.

4.3. Transformation of the Two Machine System into the OMIB Response

The transformation of the generator power and angle responses of the two machine power system, to the one machine infinite bus (OMIB) representation is investigated. The transformation is analogous to the step in the SIME algorithm where the generators of a multi-machine system are sorted into two groups of machines, and then COI responses of the two groups are combined to form the equivalent OMIB response. The following discussions emphasize that the SIME derivation of an OMIB response does

not require any simplification or modification of the underlying detailed power system model.

The SIME algorithm is a foundation of the novel EBSIME algorithm that is introduced in this research. Thus it is important to understand how the dynamic responses of a multi-machine system can be transformed into a single representative response on a simple system. For illustrative purposes the dynamic response of the two machine system is transformed into an equivalent OMIB response. This transformation is the same in principle to the transformation of the responses of a general multi-machine system to an equivalent OMIB response.

In the two-machine system the transmission angle is the OMIB rotor angle, that is:

$$\delta_{12} = \delta_1 - \delta_2 \triangleq \delta_{OMIB} \tag{4.58}$$

Since the two machines swing against one another when a fault is applied the OMIB electrical power is the difference in generator electrical powers weighted by their inertia constants [92]:

$$P_{eOMIB}(t) = H_{OMIB}\left(\frac{P_{e1}(t)}{H_1} - \frac{P_{e2}(t)}{H_2}\right) \tag{4.59}$$

The OMIB machine inertia is the parallel combination of the machine inertias because the generators swing in anti-phase with each other [92]:

$$H_{OMIB} = \frac{H_1 H_2}{H_1 + H_2} \tag{4.60}$$

Similarly the OMIB mechanical power is:

$$P_{mOMIB}(t) = H_{OMIB}\left(\frac{P_{m1}(t)}{H_1} - \frac{P_{m2}(t)}{H_2}\right) \tag{4.61}$$

The OMIB acceleration power is defined by

$$P_{aOMIB(}t) = P_{mOMIB}(t) - P_{eOMIB}(t) \tag{4.62}$$

Equations (4.58) to (4.62) show that translating the responses of two generators to the OMIB representation does not require any model simplification or other modifications to the system model. Just as the COI responses of the two machine groups are derived from the responses of all the machines in the system, similarly the OMIB responses for the generator power, speed and angle are derived by various linear combinations of the responses of the two machine groups. The latter responses are obtained from the simulations performed on detailed models of the system.

4.3.1. OMIB Power Angle Equations for the Two Machine System

Equations (4.58) to (4.60) are applied to derive the OMIB responses for the two machine system, under the base-line operating condition. The discussion focuses on the OMIB generator power versus angle characteristic since these responses are used to assess forward-swing transient stability using the SIME TSA. Although the discussion is based on the system during steady-state operation, the same concepts apply when the system operates in the fault and post-fault network states.

4.3.1.1. OMIB Power-Angle Equations When the SVC is Offline

When the SVC is disconnected from the two machine system the OMIB electrical power is determined by applying equations (4.10) and (4.11) to equations (4.59) and (4.60). At any given operating point this yields:

$$P_{eOMIB} = H_{OMIB}\left(\frac{G_{11}E_{q1}^{'2}}{H_1}-\frac{G_{22}E_{q2}^{'2}}{H_2}\right)+G_{12}E_{q1}^{'}E_{q2}^{'}\left(\frac{H_2-H_1}{H_1+H_2}\right)\cos\delta_{12} + E_{q1}^{'}E_{q2}^{'}B_{12}\sin\delta_{12} \quad (4.63).$$

Equation (4.63) shows that the OMIB electrical power as a function of the OMIB angle has three distinct parts: a constant offset (K), a cosine (C) and a sine component (S):

$$P_{eOMIB} = K + C\cos\delta_{12} + S\sin\delta_{12} \quad (4.64).$$

In the base-line operating condition $H_1 \approx H_2$, and generally $G_{12} << B_{12}$. These factors contribute to the cosine term being smaller than the sine term. If the difference in generator inertias is greater, then the coefficient of the cosine, and the constant term will be greater. P_{mOMIB} is also dependent on the relative inertia of the two machines according to (4.61). The sensitivity of P_{mOMIB} and the coefficients to the variation in the G2 inertia are shown in Table 4-4. P_{mOMIB} and the constant part (*K*) of (4.63) are most sensitive to changes in the generator inertia. Both values increase, but the change in P_{mOMIB} is greater. Figure 4-4 shows that the greater disparity between H_1 and H_2 decreases the steady-state OMIB deceleration area - the area between P_{eOMIB} and P_{mOMIB}. The area reflects the ability of the system to absorb kinetic energy before forward-swing instability happens.

This property can be observed in the OMIB electrical power rotor angle characteristic of Figure 4-3 where the steady state OMIB electrical power versus angle characteristic is displayed. The characteristics are similar for the post fault network, where the available

acceleration area between the P_{mOMIB} and P_{eOMIB} curves reduces for the increasing imbalance H_1 and H_2.

TABLE 4-4. STEADY STATE OMIB ELECTRICAL POWER COEFFICIENTS FOR THE CONTROL CASE WHEN THE SVC IS OFFLINE

Parameter (pu)		Col 1	Col 2	Col 3
		$H_1 \approx H_2$ (Base-line)	$H_2 = 2H_1$	$H_2 = 5H_1$
P_{mOMIB}		-0.48	4.59	9.29
Coefficient of equations (4.63) and (4.64)	K (constant term)	-1.08	3.07	6.91
	C (cosine term)	-0.07	0.88	1.77
	S (sine term)	2.87	2.87	2.87

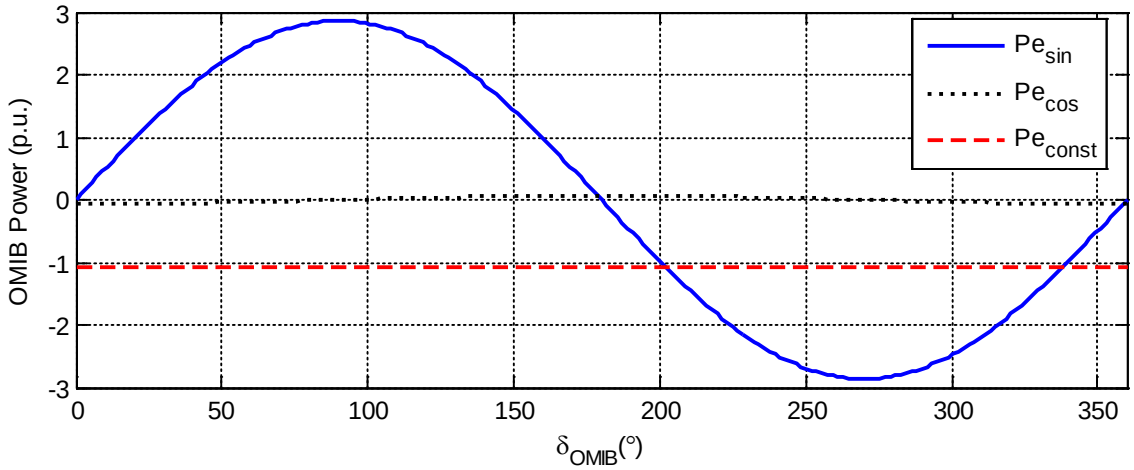

Figure 4-3. The sine, cosine and constant components of the OMIB electrical power-angle characteristic when the SVC is offline in the base-line operation.

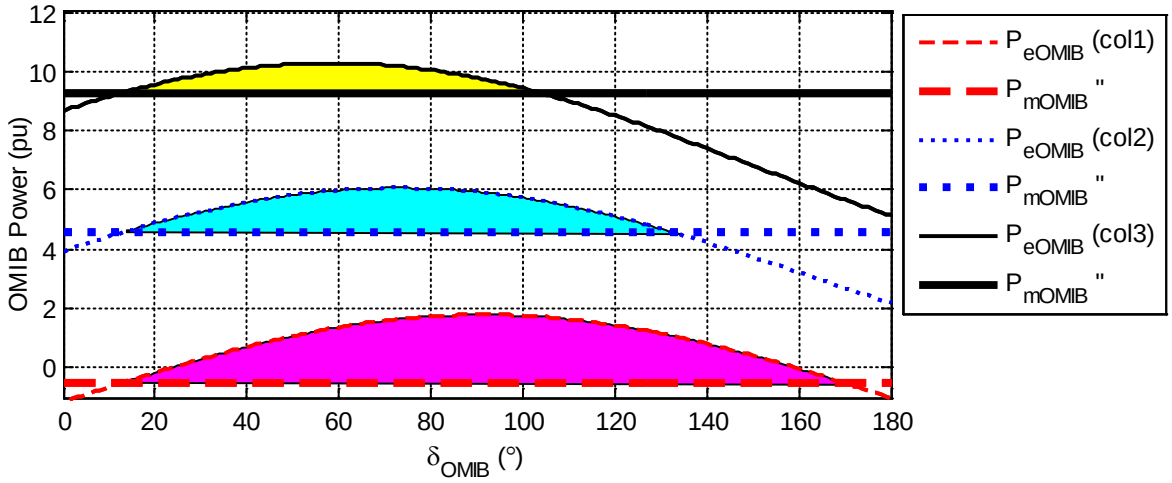

Figure 4-4. Variation in steady-state electrical and mechanical OMIB power where G2 inertia constant is varied as per columns 1, 2 and 3 in Table 4-4.

4.3.1.2. *OMIB Power-Angle Equations When the SVC is Online*

When the SVC compensation is connected to the midpoint of the two machine system, the OMIB electrical power is derived by substituting for P_{e1} and P_{e2} from equations (4.39) and (4.40) into equations (4.59) and (4.60). This yields:

$$P_{eOMIB} = P_{CONST} + P_{COS} + P_{SIN} \tag{4.65},$$

where

$$P_{CONST} = H_{OMIB}\left(\frac{G_{11}E'_{q1}}{H_1} - \frac{G_{22}E'_{q2}}{H_2}\right) \tag{4.66},$$

$$P_{COS} = H_{OMIB}\left(\frac{E'_{q1}V_S G_{1S}\cos\delta_{1S}}{H_1} - \frac{E'_{q2}V_S G_{2S}\cos\delta_{2S}}{H_2}\right) \tag{4.67},$$

and

$$P_{SIN} = H_{OMIB}\left(\frac{E'_{q1}V_S B_{1S}\sin\delta_{1S}}{H_1} - \frac{E'_{q2}V_S B_{2S}\cos\delta_{2S}}{H_2}\right) \tag{4.68}.$$

Equations (4.65) and (4.58) reveal that when the SVC is connected to the system, the OMIB electrical power is dependent on δ_{1S} and δ_{2S}, the transmission angles between the SVC and G1 and G2 respectively. These angles are determined by the SVC constraints outlined in equations (4.43), (4.42) and (4.58). The characteristics of δ_{1S} and δ_{2S} versus δ_{OMIB}, for the base-line operation with unlimited SVC capacity, are displayed in Figure 4-5. In the figure δ_{1S} and δ_{2S} vary approximately linearly with respect to δ_{OMIB}. However beyond $\pm 100°$ as δ_{OMIB} draws towards the solution limits and δ_{1S} and δ_{2S} become very sensitive to changes in δ_{OMIB}. δ_{1S} and δ_{2S} reach an asymptote at $167°$ and $-173°$.

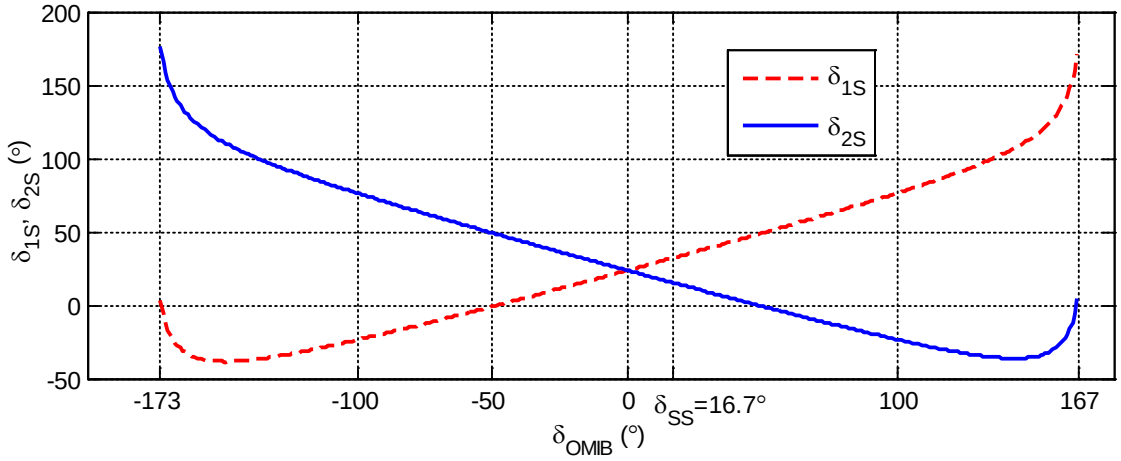

Figure 4-5 The relationship between δ_{1S}, δ_{2S} and δ_{OMIB} for the steady-state base-line case when the SVC is online with unlimited capacity.

When δ_{OMIB} is 0°, power is transferred to supply the loads L_7 and L_9, yet there is no transfer over the tie-line at this operating point. Due to the system symmetry equal amounts of active power are transferred from G1 and G2 to the SVC. As such δ_{1S} and δ_{2S} are equal and non-zero for this system condition.

The values G_{11} and G_{22} change with the network state. From Figure 4-6 and (4.65), for positive values of δ_{OMIB}, P_{SIN} makes a positive contribution to P_{eOMIB} and P_{COS} is negative, but small.

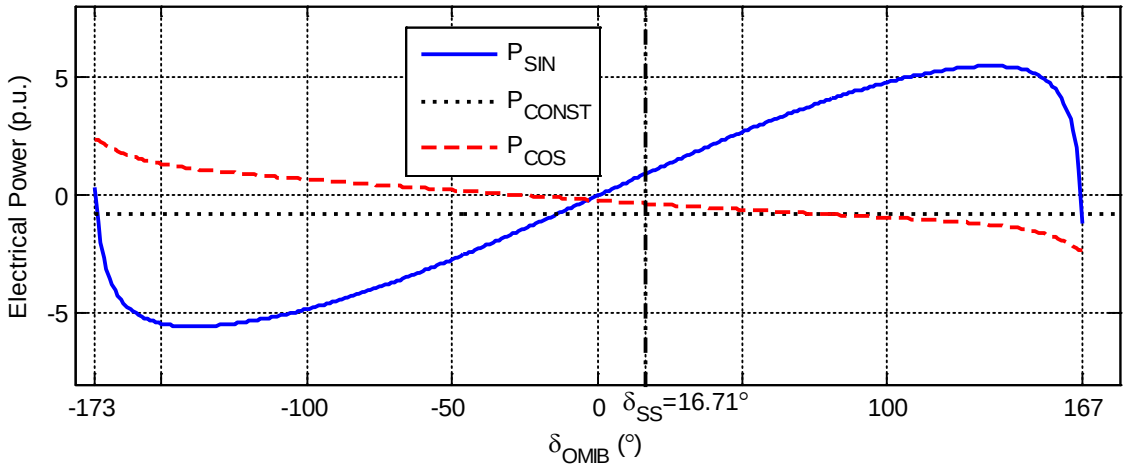

Figure 4-6. The sine (P_{SIN}) and cosine (P_{COS}) components of the $P_{eOMIB} - \delta_{OMIB}$ curve, for the base-line system in the pre-fault state.

Figure 4-7 shows the steady-state OMIB electrical power versus angle responses for the system under base-line conditions. It compares the acceleration power-angle curves for the following pre-fault scenarios: the SVC capacity is (i) infinite; (ii) ±400MVar; (iii) ±200MVar; and finally the SVC is disconnected.

It is expected that the power transfer capability should increase when the SVC is connected to the system since it injects reactive power to maintain the voltage at the middle of the transmission line to the set-point level. In Figure 4-7 the improvement in the steady-state power transfer capability is clear when the SVC capacity is unlimited. However, its impact is much less significant when the SVC capacity is limited to ±400 MVar.

For the cases where the SVC is offline, and where the SVC is online with $\pm$200MVar and $\pm$400MVAr capacity the peak value of P_{eOMIB} happens at about $95°$. If the

transmission is increased beyond $95°$ the value of P_{eOMIB} decreases. For the case where the SVC with unlimited capacity is connected, as the peak value of P_{eOMIB} happens when $\delta_{OMIB} = 130°$. If the transmission angle increases beyond $130°$ the $P_{eOMIB} - \delta_{OMIB}$ rapidly decreases towards an asymptote at $167°$, beyond which no solution for P_{eOMIB}. The $P_{eOMIB} - \delta_{OMIB}$ curve is similar for the post-fault network, and directs the dynamic change in P_{eOMIB} after a fault is cleared as described in examples in the following sections.

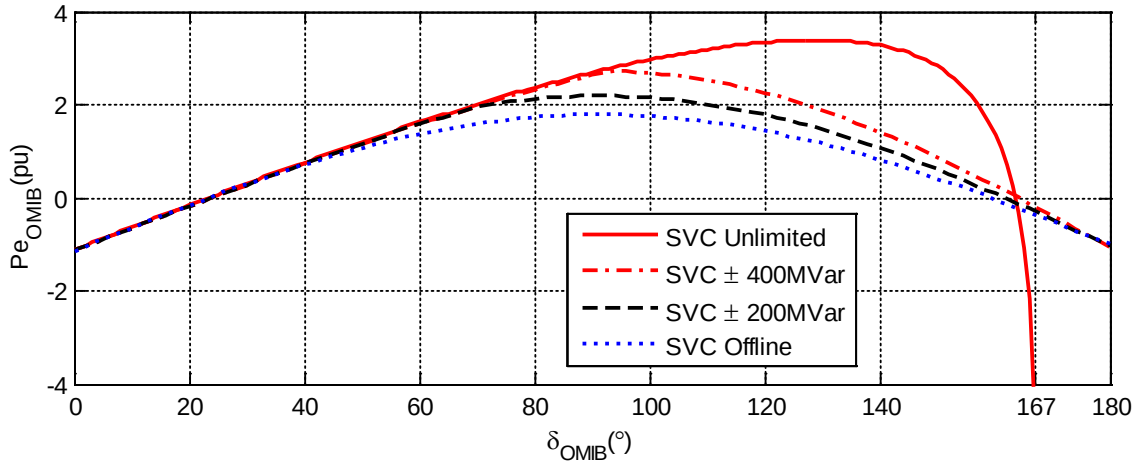

Figure 4-7. OMIB electrical power versus angle for the base-line system in the pre-fault state when the SVC is online with 1) unlimited capacity, 2) ±400MVar capacity, 3) ±200MVar capacity and 4) the SVC offline.

4.4. Dynamic Network Behaviour of the Two Machine System

In the following sections the network equations presented in section 4.2 and 4.3 are reconciled with the swing equations to describe the dynamic behaviour of the generators in the two machine power system. So far the network equations have only been investigated for the base-line steady-state operating condition. Transient stability assessment is applied to the scenarios described in Table 4-5. A scenario with an infinite capacity SVC is not considered since it was found to make negligible improvement to the *post-fault* electrical power angle curve, for the three-phase fault applied at the sending-end.

In the assessment attention is paid to the order of events leading to transient stability or instability. To allow key concepts to be demonstrated the 9-bus two machine system is idealized: The system is lossless, apart from the loads. Generator mechanical and

electromagnetic damping effects are neglected in this model. Consequently although the oscillations are bounded they do not decay. As there are no governors or automatic voltage regulators the system response may indicate longer term frequency instability – however this is beyond the scope of the transient stability problem. While the two machine system is small it can potentially provide useful insight into the behaviour of larger power systems.

TABLE 4-5. THE INVESTIGATED SCENARIOS

Scenario ID	Steady-State	Fault State	Post-Fault State	SVC Configuration	Fault Clearing Time (ms)	Transient Stability Assessment
1A.S	As described in Table 4-2	A three-phase fault is applied to the bus 6 (sending) end of circuit #2 between buses 6 & 7	The circuit breakers at both ends of circuit #2 between buses 6 and 7 are simultaneously opened.	Off-line	120	Stable
1A.MS					150	Marginally Stable
1A.U					190	Unstable
1B.S				±200MVAr Online	120	Stable
1B.MS					150	Marginally Stable
1B.U					190	Unstable

4.4.1. Generator Dynamic Response to a Sending-End Three Phase Fault

In these investigations the classical second order generator model is used to represent the generators of the 9-bus two machine power system. With this model the internal generator voltages, E'_{q1} and E'_{q2} are maintained constant at their initial steady-state values. Using this model the following equation is used to represent the motion of each generator rotor, as derived in section 2.1:

$$\frac{2H_i}{\omega_0}\frac{d^2\delta_i}{dt^2} = P_{mi} - P_{ei} = P_{ai} \tag{4.69}$$

where *i* is the generator number (i.e. 1 or 2), H_i is the inertia constant of generator *i* in pu-s, ω_0 is synchronous speed in electrical rad/s, and δ_i is the angular position of the rotor of generator *i* in electrical radians with respect to the synchronously rotating reference. P_{mi}, P_{ei} and P_{ai} are the per unit input mechanical, output electrical, and acceleration powers of each of the generators. P_{ei} is determined by equations (4.10) and (4.11) where the SVC is disconnected from the system, and equations (4.36) and (4.37)

when it is connected. No governors are included in the system, thus P_{mi} remains fixed at the initial steady state value.

$$\frac{d\delta_i}{dt} = \omega_0 \left(\omega_{ri} - 1\right) \tag{4.70}$$

$$\frac{d\omega_{ri}}{dt} = \frac{1}{2H_i}\left(P_{mi} - P_{ei}\right) \tag{4.71}$$

where ω_{ri} is the rotor velocity of generator *i.*

Equation (4.71) shows that the angular acceleration of generator *i* is proportional to the accelerating power, $P_{ai} = P_{mi} - P_{ei}$, absorbed by its rotor. From equation (4.71), during the steady-state $P_{mi} = P_{ei}$ and there is no acceleration of the generator rotors. Consequently each generator is spinning at synchronous speed and its rotor angle is fixed.

When a fault is applied to the two machine system, the network structure changes. The associated voltage depression at the fault location will cause the electrical power output of the generators to decrease. The resulting mismatch between P_{mi} and P_{ei} will cause both generators to accelerate above synchronous speed and their rotor-angles will increase. The network equations (4.10), (4.11), (4.39) and (4.40) indicate that the decrease in P_{ei} immediately after the fault is dependent on the equivalent network matrix during the fault, which in turn is influenced by the location and the severity of the fault[4].

During the fault if the SVC is disconnected from the system, or if the SVC is connected and has reached a limit, then P_{ei} is calculated by equations (4.10) and (4.11). For a three phase fault on the transmission line, since no power can be transmitted over the entire line, the terms B_{12} and G_{12} from equations (4.10) and (4.11) are 0 pu. Thus the electrical power output from the generators becomes:

$$P_{e1} = G_{11}E'^{2}_{q1} \tag{4.72}$$

and

$$P_{e2} = G_{22}E'^{2}_{q2} \tag{4.73}.$$

This implies that during the fault, the power output from G1 and G2 is fixed and independent of the generator transmission angle.

In the alternative but unlikely situation that the SVC is connected and does not reach its limit during the fault, the generator electrical power is calculated by equations (4.39) and (4.40). If the three phase fault occurs between G1 and the SVC (i.e. close to node 6) the terms B_{1S} and G_{1S} will become 0 pu. In this situation the electrical power output

[4] *It is assumed that the network state changes instantaneously when the fault is applied.*

from G1 is calculated by equation (4.72). Alternatively if the fault were to occur between G2 and the SVC (i.e. close to node 8) then the terms B_{2S} and G_{2S} will become 0 pu, and P_{e2} is calculated from equation (4.73). This indicates that during the fault, if the SVC is online and has not reached its maximum capacity, then the electrical power output from the generator nearest to the fault will be constant. However the electrical power from the other generator will depend on the angle between the generator furthest from the fault and the SVC.

When the fault is cleared the voltages recover and P_{ei} will increase to values determined by the post-fault network structure, the generator transmission angle and equations (4.10) and (4.11), or (4.39) and (4.40). Immediately after fault clearance the generators will be running above synchronous speed and the generator angles will continue to increase. The changing transmission angle will cause P_{ei} to oscillate according to the equation (4.69).

4.4.2. TSA of Stable Scenario 1A.S - SVC Offline

The dynamic system response for scenario 1A.S is shown in Figure 4-8.

Pre-fault:

- The system is initially in the steady-state.
- At t=1s a three-phase fault is applied near to bus 6.

During the fault:

- P_{e1} falls to 0MW and P_{e2} drops by about 300 MW from 1424MW, so both machines accelerate.
- Consequently $P_{a1} > P_{a2}$ causing $\omega_1 > \omega_2$;
- This causes δ_{12} to increase.

Post-fault:

- The fault is cleared at t = 1.12s where P_{e1} and P_{e2} increase to a value slightly below their respective mechanical powers.
- Here the decelerating force on G1 is temporarily negligible, the speed of G1 is relatively constant ($\omega_1 \approx \omega_{clr}$), and above synchronous speed.
- Meanwhile P_{e2} continues to fall below P_{m2}. This causes G2 to accelerate up to ω_1 at t = 1.9s. Synchronism is maintained on the forward-swing at t = 1.9s, as both machines attain the same post-fault speed. As there are no governors the speed of both generators continues to increase.

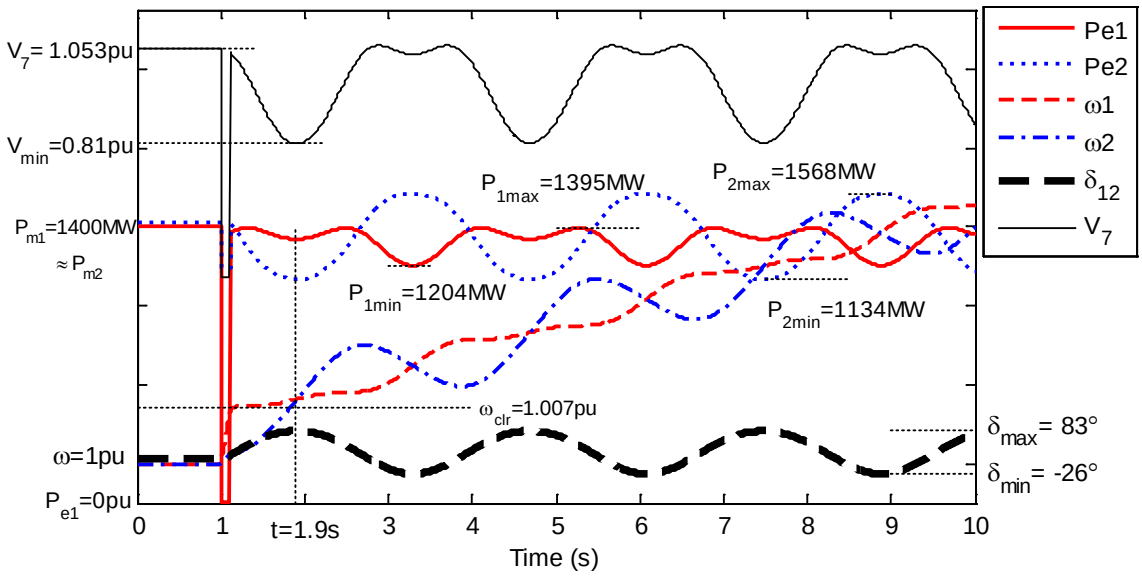

Figure 4-8. The dynamic responses for stable scenario 1A.S

The system remains synchronized (i.e. stable) for the full 10s of the simulation. The ensuing power swings on G2 span 434MW, approximately 30% of the G2 power. The power swings on G1 are smaller, spanning 191MW, 15% of the G1 power. The voltage dips to 0.81pu, an acceptable level for voltage stability as discussed in section 1.3.2. The corresponding OMIB responses for acceleration power, rotor angle and speed are shown in Figure 4-14.

4.4.3. TSA of Marginally Stable Scenario 1A.MS: SVC Offline

The dynamic system response for scenario 1A.MS is shown in Figure 4-9. In this scenario the dynamic response of the system is transiently stable, but the response is unacceptable due to low voltage levels after the clearance of the fault. This scenario brings to attention an important point: following a transient disturbance although the machines may maintain synchronism (i.e. rotor angle stability) the dynamic performance of the system may be unacceptable due to other factors, such as inadequate voltage performance. Consequently any complete assessment of dynamic performance limits must take into account factors other than rotor-angle stability. It is emphasized that this work is concerned only with rotor-angle stability.

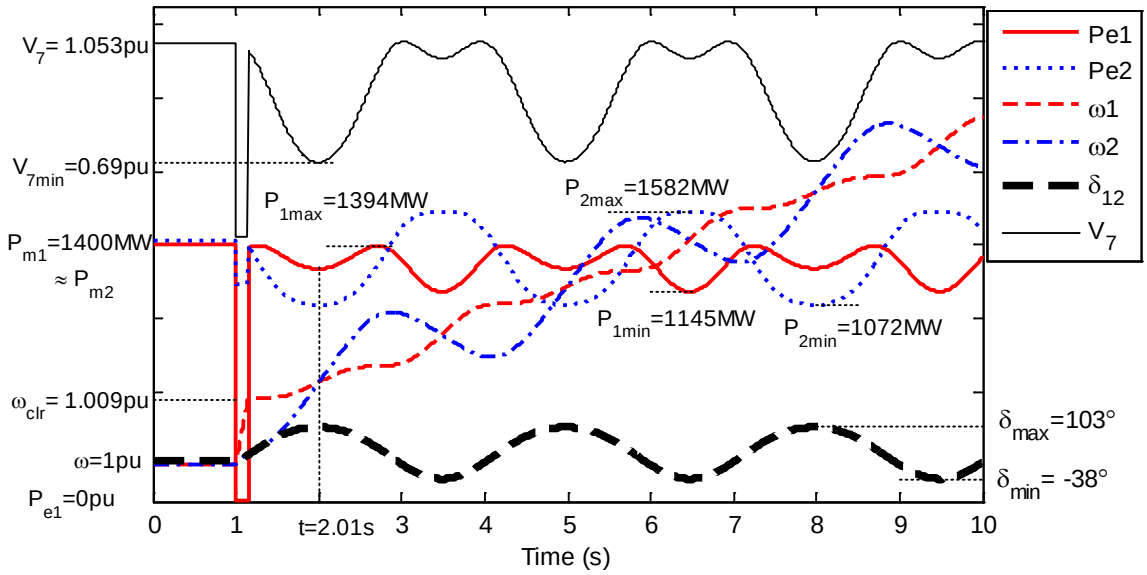

Figure 4-9. The dynamic responses for the marginally stable scenario 1A.MS

The steady-state and fault-state operating conditions are the same as scenario 1A.S, although at t=1.15s δ_{12} and $\omega_1 = \omega_{clr}$ are more advanced at fault clearance as the fault is applied for 30ms longer. The qualitative features of the response are similar to those of 1A.S.

Post-Fault

- The fault is cleared at t = 1.15s.
- As $P_{e2} < P_{m2}$ G2 accelerates, while G1 remains constant.
- $\omega_1 < \omega_2$ causing δ_{12} to increase.
- At t=2.01s synchronism is maintained on the forward-swing since $\omega_1 = \omega_2$.
- The generator rotors oscillate with respect to each other with a period of about 3s as the system is undamped.

The generators remain synchronized for the entire 10s simulation period. The voltage dips to the unacceptable level 0.69 pu, which is less than the voltage stability threshold, as mentioned in section 1.3.2.

A comparison of scenario 1.A.MS to scenario 1.A.S shows that when the system is operated under marginally stable conditions:

- The range of the G1 power swing increases by 58MW, from 191MW to 249MW, 18% of G1 power.
- The range of the G2 power swing increases by 76MW, from 434MW to 510MW, 35% of the G2 power.

- The speed of G1, at fault clearance, is slightly higher at 1.009pu in the multi-swing stable case, compared to 1.007pu in the stable case.
- The maximum transmission angle increases from 83° to 103°.

4.4.4. TSA of Unstable Scenario 1A.U: SVC Offline

The dynamic behaviour of the system for scenario 1A.U is shown in Figure 4-10. Until $t = 1s$ and $Y_{SVC0} = 0\,pu$, the behaviour before and during the fault is the same as scenario 1A.S. The difference is that in scenario 1A.U there is greater divergence in machine speeds and angles due to the longer fault duration at fault clearance.

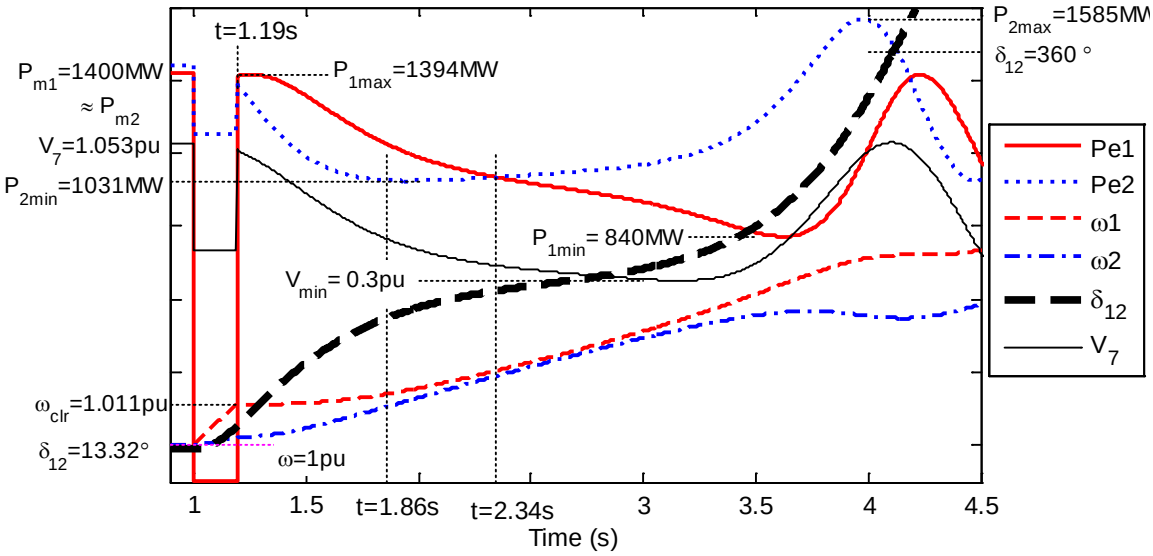

Figure 4-10. The dynamic responses for the unstable scenario 1A.U.

Post-fault

- After fault clearance, at t = 1.19s, P_{e1} and P_{e2} rise to values slightly below P_{m1} and P_{m2} respectively.
- Due to a combination of δ_{12} and the weakened post-fault network both machines continue to accelerate.
- Since $P_{e2} < P_{e1}$, the acceleration of machine 2 is higher than that of machine 1 and consequently ω_2 approaches ω_1.
- At t = 1.86s, before ω_2 can reach ω_1, P_{e2} reaches a minimum and then begins to increase slowly. In contrast P_{e1} continues its relatively fast decline.
- From t = 2.34s, whilst ω_1 is still faster than ω_2, machine 1 accelerates away from machine 2. Consequently, ω_2 is unable to match ω_1.

- Synchronism is lost at t = 4.1s when δ_{12} exceeds 360°. From the fault application to loss of synchronism δ_{12} increases monotonically, thus instability occurs on the *initial* swing.

The differences from the marginally stable case 1A.MS are that for scenario 1A.S:

– The speed of G1 is more advanced when the fault is cleared, at $\omega = 1.011 pu$,

– V_7 drops to an unacceptably low value of 0.3pu following the clearance of the fault, and oscillates between 0.3pu and 1.0pu.

– The ensuing power swings on G1 span a range of 554MW, 304MW larger than in the marginally stable case. $P_{1\max}$ is unchanged from scenario 1A.MS, so the increased swing is caused by decrease in $P_{1\min}$, which is caused by the extended voltage sag at the midpoint.

– The power swings on G2 are also 554MW, 44MW larger than the marginally stable case. The G1 swings are larger since it is closer to the fault.

4.4.5. TSA of Stable Scenario 1B.S: SVC Online

The dynamic response of scenario 1B.S from Table 4-5 is represented in Figure 4-11. The steady-state system operation is the same as scenario 1A.S. V_{SVC} is equivalent to V_7 - the voltage at node 7 - except here the SVC is online.

<u>During the fault</u>

- The fault causes the electrical power outputs of G1 & G2 to drop to $P_{e1} = 0.53 MW$ and $P_{e2} = 1225 MW$ respectively, causing both generators to accelerate. Since the acceleration on G1 is much higher than G2 the increase in rotor-angle and speed during the fault is significantly higher for G1 than G2.
- δ_1 increases much faster than δ_2, which causes the transmission angle, δ_{12}, to increase.
- V_{SVC} falls to 54% of the setpoint value ($V_{ref} = 1.053 pu$) thus the SVC increases its susceptance, Y_{SVC}, to its maximum value in an attempt to restore the voltage to V_{ref}. The SVC operates at the limit during the fault thus the behaviour of P_{e1} and P_{e2} are governed by equations (4.72) and (4.73).

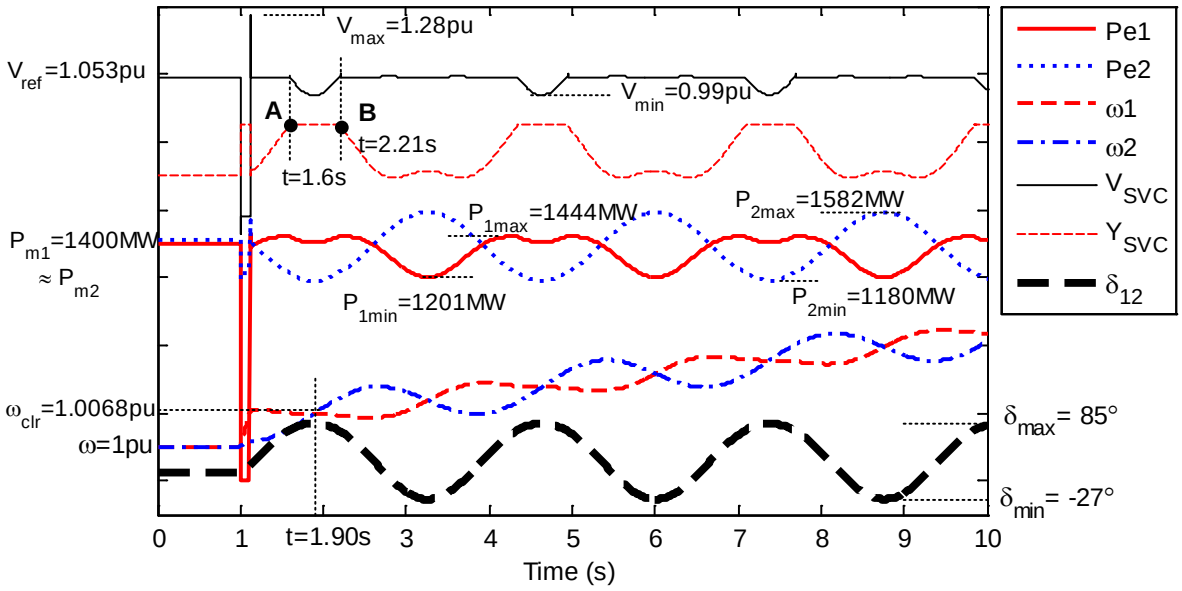

Figure 4-11. The dynamic responses for the stable scenario 1B.S

Post-Fault

- Immediately after the fault is cleared, at t = 1.12s, V_{SVC} is rapidly restored to V_{ref} and Y_{SVC} falls back within its limits.
- P_{e1} and P_{e2} recover to values near to their respective steady-state values.
- P_{e1} increases above P_{m1} and G1 experiences a small deceleration.
- $P_{e2} < P_{m2}$ thus G2 accelerates.
- Yet, $\omega_1 > \omega_2$ so δ_{12} continues to increase.
- Following the post-fault reduction in Y_{SVC} the SVC begins to increase the output susceptance in order to maintain the SVC voltage at V_{ref}. However, the SVC reaches its upper limit at t = 1.6s (point A).
- The SVC remains saturated for 0.67s, and V_{SVC} dips to a minimum of 0.99 p.u. Simultaneously there is a dip in P_{e1}.
- At t=1.9s, $\omega_1 = \omega_2$ revealing that stability is maintained after the forward angular swing. After this time δ_{12} begins to decrease as $\omega_1 < \omega_2$; and V_{SVC} starts to increase toward V_{ref} until t= 2.21 s (point B) when the SVC is able to again regulate the SVC voltage – since Y_{SVC} falls within its limits.

A comparison of scenario 1B.S to 1A.S shows that switching the SVC online causes:

– the range of the G1 power swing to be 243MW instead of 191MW, 52MW greater

– the range of the G2 power swing to be 402MW instead of 434MW, 32MW smaller

– 0.18pu improvement in the voltage sag (0.99pu instead of 0.81pu) at the SVC connection point
– the speed of G1 at the time of fault clearing, $\omega_{clr} = 1.0068\,pu$, is slightly lower than in scenario 1A.S.

4.4.6. TSA of Marginally Stable Scenario 1B.MS: SVC Online

Figure 4-12 shows the system response for scenario 1B.MS from Table 4-5. The steady-state and fault states are similar to scenario 1B.S, although ω_1, ω_2 and δ_{12}, are further advanced due to the additional fault clearing time. Like scenario 1A.MS the rotor-angle is stable in this scenario.

Post-fault

- The fault is cleared at t = 1.15s and V_{SVC} increases momentarily above V_{ref} before being restored to this reference value.
- As $P_{e1} > P_{m1}$, and $P_{e2} < P_{m2}$ G1 experiences a slight deceleration and G2 accelerates
- $\omega_1 > \omega_2$ causing δ_{12} to increase. Y_{SVC} is increased to maintain V_{SVC} at the set-point V_{ref} .
- At t = 1.48s, point A, Y_{SVC} reaches its maximum reserve and the SVC remains saturated until t = 2.51s (point C).
- During saturation V_{SVC} drops to a minimum of 0.84p.u at t = 2.12s (point B). This level of voltage sag is acceptable. At point B, synchronism is maintained on the forward-swing since the speeds of the two machines equalise.
- The SVC periodically saturates and the generator speeds converge every 2s.

A comparison of scenarios 1A.MS and 1B.MS shows that connecting the SVC online causes:

- The average power output from G1 to increase by 25MW, from 1270MW to 1295MW
- The average power output from G2 to increase by 30MW, from 1327MW to 1360MW
- The range of the G2 power swing remains about the same at 511MW
- The range of the G1 swing increases by 53 MW, from 249MW to 302MW

- The speed at the time of fault clearing, ω_{clr}, and therefore maximum transmission angle, are similar
- The minimum voltage at the SVC terminal is improved by 0.15pu from 0.69pu to 0.84pu. Consequently, the voltage response of the 1B.MS scenario is acceptable whereas it is not in the 1A.MS scenario.

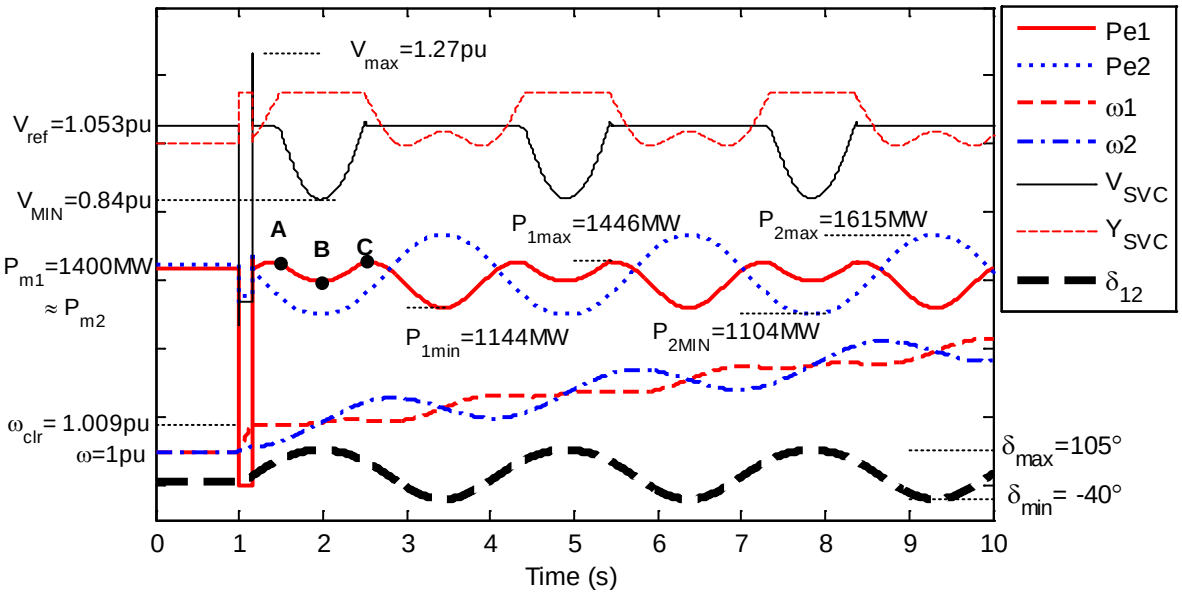

Figure 4-12. The dynamic responses for the marginally stable scenario 1B.MS

4.4.7. TSA of Unstable Scenario 1B.U: SVC Online

Figure 4-13 shows the dynamic responses for scenario 1B.U, described in Table 4-5. The system behaviour in the steady-state and fault state is the same as scenario 1B.S, although the machine speeds and δ_{12}, are more advanced due to the longer fault clearing time.

Post-fault

- The fault is cleared at 1.19s
- V_{SVC} overshoots momentarily to a peak voltage of 1.25pu before returning to V_{ref}
- Due to the increase in δ_{12}, Y_{SVC} increases to maintain the V_{SVC} at V_{ref}, but reaches its maximum at t = 1.4s (point A) until t = 3.21s (point B)
- During this interval the V_{SVC} drops to an unacceptably low value of 0.37p.u, and is below 0.8pu for 1.44s.

- From t=1.19s to $t_c = 2.13s$ (point C), the accelerating power of G1 is less than that of G2. Even so, ω_1 remains higher than ω_2 at t_c . After $t = t_c$, G1 accelerates with respect to G2 - their respective rotor speeds diverge and synchronism is lost during the forward-swing.
- Loss of synchronism is verified at t=3.4s when the transmission angle exceeds 360°.

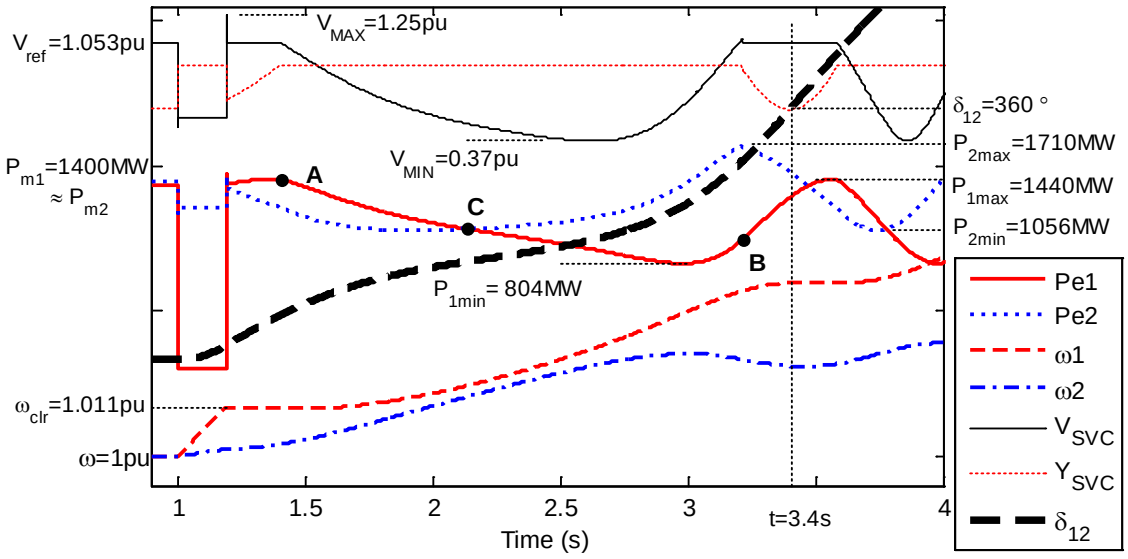

Figure 4-13. The dynamic responses for the unstable scenario 1B.U

Qualitatively the responses between scenario 1A.U (with no SVC) and 1B.U (with the SVC online) are very similar, but with some minor differences. In scenario 1B.U:

- The range of the subsequent power swings on G1 span 600MW, 46MW more than in scenario 1A.U
- The power swings on G2 span 654MW, 100MW more than scenario 1A.U. This is associated with an increase in the average G2 power output after fault clearance, from 1308MW in scenario 1A.U to 1383MW in scenario 1.BU.

4.4.8. Summary of TSA on the Two Machine System

Investigations on the scenarios in Table 4-5 provide useful insights into the dynamic behaviour of the two machine system following a transient disturbance. The analysis predominantly reveals how the generators respond to a three phase fault that occurs at the sending-end of the transmission line, how SVC compensation affects the dynamic behaviour of the system, and the associated mechanisms of stability or instability.

In the steady-state operation the electrical and mechanical shaft power of the generators are equal, the system is in equilibrium and the generators are synchronized. During fault application the two generators each absorb kinetic energy and accelerate. As G1 is located closer to the fault it tends to experience greater acceleration than G2. Thus at the time of fault clearance the speed and angle of G1, both advance ahead of G2. If the SVC is connected to the system, during the fault the SVC susceptance tends to rapidly reach the capacitive limit.

In the post-fault system for the stable scenarios the acceleration of both generators reduce, however as initially $\omega_1 > \omega_2$, δ_{12} continues to increase. The increase in δ_{12} causes G2 to experience significant acceleration such that ω_2 reaches ω_1 in the forward power swing with the result that the machines remain synchronized.

Irrespective of whether the SVC is online, the network is prone to instability on the forward-swing for the applied fault. In the unstable scenarios P_{e1} tends to decrease. This implies that δ_{12} following fault clearance is such that $P_{e1}\left(\delta_{12}\right) > P_{e1\max}$ as shown in Figure 4-7. G1 tends to accelerate with respect to G2 before the two machines can attain the same speed – consequently synchronism is lost during the forward-swing.

On the other hand if the machines can return to the same speed by the end of the forward-swing then rotor-angle stability of the system can be maintained. The marginally stable scenario 1A.MS shows that system operation may be transiently stable, but the system voltage response may be unacceptable. Scenario 1B.MS shows that connecting an SVC can improve the post-fault voltage performance.

4.5. TSA of the Two Machine System Using the SIME Analysis

This section introduces the SIME method for transient stability assessment by applying it to the two machine powe r system. The SIME technique derives an equivalent time-varying OMIB response from the time-domain simulations of a multi-machine system. As there are two machines in the system the machine groups are obvious, and the COI equations are already calculated. The COI equations are re-applied to the pair of machine responses, as indicated in Appendix B, to calculate a single time-varying OMIB response which represents the dynamic behaviour of the entire power system. No model reduction is required.

In this section the two machine power system is used to investigate the derivation of the time-varying OMIB response, with emphasis on the fact that no model reduction is required. It is an ideal platform for investigating this process because it isolates the derivation of the OMIB response from the task of splitting the system machines into two groups.

This section relates the dynamic behaviour of the two machine power system to the OMIB response. This is done by formulating the dynamic OMIB equations, and comparing them with the OMIB responses that are calculated directly from the PSS®E TDS, at each time step of a simulation. The scenarios described in Table 4-5 are used to assess how the dynamic behaviour of the full system response translates to the dynamic behaviour of the equivalent OMIB response. They are also used to demonstrate the application of the SIME early stop criteria (ESC) and the estimation of the SIME transient stability margins.

4.5.1. Derivation of the OMIB Dynamic Swing Equations

The dynamic OMIB equations for the two machine power system are formulated by substituting the equations for generator power, speed and rotor angle, described in section 4.4.1, into the OMIB transformation equations, presented in section 4.3. Differentiating (4.58) yields:

$$\frac{d\delta_{12}}{dt} = \frac{d\delta_1}{dt} - \frac{d\delta_2}{dt} = \frac{d\delta_{OMIB}}{dt} \tag{4.74}.$$

Substituting for $\frac{d\delta_i}{dt} = (\omega_i - 1)\omega_0$ from equation (4.69) into (4.74) it follows that:

$$\frac{d\delta_{OMIB}}{dt} = (\omega_1 - \omega_2)\omega_0 = \omega_{OMIB}\omega_0 \tag{4.75}$$

where $\omega_{OMIB} \triangleq \omega_1 - \omega_2$. Differentiating (4.75) again:

$$\frac{d^2\delta_{OMIB}}{dt^2} = \frac{d^2\delta_1}{dt^2} - \frac{d^2\delta_2}{dt^2} = \omega_0 \frac{d\omega_{OMIB}}{dt} \tag{4.76}$$

$$\therefore \frac{d\omega_{OMIB}}{dt} = \frac{1}{\omega_0}\frac{d^2\delta_{OMIB}}{dt^2} \tag{4.77}.$$

Recalling equation (4.69) the electrical power output from G1 and G2 is

$$P_{e1} = P_{m1} - \frac{2H_1}{\omega_0}\frac{d^2\delta_2}{dt^2} \tag{4.78}$$

and $$P_{e2} = P_{m2} - \frac{2H_2}{\omega_0}\frac{d^2\delta_2}{dt^2} \quad (4.79).$$

Substituting (4.78) and (4.79) into equation (4.59) the OMIB electrical power is

$$P_{eOMIB} = H_{OMIB}\left(\frac{P_{m1}}{H_1} - \frac{P_{m2}}{H_2} - \frac{2}{\omega_0}\left(\frac{d^2\delta_1}{dt^2} - \frac{d^2\delta_2}{dt^2}\right)\right) \quad (4.80).$$

Substituting $\delta_{OMIB} = \delta_1 - \delta_2$ to (4.80) yields

$$P_{eOMIB} = H_{OMIB}\left(\frac{P_{m1}}{H_1} - \frac{P_{m2}}{H_2} - \frac{2}{\omega_0}\frac{d^2\delta_{OMIB}}{dt^2}\right) \quad (4.81).$$

Substituting from equation (4.61) into (4.81) yields

$$P_{eOMIB} = P_{mOMIB} - 2\frac{H_{OMIB}}{\omega_0}\frac{d^2\delta_{OMIB}}{dt^2} \quad (4.82).$$

Then the OMIB acceleration power is

$$P_{aOMIB} = P_{mOMIB} - P_{eOMIB} = 2H_{OMIB}\frac{d\omega_{OMIB}}{dt} \quad (4.83).$$

During the application of the three phase fault P_{e1} and P_{e2} are constant values dictated by equations (4.72) and (4.73). Thus, during a three-phase fault the OMIB electrical power is:

$$P_{eOMIB}(t) = H\left(\frac{G_{11}E'_{q1}}{H_1} - \frac{G_{22}E'_{q2}}{H_2}\right) \quad (4.84).$$

4.6. SIME TSA for Stable Scenarios on the Two Machine System

This section outlines the relationship between the OMIB swing equations for the two machine system that is presented in section 4.5.1, and the TDS OMIB responses of the stable scenarios 1A.S, 1A.MS, 1B.S and 1B.MS which are defined in Table 4-5. The conclusions from the dynamic assessment of the stable scenarios, in section 4.4.8, are related to the behaviour of the corresponding OMIB time responses in the steady-state, fault- and post-fault operation of the system. Figure 4-14 shows the OMIB acceleration power, angle and speed responses for the four scenarios, as calculated from the equations in section 4.5.1.

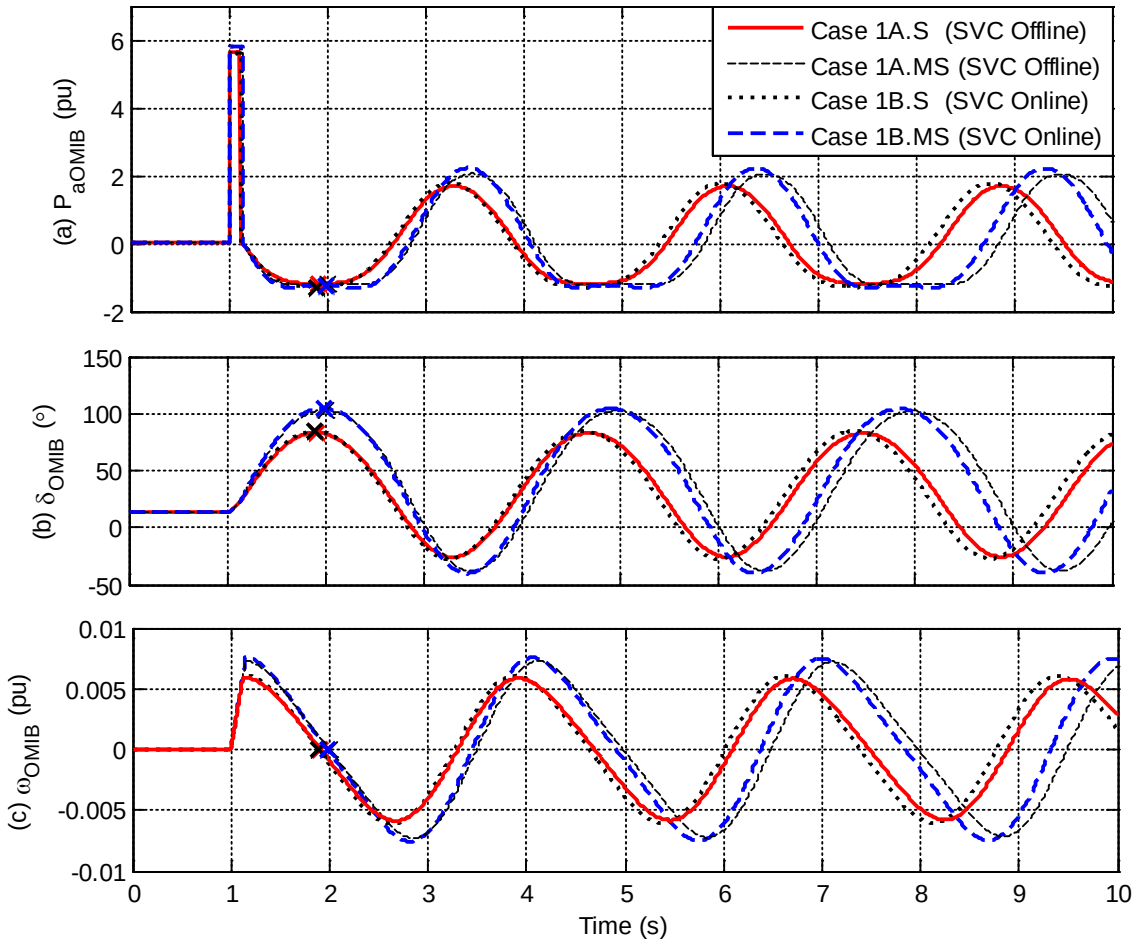

Figure 4-14. The OMIB a) acceleration power, b) rotor speed, and c) rotor angle responses for the stable scenarios 1A.S, 1A.MS, 1B.S and 1B.MS

Steady-State

Each scenario begins in the steady-state operation where the system is in equilibrium and both generators operate at synchronous speed, where $P_{eOMIB} = P_{mOMIB}$ and P_{aOMIB} is zero. For all scenarios the initial OMIB angle is 13.32˚.

Fault-State

From the section 4.4.8, during the fault, G1 experiences a larger acceleration than G2, and P_{e1} and P_{e2} are constant values. Thus, by equation (4.83), P_{aOMIB} is positive and constant during the fault. Moreover, since P_{aOMIB} is constant, because of equations (4.83) and (4.82) respectively, ω_{OMIB} will accelerate uniformly from 0pu, and by (4.75) δ_{OMIB} will increase quadratically during the fault period. Comparing P_{aOMIB} of scenario 1A.S and 1A.MS against scenarios 1B.S and 1B.MS, it is observed that the SVC compensation causes a small increase in P_{aOMIB} during the fault period.

Post-fault

In section 4.4.8 it is observed that for the stable scenarios 1A.S, 1A.MS, 1B.S and 1B.MS, immediately after fault clearance $P_{e1} \approx P_{m1}$ and $P_{e2} \approx P_{m2}$. After the fault is cleared P_{aOMIB} returns to zero. This is consistent with the observation in Figure 4-17 (a), noted in section 4.4.8, that the speed of G2 increases to match that of G1 during the forward-swing following fault clearance. This is consistent with the observation from Figure 4-17 (c) that ω_{OMIB} returns to zero (i.e. synchronous speed) at the end of the forward-swing following fault clearance.

With respect to the analysis in section 4.4, the OMIB responses in Figure 4-14 (a) indicate that when P_{aOMIB} is positive G1 experiences a larger acceleration than G2. Conversely, when P_{aOMIB} is negative G2 experiences a larger acceleration than G1. Essentially P_{aOMIB} can be viewed as the acceleration power of group 1 with respect to group 2. This interpretation is confirmed by equation (4.83). The OMIB responses also show that when ω_{OMIB} = 0pu the speeds of the generators are equal, and the system remains synchronized. Furthermore, equation (4.75) indicates that when the speed difference between G1 and G2 is zero δ_{OMIB} reaches a local maximum or minimum. Equation (4.82) shows that P_{aOMIB} (and thus P_{eOMIB}) is dependent on δ_{OMIB}. This behaviour is expected from the OMIB electrical power equations (4.63) and (4.65).

4.6.1. OMIB Power-Angle Curves for the Stable Scenarios

The SIME method applies the EAC, described in section 2.3, to the OMIB power-angle responses to assess the transient stability of the two machine system. Here, the OMIB responses of the stable scenarios are examined in the power- angle domain. Figure 4-15 shows the OMIB acceleration power versus angle response for scenario 1A.S.

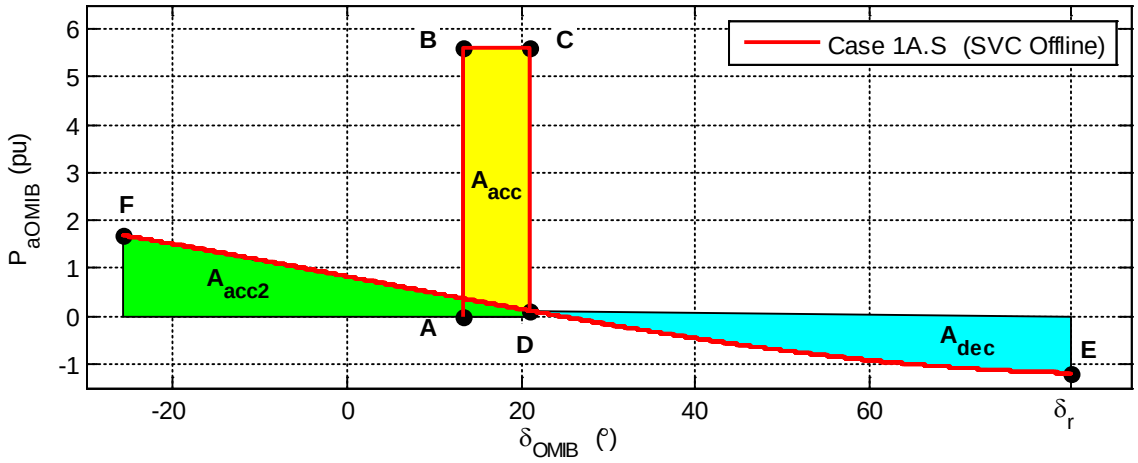

Figure 4-15. The OMIB power-angle characteristic for the stable scenario 1A.S

Steady-State

The steady-state operating point is at point A, where the system is in equilibrium. As both generators run at synchronous speed, $P_{eOMIB} = P_{mOMIB}$, thus P_{aOMIB} is zero. The initial OMIB rotor angle is 13.32°.

Fault-State

When the fault is applied after t=1s, by equation (4.83) P_{aOMIB} increases to a positive value (point to A to B) and is constant during the fault (point B to C).

Post-Fault State

When the fault is cleared at t=1.12s P_{aOMIB} falls from point C to point D. At D $\omega_{OMIB} > 0$, thus δ_{OMIB} continues to increase which causes P_{aOMIB} to fall below 0 pu as dictated by equations (4.63) and (4.65). This eventually causes ω_{OMIB} to decrease to 0 pu at point E, which is when the speeds of the two machines equalise at the end of the forward-swing. Here δ_{OMIB} reaches the maximum angle, δ_r, before decreasing again as ω_{OMIB} falls below 0pu. As the system is undamped the $P_{aOMIB} - vs - \delta_{OMIB}$ trajectory continues to oscillate along the post-fault curve between points E and F.

On the $P_{aOMIB} - vs - \delta_{OMIB}$ curve the area bounded by points A, B, C and the δ_{OMIB} axis is the acceleration area (**A_{acc}**); and the area bounded by points D, E and the δ_{OMIB} axis is the deceleration area (**A_{dec}**). According to the EAC, in section 2.3 when the trajectory of $P_{aOMIB} - vs - \delta_{OMIB}$ reaches point E the deceleration area is equal to the acceleration area. For stability a larger acceleration area requires a larger deceleration area, which will increase δ_r. In the case of a lossless system the area (**A_{acc}**) and the area formed between points F, D and the δ_{OMIB} axis (**A_{acc2}**), are equal.

Figure 4-16 shows an overlay of the $P_{aOMIB} - vs - \delta_{OMIB}$ curves for scenarios 1A.S, 1A.MS, 1B.S and 1B.MS. Comparison of scenario 1A.S and 1A.MS shows that the additional 30ms clearing time increases the acceleration area significantly, causing a noticeable increase in the return angle, from $\delta_{r1A.S}$ to $\delta_{r1.MS}$. Comparison of scenarios 1B.S and 1B.MS to scenarios 1A.S and 1A.MS shows that during the fault the SVC compensation increases P_{aOMIB} by a small amount. The SVC provides negligible improvement to the post-fault network as the $P_{aOMIB} - vs - \delta_{OMIB}$ characteristics are virtually the same. Between scenarios 1A.S and 1B.S the SVC causes a small rise in the return angle from $\delta_{r1A.S}$ to $\delta_{r1B.S}$, and similarly for scenarios 1A.MS and 1B.MS.

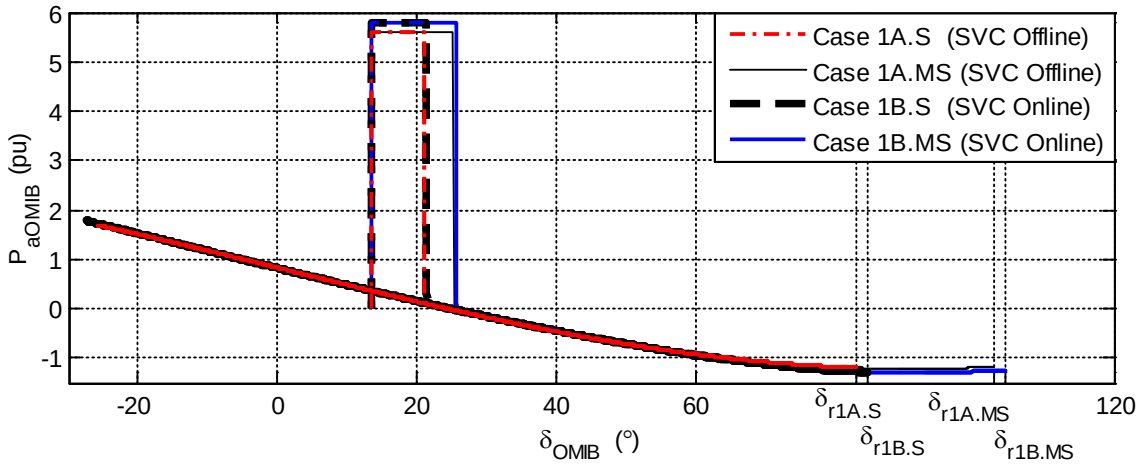

Figure 4-16. The OMIB power-angle characteristics of stable scenarios 1A.S, 1A.MS, 1B.S and 1B.MS on the two machine power system.

4.6.2. Application of the SIME ESC to the Stable scenarios

The SIME method applies criteria 1 to the OMIB response for the early detection of forward-swing stability [1] described in section 2.3.2. According to criteria 1 the stable ESC identifies forward-swing stability at the first time t_r, after fault clearance, when the OMIB rotor-speed is zero, $\omega_{OMIB} = 0$. At this instant the accelerating power must be also negative (i.e. $P_{aOMIB}(t_r) < 0$).

For scenarios 1A.S, 1B.S and 1B.MS the TDS are run for 10s before the scenario is classified as forward-swing, back-swing or multi-swing stable. However Figure 4-14 indicates with a cross 'X' the point at which the stable ESC can be applied for early detection of forward-swing stability in each of the scenarios. These times are listed in Table 4-6.

TABLE 4-6. THE ESC SIMULATION STOP TIME FOR THE STABLE SCENARIOS (NOTE: RUN-IN TIME OF 1S IS EMPLOYED)

Scenario	SVC Configuration	t_{ESC} (s)
1A.S	Offline	1.91
1A.MS	Offline	2.13
1B.S	Online	1.95
1B.MS	Online	2.13

4.6.3. Calculation of the SIME Stable Margin

As per equation (2.24) the SIME stability margin is calculated from the OMIB power-angle curve of a stable scenario. To reiterate, the SIME inertia normalised stable margin is defined as:

$$\begin{aligned} \eta_s &= \frac{\text{Unused Deceleration Area}}{2H_{OMIB}} \\ &= \frac{1}{2H_{OMIB}} \int_{\delta r}^{\delta \lim} P_{aOMIB} d\delta \end{aligned} \tag{4.85}$$

where δ_r is the OMIB return angle; and $\delta_{\lim}$ is the estimated OMIB rotor-angle limit. $\eta_S > 0$ when the system is stable.

Figure 4-17 shows an example of the unused deceleration area for scenario 1A.S. It is not possible to calculate this area by using actual simulation data. The path of the power angle curve must be extrapolated from the forward-swing return angle, δ_r, to the angle of instability, $\delta_{\lim}$, where P_{aOMIB} is zero. A linear least squares (LLS) estimation algorithm is applied to fit a quadratic function to the P_{aOMIB} - δ_{OMIB} response spanning from the clearing angle, δ_{clr} to δ_r [75]. An initial investigation indicates that about 400 points, equally spaced on the rotor-angle axis, yields a quadratic function which is sufficiently accurate and usually insensitive to relatively small deviations in the power-angle curve. This is the number of data points used in all calculations in the thesis, although it is configurable in the software. It is possible for a scenario to be so stable that it is not possible to produce a reliable margin measure. If the estimated curve does not intersect the rotor angle axis (i.e. at $P_{aOMIB} = 0$, for $\delta > \delta_r$), then the scenario is classified as "too stable" for the purpose of margin calculation.

Figure 4-17 shows the area that is used to calculate the SIME stability margin for scenario 1A.S, and also the curve that is formed by the quadratic approximation. In this scenario δ_r is 83.1°, $\delta_{\lim}$ is approximated at 170.6°, and the corresponding stability margin is 0.2158 rad-pu. Table 4-7 shows a summary of δ_r, $\delta_{\lim(estimated)}$ and the stability margin for each of the stable scenarios.

From section 2.3 it is implied that a larger stable margin is indicative of the larger unused deceleration area and that the scenario is more stable. Based on this interpretation the results of Table 4-7 rightly indicate that scenario 1A.S is the most stable scenario, with the largest margin, and smallest return angle, whereas scenario 1B.MS is the least stable scenario.

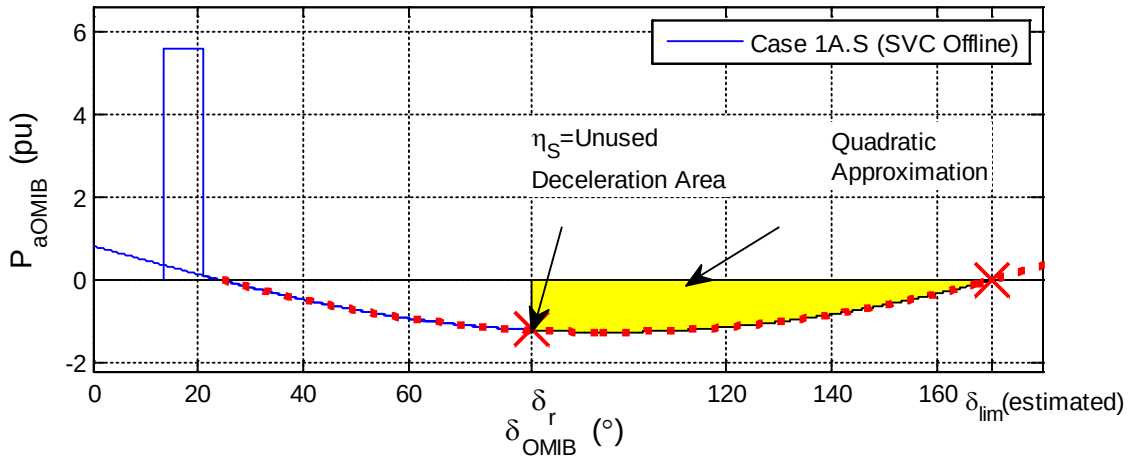

Figure 4-17. The OMIB power-angle curve of scenario 1A.S, featuring the quadratic approximation required to calculate the SIME stability margin.

TABLE 4-7. SUMMARY OF THE SIME MARGINS FOR THE EXAMPLE STABLE SCENARIOS ON THE TWO MACHINE POWER SYSTEM

(1)	(2)	(3)	(4)	(5)	(6)
Scenario	η_s (rad-pu)	δ_r (°)	$\delta_{\lim(estimated)}$ (°)	$\delta_{\lim(actual)}$ (°)	$\delta_{\lim(estimated)} - \delta_{\lim(actual)}$ (°)
1A.S	0.2158	83.1	170.5	158.4	12.1
1A.MS	0.1198	102.8	161.5	158.4	3.1
1B.S	0.2003	94.2	193.7	150.4	43.3
1B.MS	0.0499	120.0	165.8	150.4	15.4

From Figure 4-17 it is evident that the estimated value of the stable margin is influenced by δ_r and $\delta_{\lim(estimated)}$. In these scenarios, a larger clearing time is generally the cause of a larger δ_r, however in section 4.6 it is also observed that including the SVC compensation causes a larger δ_r. Column (5) of Table 4-7 lists the actual values of $\delta_{\lim}$, which are obtained from the analysis of the unstable scenarios 1A.U and 1B.U. It is apparent that for the stable scenarios 1A.S and 1B.S the estimated value of $\delta_{\lim}$, is significantly larger than the actual value. This is an example of the reduced accuracy of the estimated SIME stable margin, mentioned in [1], which evidently becomes more pronounced for more stable operating conditions. Finally, it is interesting to note that scenario 1A.S is classified as more stable than scenario 1B.S, despite the compensation provided by the SVC. This is explored in more detail in section 5.3.

4.7. SIME TSA for Unstable Scenarios on the Two Machine System

This section relates the OMIB swing equations, presented in section 4.5.1, to the TDS OMIB responses of the unstable scenarios 1A.U and 1B.U, defined in Table 4-5. Figure 4-18 shows the OMIB acceleration power, angle and speed responses for the unstable scenarios. The mechanism of instability for scenario 1A.U is described below.

Steady-State

During the 1s run-in period OMIB responses are exactly the same as for the stable scenarios.

Fault-State

As discussed in section 4.4.8, during fault application the system behaviour is essentially the same as for the stable scenarios - P_{aOMIB} becomes large and positive during the fault, and as per equation (4.82) this causes ω_{OMIB} and δ_{OMIB} to increase linearly and quadratically respectively.

Post-Fault

When the fault is cleared at t = 1.19s, P_{aOMIB} falls to 0pu due to a combination of the current value of δ_{OMIB}, and the post-fault network structure. Since ω_{OMIB} is positive after the fault, it follows from equation (4.82), that δ_{OMIB} continues to increase. This causes P_{aOMIB} to become negative based on equation (4.63). When the SVC is online equation (4.65) applies instead.

- However, P_{aOMIB} becomes positive before ω_{OMIB} returns to zero. Since P_{aOMIB} is positive, according to equation (4.83), ω_{OMIB} also increases. Consequently the OMIB rotor speeds and angles of the two machines diverge and thus loss of synchronism is indicated at $t = t_{\lim 1}$.
- Due to the sinusoidal dependence of P_{aOMIB} on δ_{OMIB} the monotonic increase in δ_{OMIB} leads to the observed oscillation in P_{aOMIB}. By equation (4.83) ω_{OMIB} increases when P_{aOMIB} is positive, and decreases when P_{aOMIB} is negative. However the deceleration is never sustained for long enough for ω_{OMIB} to return to 0pu. By equation (4.75) δ_{OMIB} increases monotonically, since ω_{OMIB} remains positive from the time the fault is applied.

The OMIB response to scenario 1B.U is similar except that loss of synchronism is indicated at $t = t_{\lim 2}$. For reasons explained in section 5.3 the SVC causes the scenario 1B.U to be less stable as $t_{\lim 2} < t_{\lim 1}$.

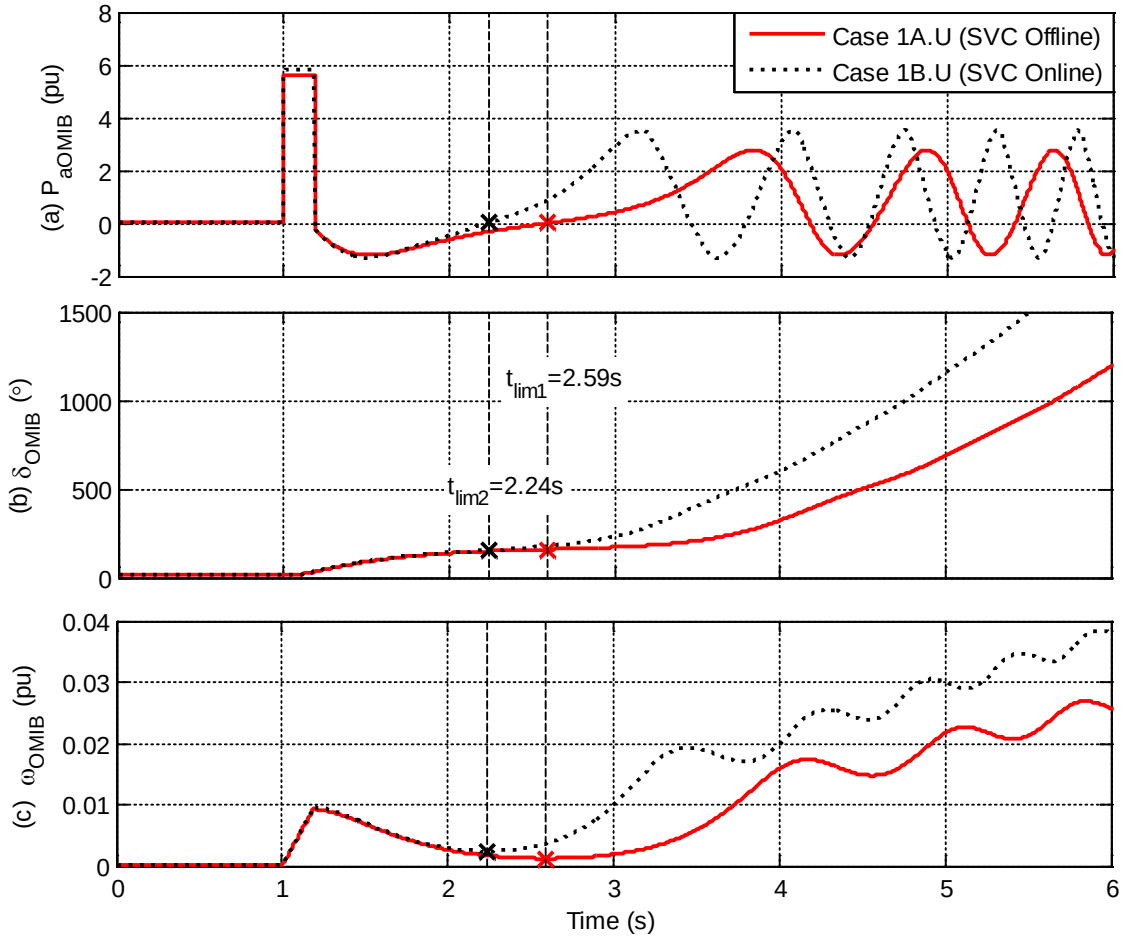

Figure 4-18. The OMIB response of (a) acceleration power, (b) rotor angle and (c) rotor speed for the unstable scenarios 1A.U and 1B.U.

4.1.1. *Application of the SIME ESC to the Unstable Scenarios*

The SIME method applies criteria 2, described in section 2.3.2 and demonstrated in Figure 2-4b), for early detection of forward-swing instability. For the unstable scenarios in Figure 4-18 this occurs at $t = t_{\lim i}$, where ω_{OMIB} is at a positive local minimum value. After this point the speed difference between the two machines increases. This is the first point in each simulation, after the fault, that P_{aOMIB} changes from decelerating (negative value) to accelerating (positive value). A limitation of criteria 2 is that for very unstable scenarios the acceleration power may not fall below zero at all, in which case the unstable ESC is not applicable. However in such instances, instability will be quickly identified by observing when the transmission angle between any two machines exceeds a large threshold, such as 360°. The responses in Figure 4-18 indicate when the

ESC detects forward-swing instability. The ESC stopping point is indicated by a cross on each of the responses. The stopping times are listed in Table 4-8. The time savings achieved by ESC, in comparison to the method of monitoring the generator angles, are also listed. In both scenarios the ESC method saves approximately one third of the simulation time.

TABLE 4-8. SUMMARY OF THE SIMULATION TIMES WHEN INSTABILITY IS IDENTIFIED BY GENERATOR ANGLE DEVIATION EXCEEDING 360˚ AND THE SIME UNSTABLE ESC ($t_{\lim}$)

Scenario	t_{360} (s)	t_{lim} (s)	Simulation time saved (s)
1A.U	4.11	2.59	1.52
1B.U	3.40	2.24	1.16

4.1.2. *OMIB Power-Angle Curves for the Unstable Scenarios*

This section provides a brief assessment of the OMIB responses of the unstable scenarios 1A.U and 1B.U in the power-angle domain. Figure 4-19 shows the P_{aOMIB} - δ_{OMIB} curves for scenarios 1A.U and 1B.U. The steady-state operation is the same as the stable scenarios (see section 4.6.1). During the fault P_{aOMIB} becomes positive, indicating that G1 is absorbing kinetic energy, and consequently δ_{OMIB} increases during the fault. From equations (4.75) and (4.83) both ω_{OMIB} and δ_{OMIB} increase during the fault.

When the fault is cleared, P_{aOMIB} falls to a value determined by the post-fault power angle characteristics for each scenario. δ_{OMIB} continues to increase since ω_{OMIB} is positive. For both scenarios when δ_{OMIB} increases to about 90˚ P_{aOMIB} reaches a local minimum, before it starts to increase again. Eventually in both scenarios, P_{aOMIB} increases to 0pu and becomes positive again, since ω_{OMIB} is unable to reduce to 0pu before this point.

Figure 4-19 shows that the acceleration area (A_{acc}) of scenario 1B.U, with the SVC online, is marginally greater than for scenario 1A.U, with the SVC offline. The deceleration areas (A_{dec}) of both scenarios are similar, however it is slightly smaller in

scenario 1B.U as $\delta_{lim1B.U}$ is lower than $\delta_{lim1A.U}$. Contrary to expectations, connecting the SVC to the midpoint of the transmission line does not enhance the stability of the system in the event of a sending-end fault. This behaviour is investigated in further detail in section 5.3.

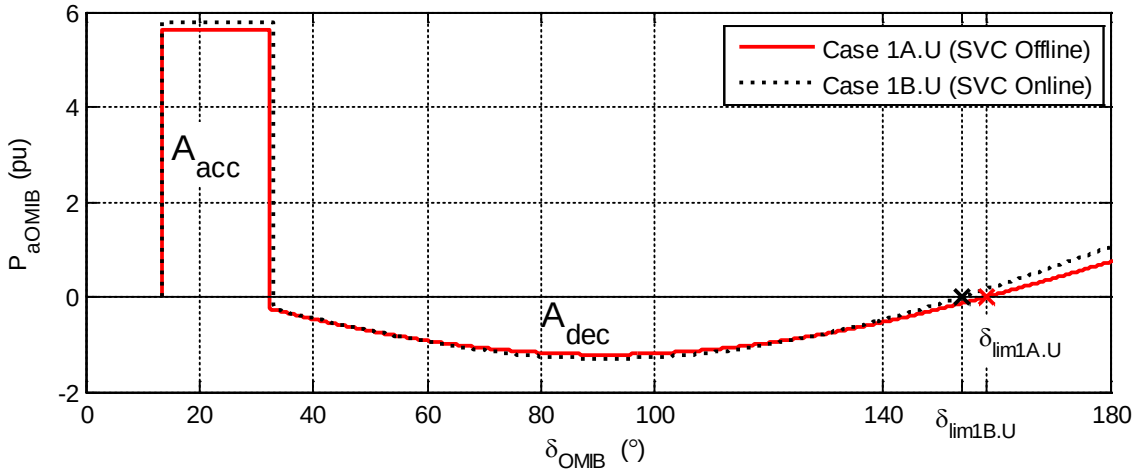

Figure 4-19. The OMIB acceleration power curves for scenario 1A.U and 1B.U.

4.1.3. *Calculation of the Unstable SIME Margin*

The SIME method employs the following unstable margin adapted from the EAC described in section 2.3.1:

$$\eta_u = -\frac{1}{2H_{OMIB}}\left(A_{acc} - A_{dec}\right) = \frac{1}{2H_{OMIB}} \int_{\delta 0}^{\delta \lim} P_{aOMIB} d\delta \tag{4.86}$$

where $\delta_0 = \delta(t=0)$, $\delta_{lim} = \delta(t_{lim})$ and where A_{acc} and A_{dec} are the acceleration and deceleration areas in the $P_{aOMIB} - vs - \delta_{OMIB}$ curve. $\eta_u < 0$ when the system is unstable. Figure 4-20 shows δ_0, δ_{lim}, A_{acc} and A_{dec} which are used to calculate η_u for scenario 1A.U. The unstable margins for scenarios 1A.U and 1B.U are listed in Table 4-9.

TABLE 4-9. SIME MARGIN AND UNSTABLE ANGLE FOR THE UNSTABLE SCENARIOS ON THE TWO MACHINE POWER SYSTEM

Scenario	SVC configuration	η_u (rad-pu)	$\delta_{\lim}$ (°)
1A.U	Offline	-0.00658	158.4
1B.U	Offline	-0.02183	154.1

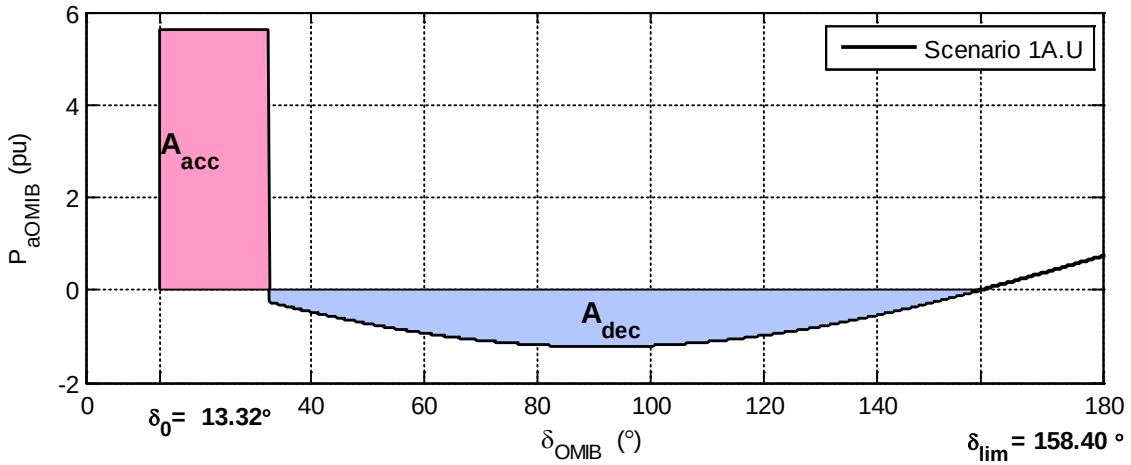

Figure 4-20.The $P_{aOMIB} - vs - \delta_{OMIB}$ curve showing the acceleration and deceleration areas and angles used in the scenario 1A.U unstable margin calculations.

4.8. Chapter Conclusion

The 9-bus two machine system is used to demonstrate that the SIME algorithm does not require any simplification of the fully detailed power system model. The steady-state network equations for the two machine system are presented as a function of transmission angle, and a closed form solution is derived from first principles. The equations that dictate the dynamic system behaviour are used to explain the mechanisms leading to transient stability or instability for a range of scenarios where a fault is applied at the sending-end of the interconnector.

The discussion demonstrates some important points:

- a rotor-angle stable scenario may be unacceptable due to inadequate voltage performance;
- a SVC may increase the power transfer of the system under steady-state conditions, but does not necessarily improve transient stability limits. This is explained in Chapter 5.

The discussion demonstrates how the responses of the two machines are translated to an equivalent OMIB response by the SIME method. For the investigated scenarios transient instability occurs only on the forward-swing. In this circumstance simulation time is saved by applying the SIME ESC for both stable and unstable scenarios, and calculation of the SIME stable and unstable margins are clearly demonstrated. Furthermore, the investigations indicate that the stable SIME margins are less accurate than the SIME unstable margin due to the estimation involved in the former. Therefore, the accuracy of linear prediction of the transient stability limit, using one or more stable margins, is likely to be less reliable than if unstable margins are employed.

Chapter 5 Transient Stability Sensitivity Analysis: The Two Machine System

The SIME algorithm is practically applied on the two machine 9-bus system, introduced in Chapter 4, to determine the transient stability limits (TSLs). The length of the two-machine system has been selected to mimic the physical characteristics of the major corridors on the Australian system. It is found that back-swing instability on this system causes the benefits of the SIME stability margins and early-stopping criteria (ESC) to be lost [93]. An objective of this chapter is to identify the conditions causing back-swing instability. Then, if such conditions can be pre-determined the Enhanced Binary-SIME (EBSIME) algorithm could be adapted to overcome the limitations by reverting to a plain binary-search to reliably determine the TSLs [93].

An outcome of this investigation is that the fault location has a predominant influence on whether the system is subject to the forward- or back-swing mechanisms of transient instability. Under many circumstances when the interconnector power transfer is high, it is frequently the case that a sending-end fault will result in forward-swing instability, and a receiving-end fault will result in back-swing instability.

These studies find that a fault applied near to the sending-end of a long transmission line yields a lower TSL than an equivalent fault applied at the receiving-end. The asymmetry in the critical fault clearing times (CCT) due to the different fault location, is accentuated when an SVC is connected at the midpoint of the line, and when the power transfer is increased. Similar behaviour is observed on the simplified model of the South-East Australian Power system (AU14GEN) in Chapters 9 and 10.

The influence of various parameters of the TSL of the two-machine system is investigated by:
1) a modified 5-bus version of the 9-bus system which relates network power equations and parameters to the OMIB responses; and
2) transient stability sensitivity analysis (TSSA) based on the SIME margins.
Note that the 5-bus version is employed because it is amenable to mathematical analysis.

5.1. Parameters of the 5-Bus Two Machine Approximation Model

Figure 5-1 shows a modified 5-bus version of the 9-bus two machine system introduced in Chapter 4 It is parameterised in terms of the length of the parallel interconnecting transmission lines (L), the power transfer (P_T) and the total system load (P_L). The transmission line susceptance is omitted since it has a relatively small effect on the transient performance. In the 5-bus system model, the load and reactive compensation for area 1 are connected to bus 4; and in area 2 they are connected to bus 5. The SVC is connected to bus 3. The purpose of this model simplification is to make it analytically tractable. The relationship between the bus numbers in the 9- and 5-bus systems are listed in Table 5-1.

TABLE 5-1. RELATIONSHIP BETWEEN THE BUS NUMBERS IN THE 9- AND 5-BUS TWO MACHINE SYSTEMS

	9-bus model	5 bus model
Bus number	1	1
	2	2
	3, 4, 5, 9	Omitted
	6	4
	7	3
	8	5

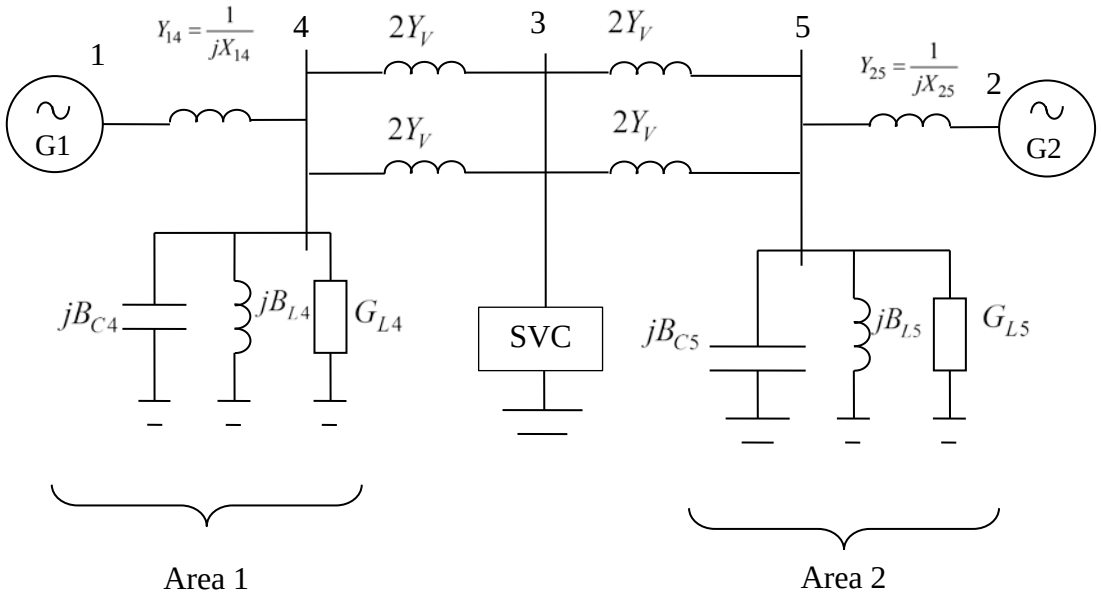

Figure 5-1. The 5-bus two machine power system model

Let x_l = impedance per km of each circuit of the double circuit transmission line between nodes 4 & 5. $X_V = Lx_l$ is the total impedance of each separate circuit on the double circuit transmission line between nodes 4 & 5, as indicated in Figure 5-2.

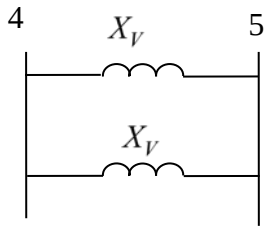

Figure 5-2. Line reactance of the double circuits between nodes 4 & 5 on the 5-bus system with intermediate bus 3 omitted.

Let
$$Y_V = -\frac{j}{Lx_l} = -\frac{j}{X_V} \tag{5.1}$$

$$\begin{aligned} Y_{34} &= \text{total admittance between nodes 3 \& 4} \\ &= 2N_{C34}Y_V \end{aligned} \tag{5.2}$$

$$\begin{aligned} \text{where } N_{C34} &= \text{number of energised circuits between nodes 3 \& 4} \\ &= \{1,2\} \end{aligned} \tag{5.3}$$

Similarly:

$$\begin{aligned} Y_{35} &= \text{total admittance between nodes 3 \& 5} \\ &= 2N_{C35}Y_V \end{aligned} \tag{5.4}$$

$$\begin{aligned} \text{where } N_{C35} &= \text{number of energised circuits between nodes 3 \& 5} \\ &= \{1,2\} \end{aligned} \tag{5.5}$$

Finally:

$$X_{14} = X_d^{'} + X_{tr} + 10x_l = X_{25} \tag{5.6}$$

thus:
$$Y_{14} = -\frac{j}{X_{14}} \text{ and } Y_{25} = -\frac{j}{X_{25}} \tag{5.7}$$

The system loads are represented by constant admittance. The loads connected to buses 4 and 5 are adjusted to vary the inter-area power transfer such that:

$$P_T = \frac{P_{L5} - P_{L4}}{2} \tag{5.8}$$

$$P_L = P_{L4} + P_{L5} = \text{constant} \tag{5.9}$$

The active power of the loads is adjusted according to:

$$P_{L5} = \beta P_L \tag{5.10}$$

$$P_{L4} = (1-\beta)P_L \tag{5.11}$$

where $0 \le \beta \le 1$. Consequently the transfer from area 1 to 2 can be expressed in terms of β:

$$P_T = \frac{2P_{L5} - P_L}{2} \tag{5.12}$$

$$P_T = \left(\beta - \tfrac{1}{2}\right) P_L \tag{5.13}$$

The reactive power of both the loads and reactive compensation are constant. Under steady state conditions, the voltages at all system buses are approximately 1 p.u. thus:

$$Q_{L4} = B_{C4} + B_{L4} = \text{constant} \tag{5.14}$$

$$Q_{L5} = B_{C5} + B_{L5} = \text{constant} \tag{5.15}$$

$$Q_L = Q_{L4} + Q_{L5} \tag{5.16}$$

5.1.1. Admittance Matrix as a Function of the System Parameters

The network admittance matrix of the 5-bus two machine system model is:

$$Y_N = \begin{bmatrix} Y_{11N} & 0 & 0 & -Y_{14N} & 0 \\ 0 & Y_{22N} & 0 & 0 & -Y_{25N} \\ 0 & 0 & Y_{33N} & -Y_{34N} & -Y_{35N} \\ -Y_{14N} & 0 & Y_{43N} & Y_{44N} & 0 \\ 0 & -Y_{25N} & -Y_{35N} & 0 & Y_{55N} \end{bmatrix} \tag{5.17}$$

where Y_{iiN} is the sum of all admittances connected to the *i*th node. The non-zero elements from the matrix of equation (5.17) are expressed in terms of the system parameters of interest which include the system load, namely L, β, N_{C34} and N_{C35}. In the following discussion the network parameters Y_{34N}, Y_{25N}, Y_{35N}, Y_{11N}, Y_{22N}, Y_{33N}, Y_{44N} and Y_{55N} are derived as a function of the system parameters.

From Figure 5-1 and equations (5.7) and (5.17):

$$Y_{14N} = -Y_{14} = \frac{j}{X_{14}} = \text{constant} \tag{5.18}$$

$$Y_{25N} = -Y_{25} = \frac{j}{X_{25}} = \text{constant} \tag{5.19}$$

Let $$B_{14} = \frac{1}{X_{14}} \text{ and } B_{25} = \frac{1}{X_{25}} \tag{5.20}.$$

From equations (5.2), (5.4) and (5.17) it follows that:

$$Y_{11N} = Y_{14N} \tag{5.21}$$

$$Y_{22N} = Y_{25N} \tag{5.22}$$

$$Y_{34N} = -j\left(\frac{2N_{C34}}{Lx_l}\right) \tag{5.23}$$

$$Y_{35N} = -j\left(\frac{2N_{C35}}{Lx_l}\right) \tag{5.24}$$

From equations (5.23) and (5.24):

$$\begin{aligned} Y_{33N} &= Y_{34N} + Y_{35N} \\ &= -\frac{j2N_{C34}}{Lx_1} - \frac{j2N_{C35}}{Lx_1} \\ &= -\frac{2j}{Lx_1}\left(N_{C34} + N_{C35}\right) \end{aligned} \tag{5.25}$$

and $$Y_{44N} = P_{L4} + Q_{L4} + Y_{14N} + Y_{34N} \tag{5.26}.$$

Expanding equation (5.26):

$$Y_{44N} = \left(1-\beta\right)P_L + j\left(B_{L4} + B_{C4} + B_{14} - \frac{2N_{C34}}{Lx_1}\right) \tag{5.27}$$

Similarly:

$$Y_{55N} = P_{L5} + Q_{L5} + Y_{25N} + Y_{35N} \tag{5.28}$$

which upon expansion gives:

$$Y_{55N} = \beta P_L + j\left(B_{L5} + B_{C5} + B_{25} - \frac{2N_{C35}}{Lx_1}\right) \tag{5.29}.$$

5.1.2. Three-Port Admittance Matrix as a Function of the System Parameters

Equations (4.3) and (4.4) can be applied to the network equation (5.17) to derive the reduced three port matrix, Y'', for the 5-bus two-machine model.

$$Y'' = \begin{bmatrix} Y_{11} & Y_{12} & Y_{1S} \\ Y_{12} & Y_{22} & Y_{2S} \\ Y_{1S} & Y_{2S} & Y_{33} \end{bmatrix} = \begin{bmatrix} Y_{11N} - \frac{Y_{14N}^2}{Y_{44N}} & 0 & -\frac{Y_{14N}Y_{35N}}{Y_{44N}} \\ 0 & Y_{22N} - \frac{Y_{25N}^2}{Y_{55N}} & -\frac{Y_{25N}Y_{35N}}{Y_{55N}} \\ -\frac{Y_{14N}Y_{34N}}{Y_{44N}} & -\frac{Y_{25N}Y_{35N}}{Y_{55N}} & Y_{33N} - \left(\frac{Y_{34N}^2}{Y_{44N}} + \frac{Y_{35N}^2}{Y_{55N}}\right) \end{bmatrix} \tag{5.30}.$$

Each matrix element in equation (5.30) can be written as a function of the system parameters by substituting in equations (5.17) to (5.29) from section 5.1.1. The expanded element values are:

$$
\begin{aligned}
Y_{11} &= G_{11} + jB_{11} \\
&= \frac{B_{14}^2 (1-\beta) P_L}{(1-\beta)^2 P_L^2 + \left(B_{L4} + B_{C4} + B_{L4} - \frac{2N_{C34}}{Lx_1} \right)^2} \\
&\quad + j \left(B_{L4} - \frac{B_{L4} + B_{C4} + B_{14} - \frac{2N_{C34}}{Lx_1}}{(1-\beta)^2 P_L^2 + \left(B_{L4} + B_{C4} + B_{L4} - \frac{2N_{C34}}{Lx_1} \right)^2} \right)
\end{aligned}
\tag{5.31}
$$

$$
\begin{aligned}
Y_{22} &= G_{22} + jB_{22} \\
&= \frac{B_{25}^2 \beta P_L}{\beta^2 P_L^2 + \left(B_{L5} + B_{C5} + B_{25} - \frac{2N_{C35}}{Lx_1} \right)^2} \\
&\quad + j \left(B_{25} - \frac{B_{25}^2 \left(B_{L5} + B_{C5} + B_{25} - \frac{2N_{C35}}{Lx_1} \right)}{\beta^2 P_L^2 + \left(B_{L5} + B_{C5} + B_{25} - \frac{2N_{C35}}{Lx_1} \right)^2} \right)
\end{aligned}
\tag{5.32}
$$

$$
\begin{aligned}
Y_{SS} &= G_{SS} + jB_{SS} \\
&= \left(2N_{C35}\right)^2 \frac{(1-\beta) P_L}{(1-\beta)^2 P_L^2 + \left(B_{L4} + B_{C4} + B_{14} - \frac{2N_{C34}}{Lx_1} \right)^2} \\
&\quad + \left(\frac{2N_{C35}}{L_{x1}} \right)^2 \frac{\beta P_L}{(\beta P_L)^2 + \left(B_{L5} + B_{C5} + B_{25} - \frac{2N_{C35}}{Lx_1} \right)^2} \\
&\quad - \frac{2j}{Lx_1} \left(N_{C34} + N_{C35} \right) \\
&\quad - j \left(\frac{2N_{C34}}{Lx_1} \right)^2 \left(\frac{B_{L4} + B_{C4} + B_{L4} + 2\frac{N_{C34}}{Lx_1}}{(1-\beta)^2 P_L^2 + \left(B_{L4} + B_{C4} + B_{14} - \frac{2N_{C34}}{Lx_1} \right)^2} \right) \\
&\quad - j \left(\frac{2N_{C35}}{Lx_1} \right)^2 \left(\frac{B_{L5} + B_{C5} + B_{L5} + 2\frac{N_{C35}}{Lx_1}}{\beta^2 P_L^2 + \left(B_{L5} + B_{C5} + B_{25} - \frac{2N_{C35}}{Lx_1} \right)^2} \right)
\end{aligned}
\tag{5.33}
$$

$$
\begin{aligned}
Y_{1S} &= G_{1S} + jB_{1S} \\
&= \left(\frac{2B_{14}N_{C34}}{Lx_l}\right)\frac{-(1-\beta)P_L}{(1-\beta)^2 {P_L}^2 + \left(B_{L4} + B_{C4} + B_{14} - \dfrac{2N_{C34}}{Lx_l}\right)^2} \\
&\quad + \left(\frac{2B_{14}N_{C34}}{Lx_l}\right)\frac{j\left(B_{L4} + B_{C4} + B_{14} - \dfrac{2N_{C34}}{Lx_l}\right)}{(1-\beta)^2 {P_L}^2 + \left(B_{L4} + B_{C4} + B_{14} - \dfrac{2N_{C34}}{Lx_l}\right)^2}
\end{aligned} \tag{5.34}
$$

$$
\begin{aligned}
Y_{2S} &= G_{2S} + jB_{2S} \\
&= \frac{-\beta P_L \dfrac{2B_{25}N_{C35}}{Lx_l}}{\left(\beta P_L\right)^2 + \left(B_{L5} + B_{C5} + B_{25} - \dfrac{2N_{C35}}{Lx_l}\right)^2} \\
&\quad + \frac{j\left(B_{L5} + B_{C5} + B_{25} - \dfrac{2N_{C35}}{Lx_l}\right)\dfrac{2B_{25}N_{C35}}{Lx_l}}{\left(\beta P_L\right)^2 + \left(B_{L5} + B_{C5} + B_{25} - \dfrac{2N_{C35}}{Lx_l}\right)^2}
\end{aligned} \tag{5.35}
$$

By representing the equivalent three-port admittance matrix elements as a function of these sensitivity parameters, the generator electrical power and the OMIB electrical power equations, as described in sections 4.3 and 4.4, can be related to the parameters of the 9-bus two machine model.

5.2. Investigated Parameters on the 9-Bus Two Machine System

The 9- and 5-bus two machine power system models are employed to develop insights into the influence and behaviour of the SVC on the transient stability of the system. The equations of the 5-bus model are used to develop analytical insights into the behaviour of the larger 9-bus system. All graphs and simulations are generated using the 9-bus model. The investigated factors are:

- the level of power transfer;
- the fault location;
- the SVC pre-fault capacitive reserve;
- the fault clearing time;
- the generator inertias; and
- the system loading.

The resultant OMIB responses are examined to determine if there are patterns that could be exploited to enhance the SIME method. One objective is to identify a way to systematically enhance the SIME methodology to robustly handle network conditions where SVCs are critical to transient stability. In these investigations, the SIME margins and the quantities involved in their calculation provide a way to quantify how far a given system operating condition is from the TSLs. The SIME margins and OMIB derivation are a core aspect of the EBSIME algorithm, thus it is important to examine them on a simple system. The results of this analysis can potentially be applied to larger power systems.

The above-listed system parameters are varied, one at a time, from the base-line condition of case 1 in Table 5-5. Cases 1A to 2C correspond to the scenarios investigated in Chapter 4. The CCTs have been calculated using a binary-search where time-domain simulations (TDS) are run over a 10s period. The CCT results in Table 5-5 are analysed in this chapter.

TABLE 5-2. DESCRIPTION OF APPLIED FAULTS AND LOCATION

Row No.	Fault-State	Description
1	Sending-end fault	A three-phase fault is applied near to the bus 6 end of circuit #2 between buses 6 & 7. This corresponds to a fault at bus 4 on the 5-bus system
2	Receiving-end fault	A three-phase fault is applied near to the bus 8 end of circuit #2 between buses 7 & 8. This corresponds to a fault at bus 5 on the 5-bus system

TABLE 5-3. FAULT CLEARANCE METHODS

Row No.	Description
1	Clear sending-end fault: The circuit breakers at both ends of circuit #2 between buses 6 and 7 are simultaneously opened.
2	Clear receiving-end fault: The circuit breakers at both ends of circuit #2 between buses 7 and 8 are simultaneously opened.

TABLE 5-4. GENERATOR INERTIA CONSTANTS (SEE APPENDIX D)

Row No.	Applicable Cases	H1 (pu on 900MVA base)	H2 (pu on 900MVA base)
1	1 to 7B	6.175	6.5
2	8A and 8B	3.0875	3.25

TABLE 5-5. INVESTIGATED CASES ON THE 9-BUS TWO MACHINE SYSTEM

Case ID	Variable Parameter	SVC Capacitive Reserve	Steady-State	Fault Location	Post-Fault State	CCT (ms)
1	Base-case	Offline	Table 5-6, column (col) 1 L=440km, 100MW transfer	Sending-end Fault. Table 5-2, row 1	Table 5-3, row 1	188
2A	SVC capacity	±200MVar				183
2B		±400MVar				175
2C		Unlimited				141
3A	L=220km	Offline	Table 5-6 col 2 100MW Transfer			343
3B		±200MVar				339
3C		±400MVar				333
3D	L=110km	Offline	Table 5-6 col 3 100MW transfer			556
3E		±200MVar				550
3F		±400MVar				542
4A	L=440km Receiving-end Fault	Offline	Table 5-6 col 1 100MW transfer	Receiving-end Fault Table 5-2 row 2	Table 5-3, row 2	210
4B		±200MVar				247
4C		±400MVar				274
4D		±200MVar	Table 5-7 0MW (col 1)			241
4E			Table 5-7 25MW (col 3)			258
4F			Table 5-7 50MW (col 4)			272
4G			Table 5-7 150MW, (col 5)			219
4H			Table 5-7 200MW, (col 2)			183
5A	0MW	Offline	Table 5-7 col 1, L=440km,	Sending-end Fault Table 5-2, row 1	Table 5-3, row 1	270
5B		±200MVar				262
6A	200MW	Offline	Table 5-7 col 2,L=440km			73
6B		±200MVar				77
6C	50MW	±200MVar	Table 5-7 col 4, L=440km			225
6D	150MW	±200MVar	Table 5-7 col 5, L=440km			135
7A	Half Generation and Load	Offline	Table 5-7 col 6, L=440km	Sending-end Fault. Table 5-2, row 1	See Table 5-3, row 1	435
7B		±200MVar				444
8A	Half Generator Inertia	Offline	Table 5-6 col 1, L=440km			133
8B		±200MVar				129

TABLE 5-6. STEADY-STATE NETWORK VALUES OF THE 9-BUS SYSTEM FOR VARIATION IN THE INTERCONNECTOR LINE LENGTH

Network Values	Variation in Interconnector Length (L, in km)			Unit
	L = 440 (Base Line) (Col 1)	L = 220 (Col 2)	L=110 (Col 3)	
Power Transfer	100	100	100	MW
E'_{q1}	1.040	1.045	1.046	pu
E'_{q2}	1.019	1.024	1.027	pu
$V_7 = V_{SVC}$	1.053	1.019	1.011	pu
δ_1	26.79	20.87	17.06	deg
δ_2	13.47	13.15	13.00	deg
$\delta_7 = \delta_{SVC}$	-3.83	-6.68	-8.50	deg
P_{m1}	14.00	14.00	14.00	pu
P_{m2}	14.24	13.98	13.86	pu

TABLE 5-7. STEADY-STATE NETWORK VALUES OF THE 9-BUS SYSTEM FOR VARIATION IN THE INTERCONNECTOR TRANSFER AND SYSTEM LOAD

Network Values	Variation in Power Transfer					½ Load & Generation	Unit
Power Transfer	**0 (Col 1)**	**200 (Col 2)**	**25 (Col 3)**	**50 (Col 4)**	**150 (Col 5)**	**100 (Col 6)**	**MW**
E'_{q1}	1.038	1.048	1.038	1.039	1.043	0.986	pu
E^1_{q2}	1.017	1.024	1.017	1.018	1.021	0.965	pu
$V_7 = V_{SVC}$	1.062	1.021	1.062	1.060	1.041	1.071	pu
δ_1	14.15	41.96	17.17	20.27	33.88	17.05	deg
δ_2	13.56	13.12	13.56	13.54	13.34	7.47	deg
$\delta_7 = \delta_{SVC}$	-10.11	3.77	-8.62	-7.08	-0.27	-0.31	deg
P_{m1}	14.00	14.00	14.00	14.00	14.00	7.00	pu
P_{m2}	14.31	13.94	14.31	14.30	14.13	7.53	pu

5.3. Variation in SVC Capacity – Sending-End Fault – Forward-Swing Instability

The influence of variation in the SVC capacity on the TSLs of the two machine power system is investigated by comparing the system responses of case 1, from Table 5-5, against the responses of cases 2A, 2B and 2C. In each of these cases the sending-end fault causes transient instability to occur on the forward-swing. A comparison shows that the CCT decreases as the SVC capacity is increased. This behaviour is counter-intuitive and can be explained from Figure 5-3. Similar behaviour was observed in Chapter 4.

Figure 5-3 shows the OMIB acceleration power-angle characteristic from the time response of three unstable scenarios corresponding to cases 1, 2A and 2B. In each scenario the applied fault is cleared after 190ms. The post-fault characteristic for case 2C where the SVC has unlimited capacity is also shown. It was calculated using the procedure described in section 4.3.1.2.

Figure 5-3 shows that during the fault the increased SVC capacity causes P_{aOMIB} to increase. Therefore, δ_{OMIB} is further advanced at fault clearance and the acceleration area formed during the fault is larger.

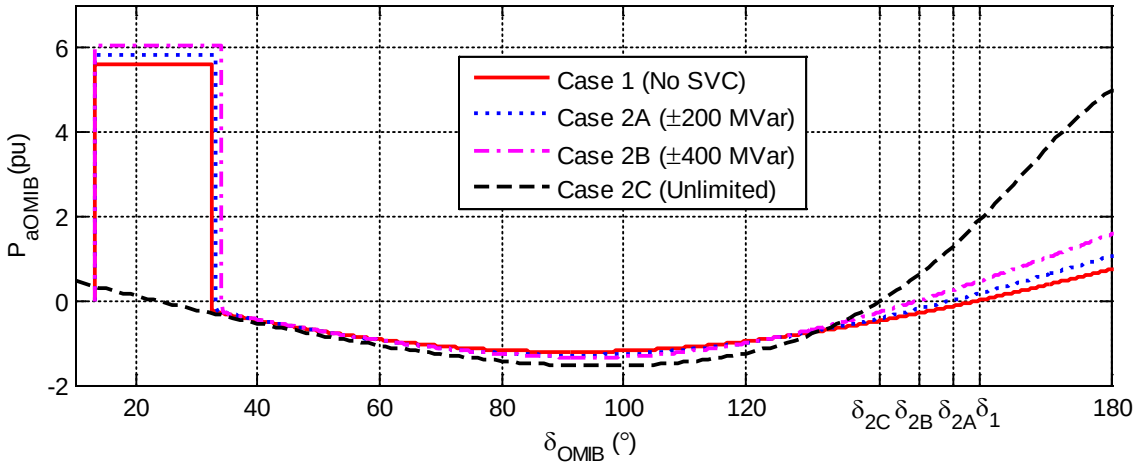

Figure 5-3. Overlay of the OMIB acceleration power versus angle characteristics for unstable scenarios from cases 1, 2A and 2B with fault clearing time of 190ms; and the post-fault response of case 2C.

In each case P_{aOMIB} instantaneously becomes negative when the fault is cleared. According to the ESC, instability occurs when P_{aOMIB} changes from a negative to positive value and δ_{OMIB} rises. The angles at which P_{aOMIB} crosses the zero-axis (where

$P_{aOMIB} = 0$) are δ_1, δ_{2A}, δ_{2B} and δ_{2C} for cases 1, 2A, 2B and 2C respectively. As the available reactive capacity of the SVC increases the unstable angle reduces. The post-fault $P_{aOMIB} - \delta_{OMIB}$ characteristic is similar for each of the displayed cases. Lowering the unstable angle causes a small reduction in the available deceleration area when the available SVC capacity is increased. The combination of a larger acceleration area, and smaller deceleration area reduces the CCT. One way of arresting the increase in acceleration area could be to prevent the SVC susceptance from changing during the fault period. It is important to note that the details of the SVC control strategies may affect these conclusions.

5.4. Variation in SVC Capacity – Receiving-End Fault – Back-Swing Instability

The effect of fault location on the transient stability of the two machine power system is explained using TDS of stable and unstable scenarios from cases 4A and 4B. The investigated scenarios are listed in Table 5-8 with reference to Table 5-5, and are used to demonstrate the key mechanisms of instability for a fault applied at the receiving-end of the line. This fault tends to cause the system to be constrained by back-swing instability. Then the rudimentary early stop criteria (ESC) of the SIME assessment are inaccurate.

Sensitivity analysis using the SIME margins is not presented for cases 4A, 4B and 4C featuring the receiving-end fault, as the back-swing constraint causes all scenarios to produce a SIME margin that is considered too stable for SIME analysis. The CCTs listed in Table 5-5 for cases 4A, 4B and 4C indicate that increasing the SVC capacity causes the system to become more stable when a receiving-end fault is applied. This contrasts to the tendency for the CCT to reduce with increasing SVC capacity for a sending-end fault.

TABLE 5-8. SCENARIO SPECIFICATIONS TO INVESTIGATE OF THE MECHANISM OF INSTABILITY FOR A RECEIVING-END FAULT ON THE TWO MACHINE SYSTEM

Scenario Identifier	Case No.	Fault Clearing Time	Stability Diagnosis
4A.S	4A	120ms	Stable
4A.U		270ms	Unstable
4B.S	4B	120ms	Stable
4B.U		270ms	Unstable

5.4.1. Receiving-End Fault: SVC Offline

5.4.1.1. *Stable Scenario 4A.S*

The transient response for stable scenario 4A.S, shown in Figure 5-4, is similar to that of scenario 1A.S described in section 4.4.2. The key features of the response are listed below:

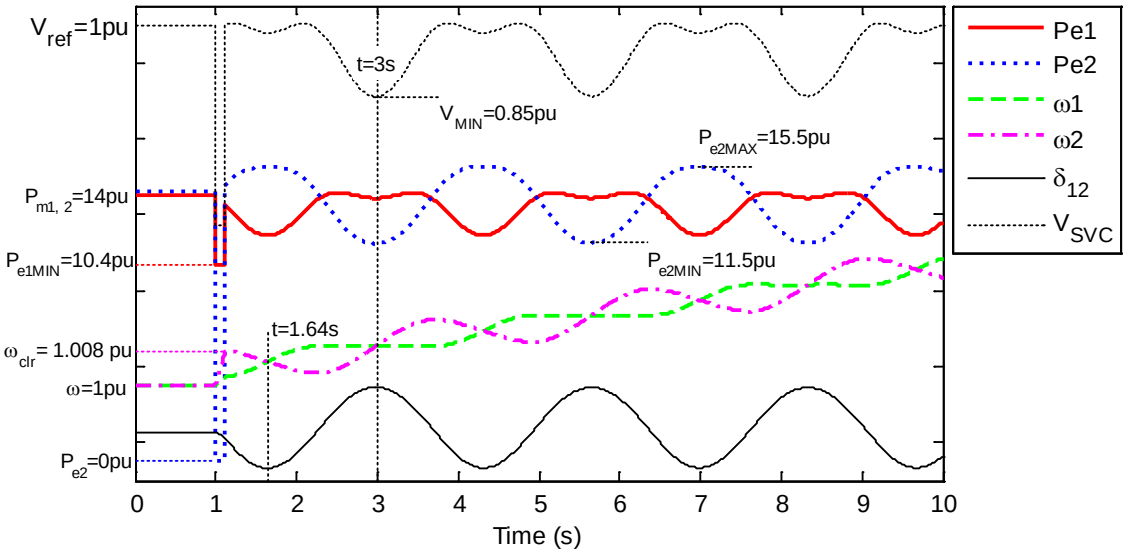

Figure 5-4. Dynamic responses for the stable scenario 4A.S, where the receiving-end fault is cleared after 120ms.

Pre-fault:

At t=1s, a three-phase fault is applied near to bus 8.

During the fault:

- P_{e1} falls to 10.4 pu, while the P_{e2} falls to 0pu, causing both generators to accelerate.
- As the acceleration of G2 is greater than for G1, δ_2 and ω_2 advance ahead of G1.
- Since $\omega_2 > \omega_1$ during the fault, δ_{12} decreases.

Post-fault

- At t = 1.12s, P_{e1} and P_{e2} initially increase due to the falling δ_{12}.
- As δ_{12} continues to fall, P_{e2} rises above P_{m2} and G2 decelerates.
- Simultaneously, P_{e1} decreases below P_{m1} and G1 accelerates.
- At t = 1.64s, the speeds of G1 and G2 equalise on the forward-swing. This is maintained for the full integration period.

- Since governors are not represented, there is a net acceleration on both generators; so ω_1 and ω_2 continually increase together after the fault.

At t=3s, the voltage drops to 0.85 pu, which is an acceptable voltage level. The magnitude of the P_{e2} oscillations span 400MW, or 28.6% of the generator output. The power swing is large because the system model is undamped and has minimal losses.

5.4.1.2. *Unstable Scenario 4A.U*

As shown in Figure 5-5, instability for scenario 4A.U occurs during the back-swing. The dynamic system response is the same as case 4A.S in the steady-state and fault-states. The additional 150ms in the fault duration of 4A.U causes greater variation in δ_{12}, ω_1 and ω_2 than for 4A.S by the time the fault is cleared.

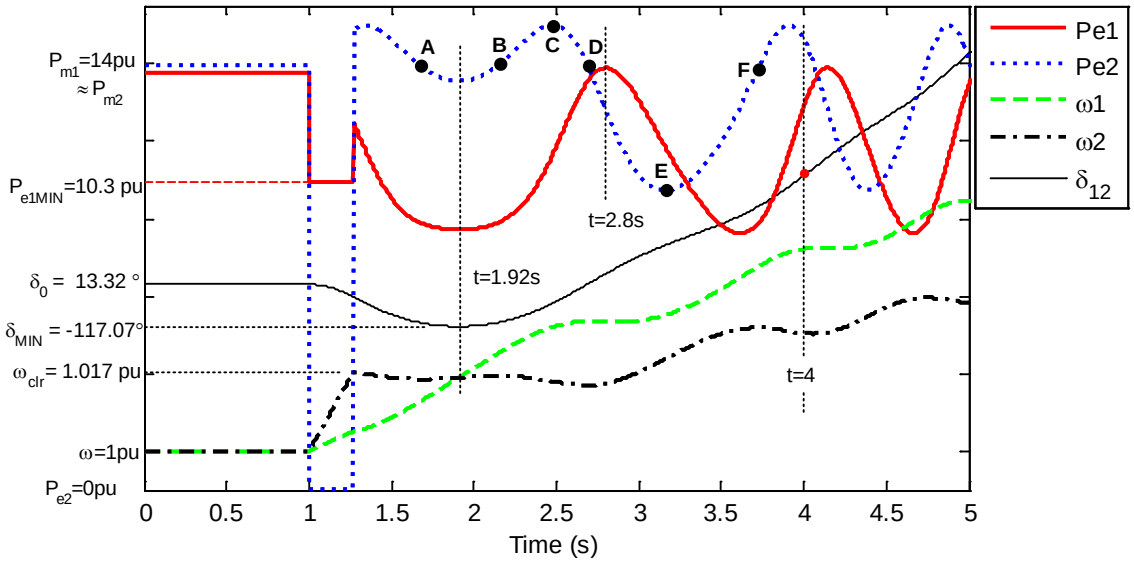

Figure 5-5. Dynamic responses for the unstable scenario 4A.U where the SVC is offline, and the receiving-end fault is cleared after 270ms.

The sequence of events leading to instability following fault clearance are:

Post-fault

- At t=1.27s, when the fault is cleared P_{e2} instantaneously increases above P_{m2} and G2 experiences a small deceleration.
- $\omega_2 > \omega_1$ and δ_{12} decrease causing P_{e2} to fall.
- P_{e1} increases by 200MW; since $P_{e1} < P_{m1}$, ω_1 rises.
- At point A, where t = 1.68s, since $P_{e2} < P_{m2}$, G2 accelerates again.
- At = 1.92s, the generator speeds equalise momentarily on the forward-swing.
- If the SIME ESC were applied to this case, it would be falsely concluded at t=1.92s that the system is stable.

Post forward-swing speed equalization: G1

- ω_1 continues to rise such that $\omega_1 > \omega_2$. This causes δ_{12} to increases for the first time since fault clearance. Simultaneously, P_{e1} and P_{e2} reach a local minimum.
- For 1.92s < t <2.8s, G1 accelerates (ω_1 rises) since $P_{e1} < P_{m1}$.
- At t = 2.8s, G1 briefly decelerates causing ω_1 to fall before rising again.
- This reoccurs at t = 4.15s.

Post forward-swing speed equalisation: G2:

- In contrast, G2 experiences a small acceleration in the interval $1.92s < t < 2.16s$, before decelerating again.
- The rising δ_{12} causes P_{e2} to peak at 11pu at point C, where t = 2.48s, before decreasing again.
- Between points B and D, $P_{e2} > P_{m2}$ and so the machine experiences a small deceleration.
- At point D, where t = 2.69s, P_{e2} drops below P_{m2}, causing G2 to resume acceleration (ω_2 rises).
- At point E, where t = 3.16s, P_{e2} dips to 10.1pu, before increasing again.
- By point F, where t = 3.72s, P_{e2} increases above P_{m2} causing G2 to decelerate.
- Since ω_2 is already less than ω_1, the speeds of the two generators cannot equalise. ω_1 and ω_2 continue to diverge.
- At t = 4s, δ_{12} diverges beyond 360˚. The machines lose synchronism on the back-swing.

5.4.2. Receiving-End Fault: SVC Online

5.4.2.1. *Stable Scenario 4B.S*

Scenario 4B.S is shown in Figure 5-6. The steady-state operation is the same as scenarios 4A.S and 4A.U.

During the fault:

- Initially, the SVC voltage (V_{SVC}) drops to 0.47 pu then settles at 0.54 pu.
- The SVC susceptance (Y_{SVC}) increases to the maximum capacity in an attempt to maintain V_{SVC} at the set point, V_{ref}.
- As in scenario 4A.S, since $P_{e1} > P_{e2}$, δ_{12} initially decreases.

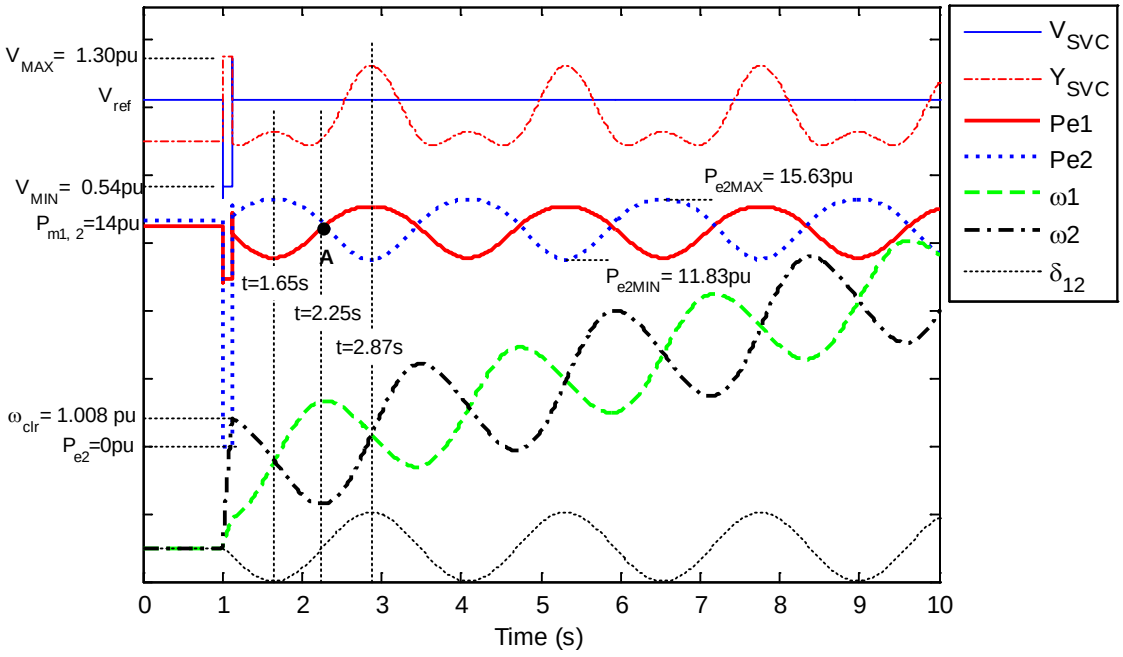

Figure 5-6. Dynamic responses for the stable scenario 4B.S when the SVC is online with ±200MVar capacity and the receiving-end fault is cleared after 120ms.

Post-fault:

- At t = 1.12s, V_{SVC} initially overshoots to 1.3 pu, then returns to V_{ref} so the SVC remains operating within its limits.
- Like scenario 4A.S the speeds of the two machines equalise on the forward-swing at t = 1.65s.
- At t = 2.08s, Y_{SVC} reaches a local minimum and δ_{12} reaches 0˚ before Y_{SVC} rises again.
- When δ_{12} rises above 0˚, Y_{SVC} increases at a faster rate to maintain V_{SVC} at V_{ref}.
- After point A, where t = 2.25s, $P_{e1} > P_{m1}$ causing G1 to decelerate; and $P_{e2} > P_{m2}$, causing G2 to accelerate.
- The generator speeds equalise on the back-swing at t = 2.87s. Here P_{e1}, Y_{SVC} and δ_{12} reach a maximum; P_{e2} reaches a minimum.
- Stability is maintained.

Since V_{SVC} remains at V_{ref}, the system is voltage stable. As the system is undamped P_{e2} experiences power swings that are about 28.5% of the input generation.

5.4.2.2. *Unstable Scenario 4B.U*

As shown in Figure 5-7 instability of scenario 4B.U is detected during the back-swing. The steady-state and fault-states are similar to those of scenario 4B.S. The longer fault clearing time of 270ms causes a larger deviation in δ_{12}, ω_1 and ω_2 at fault clearance.

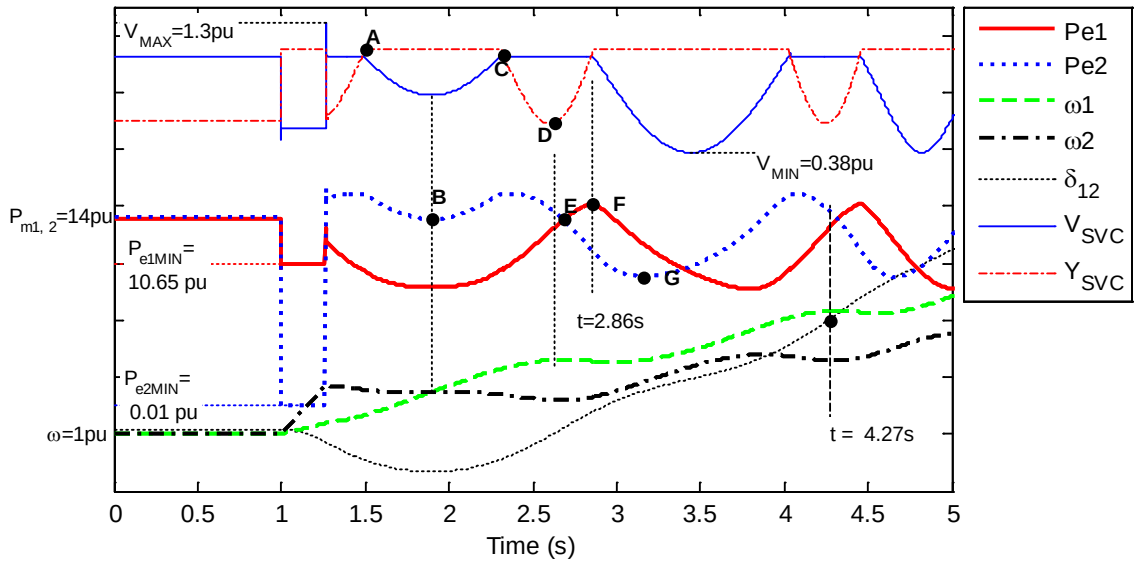

Figure 5-7. Dynamic responses for the unstable scenario 4B.U where the SVC is online with ±200MVar capacity, and the receiving-end fault is cleared after 270ms.

The sequence of events leading to instability following fault clearance are:

Post-fault:

- At t = 1.27s, V_{SVC} initially overshoots V_{ref} by 1.3 pu before being restored.
- Since $\omega_2 > \omega_1$, δ_{12} continues to decrease. This causes P_{e1} to instantaneously drop below P_{m1}, so G1 accelerates (ω_1 rises).
- Conversely, $P_{e2} > P_{m2}$ immediately following fault clearance so G2 decelerates (ω_2 falls).
- V_{SVC} is maintained at V_{ref} until point A (t = 1.5s) when the SVC reaches its capacitive limit.

Forward-swing stability

- Although V_{SVC} sags, the large acceleration by G1 enables the speeds of the two machines to equalise on the forward-swing at point B (t = 1.90s).
- P_{e1} and P_{e2} each reach a local minimum at point B. At this point it would incorrectly conclude that the system is stable according to the FS ESC.
- At point C (t = 2.32s), V_{SVC} is restored to V_{ref}.

Back-swing instability

- The back-swing commences after t = 1.9s, where δ_{12} begins to rise.

- Since $P_{e1} < P_{m1}$, ω_1 continues to increase. Conversely, for G2, $P_{e2} < P_{m2}$ and so ω_2 decreases. Thus δ_{12} continues to increase.
- At point D, where t = 2.62s, Y_{SVC} reaches a local minimum and $\delta_{12} = 0°$.
- At point E, where t = 2.69s, P_{e1} increases above P_{m1}, causing G1 to decelerate. Concurrently, $P_{e2} < P_{m2}$ causing G2 to accelerate.
- Since δ_{12} increases, Y_{SVC} rises to maintain V_{SVC} at V_{ref}.
- Y_{SVC} rapidly reaches the limit at point F, where t= 2.86s. Consequently, V_{SVC} collapses to 0.38 pu at t = 3.27s, and the system becomes voltage unstable.
- Although G2 accelerates at point G, where t = 3.02s, there is insufficient synchronizing power for ω_2 to reach ω_1.
- Synchronism is lost at t = 4.27s where the machines diverge and δ_{12} exceeds 360°.

5.4.3. Common Events Leading to the Back-Swing Mechanism of Instability

The time-varying responses of scenarios 4A.S, 4A.S, 4B.S and 4B.U described in sections 5.4.1 and 5.4.2 show that the three-phase fault applied at the receiving-end of the two-machine system tends to cause back-swing instability. This behaviour is independent of the SVC connection. The common characteristics of the scenarios are:

<u>During the fault:</u>

- G2 experiences a larger acceleration as, electrically, it is closer to the fault; causing $\omega_2 > \omega_1$ during the fault. Thus δ_{12} decreases during the fault.

<u>Post-fault:</u>

- In the forward-swing, G1 has sufficient kinetic energy to accelerate to the same speed as G2.
- After the speeds equalize, G1 continues to accelerate and G2 continues to decelerate, such that $\omega_1 > \omega_2$.
- Instability happens when there is insufficient synchronizing torque for the speed of G2, ω_2, to accelerate and equalise again with the speed of G1, ω_1; thus the machines lose synchronism on the back-swing.

The implications for the SIME method are:

- The ESC will incorrectly identify all scenarios with a back-swing instability constraint to be forward-swing stable.

- Any SIME margin estimated from the dynamic response will refer to forward-swing transient stability, and therefore be an irrelevant indicator of the system behaviour.

5.4.4. OMIB Responses for a Receiving-End Fault on the Two Machine System

Figure 5-8 shows the time-varying OMIB rotor angle, speed and acceleration-power responses for the four scenarios described in Table 5-8.

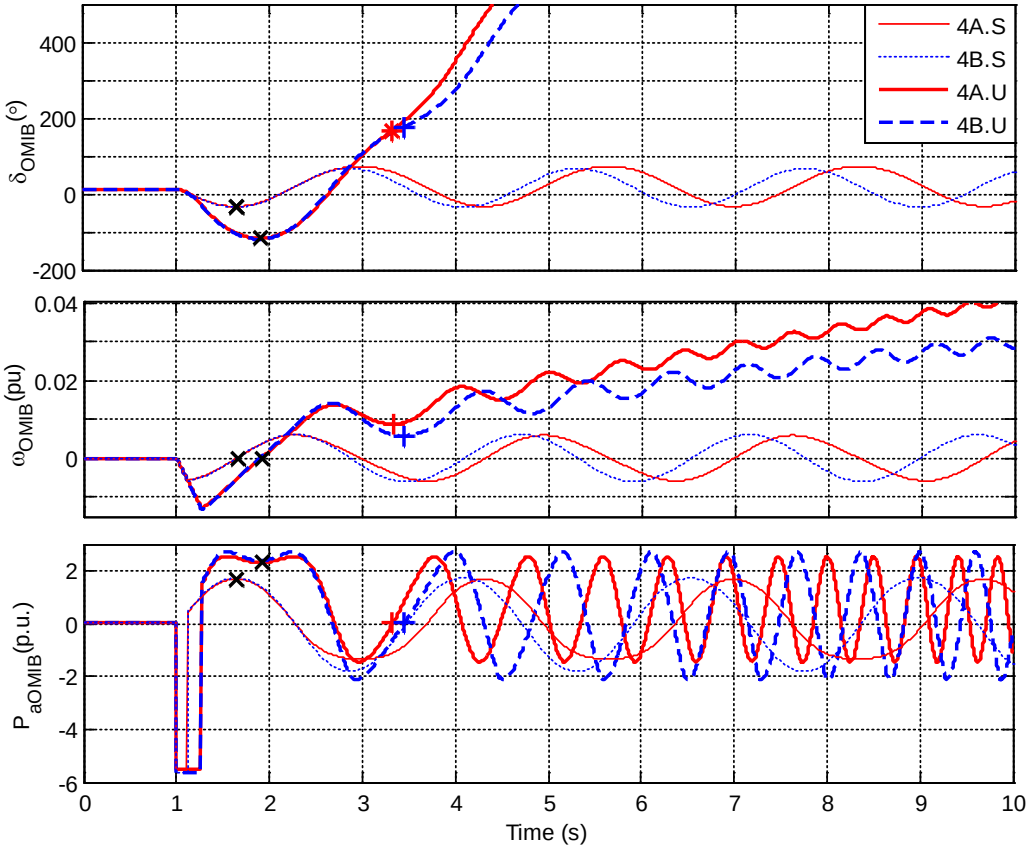

Figure 5-8. OMIB responses for scenarios 4A.S, 4A.U, 4B.S and 4B.U; "x" marks when the ESC identifies forward-swing stability; "+" indicates when a scenario actually becomes unstable on the back-swing.

For all scenarios, during the fault:

- ω_{OMIB} falls because $\omega_2 > \omega_1$ and P_{aOMIB} is negative. This is opposite to the OMIB responses for the sending-end fault in section 4.7.
- After fault clearance $|\omega_{OMIB}|$ decreases because $|\omega_2 - \omega_1|$ decreases, and $\omega_{OMIB} < 0$ because $\omega_2 > \omega_1$.

Stable scenarios 4A.S and 4B.S:

- Forward-Swing stability is correctly detected when ω_{OMIB} is 0 pu at t=1.65s.
- After this $P_{aOMIB} > 0$, so ω_{OMIB} and δ_{OMIB} rise.
- The system remains stable as ω_{OMIB} periodically returns to 0 pu.

Back-swing unstable scenarios 4A.U and 4B.U:

- The speeds of the machine groups equalise on the forward-swing when t = 1.9s. At this point the SIME ESC would falsely indicate that the system is stable.
- In scenario 4A.U at t = 2.71s and in scenario 4B.U at t = 2.68s, P_{aOMIB} becomes negative and thus ω_{OMIB} reaches a local maximum of 0.014 pu at these instants.
- In scenario 4A.U, P_{aOMIB} becomes positive at t = 3.33s; in scenario 4B.U this happens at t =3.25s. This transition occurs before ω_{OMIB} can return to 0 pu, and results in G1 accelerating away from G2, causing transient instability on the back-swing.
- In both scenarios, δ_{OMIB} increases indefinitely and the machines lose synchronism when $\delta_{OMIB} > 360°$.

5.4.5. The OMIB Power-Angle Curves For the Receiving-End Fault

In Figure 5-9 the OMIB acceleration power-angle response for the unstable scenario 4A.U is used to demonstrate back-swing instability. It is superimposed on the trajectory of the unstable forward-swing constrained scenario 1A.U from Chapter 4. Both scenarios begin in the steady-state at point A, with the transmission angle of 13.32°. The key steps of scenario 4A.U are as follows:

During the receiving-end fault (scenario 4A.U)

- $P_{aOMIB} < 0$ as G2 experiences a larger acceleration than G1.
- Thus δ_{OMIB} falls; and the fault clears when $\delta_{OMIB} = -25°$.

Post-fault (scenario 4A.U):

- P_{aOMIB} instantaneously becomes positive; δ_{OMIB} decreases since $\omega_{OMIB} < 0°$.

The speeds of G1 and G2 equalise on the forward-swing at point C, where $\delta_{OMIB} = -117°$. Since the scenario is forward-swing stable, the deceleration area (between points B', C and the δ-axis where $P_{aOMIB} = 0$) and the acceleration area during the fault (between points A', B and the δ-axis) are equal.

- After this, $\omega_{OMIB} > 0°$ so δ_{OMIB} rises following a trajectory from C to A.
- At point A, when δ_{OMIB} increases to 17˚, P_{aOMIB} becomes negative.
- From points A to D, ω_{OMIB} reduces towards 0 pu since $|\omega_2 - \omega_1|$ reduces.
- At point D, P_{aOMIB} becomes positive before ω_{OMIB} can reach 0 pu, and the system loses synchronism on the back-swing when $\delta_{OMIB} = 166°$.
- Since the acceleration area, between points C-to-A and the δ-axis, is greater than the deceleration area, between points A-to-D and the δ-axis, the system is transiently unstable.

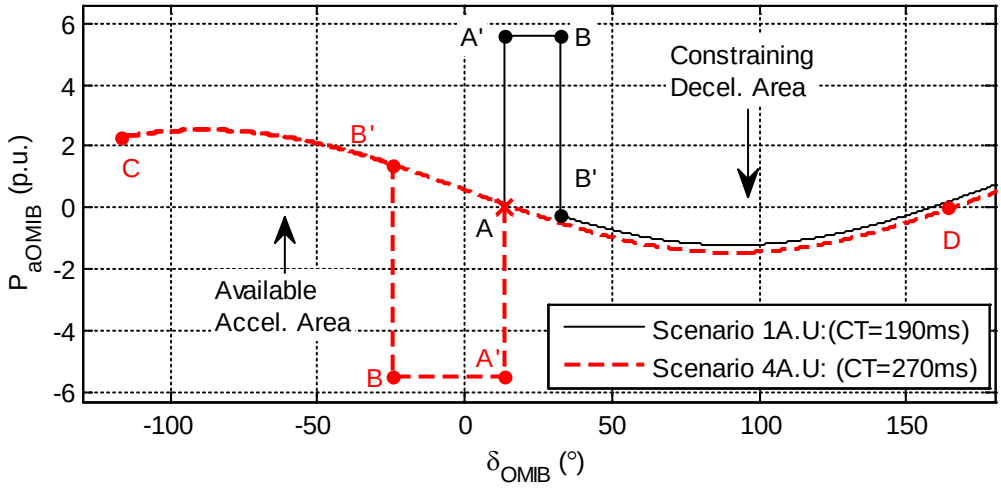

Figure 5-9. $P_{aOMIB} - \delta_{OMIB}$ curves for the unstable scenarios 1A.U (sending-end fault) and 4A.U (receiving-end fault).

It is noted that for the scenario to be stable, during the back-swing it must be possible for the acceleration area (between points C-to-A and the δ-axis) and the deceleration area (between the points A-to-D and the δ-axis) to be equal. For scenarios 1A.U and 4A.U the available deceleration area is much smaller than the available acceleration areas, where $P_{aOMIB} > 0$. Thus, the system operation is constrained due to insufficient deceleration area. For scenario 4A.U, the constraining deceleration area occurs on the subsequent back-swing. For scenario 1A.U the constraining deceleration area occurs on the forward-swing.

Figure 5-10 shows the post-fault OMIB acceleration power-angle characteristics for the receiving-end fault when the SVC is offline; and when the SVC is online with various SVC capacities. The post-fault curves for cases 4A and 4B, and the parts of the curves associated with the forward and back-swing phases, are indicated.

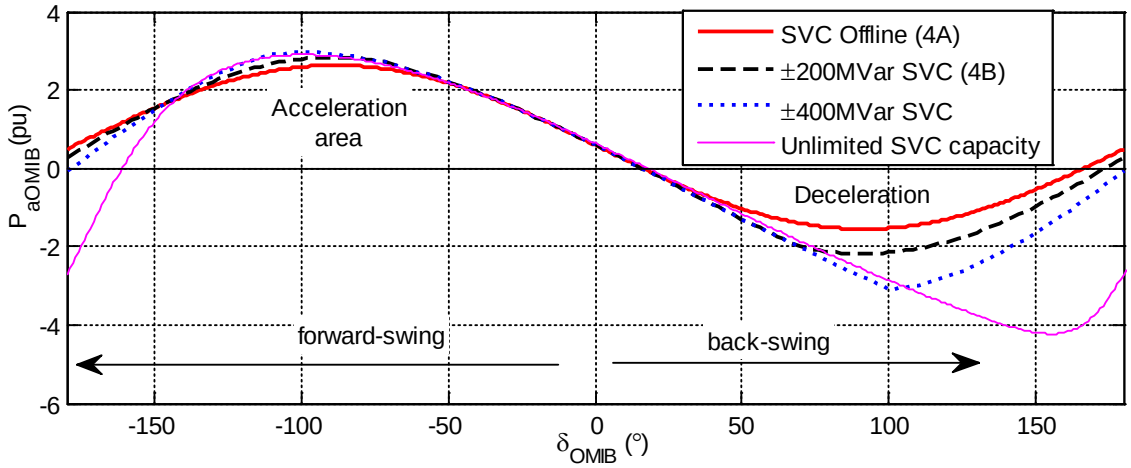

Figure 5-10. OMIB acceleration power versus angle curves for the receiving-end fault where 1) the SVC is off-line; or otherwise online with 2) ±200MVar, 3) ±400MVar and 4) unlimited SVC capacity.

The areas between $P_{aOMIB} > 0$ and the δ-axis are associated with the forward-swing, and are referred to as the *acceleration area*. The areas between $P_{aOMIB} < 0$ and the δ-axis are associated with the back-swing, are the *deceleration area*. Table 5-9 lists the *acceleration* and *deceleration areas*, and the maximum and minimum values of P_{aOMIB} for each case from Figure 5-10. The *acceleration area* represents the capacity of G1 to speed up and equalise with the speed of G2 on the forward-swing. The *deceleration area* represents the capacity of G2 to accelerate and equalise with the speed of G1 during the back-swing.

TABLE 5-9. ACCELERATION AREA, DECELERATION AREA, MAXIMUM AND MINIMUM POST-FAULT VALUES OF P_{AOMIB} FOR VARIATION IN SVC CAPACITY

Row No.	SVC capacity	Forward-Swing		Back-Swing	
		$P_{aOMIBmax}$ (pu)	Accel. Area (pu- rad)	$P_{aOMIBmin}$ (pu)	Decel. Area (pu- rad)
1	Offline	2.63	6.02	-1.55	2.62
2	±200MVar	2.85	6.17	-2.18	3.76
3	±400MVar	2.96	6.20	-3.09	4.98
4	Unlimited	2.90	5.90	-4.23	7.67

Figure 5-10 and Table 5-9 show that the deceleration area and $|P_{aOMIB\min}|$ rise as the SVC capacity increases; in contrast the *acceleration area* and $P_{aOMIB\max}$ vary only slightly with SVC capacity. This is more exaggerated as the SVC capacity increases. In rows 1 to 3 in Table 5-9, the *deceleration area* < *acceleration area*, indicating that transient stability is constrained on the back-swing. For the ideal SVC where there is

unlimited reactive capacity (row 4), *acceleration area* < *deceleration area*, and the system is constrained by forward-swing transient instability.

5.4.6. Relationship of Power Transfer to CCT for the Receiving-End Fault

Case 4B and cases 4D to 4H from Table 5-5 are used to explore the relationship between power transfer and CCT, where a three-phase fault is applied at the receiving-end of the interconnector. The findings are significant, as similar anomalous behaviour is observed on the simplified model of the South-East Australian Power (AU14GEN) system in Chapters 9 and 10. Figure 5-11 shows an overlay of the power-angle curves for a set of marginally unstable scenarios. Since the choice of reference angle is arbitrary, in the following sections δ_{OMIB} has been arbitrarily defined such that P_{aOMIB} is positive during the fault. This is opposite to the choice made in Figure 5-9 for scenario 4A.U. In each scenario:

- The $P_{aOMIB} - \delta$ trajectory begins when P_{aOMIB} is 0 pu.
- During the fault G2, at the receiving-end, accelerates. P_{aOMIB} is positive and δ increases.
- When the fault clears, δ continues to increase. $P_{aOMIB} < 0$ as G2 slows down.

For the cases with power transfers between 0MW and 25MW, G2 has *insufficient capacity to decelerate* to the same speed as G1. The machines lose synchronism on the forward-swing when δ rises above 180°, and G2 accelerates ahead of G1.

For the cases with transfers between 50MW and 200MW, the receiving-end generator has *sufficient capacity to decelerate* to the same speed as G1 at the end of the forward-swing. After this:

- δ falls as G2 continues to slow down, until it is slower than G1 and $P_{aOMIB} > 0$, causing G2 to accelerate.
- At this point G2 has *insufficient potential energy* to equalise with the speed of G1.
- Stability is lost on the back-swing where G1, at the sending-end, continues to accelerate ahead of G2, and δ falls below -180°.

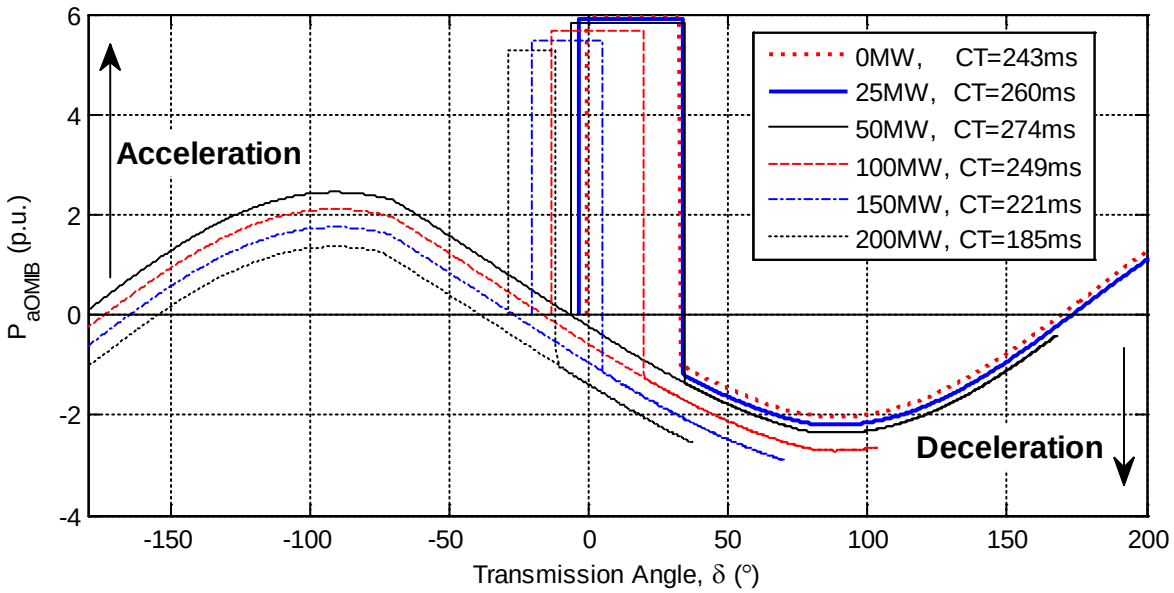

Figure 5-11. OMIB acceleration power versus angle for marginally unstable scenarios where the receiving-end fault is applied on the two machine system

Figure 5-12 shows an overlay of the post-fault $P_{aOMIB} - \delta$ curves for the unstable scenarios in Figure 5-11. Increasing the power transfer over the interconnector causes the characteristics to be negatively offset. This causes the deceleration area to increase, and the acceleration area becomes smaller. Table 5-10 lists the areas between the $P_{aOMIB} - \delta_{OMIB}$ curve and the δ-axis. For each case the constraining areas are underlined.

Figure 5-13 plots the constraining area against the interconnector power transfer. Two operating regions are apparent:

- region 1: transient stability is constrained on the forward-swing, where there is insufficient *deceleration* area to restore synchronism;
- region 2: transient stability is constrained on the back-swing, where there is insufficient *acceleration* area to restore synchronism.

In region 1 the *deceleration* area is proportional to the power transfer. In region 2 the *acceleration* area is inversely proportional to the transfer. Overall there is a piece-wise linear relationship between the constraining area and power transfer. Table 5-10 shows a similar relationship between the CCT and the power transfer. In region 1, the CCT and power transfer increase together; in region 2 the CCT is inversely proportional to the transfer. This indicates that the CCT is proportional to the constraining acceleration or deceleration area, and is verified mathematically in section 5.5.1.

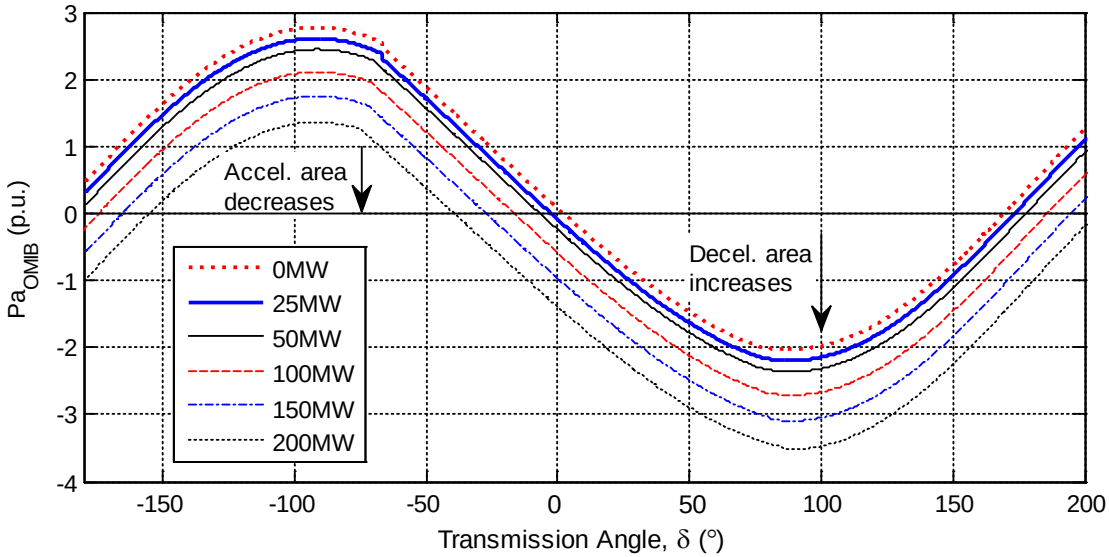

Figure 5-12 OMIB acceleration power versus angle curves for marginally unstable cases where the receiving-end fault is applied on the two-machine system

TABLE 5-10. AVAILABLE ACCELERATION AND DECELERATION AREAS FOR CASES 4B, AND 4D TO 4H

Case	4D	4E	4F	4B	4G	4H
Power Transfer (MW)	**0**	**25**	**50**	**100**	**150**	**200**
Accel. Area (pu-rad)	5.6660	5.1288	4.6248	3.6253	2.668	1.7621
Decel. Area (pu-rad)	3.7260	4.22	4.7235	5.89	7.28	8.97
CCT (ms)	241	258	272	247	219	183
Constraining swing B=Back-swing F=Forward-swing	F	F	B	B	B	B
Operating Region	1		2			

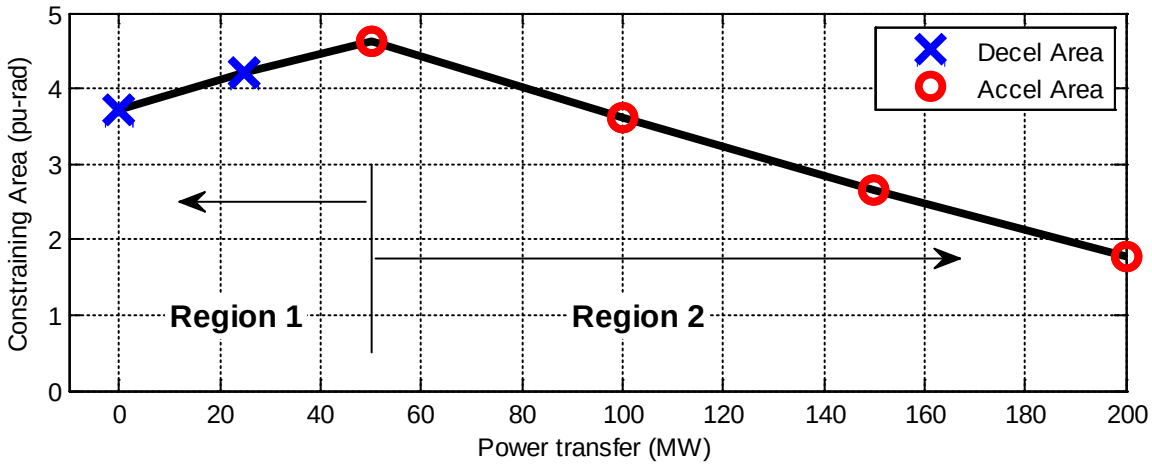

Figure 5-13. Constraining area versus power transfer, for a receiving-end fault, on the two-machine system (cases 4B, and 4D to 4H)

5.4.7. Ratios to Predict the Constraining Mechanism of Instability

Table 5-11 lists a set of ratios calculated from the OMIB responses of the 9-bus two machine system that may be used to predict if a scenario is constrained by forward or back-swing instability. It uses parameters that are associated with the OMIB acceleration and deceleration areas after the receiving-end fault is cleared. Row 1 shows the ratio of the available post-fault acceleration and deceleration areas for the range of investigated transfers. A ratio greater than 1 indicates that system operation is constrained by forward-swing instability; less than 1 if the operating conditions are constrained by back-swing instability. This ratio provides an accurate result and useful insights into the mechanism of instability. However it is difficult to obtain from complex multi-machine power systems as it is likely that the available acceleration and deceleration areas will need to be estimated.

TABLE 5-11. RATIOS TO PREDICT FORWARD OR BACK-SWING MECHANISM OF INSTABILITY FOR THE RECEIVING-END FAULT

Row No.	Power Transfer	0 MW	25 MW	50 MW	100 MW	150 MW	200 MW
1	$\frac{accel\ area}{decel\ area}$	1.5206	1.2161	0.9791	0.6152	0.3664	0.1965
2	$P_{a\min}$ (pu)	-2.0304	-2.1962	-2.3588	-2.7110	-3.0944	-3.5212
3	$P_{a\max}$ (pu)	2.7700	2.6073	2.4470	2.1081	1.7480	1.3581
4	$P_{a\max} \div \lvert P_{a\min} \rvert$	1.3643	1.1872	1.0374	0.7776	0.5649	0.3857

Row 4 takes an alternative approach, using the ratios of the minimum and maximum values of P_{aOMIB} ($P_{a\min}$ and $P_{a\max}$ in rows 2 and 3). Row 4 indicates that the forward-swing constrained scenarios tend to have a ratio of greater than 1; scenarios constrained on the back-swing have a ratio of less than 1. The exception is the back-swing scenario with 50MW power transfer, where the ratio exceeds 1 by 3.7%. On large power systems the effect of system damping and other non-linearities are likely to reduce the accuracy of this ratio as the P_{aOMIB} response will tend to vary from the sinusoidal shape. Nevertheless these results suggest that it may be possible to construct indices to predict the likely mechanism of instability.

5.4.8. SIME Assessment of Cases Constrained by Back-Swing Instability

Although the SIME method proposes ESC and SIME margins for stable scenarios they are not applied in the SIME limit searching method [1, 94]. Pavella et al [1] reason that a stable scenario cannot provide a SIME response as the stable system does not separate into two aggregate machine groups. The EBSIME algorithm for TSL searching, presented in this research, allows stable scenarios to be represented by the OMIB responses, and uses the corresponding SIME margins to accelerate the search. As mentioned earlier, in the EBSIME approach the machine groups identified for an unstable response are used in the analysis of stable cases too.

The SIME margins and ESC are derived from the EAC [1] and are intended to assess forward-swing (in)stability. Pavella et al [1] propose SIME-based techniques to extend the SIME margins and ESC for multi-swing analysis. The EBSIME algorithm does not adopt this approach as the interpretation of SIME for multi-swing stability analysis is unclear.

Figure 5-14 demonstrates how a forward-swing stable SIME margin is calculated from scenario 4A.U, which is actually found to be unstable during the back-swing. Table 5-12 lists the margins and a comparison of the stopping time for the scenarios defined in Table 5-8. In this situation the margin and ESC could be considered misleading as all 4 scenarios are categorized as forward-swing stable. If the simulation of scenarios 4A.U and 4B.U is continued the ESC would eventually recognize the conditions for instability after t=3.3s, and t=3.4s respectively.

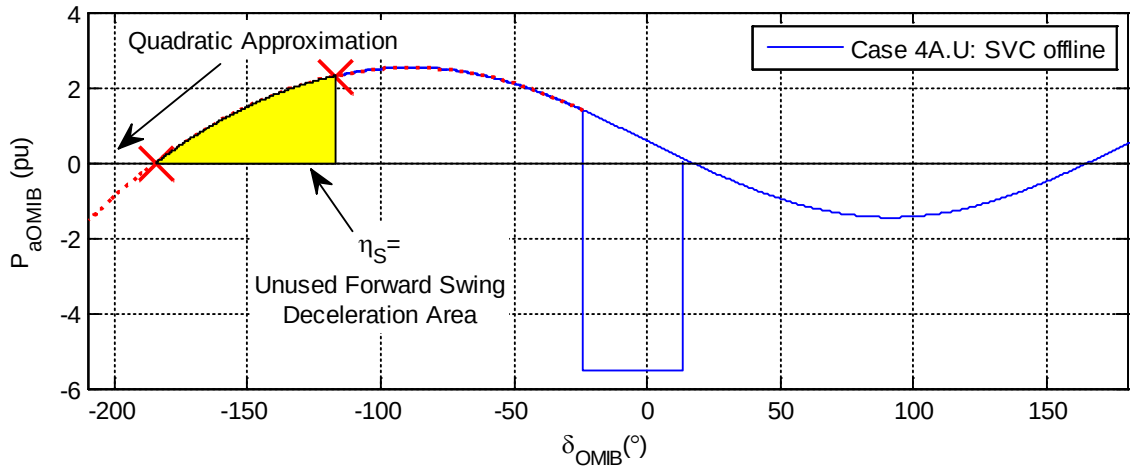

Figure 5-14. OMIB acceleration power angle curve for case 4A.U; the yellow area is used to estimate the forward-swing margin.

For scenarios 4A.S and 4B.S, application of the ESC saves more than 8 sim-s. It provides an early indication that scenarios 4A.U and 4B.U are forward-swing stable at t≈1.91s. If the simulation is continued instability will be identified at t≈3.4 s, 0.6 sim-s sooner than the conventional COI stop criteria.

The EBSIME algorithm uses the SIME ESC and margins to locate the forward-swing limit, prior to determining the multi-swing stability limit. However, where back-swing instability is identified the algorithm reverts to a plain binary search [93], to avoid conflicting information provided by the ESC.

TABLE 5-12. SIME MARGIN AND ESC RESULTS FOR THE RECEIVING-END FAULT SCENARIOS

Scenario Identifier	SIME Margin (pu-rad.s^{-1})	$t_{ESC\ stable}$ (s)	$t_{ESC\ unstable}$ (s)	t_{COI} (s)
4A.S	Too Stable	1.915	N/A	10
4A.U	0.2521	1.915	3.325	4.03
4B.S	Too Stable	1.655	N/A	10
4B.U	0.2499	1.902	3.447	3.98
Times include 1s run-in period before the fault is applied				
$t_{ESC\ unstable}$ assumes that the stable ESC has been ignored and instability is consequently identified on the back-swing according to the SIME unstable ESC				
t_{COI} is the time the system loses synchronism based on the COI instability criteria				

5.5. Asymmetry in the CCT due to Variations in Fault Location

On the 9-bus two machine system, the sensitivity of the CCT to variation in quantities such as the SVC capacity, or power transfer, is different for a fault applied at the sending-end of the interconnector compared to a similar fault applied at the receiving-end. Figure 5-15 shows that when a three-phase fault is applied at the receiving-end the CCT is extended by 35ms with the addition of a SVC with capacity ±200MVar. Conversely, for the same fault applied at the sending-end of the interconnector the CCT is 6ms less with the addition of the same SVC. The asymmetry in the variation of CCT to power transfer is explored in section 5.5.3. Similar observations are encountered in Chapters 9 and 10 in the studies on the AU14GEN system.

For each case the CCT is related to the constraining *acceleration* or *deceleration area* for the post-fault network. The areas can be determined from the P_{aOMIB} versus δ_{OMIB} curve for the post-fault network operating state.

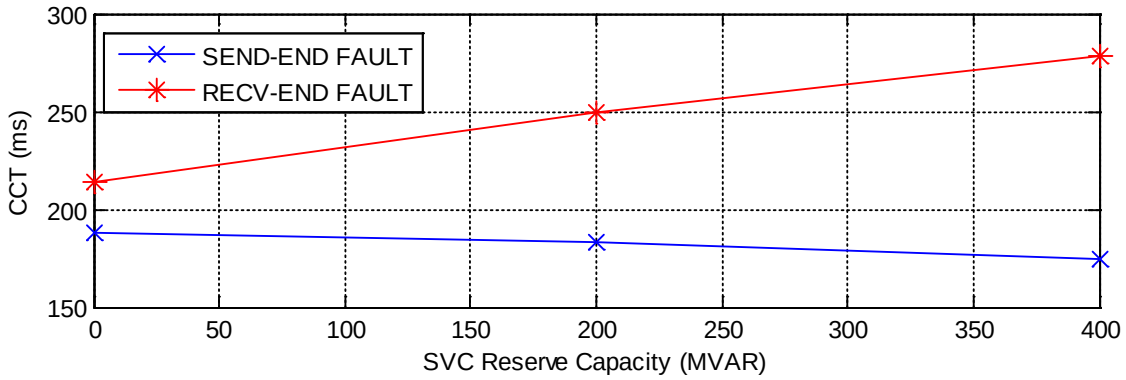

Figure 5-15. Sensitivity of CCT to variation in SVC capacity for cases 1, 2A and 2B (sending-end fault) and 4A, 4B and 4C (receiving-end fault).

When the SVC is online, assuming that it saturates in the post-fault state, the two machine system can be represented by equation (4.63) for a passive 2-port network the OMIB electrical power can be generalized to:

$$P_{eOMIB} = C\cos\delta_{12} + S\sin\delta_{12} + P_C \tag{5.36}$$

where

$$P_C = H\left(\frac{G_{11}E_{q1}^{'2}}{H_1} - \frac{G_{22}E_{q2}^{'2}}{H_2}\right) \tag{5.37}$$

$$C = G_{12}E_{q1}^{'}E_{q2}^{'}\left(\frac{H_2 - H_1}{H_1 + H_2}\right) \tag{5.38}$$

and

$$S = E_{q1}^{'}E_{q2}^{'}B_{12} \tag{5.39}.$$

Table 5-13 lists the post-fault network values of P_C and S for cases 1, 2A, 2B, 4A, 4B and 4C. C is negligible in comparison to P_C and S. So equation (5.36) can be simplified to:

$$P_{eOMIB} \approx S\sin\delta_{12} + P_C \tag{5.40}.$$

Equation (5.40) also applies when the power transfer is varied instead of the SVC capacity.

For the two fault locations, the S and C coefficients are approximately the same. The difference in P_C between the two fault locations is significant, and it widens as the SVC reserve capacity is increased. The different mechanisms of instability and the asymmetry between the acceleration and deceleration areas can be attributed to:

$$\Delta P_C = P_{CR} - P_{CS} \tag{5.41},$$

where P_{CR} and P_{CS} are the post-fault values of P_C for the receiving and sending-end faults respectively.

TABLE 5-13. SINE, COSINE AND CONSTANT TERMS FOR THE POST-FAULT 9-BUS TWO-MACHINE SYSTEM

	Case	1	2A	2B	4A	4B	4C	Units
	Fault Location	Sending-End Fault			Receiving-End Fault			
	SVC Capacity	Offline	±200	±400	Offline	±200	±400	MVar
Term	S (sine)	1.992	2.402	3.016	1.994	2.408	3.034	p.u.
	C (cosine)	-0.049	-0.062	-0.082	-0.049	-0.062	-0.082	p.u.
	P_C (constant)	-1.261	-1.587	-2.123	-1.023	-0.783	-0.383	p.u.

5.5.1. Asymmetry of ΔPC to CCT For Variation in SVC Reserve Capacity

The relationship between the variation in SVC capacity, ΔCCT_{R-S} and ΔP_C is shown in Figure 5-16 where $\Delta CCT_{R-S} = CCT_R - CCT_S$ (5.42).

ΔP_C and ΔCCT_{R-S} are both proportional to SVC capacity. Figure 5-16 shows a quadratic relationship between ΔP_C and ΔCCT_{R-S}.

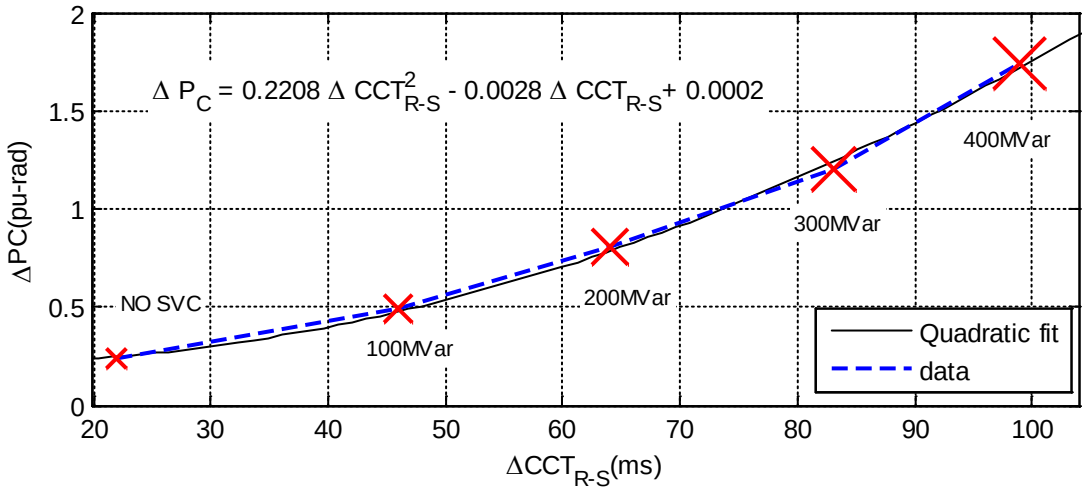

Figure 5-16. ΔP_C versus ΔCCT_{R-S} for variation in SVC capacity on the 9-bus two-machine system

From equation (5.40) the post-fault OMIB acceleration power for a sending-end fault can be expressed as:

$$P_{as} \approx P_{mcs} - S_S \sin \delta_{12} \tag{5.43}$$

where

$$P_{mcs} = P_{mOMIB} - P_{CS} \tag{5.44}$$

And for a receiving-end fault:

$$P_{ar} \approx P_{mcr} - S_R \sin \delta_{12} \tag{5.45}$$

where $$P_{mcr} = P_{mOMIB} - P_{CR} \quad (5.46).$$

For the two fault locations Figure 5-17a shows an overlay of the constant and sinusoidal parts of equation (5.43) when the SVC is offline. Table 5-13 shows that the amplitude of the sine curve, S, is the same for both faults such that:

$$S = S_S \approx S_R \quad (5.47).$$

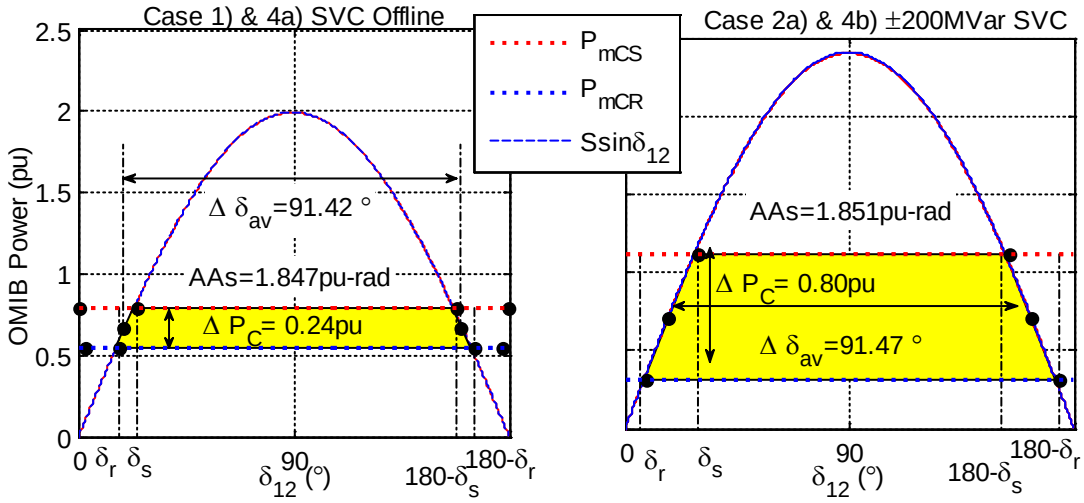

Figure 5-17. Sine and constant components of the $P_{aOMIB} - \delta_{OMIB}$ characteristic for the baseline operating condition with a) SVC disconnected, and b) ±200MVar SVC online.

For a sending-end fault, the area between P_{mcs} and $S_S \sin\delta_{12}$ is the available deceleration area. P_{mcs} intersects $S\sin\delta_{12}$ at the angles δ_S and $\pi - \delta_s$. Similarly, the area between $S\sin\delta_{12}$ and P_{mcr} is the available deceleration area for a receiving-end fault, and P_{mcr} intersects $S\sin\delta_{12}$ at the angles δ_r and $\pi - \delta_r$. The difference between the deceleration areas of the two faults is the shaded trapezium, ΔAA_{R-S}, in Figure 5-17a where

$$\Delta AA = AA_R - AA_S \quad (5.48).$$

P_{mOMIB} is the same for both faults and ΔP_C is the height of the trapezium. It follows that:

$$\Delta AA_{R-S} = \Delta P_C \Delta\delta_{av} \quad (5.49)$$

where

$$\Delta\delta_{av} = \pi - \delta_s - \delta_r \quad (5.50).$$

Figure 5-17b shows that increasing the SVC capacity causes S to increase. P_{mcs} increases and P_{mcr} decreases such that ΔP_C widens. $\Delta\delta_{av}$ is approximately unchanged. Since ΔP_C is the dimension of the trapezium that varies with the SVC capacity:

$$\Delta P_C \propto \Delta AA_{R-S} \tag{5.51}$$

There is a 0.004 pu-rad decrease in AA_S when the 200MVar SVC is switched online. This corresponds to a decrease in CCT_S from 188ms to 183ms. The increase in ΔAA is primarily due to the increase in AA_R.

The following relationship, which applies during the fault, can be deduced from the generator swing equations:

$$\frac{4H\left(\delta_c - \delta_0\right)}{\omega_0\left(P_m - P_e\right)} = t_c{}^2 \tag{5.52}$$

For an arbitrary three phase fault, let the acceleration area be AA_f. The rectangular area AA_f is proportional to $\delta_c - \delta_0$, where δ_0 and δ_c are the steady-state angle and fault-clearing angle respectively; t_c is the fault clearing time. From (5.52):

$$AA_f \propto t_c^2 \tag{5.53}$$

From the EAC AA_f is the critical deceleration area formed during the fault when $t_c = CCT$. AA_f can be reasonably approximated by the post-fault network value of either AA_R or AA_S depending on the fault location. Since AA_S is relatively constant for variations in the SVC capacity from equations (5.51) and (5.53) it can be deduced that:

$$\Delta P_C \propto \Delta CCT_{R-S}^2 \tag{5.54}$$

This quadratic relationship is observed in Figure 5-16. It is also observed on the AU14GEN system when the reactive capacity of an SVC, at the South Australian end of the Victoria to South Australia interconnector, is doubled. The cases constrained by forward-swing instability show that the doubling the SVC capacity has negligible impact on the CCT. Otherwise, in the cases constrained by back-swing transient instability the increase in the CCT is significant. The resultant asymmetry can be attributed to the consequent variation in ΔP_C.

5.5.2. Power Transfer and the Assymetry of the Sine, Cosine and Constant components of OMIB Electrical Power

This section investigates how variation in power transfer influences the equation for P_{eOMIB}. The 5-bus two-machine approximation model derived in section 5.1 is used as a basis for the investigation. The equations from the model provide insight into how variations in the system parameters influence the sine, cosine and constant components of P_{eOMIB}, as discussed in section 5.5. The parameter β, introduced in equations (5.8) to

(5.13), is a scaling factor that represents power transfer in terms of the load distribution in the areas 1 and 2 of the two machine system. From equation (5.13), β is proportional to power transfer, and the corresponding values of interest are listed in Table 5-14. The post-fault networks for case 2A and 6B from Table 5-5, which respectively feature a sending and receiving-end fault are used to demonstrate the findings.

TABLE 5-14. POWER TRANSFER AND THE CORRESPONDING VALUE OF β

	Power Transfer (MW) from Area 1 to 2		
	0	100	200
β	0.5	0.537	0.572

It is useful to understand how power transfer causes variation to P_{eOMIB}, and consequently the P_{aOMIB} - δ_{OMIB} acceleration and deceleration areas, since these areas are proportional to the TSLs of the two machine system. The following conductances and susceptances are defined based on equations (4.66), (4.67) and (4.68) which relate to the constant, sine (S) and cosine (C) components of P_{eOMIB} (P_C):

$$\Delta G_{CONST} = G_{11} - G_{22} \tag{5.55}$$

$$\Delta G_{COS} = G_{1S} - G_{2S} \tag{5.56}$$

and

$$\Delta B_{SIN} = B_{1S} - B_{2S} \tag{5.57}.$$

These equations are based on the conditions in Table 5-7 where E'_{q1}, E'_{q2} and $V_s \approx 1pu$, since $H_1 \approx H_2$. Note $H_1 \approx H_2$ for all cases except 8A and 8B in Table 5-5.

Equations (5.55), (5.56) and (5.57) are proportional to P_C, S and C from equations (5.37), (5.38) and (5.39). Figure 5-18 shows ΔG_{COS}, ΔB_{SIN} and ΔG_{CONST} for the two cases as a function of power transfer. In both cases ΔG_{COS} and ΔB_{SIN} are relatively insensitive to the changes in transfer. Significantly, the constant component ΔG_{CONST} is most sensitive to power transfer. Both cases feature the slope of -1.045pu per 100MW.

The comparative sensitivity of ΔG_{CONST}, and the insensitivity of ΔG_{COS} and ΔB_{SIN}, to β is apparent when considering the formulae for the conductances G_{11}, G_{22}, G_{1S} and G_{2S}; and susceptances B_{1S} and B_{2S} in equations (5.30) to (5.35). In (5.32) G_{22} is directly proportional to β, and in (5.31) G_{11} is directly proportional to (1-β). Thus when the power transfer is increased, β increases, G_{11} falls and G_{22} rises. Similarly in (5.34) and (5.35), $G_{1S} \propto \beta$ and $G_{2S} \propto 1-\beta$. G_{1S} will tend to fall, and G_{2S} will tend to rise, when power transfer is increased. G_{11} and G_{22} have a larger magnitude and are

therefore more sensitive to changes in transfer than G_{1S} and G_{2S}. In (5.34) and (5.35), β^2 is present only in the denominator term of B_{1S} and B_{2S}, therefore β has negligible impact on ΔG_{COS} and ΔB_{SIN}. Figure 5-19 shows the conductances and susceptances as a function of transfer.

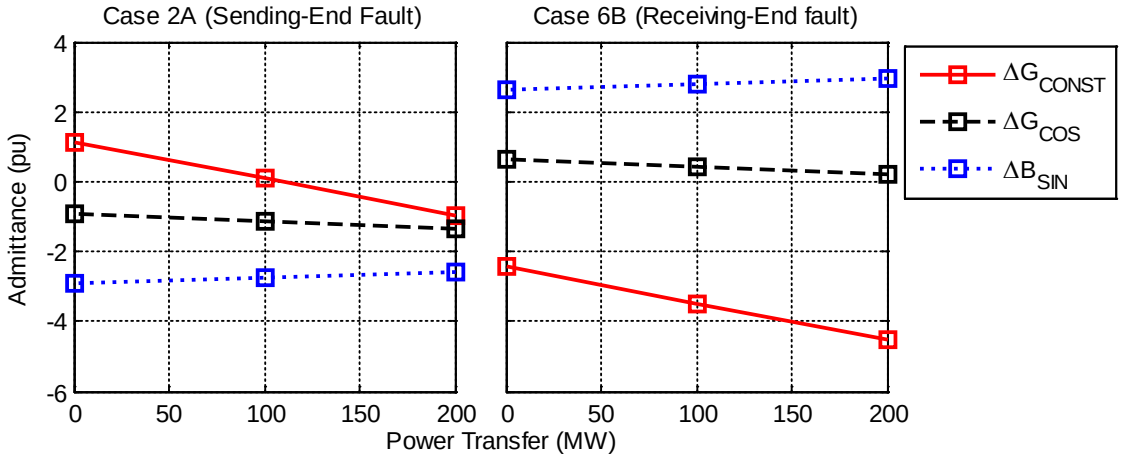

Figure 5-18. Constant, sine and cosine coefficients for the post-fault P_{eOMIB} for cases 2A and 6B, as a function of power transfer - calculated from the 9-bus model

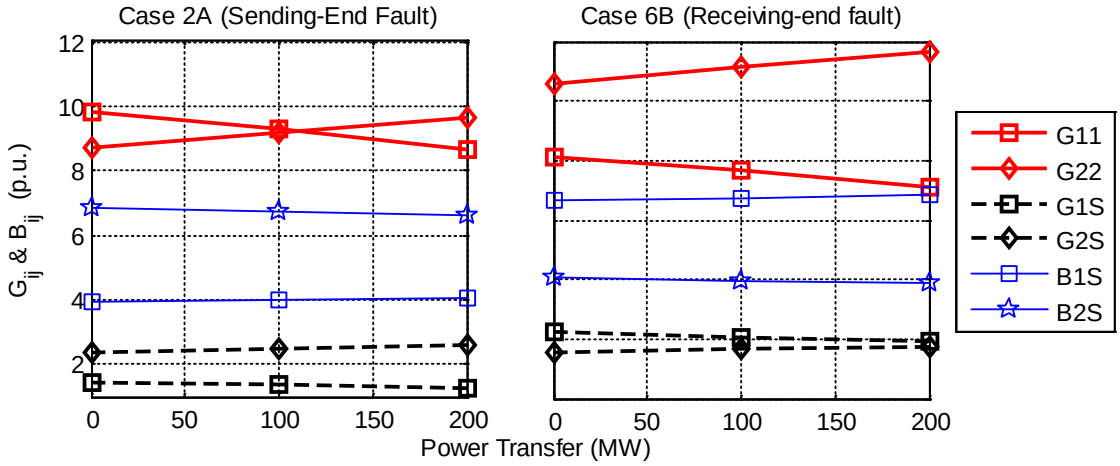

Figure 5-19. Post-fault network admittances for the P_{eOMIB} as a function of power transfer calculated from the 9-bus model

For both cases there is a linear relationship between G_{11} and the power transfer. Furthermore the rate of change of G_{11} with respect to power transfer is the same, and similarly for G_{22}. It can be concluded that there is a linear relationship between the power transfer and P_C, since ΔG_{CONST} is proportional to P_C. Table 5-15 lists P_C for the different transfer levels, which were calculated using equation (5.37).

Thus:

$$P_{CS} = -0.6P_T - 0.96 \quad (5.58)$$

$$P_{CR} = -0.6P_T - 0.16 \quad (5.59)$$

Substituting (5.58) into (5.44) and P_{mCS} can be expressed as:

$$P_{mCS} = 0.6P_T + (P_{mOMIB} + 0.96) \quad (5.60).$$

Similarly, substituting (5.59) into (5.46) yields:

$$P_{mCR} = 0.6P_T + (P_{mOMIB} + 0.16) \quad (5.61).$$

Substituting equations (5.58) and (5.59) into (5.41) it is apparent that ΔP_C is independent of power transfer and has the constant value of 0.8pu. As load-scaling is used to vary power transfer the value of P_{mOMIB} is relatively constant. Therefore (5.60) and (5.61) indicate that P_{mCS} and P_{mCR} are linearly proportional to P_T . These conclusions are important in the following investigation where the asymmetry of the CCT is related to variation in power transfer.

TABLE 5-15 VARIATION OF P_C TO POWER TRANSFER FOR CASES 2A AND 6B

Case	Parameter description	Power Transfer (P_T)			
		50MW	100MW	150MW	200MW
		P_C (pu)			
2A	Sending-end, P_{CS}	-1.27	-1.59	-1.90	-2.22
6B	Receiving-end, P_{CR}	-0.47	-0.78	-1.10	-1.41

5.5.3. Asymmetry of CCT To Power Transfer

Figure 5-20 shows that for the base-line operation the CCT decreases as power transfer over the interconnector is increased. For a 50MW transfer, the CCT for the receiving-end fault is approximately 50ms longer than for a fault applied at the sending-end. This difference increases to 110ms when the transfer is increased to 200MW. The increasing difference in the CCTs is due to the back- and forward-swing mechanisms of instability associated with the two different fault locations.

In section 5.5.1, AA_f is defined as the acceleration area for an arbitrary three-phase fault, where AA_f is the critical deceleration area formed during the fault when the clearing time is $t_c = CCT$. From equations (5.52) and (5.53) the following is deduced:

$$\frac{AA_S}{AA_R} \propto \left(\frac{\delta_{cs}-\delta_0}{\delta_{cr}-\delta_0}\right)\frac{P_{ar}}{P_{as}} = \left(\frac{CCT_{SEND}}{CCT_{RECV}}\right)^2 \tag{5.62}$$

where δ_{cs} and δ_{cr} are the critical clearing angles for the sending and receiving-end faults respectively. P_{as} and P_{ar}, from equations (5.43) to (5.46), are the OMIB acceleration powers for the respective fault locations. They vary linearly with the power transfer (see equations (5.58) to (5.61)). Equation (5.62) indicates that the ratio $CCT_S : CCT_R$ has quadratic relationship to the power transfer.

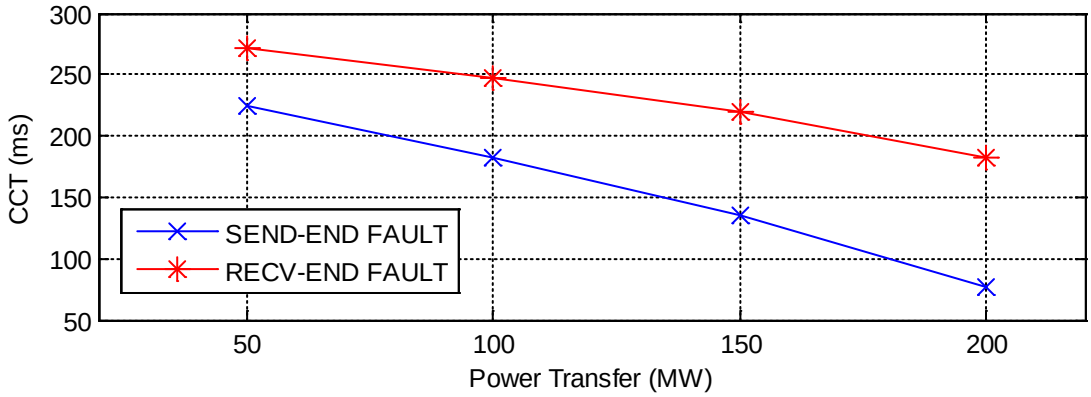

Figure 5-20. CCT versus power transfer for sending-end (SEND-END) fault cases 2A, 6B, 6C and 6D and receiving-end (RECV-END) fault cases 4B, 4F, 4G and 4H.

Figure 5-21 shows the relationship between the ratios $AA_S : AA_R$ and $\left(CCT_S : CCT_R\right)^2$ and the power transfer. There is an approximately linear relationship between $\left(CCT_S : CCT_R\right)^2$ and the transfer as described by (5.62). As both ratios are less than 1 $AA_S < AA_R$ and $CCT_S < CCT_R$. Increasing the power transfer causes both ratios to decrease, which indicates an increasing disparity between the available deceleration and acceleration areas of the two fault locations. At transfers above 150MW the variation in $AA_S : AA_R$ is large, such that a small increase in power transferred causes significant reduction in AA_S with respect to AA_R. The reduction in AA_S for an incremental increase in the power transfer is more gradual at lower transfers. In Chapter 10 the relationship between $\left(CCT_S : CCT_R\right)^2$ and power transfer is investigated on the AU14GEN system and a similar result is observed.

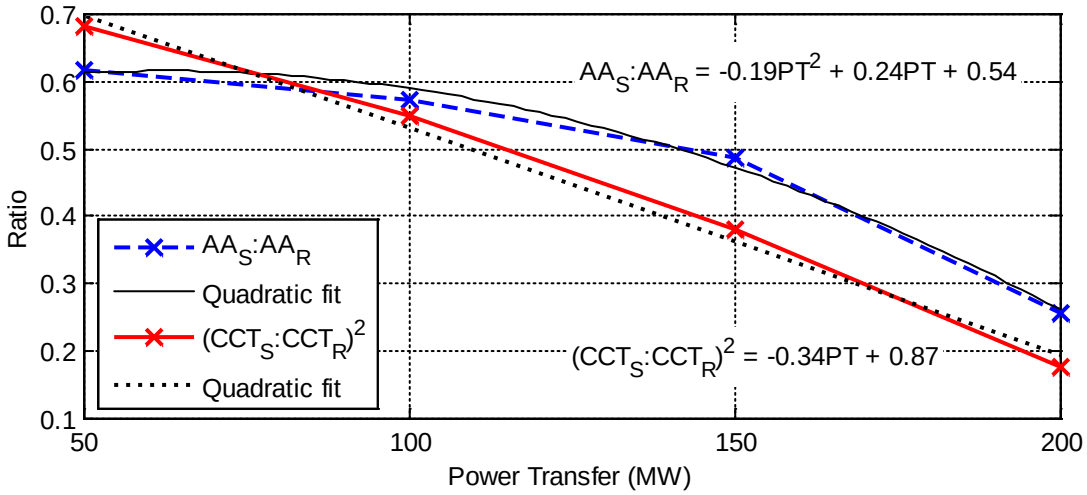

Figure 5-21 The ratios of available deceleration areas and CCT^2 as a function of power transfer

5.6. Variation in the Power Transfer

This section investigates how power transfer influences the TSLs on the two machine power system. The following sections explore the factors that influence the shape of the OMIB acceleration power-angle curve.

5.6.1. Influence of the Power Transfer on the Acceleration and Deceleration Areas: Sending-End Fault

Figure 5-22 shows an overlay of the post-fault network P_{aOMIB} versus δ_{OMIB} characteristics for three different transfers. The calculated acceleration and deceleration areas are summarized in Table 5-16. For each case the system operation is constrained by the available deceleration area because it is smaller than the acceleration area. As discussed in section 5.6.1, P_{eOMIB}, and therefore P_{aOMIB}, is composed of a sine, a cosine and a constant term (P_C). Increasing the transfer causes P_C to decrease, whereas the sine and cosine terms remain unchanged. Consequently, P_{aOMIB} shifts upwards, reducing the available deceleration area, which in turn reduces the CCT.

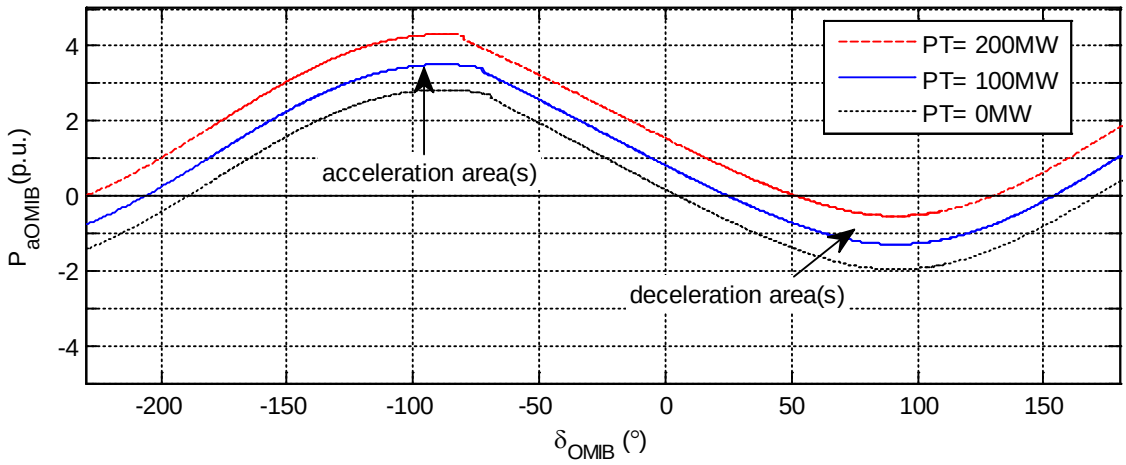

Figure 5-22. $P_{aOMIB} - \delta_{OMIB}$ curves for variation in power transfer with ±200Mvar SVC capacity

Figure 5-23 shows an overlay of the OMIB acceleration power versus angle response for each of the scenarios in Table 5-16. Here, the reference angle δ_{OMIB} is arbitrarily defined such that P_{aOMIB} is positive during the fault. This is opposite to the choice made for the receiving-end fault.

- When each scenario starts, P_{aOMIB} is 0pu.
- During the fault, δ_{OMIB} advances as the contingency at the sending-end fault causes G1 to experience a constant acceleration that is larger than the acceleration on G2.
- In each scenario, the speed of the two machines is unable to equalise on the forward-swing and synchronism is lost. This is consistent with Figure 5-22 which shows that the available deceleration area, concerned with forward-swing instability, is smaller than the available acceleration area. Therefore it limits the system response.

TABLE 5-16. AVAILABLE ACCELERATION AND DECELERATION AREAS OF SELECTED MARGINALLY UNSTABLE SCENARIOS AT VARIOUS POWER TRANSFERS

Case ID (see Table 5-5)	Scenario Identifier	Fault Clearing Time (ms)	Power Transfer (MW)	Available Deceleration Area (pu-rad)	Available Acceleration Area (pu-rad)
6B	6B.U	79	200	0.41	11.74
2A	2A.U	190	100	1.60	8.60
5B	5B.U	266	0	3.21	6.13

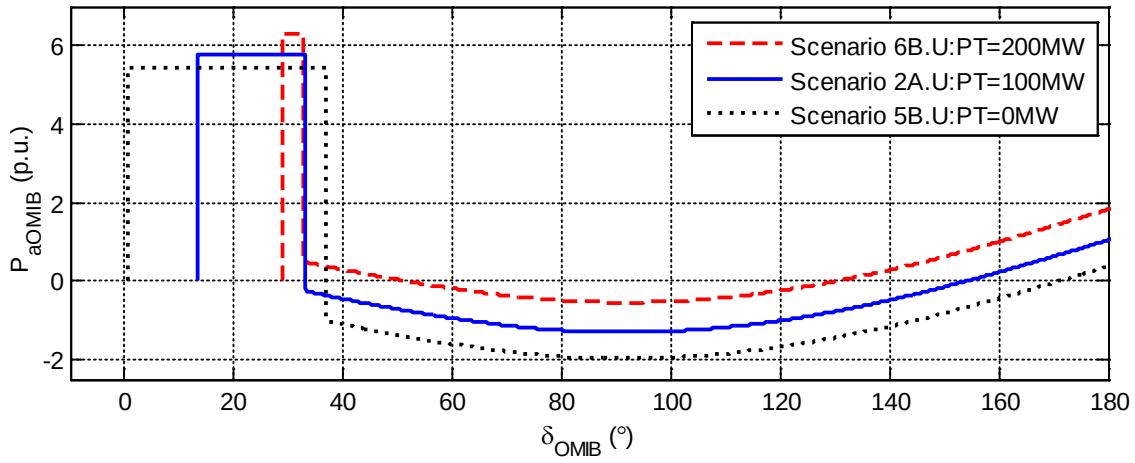

Figure 5-23. $P_{aOMIB} - \delta_{OMIB}$ responses for the marginally unstable scenarios in Table 5-16.

5.6.2. Sensitivity of the CCT to Variation in the Power Transfer

Figure 5-24 shows the sensitivity of SIME margins to the fault clearing time, for variation in the power transfer on the 9-bus two machine power system. The CCT occurs where $\eta = 0$ pu-rad. As might be expected, the results indicate that a higher power transfer subjects the system to greater stress, thus lowering the CCT. As noted in section 5.3, switching the SVC online with ±200MVar available reactive capacity tends to reduce the CCT, although the reduction is small. The sensitivity analysis shows the cases where a fault is applied at the sending-end of the system. For this type of fault the available acceleration area is smaller than the available deceleration area. Thus instability occurs on the forward-swing and so the SIME margins are meaningful.

Conversely, as discussed in section 5.4.3, when a receiving-end fault is applied to the system back-swing transient instability tends to constrain the system operation as the available deceleration area is smaller than the available acceleration area. It is not meaningful to estimate a forward-swing SIME margin for cases constrained by back-swing instability.

Figure 5-20 shows the relationship between power transfer and the CCT for cases 4B, 4F, 4G and 4H featuring a receiving-end fault, and cases 5B, 6B, 6C and 6D featuring a sending-end fault. For a 50MW transfer, the constraining deceleration area, of case 4F, is larger than the constraining acceleration area, of case 6C. Consequently, the CCT for case 4F is 50ms longer than case 6C. The CCT of cases 4F, 4G and 4H are longer than cases 6B, 6C and 6D for similar reasons.

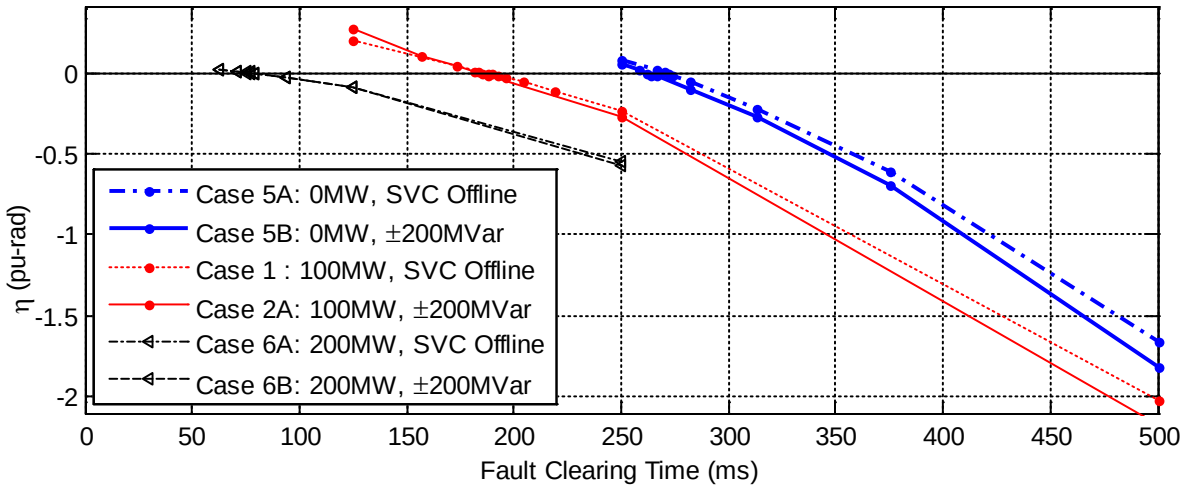

Figure 5-24. Sensitivity of the SIME margins to fault clearing time, for variation in power transfer on the two-machine 9-bus system

5.7. Variation in the Total System Load

Reducing the system load increases the amplitude of the post-fault $P_{aOMIB} - \delta_{OMIB}$ curve. This improves the capacity of the generators to maintain synchronism following a disturbance and increases the TSLs. The effect of varying the system load on the TSLs of the two machine system was considered by comparing cases 2A and 7B from Table 5-5. In case 2A the system load and generation is close to maximum capacity; in case 7B it is halved.

Equations (5.8) to (5.13) describe the relationship between the total system load, P_L, and the load dissipated at buses 4 and 5 in the equivalent 5-bus model. Equations (5.30) to (5.35) show the relationship between P_L and the admittances used to calculate P_{eOMIB} when the SVC is online. Table 5-17 and Table 5-18 compare how the three and two-port equivalent network admittances for the 5-bus model vary for the 2 cases. During the fault the SVC is saturated, thus P_{eOMIB} is described by equation (4.63).

When the load is halved, Table 5-17 shows a small increase in B_{1S} and B_{2S}. Table 5-18 shows that the self-conductance, G_{22}, and susceptance, B_{12}, are halved. Since $H_1 \approx H_2$, it is meaningful to consider ΔG_{COS}, ΔB_{SIN} and ΔG_{CONST} from equations (5.55) to (5.57). Their values are listed in Table 5-19. The post-fault magnitude of ΔB_{SIN} is much larger than ΔG_{COS} and ΔG_{CONST}. Therefore the sine component of P_{eOMIB}, equation (5.39), is the dominant term. Halving the load causes ΔB_{SIN} to reduce by

10%, which causes a proportional reduction in the sine component of P_{eOMIB}, effectively increasing the available deceleration area under the post-fault P_{aOMIB} - δ_{OMIB} curve.

TABLE 5-17. POST-FAULT THREE-PORT NETWORK PARAMETER VALUES FOR THE 9-BUS MODEL

Case ID	G_{11} (pu)	G_{22} (pu)	G_{1S} (pu)	G_{2S} (pu)	B_{1S} (pu)	B_{2S} (pu)
2A	9.17	9.01	1.25	2.46	3.66	6.69
7B	4.60	5.26	0.63	1.43	3.99	7.31

TABLE 5-18. FAULT-STATE TWO-PORT NETWORK ADMITTANCE VALUES BY THE 9-BUS MODEL

Case ID	G_{11} (pu)	G_{22} (pu)	G_{12} (pu)	B_{12} (pu)
2A	0	11.26	0	-6.393
7B	0	6.73	0	-3.191

The P_{aOMIB} - δ_{OMIB} curves from two marginally unstable scenarios for cases 2A and 7B are compared in Figure 5-25 with the fault clearing time and steady-state transmission angle listed in Table 5-20. The starting angle is lower for the case 7B as the load is less than in 2A.

<u>During the fault:</u>

Since G_{11} is 0pu P_{eOMIB} is entirely influenced by the constant term G_{22}. Halving the load causes P_{aOMIB} to halve. Thus the generators accelerate half as much, thereby reducing the severity of the fault on system.

<u>Post-Fault State:</u>

The load reduction causes the amplitude of the post-fault $P_{aOMIB} - \delta_{OMIB}$ curve to increase, thus improving the capacity of the generators to maintain synchronism following the disturbance. Overall, halving the system load significantly increases the TSL.

TABLE 5-19. EQUIVALENT ADMITTANCE TERMS TO APPROXIMATE P_{eOMIB} FOR VARIATION IN LOAD

Load	Case ID	ΔG_{CONST} (pu)	ΔG_{COS} (pu)	ΔB_{SIN} (pu)
Full	2A	0.16	-1.21	-3.03
50%	7B	-0.66	-0.81	-3.32

TABLE 5-20. FAULT CLEARING TIMES FOR THE MARGINALLY UNSTABLE SCENARIOS TO DEMONSTRATE OMIB RESPONSES FOR VARIATION IN LOAD

Scenario Identifier	Case No.	Fault Clearing Time (ms)	Steady-State (°)
2A.U	2A	185	13.32
7B.U	7B	446	9.57

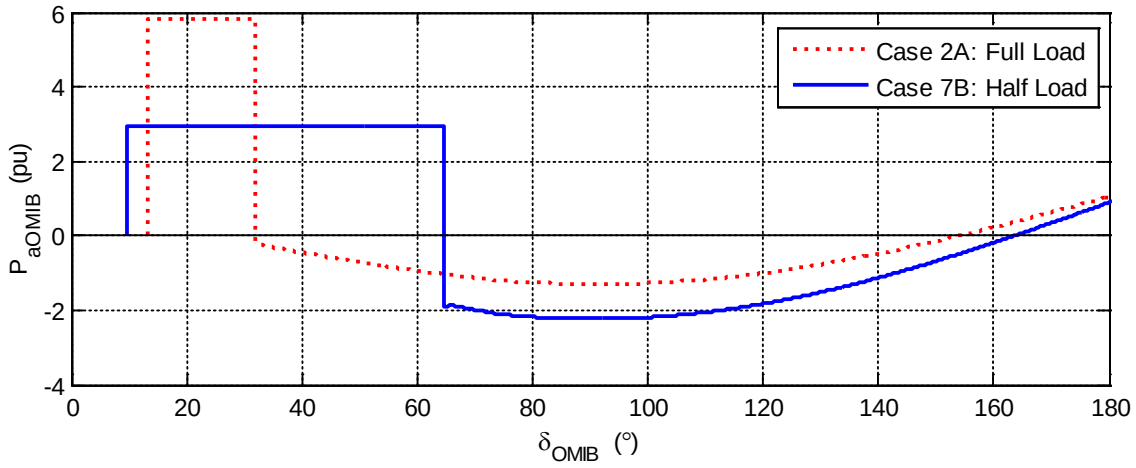

Figure 5-25. $P_{aOMIB} - \delta_{OMIB}$ curves for variation in system load on the two machine system

5.7.1. Sensitivity of the CCT to Variations in the Total System Load

Figure 5-26 shows the relationship between the SIME margins in cases 1, 2A, 7A and 7B and the fault clearing time. Cases 7A and 7B show that halving the system load almost doubles the CCT (where η=0). Again, switching the SVC online causes negligible change to the CCT. In case 7B, for the clearing time of 250ms, the stable margin is much larger than in 7A. This demonstrates that the procedure to estimate the SIME margin for stable scenarios is prone to inaccuracy. In particular, there is a tendency to overestimate the degree of stability.

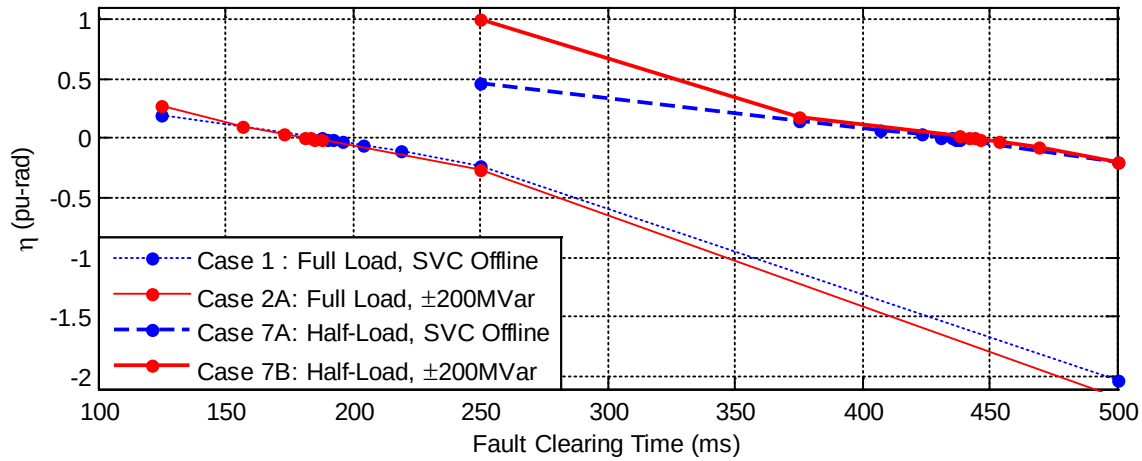

Figure 5-26 Sensitivity of the SIME margins to fault clearing time, for variation in the total system load on the 9-bus two machine system

5.8. Variation in the Transmission Line Length

In cases 3A and 3D, for a fault applied at the sending-end of the two machine system, the transmission line length, L, is reduced from 440km to 220km, then 110km, as shown in Table 5-5, to explore how the length affects the TSL of the two machine system. Figure 5-27 shows that for cases 1, 3A and 3D, where the SVC is offline, the CCT is inversely proportional to the line length, i.e. the CCT rises as the length shortens.

Figure 5-28 shows an overlay of the post-fault P_{aOMIB}–δ_{OMIB} curves for cases 1, 3A and 3D. The figure indicates that the available deceleration area between P_{aOMIB} and the zero-axis is approximately inversely proportional to the change in L. For example,

1) when L is decreased from 440km to 220km the area between the curve and the zero-axis approximately doubles;

2) when L is decreased from 440km to 110km the area approximately quadruples. Increasing the available deceleration area increases the CCT.

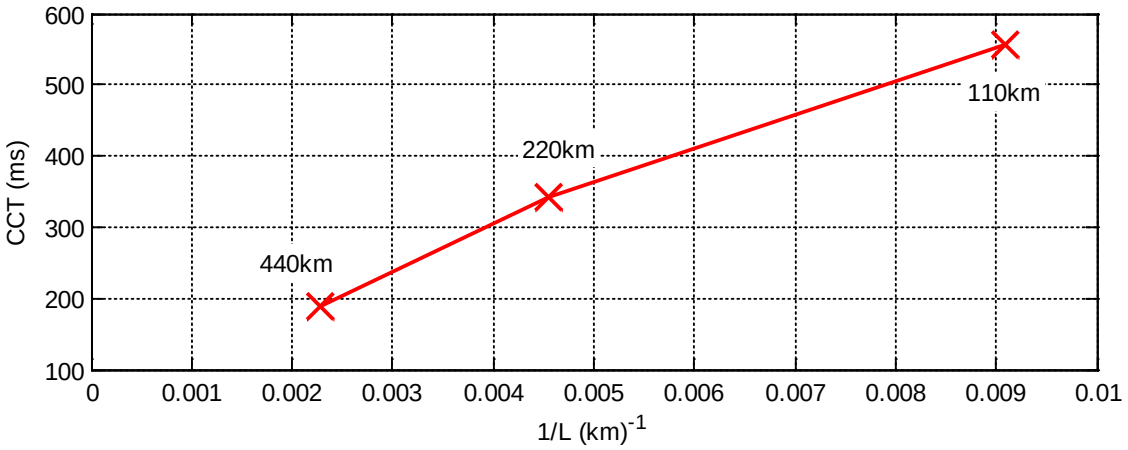

Figure 5-27. CCT versus inverse transmission line length where the SVC is offline, on the 9-bus two machine system

The available deceleration area is proportional to the magnitude of P_{aOMIB} and P_{eOMIB}. From the 5-bus machine model the interconnector susceptance, Y_v, is represented as a function of L. Equation (5.1) shows that Y_v is inversely proportional to L. When L is halved in case 3A, the magnitude of Y_v doubles. When L is reduced to 110km in case 3D, Y_v becomes four times larger than the base-line value. Therefore, Y_v is proportional to P_{eOMIB}.

In summary Y_v, P_{eOMIB}, and the available deceleration area are inversely proportional to the transmission line length. As a first order approximation:

$$CCT(L) = \frac{K}{L} \tag{5.63}.$$

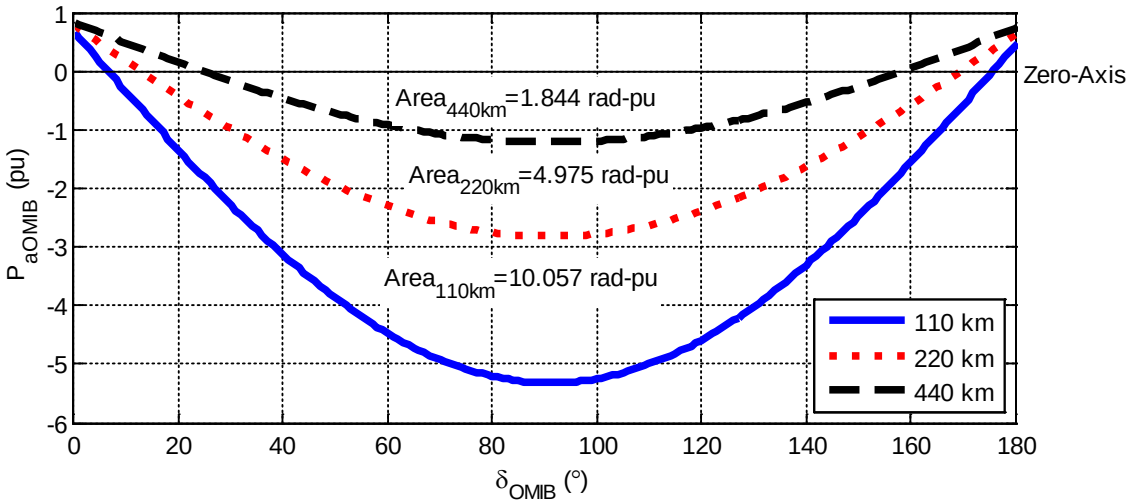

Figure 5-28. Post-fault $P_{aOMIB} - \delta_{OMIB}$ characteristics for the two machine system, for variation in the transmission line length, when the SVC is offline.

Figure 5-29 shows the relationship between the SIME margin and fault clearing time for the different transmission line lengths, and the variation in the SVC reserve capacity. The graph indicates that halving the total length from 440km to 220km increases the CCT by about 125ms. Shortening the length to 110km increases the CCT by about 350ms when compared with case 1 in which the line length is 440km. In all cases the CCT is slightly reduced when the SVC is online, as discussed in section 5.3.

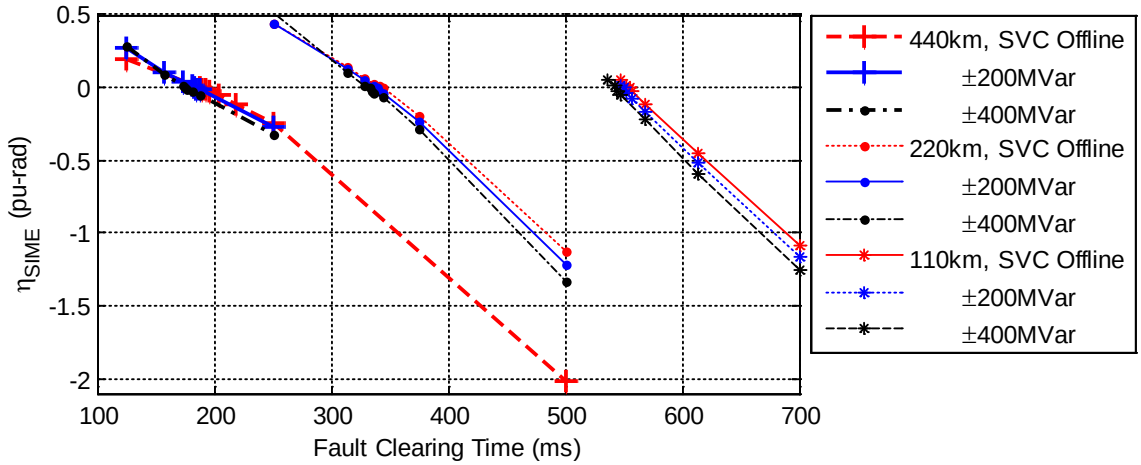

Figure 5-29. Sensitivity of the SIME margins to variation in fault clearing time, for various transmission line lengths in the 9-bus two-machine system

5.9. Variation in the Machine Inertia

The machine inertia constant, H, describes the tendency of a generator to remain in its current state of motion. A larger H indicates that the machine will be more resistant to change in motion; a smaller H indicates that the machine will be less resistant. This section investigates how variations in H affect the TSLs in the two machine power system.

In cases 1 to 7B from Table 5-5 the machine inertia constants for the two generators typically relate to steam-turbine driven generators [13]. In case 8A and 8B the generator inertias of both machines are halved, as shown in Table 5-4 [13]. The dynamic behaviour of the system for cases 2A and 8B are compared in the following analysis. From equation (4.69) the swing equations can be rearranged to:

$$\alpha_i = \frac{d\delta_i^2}{dt^2} = \frac{P_{a_i}}{2H_i\omega_0} \tag{5.64}.$$

Therefore, for each generator:

$$\alpha_i \propto \frac{1}{H_i} \tag{5.65}$$

where α_i is the angular acceleration of the *i*th generator.

Equation (5.65) indicates that if H_1 and H_2 are halved with respect to the case 2A values, each generator will accelerate twice as much during the fault. This will double the speed deviation of both generators and the transmission angle when the fault is cleared. Generators with a lower machine inertia will tend to reduce the transient stability limits. From equation (4.60) halving the inertia constant of both generators will halve H_{OMIB} as follows:

$$H_{OMIBhalf} = \frac{\frac{H_1 H_2}{4}}{\frac{H_1+H_2}{2}} = \tfrac{1}{2} H_{OMIB} \tag{5.66}.$$

When H_1 and H_2 are halved and (5.66) is applied to equation (4.59), P_{eOMIB} is unchanged since the change in inertia cancels out:

$$P_{eOMIB}(t) = H_{OMIBhalf}\left(\frac{2}{H_1}P_{e1}(t) - \frac{2}{H_2}P_{e2}(t)\right) = H_{OMIB}\left(\frac{P_{e1}(t)}{H_1} - \frac{P_{e2}(t)}{H_2}\right) \tag{5.67}.$$

Therefore P_{eOMIB} is independent of inertia, and the $P_{eOMIB} - \delta_{OMIB}$ characteristics for cases 8B and 2A are the same.

Figure 5-30 shows an overlay of the $P_{eOMIB} - \delta_{OMIB}$ responses of two unstable scenarios from case 2A and case 8B. In both scenarios the fault clearing time is 190ms. During the fault:

- Case 2A: δ_{OMIB} increases from 13.32˚ to 33.07˚, advancing 19.75˚.
- Case 8B: δ_{OMIB} increases from 13.32˚ to 52.56˚, advancing 39.2˚.

As per equation (5.64) halving the machine inertia doubles the rate of change of the transmission angle. Both scenarios follow the same post-fault $P_{eOMIB} - \delta_{OMIB}$ trajectory aside from the different fault clearance angles.

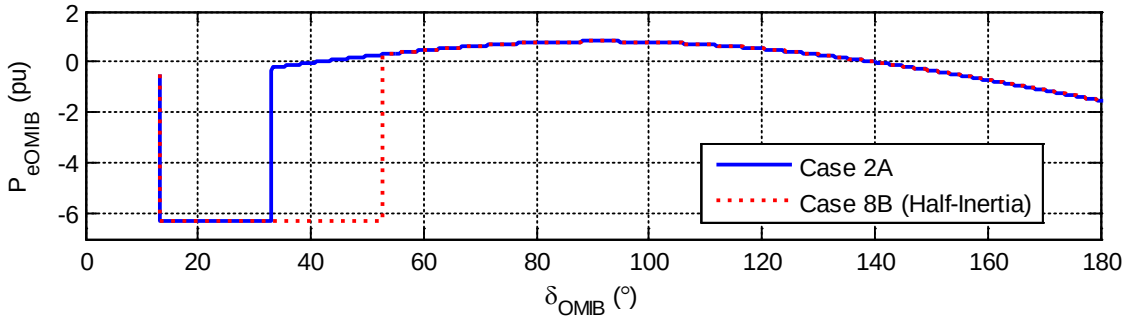

Figure 5-30. OMIB electrical power versus angle curves for cases 2A and 8B, where CT =190ms

Figure 5-31 shows an overlay of the OMIB time responses for the two scenarios. In case 8B the speed deviation, ω_{OMIB}, doubles during the fault compared to case 2A. In case 8B, δ_{OMIB} is twice as large as case 2A.

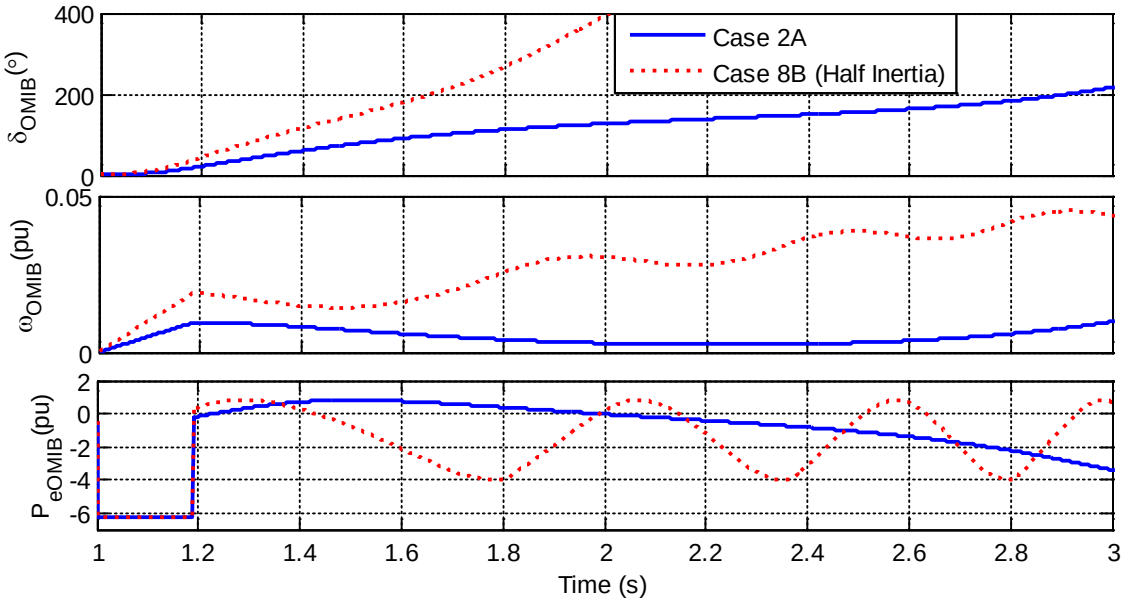

Figure 5-31. OMIB rotor angle, speed, and electrical power versus time responses for cases 2A and 8B where the fault is cleared after 190ms.

5.9.1. Sensitivity of the CCT to Variations in Generator Inertia

The relationship between the CCT and generator inertia in the two machine power system is investigated. Figure 5-32 shows the relationship between the SIME margins for cases 1, 2A, 8A and 8B. The results show that when the inertia of both generators is halved, the CCT decreases significantly. As listed in Table 5-5 halving the inertia of the two machines makes the system less stable, reducing the CCT by about 55ms.

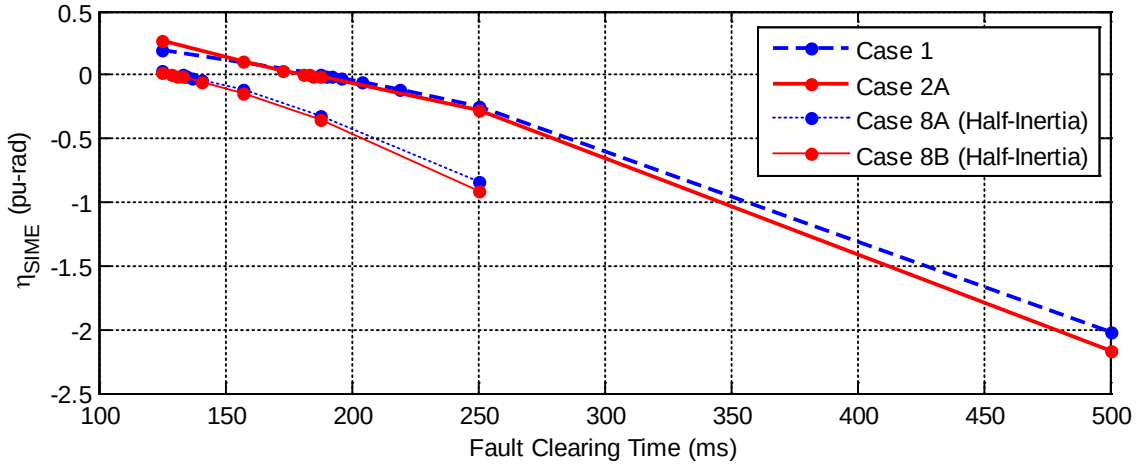

Figure 5-32. Sensitivity of the SIME margins to fault clearing time, where the machine inertia of the generators are varied on the 9-bus two-machine system

5.10. Chapter Conclusion

In this section the SIME algorithm is practically applied on the two machine 9-bus system to determine the transient stability limits (TSLs). The length of the transmission lines in the two-machine system has been selected to emulate the long transmission lines of the major corridors on the Australian system that are constrained by transient instability. This chapter investigates the conditions causing back-swing instability, because if such conditions can be pre-determined the Enhanced Binary-SIME (EBSIME) algorithm could be adapted to overcome the limitations by reverting to a plain binary-search to reliably determine the TSLs. The outcomes of this chapter are as follows:

Sensitivity Analysis using the SIME margins

The SIME algorithm is applied to determine the TSLs on the two machine 9-bus system. Sensitivity analysis with the SIME margins provides useful insights into the relationship between the system parameters and the TSLs. However the SIME margins are not meaningful if the system operation is constrained by back-swing instability.

Effect of Fault Location

The fault location affects the mechanism by which transient instability occurs, and therefore influences the TSLs. Similar behaviour is observed on the simplified model of the South-East Australian Power system (AU14GEN) in Chapters 9 and 10.

Effect of Fault Location: Sending-End Fault

For a three-phase fault applied at the sending-end of the interconnector the CCT tends to decrease when the power transfer is increased, and the system is constrained by forward-swing instability. As discussed in sections 5.4.5 and 5.4.6 this is because the available deceleration area formed by the OMIB acceleration power-angle curve constrains the system operation - it is smaller than the available acceleration area. The CCT is proportional to the available deceleration area, which decreases as the power transfer is increased.

Effect of Fault Location: Receiving-End Fault

When a three-phase fault is applied at the receiving-end of the system, transient instability is constrained on the back-swing, and the CCT decreases when power transfer is increased. In sections 5.4.5 and 5.4.6, the available acceleration area formed by the OMIB acceleration power-angle curve is shown to be smaller than the available deceleration area, thereby constraining the system operation. The CCT is proportional to the available acceleration area which decreases when the power transfer is increased.

The exception is for low transfers where forward-swing transient instability constrains the system operation. The available deceleration area is smaller than the available acceleration area, and the CCT is instead proportional to the power transfer. If back-swing instability can be identified a priori, the limitations of the SIME method can be readily avoided by reverting to a plain binary-search to reliably determine the TSLs.

The Relationship of ΔCCT to ΔPT

The CCT for a fault applied to the receiving-end of the system tends to be higher than an equivalent fault applied at the sending-end. The asymmetry in the CCTs due to the different fault locations is accentuated when:

1) a SVC is connected at the midpoint of the line, and

2) the power transfer is increased.

Similar findings are observed on the AU14GEN system in Chapter 10.

Chapter 6 Comparison of the SIME and EBSIME TSL Searches

The SIME method has many attractive properties for application to the transient stability limit (TSL) search. It can perform fast transient stability assessment (TSA), provide transient stability margins (TSM), and most significantly does not require any simplifications of the detailed model of the power system being investigated. Linear prediction of the limit using the SIME stability margins also provides a means for accelerating a limit search. However, the SIME method has a significant weakness. Its success is dependent on the heuristic tuning of the algorithm parameters to the investigated network model, the operating conditions and critical fault locations.

This chapter introduces the Enhanced Binary-SIME (EBSIME) algorithm for the TSL search and highlights how it addresses the short-comings of the SIME method. It engages the best features of the SIME method by estimating TSMs and using them to predict the limit. The SIME TSL search is improved by ensuring that the correct solution is reached without the need for system specific algorithmic tuning. This is achieved by using a bisection step - locating the mid-point between the current search bounds - to continue the search if linear limit prediction using the SIME margins causes the search to diverge from the limit. The EBSIME algorithm for TSL searching is the novel contribution of this thesis and is described in detail in Chapters 7 and 8.

This chapter directly compares the EBSIME algorithm and the SIME method for TSL searching. Due to the heuristic nature of the SIME algorithm for TSL searching, it was not possible to implement a version the SIME algorithm for the thesis. However aspects of the SIME and EBSIME methods are compared on the 4-machine system in section 6.1.2. Observations of the SIME method for TSL searching are based on the SIME text book [1] and a copy of the original SIME source code generously provided by the University of Liege [95]. This source code and specific details of heuristic tuning methods that it contains are confidential and are therefore not provided in this thesis.

6.1. Differences Between the SIME and EBSIME Searches

Table 6-1 compares the defining features of the SIME method and the EBSIME algorithm for TSL searching. The weaknesses of the SIME method are juxtaposed against the alternative solution proposed by the EBSIME algorithm. Where possible, cross-references are provided to the relevant chapters in the thesis where the algorithm principles are explained. Each discussion point is expanded in the following subsections.

The term *machine groups* (MG), introduced here, describes the pattern by which the system machines lose synchronism and separate into two groups of machines. The MG are used to calculate the one machine infinite bus (OMIB) responses, also referred to as the SIME response. In literature the MG are alternatively referred to as the mode of disturbance (MOD), or as the critical and non-critical machines (see Chapter 2).

The term *bisection step* is also introduced. Bisection is defined as a method of determining the search variable (SV) for the next search scenario to be considered. The SV may be the fault clearing time (CT), or the power transfer over an interconnector. If the current scenario is identified as transiently stable, bisection returns the mid-point between the current SV and the upper search bound. Otherwise if the scenario is identified as unstable, then bisection yields the mid-point between the lower search bound and the current SV.

TABLE 6-1. SHORT-COMINGS OF THE SIME METHOD FOR TSL SEARCHING AS ADDRESSED BY THE EBSIME ALGORITHM (REFER TO CROSS-REFERENCES FOR CLARIFICATION)

Item No.	Thesis Sections	Feature	The SIME Approach	The EBSIME Algorithm approach
1	6.1.1 2.3.2 7.4.2 7.4.3	**Application of the SIME Early Stop Criteria (ESC)**	The unstable SIME ESC is extended to assess a TDS for transient instability beyond the forward-swing (FS). To facilitate this the following parameters, which require heuristic tuning to the investigated power system, are necessary: K - the number of MG assessed by the SIME ESC at every time step; $\delta_{\min}$ - the threshold OMIB angle that must be exceeded if a scenario is to be classified as unstable. The stable SIME ESC is not applied. If instability is not flagged before the end of the TDS then the scenario is stable. (This means that for every stable scenario a full length TDS is required.)	The SIME ESC is applied for forward-swing (FS) transient stability assessment - both stable and unstable SIME ESC are applied during the search. The MG, defined from one unstable search scenario only, is used during the entire search. Tuned parameters are not necessary. Centre of Inertia (COI) stop criteria is applied to the first search scenario, and in the final search phase to assess transient stability beyond the FS. If the system operation is constrained by instability on the back-swing, or subsequent swings, the SIME ESC will lead to an optimistic TSA. However, as discussed in 2.1.3 the COI stability criteria ensures that the actual TSL is located.

Item No.	Thesis Sections	Feature	The SIME Approach	The EBSIME Algorithm approach
2	**6.1.2** **2.6.1.1** **7.4.1**	**Machine Groups (MG)**	At every time-step $t(n)$ of a TDS, *K* MG and associated OMIB values are formulated for $t(n-1)$ and $t(n)$. The simulation stops when one of the K OMIB responses satisfies the unstable SIME ESC, that $P_{aOMIB}(n-1)<0,\quad P_{aOMIB}(n)>0$ and $\omega_{OMIB}(n)>0.$ The corresponding MG are used for the SIME margin calculations. Every unstable scenario encountered during a SIME TSL search, could yield a different 'critical' MG, particularly for larger multi-machine power systems.	Only one MG are required for the entire EBSIME TSL search. The MG are identified from the first (unstable) TDS in the search (i.e. i=1), which is assessed by the COI stop criteria. They are determined at the last time step when the TDS has stopped.
3	**6.1.4** **2.3.1** **2.6.1.1** **7.4.5** **7.5.5**	**Transient Stability Margins**	The SIME margins are based on the EAC for forward-swing TSA in section 2.3.1. Further investigation of these margins is required for a reliable multi-swing TSA. [1]. 3 types of margins are considered: stable, unstable and too unstable. Each has a unique dimensions and physical interpretation. It is not meaningful to combine different types of margins for limit prediction and transient stability sensitivity analysis (TSSA) applications.	The transient (in)stability margins described in section 2.3.1 are applied to assess forward-swing transient (in)stability. The unstable and stable forward-swing margins have the same dimension and physical meaning and are based on the EAC. They use the same MG, thus any pair of margins can be used for the linear limit prediction, or for TSSA applications.

Item No.	Thesis Sections	Feature	The SIME Approach	The EBSIME Algorithm approach
4	**6.1.5** **3.6.1.1** **7.4.4**	**Search Initialization**	The aim is to identify an unstable scenario with a defined unstable SIME margin. The unstable SIME ESC is applied to assess transient instability, as described in section 6.1.1. A descending linear search is used to identify this scenario. The search initialization performance depends on the step size of the linear search. If a TDS is too unstable for a defined SIME margin, limit prediction using the quantity $P_{a\min}$ (see section 6.1.4) is used to accelerate the search for an acceptable unstable scenario.	The aim is to locate an unstable scenario with a defined FS unstable SIME margin. The first scenario (k=1) is assessed using the COI stability criteria. 1) If the first scenario has a defined unstable SIME margin, search initialization is complete. The next SV is determined by bisection of the search bounds. 2) If the first scenario does not have a defined FS unstable SIME margin, iterative bisection is applied to locate a suitable scenario. From scenario k=2 onwards, the SIME ESC is applied for TSA. 3) If the first scenario is transiently unstable, but FS stable by the SIME ESC – then system operation is constrained by back-swing instability. The EBSIME search will switch to a binary search to locate the TSL.

Item No.	Thesis Sections	Feature	The SIME Approach	The EBSIME Algorithm approach
5	**6.1.6** **7.4.4** **7.5**	**Limit Prediction -to determine the SV for the next scenario**	Limit prediction for the multi-swing limit is performed using a pair of TSMs from the current scenario and the previous unstable scenario. The two margins must be calculated using the same MG, and for the same power swing. If the current scenario is: 1) *stable*, the OMIB response is calculated using the MG of the previous unstable scenario 2) *unstable* the OMIB response of the previous scenario is recalculated using the MG of the current scenario. The TDS of the previous scenario must be continued if necessary to calculate the correct SIME margin with revised MG.	Linear prediction for the forward-swing limit (FSL) is performed using a pair of TSMs from the current and previous search scenarios. The scenarios may be either stable or unstable, as long as a SIME margin is defined. All margins are calculated for FS TSA, and using the same MG. Therefore any pair of margins calculated during the search are compatible for limit-prediction and TSSA applications.
6	**6.1.7** **7.5.7**	**Search Divergence**	If a predicted limit diverges from the TSL, heuristic decisions that are system dependent and fault dependent are taken to redirect the search.	If limit prediction causes the search to diverge from the FSL, bisection with the current search bounds is used to redirect the search. If search divergence occurs more often than the allowed threshold, the search reverts to a binary search to locate the actual TSL.

Item No.	Thesis Sections	Feature	The SIME Approach	The EBSIME Algorithm approach
7	**6.1.8** **7.6**	**Locating a provisional limit**	The search ends by locating a provisional limit when the distance between the upper and lower search bounds drop below the search tolerance. The provisional limit assumes that K and $\delta_{\min}$ have been selected correctly.	The limit prediction phase ends when the distance between the search bounds falls within the tolerance. The provisional limit that is returned is FS stable. It needs to be verified that it is also the TSL.
8	**6.1.9**	**Confirmation of the Provisional Limit**	Further heuristically determined search steps are required if the provisional limit is not the TSL.	The TDS' of the provisional limit and of the of the FS upper bound are continued and assessed for transient instability using the COI instability criteria. If the provisional limit is transiently stable, and the upper search bound is transiently unstable then the provisional limit is the TSL. Otherwise, it is concluded that the system operation is constrained by multi-swing transient instability. Thus instability occurs after the forward-swing. The EBSIME algorithm revert to a binary search to find the TSL, which assesses the TDS using the reliable COI (in)stability criteria.

6.1.1. Application of the SIME Early Stop Criteria (ESC)

In a TSL search the dynamic response of multiple search scenarios are assessed for transient (in)stability. The SIME method for TSL searching uses criteria 2 described in section 2.3.2 for fast assessment of multi-swing transient instability. By this criteria instability is identified when

$$P_{aOMIB}(t_u) = 0\,,\ \left.\frac{dPaOMIB}{dt}\right|_{t=tu} > 0 \text{ and } \omega_{OMIB}(t) > 0 \text{ for } t < t_f < t_u \qquad (6.1)$$

where

t_f is the time when the fault is applied,

t_u is the time when the system loses synchronism,

P_{aOMIB} is the OMIB acceleration power, and

ω_{OMIB} is the OMIB rotor speed.

The assessment requires OMIB values to be calculated for the TDS time-steps $t(n)$ and $t(n\text{-}1)$, where n is the current simulation point.

The method for fast TSA using the unstable SIME ESC is interrelated with the procedure for identifying the MG to define the OMIB response, and thereby to calculate SIME margins for a given search scenario. At each time-step of a scenario the SIME procedure considers several possible MG. K is the number of MG that are assessed by the SIME ESC at every time step and the unstable SIME ESC is applied to test each pair of values for transient instability. K is a heuristically selected value, and varies with the investigated power system.

As a large range of MG may be considered, particularly for larger multi-machines power systems, it is possible for an incorrect diagnosis of stability to be made by the SIME ESC. To safeguard against mistakes the SIME method requires that for instability δ_{OMIB} must exceed the pre-assigned threshold angle $\delta_{\min}$. As soon as the instability criteria is satisfied the simulation will cease. If a TDS runs for the full simulation period without detecting instability then the scenario is multi-swing stable. The stable SIME ESC for fast assessment of stable scenarios is not used [1].

This method for TSA is applied to all scenarios in the SIME TSL search. The tuned values, $\delta_{\min}$ and K, affect the search performance. The choice of $\delta_{\min}$ and K depend on the network model, the fault location and the operating condition. This represents a further complication. Heuristic parameter tuning is undesirable as for each given network model it involves manually assessing many operating conditions and contingencies, and managing large amounts of data.

In contrast the EBSIME algorithm for TSL searching applies two different approaches to TSA throughout the search: stop criteria based on the centre of inertia (COI) angle as described in section 2.1.3 and the SIME ESC for fast assessment of forward-swing transient (in)stability as described in section 2.3.2.

The COI stability criteria is based on section 2.1.3 and compares the rotor angle of all system machines to the COI angle for the entire network, at every time step. If the rotor angle of any machine diverges from the COI angle by more than the customisable angle, δ_{COImax}, then the scenario is unstable and the TDS will halt at time $t = t_{obs}$. In this thesis $\delta_{COImax} = 180°$ is used in all investigations. If all machine angles remain within the stability threshold for the full simulation period then the scenario is transiently stable.

The EBSIME algorithm applies the SIME ESC in a way that tuned parameters are unnecessary. This is achieved by using one MG to calculate all the OMIB responses throughout the search. The MG are defined from the first (and most unstable) search scenario at the instant when instability is detected, i.e. $t = t_{obs}$. The EBSIME algorithm applies the time-saving advantages of the SIME ESC, and the reliability of the COI TSA criteria to achieve a fast, robust and accurate TSL search.

6.1.2. Identification of Machine Groups (MG) on the Basis of Ordered Machine Angles

In the EBSIME algorithm the MG is determined from the first unstable search scenario using the following procedure. At $t = t_{obs}$ the machine angles are arranged in descending order:

$$\delta_i > \delta_{i+1},\ i = 1,...N-1 \tag{6.2}$$

where δ_i is associated with machine $m(i)$,

and N is the number of online machines.

The difference between adjacent machine angles is $\Delta\delta_i = \delta_{i+1} \geq 0,$ (6.3).

j is found such that: $\Delta\delta_j = \max(\Delta\delta_i)$ (6.4).

Then, the machines in group 1 are:

$$G_1 = \{m(1),...m(j)\} \tag{6.5}$$

and in group 2:

$$G_2 = \{m(j+1),...m(N)\} \tag{6.6}.$$

In the SIME method to search for the TSL K MG are determined at every time-step, $t(n)$, of a TDS. The same procedure described by equations (6.2) to (2.52) is applied,

but instead the K largest values of $\Delta\delta_i$ are used to find j and then to identify K MGs. The first MG to satisfy the unstable SIME ESC is the MG for the current unstable scenario.

6.1.3. Example of SIME ESC and Machine Grouping

For clarity the above described machine grouping procedure is explained on the following 4-machine example system. This 4-machine system is explored thoroughly in Chapter 7. The system parameters are described in Appendix C. In this 50Hz system 200MW is transferred from area 1 to area 2. A 3 phase fault is applied at t=0s to the node 7 end of circuit #1 between buses 7 and 8. The fault is cleared after 375ms by simultaneously opening the breakers at both ends of circuit #1. Governors are not represented in the system. Power system stabilizers and AVR controls are included at each generator.

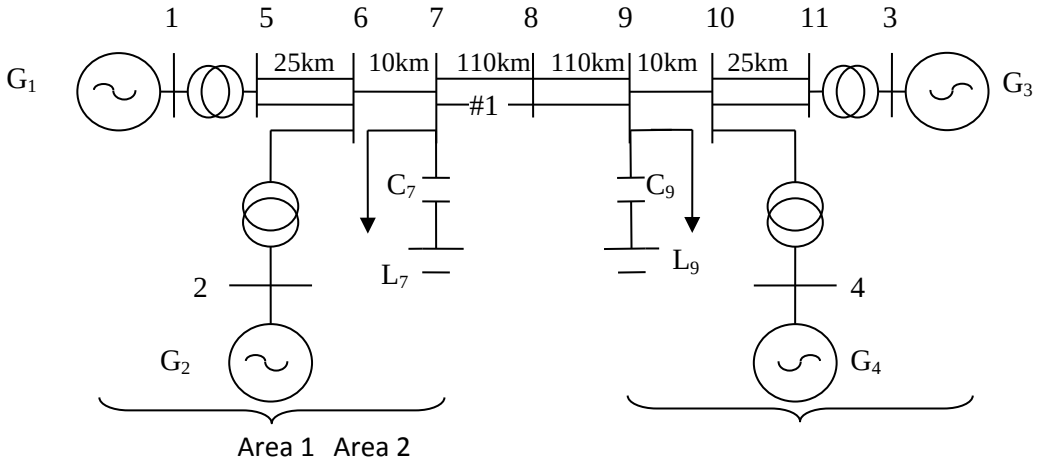

Figure 6-1. The 2-Area 4-machine test system

Figure 6-2 shows the generator angles of each of the machines, and the equivalent COI angle. The 3 possible MGs for which the unstable SIME ESC can be assessed at every time step are listed in Table 6-2. The equivalent OMIB rotor angle, speed and acceleration power responses for the three MG are compared in Figure 6-3.

TABLE 6-2. CONSIDERED MACHINE GROUPS (MG) FOR THE 4-MACHINE SYSTEM

Machine Groups ID	Generators in Group 1	Generators in Group 2
MG1	G1, G2	G3, G4
MG2	G1	G2, G3, G4
MG3	G1, G2, G3	G4

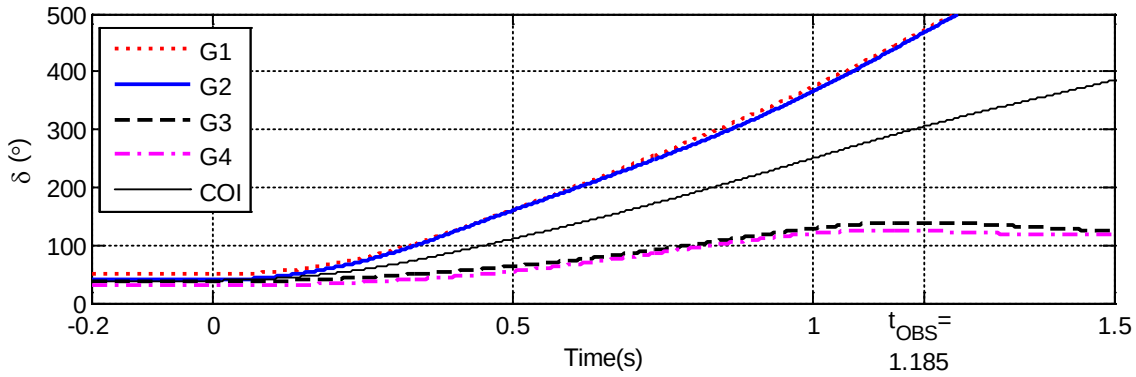

Figure 6-2. The generator rotor angles on the 4-machine system where a 3 phase fault is applied at t=0s, and cleared after 375 ms

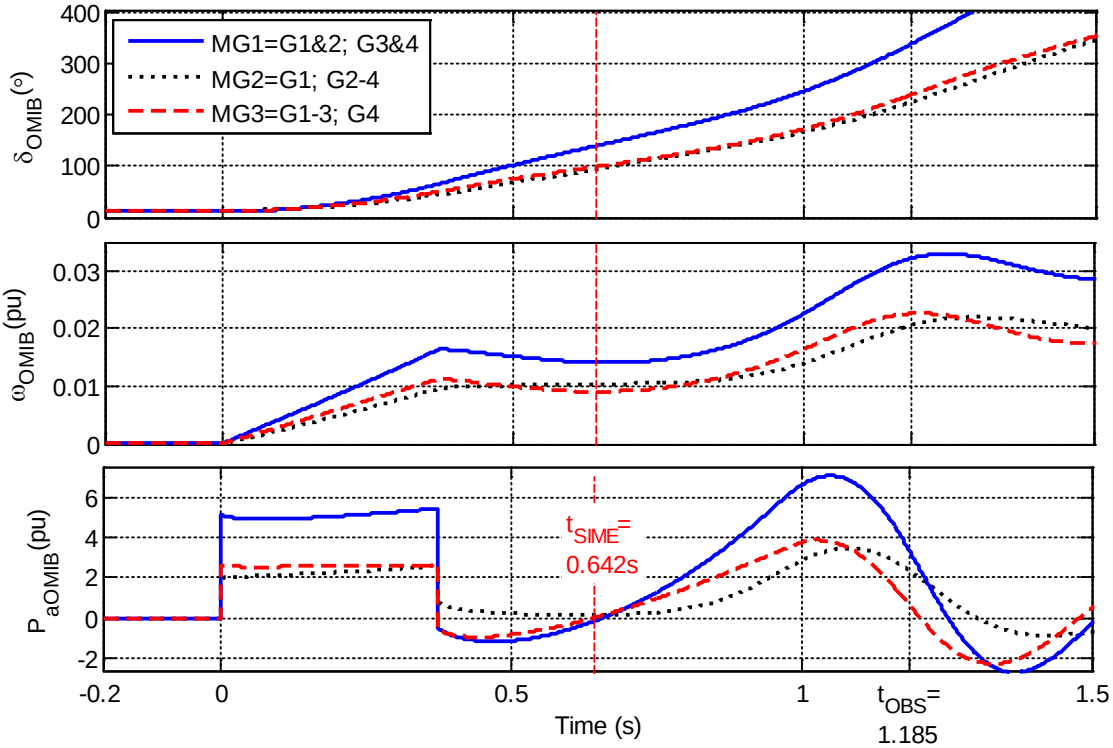

Figure 6-3 Demonstration of the SIME ESC on the 4-machine power system - the critical MG is identified at t=0.642s

Figure 6-2 also shows that the natural grouping of this system is G1 and G2; and G3 and G4. This is reflected by MG1, so at every time step MG1 is considered first for the SIME TSA. However, MG3 is the first to satisfy the unstable SIME ESC at t=0.642s when P_{aOMIB} changes from negative to positive and $\omega_{OMIB} > 0$. This assumes that $\delta_{OMIB} = 99° > \delta_{\min}$. Although, if $99° < \delta_{\min} < 140°$, or alternatively if K=1 were selected, MG1 would satisfy the SIME ESC first at t=0.66s. Further, if $\delta_{\min} > 140°$, MG3 would be the critical grouping, and second-swing instability would be instead be identified at t=1.48s, as the next time the unstable ESC is satisfied and $\delta_{OMIB} > 140°$. This demonstrates the dependence of the SIME method on parameters *K* and $\delta_{\min}$.

The EBSIME TSL search uses one MG to calculate the OMIB responses for the entire search. No parameter tuning is required. The MG is identified using the first and most unstable search scenario. At $t = t_{obs}$, when the TDS is halted by the unstable COI-based TSA criteria mentioned in section 6.1.1, steps 1-4 in the above list are applied. The MG is determined by partitioning the machines on either side of the maximum $\Delta\delta_i$. In the above example, the COI instability criteria is satisfied at $t_{obs} = 1.185s$. The largest angle separation at this time is 327˚ between G2 and G3, therefore MG1 will applied for all scenarios in the remaining search.

A concern of applying only one MG is that through the course of the search, the relevant MG may change, particularly in a power transfer limit search. Although the MG can change under less stressed operating conditions, the EBSIME algorithm can still find the TSL by resorting to a plain binary search when the SIME limit prediction diverges from the FSL. Chapters 9 and 10 present some case studies where the EBSIME algorithm locates the correct TSL in spite of variation in the MG for different power transfers.

6.1.4. Transient Stability Margins

The SIME TSL search uses the calculations of both forward- and multi-swing TSMs to accelerate the search using pairs of margins to linearly predict the limit. Stable margins are calculated by estimating the unused deceleration area under the $P_{aOMIB} - \delta_{OMIB}$ curve from the swing of interest (see equation (2.24)). Unstable margins are calculated from the kinetic-energy based equation (2.26). When a scenario is too unstable to provide a measure for (2.26) the minimum post-fault OMIB acceleration power $\left(P_{a\min}\right)$ of the forward power swing, demonstrated in Figure 6-4, is used as an alternative margin measure. It is the intent of the SIME TSL search to use linear extrapolation applied to a pair of points, $(P_{a\min 1}, SV_1)$ and $(P_{a\min 2}, SV_2)$, to accelerate the location of an unstable scenario with a defined SIME margin. Figure 6-4 demonstrates that the unstable SIME ESC can still be applied to identify instability for a very unstable scenario, however it may be identified on a subsequent power-swing (i.e. at $t_{SIME} = 1.256s$ in this example).

As mentioned in section 4.6.3, there are a number of concerns when SIME margins are used for the TSL search:

- The three proposed SIME margins –unstable, stable and too unstable $\left(P_{a\min}\right)$ – each have different dimensions. They cannot be combined in interpolation or extrapolation equations to provide an estimate of the limit;

- The multi-swing SIME margins are an adaptation of the EAC-based margins for FS stability. Despite the work of Pavella and Yin et al [1, 96] the interpretation and use of the multi-swing stability SIME margins is a topic that requires further investigation.

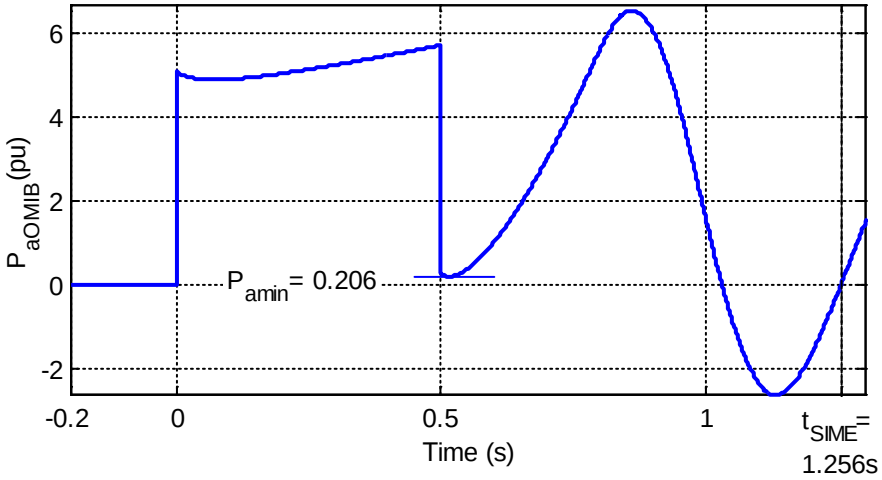

Figure 6-4. From the 4-machine example, for a CT=500ms the scenario is too unstable for a SIME margin to be defined; instead. $P_{a\min}$ *is used*

The EBSIME algorithm uses a different set of SIME margins in the TSL search for the above reasons. Equation (2.24) is used to calculate the margin for stable scenarios, however it is restricted to FS stability assessment. The FS unstable margin is calculated using (2.25). The stable and unstable SIME margins used here both describe the areas within the $P_{aOMIB} - \delta_{OMIB}$ curve, and thus their dimensions and interpretation are consistent (pu-rad).

6.1.5. Search Initialization

The aim of the SIME TSL search initialization is to locate an unstable scenario with a defined SIME margin. Since the SIME TSL search only applies ESC for fast assessment of unstable scenarios, the algorithm aims to maximize the number of unstable scenarios that are assessed. Therefore it begins with a descending linear search. During the linear search the unstable SIME ESC is applied to assess the transient stability of each investigated scenario. If a suitable scenario is not identified before a stable scenario is encountered then the SIME TSL search must be restarted, and the parameters of the linear search reviewed. Otherwise if the sought-after scenario is identified, the next SV is determined by another descending linear step.

The aim of the EBSIME TSL search initialization is to locate an unstable scenario with a defined forward-swing unstable SIME margin. The first search scenario must be transiently unstable and is confirmed as being unstable using the COI-based stability criteria. It is used to determine the MG for the search. If the first scenario:

1) has a defined unstable SIME margin, then bisection is used to determine the SV for the next scenario and initialization is complete;
2) does not have a defined unstable SIME margin, then bisection is used to determine the SV for the next search scenario in the initialization phase. And similarly for all succeeding scenarios until a FS unstable scenario with a defined unstable margin, is found;
3) has a defined FS stable margin – this indicates that the system operation is constrained by back-swing instability.

After the first scenario and during initialization, the TDS are assessed using SIME ESC for FS transient (in)stability. If a scenario with an unstable SIME margin cannot be located during initialization, or if back-swing instability is recognized, the algorithm will revert to a plain binary search to locate the TSL.

6.1.6. Limit Prediction

In the SIME and the EBSIME TSL searches the iterative limit prediction phase follows the search initialization. In general, a pair of points (SV_{k1}, m_{k1}) and (SV_k, m_k) from the current search scenario (k) and a previous scenario (k-1), are used to linearly predict the TSL limit; where m_k and m_{k1} are SIME margins. The predicted value becomes the SV for the next search scenario:

$$SV_{next} = SV_k - m_k \frac{SV_{k1} - SV_k}{m_{k1} - m_k} \quad (6.7).$$

In the SIME TSL search the iterative limit-prediction procedure has the following constraints. For the current and previous search scenarios, the OMIB responses and SIME margins must be calculated:

- using the same MG; and
- for the same power swing (i.e. forward, back, or second-swing); and
- at least one of the scenarios must be unstable.

To satisfy point a) if the current scenario is stable, the OMIB response, and SIME margin, is calculated using the MG of the previous unstable scenario. Otherwise if the current scenario is unstable, the OMIB response of the previous scenario must be

recalculated using the MG of the current scenario. The simulation of the previous scenario must be resumed while applying the updated MG, and continued to ensure that the correct SIME margin is calculated. The limit prediction step will fail if:
1) the current scenario loses stability on a different swing to the last unstable scenario;
2) the next scenario is too stable for a valid stable margin estimate; or
3) the predicted limit falls outside the search bounds.

In the EBSIME algorithm limit prediction is less complicated since, for all scenarios, the OMIB responses are calculated from the same MG. Linear limit prediction is performed using the FS margins from the two most recently traversed scenarios, irrespective of whether they are stable or unstable. As with the SIME TSL search, the limit prediction can stall if a scenario is too stable for a SIME margin to be defined, or the search may diverge from the forward-swing limit (FSL) if the limit prediction is outside the search bounds.

6.1.7. Search Divergence from the Limit

If the SIME limit prediction step diverges from the TSL, the SIME TSL search uses tuned measures, based on past heuristic observations of the OMIB responses on the investigated system, to locate the next scenario [1, 95]. Although the SIME TSL search may rapidly locate the TSL, implementation of the limit prediction phase is strongly reliant on algorithmic tuning. It uses procedures to advance the search that are not documented in publically available literature.

For the EBSIME algorithm, if the linear prediction step diverges from the limit then bisection is used to determine the next search scenario. If search divergence occurs too often then the EBSIME algorithm will revert to a plain binary search to complete the TSL search.

6.1.8. Locating the Provisional TSL

The SIME limit prediction phase provides a provisional TSL when the distance between the search bounds falls below the search tolerance. The lower search bound is the limit since the SIME ESC is applied to assess multi-swing (in)stability. If $\delta_{\min}$ and K are correctly tuned then the provisional limit is the TSL, otherwise the provisional limit needs to be verified for transient stability.

The EBSIME algorithm returns a provisional limit at the end of the limit prediction search phase when the distance between the search bounds falls below the tolerance. The lower bound is the provisional FS stability limit. Alternatively, if an excessive number of bisection steps have been necessary due to search divergence, the EBSIME algorithm will revert to a plain binary search to ensure an accurate and robust solution to the search.

6.1.9. Confirmation of the Provisional Limit

If $\delta_{\min}$ and K are correctly tuned for the SIME TSA, then the provisional limit returned by the SIME search is the TSL. Otherwise, user-tuned decisions are required to locate the TSL.

If the EBSIME algorithm provides a provisional limit, it must be verified that the provisional limit is also the transient stability limit. This requires continuing the TDS of the provisional limit and the upper search bound, on exit, and assessing them using the COI-based criteria. If the provisional limit is transiently stable, and the upper search bound is transiently unstable then the provisional limit is the TSL.

Otherwise, the search must continue with a plain binary search for the actual TSL. Prior to continuing with the binary search the search bounds are updated by resuming the simulations of previous TDS. The aim is to verify a transiently stable scenario and an unstable scenario. This transition from the limit-prediction search phase to the plain-binary search is described in Chapter 7. Similar steps apply if excessive search divergence was encountered in the limit prediction phase, the lower FS search bound is treated as the provisional limit.

The TDS at the provisional limit is resumed first and rigorously assessed for transient stability using the COI-based stability criteria. When updating the search bounds there are three possibilities:

1) The provisional limit is transiently stable and:
   a) the upper search bound is unstable (the provisional limit is the TSL)
   b) the upper bound is FS unstable but actually transiently stable. This is concerning as the unstable SIME ESC contradicts the COI transient stability criteria. To locate a transiently unstable scenario, the TDS of previous FS unstable scenarios are continued and assessed for transient instability in order of increasing SV until a transiently unstable scenario is found.

2) The FS stable provisional limit is transiently unstable, indicating that the provisional limit becomes unstable on a subsequent swing. To locate a transiently stable scenario, the TDS of previous FS stable scenarios are continued and assessed for transient stability in order of decreasing SV.

For cases 1b) and 2a) the lower and upper bounds for the binary search are the stable scenario with the highest SV, and the unstable scenario with the lowest SV. The binary search continues the EBSIME TSL search, ending when the distance between the search-bounds of the binary-search falls below the search tolerance.

6.2. Chapter Conclusion

The SIME method proposes a fast and accurate method for TSA that does not require any simplification of a power system model. It defines forward- and multi-swing transient stability margins that can potentially be used to linearly predict the TSLs and accelerate the search. The fast TSA relies on search parameters tuned to the investigated power system to ensure a correct diagnosis of transient stability.

The automated SIME TSL search is composed of many search steps based on heuristic decisions and algorithmic tuning. The success of the search is dependent on factors that must be fine-tuned for each investigated network model, over a large range of operating conditions and contingencies. Tuning the algorithm is a computationally complex and time-consuming task due to the large amounts of data that must be simulated and assessed, especially for large complex power system models. These procedures are not documented publically.

A corollary is that there are too many unknowns in the SIME algorithm, as documented publically. Thus any attempt to implement SIME algorithm would be to re-invent it, and therefore impact on the algorithm's performance. Tuning and timing of the SIME TSL search depends on the network topology, the fault locations and operating conditions. The EBSIME algorithm does not have any such unknown heuristics that impact on the search algorithm's performance and robustness.

The EBSIME algorithm for TSL searching provides a fast, accurate and robust approach to TSL searching by adapting the strengths of the SIME method for TSL searching, and avoiding dependence on heuristic methods. This is achieved by using COI-based TSA criteria to choose the MG used to calculate the OMIB responses and SIME margins for all search scenarios. The SIME ESC and limit prediction are applied to accelerate the search. Divergence from the limit is handled by using bisection of the search bounds to advance to the next search step. If the EBSIME search diverges too often, or if multi-swing instability is the limiting factor, then the algorithm will revert to a binary search to accurately locate the TSL.

Chapter 7 The Enhanced Binary-SIME (EBSIME) Algorithm

This chapter introduces the EBSIME Algorithm for transient stability limit (TSL) searching. The EBSIME Algorithm provides a fast, flexible and robust approach to the TSL search and proposes potential enhancements to the standard SIME algorithm [1] and the plain binary search. The EBSIME algorithm is explained by example, to locate the critical fault-clearing time (CCT) of the IEEE two-area four-machine test system for a given operating condition. Emphasis is placed on integrating the method with a standard TDS program. The time-saving benefits and accuracy of the EBSIME search are compared against a plain binary-search. The potential online and offline applications of the proposed algorithm are outlined in Section 1.4.

7.1. Introduction to the EBSIME TSL Search

The SIME method provides a fast and flexible approach to estimating transient stability margins (TSM) and predicting transient stability limits (TSL) for multi-machine power systems. This is achieved by combining the features of time-domain methods and the Equal Area Criterion (EAC) [13]. A key feature of the SIME method [1], is that it employs fully detailed device and controller models in the analysis and does not make any simplifying assumptions. It is peripheral to the time-domain simulation (TDS) software and therefore has the potential to be implemented as an add-on to commonly used commercial transient stability packages without requiring access to, or modification of, the TDS source code. The limit and margin information it provides also make it useful for transient stability sensitivity analysis and control applications.

However, the original SIME method is prone to failure due to its dependence on algorithmic parameters that must be tuned for the power system under investigation. Furthermore, limit prediction using the SIME margins may cause divergence and thus search failure.

The EBSIME algorithm proposes an improvement to the SIME method for the TSL search. The proposed algorithm does not require any system- or fault-specific parameter tuning, and if the SIME limit prediction procedure fails to converge, bisection steps are employed to complete the search, ensuring that the correct limit is found. The search algorithm can be applied to search for both CCTs and PTLs. For TSL searching the EBSIME algorithm is superior to the binary as it robustly locates the limit with the same accuracy, but in a shorter search time.

In the following sections the EBSIME algorithm is explained using the example problem described in section 7.2. The superior performance of the EBSIME algorithm is compared against that of a standard binary-search. It is not possible to compare the performance of the EBSIME method against the SIME method, due to the latter's dependence on parameter tuning. Transient stability sensitivity analysis (TSSA) using the acquired margins are demonstrated at the end of the chapter.

7.2. Example: Problem Definition

The EBSIME method for TSL searching is demonstrated on the IEEE 2-Area 4-machine system model [13, 91] in Figure 6-1. In the base-line operating condition 200MW is transferred from area 1 to area 2, and the system frequency is 50Hz. A 3 phase fault is applied to the node 7 end of circuit #1 between buses 7 and 8. The fault is cleared by simultaneously opening the breakers at both ends of circuit #1. Governors are not

represented in the example, and the SVC is disconnected. The objective is to determine the CCT for this case using the EBSIME search, thus the transient stability search variable (SV) is the fault clearing time (CT). The methodology can be extended to a search for the PTL where the SV is the power transfer (PT). The system includes power system stabilizers and AVR controls on each generator. The system parameters and controls are given in Appendix C. The two-machine system investigated in Chapters 4 and 5 is based on this model.

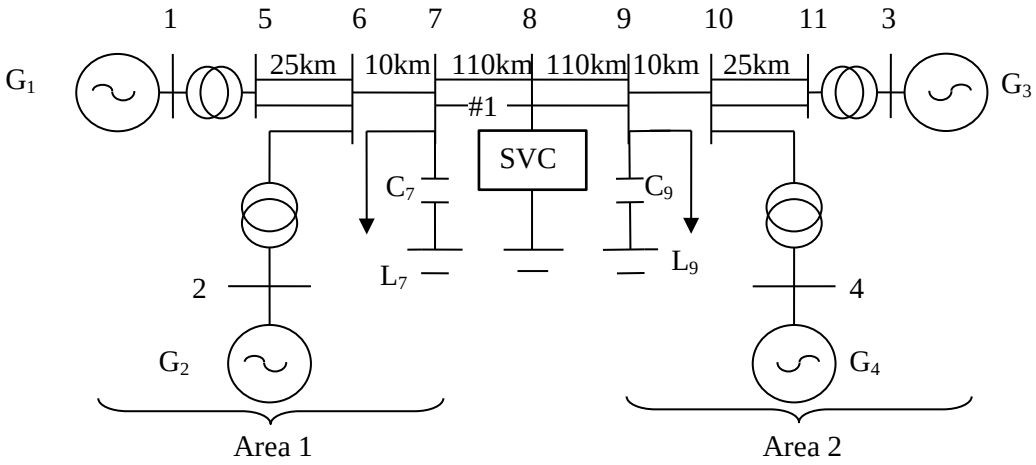

Figure 7-1. The 2-Area 4-machine system.

7.3. Overview of the EBSIME TSL Search

The EBSIME TSL search combines the best features of the SIME and binary-search methods. The SIME method reduces the search simulation time, without requiring any model reduction, by applying the forward-swing early stop criteria (ESC) for transient stability assessment (TSA). Furthermore it applies the approximately linear relationship between the SIME stability margins and SV, to accelerate convergence to the limit. The binary-search component ensures the success of the limit search by selecting a suitable starting point for the iterative limit prediction procedure and intervening to complete the search if SIME based limit prediction causes divergence. An overview of the EBSIME TSL search is shown in Figure 7-2.

The two principle stages of the EBSIME algorithm are the forward-swing stability limit (FSL) search (Figure 7-2, step 1) and the multi-swing transient stability limit (MSL) search (Figure 7-2, step 2b). The latter is required if TDS reveal that the FSL is multi-swing unstable (Figure 7-2, step 2a); if the FSL search tolerance is reached yet the upper search bound is multi-swing stable, or if the FSL phase of the search diverges. The procedure to perform a MSL search is included in Figure 7-2. Step 1 of the FSL search is described in Figure 7-3 and Figure 7-4.

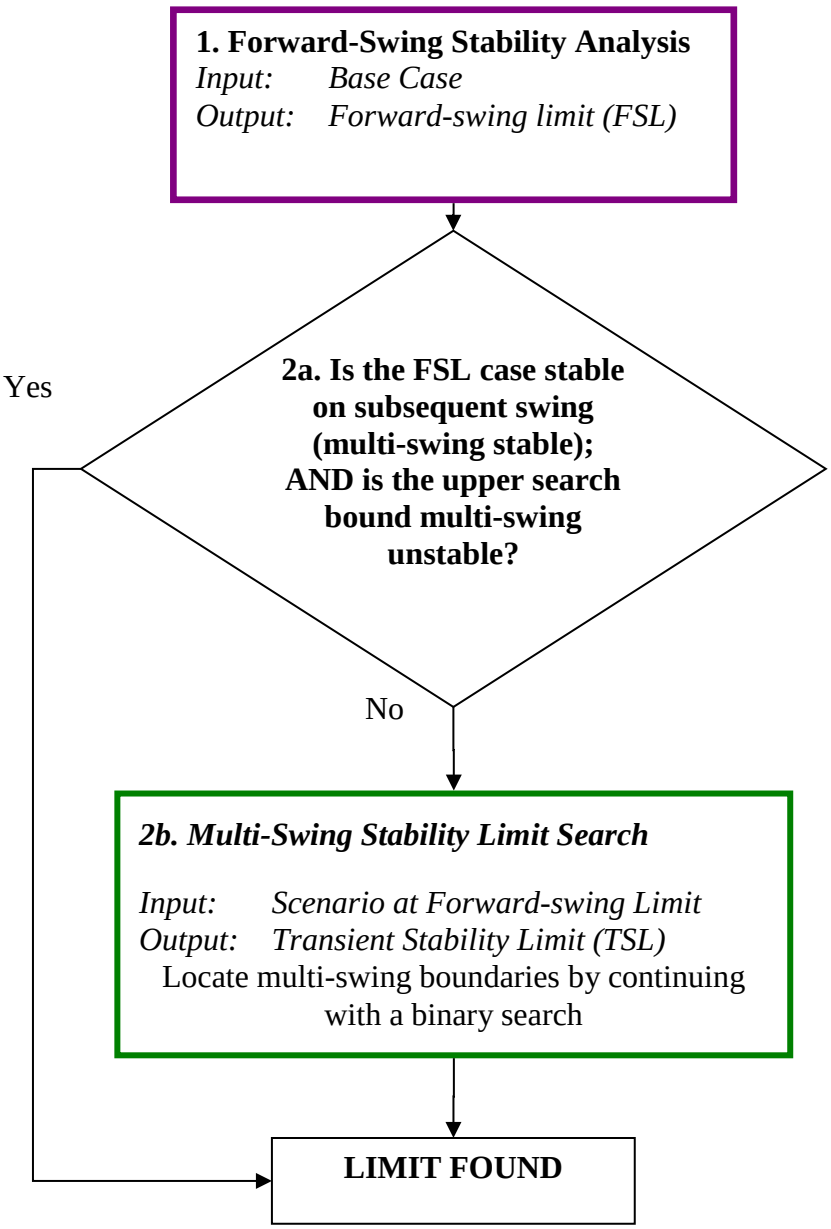

Figure 7-2. Overview of the EBSIME search algorithm for the TSL search

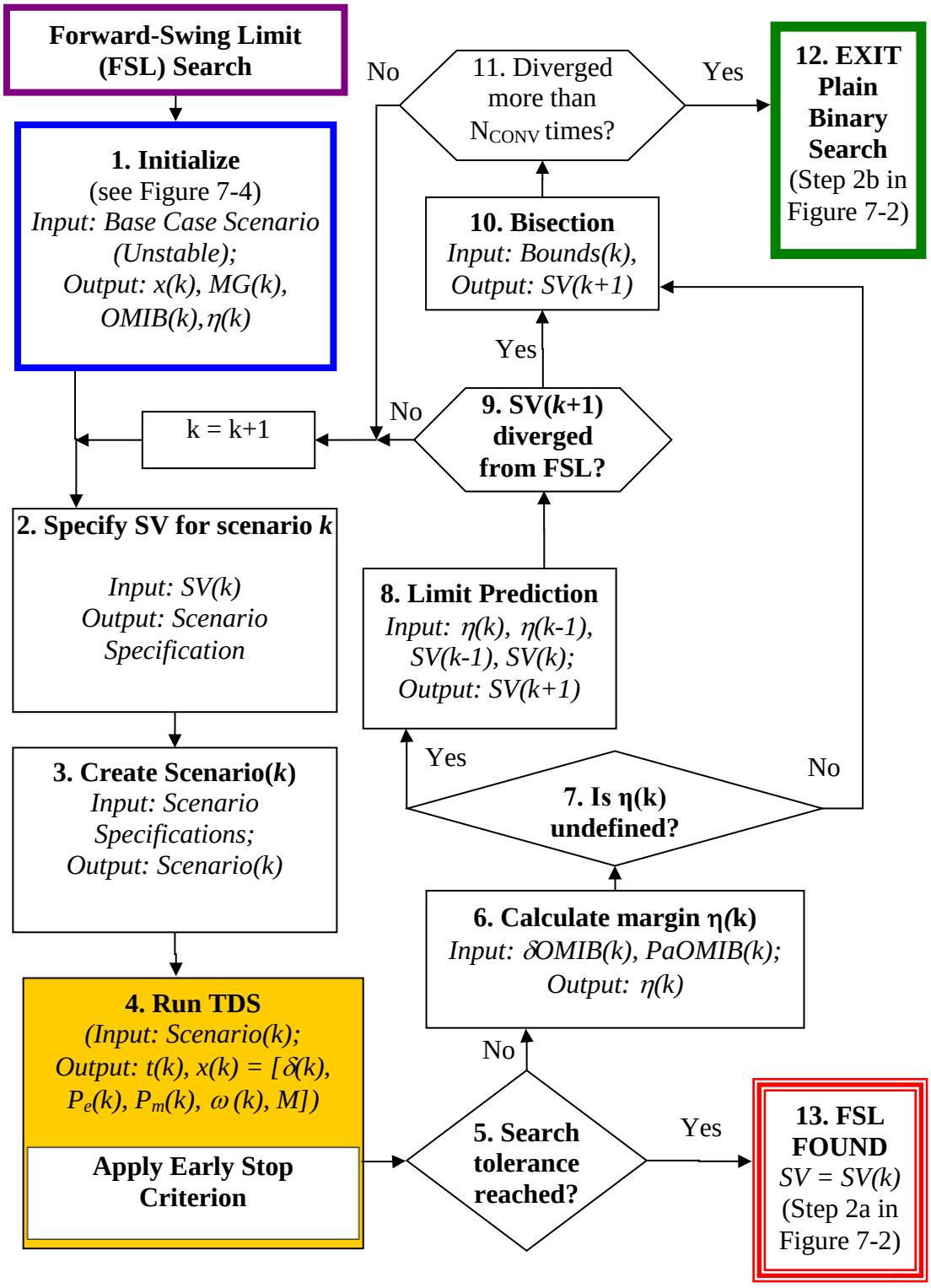

Figure 7-3. Core elements of the EBSIME Search Algorithm for the TSL Search. The search variable (SV) is either clearing time (CT) or power transfer (PT)

7.4. Initialization of the EBSIME TSL Search

The aim of the FSL search initialization procedure is to select the first unstable scenario that can be used for the iterative FSL prediction search phase. Initialization is represented at step 1 of Figure 7-3. The entire initialization procedure is described in Figure 7-4, commencing at Step 1A where the first scenario with the SV at the upper search bound is assessed. A TDS (Step 1B of Figure 7-4) is conducted and instability is detected by applying the COI criteria. A criterion of the desired first scenario is that it must be unstable (Step 1C of Figure 7-4). If instead the first scenario is stable then the search must be restarted with a larger upper search bound.

Bisection is defined as a method of determining the SV for the next search scenario to be considered. If the current search scenario is identified as transiently stable, bisection returns the middle-point between the current SV and the upper search bound. Otherwise if the scenario is identified as unstable, then bisection yields the mid-point between the lower search bound and the current SV.

Bisection is used to determine the starting scenario. For the example described in section 7.2, an initial CT of 500ms is chosen; it is assumed that the system is stable with a CT of 0ms. The latter assumption is expected to be correct in the vast majority of cases. However, if it is incorrect the algorithm will still succeed in identifying whether the system is inherently unstable.

7.4.1. Determination of the Machine Group from the Initial Scenario

The SIME approach is based on the assumption that loss of synchronism is caused by the irrevocable angular separation of a system into two groups of machines (MG) [1]. The MG is needed to calculate the OMIB response for each search scenario. Then the SIME ESC can be applied to the TDS for fast assessment of forward-swing stability.

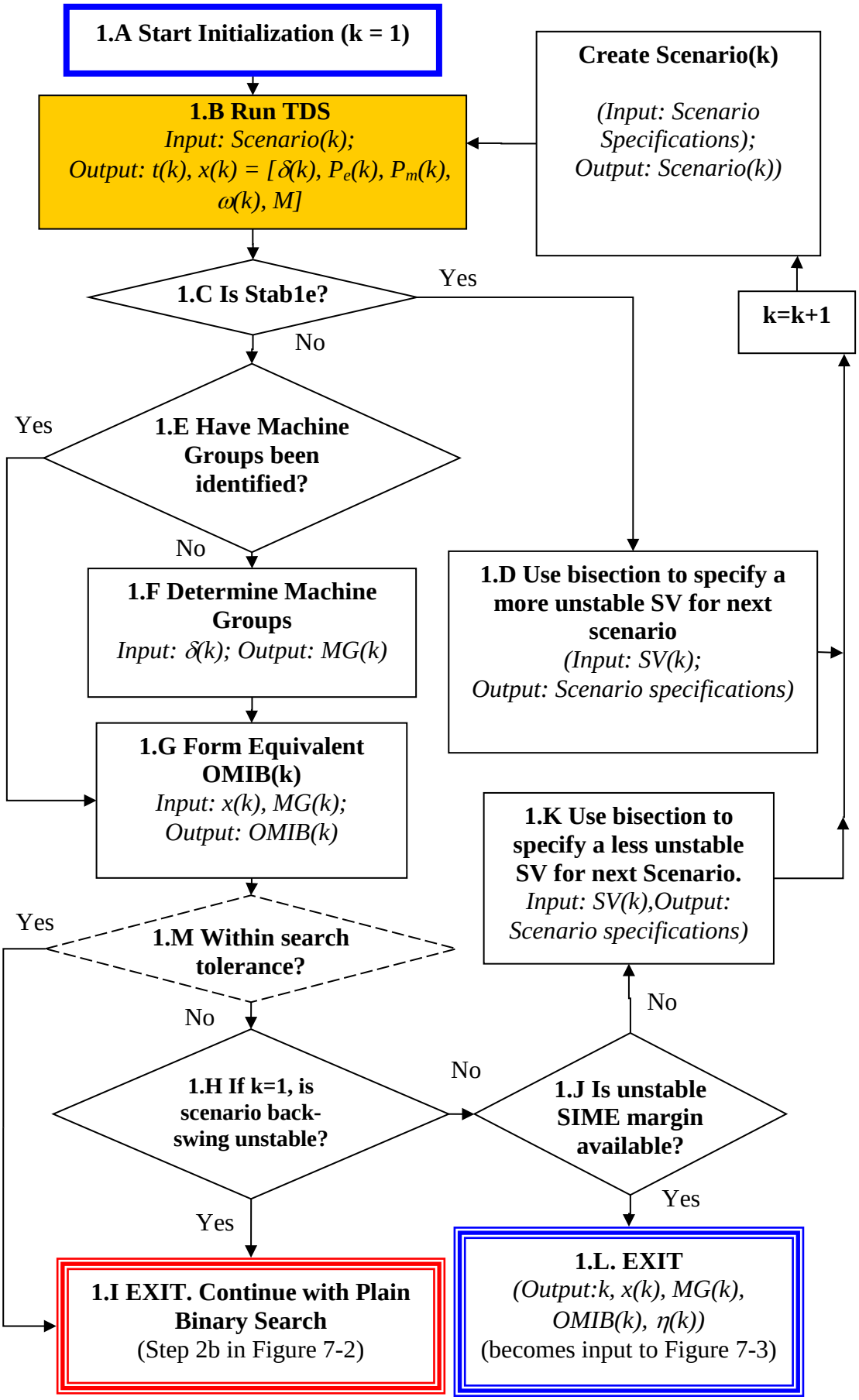

Figure 7-4. The initialization phase of the EBSIME search algorithm for transient stability limit searching. Step 1 in Figure 7-3.

In the EBSIME algorithm the MG is determined from the first unstable search scenario using the following procedure. In this scenario the MG is identified at the instant, $t=t_{obs}$, when transient instability is identified by the COI stability criteria. At $t = t_{obs}$ the machine angles are arranged in descending order [97]

$$\delta_i > \delta_{i+1},\ i = 1,...N-1 \tag{7.1}$$

where δ_i is associated with machine $m(i)$,

and N is the number of online machines.

The difference between adjacent machine angles is $\Delta\delta_i = \delta_{i+1} \geq 0,$ (7.2).

j is found such that $\Delta\delta_j = \max(\Delta\delta_i)$ (7.3)

Then, the machines in group 1 are:

$$G_1 = \{m(1),...m(j)\} \tag{7.4}$$

and in group 2:

$$G_2 = \{m(j+1),...m(N)\} \tag{7.5}.$$

Figure 7-5 demonstrates the MG selected for the example in Figure 6-1.

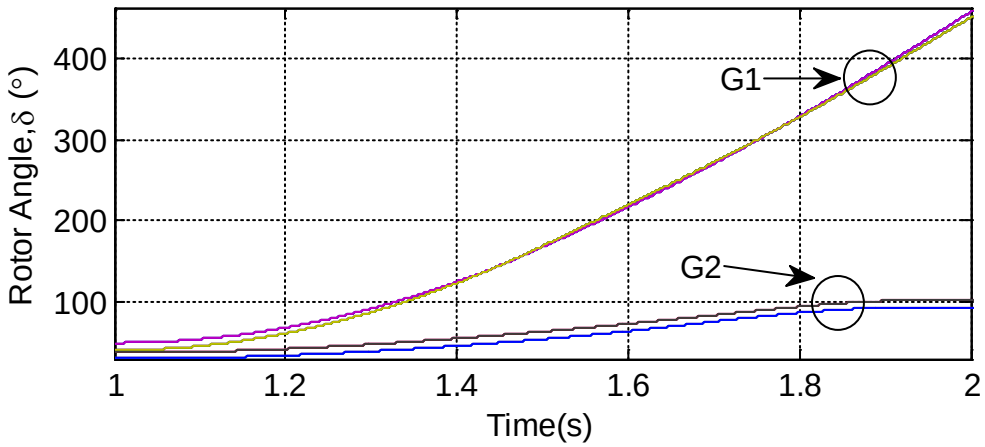

Figure 7-5: EBSIME algorithm: the MG are determined from the first unstable scenario

As indicated in step 1E of Figure 7-4 the same MG is used for all subsequent SIME calculations throughout the entire search. By using the same MG the margins that are calculated for all scenarios, whether stable or unstable, are compatible for limit prediction and for sensitivity analysis applications.

This differs from the SIME method for the TSL search where different MG may potentially be calculated for each unstable scenario, and TSA is dependent on the tuned parameters K and $\delta_{\min}$ (see Table 6-1). THE EBSIME algorithm handles this situation by avoiding the use of tuned parameters, and only using the MG identified during search initialization.

7.4.2. Forming the Equivalent OMIB Responses

Once the MG are identified the OMIB response for the first unstable scenario can be calculated using the COI equations (see section 2.1.3) and the SIME equations (see section 4.3). This is indicated at step 1G of Figure 7-4. For all subsequent scenarios the OMIB response may be calculated coincidentally with the TDS at each time-step. This enables the SIME ESC to optionally be applied to accelerate the search during the initial and limit prediction search phases.

7.4.3. Handling the Identification of Back-Swing Mechanism of Instability

As Chapter 5 explains, for scenarios where the power system tends to be constrained by back-swing instability, the SIME ESC will provide a misleading transient stability assessment. In this situation the SIME ESC will classify all such scenarios as forward-swing stable irrespective of whether it is transiently stable or unstable.

In step 1H of Figure 7-4 it is known that the system is unstable. A test is performed to determine if the system is unstable according to the ESC. If not then it must be that the system becomes unstable either on the back-swing or on a subsequent swing. Under this condition the EBSIME algorithm will revert to a plain binary search, using bisection to determine the next SV as in step 1I in Figure 7-4.

Otherwise the search initialization will continue. If any ensuing scenarios happen to be constrained by back-swing instability the EBSIME algorithm will still return a robust and accurate result, as it reverts to a plain binary search at the end of the EBSIME search (step 2b in Figure 7-2).

7.4.4. Choosing the First Search Scenario for the Limit Prediction Procedure

The third purpose of the initialization is to identify a scenario that can be used for the SIME limit prediction. The requirements for this scenario are that it must be forward-swing unstable for which a SIME stability margin can be determined. The first search scenario to satisfy this criteria (step 1J in Figure 7-4) will cause initialization to end at step 1L in Figure 7-4. Otherwise bisection is used to locate the first unstable scenario that satisfies the initialization criteria (step 1K in Figure 7-4).

For the example Figure 7-6 shows that the first search scenario, where CT is 500ms, is too unstable to define a SIME margin because the deceleration area is zero.

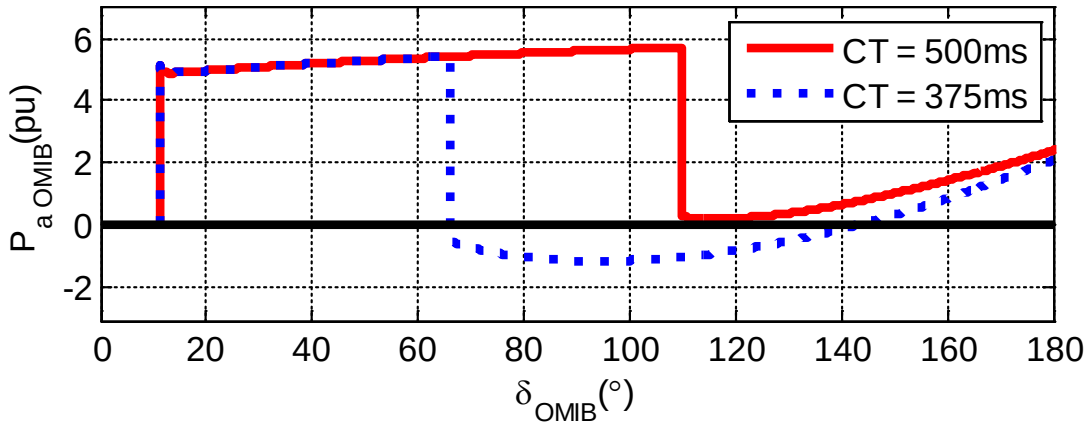

Figure 7-6. $P_{aOMIB} - \delta_{OMIB}$ characteristic for the unstable scenarios where the SIME margin is defined for CT=375ms, and undefined for CT = 500ms.

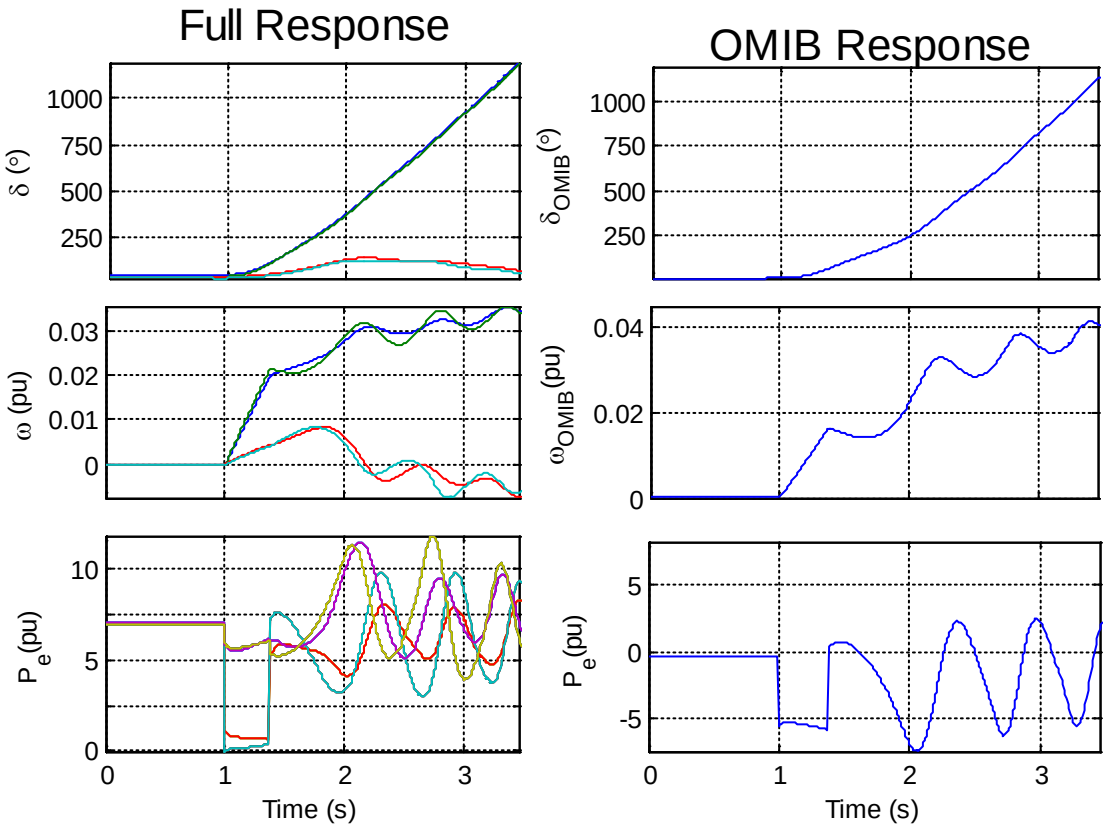

Figure 7-7. Full system and equivalent OMIB responses for rotor angle, speed deviation and electrical power, when the CT is 375ms

Bisection is used to obtain the CT of (0 + 500)/2 = 250ms for the next scenario (step 1K in Figure 7-4). However, TDS shows this scenario is stable and is thus unsuitable. The next selected scenario has a CT of (250 + 500)/2 = 375ms. Figure 7-6 shows that the acceleration power of this unstable scenario drops below zero and thus it is possible to

calculate the unstable SIME margin. This is an acceptable starting point. The OMIB characteristics for the starting scenario are shown in Figure 7-7.

If a suitable initial search scenario cannot be identified before the search tolerance is reached the algorithm then the FSL has been found during the initialization phase and the algorithm reverts to the plain binary search to confirm this is the actual TSL. This is indicated in step 1M in Figure 7-4 .

7.4.5. Calculating the Forward-Swing Unstable Margin

When the first satisfactory unstable scenario is found the corresponding unstable SIME margin can be determined by applying equation (2.25) to the OMIB acceleration-power angle curve (step 1L in Figure 7-4). The calculated margin is normalized by dividing it by the OMIB machine inertia constant, M, to make it independent of the system generation capacity [1]. The margin for CT=375ms is $\eta(3) = -0.03335$ *pu-rad* .

7.5. Iterative Search Procedure

The iterative part of the EBSIME algorithm is shown in Figure 7-3, steps 2 to 11. The aim of this procedure is to locate the FSL by iteratively applying linear extrapolation or interpolation with pairs of SIME margins to estimate the limiting value of the SV. In the example the SVC is the fault clearing time, CT. The FSL is found when the search satisfies the convergence criteria described in section 7.5.8. If the iterative part of the search diverges from the FSL, then bisection is used to determine the SV for the next scenario and continue the search.

If the next estimate of the limit falls outside of the current FS search bounds then bisection is used to determine the SV for the next scenario. This provides a robust guard against divergence of the search.

7.5.1. Calculating the Value of the Search Variable (SV)

After the initial SIME scenario has been located bisection is used to locate the second search scenario. This is shown in Figure 7-3 step 2. In the example problem, the next scenario has a CT of (375 + 250)/2 = 313ms. For all subsequent scenarios SIME limit prediction is used to locate the next search operating condition, unless the next predicted value of the SV is outside of the current search bounds, or the FSL is found.

7.5.2. Assessing the TDS with the SIME Early Stop Criteria

For each successive search scenario a solved load flow and TDS are required (steps 3 & 4 in Figure 7-3). The SIME ESC are applied to accelerate the search by reducing the scenario simulation time. To apply the SIME ESC, the SIME method must be implemented with the TDS software to calculate the equivalent OMIB response at each time step of the TDS.

7.5.3. Forward-Swing Assessment of an Unstable Scenario

For the example problem when the ESC is applied to the scenario with a CT of 313ms, the scenario is found to be unstable at 0.57 simulation seconds (sim-s) after the applied fault. This is shorter than the simulation time required by the COI instability criterion which detects instability 1.27 sim-s after the fault.

7.5.4. Limit Prediction Where the Current Search Scenario is Unstable

The CCT or PTL is predicted by linear interpolation or extrapolation using the TSMs $\eta(k)$ and $\eta(k-1)$. The relationship of the forward-swing margin to CT or PT is approximately linear. In the example the margins corresponding to CTs of 313ms and 375ms provide an estimated CCT of 286ms, as shown in Figure 7-8.

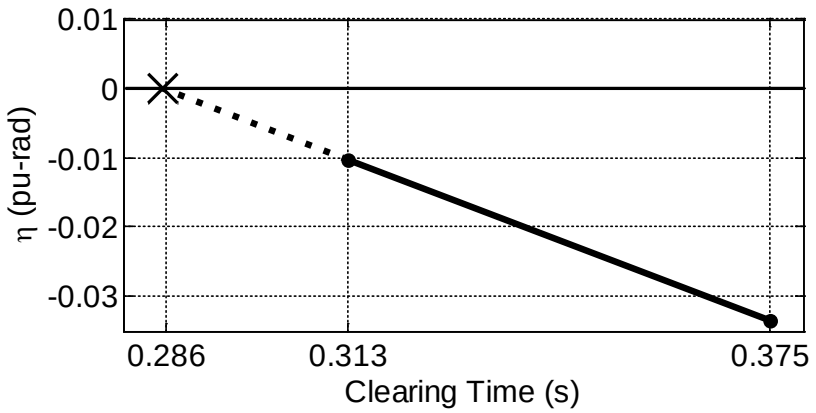

Figure 7-8. The SIME margins corresponding to the scenarios with CT of 313ms and 375ms are used to predict the CCT.

7.5.5. Forward-Swing Assessment of a Stable Scenario

Performing steps 3 to 8 of Figure 7-3 the scenario with CT at 286ms proves to be forward-swing stable. The stable margin is the shaded area in Figure 7-9. It is not

possible to calculate this area by using actual data; rather the unused deceleration area is approximated with a quadratic function [98]. It is possible for a scenario to be too stable to produce a reliable margin measure (Figure 7-3, step 7). In such circumstances bisection should be applied to locate the next SV.

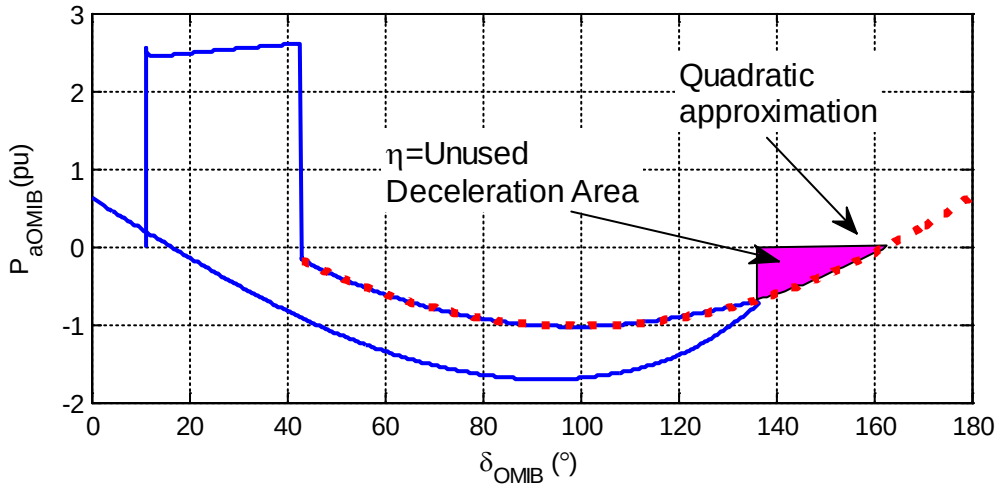

Figure 7-9. The OMIB power angle response for a stable scenario where CT = 286ms.

7.5.6. Limit Prediction When the Current Search Scenario is Stable

The margin of the current stable scenario, *k*, is used together with the most recent scenario that has a defined margin (usually scenario *k*-1) to linearly predict the limit. The other scenario may be either stable or unstable.

7.5.7. Handling Divergence from the Forward-Swing Limit

On some occasions the EBSIME search may stall due to the next search step diverging from the FSL (step 9 in Figure 7-3). For example, the predicted limit may occur on or outside of the current search bounds. In such situations the next SV is determined by bisection (step 9 in Figure 7-3). If the predicted limit diverges more than a prescribed number of times, N_{conv}, then the iteration phase of the search will end and the search will continue with a plain binary-search for the multi-swing stability limit (MSL). While N_{conv} may influence the total search time, the EBSIME search will return a robust solution, irrespective of this value. In this thesis $N_{conv} = 3$ is used.

7.5.8. Determining Convergence to the Forward-Swing Limit

The FSL can be identified by repeating steps 2 to 11 in Figure 7-3. As indicated in Figure 7-3 steps 5 and 13, the iterative part of the search ends when the difference between the upper and lower search bounds, falls within the search tolerance.
If this condition is satisfied then the TDS of the current scenario must be continued and tested for multi-swing instability, against the COI stability criteria. In the example, the FSL is identified at 290ms. When the TDS is continued, the COI criteria confirms that it is also multi-swing stable to the prescribed maximum simulation time. Typically the prescribed simulation time for assessing transient stability is 10 to 20 seconds.

7.6. Multi-Swing Stability Limit (MSL) Search Phase

The EBSIME algorithm will commence the MSL search phase if:

1) a suitable scenario to commence the limit-prediction procedure cannot be identified during the initialization
2) during the FSL search phase it is found that the limit prediction falls outside of the current search bounds more than the prescribed number of times, Nconv
3) the provisional FSL is found.

When the MSL search phase is required the EBSIME algorithm continues with a plain binary search to ensure a robust solution for the actual TSL. This referred to as the residual binary search.

7.6.1. Initializing the Search Bounds for the MSL Search Phase

Prior to commencing the binary search for the MSL, the search bounds must be updated to identify a multi-swing stable lower-bound scenario and an unstable upper-bound scenario. After they are identified the MSL search phase can continue. The search bounds are established by continuing the TDS of scenarios that were simulated during the FSL search phase. The following iterative procedure, to initialize the MSL search bounds, is depicted in Figure 7-10:

Step 1. Consider the lower search bound when the FSL search phase has ended at scenario $k=k_n$, where n is the iteration number corresponding to the scenario. Scenario k is the FS stable scenario with the highest SV. Resume the TDS of this scenario and assess transient stability using the COI stability criteria.

Step 2a) If scenario k is multi-swing stable, then the SV is the lower search bound, otherwise

Step 2b) the SV is the upper search bound.

For step 2a) an upper bound remains to be found. To locate it the lowest SV identified as FS unstable during the FSL search phase is resumed, and transient stability is assessed using the COI stability criteria. If scenario k is transiently unstable then the corresponding SV is the upper bound (UB). Otherwise if scenario k is multi-swing stable then the lower bound (LB) is updated to the value of the corresponding SV, $k = k + 1$ and step 2a is repeated. If all scenarios are identified as multi-swing stable then the upper search bound is the same as its initial value at the start of the EBSIME search (i.e. 500ms).

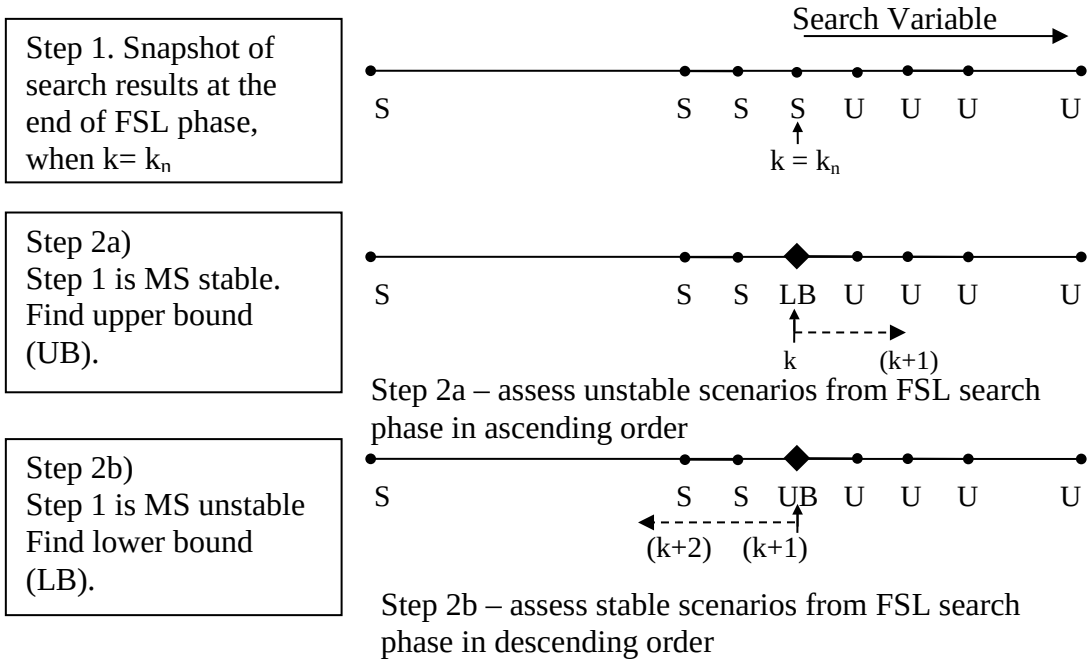

Figure 7-10. The procedure to initialize the search bounds for the MSL search phase, where LB = lower bound, and UB = upper bound, S=FS stable scenario, U = FS unstable scenario.

If the FSL is unstable on a subsequent swing then step 2b) is required, and the lower search bound remains to be found. To locate it the TDS of the FS stable scenario with the highest SV is continued, and transient stability is assessed using the COI stability criteria. If the TDS is multi-swing stable then the lower bound is set to the value of the SV. Otherwise, the upper search bound is assigned the value of the corresponding SV at $k = k + 1$ and step 2b is repeated. If all stable scenarios from the FSL search phase are identified as multi-swing unstable then the lower bound is set to the initial value from the start of the search (i.e. 0 ms).

The aim of this procedure is to minimize the total simulation time required for the remaining search by using scenarios that have been partly simulated during the FSL search phase. The binary-search for the MSL commences when the procedure to update the binary search bounds is complete.

7.7. Application of the EBSIME TSL Search to a Four Machine System

The following sections provide an example of the EBSIME algorithm, applied to the example problem defined in section 7.2. The total simulation time (TSIM) is compared against that of a plain binary search.

Table 7-1 summarizes the search traversal of the EBSIME algorithm when it is applied to locate the CCT for the example problem. In the table, *k* is the search scenario number, and TSIM describes the time taken to assess the transient stability of each scenario in simulation seconds (sim-s). TSIM includes a 1s run-in period for each traversed scenario prior to the fault application.

Search initialization occurs in steps 1 and 2 of Table 7-1. The iterative limit prediction phase occurs in steps 3 to 7. At step 7 the distance between the search bounds falls within the 2ms search tolerance, and the FSL is identified as CT = 290ms.

At the end of the FSL search scenario k=7 with CT = 290ms is the lower search bound, and k=6 is the upper search bound with CT = 292ms. To identify the initial search bounds for the MSL search bounds the TDS for k=7 is resumed. The COI stability criteria assesses this scenario to be multi-swing stable, the lower search bound is identified as 290ms (as per step 2a in 7.6.1).

At step 8, the TDS for k=6, the scenario corresponding to the upper search bound at the end of the FSL search, CT = 292ms, is resumed (as per step 2a described in section 7.6.1). The COI-based stability criterion verifies this scenario to be MS unstable therefore 292ms is the initial upper MSL search bound. Since the difference between the initial MSL search bounds is within the 2ms search tolerance, the EBSIME search ends, identifying the actual transient stability limit as CT = 290ms.

Figure 7-11 compares the convergence of the EBSIME algorithm to locate the CCT of 290ms with that of a plain binary search. Both approaches use a search tolerance of 2ms. In the EBSIME algorithm the SIME ESC is applied during both the initialization

and limit prediction phased. The search concludes when the distance between the upper and lower search bounds falls below 2ms. Scenario 7 is verified as multi-swing stable as the system machines remain synchronized following the full 10s simulation period. The binary-search is completed in 47.9 sim-s. The EBSIME search is completed in 22.77 sim-s, 52% faster than the binary-search.

TABLE 7-1 EBSIME CCT SEARCH FOR THE EXAMPLE PROBLEM IN SECTION 7.2 WHERE 200MW POWER IS TRANSFERRED FROM AREA 1 TO 2

k	CT(k) (ms)	η(k) (rad-pu)	η(k-1) (rad-pu)	Predicted CCT(k) (ms)	TSIM (sim-s)	Search Bounds		Comment
						Lower (ms)	Upper (ms)	
1	500	>0	-	-	1.98	0	500	Too unstable; bisection step to obtain CT = 250ms.
2	250	>0	-	-	1.82	250	500	Scenario found to be FS stable by ESC; bisection step to obtain CT = 375ms.
3	375	-0.03335	-	-	1.66	250	375	Bisection step to obtain CT = 313ms.
4	313	-0.01022	-0.03335	286	1.88	250	313	1st SIME step
5	286	0.00179	-0.01022	292	2.13	286	313	2nd SIME step
6	292	-0.00193	0.00179	290	2.32	286	292	3rd SIME step
7	290	0.00063	-0.0020	290	2.35	290	292	4th SIME step
FSL found at 290ms. Initialize search bounds for the binary search to locate the MSL.								
7	290	-	-	-	7.65	290	500	Continue simulation k=7, with COI stability assessment
8	292	-	-	-	3.33	290	292	Continue simulation k=6 with COI stability assessment
Multi-swing limit found at 290ms								
Total simulation time (sim-s)					22.77			

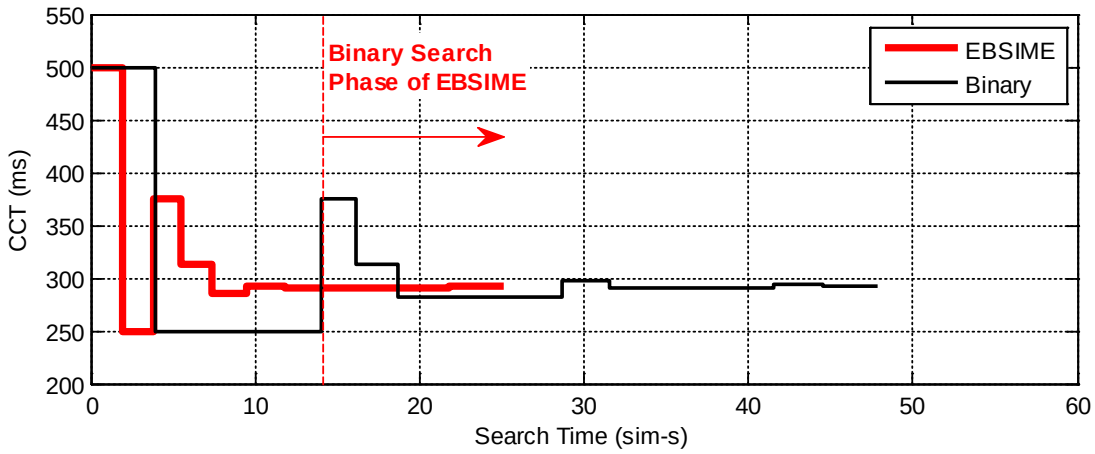

Figure 7-11. Convergence of the Binary and EBSIME searches towards the CCT of 290ms for the section 7.2 problem, where 200MW power is transferred from area 1 to 2

7.8. Performance of the EBSIME Search on the Four Machine System

Table 7-2 compares the performance of the plain binary search and the EBSIME algorithm for a range of operating conditions on the IEEE 4-machine system operating at 50Hz. The results include the total simulation time of each search, as well as the identified CCTs. For all of the investigated operating conditions a contingency is applied at the sending-end of the long transmission line (node 7) only. In cases 8 to 11 governors are connected to each of the generators to regulate the mechanical input power and speed. The SVC and governor control models are given in Appendix C.

The application of a three-phase fault at the receiving-end of the transmission line (i.e. node 9) was considered. However as discussed in chapter 5 this operating condition tends to be constrained by back-swing instability. Under these conditions, it is difficult to locate a scenario with a valid forward-swing unstable SIME margin during the search initialization. The SIME ESC will tend to classify back-swing constrained scenarios as "too stable". Under these circumstances bisection is used to complete the TSL search, and the EBSIME search is essentially the same as a binary search. While the EAC may potentially be extended to estimate margins for back-swing instability they are not investigated in this thesis.

TABLE 7-2. PERFORMANCE OF THE EBSIME ALGORITHM AND A BINARY SEARCH FOR THE CCT FOR VARIOUS OPERATING CONDITIONS (FAULTS AT SENDING-END)

Case No.	Power Transfer (MW)	Description (relative to BASE CASE)	EBSIME search		Standard Binary-search		$\frac{TSIM\ EBSIME}{TSIM\ Binary}$
			TSIM (sim-s)	CCT (ms)	TSIM (sim-s)	CCT (ms)	
1	100**	Vary Power transfer	88.5	337	62.8	337	1.42
2	200	BASE CASE	22.8	290	49.7	290	0.44
3	300	Vary Power transfer	28.7	234	70	233	0.41
4	400	Vary Power transfer	24.9	172	60.6	171	0.41
5	100**	200 MVar SVC at bus 8	34.3	340	67.3	339	0.51
6	200	200 MVar SVC at bus 8	22.8	296	61.8	296	0.37
7	300	200 MVar SVC at bus 8	23.0	242	62.9	243	0.37
8	100	Governors on	21.6	367	70.2	366	0.31
9	200	Governors on	19.1	308	63.0	308	0.30
10	300	Governors on	21.1	251	33.1	250	0.64
11	400	Governors on	22.8	185	68.1	185	0.33
12	200	90% of base load	23.1	326	55.2	325	0.42
13	200	80% of base load	24.8	364	62.9	364	0.39
14	200	70% of base load	23.1	406	48.0	407	0.48
15	200**	Half Line Length	75.1*	401	76.1	401	0.99
16	200**	2 x Line Length	38.2*	158	43.7	157	0.87
*Search diverged from the FSL, so EBSIME method completed with binary search. **System operation is constrained by multi-swing transient instability.							

7.8.1. Performance of the EBSIME Algorithm for the Investigated Cases

All cases, except for 1, 5 and 15 in Table 7-2 are constrained by forward-swing instability. Case 9 features the greatest improvement in search time, where the EBSIME algorithm takes 30% of the time of the binary search to locate the TSL. On average the EBSIME algorithm is 46% faster than the binary search.

For the cases constrained by forward-swing instability, the EBSIME search is fast. This is because at the end the FSL search phase only two scenarios, the lower and upper

search bound, need to be resumed and assessed by the COI stability criteria to verify the TSL.

The EBSIME algorithm is significantly faster than the binary search for all cases except 1 and 15 in Table 7-2. For both cases the system operation is constrained by transient instability on the second (forward) power-swing after fault clearance when the area 1 machines accelerate ahead of the area 2 machines.

Case 1 demonstrates the worst performance for the EBSIME search. The EBSIME algorithm quickly locates the FSL at 345ms within 14.72 sim-s, however the FSL is transiently unstable when assessed by the COI criteria. The actual CCT is 8ms lower at CT=337ms. An additional 17.88 sim-s are required to update the lower and upper search bounds for the MSL search phase - 250ms and 340ms respectively. The remaining binary search takes 55.85 sim-s. Five additional stable scenarios and one unstable scenario are run during the binary search causing the lengthy search time.

In case 15, the FSL search phase diverges from the CCT thrice. After 14.29 sim-s the EBSIME algorithm reverts to a binary search. It takes 13.62 sim-s to update the initial lower and upper search bounds -375ms and 438ms respectively – prior to commencing the binary search phase. The remaining binary search takes 47.18 sim-s, 30 sim-s are due to for 3 stable scenarios, and 17.18 sim-s for 2 marginally unstable scenarios.

If a scenario is subject to multi-swing instability this does not imply that the EBSIME search will take longer than a plain binary search. In case 5 the system operation is constrained by second-swing instability, but the EBSIME search takes half as long as the plain binary search. In the EBSIME search the FSL is 346ms and is located within 12.6 sim-s. It takes 11 sim-s to update the lower and upper search bounds of 340ms and 346ms. Then the remaining binary search takes 10.7 sim-s. In case 5 the EBSIME TSL search is faster as more unstable scenarios are traversed during the final binary search phase. Importantly the EBSIME algorithm converges to the TSL.

7.8.2. Performance of the EBSIME Algorithm for TSL Searching

The advantages and disadvantages of the EBSIME algorithm for TSL searching, as determined from the investigations on the 4-machine power system, are summarized in Table 7-3 and Table 7-4.

TABLE 7-3. ADVANTAGES OF THE EBSIME ALGORITHM FOR TSL SEARCHING

Characteristic	Advantage
Tuned parameters not required for transient stability assessment (TSA)	Transient stability is assessed by 1) the SIME ESC during the initialization and FSL prediction phases; and 2) the COI transient (in)stability criteria for the initial scenario, and in the binary search. Both methods of TSA do not use tuned parameters to verify transient stability. Application of the COI stability criteria at the end of the search ensures that MS instability is considered, and thus the actual TSL is located.
Robust	Bisection of the search bounds is used to redirect the EBSIME search: when the SIME limit prediction diverges from the FSL, and if the FSL is not the actual TSL. This consistent approaches means that heuristic measures are not required when the search diverges, and that the search will advance until the TSL is accurately located.
Tuned parameters not required to end the search	The FSL search phase and the binary search both end when the distance between the SV search bounds falls below the search tolerance. The EBSIME avoids the use of search parameters that must be tuned, such as a threshold SIME margin, to end the search.
Faster search	On the 4 machine power system, where the system operation is constrained by FS instability, the EBSIME algorithm is 30% to 70% faster than the plain binary search. The EBSIME algorithm can also provide significant time savings for system operation that is constrained by MS instability, as demonstrated by cases 5 and 15 in Table 7-2.
The same set of machine groups (MG) throughout the search	The EBSIME algorithm uses one MG throughout the entire search allows the SIME margins from any pair of scenarios to be used for limit prediction, thereby accelerating the search. Furthermore, it is then possible for the calculated margins to be used for transient stability sensitivity analysis and control applications.

TABLE 7-4. DISADVANTAGES OF THE EBSIME ALGORITHM FOR TSL SEARCHING

Characteristic	Disadvantage
Back-swing instability	If the system operation is constrained by back-swing instability, then the EBSIME algorithm cannot identify a scenario with an unstable SIME margin to commence the limit prediction phase. In this situation, the EBSIME search is the same as the binary search.
Search delays	If the system operation is constrained by multi-swing transient instability, the EBSIME algorithm may take longer than the plain binary-search to locate the TSL. If the TSL is less than but close to the FSL, the additional stable scenarios will lengthen the search simulation time. However, the additional search time is small in comparison to the time savings that can be achieved over a range of operating conditions and contingencies.

7.9. Application to Transient Stability Sensitivity Analysis (TSSA)

The EBSIME algorithm can be applied to perform TSSA, and is demonstrated on the IEEE four-machine network model. The SIME margins generated by the EBSIME algorithm are used to investigate the sensitivity of the CCTs to the parameters listed in column 1 of Table 7-5. The TSSA shows the useful auxiliary insights that the EBSIME algorithm can provide. The sensitivity data is taken from the limit searches in Table 7-2.

TABLE 7-5. FACTORS INVESTIGATED IN THE TRANSIENT STABILITY SENSITIVITY ANALYSIS

Varied Parameter (Column 1)	Investigated Parameter Values (variations from the base case) (Column 2)
Power transfer (from area 1 to area 2)	100MW, 300MW, 400MW
SVC	The 200MVar SVC at node is either on or off-line
Governor	The generator governors are connected
Total active load	90%, 80%, 70% of base load
Transmission line length between buses 7 & 9	Half or double the base length

7.9.1. Transient Stability Senstivity Analysis Methodology

The example problem definition in section 7.2 is the base-scenario for the TSSA. The following method is used to relate the sensitivity of CCTs to variations in the investigated system parameters:

1) Adjust the load flow from the base scenario to reflect the investigated parameter value(s). In general, one parameter value is varied per investigation, however in some studies two parameters are varied.
2) Solve the load flow for the investigated case.
3) Use the EBSIME algorithm to obtain the SIME margins and to search for the CCT corresponding to the solved load flow
4) Repeat steps 1 to 3 for each investigated parameter value in column 2 of Table 7-5.

For each investigated parameter value the SIME margins are plotted as a function of the fault clearing time. The following sections discuss the sensitivity results between the SIME margins, fault clearing times and variations in the parameters described in column 1 of Table 7-5.

7.9.2. Sensitivity of the SIME margins to Fault Clearing Time (CT) for Variation in the Power Transfer

Figure 7-12 describes the relationships between the SIME margins, fault clearing times, and power transfers investigated by cases 1 to 4 in Table 7-2. The sensitivity results show that a larger interconnector transfer will yield a lower CCT. Increasing the power transfer tends to reduce the available deceleration energy of the system generators. Thus, the capacity of the system machines to resynchronize following the disturbance is reduced. This behaviour is reflected in Figure 7-12 where at $\eta=0$ the (forward-swing) CCT decreases with increasing power transfer.

Table 7-2 notes that the 100MW case is multi-swing unstable, and the actual CCT is 337ms. Transient stability is constrained by forward-swing instability for the other power transfers in Figure 7-12. For each level of transfer the unstable scenarios show a clear linear relationship between the fault clearing times and the margins. At 300MW transfer for CT=125ms, the stable margin is lower than the value extrapolated from the unstable margins. For the 400MW case, the stable margin increases when the CT changes from 125ms to 144ms. These deviations in the stable SIME margins are because the SIME stable margin is an approximation.

Limit prediction using any pair of SIME margins provides a reliable guess of the FSL, and is sufficient to accelerate the EBSIME search. For both cases the EBSIME search is 60% faster than the binary search.

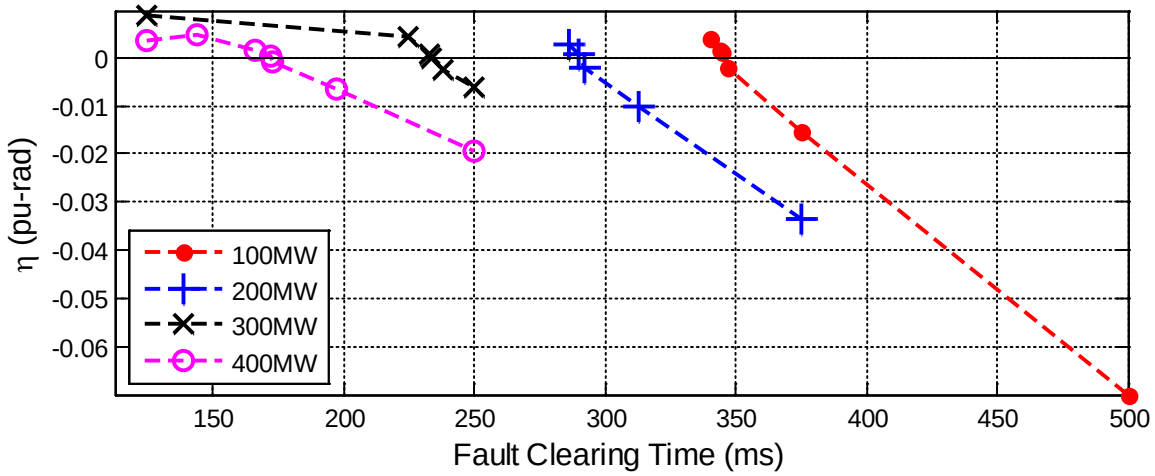

Figure 7-12. Sensitivity of the SIME margin to variations in the clearing time, and power transfer on the 4-machine system (SVC off-line)

7.9.3. Sensitivity of the SIME margins to Fault Clearing Time for Variation in the SVC Capacity

In cases 5 to 7 in Table 7-2, a SVC with 200MVar capacity is connected to the 4-machine system at bus 8 for a range of power transfers. For each case the reference voltage at the SVC node is the same as the steady-state voltage when the SVC is offline. Observing the CCTs for cases 1 to 3 and 5 to 7, from Table 7-2, it is apparent when the SVC is online, there is negligible increase to the CCT. For the power transfers of 100MW, 200MW and 300MW the respective increases in the CCT, due to the SVC, are only 3ms, 6ms and 8ms. Furthermore connecting an SVC for voltage regulation, at the mid-point of the system has negligible influence on the TSLs for a sending-end contingency. It is significant that the IEEE 4-machine model with its use of sixth order machine modelling, AVR excitation, power system stabilizers and SVC controls, yields these results.

The results are similar to those in Chapter 5 in which very simple generator and SVC models were used. On the two-machine system, the TSLs were also lower for contingencies applied close to the sending-end of the system, due to the reduced acceleration area formed under the power-angle curve of the post-fault network. Figure 7-13 shows that when the SVC is connected there is an approximately linear relationship between the CT and SIME margin. This indicates that when the SVC is connected that pairs of SIME margins will be useful for the limit prediction procedure

in the EBSIME search, even the margin of the most stable scenario at 300MW transfer. Comparison of Figure 7-12 and Figure 7-13 shows that the variation in margin is very similar with, or without, the SVC online.

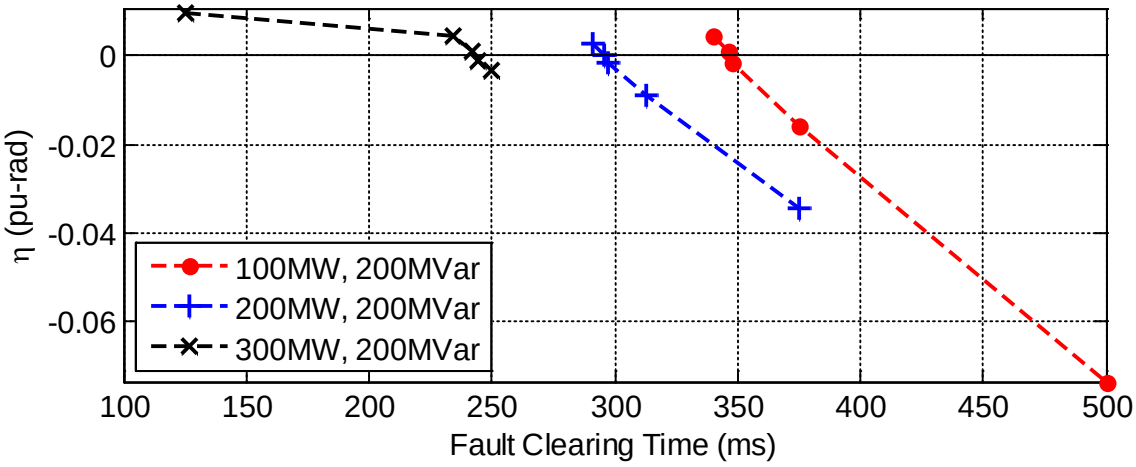

Figure 7-13. Sensitivity of the SIME Margin to variation in the fault clearing time and power transfer when the SVC is connected to the 4-machine system.

7.9.4. Sensitivity of the SIME margins to Fault Clearing Time when Governor Controls are included

Figure 7-14 shows the TSSA results from cases 8 to 11 in Table 7-2, where generator governor controls are employed. Each case is constrained by forward-swing instability. Comparison of Figure 7-14 against Figure 7-12 shows that including governors raises the CCT. The governors adjust mechanical shaft power to restore the generators to synchronous speed, effectively reducing the amount of acceleration and deceleration energy exchanged between system machines in the event of a disturbance.

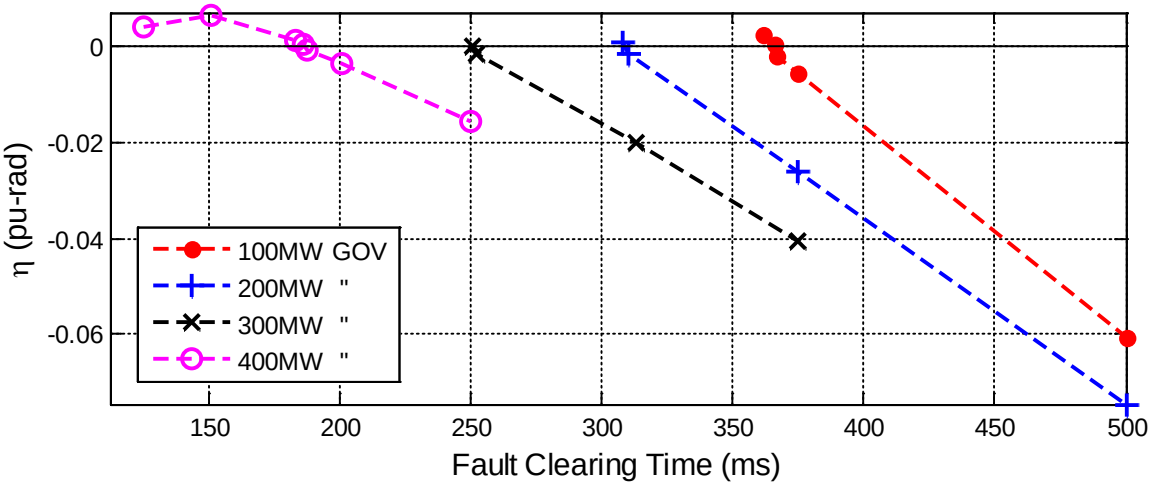

Figure 7-14. Sensitivity of the SIME margins to variation in fault clearing time, and power transfer with governors connected to the 4-machine system

For the 400MW case, the stable margin at fault clearing time of 125ms, provides a lower stable SIME margin than would be extrapolated from the unstable margins. This can be attributed to the approximation that is required to calculate SIME margins for very stable scenarios. Yet, Table 7-2 shows that in this case the simulation time of the EBSIME algorithm is 60% faster than the binary search.

7.9.5. Sensitivity of the SIME margins to Fault Clearing Times for Variation in the Total System Load

In cases 12 to 14 in Table 7-2 the total system load is decreased by reducing the system load and generation by the same proportion. By reducing the generation each of the system machines experience a smaller acceleration during the three phase fault. This effectively increases the capacity of the system machines to decelerate after the fault is cleared, thereby increasing the CCT. Figure 7-15 shows the sensitivity of the SIME margins to the fault clearing time for the load variations. Each case is constrained by forward-swing instability.

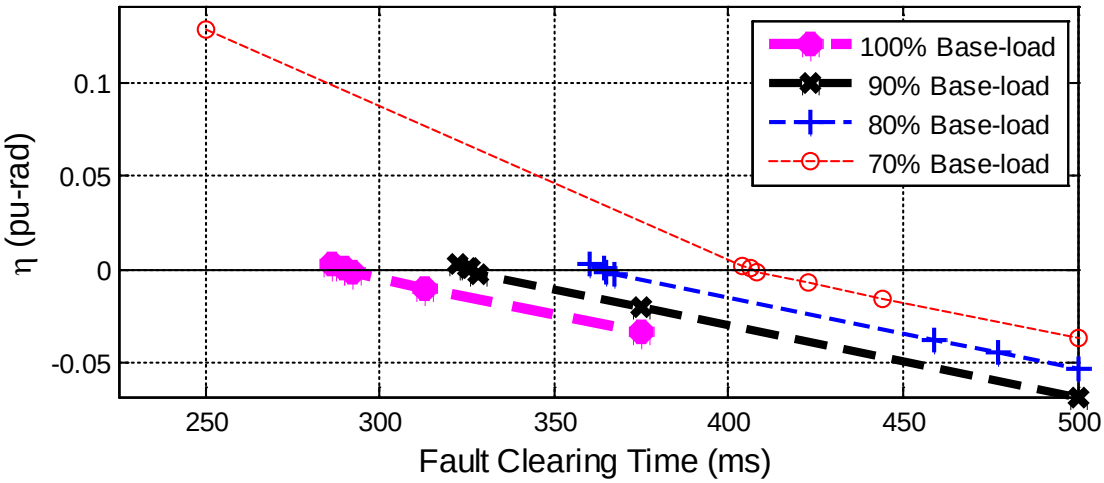

Figure 7-15. Sensitivity of the SIME margin to variation in fault clearing time, and the total system load and generation capacity on the 4-machine system

7.9.6. Sensitivity of the SIME margin to Fault Clearing Time for Variation in the Transmission Line Length

In this analysis the total length of the transmission line between nodes 7 and 9 is varied between half (110km) and double (440km) the base line length (220km). The transmission line length is proportional to the total line reactance between area 1 and 2 in the test system. It is also proportional to the interconnector line charging susceptance, although the effects of line charging are negligible in comparison to line reactance. Increasing the line length will reduce the power transfer and the capacity of the system

to decelerate after fault clearance. A longer line will degrade the transient stability of the system, and reduce the CCT. The converse is true where the line-length is halved.

Figure 7-16 displays the TSSA data from cases 13 to 15. The results show that as the line length increases, the CCT decreases. When line length is halved the mechanism of transient instability tends to occur on the second swing. Even though the actual CCT is 50ms less than the FSL Figure 7-16 reflects the significant increase in CCT, from the base line value, when the line length is halved.

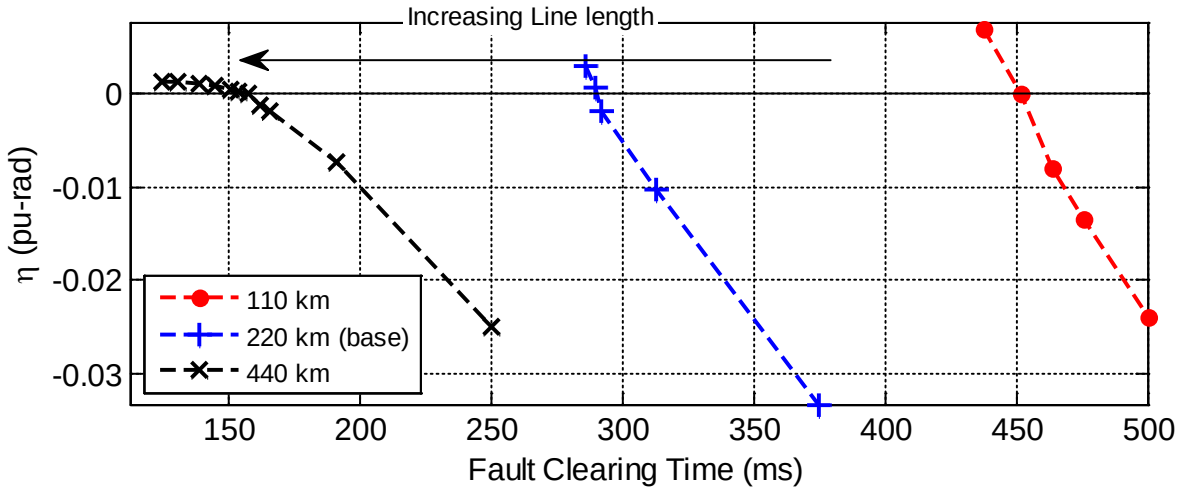

Figure 7-16. Sensitivity of the SIME margin to variation in the fault clearing time and interconnector line length on the 4-machine system

7.10. Chapter Conclusion

The EBSIME algorithm provides a fast, accurate and robust approach to locating the TSLs of multi-machine power systems. It combines the reliability and accuracy of the binary-search and the time saving techniques of the SIME method for a superior approach to TSL searching. The proposed EBSIME algorithm can be used to search for both CCTs and PTLs. It is the preferred method for TSL searching for the following reasons:

The EBSIME technique [97] enhances the robustness of the basic SIME method [1] by:

- Switching to a bisection step, i.e. locating the mid-point between the current SV and the current upper or lower search bound depending on whether the SV is stable or unstable when the SIME limit prediction cannot be applied;
- It does not require a priori tuning of the system and fault dependent parameters.

The EBSIME algorithm improves the plain binary search by:

- Using linear limit prediction steps with pairs of estimated TSMs to accelerate the search for TSLs.
- Providing significant time-savings for a large range of operating conditions;
- Even when search redirection is required the EBSIME algorithm can achieve a faster search time. This is demonstrated on the 4-machine system, and on the 14-generator model of the South-East Australian power system in Chapter 9.

The search methodology can be extended to provide information for control and TSSA applications. When the EBSIME algorithm is applied to the 4-machine system the TSSA shows that there is a relatively linear relationship between the SIME margins and the CTs for variations in a number of system parameters. The linearity is generally clearer for unstable scenarios. The TSSA results reiterate the Chapter 5 finding, that where a SVC is connected to a long interconnector there is no appreciable improvement in the transient stability when a fault is applied at the sending-end of the system.

Chapter 8 Design and Implementation of the AUSIME Software

The software developed in this research (AUSIME) is a flexible and reliable automation tool that is able to accurately locate transient stability limits (TSL) with the Enhanced-Binary SIME (EBSIME) algorithm. The software integrates the EBSIME algorithm with the PSS®E TDS software thereby ensuring reliable search results. The algorithm has been implemented as a peripheral plug-in to the core PSS®E TDS software by using the PSS®E Application Program Interface (API) and automation facilities, without requiring access to, or modification of, the PSS®E source code. The AUSIME software is designed with research and production purposes in mind, and enables the algorithm to be investigated and compared with other search methods. This chapter describes the key design features of the AUSIME software and how it is implemented.

8.1. Design Choices for the AUSIME Software

The implementation of the AUSIME software provides the following facilities for research purposes:

- Flexible text-based configuration of a TSL search (input instructions)
- Comprehensive TSL search summaries
- Options to save generator, OMIB and COI response data into compact binary files. Facilities have been implemented to view the data in these files with MATLAB® [99];
- Options to report the actual (wall-clock) execution and simulation times, for each search iteration individually and cumulatively;
- Options to select the detail of diagnostic and error reporting;
- Options to redirect search traversal based on the assessment of forward-swing, or multi-swing, stability;
- Options to specify machine groups for OMIB calculations

Dynamically allocatable storage is used to facilitate the analysis of power systems of widely differing sizes, and to efficiently handle the large volumes of data involved.

8.1.1. Modular Architecture of the AUSIME Software

The AUSIME software has been designed with the modular software architecture shown in Figure 8-1. It is composed of two loops - an inner search loop and an outer loop. The outer search loop (blue boxes) is implemented in Python code modules [11, 100], and the inner loop (orange boxes) is implemented as a PSS®E user-defined model in Fortran 95 [11, 101]. The decision-making calculations for the EBSIME algorithm are implemented within the Fortran 95 modules in the inner search loop. This allows variations in the algorithm, such as alternative approaches to ESC or limit prediction, to be implemented and explored in a straight forward manner.

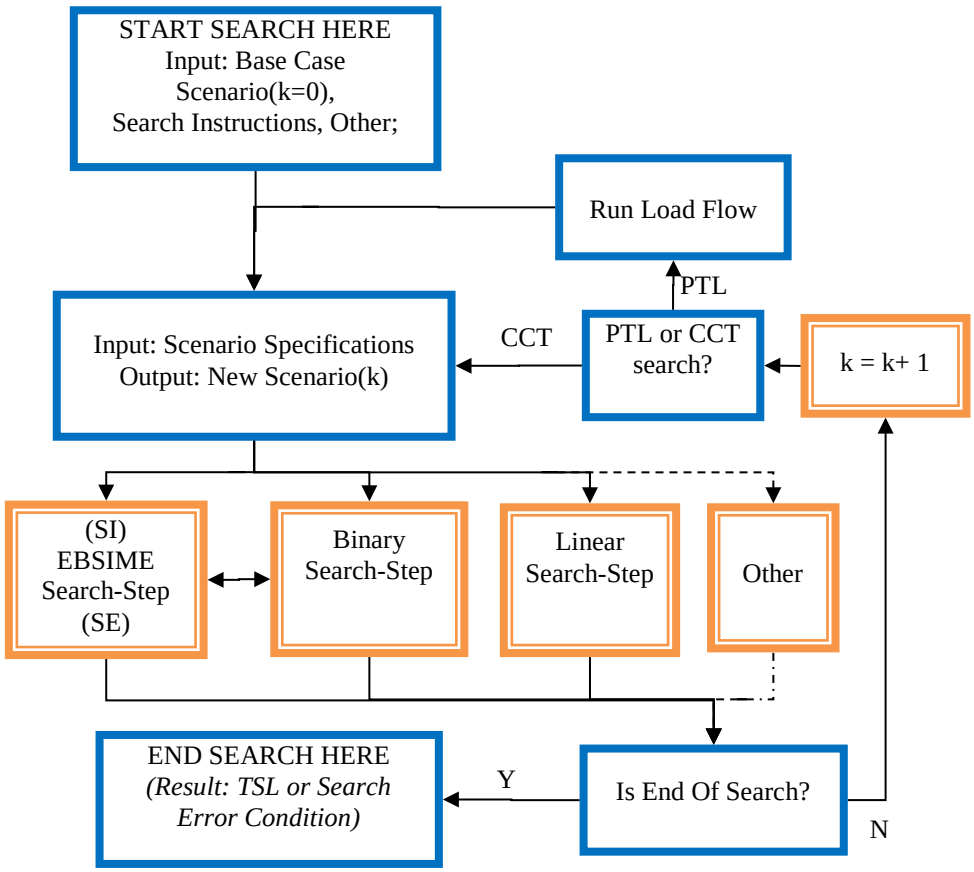

Figure 8-1. Modular architecture of the AUSIME software – the outer loop modules are highlighted in blue, the inner loop modules are highlighted in orange.

The inner search loop applies the EBSIME algorithm to each scenario that is simulated by TDS during the search. During each TDS the inner loop performs OMIB calculations to accelerate transient stability assessment, and to advance the search. The modular architecture allows for alternative search approaches, such as a linear or binary search, to be invoked by the TDS to determine the next search step. This is useful for research and comparing search algorithms.

The outer-loop interprets the user-specified text-based search instructions. It handles the transitions between iterations as the search progresses, directs PSS®E to solve load flows and invokes PSS®E dynamic simulations at the appropriate times. For a CCT search a set of instructions in the PSS®E command language are generated by the Python supervisory software. These instructions include the type, location, duration of the fault, and how the fault is cleared. The PSS®E software is then requested to execute the instructions. For a PTL search a load flow solution (.RAW) and a PSS®E command file (.IDV) are both generated and solved for each search scenario. The supervisory outer loop manages the auxiliary inner- and outer-loop configuration files that interface with the inner loop. It recognizes when the multi-swing limit has been reached, and finishes the search at an appropriate point.

8.1.2. Using The PSS®E Simulation Software

PSS®E provides tools to solve network load-flows and to perform TDS of multi-machine power systems. These facilities can be executed by manual interaction or in automation mode from the DOS command prompt. In automation mode a set of instructions in the PSS®E command language are provided in a text file. The PSS®E software is required to execute these PSS®E instructions via an operating system command. The automation mode is used to solve PSS®E load-flows and run PSS®E dynamic simulations within the overarching AUSIME software.

PSS®E provides a standard library of dynamic models that represent the physical behaviour of common power system equipment. Where the supplied models cannot accurately represent a desired piece of equipment, user-written models can be provided. These models are written in a programming language supported by PSS®E and must adhere to a number of rules to be able to properly integrate with the PSS®E simulation engine. The source code for the user-defined model is compiled and then linked with PSS®E. By this means the user-defined model is embedded in PSS®E without requiring direct access to the PSS®E source code. This user-defined modeling facility is used to implement the EBSIME algorithm.

Although EBSIME is not a device, the modelling interface to PSS®E has sufficient flexibility to support the implementation of the EBSIME algorithm. Thus a PSS®E user-written model called AUSIME has been developed to perform the inner-loop functions of the EBSIME algorithm.

The AUSIME model is implemented using the Fortran 95 programming language. The mechanics of the AUSIME inner search loop are implemented with a set of Fortran 95 code modules. They are compiled to produce a set of object files (.obj) using the Lahey-Fujitsu Intel® Fortran 95 compiler 10.1. PSS®E provides a batch file, ‘cload4.bat’, that is used to link the object files with the main PSS®E simulation engine to perform the AUSIME inner loop calculations.

The inner search loop of the EBSIME algorithm is declared to PSS®E as a user defined model in the PSS®E dynamic (.dyr) file. The model describes an object that observes the system algebraic and state variables at every time-step. In the dynamics data file (.dyr) of an investigated power system, the inner-loop user-defined model is declared with the following line record:
0 'USRMDL' 0 'AUSIME' 8 0 0 0 0 0 /

The syntax of this statement is explained in section F.5.1. An example of the commands used to compile and link the AUSIME user-defined model with PSS®E is shown in Figure F-14.

The PSS®E software is embedded with a Python interpreter. It allows PSS®E to be conveniently accessed and controlled from the Python environment. Python is a community-supported, interpretive, interactive, object-oriented programming language that can be used to link programs and processes that have been written with different coding languages [100]. Python scripts can be used to facilitate sophisticated control of PSS®E. They enable looping and decision making based on the results of PSS®E analyses [102]. In the implementation of the EBSIME algorithm Python scripts are used to drive the AUSIME outer search loop. They are used to create the appropriate input files to the inner search loop, translate the outer-loop configuration file generated by the inner loop, and determine search actions for the next scenario.

8.1.3. Convenient Assessment of the Search Results With MATLAB®

For investigations of the EBSIME algorithm, it is useful to review the OMIB, COI and original machine time responses that are generated from each search scenario. For a given TDS, time-step by time-step the AUSIME software simultaneously calculates and records each of these responses into a set of binary files. A separate binary file is assigned to the complete OMIB, COI and original machine time responses. It is advantageous to record the data in this format as, in contrast to other file formats, the file size is small and the writing time is minimal. The record function is implemented in Fortran 95 within the inner search loop, as part of the AUSIME user-defined model. A set of executable program files have been written in the Fortran 95 language, to enable translation of the binary files produced by Fortran into a MATLAB® compatible format that can be reviewed with MATLAB's sophisticated graphical display functions. The recorded responses can be conveniently investigated using the full range of MATLAB® data processing and graphical display facilities.

8.2. A High Level Overview of the AUSIME Inner Search Loop

The AUSIME inner search loop performs the calculations required to determine the next search step using the EBSIME algorithm, or by alternative search methods. As the inner search loop is implemented as a PSS®E user-defined dynamic model, it is called at every time-step of a TDS. Figure 8-2 provides an overview of the inner loop. Step 1 is performed once, at the beginning of the TDS, and step 2 at every TDS time-step. Steps 3 & 4 are each performed once at the end of the TDS. These steps are performed for each of the outer-loop search iterations.

The first time the inner search loop is run for a search scenario the data records and variables describing the scenario are initialized (Step 1). The inner loop reads a text-based *input* configuration file that was generated by the outer supervisory loop. The search conditions for the current scenario are read and loaded into working memory. After initialization (step 2) OMIB, COI and SIME calculations are performed at every time step until the end of the integration period ($t_i > T_{MAX}$), or until the ESC is satisfied ($t_i > T_{ESC}$).

Subsequent calculations depend on the search phase, which may be in initialization (phase A), forward-swing limit prediction (phase B), or locating the multi-swing limit (phase C). At the end of the TDS (Step 3) post-processing of the current scenario, and preparation for the next scenario, are performed. The results of the inner search loop are communicated to the outer loop by generating a text-based outer-loop configuration file at the end of the TDS (Step 4).

Figure 8-2 describes the inner workings of the orange EBSIME module shown in Figure 8-1. Alternative search methods, such as the binary, linear or other searches can be implemented in a similar way. The following sections describe the AUSIME software, and the PSS®E TDS operation environment in more detail. Section 8.3.4 describes the syntax of the inner- and outer-loop configuration files. Examples of both types of configuration file are shown in Figure F-7 to Figure F-9. They each provide insight into the types of information that are calculated and used to drive the EBSIME TSL search, and to produce the accompanying report and data files.

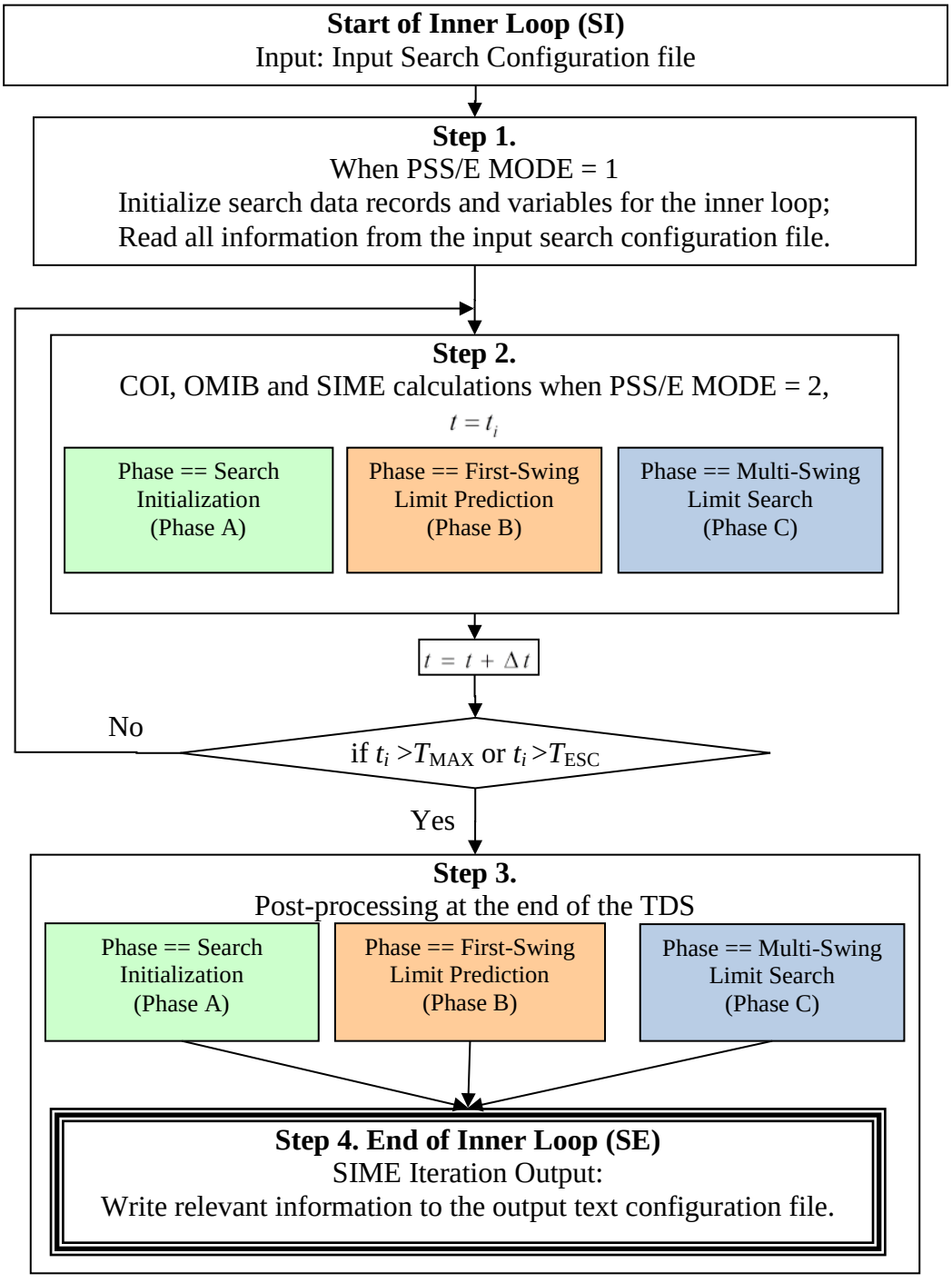

Figure 8-2. A high level flowchart of the AUSIME Inner Loop. The actions performed in steps 2 and 3 depend on the search phase A, B or C.

8.2.1. Programming the AUSIME Software to Operate within the PSS®E TDS Environment

The AUSIME (inner loop) software is programmed as a user-defined model for the PSS®E dynamic model library. During a TDS, when the AUSIME model is invoked it monitors certain PSS®E flags, constants, and parameter values so that it can perform

calculations in the appropriate sequence, and make decisions to autonomously drive the EBSIME search. The "MODE" flag, shown in Figure 8-2, is an example of a PSS®E variable that is used by AUSIME to guide the inner loop process. The next sections describe the range of PSS®E procedures, flags and data structures that are used to implement the EBSIME search.

8.2.2. The PSS®E Dynamic Simulation Sequence

Running a PSS®E dynamic simulation study involves two phases: setting up the system model and running simulations using it. The system model data for a dynamic simulation is comprised of:

1) a solved load-flow case – with a positive sequence representation of the network

2) dynamics data for equipment models which may be either PSS®E built-in or user-written models; and

3) PSS®E automatically generates a subroutine that specifies the user-defined subroutines that are to be called by the main PSS®E engine.

Running a PSS®E dynamic simulation typically involves the sequence of tasks shown in Figure 8-3.

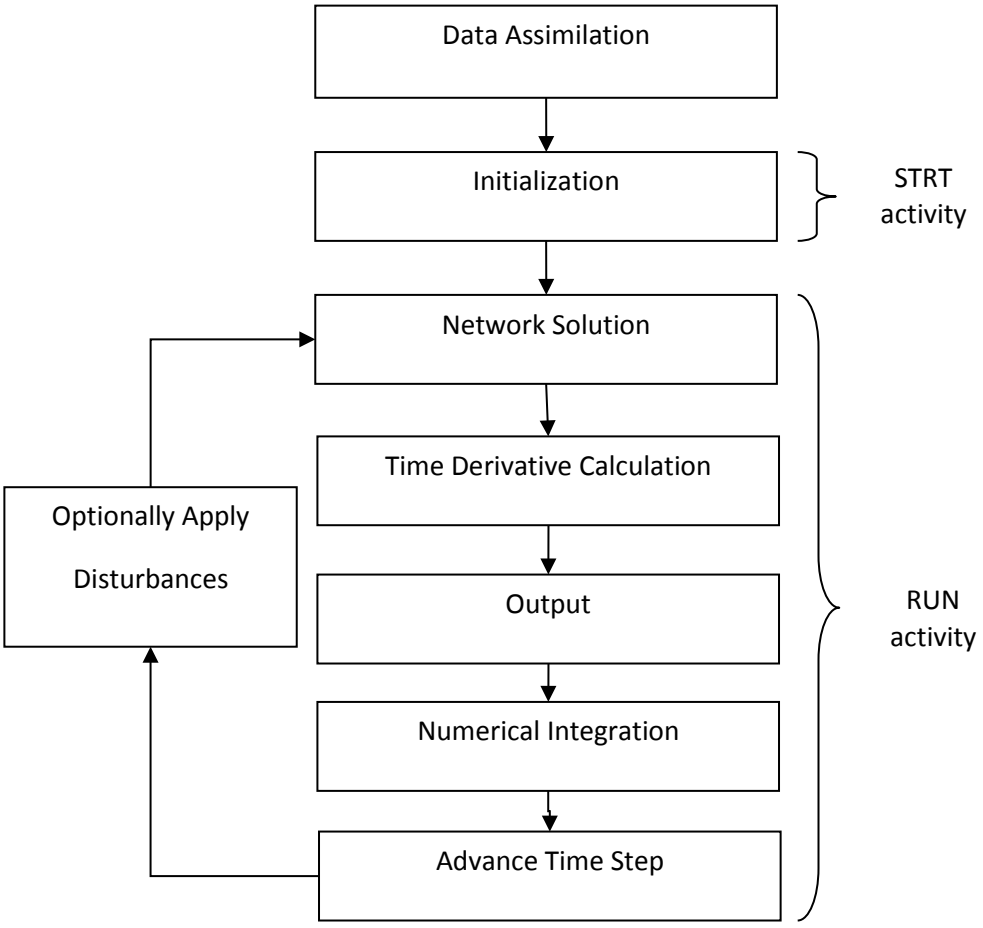

Figure 8-3. Basic flow of the PSS®E dynamic simulation sequence [102]

For *data assimilation* PSS®E reads the input dynamic data into working memory and builds the connection subroutines. In *initialization*, PSS®E checks the consistency of the load-flow and dynamics data for the initial condition operating point, computes the initial values of all system variables and verifies if all variables are within their operating limits (phase 1). If the system model is satisfactory then execution of the TDS can commence via the PSS®E RUN activity.

8.2.3. Accessing PSS®E Simulation Data Via the User-Defined Model

In the inner search loop, access to the state and algebraic variables of the system model is required at every time step of a dynamic simulation. PSS®E allows user-defined models to access TDS arrays and common operational variables - such as generator rotor angles, speed, and power output – via the built-in 'COMON4.INS' module.

Significant PSS®E control flags sent from PSS®E to the user-defined model are MODE and KPAUSE. The flags and the meaning of their values to the PSS®E TDS are summarized in Table 8-1. They provide information about the present phase of operation of a dynamic simulation at any instant in time.

The AUSIME user-defined model only performs computations during MODEs 1 and 2. MODE = 1 tells the model that the TDS for a search scenario is being initialized. Under this condition the AUSIME model reads search information for the current scenario into memory, and creates output files such as the binary time response files, and the outer-loop configuration file. The search report and timing files are created and initialized, or reopened if they already exist. This corresponds to step 2 in Figure 8-2.

MODE = 2 tells the user-defined model that the TDS is in the process of performing the time derivative calculations for the system state variables. In this MODE the AUSIME user-defined model will perform the COI and OMIB calculations for the current time-step, and write the computed results to corresponding the binary time response files. This corresponds to step 2 in Figure 8-2.

If MODE= 2 and the current simulation time exceeds T_{MAX} or T_{ESC} the model will perform the necessary computations to determine the next search step (step 3 in Figure 8-2). The actions performed depend on the search phase, and may involve calculating the next search variable (SV) by interpolation/extrapolation from the current and previous search margins; or otherwise computing the SIME margin for the current scenario and determining the next search step by limit prediction using the current and previous SVs and the corresponding margins. Additionally, the user-defined model

writes useful search information for the current scenario to the search traversal and timing report files. This corresponds to step 4 in Figure 8-2.

The *KPAUSE* flag indicates to the AUSIME model if a normal simulation step is being performed by the TDS, or otherwise if it is at an instant before or after a switching event – such as the application or clearance of a fault. *KPAUSE* is monitored by the AUSIME model to ensure that the time-steps at switching are not duplicated in the recorded OMIB, COI and dynamic data responses.

Figure 8-4 and Figure 8-5 summarizes how the values of the MODE and KPAUSE flags are used to guide execution of TDS within the PSS®E framework. To calculate a TDS, the PSS®E STRT (initialization) activity is first executed, followed by the RUN activity. During both activities the CONEC and CONET subroutines that are built-in to PSS®E, are called several times. The tasks they perform are also directed by the values of MODE and KPAUSE.

TABLE 8-1. INTERPRETATION OF THE PSS®E CONTROL FLAGS DURING THE DYNAMIC SIMULATION SEQUENCE

Flag	Value	Significance
MODE	1	Calculate the initial values of all state variables and algebraic variables. Used by AUSIME during scenario initialization.
	2	Calculate and store: - the time derivatives of all state and algebraic variables; - the present output signal value for each stabilizer, minimum excitation; - limiter and maximum excitation limiter model. Used by AUSIME during TDS to: - perform EBSIME calculations for next search variable; - record time response data to binary files; - record search traversal information to the output report file.
	3	Compute and store: - the present output signal value for each stabilizer, minimum excitation limiter and maximum excitation limiter model. - the present value of turbine mechanical power. Used by AUSIME model during binary-search phase.
	4	Special calculations to initialize induction motor and dc transmission models. Not used by AUSIME model.
KPAUSE	0	Call PSS®E models under normal time step conditions
	1	Call PSS®E models at the time-step, $t = t_{PAUSE}^{-}$, immediately prior to a switching event. Used by AUSIME model to avoid duplication of data at the switching instant
	2	Call PSS®E models at the time-step, $t = t_{PAUSE}^{+}$, immediately after a switching event. Used by AUSIME model to avoid duplication of data at the switching instant

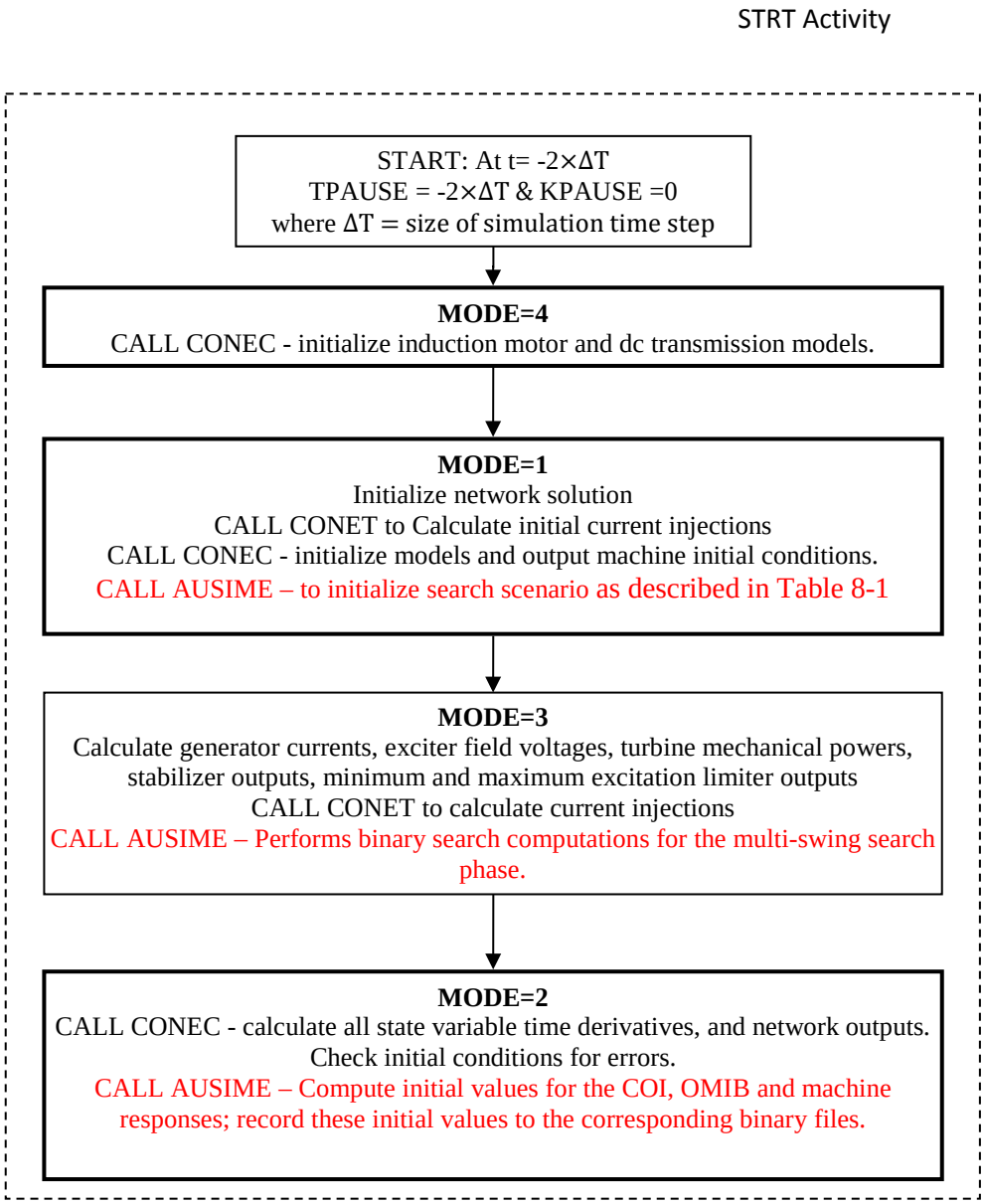

Figure 8-4. Sequence of actions of the PSS®E initialization activity, 'STRT', as dictated by the MODE and KPAUSE control flags. Adapted from [102]

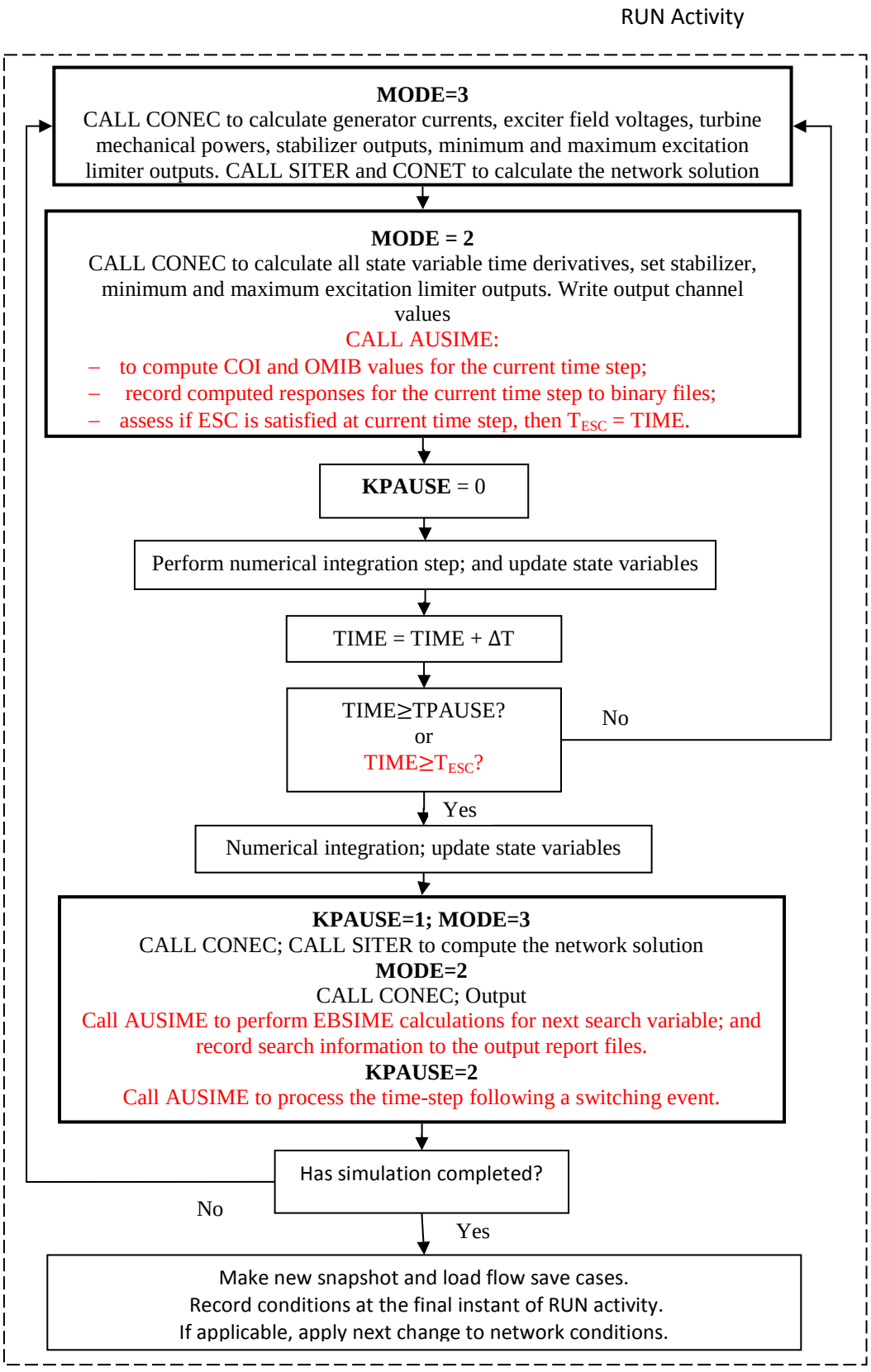

Figure 8-5. Sequence of actions of the PSS®E 'RUN' dynamic simulation activity as dictated by the MODE and KPAUSE control flags. Adapted from [102]

8.2.4. Accessing The PSS®E Data Structures

The PSS®E dynamic simulation data is stored in a group of arrays related to buses, machines, loads and other components that are used in the calculation and display of other PSS®E variables. The PSS®E TDS uses four large general purpose storage arrays:
CON – for model parameters at the current time step
STATE – for state variables
VAR – for algebraic variables at the current time step; and
ICON – integer quantities that may be either constant or algebraic variables.
As mentioned earlier the above arrays and facilities for accessing them are provided in PSS®E.

PSS®E provides the starting address in each of the arrays when a user-defined model is called. Each reference to a PSS®E model, either from the built-in library or user-written, may be assigned a small contiguous block of space in one or more of these arrays - in working memory. The storage space and address allocated to each device depend on how the dynamic simulation input files are specified and the order that PSS®E subroutines and user-defined models are called during initialization. As a TDS is executed, the location and space allocated to system parameters remain the same, however the values will vary with the simulation.

For the SIME calculations, at each time-step, the rotor angle, speed, electrical and mechanical power quantities are determined from the PSS®E arrays respectively named ANGLE, SPEED, PELEC and PMECH. The base power of each machine is stored in the PSS®E array named MBASE. PSS®E also provides facilities to access machine inertia constants of each generator. By making use of PSS®E API functions AUSIME can access the inertia constant, H, of each generator.

8.3. Flow of Control during Execution of the Inner Search Loop

The processes that are used to implement the inner search loop are shown in Figure 8-6. For each search iteration the inner loop is executed at every time-step of the PSS®E TDS, where ‘k’ is the scenario counter. For a TDS the first time the inner loop is called the inputs to the model are 1) the inner-loop configuration text file and 2) the PSS®E MODE and KPAUSE flags. When MODE=1 the inner-loop configuration file is read into the PSS®E working memory.

Steps 2 and 3 from Figure 8-6 and Figure 8-7 are each implemented in separate Fortran 95 modules within the AUSIME model. For each step the three phases A, B and C are implemented by separate subroutines. The multi-swing limit (MSL) search phase is shown in Figure 8-7. The inner loop actions are the same as step 3C, with the exception that post-processing is performed in MODE = 3.

8.3.1. Step 2: Step-by-Step Processing in the Inner Loop

When the time-step by time-step processing begins, MODE = 2. If the EBSIME search algorithm is in the initial phase, then step 2A of Figure 8-6 is performed. Otherwise if the search is in the forward- or multi-swing phases, then steps 2B or 2C of Figure 8-6 are processed respectively.

In step 2B of Figure 8-6 the ESC and COI stop criteria are both applied to test for transient (in)stability, and the OMIB, COI and dynamic machine responses are stored into working memory. It is similar for step 2A of Figure 8-6, except in the first search scenario where the scenario counter k=1, only the COI stop criteria is applied - the OMIB value is not calculated. Step 2C is similar to step 2B in Figure 8-6, except in step 2C only the COI stop criteria is used to assess transient stability. When a fault is applied or cleared, PSS®E performs dynamic calculations twice at the time step when switching occurs. As mentioned earlier, to prevent consequential duplication errors, the KPAUSE flag is monitored to ensure that time-steps at the switching instant are not duplicated in the OMIB, COI and dynamic data responses.

8.3.2. Step3: Scenario Post-Processing in the Inner Loop

The first indication of transient (in)stability by any stop criteria halts the TDS. At this time post-processing at the end of the TDS is performed (step 3 in Figure 8-7). If the search is in the initialization phase, then post-processing is performed by step 3A. If it is in the forward-swing limit prediction phase, then post-processing is performed by step 3B. If it is in the multi-swing limit phase, then post-processing is performed by step 3C. Step 3A, 3B and 3C implement the actions described in sections 7.4, 7.5 and 7.6 respectively.

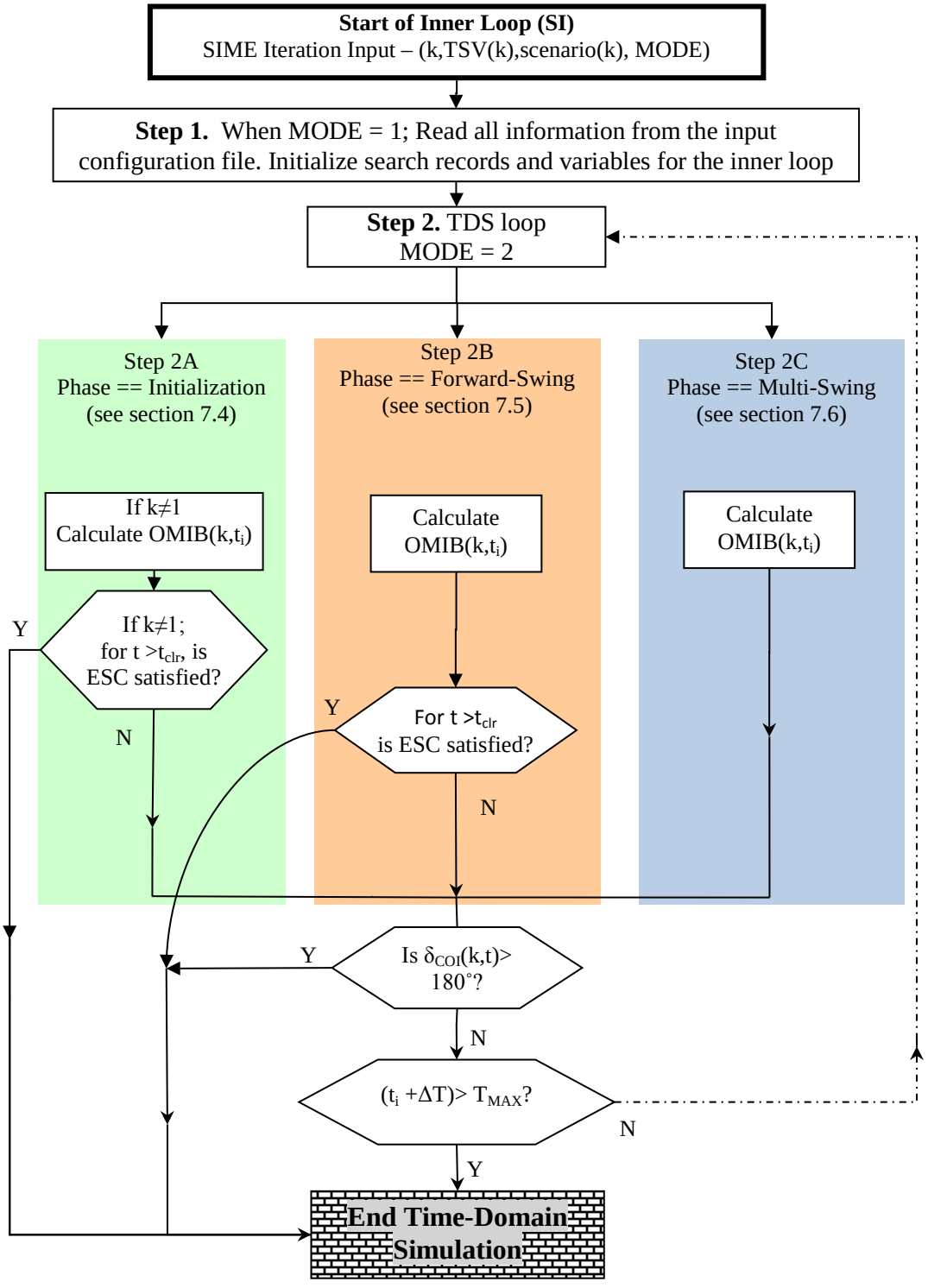

Figure 8-6. Inner Loop: Steps 1 and 2 of the implementation of the EBSIME search iteration algorithm

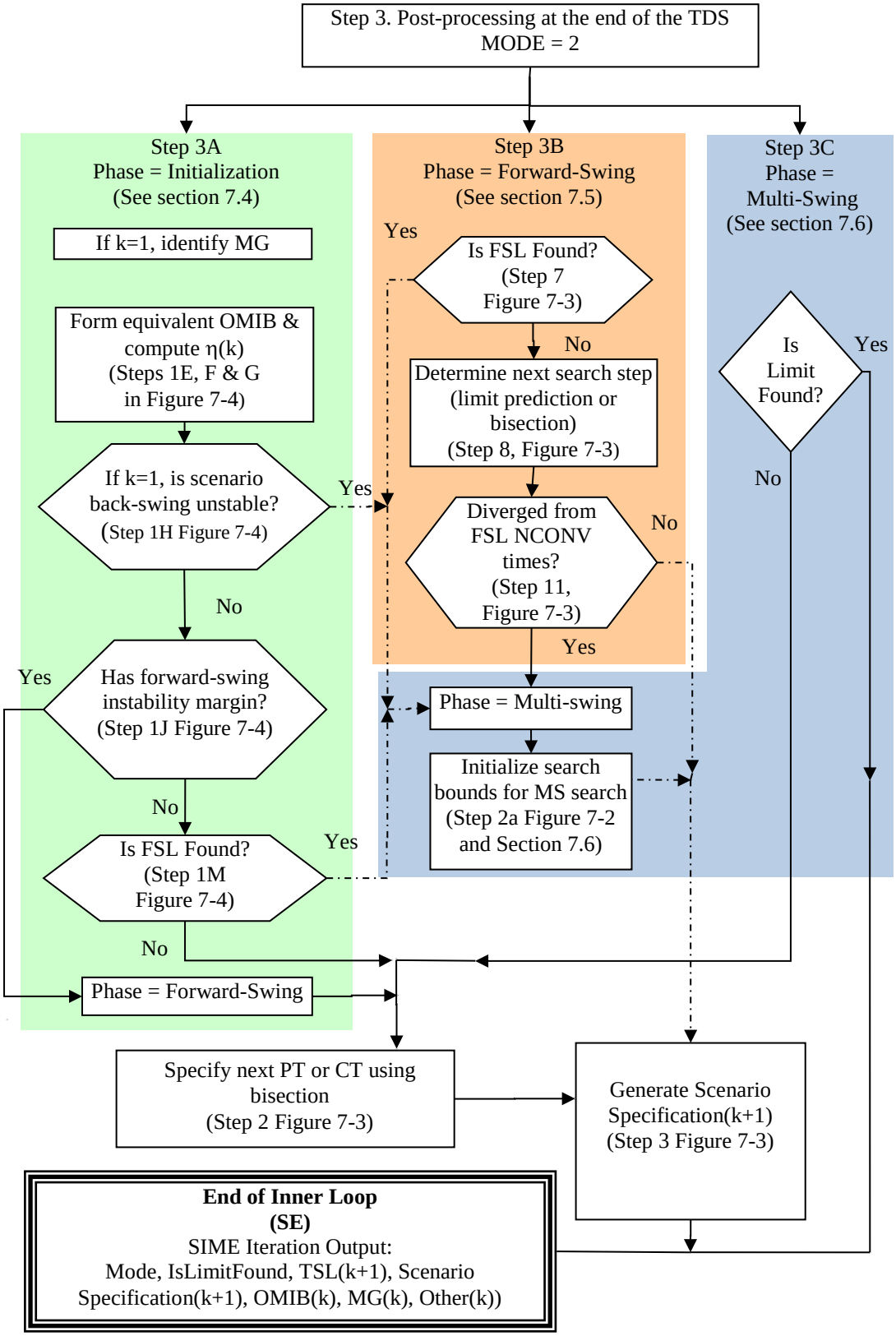

Figure 8-7. Inner Loop: Step 3 of the implementation of the EBSIME search iteration algorithm

8.3.2.1. *Determining the SIME Machine Groups*

In the EBSIME algorithm the machine groups used to calculate OMIB responses during Step 3A in Figure 8-7 are defined from the first search scenario. With this approach limit prediction from any pair of SIME margins can be performed during the search. Recalculation of the SIME margin and OMIB responses for previous search scenarios is unnecessary.

During conceptualisation of the EBSIME algorithm, an alternative method of determining the machine groups (MG), similar to the original SIME method was considered. In this approach, the applied MG might vary between search iterations. The MG from the most recent unstable scenario is used to calculate the SIME margins for the pair of search scenarios used in limit prediction. However, as mentioned in Chapter 7 investigations revealed that this approach tends to yield more reliable results than updating the MG at every unstable scenario. The OMIB responses appear to be most meaningful when they are formulated with MG from a very unstable scenario.

Furthermore, the TDS of previous scenarios may need to be resumed to correctly compute the SIME margin with the newly identified machine group. These two key findings, and the need to tune SIME algorithm search parameters to both the system and fault under investigation, justifies the decision not to apply the original SIME approach of changing the MG in the EBSIME algorithm during the course of the search.

The original SIME method for limit searching also requires that at least one of the scenarios used in limit prediction to be unstable for a more accurate limit prediction. This criteria was considered for the EBSIME algorithm, where limit prediction involved the most recent unstable scenario in each calculation. However, for a range of operating conditions and contingencies on a test power system model[5], it was found that this condition does not always accelerate a search. In some circumstances it caused very slow convergence to the forward-swing limit. Thus this criteria was also omitted from the EBSIME algorithm.

8.3.2.2. *Calculating the SIME Margins*

The EBSIME algorithm calculates the SIME margin for the current search scenario during step 3 of the inner search loop. The unstable SIME margin is calculated by applying the trapezoidal integration method to calculate the difference between the acceleration and deceleration areas of the OMIB power -angle curve. It is calculated

[5] The IEEE simplified 14-generator South-East Australian power system, introduced in Chapter 9.

from the actual OMIB acceleration power (P_{aOMIB}) and rotor angle time-responses generated by the TDS.

As mentioned in section 7.7 the stable margin is the unused deceleration area, and the boundaries of this area must be approximated. The quadratic approximation function used for this purpose is shown in Figure 8-8. The path of the OMIB power angle curve must be extrapolated from the end of the forward-swing δ_r, to the angle of instability, δ_u, where P_{aOMIB} is zero. A linear least squares (LLS) estimation algorithm is applied to fit a quadratic function to the OMIB power-angle response spanning from the clearing angle, δ_{clr} to δ_r. The LLS and quadratic fit operations are performed using subroutines from SLATEC [75], a highly respected publicly available library of mathematical and statistical routines written in Fortran 77.

Initial investigations on the 4-machine system indicate that 400 points, equally spaced on the rotor-angle axis between δ_{clr} and δ_r, yields a quadratic function that is sufficiently accurate and insensitive to relatively small deviations in the power-angle curve. In the AUSIME software 400 data points are used to extrapolate and calculate the stable margin. However, if the estimated quadratic curve does not intersect the rotor angle axis (at $P_a = 0$, for $\delta > \delta_r$), then the scenario is classified as too stable for the margin calculation.

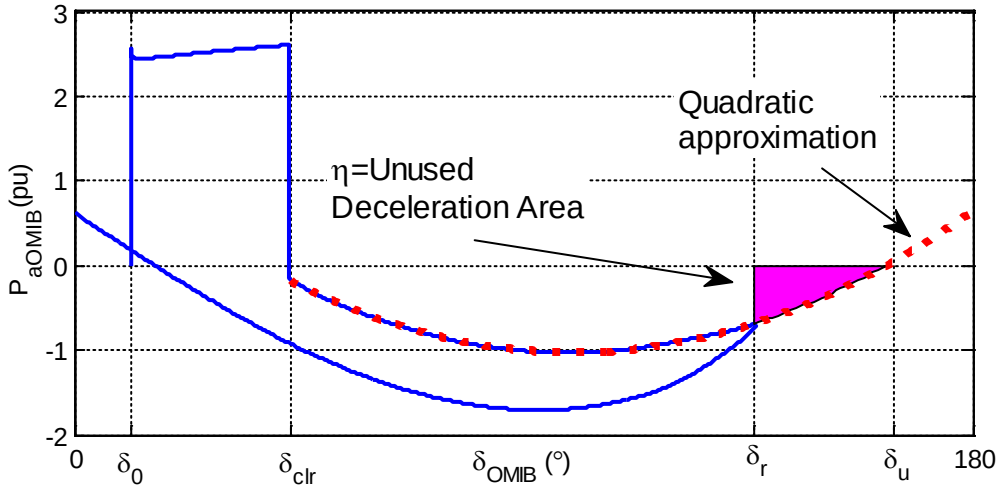

Figure 8-8. The OMIB power angle response showing extrapolation for the stable margin, discussed in section 7.5.5.

8.3.2.3. *Search Redirection Upon Convergence Failure*

When the forward-swing limit is predicted some tests are performed to detect if the search fails to converge. As explained in section 7.5.7, if the predicted limit is outside of

the search bounds then the TDS of the current scenario is resumed and the COI stop criterion is applied. If the predicted limit falls outside the current search limit more than a user-prescribed number of times, the SIME method is abandoned and the search is completed using the binary-search algorithm.

8.3.2.4. *Facility for Alternative Search Approaches in the AUSIME software*

For research purposes it is possible to direct the AUSIME software to run alternative versions of the EBSIME search for the TSL. The description of how to specify these alternative options is explained in section 8.4.1.1.

8.3.3. Allocation of Dynamic Simulation Data in the Inner Search Loop

The inner search loop tool employs a number of data structures to perform SIME calculations on the TDS and to store associated data. The defined structures are used as containers to process the different groups of information that are generated by the PSS®E TDS and handled by the inner SIME search loop. These containers, and the core variables within them, are graphically shown in Figure 8-9 to Figure 8-12.

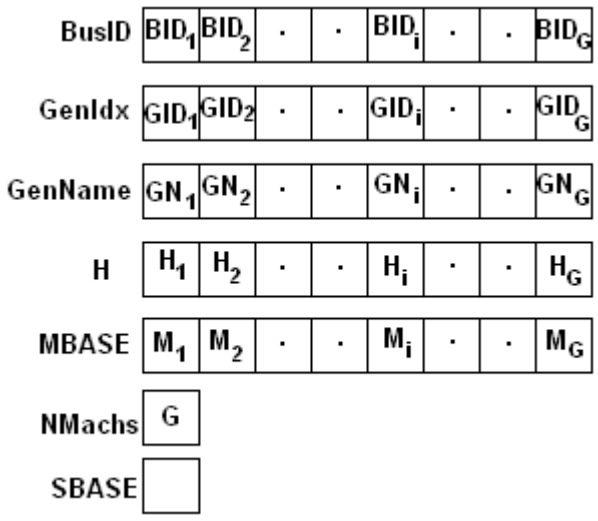

Figure 8-9. GeneratorParamType - storage of constant PSS®E TDS generator and bus variables

Figure 8-9 represents the data structure GeneratorParamType that is used to store data extracted from the PSS®E TDS (see section 8.2.4). The record incorporates a set of allocatable arrays that contain information on the PSS®E bus and generator integer identifiers (BusID & GenIdx), generator types (GenName), machine inertia (H), and

machine base power (MBASE) of each system generator. It also stores information on the number of system machines (NMachs, G), and the system base power (SBASE). A set of Fortran 95 subroutines have been coded to read the relevant information from the PSS®E data structure, and to store and access it using this data structure. The GeneratorParamType record is generated during the initialization of the PSS®E simulation and is unchanged subsequently.

For each individual time-step, the time-varying generator variables calculated by PSS®E are stored in the data structure called 'GeneratorVarType', represented in Figure 8-10. It contains a set of allocatable arrays - the size of the arrays is NMachs (G). δ, ω, Pe, Pm, Pa and the online status (ONSTAT) for each generator are read from the PSS®E data structures and duplicated in this record. The value of the current time step (tstep) is also saved with this information.

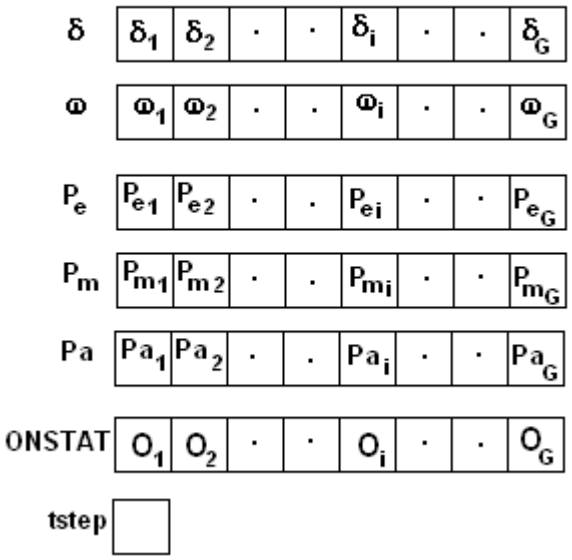

Figure 8-10. GenVarType - stores the generator variables at a given time-step

8.3.3.1. *Allocation and Storage of OMIB Data in the Inner Loop*

The full set of OMIB responses for a scenario are stored in the OMIBResponseType data structure shown in Figure 8-11. This record is composed of a set of allocatable arrays to store the complete time response of each OMIB variable, for the current search scenario, and the associated time vector. The size allocated to the arrays is Nstep, the maximum number of time steps that a TDS will require. Less steps are used for unstable scenarios, or where the ESC is applied. The period between time steps (Tinterval), and the count (i) of the current time step processed by the TDS are also recorded. The information stored in this record is used to calculate the SIME margins for the associated scenario.

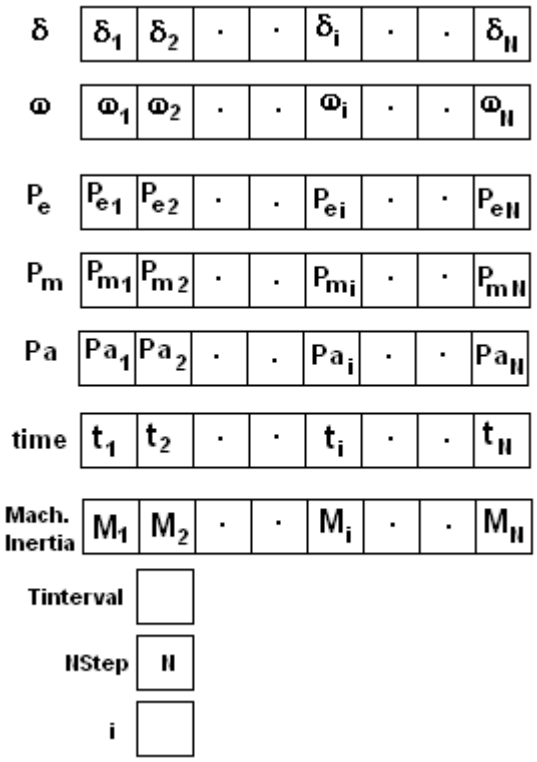

Figure 8-11. OMIBResponseType – stores the OMIB time responses for a scenario

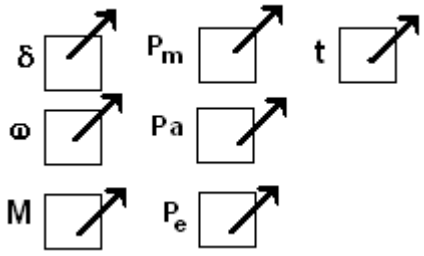

Figure 8-12. OMIBStepType - points to addresses in memory of the OMIB response data elements for the current (ith) time-step.

The OMIBStepType data structure operates in partnership with the OMIBResponseType structure. It is a set of pointer variables that point to the CPU memory address of the OMIB values, at the current (*i*th) time step. The inner-loop user-defined model uses the pointers to keep track of the instantaneous length of the OMIB response data, as the simulation time proceeds.

For the first search scenario the OMIB response is not calculated until after the end of the TDS. The machine group to calculate the response cannot be defined until after COI instability is detected. In this situation, the instantaneous value for each generator variable from Figure 8-10 is progressively recorded to a single binary file. At the end of the TDS the binary file is saved, then closed and reopened with the file handler repositioned at the beginning of the file. The file is re-read from start to finish. The

OMIB response for the variables indicated in Figure 8-10 are simultaneously calculated and stored in the OMIBResponseType structure.

In Fortran, writing and reading TDS data to and from binary files is relatively fast, and the file size is minimal. Such binary files are recorded for all scenarios. This facility has aided investigations on the preferred machine grouping approach.

8.3.3.2. *Storage of Machine Group Data in the Inner Search Loop*

The data structure for handling machine group information is MGType shown in Figure 8-13. Each MGType describes one machine group definition. It contains an allocatable integer array (MachinesSorted), where the size of the array is the number of online machines in the network (NOnline). The array stores a list of machine identifiers partitioned into the two groups. The index value *isplit* indicates the last machine in group 1. Allocatable arrays for the Bus ID, Generator ID (GenID) and generator type[6] (GenType) information are also provided in the MGType record as this information is needed to extract PSS®E TDS data to perform SIME calculations (see section 8.2.4). For BusID, GenID and GenName arrays of pointer variables are used to point to the values in the memory, rather than to duplicate data.

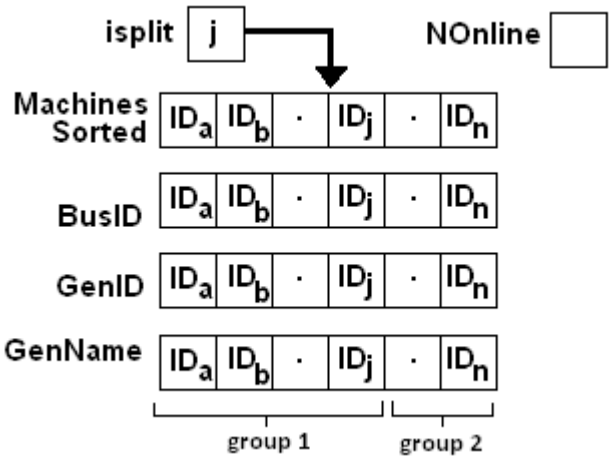

Figure 8-13. MGType -stores machine grouping information

8.3.4. Inner and Outer Loop Configuration Files

To automate the EBSIME search, the inner search loop respectively reads text-based input from an inner loop configuration file and generates a configuration file for the outer loop to enable the outer loop to generate the next scenario. The *inner loop configuration file* is generated by the outer supervisory loop. It provides information about the current scenario that is to be simulated.

[6] In the software the generator type is referred to as GenName.

The *outer loop configuration file* provides information for the next search scenario. The supervisory outer loop prepares load-flow information for the next scenario, and generates the next inner loop configuration file. The process repeats until the search ends. User-written versions of the inner and outer loop configuration files can be adapted for debugging purposes to manually execute the EBSIME algorithm.

The inner loop configuration file and the outer loop configuration file have similar formats. They are composed of a set of search parameters that describe the current or next iteration. Each keyword is followed by a comma-separated parameter value, one per line. Keywords are not case-sensitive and listed in no particular order. Some keywords are mandatory; others are optional, depending on the search progression. The outer- and inner-loop configuration files are distinguished from one another by the keyword LOOP. A LOOP value of 0 in the file indicates it is outer loop configuration file, whereas a LOOP value of 1 indicates it is an inner loop configuration file. Additionally the inner loop configuration file must specify the file location of the outer loop configuration file with the keyword CONFIGFILE_OUT.

The keywords and their associated values are described in Appendix E. Table E-3 explains the keywords required for both inner- and outer-loop configuration files. Table E-4 describes the keywords related to the report and log files that may be generated by the AUSIME model. All filenames are specified with respect to the root directory from which the AUSIME tool is executed. Table E-5 describes variables that are used in the SIME search.

The SIME keywords are categorized into two parts:

1) keywords that describe the SIME margin and its associated properties after the current scenario has been assessed; and
2) keywords that describe the SIME margin of the previous scenario that is used in the limit prediction step.

Table E-6 describes the keywords that have an integer instruction code, and the meaning of the defined code values. In the user-defined model, each of these options is defined as a constant parameter associated with a unique integer identifier that also appears in the inner- and outer-loop configuration files. Examples of the inner- and outer-loop configuration file are shown in Appendix F.

8.3.5. Information Generated by the Inner Search Loop

Depending on the search instruction, the inner search loop (PSS®E user-defined model) is capable of writing search information to a set of text-based reports. TDS, OMIB and

COI responses calculated during the search can be recorded to binary files as mentioned in section 8.1.3. Unless otherwise specified, all output files are created in the folder specified by the keyword SAVEFOLDER described in Table E-4.

8.3.5.1. *Search Traversal Report*

The search traversal report shows the main steps in the path taken by the EBSIME algorithm to locate the TSL. If DEBUGLVL > 0, the traversal report is created at the address specified by SIMEINFO_<FILENM>_TXT. At each iteration the information described in Table 8-2 is reported in a single line record. The records are listed in order of search scenarios. If the predicted FSL falls outside of the current search bounds and redirection (by means of bisection) is required, the violating prediction is listed next to the redirected search step. An example of a traversal report, which includes redirection due to divergence from the FSL, is provided in Figure F-1. The report is similar for the alternative search options, but only the relevant fields are included.

TABLE 8-2. SEARCH TRAVERSAL REPORT - FIELDS TO DESCRIBE EACH ITERATION

Field Name	Definition/ Possible Values
Iter. No	Iteration number (k)
n(k-1)	Margin for the previous scenario (used in limit prediction)
n(k)	Margin for the current scenario
SV	Transient stability Search Variable: either interconnector power transfer or fault clearing time: 'PT' – for power transfer limit search 'CT' – for CCT search
SearchMode	Phase of the EBSIME Search: 'INITIAL' – for search initialization phase 'FIRST-SWING' - for SIME-based FSL prediction phase 'BINARY' – for binary search
Stability Assessment	Transient stability assessment of the current scenario: 'S' if the scenario is classified as stable 'U' if the scenario is classified as unstable.
Predict TSV	SV for the next search scenario Either determined by SIME limit prediction or bisection step
TSA Method	Transient stability assessment that is used to assess the current scenario: 'COI' – if centre of inertia stability criteria is used 'ESC' – if forward-swing early stop criteria is used
LO	The lower search bound
HI	The upper search bound
MOMIB	Twice the OMIB machine inertia used to calculate the SIME response for the scenario.

8.3.5.2. *Search Timing Report*

The search timing report records the time taken to simulate the TDS for each search iteration. The report is written to the file associated with TSIM_FILENM_TXT in the inner loop configuration file. The file is written only if ISRecordTSIM = 1 and DEBUGLVL > 0.

Table 8-3 describes the information that is described in each record. All search times refer to the inner search loop only. The time required for the outer loop process is considered negligible, and thus the outer loop timing is not included. An example of the search execution time report is shown in Figure F-2.

TABLE 8-3. SEARCH TIMING REPORT – FIELDS TO DESCRIBE EACH LINE RECORD

Field Name	Description
Iter. No	Iteration number (k)
TWALL	Real-time in seconds according to the CPU wall clock, taken to run the TDS for the current iteration.
TWALL Cumulative	Real-time in seconds according to the GPS wall clock, taken to run all TDS for the search so far.
TSIM	Duration in simulation seconds of the current TDS.
TSIM Cumulative	Accumulated simulation time, in sim-s, for all TDS so conducted to date.
TSA Method	Stability method used to assess transient stability: 'COI' – if centre of inertia stability criteria is used 'ESC' – if forward-swing early stop criteria is used
Search Variable	The current value of the search variable: in MW for a PTL search; in ms for a CCT search.
Stability Assessment	Stability classification for the current scenario: S - if scenario is stable; or U – if the scenario is unstable.

8.3.5.3. *Machine Group Report*

The machine group report provides information on the machine group used during the search. In the EBSIME search algorithm, the machine group is derived from the first search scenario. The machine group report is written to a file called '<CaseID>_MACH_GRP.TXT', where the field *CaseID* is explained in Table E-1. An example of the machine group report is shown in Figure F-3.

8.3.5.4. *Diagnostic and Error Reporting*

The integer keyword DEBUGLVL, listed in Table E-6 selects between the four debugging levels available for the inner search loop. At the lowest level no debug information is written to file by the user-defined model. At the highest level all formal reports are generated. All trace statements used to develop the inner loop software are printed to a log file and the PSS®E console. Any errors or warnings that occur during execution of the inner-loop are written to an error report file.

To facilitate the debugging feature, the inner search loop creates an error report file and a log file when the search begins. The names of these two files are specified in the inner loop configuration file with the keywords ERROR_FILENM and LOG_FILENM. However, ultimately the names of the error and log files are specified as input parameters when the AUSIME software is called from the command line (see section 8.4.3).

In general, the error report is blank, unless an error occurs during search execution. If this happens the search will terminate, and an error message will be written in this file. The error message includes the name of the AUSIME subroutine where the error was detected. The inner loop uses a global 'ErrorCode' parameter to classify if a user or software error is identified and to indicate the type of error. In normal correct operation the *ErrorCode* value is 0. If an error occurs during execution of the inner loop the *ErrorCode* will be assigned a non-zero integer that describes the type of error.

The log file is essential for developing the implementation of EBSIME algorithm. It is a useful tool for implementing future search methods within the AUSIME framework. The inner loop model includes a library of subroutines that enables trace statements to be easily, and uniformly, reported at any point during the search traversal.

8.3.6. Binary Files Generated For Analysis with MATLAB®

The inner search loop generates a set of binary data files that record the content of the data structures described in section 8.3.3. The binary files are created in the location described by the keyword SAVEFOLDER, from Table E-1.

8.3.6.1. *Generator Parameters Binary File*

Each time the AUSIME tool is executed a binary file titled 'GeneratorParams.bin' is created.

It records the following steady-state information for each online machine, with the parameters of each record in the following order:

`SBASE, MBASE, H, GenIdx, BusID, GenName`

This information is a direct translation of the GenParamType variable in Figure 8-9. It provides a link between the generator variable data and auxiliary information, such as the generator names and numbers. This data is essential to providing a meaningful analysis of the saved results outside of the AUSIME tool.

8.3.6.2. *Generator Variable Binary Files*

For each search iteration, a binary file containing the time-series data of each variable in the GenVarType record, Figure 8-10, is created. For a CCT search the title of each created file is:

'<CASEID>_ CT_<CT>_ms_IT<IterNo>_GENVAR1.BIN'.

Otherwise for the PTL search, it is:

'<CASEID>_PT_<PT>_MW_IT<IterNo>_GENVAR1.BIN'.

where

<CT> is a placeholder for the scenario clearing time in ms;

<PT> is a placeholder for the scenario power transfer in MW;

<IterNo> is a placeholder for the search iteration number; and

<CASEID> is a placeholder for a string descriptor of the current search, as described in Table E-1.

The created files make the generator rotor angle, speed, electrical, mechanical and acceleration power response, for every machine available for analysis after the AUSIME search. Used together with generator parameters binary file, the SIME responses of each scenario can be independently explored with MATLAB®. At each time-step the data from the GenVarType structure is written to file in the following order:

`tstep, Pe, Pm, Pa,` $\delta, \omega,$ `ONSTAT`

Aside from `tstep,` each of the listed parameters represents an array of length NMachs, the number of online generators in the network model.

8.3.6.3. *COI Response Binary Files*

For each iteration, a binary file is created containing the time-evolving COI responses calculated from the generator variable data, Figure 8-10. The naming convention used for the COI response files is similar to that described in section 8.3.6.2, except a post-script of '_COI.BIN' is used (instead of '_GENVAR1.BIN').

At each time-step the following COI values for Figure 8-10 are written to the binary file in the listed order:

`tstep, Msum, δCOI, ωCOI, PeCOI, PmCOI, PaCOI`

where `Msum` is the sum of machine inertia from all online generator in the system. The following variables are are arrays of length NMachs:

`δCOI, ωCOI, PeCOI, PmCOI, PaCOI`

8.3.6.4. *OMIB Response Binary Files*

For each search iteration, a single binary file is created that contains the time-evolving OMIB responses described by the OMIBStepType derived type in Figure 8-10. The naming convention used for the OMIB binary files is similar to the convention described in section 8.3.6.2, except a post-script of '_OMIB.BIN' is used. At each time-step the values from the OMIBStepType of Figure 8-12 are written to the binary file in the listed order:

`tstep, M, δOMIB, ωOMIB, PeOMIB, PmOMIB, PaOMIB`

8.3.6.5. *Machine Groups (MG) Binary File*

The MG binary file is a direct translation of the data stored in the MGListType structure, described in section 8.3.3.2. When the AUSIME tool is executed a single binary file, named '<CaseID>_MACH_GRP.BIN' is created. This file can be used to pre-select and use the MG in subsequent EBSIME searches.

8.3.6.6. *Tools for Converting Binary files into MATLAB® format*

Auxiliary applications to translate the binary data into a MATLAB® readable format have been written in Fortran 95, and provided with the AUSIME package. The name and function for each tool is described in Table 8-4. The input arguments are described in Table 8-5. The output variables that are made available in generated MATLAB® m-files are described in Table 8-6. The variables in rows 1 to 6 are available in the m-files generated by each of the conversion tools. The GenerateMFile_genvars application additionally makes the variables listed in rows 7 to 12 accessible.

Figure F-18 shows how the conversion commands are executed form the DOS command prompt. MATLAB® scripts demonstrating how the generated m-files may be used are presented in Figure F-19.

TABLE 8-4. GENERAL DESCRIPTION OF THE BINARY TO MATLAB® CONVERSION TOOLS

Tool Name	Function
GenerateMFile_genvars.exe	Generates a MATLAB® m-file describing time-varying variables for each generator in the system model. M-file naming convention: <CaseID>_G<Index>.m where <Index> is substituted with the machine index. Executing this file makes select generator variables, for a given scenario, available to MATLAB®.
GenerateMFile_COI.exe	Writes COI responses to a MATLAB® m-file. M-file naming convention: <CaseID>_COI.m Executing this m-file makes the COI time responses for a given scenario, available to MATLAB®.
GenerateMFile_OMIB.exe	Write OMIB responses to a MATLAB® m-file. M-file naming convention: <CaseID>_OMIB.m Executing this m-file makes the OMIB time responses for a given scenario, available to MATLAB®.

TABLE 8-5. BINARY TO MATLAB® M-FILE CONVERSION TOOLS - INPUT ARGUMENTS

Tool Name	Input arguments
GenerateMFile_genvars.exe	1 – Binary File Name 2 – Output folder 3 – CaseID 4 – Location of file GeneratorParams.bin
GenerateMFile_COI.exe	1 – Binary COI File Name 2 – Output folder 3 – CaseID
GenerateMFile_OMIB.exe	1 – Binary OMIB File Name 2 – Output folder 3 – CaseID

TABLE 8-6. BINARY TO MATLAB® M-FILE CONVERSION TOOLS - GENERATED VARIABLES

Row No.	AUSIME Variable	MATLAB® equivalent
1	time	t
2	δ	delta
3	ω	omega
4	P_e	Pe
5	P_m	Pm
6	P_a	Pa
7	ONSTAT	ONSTAT
8	MBASE	MBASE
9	SBASE	SBASE
10	BusID	BusID
11	GenIdx	GenIdx
12	H	H

8.4. Design Choices for the Supervisory Outer Search Loop

The AUSIME outer search loop provides the interface between the user and the AUSIME software, and fully automates the TSL search using the EBSIME algorithm. It supervises consecutive search iterations executed by the inner loop. It also reads and translates the main search instructions, tracks changes in key parameters as the search progresses, and provides an interface between the inner loop dynamic simulations. The outer loop functions are summarized by the blue boxes in Figure 8-1. The outer loop is designed to read and translate a set of text-based search instructions from a user supplied text file and for each search scenario it:

- generates a text-based inner-loop configuration file to be read by the AUSIME inner search loop each time a TDS is run;
- generates a PSS®E command file (.IDV) with the instructions for each TDS; and
- reads the outer loop configuration files generated by the inner search loop.

The AUSIME outer loop software is also intended to prepare PSS®E load flow data files (.RAW) that are required to run each TDS. It is noted that at the time of writing this function has not been implemented yet, all load-flows are manually prepared.

PSS®E versions 30 and above allow PSS®E load flows and TDS to be executed using Python scripts. As such, the outer search loop is designed and implemented using the Python programming language.

8.4.1. Input files to the Outer Search Loop

The AUSIME outer loop software requires a number of input files that contain search instructions. After setting up the initial files correctly, many search studies can be readily executed. The input files are described in the following sections.

8.4.1.1. *Flexible Input Search Instruction File*

The AUSIME outer loop software receives its main instructions from the main instruction file, a text file provided by the user. It describes the type of search that is to be executed, search related options, and the locations of files and folders that are required for the search. The instructions are listed as comma-separated keyword and parameter records, with one record per line. The keywords required for the instruction file are described in Table E-1. All keywords are case insensitive. An example of the main input instruction text file is shown in Figure F-4.

8.4.1.2. *Fault Definition File*

The fault definition text file is used to describe the contingency for a TSL search. Instructions are listed as comma-separated keyword and parameter records, with one record per line. The keywords required for the fault definition file are described in Table E-2. All fields are compulsory. The information in this file is primarily used to generate the sequence of commands that PSS®E must execute, to perform the TDS. An example of the fault definition file, and the generated PSS®E command file, are shown in the Appendix F.

8.4.1.3. *Input Dispatch Information*

For a PTL search there are many ways that the interconnector power transfer may be adjusted. As such, generation and/ or load dispatch instructions need to be provided to instruct the AUSIME software on how to change the interconnector flow between search scenarios. As the feature to automate PTL searches with the AUSIME software has not been implemented yet, the following approach is suggested.

The location of the dispatch file is described in the main search instruction text file with the *DispatchFile* keyword (see Appendix F). The dispatch text file contains a set of information that enables solvable load-flow files with specific interconnector power transfer to be generated, as needed, by the AUSIME software. This information is described in Table 8-7. The dispatch instruction file describes two areas bordering the interconnector that is being investigated and whether the power transfer will be varied by load or generator dispatch. The dispatch file also describes a set of solved, base load-flow (.RAW) files with unique pre-specified interconnector flow that must be provided by the user. The power transfer of the provided load-flows should increase monotonically by a fixed, coarse, step size. Each load-flow should be manually configured to ensure that the system operates within its physical limits. During the search, the outer supervisory loop creates load-flow files with more refined transfer as needed, from the base set of load-flows. Figure 8-14 shows an example of the suggested dispatch text file for a PTL search on the 4 machine system, where the required information is listed. The *RAWFILE* keyword describes where the base set of the load-flow files are located. To automate a CCT search the dispatch text file is not required. A single load-flow, the location specified via the main search instruction file (*LoadFlowFile)*, is required. The same load-flow is used for all scenarios in the CCT search.

TABLE 8-7. PROPOSED INFORMATION FOR THE DISPATCH INSTRUCTION FILE

Keyword	Description
AREA_A	The integer identifier of the first area where load or generation will be adjusted. The direction of transfer is from area A to B.
AREA_B	The integer identifier of the second area in which load or generation will be adjusted.
ADJUST	Describes how the power transfer will be varied over the target interconnector to achieve a target transfer. 'LOAD' – indicates power transfer adjustment by scaling load, 'GENERATION' – indicates power transfer adjustment by scaling generation.
RAWFILE	The file location of a sequence of load flow cases with monotonically increasing power transfer. Each load flow file record has the format RAWFILE, <PT>, <RawFileName> where <PT> is the power transfer in MW and RawFileName is the name of the PSS®E load flow raw data file.

```
AREA_A, 1
AREA_B, 2
ADJUST, LOAD
RAWFile, 0, ..\PSSEFILES\MediumLoad_0MW.raw
RAWFile, 100, ..\PSSEFILES\MediumLoad_100MW.raw
RAWFile, 200, ..\PSSEFILES\MediumLoad_200MW.raw
```

Figure 8-14. An example of the dispatch text file

8.4.2. Outer Loop Data Structures

The outer loop data structures have three main purposes:
1) to store data read from the user supplied search instruction files into working memory;
2) to provide sufficient information to correctly generate inner-loop configuration and PSS®E command files; and
3) to store information read from the outer-loop configuration files produced by the inner-loop into working memory that is required to prepare data for the next scenario.
The outer loop implementation makes extensive use of the Python 'dictionary' data structure. The dictionary structure comprises a set of keys and associated values. The dictionary is indexed by its keys. A foundational data structure defined for the outer-loop implementation is a dictionary called *KeyItem*.

The KeyItem variable stores information read from a single line record of one of the outer loop text files described in sections 8.3.4 and 8.4.1. It provides sufficient information to check that the value specified by the line record matches the expected data type. It provides a boolean field, '*UserSpecified*', which must be 'true', to check

that *required* keywords are specified in the text file. The key-value pairs stored in the KeyItem object are summarized in Table 8-8.

An example application of the KeyItem data-type to represent the 'SearchMode' keyword is shown in Figure 8-15. The SearchMode field is a *string* variable that *must* be specified by the user. As such it has no default *value* and the *UserSpecified* is 'FALSE' as the *value* is not yet assigned.

TABLE 8-8. THE KEYITEM OBJECT USED TO REPRESENT EACH FIELD

Key	Value
Type	The required data type for the Value .
IsRequired	'True' if the keyword and value must be defined in the input text file; otherwise 'false'
Value	The value associated with the keyword. The value must match the Type. In case IsRequired= 'false', the initial value is the default.
UserSpecified	In the case where a field is optional: 'True' if a valid value is assigned to the keyword in the input text file; 'False' to indicate that the default value is used.

'Type'	'IsRequired'	'Value'	'UserSpecified'
STRING	TRUE		FALSE

Figure 8-15. The SearchMode field as represented by a KeyItem variable

The outer-loop implementation uses three higher level dictionary structures to store data from the search text files:

- The *SearchInfoItem* data type is designed to store information read from the main search instruction file described in Table E-1.
- The *FaultInfoItem* data type holds the information read from the fault definition file described in Table E-2.
- The *ScenarioItem* data type progressively stores information for the inner- and outer-loop configuration files, as described in section 8.3.4. It saves data associated with the keywords described in Table E-3 to Table E-6.

In the SearchInfoItem, FaultInfoItem and ScenarioItem objects each keyword is represented by a key and a KeyItem value. The key is the name of the described field and KeyItem describes the properties associated with it. Figure 8-16 shows an example of a part of a SearchInfoItem variable after the main search instruction text file has been read. The fields SearchMode, TSVType and GenerateReport from Table E-1 are

represented. The left column describes fields represented by the SearchInfoItem dictionary; the remaining describe the field properties. The information in the FaultInfoItem dictionaries is similar.

KEY	KeyItem Values			
SearchMode	'Type'	'Value'	'IsRequired'	'UserSpecified'
	STRING	BINARY-SIME	TRUE	TRUE
TSVType	'Type'	'Value'	'IsRequired'	'UserSpecified'
	STRING	CCT	TRUE	TRUE
GenerateReport	'Type'	'Value'	'IsRequired'	'UserSpecified'
	INTEGER	1	FALSE	FALSE
• • •		• • •		

Figure 8-16. An example of the SearchInfoItem structure

The ScenarioItem is similar, but an additional boolean field 'IsWrite' is added to the KeyItem object. This field is necessary as the ScenarioItem is used to respectively read data from the outer-loop configuration files, and write data to the inner-loop configuration files. Between the two file types, different keywords are required. When 'IsWrite' is true, this indicates that the described field will be written to the inner-loop configuration file.

The *ScenarioList* is a higher level dictionary that uses the SVs as keys paired with ScenarioItem values. The purpose of this structure is to keep track of the data from all traversed scenarios. As the search proceeds through a range of scenarios, corresponding ScenarioItems are progressively appended to the ScenarioList. This feature is useful for reviewing the results of previously traversed scenarios for reasons such as search redirection, or determining the new search bounds when the search transitions from the forward-swing to the multi-swing phase.

8.4.3. Executing a TSL search with the AUSIME Tool

The AUSIME software is driven by a high level Python script called 'AUSIMEDriver.py' here on referred to as the driver. It is called from the DOS command prompt by executing a command of the following syntax:

```
Python AUSIMEDriver.py <InstructionTextFile>
<ErrorTextFile> <LogTextFile>
```

The function of each argument is described in Table 8-9.

TABLE 8-9. AUSIME SOFTWARE ARGUMENT DESCRIPTORS

Argument	Description
InstructionTextFile	The location of the main search instruction file - relative to the current working directory (CWD).
ErrorTextFile	The location of the error report text file, will be created relative to the CWD.
LogTextFile	The location of the log (text) file, will be created relative to the CWD.

To run a search the path of the Python software and the outer loop source code must be assigned to the DOS path. It is useful to encapsulate this information in a batch file. Figure 8-17 shows a batch file that is used to execute a TSL search with the AUSIME software.

```
set PYTHONPATH=PYTHONPATH;..\outerloop\Pythoncode\

Python AUSIMEDriver.py InstructionFile1.txt AUSIME_Error.txt

AUSIME LOG.txt
```

Figure 8-17. An example of batch file commands used to execute a TSL search with the AUSIME software

8.4.4. Flow Of Control of the Outer Search Loop

A chart describing the flow of actions performed by the outer search loop is shown in Figure 8-18. Each of the main tasks are performed by a combination of subroutines defined in the Python modules. The major subroutines are mentioned in bold in Figure 8-18.

The AUSIME software is called from the DOS command-line, as per steps A & B in Figure 8-18. The supplied input arguments (see section 8.4.3) are used to create and open the global error and log files. At step C in Figure 8-18 the information provided by the main search instruction file is parsed into an instance of the *SearchInfoItem*. The inner loop AUSIME model is linked with PSS®E at step D in Figure 8-18. It must be linked every time the search is executed in a new working directory. At step E in Figure 8-18 fault information is read into an instance of the *FaultInfoItem*. In step F in Figure 8-18 the information for the first scenario is loaded into an instance of a *ScenarioItem*. It is used to generate the first PSS®E command file (.IDV) and inner-loop configuration files for the search (step G in Figure 8-18).

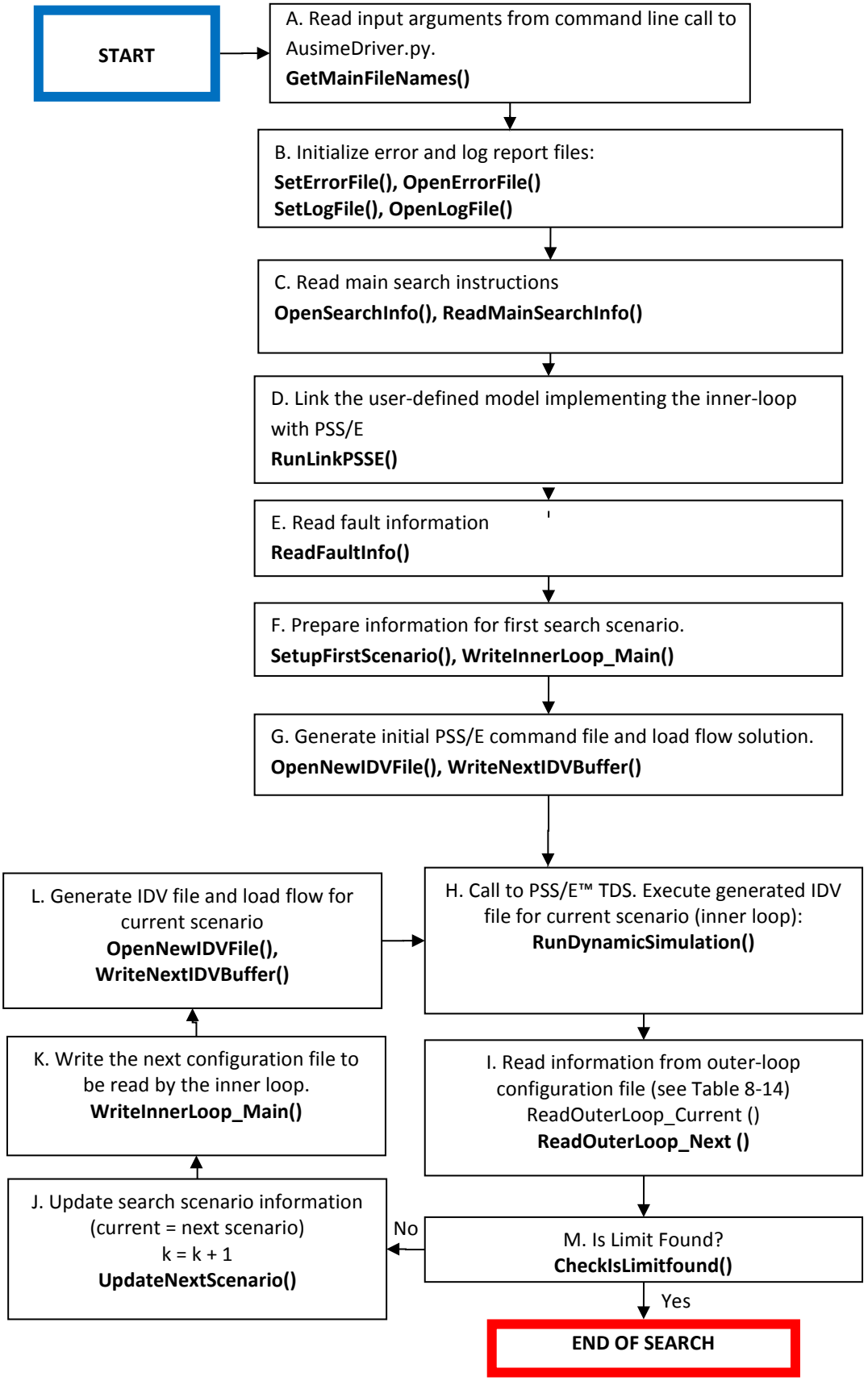

Figure 8-18. Flow of control of driver for the Outer Loop (AusimeDriver.py)

The iterative search phase begins at step H with the first call to the inner loop model. After the TDS is executed the outer-loop configuration file, generated by the inner loop, is read and interpreted by the outer loop (step I in Figure 8-18). It is used to update the search information stored in the outer loop data structure (step J in Figure 8-18). The file, and the load-flow for a PTL search, are prepared for the next search scenario. Steps H to M in Figure 8-18 are repeated until the multi-swing limit is found.

8.4.5. Python Modules of the Outer Search Loop

The subroutines used to run the outer search loop are defined in Python modules – files containing a set of data structures and subroutines designed to perform a particular task. Figure 8-19 describes the modular Python architecture used to implement the outer loop. Many AUSIME modules are built using inherited data structures or subroutines defined in other modules in the AUSIME library.

The outer loop modules can be split into the following categories based on their primary functions:

- Report error, warnings and debug messages to global error and log files;
- Parse information from a text instruction file into dynamic memory; and
- Generate text instruction files to be read by the inner loop model.

The following sections describe how the modules integrate with the driver to implement the AUSIME search procedure.

8.4.5.1. *Automating the Full Search*

The FullSearchInfoModule is used to manage automation of an entire AUSIME TSL search from start to finish. With reference to Figure 8-18 the key functions of this module are to:

1) read the main search instruction file (step C),
2) store data read from the main search instruction into working memory (step C)
3) automate the iterative part of the search (steps H to M).

To store the main search information, the module defines the SearchInfoItem structure, as described in section 8.4.2 and provides subroutines to handle the data it contains. The full set of subroutines provided by this module are summarized in Table 8-10. The RunCCTSearch subroutine is used to automate the iterative part of the CCT search. It takes a high level view of the search, and uses many key subroutines in the other Python modules to perform this task.

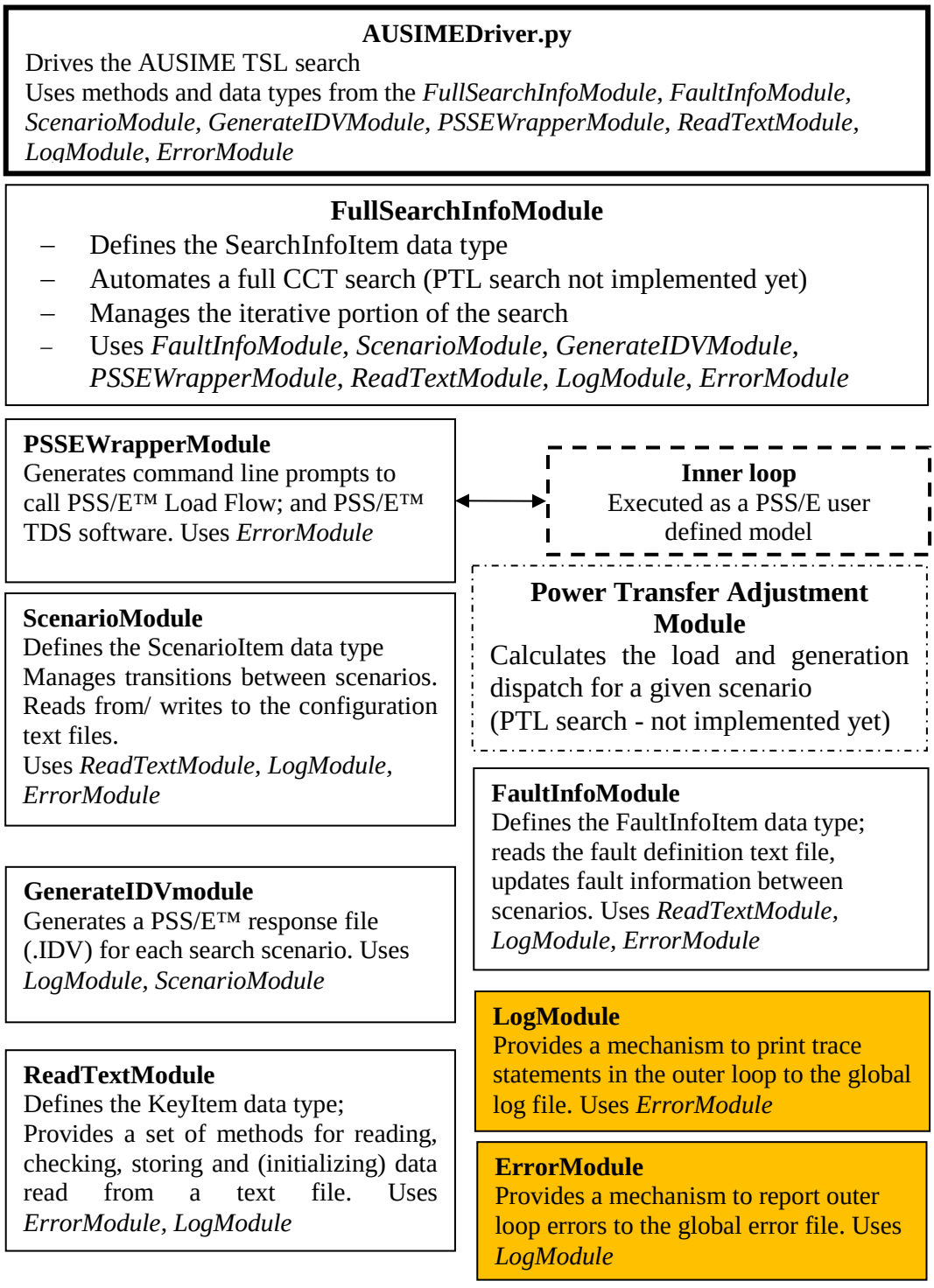

Figure 8-19. Modular architecture of the outer loop written in the Python programming language

The RunCCTSearch subroutine uses the ScenarioList dictionary, described in section 8.4.2, to keep track of the scenarios that are traversed. The ScenarioList is significant during the search redirection, and the last part of the forward-swing limit prediction phase when traversed scenarios may need to be revisited to determine multi-swing stability.

TABLE 8-10. SUBROUTINES PROVIDED BY THE FULLSEARCHINFOMODULE

Subroutine	Description
GetMainFileNames	Decodes input specified in the command line call to the AUSIME tool. See section 8.4.3.
Init_MainSearchInfo	Initializes the structure of the SearchInfoItem. Output: Initialized SearchInfoItem object
OpenSearchInfo	Opens the main search instruction text file for reading. Input: Filename of main search instruction file Output: File handle of search instruction file
Read_MainSearchInfo	Read and validate information in the main search instruction file and store it into working memory. Input: File handle of the opened file Output: SearchInfoItem
CheckMainSearchInfo	Test that the data provided by the main search instruction file describes a valid search. Input: MainSearchInfo Output: ErrorCode
RunCCTSearch	Automates the iterative part of the search (steps H to M in Figure 8-18) until the multi-swing limit is found. Input: FaultInfo, SearchInforItem, ScenarioItem for the current scenario Output: ScenarioList

8.4.5.2. *Reporting Errors, Warnings and Debug Statements*

The ErrorModule provides facilities to report errors encountered during execution of the outer search loop. It accommodates different levels of error reporting as specified by the DEBUGLVL keyword (see Table E-6). The AUSIME software employs an error reporting method where a global error report file is created. File close and open methods allow the error file to be shared with the inner loop for error reporting. The supplied subroutines are summarized in Table 8-11. Like the inner loop, a global integer variable, 'Errorcode', is used to indicate if an error occurs during execution of the outer loop. As long as it is 0, the search operates normally. Otherwise a non-zero ErrorCode indicates that an error has been identified, and the search will terminate. The LogModule provides a similar set of subroutines for writing debug statements to a globally accessible log file.

TABLE 8-11. SUBROUTINES PROVIDED BY THE ERRORMODULE

Subroutine	Description
SetErrorFile	Assigns the global error report file. Input: error file name
ReturnErrorFile	Returns the integer file handle of the assigned error file Output: file handle object
OpenErrorFile	Creates and opens a new error file
CloseErrorFile	Closes the error file
ReOpenErrorFile	After the global error file has been created, this subroutine is used to reopen it, and position the error file handle to point to the end of the file.
SetErrorLevel	Assigns the DEBUGLVL. Input: debug level code
ReportError	Records an error message to the error file. Input: Error message

8.4.5.3. *Parsing Data From Input Text Files*

The ReadTextModule is concerned with reading a single line record from an input text file, and saving the data into an instance of the KeyItem object. It defines the KeyItem dictionary (see section 8.4.2), and a range of Python methods to access the KeyItem data structure and to parse line records from a text file to working memory. The subroutines provided by this module are listed in Table 8-12. These subroutines are used by the read subroutines in the ScenarioModule and the FaultInfoModule.

The ScenarioModule is concerned with reading and writing information to, and from, the configuration text files. It defines the ScenarioItem structure which contains this information. Similarly the FaultInfoModule provides subroutines to read information from the fault definition text file. It defines the FaultInfoItem dictionary for storing information about the dynamic simulations. The values of the ScenarioItem and FaultInfoItem variables use the KeyItem structure, defined in the ReadTextModule. The contents of the two data structures are each designed to reflect the information in the fault definition file, and the configuration files. The subroutines provided by the FaultInfoModule and ScenarioModule and are summarized in Table 8-13 and Table 8-14.

TABLE 8-12. SUBROUTINES AND FUNCTIONS PROVIDED BY THE READTEXTMODULE

Subroutine	Description
InitKeyItem	Initializes a KeyItem object - defines the expected type of the key value, a default value, and a flag indicating if the item must be specified (IsRequired). Input: type, default value, IsRequired Output: KeyItem
ReadKey	Parse a single line record into key and value (string) tokens Input: text line record Output: key, value
CheckKeyItem	Check that a specified key exists in the dictionary structure, and the value is the expected type. Input: Dictionary, key, value Output: Errorcode
SetKeyItem	Assigns a key and value to a KeyItem object Input: KeyItem, key, value Output: KeyItem
IsBlankLine (function)	Returns: IsBlank = 'true' if the input line record is blank; otherwise IsBlank = 'false'. Input: Line record Output: IsBlank flag
IsComment (function)	Returns: IsComment = 'true' if the input line record is a comment line prefixed by "\"; otherwise IsComment = 'false'. Input: Line record Output: IsComment flag

TABLE 8-13. SUBROUTINES PROVIDED BY THE FAULTINFOMODULE

Subroutine	Description
INIT_FaultInfo	Initialize an instance of the FaultInfo dictionary; assign default values to the FaultInfo object Output: FaultInfo
ReadFaultInfo	Read the fault definition text file Input: FileID, MainSearchInfo Output: FaultInfo
CheckFaultInfo	Check the validity of the information stored in an instance of the FaultInfo data structure. Input: FaultInfo,MainSearchInfo

TABLE 8-14. SUBROUTINES PROVIDED BY THE SCENARIOMODULE

Subroutine	Description
CHECK_Scenario_for_Read	Checks if the data read from the outer-loop configuration file is valid Input: ScenarioItem
CheckIsLimitFound	Returns: ' ' if no limit is found 'FS' if the forward-swing limit is identified; otherwise 'MS' if the multi-swing limit is found Input: ScenarioItem; Output: IsLimitFound (string)
SET_ScenarioItem	Assigns the value for a specified key in the ScenarioItem dictionary. Input: ScenarioItem, key, value Output: Updated ScenarioItem
GET_Scenario	Return the value for a specified key in the ScenarioItem dictionary. Input: ScenarioItem, key Output: Requested Value
INIT_Scenario	Initializes an instance of the ScenarioItem dictionary, assigning optional, compulsory, and default properties for each KeyItem. Output: ScenarioItem
ReadScenarioKey	Parses a string into key and value tokens. Returns a user-error if key or value is invalid. Input: String Output: key, value, errorcode
ReadOuterLoop_Current	Reads the outer loop configuration file and updates current scenario information (such as TDS time, and SIME margins) in the ScenarioItem object after the TDS is run. Input: File handle, ScenarioItem Output: ScenarioItem
ReadOuterLoop_Next	Reads the outer loop configuration file to create the ScenarioItem for the next search scenario, prior to the TDS. Input: File handle Output: ScenarioItem
UpdateNextScenario	Prepare the ScenarioItem for the next iteration Input: SearchInfoItem, ScenarioItem Output:Next ScenarioItem

8.4.5.4. *Tools to Generate Response and Configuration Files*

The GenerateIDVModule and the ScenarioModule each provide a set of tools to generate text-based code files. In both modules the approach to code-generation is first to write the code to a string buffer, and then to write the string buffer to file. Both modules provide methods for opening and closing files, and assigning valid file handles to a new file.

The ScenarioModule provides subroutines to generate the inner- and outer-loop configuration text files for a given scenario, as per steps F and K in Figure 8-18. These subroutines are listed in Table 8-15.

TABLE 8-15. SCENARIOMODULE: TO GENERATE THE INNER-LOOP CONFIGURATION FILE

Subroutine	Description
CreateConfigFileName_InnerLoop	Generates the name of the inner- and outer-loop configuration files for the specified scenario Input: CASEID, ISEARCH, SAVEFOLDER Output: ConfigFileName_In, ConfigFileName_Out
SetupFirstScenario	Setup the ScenarioItem for the first scenario, using information from the main search instructions and fault definition file. Input: SearchInfoItem, FaultInfoItem Output: ScenarioItem
CHECK_Scenario_for_Write	Check if all values stored in a ScenarioItem object are sufficient to generate an inner-loop configuration file. Input: ScenarioItem
WriteInnerLoop_Main	Writes the code for the inner-loop configuration file to a string buffer Input:Scenario; Output: string
WriteInnerLoop	Encapsulates the following procedures 1) Create a new inner-loop configuration file; 2) Write string buffer to file; 3) Close file Input: string buffer, Scenario; Output: Name of the new inner-loop configuration file

The subroutine ‘CreateConfigFileName_InnerLoop’ creates the names for the inner- and outer-loop configuration files. The syntax of the inner-loop configuration file name is:

“AUSIME_INNERLOOP_CONFIG_<CASEID>_IT<ISEARCH>_IN.txt”.

where <ISEARCH> is the scenario number. The syntax of the outer-loop configuration filename is:

“AUSIME_INNERLOOP_CONFIG_<CASEID>_IT<ISEARCH>_OUT.txt”.

The parameterised fields in the filenames are described in Table E-3 and Table E-4.

At step F of Figure 8-18, the ScenarioItem is loaded with the data required to generate both the inner-loop configuration file and the PSS®E command file (.IDV) for the first search scenario. This is performed by the subroutine SetupFirstScenario. In all following scenarios, the search data for the next ScenarioItem is duplicated from the current one. Remaining fields are updated according to the data from the outer-loop configuration file. The subroutine ‘CHECK_Scenario_for_Write’ checks that all values required for the next inner-loop configuration file are written.

The information prepared for the inner-loop configuration file is translated for the current scenario. As in section 8.3.4 the set of data written to the inner-loop configuration file differs from the outer-loop configuration file. As such each KeyItem in the ScenarioItem structure has an additional boolean field - 'IsWrite'. The subroutine WriteInnerLoop_Main uses this flag to identify all the key-value pairs that must be written to the inner-loop configuration file, and writes them to a string buffer. Then, the subroutine WriteInnerLoop is called to create a new inner-loop configuration file, write the string buffer to file, and close the file. An example of the generated inner-loop configuration file is shown in Figure F-7.

GenerateIDVModule provides subroutines to auto-generate the PSS®E command file for a given scenario. It supports steps G and L in Figure 8-18. When a new PSS®E command file is created by the subroutine 'OpenIDVFile', the file name is:
<SAVEFOLDER><CASEID>_<SVName>_<SV><SVUNITS>_ITER
<ISEARCH>.IDV
where <SAVEFOLDER> is the destination directory where all outputs are saved;
<SVName> is either 'PT' for a PTL search, or 'CT' for a CCT search,
<SV> is the value of the search variable for the scenario,
and <SVUNITS> is either 'MW' for the a search, or 'ms' for a CCT search.

The generated PSS®E command file is composed of multiple sections that each perform a particular task in the TDS. Each section of PSS®E commands is progressively appended to the end of a string buffer. The full contents of the buffer are written to file with a single write command. Table 8-16 lists the subroutines from GenerateIDVModule that are involved with file creation, and preparing the content of the PSS®E command file. An example of the generated command file, and the subroutines that produce each part, is explained in Figure F-10 to Figure F-13.

TABLE 8-16. AUXILIARY SUBROUTINES PROVIDED BY THE GENERATEIDVMODULE

Subroutine	Description
OpenIDVFile	Creates an empty PSS®E command file, and an associated file name. Input: ScenarioItem Output: File handle, updated ScenarioItem, FileName
CloseIDVFile	Close the created command file. Input:File handle
WriteNextIDVBuffer	Writes the complete contents of the generated PSS®E command file to a string buffer. Encapsulate the code generation subroutines. Input: ScenarioItem, FaultInfo Output: StringBuffer

8.4.5.5. *Encapsulating Calls to the Command Prompt*

The PSSEWrapperModule enables PSS®E calculation tools to be called at appropriate times during execution of the outer-search loop. It provides subroutines that generate a set of DOS commands to a string buffer, and then executes them at the command prompt.

The subroutine 'RunLinkPSSE' performs Step D of Figure 8-18. It prepares a set of commands for the Lahey-Fujitsu Fortran 95 compiler, to link the object files of the AUSIME inner-loop model to PSS®E in the working directory. This action must be performed whenever the AUSIME tools are operated from a new working directory, otherwise the AUSIME tools will be unrecognized by PSS®E.

The subroutine 'RunDynamicSimulation' performs Step H in Figure 8-18. It is called for each scenario when the TDS needs to be run. It generates the following line record and executes it at the DOS command prompt:

```
pssds4 -gnikool off -inpdev <IDVFileName> ^>
<SAVEFOLDER>IT<ISEARCH>.TXT
```

<IDVFileName> is the name of the PSS®E command file generated by the outer-loop, the other fields are defined in Appendix E. This command redirects console output to a text file in the output save folder called '`IT<ISEARCH>.TXT`'. Table 8-17 summarizes the subroutines provided by this module.

TABLE 8-17. PUBLIC SUBROUTINES PROVIDED IN THE PSSEWRAPPERMODULE

Subroutine	Description
RunLinkPSSE	Generates and executes text commands to link the inner loop model object files to PSS®E using the Lahey-Fujitsu Fortran 95 compiler Input: Folder location of inner loop object files (string)
RunDynamicSimulation	Generates and executes the call to the PSS®E dynamic simulation program for the current scenario Input: PSS®E Command File Name, ISEARCH, SAVEFOLDER
RunPause	Pauses the simulation.

8.5. Chapter Conclusion

The AUSIME software is a flexible and reliable automation tool that is able to accurately locate TSLs using the EBSIME algorithm. It integrates the algorithm with the PSS®E software by using the facility for PSS®E user-defined models, consequently providing reliable and accurate TSL search results. The software incorporates a number of useful design choices:

- Flexible text-based search instruction inputs,
- Text-based output reports on the search timing, traversal and other results;
- OMIB, COI, and original time responses saved to binary file that can be converted to MATLAB® readable format;
- A modular architecture that allows the AUSIME software to automate alternative search algorithms, and to use tried and trusted open source tools;
- Dynamically allocatable storage to facilitate the analysis of power systems of widely differing sizes, and to enable efficient handling of the potentially large volumes of data involved.

The chapter includes explanations of how to 1) execute the AUSIME tool, 2) write the text-based in input files to specify the search instructions and 3) read the output report files.

The software implementation is composed of two parts – the inner search loop and the supervisory outer search loop. The inner loop is implemented as a PSS®E user-defined model using the Fortran 95 programming language, and is executed at every time step of the TDS. The supervisory outer loop makes use of the PSS®E automation feature where tools from the PSS®E API library can be invoked using the Python language. The outer loop is implemented using Python scripts. It drives the search, invokes the PSS®E dynamic simulations and keeps track of the search traversal. Text-based inner- and outer-loop configuration files are used to communicate results between the inner and outer search loops. The EBSIME algorithm has been implemented as a plug-in to the TDS software without requiring access to, or modification of, the PSS®E source code.

Chapter 9 TSA on the Simplified Model of the South-East Australian System

This chapter examines the practical application of the Enhanced Binary-SIME (EBSIME) algorithm to search for transient stability limits (TSL) on the IEEE simplified 14 generator model of the South-East (SE) Australian power system (AU14GEN) [12]. Power transfer limit (PTL) searches are conducted for 8 cases in this chapter. In four of the cases the fault is applied at the sending-end of the interconnector, and the receiving-end in the other four cases. The searches are conducted for 3 phase faults on the Queensland to New South Wales Interconnector (QNI) and the Victoria to South Australia Interconnector (VSI).

On the AU14GEN system, as in Chapter 5, it is found that a fault applied at the sending-end of an interconnector tends to constrain system operation with forward-swing instability, particularly for high power transfers. Thus, for such scenarios the SIME early stop criteria (ESC) and SIME margins can be used by the EBSIME algorithm to accelerate the search for the critical fault clearing time (CCT) or the power transfer limit (PTL). In this chapter the following are compared: 1) the performance of the EBSIME algorithm against the plain binary search to locate the TSLs, and 2) the mechanisms leading to transient instability.

There is no advantage to the EBSIME algorithm when back-swing instability is a concern. As such a detailed discussion of the AU14GEN cases featuring a receiving-end fault, and the asymmetry in the TSLs when compared to a sending-end fault (see Chapter 5) are deferred to Chapter 10.

9.1. Problem Description

Transient stability analysis (TSA) of the IEEE 14-generator SE Australian system (AU14GEN) is used to test the performance of the EBSIME algorithm. A geographical representation of AU14GEN is shown in Figure 9-1. The one-line diagram of the system is shown in Figure 9-2.

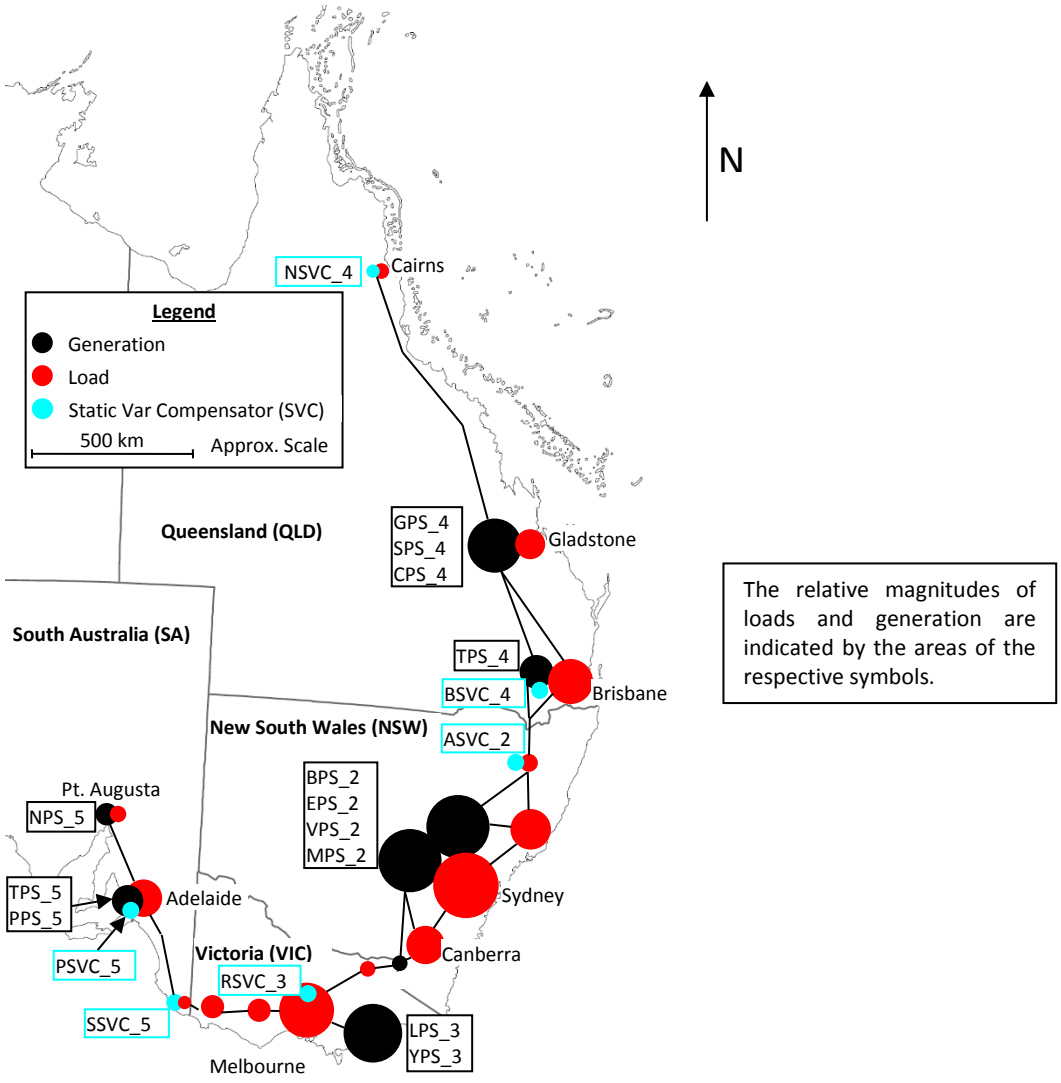

Figure 9-1. A geographical representation of the 14 generator South East Australian power system (AU14GEN)

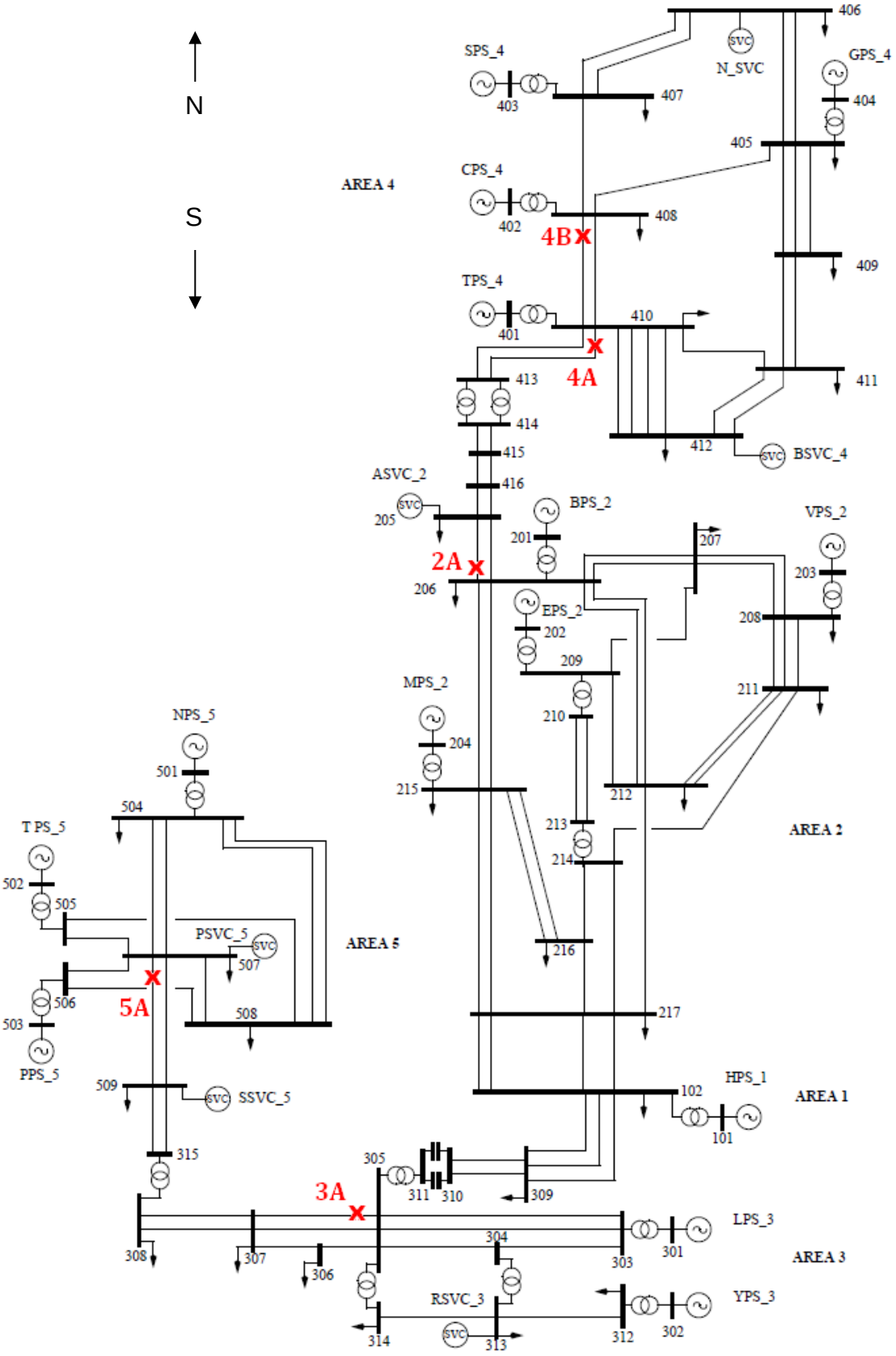

Figure 9-2. One-line diagram of the AU14GEN system

9.1.1. Base Operating Conditions

On the AU14GEN system two different base operating conditions are considered - scenario 1 and 2 from [12]. In base condition B1, the system is under heavy load and the power flows from north to south. In base condition B2, the system is under medium to heavy load, and the power flow is from the south to north. In both base conditions the slack bus is located at the Snowy Hydro power station, at bus 101. The base conditions provide a common basis to assess transient stability for a range of bi-directional power transfers over the system. Table 9-1 summarizes the total generation, load and power transfer over the major interconnectors for each base operating condition.

Variations in the power transfer over the QNI are achieved by transferring load between Queensland (QLD) and New South Wales (NSW), such that the total load remains constant. Changes in power transfer over the VSI are similarly achieved by transferring load between South Australia (SA) and Victoria (VIC). For example, consider base condition B1. To increase the power transfer from QLD to NSW from 500MW to 550MW, the NSW load should be increased by approximately 50MW, and the QLD load reduced by 50MW. In the solved load-flow the SVC reference voltage and transformers tap settings are adjusted to ensure that the SVC's operate within their reactive power limits.

TABLE 9-1. STEADY STATE BASE OPERATING CONDITIONS

Base Condition No.	Direction of Power Flow	Total System Generation (MW)	Total System Load (MW)	Interconnector Power Flow (MW) (North to South)			
				QLD to NSW	NSW to Snowy-Hydro	Snowy-Hydro to VIC	*VIC to SA*
B1	North to South	23030	22300	500	1134	1000	500
B2	South to North	21590	21000	-300	-1120	-1000	-500

9.1.2. Contingencies Investigated on the AU14GEN System

For the TSA of the AU14GEN system a three-phase fault is applied at each of the locations marked in Figure 9-2. Table 9-2 provides a summary of the investigated cases. Two different fault locations, relative to the direction of power transfer on the target interconnectors, are considered. A three-phase fault applied at the sending-end of the interconnector; and a three-phase fault at the receiving-end of the interconnector.

TABLE 9-2. SUMMARY OF INVESTIGATED CASES (PTL SEARCHES ARE CONDUCTED FOR CASES 1 TO 8; A CCT SEARCH IS CONDUCTED FOR CASE 1 ONLY)

Case No.	Base Condition	Inter-connector	Direction of Transfer		Fault Location			
					Line	Nominal Line Voltage	Bus No.	Location relative to direction of transfer
1	B2	QNI	NSW to QLD	South to North	2A	330	206	Sending-end
2		QNI			4A	275	410	Receiving-end
3	B1	QNI	QLD to NSW	North to South	2A	330	206	Receiving-end
4		QNI			4A	275	410	Sending-end
5	B1	VSI	VIC to SA	North to South	3A	500	305	Sending-end
6		VSI			5A	275	507	Receiving-end
7	B2	VSI	SA to VIC	South to North	3A	500	305	Receiving-end
8		VSI			5A	275	507	Sending-end

A PTL search is conducted for each case. Each search commences with an initial power transfer value (upper search bound) relating to the direction of power flow, and the interconnector of interest. The values used for the initial upper search bound for each case is provided in Table 9-3. The initial lower search bound is 0MW in all cases. Both PTL search methods employ a search tolerance of 5MW. A CCT search is conducted for case 1 only between the initial search bounds of 0ms and 500ms. A search tolerance of 2ms is used.

The EBSIME algorithm reverts to a binary search if the search diverges from the forward-swing limit (FSL) three times. Note that all PTL searches – EBSIME and binary, have been performed with some manual intervention, as the code to fully automate these procedures has not been written. While the CCT searches are mostly automated, the steps to identify the multi-swing limit (MSL) search bounds were performed manually. It is emphasized that the manual steps were performed in accordance with the algorithm documented in Chapter 7.

In this chapter all timing results are reported in simulation seconds, rather than wall-clock time. As such the results are independent of the computer processor. All reported dynamic simulations begin with a 1s run-in period to ensure the system is correctly initialized and stabilized. The three-phase fault is applied at t=1s at the specified location. The fault is cleared by simultaneously opening the circuit breakers at each end of the faulted line.

In the EBSIME algorithm, during the initial and FSL search phases after fault clearance the SIME ESC is applied to determine if the system is transiently stable. In the binary search, and the multi-swing limit search phase of the EBSIME algorithm, each stable simulation is run until t=10s to confirm the system is transiently stable. Unstable simulations terminate before 10s based on the COI or ESC TSA criteria.

TABLE 9-3.INITIAL PTL SEARCH BOUNDS FOR BOTH BINARY AND EBSIME SEARCH METHODS

Interconnector	Base Condition	Direction of Transfer	Upper Search Bound (MW)	Applicable cases
QNI	B2	South to North	900	1,2
QNI	B1	North to South	900	3,4
VSI	B1	North to South	750	5,6
VSI	B2	South to North	600	7,8
In all cases the lower search bound is 0MW.				

9.2. Summary of TSL searches on the Simplified SE Australian System

Table 9-4 summarizes the transient stability power transfer limits for all of the investigated cases, and compares the performance of the EBSIME and binary search algorithms. In Table 9-4, the fault clearing times were determined based on the rules specified in the National Electricity rules [6]. The rules specify that for transmission lines with a nominal line voltage between 250kV and 400kV, the maximum allowable fault clearing times are 100ms and 120ms for the sending- and receiving-end faults respectively. When the nominal line voltage is greater than 400kV, the maximum allowable clearing times are 80ms and 100ms for a sending or receiving-end fault respectively. An exception recorded in the table is case 5. The maximum allowable clearing time of case 5a (80ms) provides conditions that are too secure to enable a PTL search on the VSI. For illustrative purposes a longer clearing time of 120ms is applied in the case 5 search.

Case 7 constrains the system operation as it is inherently transiently unstable. Case 8 is the next most constraining case where the PTL is 196MW. Both of these cases indicate that the VSI is the weakest interconnector in the system for the south to north transfer (base condition B2). The least constraining is case 2 which has the highest PTL of 865MW (base condition B2).

TABLE 9-4. POWER TRANSFER LIMITS DETERMINED BY THE BINARY AND EBSIME SEARCHES

Case	Fault Location (S,R)	Fault Clearing Time (ms)	Binary Search		EBSIME search	
			PTL (MW)	TSIM(sim-s)	PTL (MW)	TSIM(sim-s)
1	S	100	647	69.3	647	77.0
2	R	120	865	84.2	Same as Binary Search	
3	R	120	701	64.8	Same as Binary Search	
4	S	100	602	61.3	602	45.0
5a	S	80	Too stable for assessment			
5	S	120	742	74.9	744	51.2
6	R	120	587	55.4	Same as Binary Search	
7	R	120	Too unstable for assessment			
8	S	100	196	40.6	199	42.9

Table 9-4 shows that the binary and EBSIME search results are the same, each within the 5MW search tolerance, but for cases 1, 4, 5 and 8 the search times are different. In cases 1 and 8, the EBSIME method takes slightly longer than the binary search. In cases 4 and 5, the EBSIME searches are 16s and 23s faster than the binary search respectively. Cases 1, 4, 5 and 8 each describe a contingency that is applied at the sending-end of the investigated interconnector. In these cases the system tends to be constrained by forward-swing instability, thus the limit-prediction steps of the EBSIME algorithm can be applied to accelerate the search for the FSL to locate the PTL. The mechanisms leading to forward-swing instability, for cases 1, 4, 5 and 8, are discussed in this chapter.

For cases 2, 3, 6 and 7, the SIME steps of the EBSIME algorithm cannot be applied. Thus the trajectory of the EBSIME algorithm is effectively the same as the plain binary search. Each of these cases are constrained by back-swing instability, therefore no SIME margin information is available and the EBSIME algorithm reverts to a binary search. The mechanisms leading to back-swing instability for these cases are discussed in Chapter 10.

In Chapter 5, it is observed that for any given case the mechanism of transient instability is dependent on the interconnector power transfer. The same findings are observed on the AU14GEN system in section 9.5 and in Chapter 10. In a CCT search, there is only one relevant mechanism of transient instability. For simplicity, a CCT search on case 1 is used to demonstrate the application of the EBSIME algorithm to the AU14GEN system. The CCT search is not considered for any other case from Table 9-2.

9.3. The EBSIME Algorithm Applied to the AU14GEN System

Section 9.3.1 provides a guided example of how the EBSIME algorithm is applied to search for the CCT in case 1 in Table 9-2. Sections 9.3.2 to 9.3.5 discuss the application of the EBSIME algorithm to search for the PTL in cases 1, 4, 5 and 8 for the conditions in Table 9-2. Significant issues faced by the EBSIME PTL search and their influence on the search results are highlighted. The performances of the EBSIME and binary search methods are compared.

9.3.1. CCT Search Case 1: 500MW from VIC to SA - Fault at 3A

The EBSIME algorithm is demonstrated for a CCT search for base condition 1 of Table 9-1, where a fault is applied to the sending-end of the VSI at point 3A in Figure 9-2. A binary search for the CCT, summarized in Table 9-5, identifies the CCT as 149ms. The binary search takes 43.21 sim-s. The corresponding EBSIME search for the CCT which takes 25.5sim-s, is described in Table 9-6.

TABLE 9-5. BINARY CCT SEARCH CASE 1: NSW TO QLD: FAULT AT 3A , PT = 500MW

k	CT (k) (ms)	Search Bounds (ms)	TSIM (sim-s)
1	500	[0,500]	3.50
2	250	[0,240]	1.52
3	125	[125,250]	10.00
4	188	[125,188]	1.69
5	157	[125,157]	2.02
6	141	[141,157]	10.00
7	149	[149,157]	10.00
8	153	[149,153]	2.15
9	**151**	**[149,151]**	**2.33**
		Total TSIM	43.21

The EBSIME search commences in the initial search phase between the search bounds of [0, 500] ms. In the first iteration a scenario with a clearing time of 500ms is assessed. Transient instability is identified by the COI stop criteria at t=1.45s. At this time, the largest angle separation occurs between the Loy Yang (LPS_3) generators at bus B301 and the rest of the system. This separation defines the machine groups (MG) that are used for the rest of the EBSIME search. Closer inspection reveals that the system actually separates into 3 sections – SA, VIC and the rest of the system. This differs from

the SIME assumption that loss of synchronism is caused by the separation between two groups of machines [1]. It is observed from Figure 9-3 that the two VIC stations, LPS_3 & YPS_3, both accelerate relative to the remainder of the system. Although, at the time when the MG are determined (t = 1.45s) the YPS_3 machine is erroneously grouped with the remaining system rather than LPS_3.

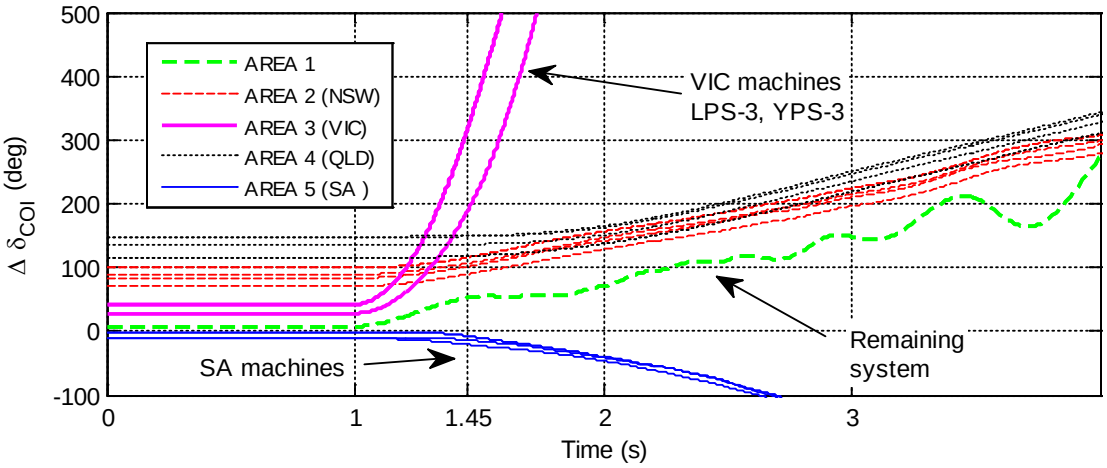

Figure 9-3. Rotor angles for 500MW transfer from VIC-SA; a three-phase fault is applied at 3A (Figure 9-2) and cleared after 500ms

TABLE 9-6. EBSIME CCT SEARCH CASE 1: VIC TO SA: FAULT AT 3A, PT = 500MW

k	η(k-1) (rad-pu)	η(k) (rad-p u)	CT (ms)	Search bounds (ms)	Predicted CCT (ms)	TSA Criteria	Stable (S)/ Unstable (U)	TSIM (sim-s)
1	-	-	500	[0, 500]	-	COI	U	1.45
2	-	-0.193036	250	[0, 250]	-	ESC	U	1.31
3	-0.193036	0.048460	125	[125, 250]	150	ESC	S	1.51
4	0.048460	0.002310	150	[150, 250]	151	ESC	S	1.80
5	0.002310	0.001249	151	[151, 250]	152	ESC	S	1.83
6	0.001249	0.000548	152	[152, 250]	153	ESC	S	1.87
7	0.0005482	0.000167	153	[153, 250]	153	ESC	S	1.91
Predicted CCT diverges. Next CT by bisection of current bounds.								
8	0.000167	-0.1004285	202	[153,202]	178	ESC	U	1.43
9	-0.1004285	-0.051870	178	[153,178]	152	ESC	U	1.52
Predicted CCT diverges. Next CT by bisection of current bounds.								
10	-0.051870	-0.029077	166	[153,166]	151	ESC	U	1.6
Predicted CCT diverges from the FSL three times. Revert to Binary Search.								
11	-	-	153	[0, 153]	-	COI	U	0.24
12	-	-	152	[0, 152]	-	COI	U	0.34
13	-	-	151	[0, 151]	-	COI	U	0.5
14	-	-	150	[150,151]	-	COI	S	8.2
							Total TSIM	25.5

The search traversal and timing are sensitive to the different MGs. In spite of the inability of the SIME method to handle three (or more) machine groups, the EBSIME CCT search is significantly faster. Appendix G shows an alternative EBSIME CCT

search for the same case where the LPS_3 and YPS_3 machines form one MG, and the remaining machines form the other. The different MG causes the SIME limit prediction to converge to a higher FSL. Consequently, the residual binary search takes longer and the EBSIME is 20% slower than the binary search.

Since the VIC machines do not decelerate before synchronism is lost a margin cannot be determined for the first scenario. Bisection of the search bounds is used to identify that the next CT is 250ms in the second iteration. It is identified as forward-swing unstable at t = 1.31s by application of the ESC to the OMIB response. An unstable margin is determined for this scenario. Thus the search can commence the iterative limit prediction cycle at the next step.

At k = 3 the next CT, determined by bisecting the search bounds, is 125ms. This scenario is determined to be forward-swing stable at t = 1.51s using the ESC. It yields an estimated stable margin of 0.04846 rad-pu. The CT of the next search step (k=4) of 150ms is estimated by interpolation of the margins and CTs for the scenarios k=2 and 3. The limit prediction search phase continues for iterations 4 to 7. At k=4, the ESC identifies the scenario to be forward-swing stable, and yields the stable margin 0.00231 rad-u. It is used with the margin of the previous scenario (k=3) to linearly predict the limit at 151ms. A similar logic applies to scenarios k = 5 & 6.

At k=7 a CCT of 153ms is predicted by extrapolation of the CTs and stable margins estimated for scenarios k = 6 & 7. Since the predicted CCT is the same as the lower search bound the search is classified as diverging. Thus the search bounds of k = 7 are bisected to obtain the next CT of 202ms. For k = 8 the predicted CCT is within the search bounds, but the search diverges again at k=9. Bisecting the search bounds of k=9 identifies the next CT at 166ms. At k=10, the predicted CCT exceeds the search bounds again. Since the search has diverged 3 times, reaching the search divergence limit, the algorithm switches to the plain binary search.

The multi-swing (MS) binary search phase is conducted from steps 11 to 14. In step 11, the step 7 simulation with CT = 153ms is continued and is confirmed to be transiently unstable. Similarly for steps 12 and 13. In step 14, the step 4 simulation is continued and is confirmed to be transiently stable. Since the difference between the search bounds is less than the 2ms tolerance, the search ends and the identified CCT is 150ms. The 25.5sim-s total search time of the EBSIME algorithm is 41% faster than the binary search. The search convergence of both methods is compared in Figure 9-4.

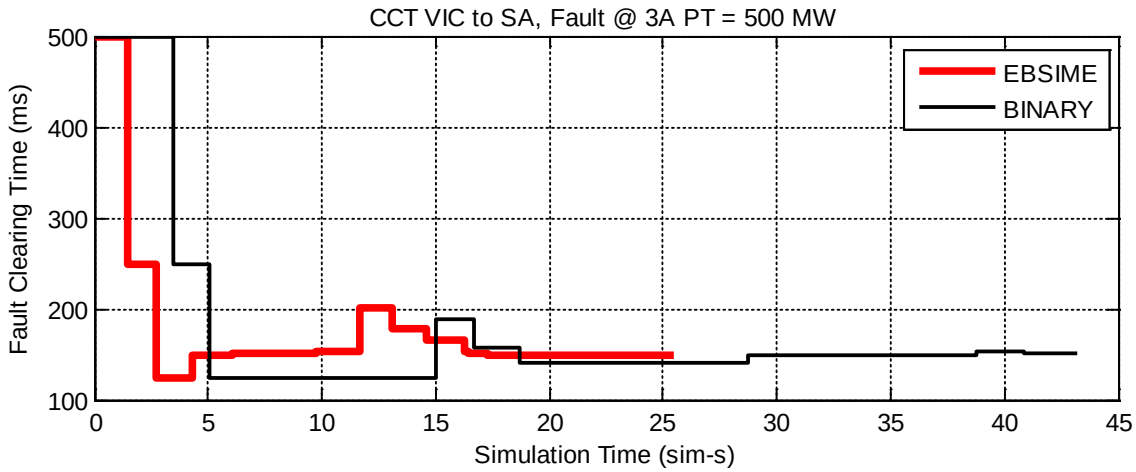

Figure 9-4. Case 1 simulation times for the EBSIME and binary CCT searches

9.3.2. PTL search Case 1: Transfer From NSW to QLD – Fault at 2A

In case 1, the binary search locates the PTL at 647MW. The full search takes 69.3s. Full details of the case 1 EBSIME PTL search are reported in Table 9-7. The search begins at scenario k=1 with 900MW power transfer over the QNI from NSW to QLD. Figure 9-5 indicates that the system is found to be unstable t=1.88s according to the COI criteria. At this time the rotor angle of one of the QLD machines deviates by more than 180° from the COI angle. According to the MG identification algorithm (see section 7.4.1) the QLD machines form one group and those of the remaining system form the other group. The selected MG yields an unstable margin of -0.0064893 pu-rad, thus the limit prediction phase begins at step 2.

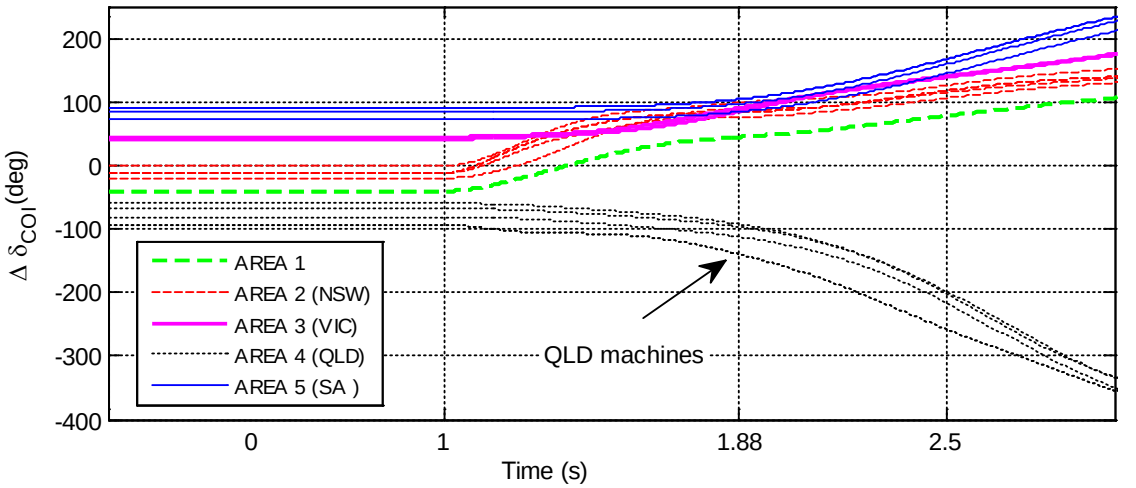

Figure 9-5. Rotor angles for 900MW transfer from NSW to QLD, CT =100ms

TABLE 9-7. EBSIME PTL SEARCH CASE 1: NSW TO QLD: FAULT AT 2A, CT = 100MS

K	η(k-1) (pu-rad)	η(k) (pu-rad)	PT(k) (MW)	Search Bounds (MW)	Predicted Limit (MW)	TSA Criteria	Stable (S)/ Unstable (U)	TSIM (sim-s)
1	-	-0.006489	900	[0,900]	-	COI	U	1.88
2	-0.006489	0.006507	450	[450,900]	675	ESC	S	1.56
3	0.006507	0.001046	675	[675,900]	718	ESC	S	1.86
4	0.001046	-0.000669	718	[675,718]	701	ESC	U	1.89
5	-0.000669	-0.000534	701	[675,701]	633	ESC	U	1.92
Predicted PTL diverges. Next CT by bisection of current bounds.								
6	-0.000534	-0.000468	688	[675,688]	595	ESC	U	1.95
Predicted PTL diverges. Next CT by bisection of current bounds.								
7	-0.000468	-0.000449	682	[675,682]	546	ESC	U	1.95
Predicted PTL diverges three times. Revert to Binary Search.								
8	-	-	675	[0,675]	-	COI	U	3.20
9	-	-	450	[450,675]	-	COI	S	8.44
10	-	-	563	[563,675]	-	COI	S	10.00
11	-	-	619	[619,675]	-	COI	S	10.00
12	-	-	647	[647,675]	-	COI	S	10.00
13	-	-	661	[647,661]	-	COI	U	6.03
14	-	-	654	[647,654]	-	COI	U	7.04
15	-	-	651	[647,651]	-	COI	U	9.28
MS Limit found at PTL = 647MW								
							Total TSIM	77.00

The next scenario, k=2, is 450MW and is determined by bisecting the search bounds. The SIME COI criteria identifies it to be forward-swing stable at t=1.56s. It yields a stable SIME margin of 0.0065065 pu-rad. The margins of scenarios k = 1 and 2 are interpolated to predict the next search step at 675MW. The next three scenarios are assessed by the SIME ESC and yield valid SIME margins that are used to iteratively determine the next search step. In each step, the information of the current *k*th scenario is paired with the previous one (k-1) to estimate the limit and the next step using linear prediction.

However at step k=5, the predicted PTL is 633MW and is below the lower search bound of 675MW. The next PT of 688MW is determined by bisecting the search bounds of scenario k=5. At scenario k=6, the limit prediction step again predicts a PTL outside the current search bounds, so the transfer for scenario k=7 again determined by bisecting the search bounds, is 682MW. At k=7 the predicted limit is again below the lower search bound. Since the search has diverged three times, the EBSIME algorithm switches to a plain binary search to locate the TSL.

The aim of initializing the multi-swing binary search phase is to update the search bounds by identifying a multi-swing stable and unstable scenario. At initialization the only confirmed bound is from scenario 1, which was assessed using the COI instability

criteria. As described in section 7.6.1 the procedure to update the search bounds for the TSL is:

Step 1) The TDS of scenario k=3, where PT=675MW, is resumed first, as it is the forward-swing stable scenario with the highest transfer.

Step 2b) The COI instability criteria classifies this scenario as multi-swing unstable at t=4.76s; thus 675MW becomes the upper search bound. To identify the lower search bound the simulation of the forward-swing stable scenario with the next highest transfer, k=2 with PT=450MW, is continued. It is classified as stable by the COI stability criteria. Therefore the residual plain binary search continues from k=10, with the search bounds [450MW, 675MW].

The FSL search phase takes 13.01 sim-s. The residual binary search component takes 64 sim-s, including identification of the binary search bounds. Here the EBSIME search is 10% (7 sim-s) slower than the binary search.

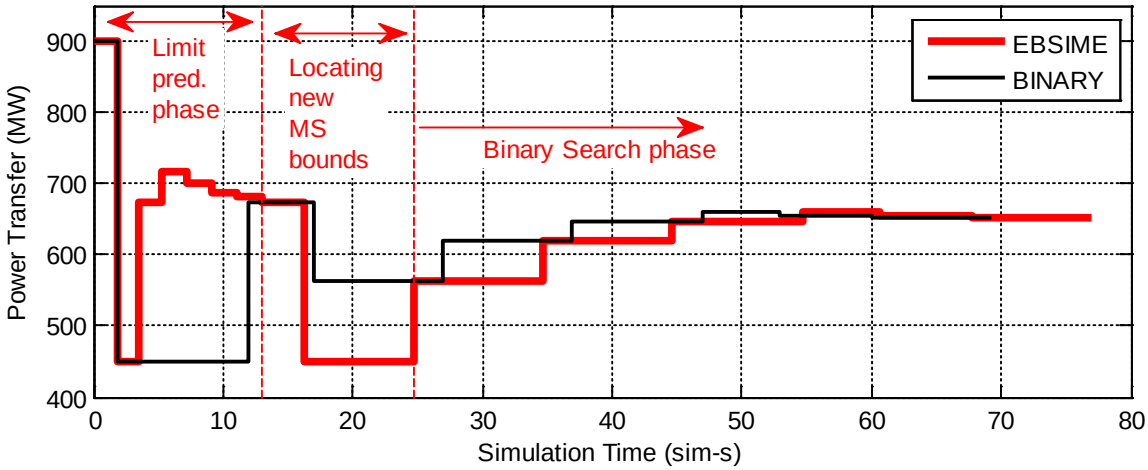

Figure 9-6. Case 1 simulation times for the EBSIME and binary PTL searches

9.3.3. PTL search Case 4: Transfer from QLD to NSW– Fault at 4A

In case 4, the binary search converges to a PTL of 602MW and takes 61.25 sim-s to complete. The EBSIME PTL search for case 4 is described in Table 9-8. This example demonstrates how the EBSIME can locate the TSL with fast and robust results, even if the SIME based limit prediction steps diverge. In the first search scenario, where 900MW of power is transferred from QLD to NSW, the COI criteria determines that the simulation becomes unstable at t=1.63s. At this time the system separates into QLD machines and the rest of the system as shown in Figure 9-7. This machine grouping is used for the entire search.

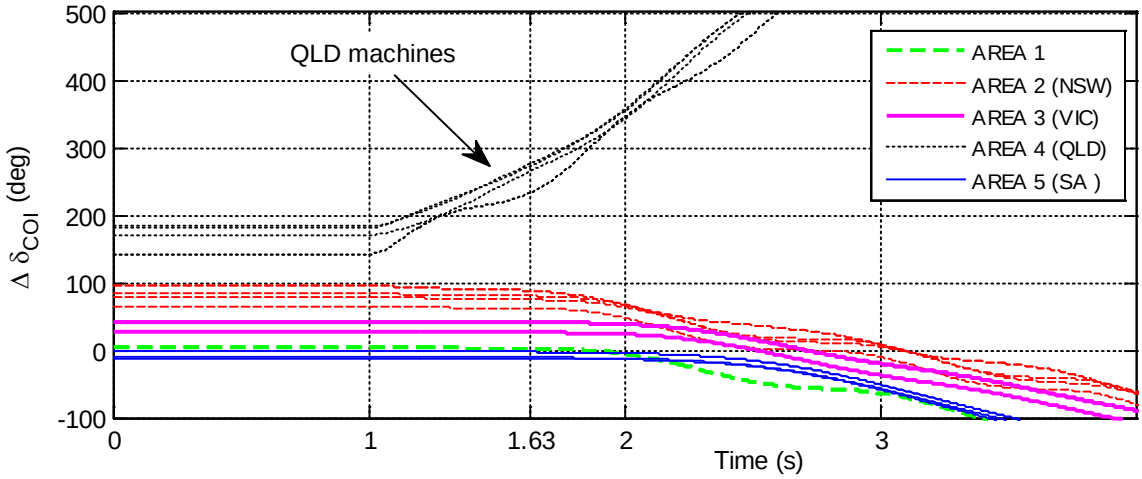

Figure 9-7. Rotor angle responses for 900MW transfer from NSW to QLD, CT =100ms

Table 9-8 shows that the limit prediction search phase commences after scenario k=1, and continues until k=7. During this time the limit prediction steps fall outside of the search bounds three times, at k =3, 6 and 7. Thus the SIME search phase is abandoned and the residual binary search is used to complete the search. The multi-swing search phase begins at scenario k=8. Scenarios k= 8 and 9 continue the simulations of steps k=7 and 4 respectively, to identify the starting bounds for the binary search. The binary search continues from step 10 to complete the search.

TABLE 9-8. EBSIME PTL CASE 4: QLD TO NSW: FAULT AT 4A, CT = 100MS

K	η(k-1) (pu-rad)	η(k) (pu-rad)	PT(k) (MW)	Search Bounds (MW)	Predicted PTL (MW)	TSA Criteria	Stable (S)/ Unstable (U)	TSIM (sim-s)
1	-	-0.012335	900	[0,900]	-	COI	U	1.63
2	-0.012335	0.000130	450	[450,900]	455	ESC	S	1.83
3	0.000130	0.000130	455	[455,900]	3651	ESC	S	1.83
Predicted PTL diverges. Next PT by bisection of current bounds.								
4	0.000130	-0.002911	678	[455,678]	465	ESC	U	1.91
5	-0.002911	0.000131	465	[465,678]	474	ESC	S	1.84
6	0.000131	0.000135	474	[474,678]	112	ESC	S	1.85
Predicted PTL diverges. Next PT by bisection of current bounds								
7	0.000135	0.000138	576	[576,678]	3000	ESC	S	2.07
Predicted PTL diverges from the FSL three times. Revert to Binary Search.								
8	-	-	576	[576,900]	-	COI	S	7.93
9	-	-	678	[576,678	-	COI	U	0.39
10	-	-	627	[576,627]	-	COI	U	2.87
11	-	-	602	[602,627]	-	COI	S	10.0
12	-	-	615	[602,615]	-	COI	U	3.24
13	-	-	609	[602,609]	-	COI	U	3.61
14	-	-	606	[602,606]	-	COI	U	4.02
MS Limit found at PTL = 602MW								
							Total TSIM	45.02

Figure 9-8 provides a visual comparison of the two search methods. The limit prediction steps from k=2 to 7 accel erate the search as they converge towards a FSL, which is lower than the actual limit. Although the EBSIME algorithm was unable to find the FSL those SIME steps that were successful ultimately resulted in the EBSIME algorithm finding the PTL in 45.02 sim-s, some 25% faster than the plain binary search.

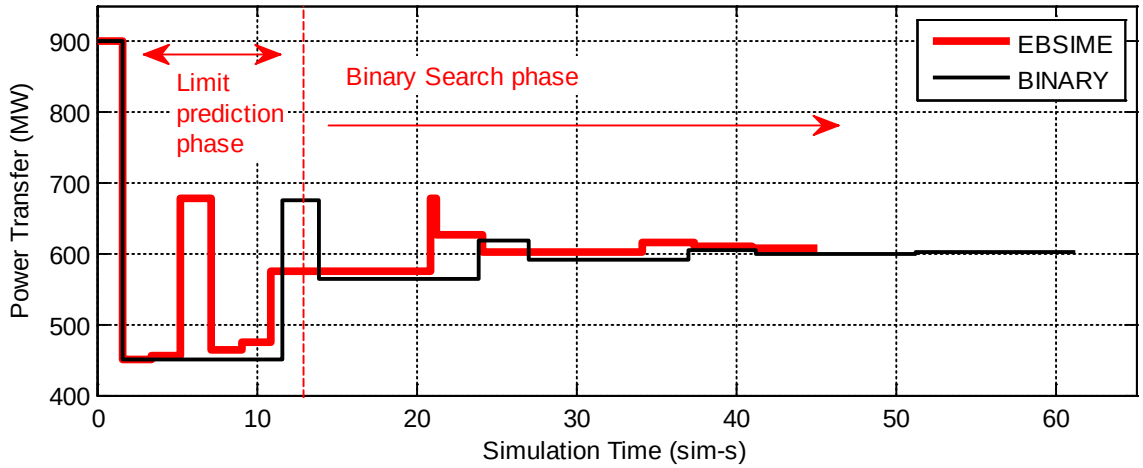

Figure 9-8. Case 4 simulation times for the EBSIME and binary PTL searches

9.3.4. PTL search Case 5: Transfer from VIC to SA– Fault at 3A

This section compares the EBSIME and binary searches when a fault is applied on the VSI. In this example the simulation time of the EBSIME algorithm is faster than the binary search. The binary search converges to the PTL at 742MW and takes 74.93 sim-s. Since the PTL is relatively high, seven out of the nine assessed scenarios in the binary search are stable and require simulation for the full 10 sim-s integration period.

The EBSIME search is described in Table 9-9. It converges to a PTL of 744MW which is within the 5MW search tolerance. The search commences at k=1, where 750MW is transferred over the VSI from VIC to SA. The COI instability criteria halts the TDS at t=2.37s, when the greatest angle separation is between the SA machines and the rest of the system, as shown in Figure 9-9, defining the MG for the search. The unstable margin -0.00134742 pu-rad is calculated for k=1, thus the limit prediction phase begins at k=2.

The PT for the next three steps are determined by bisecting the search bounds of k =1, 2 and 3. Scenarios k=2 and 3 are forward-swing stable, and the stable SIME ESC rapidly identifies stability, but both scenarios are too stable to yield a SIME margin. A stable margin is estimated for scenario 4. Limit prediction with the margins from steps k=1

and 4 determines the next PT of 696MW for scenario k=5. The SIME ESC classifies scenario 5 as forward-swing stable at t=1.9s. In scenarios k=5, 6 and 7, a SIME margin can be calculated. However, in each of these scenarios the predicted PTL is outside the search bounds. Thus the algorithm switches to a plain binary search to locate the PTL.

Initialization of the bounds for the residual binary search happens in steps k=8 and 9. As prescribed in step 1 in section 7.6.1. Scenario k=8 with PT = 710MW is resumed first as it is the forward-swing stable scenario with the highest transfer when the limit prediction phase ended. The COI stability criteria confirms that the scenario is transiently stable, and 710MW is the lower search bound.

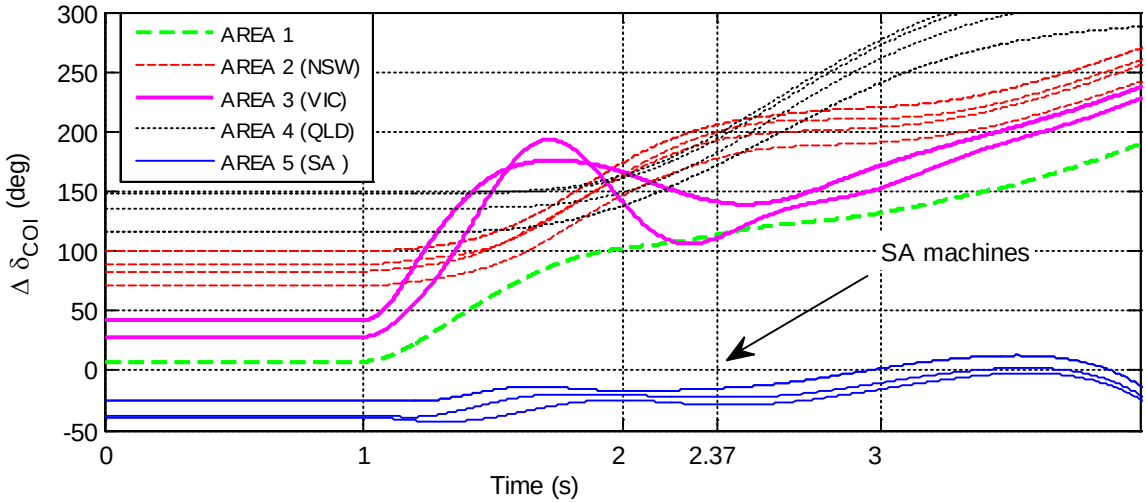

Figure 9-9. Rotor angles for 750MW transfer from VIC to SA, CT = 120ms

As per step 2a in section 7.6.1 an upper bound remains to be found. Scenario k=9 with PT=723MW on the VSI is resumed, as it is the forward-swing unstable scenario with the lowest transfer. However, significantly the COI assessment criteria classifies this scenario as transiently stable, thus the lower search bound is updated to PT=723MW.

Figure 9-10 shows the corresponding OMIB acceleration power and speed responses for this scenario. At t=2.09s, the SIME ESC classifies the scenario as forward-swing unstable as $\omega_{OMIB} > 0$ and P_{aOMIB} momentarily increases from a negative to positive value. However, the remaining part of both OMIB responses shows that the system stabilizes. This misdiagnosis is a reminder that a scenario classified by the SIME ESC as a lower search bound may be transiently unstable; or a scenario classified as an upper search bound may be transiently stable. This emphasizes the importance of relying on the COI stability criteria to check that the search bounds for the remaining binary search are correct, so that the correct TSL is identified.

Scenario k=1 has the next highest transfer at PT=750MW. It was initially assessed with the COI stability criteria, so the upper search bound is PT=750MW. The binary search commences at k=10. At k=12 the TSL is identified as 744MW. Figure 9-11 compares the simulation times of the two searches. The EBSIME search takes 51.22 sim-s. It is 23.83 sim-s (31%) faster than the binary search in spite of the incorrect SIME ESC assessment at k=6. The limit prediction phase forms less than 20% of the full search. Time was saved by avoiding assessment of many of the stable scenarios traversed by the plain binary search.

TABLE 9-9. EBSIME PTL SEARCH CASE 5: VIC TO SA – FAULT AT 3A, CT = 120MS

K	η(k-1) (pu-rad)	η(k) (pu-rad)	PT (k) (MW)	Search Bounds (MW)	Predicted Limit (MW)	TSA Criteria	Stable (S)/ Unstable (U)	TSIM (sim-s)
1	-	-0.0013474	750	[0 , 750]	-	COI	U	2.37
2	-0.0013474	-	375	[375, 750]	-	ESC	S	1.38
3	-0.0013474	-	563	[563, 750]	-	ESC	S	1.47
4	-0.0013474	0.0009869	657	[657, 750]	657	ESC	S	1.54
5	0.0009869	0.0000053	696	[696, 750]	696	ESC	S	1.9
Predicted PTL diverges. Next PT by bisection of current bounds								
6	0.0000053	-0.0005481	723	[696, 723]	696	ESC	S	2.09
Predicted PTL diverges. Next PT by bisection of current bounds								
7	-0.0005481	0.0000015	710	[710, 723]	710	ESC	S	2.27
Predicted PTL diverges three times. Revert to Binary Search.								
8	-	-	710	[710, 750]	-	COI	S	7.73
9	-	-	723	[723, 750]	-	COI	S	7.91
10	-	-	737	[737, 750]	-	COI	S	10
11	-	-	744	[744, 750]	-	COI	S	10
12	-	-	747	[744, 747]	-	COI	U	2.56
MS Limit found at PTL = 744 MW								
							Total TSIM	51.22

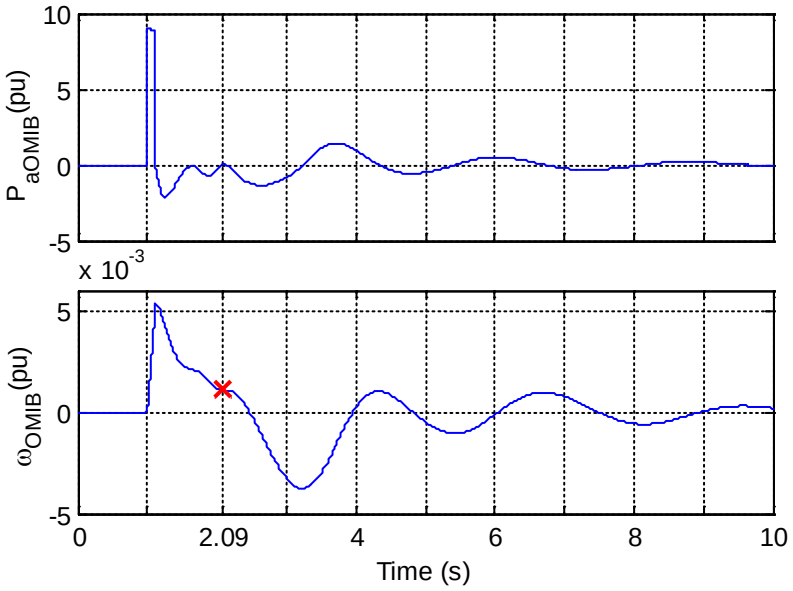

Figure 9-10. OMIB acceleration power and rotor speed response for 723MW transfer from VIC to SA, CT = 120ms

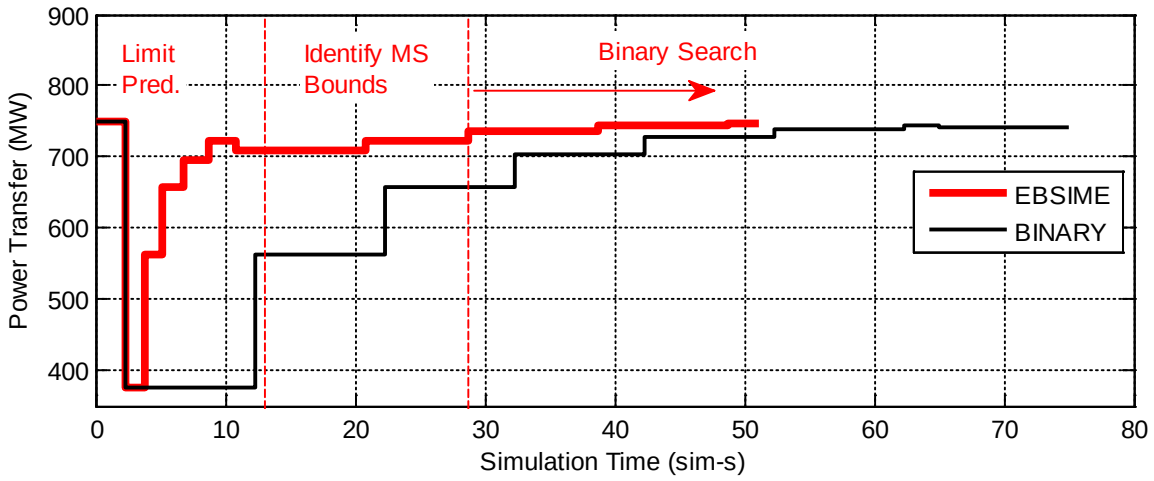

Figure 9-11. Case 5 simulation times for the EBSIME and binary PTL searches

9.3.5. PTL search Case 8: Transfer from SA to VIC – Fault at 5A

For case 8 the binary search finds the PTL of 198MW in 40.96 sim-s. The traversal of the EBSIME search, which takes 42.88 sim-s, is described in Table 9-10. The COI criteria identifies scenario k=1 as unstable at t=1.58s. The SA machines accelerate ahead of the rest of the system as shown in Figure 9-12.

The limit prediction phase begins at scenario k=2 when the first unstable margin is defined. The iterative limit prediction procedure continues unhindered until the forward-swing stable scenario k=6, where PT=192MW. The PTL predicted by this search step is 192MW, the same as the current scenario, indicating search divergence. Thus for scenario k=7, the next PT of 246MW is determined by bisection of the step 6 search bounds. However, the search also diverges from the PTL for scenarios k=7 and 8. Thus from scenario k=9 the EBSIME algorithm reverts to a plain binary search to locate the PTL.

The search bounds for the residual binary search phase are identified in steps k = 9 and 10. At scenario k=9, the TDS corresponding to PT = 192MW is the first to be resumed, as it is the lower search bound when the FSL search phase ended. The system machines maintain synchronism for the full 10 sim-s, and scenario 9 is stable according to the COI stability criteria. Therefore 192MW is the lower search bound.

To identify the upper search bound the scenario with the next highest PT of 219MW is resumed. This scenario is the upper search bound when the FSL search phase ended. The COI instability criteria verifies that scenario k=10 is unstable at t = 3.3s, 0.74 sim-s

after resuming the TDS. Thus the upper search bound for the residual binary search is 219MW.

TABLE 9-10. EBSIME PTL SEARCH CASE 8: SA TO VIC, FAULT AT 5A, CT = 100MS

K	η(k-1) (pu-rad)	η(k) (pu-rad)	PT (k) (MW)	Search Bounds (MW)	Predicted PTL (MW)	TSA Criteria	Stable(S)/ Unstable (U)	TSIM (sim-s)
1	-	-	600	[0, 600]		COI	U	1.58
2	-	-0.00548	300	[0, 300]		ESC	U	1.79
3	-0.00548	0.00039	150	[150, 300]	160	ESC	S	2.15
4	0.00039	0.00024	160	[160, 300]	177	ESC	S	2.22
5	0.00024	0.00012	177	[177, 300]	192	ESC	S	2.32
6	0.00012	0.000003	192	[192, 300]	192	ESC	S	2.56
Predicted PTL diverges. Next PT by bisection of current bounds								
7	0.000003	-0.00253	246	[192, 246]	192	ESC	U	2.07
Predicted PTL diverges. Next PT by bisection of current bounds								
8	-	-	219	[192,219]	157	ESC	U	2.3
Predicted PTL diverges three times. Revert to Binary Search.								
9	-	-	*192*	*[192, 600]*	-	*COI*	*S*	*7.44*
10	-	-	*219*	*[192, 219]*	-	*COI*	*U*	*0.74*
11	-	-	206	[192, 206]	-	COI	U	3.63
12	-	-	199	[199, 206]	-	COI	S	10
13	-	-	203	[199, 203]	-	COI	U	4.08
MS Limit found at PTL = 199 MW								
							Total TSIM	42.88
Identification of the MS search bounds is highlighted in *italics.*								

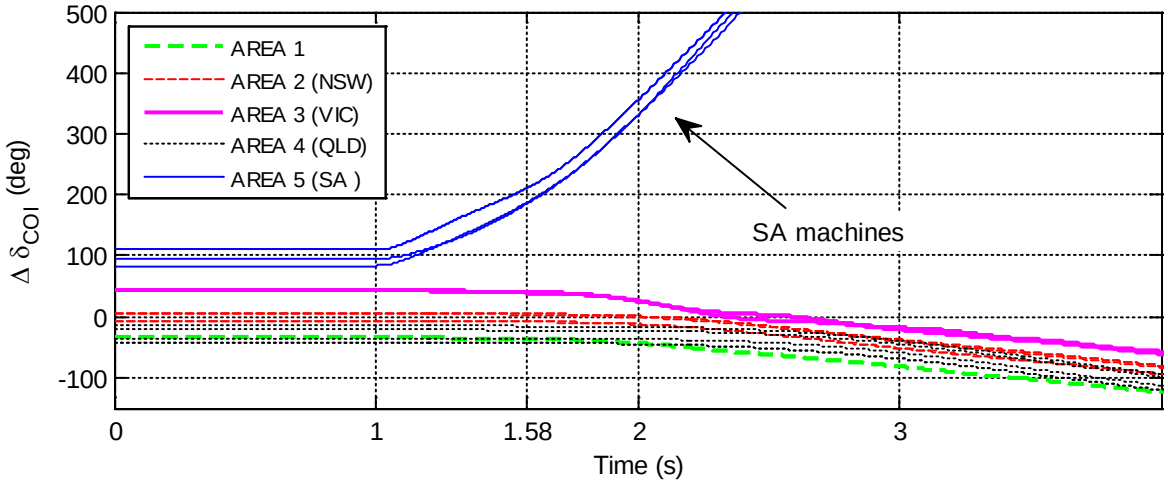

Figure 9-12. Case 8: Rotor angles for 600MW transfer from SA to VIC, fault at 5A (Figure 9-2), CT = 100ms

The search continues with plain binary steps in scenarios k=11 to 13. At k=13, the difference between the search bounds falls below the 5MW search tolerance, and the PTL is identified as 199MW after a total search time of 42.88 sim-s.

Figure 9-13 provides a visual comparison of the two search methods for case 8. The forward-swing search component consumes one third of the total search time. Despite the fast convergence to the FSL, the onerous part of the search is in verifying the multi-swing limit. The EBSIME search is 1.92 sim-s slower than the binary search.

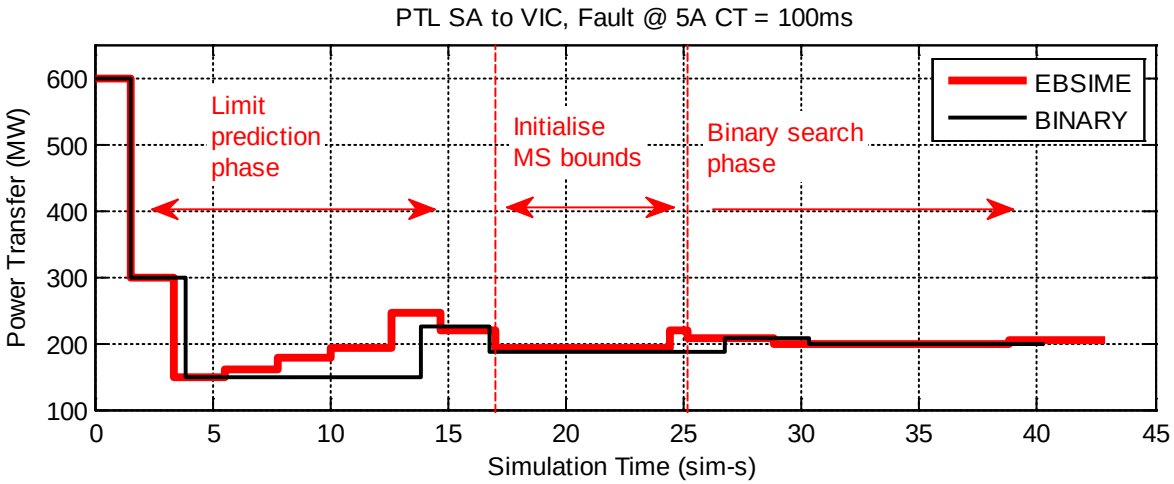

Figure 9-13. Case 8 simulation times of the EBSIME and binary PTL searches

9.3.6. Summary of the EBSIME Search Performance

In the searches discussed in sections 9.3.2 to 9.3.5, the EBSIME search first aims to locate the FSL, and then the actual limit. In all of the PTL searches the EBSIME algorithm experiences failure to converge to a FSL. However, using bisection steps the correct PTL is found. Table 9-11 provides a comparison of the FSLs and the TSLs for the searches described in section 9.3, and the corresponding search times of the binary and EBSIME. It is emphasized that failure of the SIME limit prediction during the search does not necessarily imply a search time longer than that for a plain binary search. On the contrary, in cases 4 and 5 the successful SIME steps rapidly narrow the search bounds so that the residual binary phase of the search is completed rapidly.

TABLE 9-11. COMPARISON OF THE FSLS AND TSLS FOR CASES 1, 4, 5, AND 8

Case No.	Type of Search	Forward-Swing Limit (FSL)	Transient-Stability Limit (TSL)	Binary Search Time (sim-s)	EBSIME Search Time (sim-s)
5	CCT	153ms	150 ms	43.21	25.51
1	PTL	675 MW	647 MW	69.29	77.00
4	PTL	576 MW	602 MW	61.25	45.02
5	PTL	696 MW	744 MW	74.93	51.22
8	PTL	192 MW	196 MW	40.96	42.88

It is evident from the case 5 PTL search, that ultimately a TDS must be assessed with the COI-based stability criteria for an accurate diagnosis of transient stability. This emphasizes the importance of the bisection steps and the residual binary search to conclude a SIME-based search, to ensure a robust determination of the TSL.

9.4. Relationship between CCT and Power Transfer on the AU14GEN System

To provide further insights on the transient stability of cases 1, 4, 5 and 8, the relationship between interconnector power transfer and the CCT is considered. Information for case 1 and 4, where a three-phase fault is applied on the VSI, are displayed in Table 9-12. The information for case 5 and 8 is provided in Table 9-13. In both tables, supplementary load-flow information is listed to help explain the relationships between the CCT and interconnector power transfer. For case 8, a load-flow solution could not be obtained for 700MW power transfer from SA to VIC. Thus the data is omitted.

Table 9-12 and Table 9-13 show that in cases 1, 4 and 8, and for high transfers in case 5, the CCT decreases monotonically as power transfer increases. These observations are in line with the inversely proportional relationship observed between CCT and power transfer in Chapter 5, for a sending-end fault applied to the two-machine power system.

TABLE 9-12. RELATIONSHIP BETWEEN QNI TRANSFER AND OTHER NETWORK DATA

Case	Faulted circuit	Property	Power Transfer (MW)			
			0	300	600	900
1	2A	CCT(ms)	129	120	110	0
		Steady-state transfer from bus 206 to 205 (MW)	0	300	600	900
		Voltage angle drop over line (°)	7.5	13	19.2	25.6
4	4A	CCT(ms)	218	171	100	0
		Steady-state transfer from bus 410 to 413 (MW)	0	300	615	944
		Voltage angle drop over line (°)	0.1	4.0	8.2	13.6

TABLE 9-13. RELATIONSHIP BETWEEN VSI TRANSFER AND OTHER NETWORK DATA

Case	Faulted Circuit	Property	Power Transfer (MW)				
			0	100	300	500	700
5	3A	CCT(ms)	157	161	163	149	125
		Steady-state transfer from bus 305 to 307 (MW)	1514	1600	1675	1758	1850
		Voltage angle drop over line (°)	1.9	2.0	2.1	2.2	2.4
8	5A	CCT(ms)	181	145	0	0	-
		Steady-state transfer from bus 507 to 506 (MW)	97	193	384	580	-
		Voltage angle drop over line (°)	6.4	12.1	24.1	39.6	-

In case 5, for VIC to SA transfers between 0MW and 300MW the CCT is proportional to the transfer. For transfers between 300MW and 700MW the CCT is inversely proportional to the power transfer. The variation in CCT in these two different operating ranges is caused by different constraining mechanisms of instability due to the changes in power transfer. This issue is discussed in detail in section 9.5.2.

In cases 4 and 8, the CCT is more sensitive to changes in the interconnector transfer than in cases 1 and 5. In case 4, a 300MW increase in the QNI transfer causes approximately 60ms reduction in the CCT. In contrast, in case 1 the CCT is at most reduced by 10ms for a 300MW increase in QNI transfer. In case 8 when the VSI transfer is increased from 0MW to 100MW the CCT decreases by 45ms. Yet in case 5, for VSI transfers above 300MW, a 100MW increase causes a 7.5ms reduction in the CCT.

The sensitivity of the CCT to interconnector transfer does not appear to be influenced by the variation in steady-state voltage-angle drop, or the initial power flow over a faulted circuit. This can be observed by comparing the results of cases 1 and 5. In case 1, a 300MW increase in QNI transfer causes a 6° increase in the voltage angle drop, and 300MW increase in the flow over line 2A. Yet the change in CCT is small. Conversely, in case 5 a 200MW increase in VSI transfer causes a 0.1° increase in the voltage angle drop, and ~80MW rise in the flow over line 3A. The change in CCT is also small. Thus the sensitivity of CCT to interconnector power transfer is not related to these steady-state parameters. It appears to have greater dependence on the mechanism of instability.

9.5. Mechanisms Leading to Transient Instability on the AU14GEN system

This section explores the factors that constrain the dynamic operation of the AU14GEN system for the cases where a three-phase fault is applied at the sending-end of a major interconnector. Where appropriate relevant factors such as voltage and small signal instability are highlighted. Table 9-14 provides a summary of the key factors contributing to transient instability for each of the listed cases. In each case the SVC that limits the system operation is listed in the table. For cases 1, 4, 5 and 8 this tends to be the SVC that provides reactive support at an intermediate point of an interconnector. Saturation of the limiting SVC tends to cause significant voltage reduction at the bus to which it is connected.

TABLE 9-14. MECHANISMS OF TRANSIENT INSTABILITY WHERE A THREE-PHASE FAULT IS APPLIED AT THE SENDING-END OF AN INTERCONNECTOR

Case	Fault location	Direction of transfer	Transfer Range	Constrained SVC	Cause of transient instability
1	2A	NSW to QLD	[0, 500MW]	SSVC at bus 509	SA machines accelerate ahead of the rest of the system due to a dominant inter-area mode involving the SA machines (back-swing instability)
			>500MW	ASVC at bus 205	QLD machines slow down, separating from the rest of the system (forward-swing instability)
4	4A	QLD to NSW	All transfers	ASVC at bus 205	QLD machines separate and accelerate ahead of the rest of the system (forward-swing instability)
5	3A	VIC to SA	[0,450MW]	SSVC at bus 509	VIC machines accelerate ahead of remaining system (forward-swing instability)
			>450MW		SA machines decelerate away from the rest of the system (forward-swing instability).
8	5A	SA to VIC	All transfers	SSVC at bus 509	SA machines accelerate ahead of the rest of the system (forward-swing instability)

The mechanisms of instability for cases 1 and 5 are discussed in the following sections. These cases cover a fault on the QNI and a fault on the VSI. In cases 1 and 5 there is more than one series of events leading to transient instability depending on the power transfer. The following discussions provide explanations for the relationships between the CCT and power transfer observed in Table 9-12 and Table 9-13, and provide further insights into the performance of the EBSIME algorithm for these cases. Although they are not discussed in detail, similar observations apply to cases 4 and 8. In Chapter 5 it is observed that a sending-end fault tends to be associated with a forward-swing mechanism of transient instability. This is true for cases 4, 5 and 8, and for case 1 when the interconnector transfer is high. As found in Chapter 5, the CCT is inversely proportional to the transfer for these operating conditions.

9.5.1. Case 1: Transfer from NSW to QLD - Fault at 2A

In case 1 there are two different mechanisms of transient instability. The mechanism of instability is dependent on the magnitude of power transfer over the QNI. For transfers from NSW to QLD between 0MW and 500MW, machines in the SA system tend to constrain system operation. Yet when the transfer is greater than 500MW, the QLD machines tends to limit system operation. The mechanisms leading to these results are explored in the next sections.

9.5.1.1. *Back-Swing Instability for Transfers from 0MW to 500MW: Sending-End Fault*

Figure 9-14 and Figure 9-15 show the time responses of a case 1 scenario where 500MW is transferred from NSW to QLD. After a 1s run-in period a three-phase fault is applied at point 2A in Figure 9-2, and cleared after 120ms. This scenario is marginally unstable. For NSW to QLD transfers between 0 and 500MW the mechanism of instability is similar. The scenario begins with the system in steady-state. The voltages of the SVCs at buses 205 and 509 (V_{205}, V_{509}) are each at their set point levels (V_{REF}). All machines operate at synchronous speed (ω_0).

Figure 9-14 shows the responses of key variables in the vicinity of the QNI.

<u>During the fault:</u>

- The power transfer over the QNI (P_{NQ}) falls to zero.
- Thus the NSW machines accelerate, which causes their speed (ω_{NSW}) machines to advance ahead of the other machines
- The Armidale SVC saturates (see B_{ASVC}) and

– The voltage at bus 205 (V_{205}) falls to 0.84 pu.
– The speed of the QLD machines (ω_{QLD}) at the other end of the line are relatively unperturbed.

After the fault is cleared:

– The Armidale SVC at bus 205 remains saturated
– V_{205} increases but remains below V_{REF}
– The advance in NSW rotor angle causes P_{NQ} to rapidly rise above P_{REF}, thus the NSW machines start to decelerate.

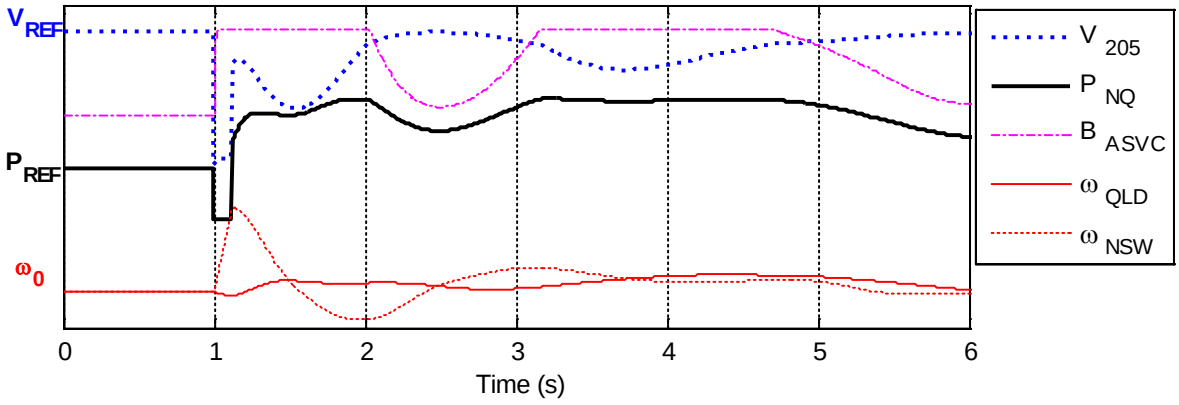

Figure 9-14. Time responses of (i) the bus 205 voltage (V_{205}), (ii) power flow in circuit #2 from bus 206 to 205 (P_{NQ}), (iii) susceptance of the Armidale SVC (B_{ASVC}) at bus 205; and (iv) rotor speeds of the generators connected to buses 201 (ω_{NSW}) and 401 (ω_{QLD}).

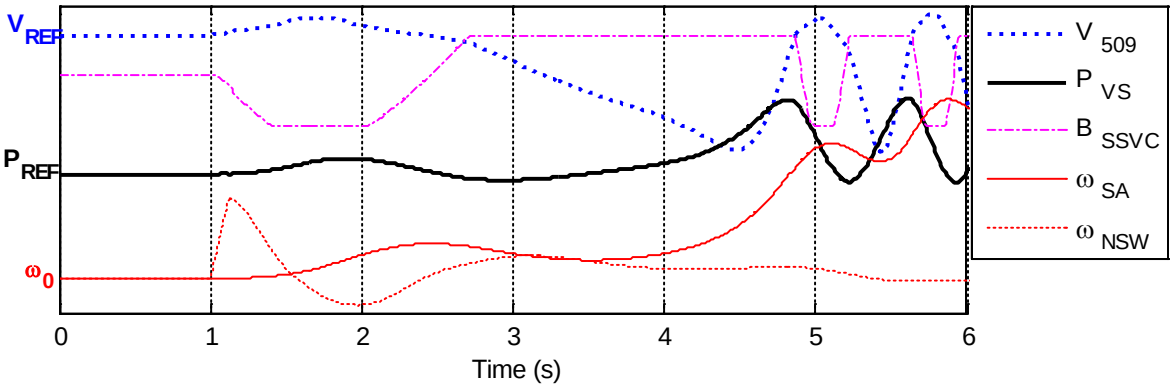

Figure 9-15. Time responses over the VSI of (i) bus 509 voltage (V_{509}), (ii) power flow in circuit #2 from bus 509 to 507 (P_{VS}), (iii) the susceptance SSVC at bus 509 (B_{SSVC}), and (iv) rotor speeds of the generators connected to buses 201(ω_{NSW}) and 503 (ω_{SA})

At t = 1.5s the NSW machines decelerate to synchronous speed. At t=2s the Armidale SVC resumes regulating and V_{205} is restored to its V_{REF}. After fault clearance, a mode of oscillation that causes the speed of the SA machines to swing in anti-phase with the NSW machines, can be observed in Figure 9-15.

During the fault, and after fault clearance:

- P_{VS} rises above P_{REF} causing the SA machines to accelerate.
- It also causes V_{509} to increase and the susceptance of the SVC at bus 509 (B_{SSVC}) to reduce. In an attempt to return V_{509} to V_{REF} the SVC reaches its lower limit at t=1.4s. The SVC remains at this operating point until t=2.1s.
- At t=1.8s, P_{VS} reaches a local maximum and then starts to decrease in response to the rising SA speed and angle of the SA machines. In turn, V_{509} reduces.
- At t=2s, V_{509} falls below V_{REF}. In response:
- B_{SSVC} increases to increase V_{509}. However the SVC at bus 509 saturates at t=2.7s and remains at this operating point until t=4.9s.
- Consequently, V_{509} dips to 0.34 pu and the SA system loses synchronism with the remainder of the system.

Instability happens when the SA machines accelerate ahead of the rest of the system, which is shown by ω_{SA} in Figure 9-15. There are insufficient synchronizing torques from the SA generators to restore synchronism between the SA and VIC machines at the other end of the VSI. Although the fault is applied on the QNI interconnection, synchronism is lost between the Victorian and South Australian systems which is at the opposite end of the system from where the fault was applied.

The equivalent SIME response becomes unstable on a back-swing because the NSW machines accelerate during the fault but are slower than the SA machines when synchronism is lost. It is the same for all NSW to QLD transfers between 0MW and 500MW. Within this transfer range, the SIME algorithm will only produce stable SIME margins even for scenarios that are unstable due to separation of the VIC and SA systems.

9.5.1.2. *Forward-Swing Mechanism of Instability for Transfers Above 500MW*

Figure 9-16 shows the time responses of a case 1 scenario where 647MW is transferred from NSW to QLD. This scenario marginally over the PTL limit. The scenario is in steady-state during the 1s run-in period. The voltage of the SVC at bus 205 is at its set

point level (V_{REF}). All machines operate at synchronous speed (ω_0). Then a three-phase fault is applied at location 2A in Figure 9-2, and cleared after 120ms.

The mechanism of instability demonstrated in this scenario is the same for all transfers from NSW to QLD that are greater than 500MW. When the fault is applied:

- The power transfer (P_{NQ}) over the QNI is reduced to 0 pu.
- The SVC at bus 205 saturates.
- This causes V_{205} to drop to 0.32 pu .
- The NSW machines experience a large acceleration ($\frac{d\omega_{NSW}}{dt}$>0) with respect to the remaining system.

After t= 1.12s when the fault clears:

- P_{NQ} increases causing
- the NSW machines to decelerate;
- and V_{205} to increase. However the SVC at bus 205 has insufficient capacity to restore V_{205} to its set-point value and so the SVC remains saturated.

At t=3.8s, although ω_{NSW} is greater than, and increasing with respect to, ω_{QLD} the power flow from NSW to QLD decreases significantly and so synchronism is lost. Following the decrease in P_{NQ} the voltage at bus 205 increases temporarily. The SVC resumes control temporarily until it again saturates at t=5.1s due to the increase in P_{NQ}.

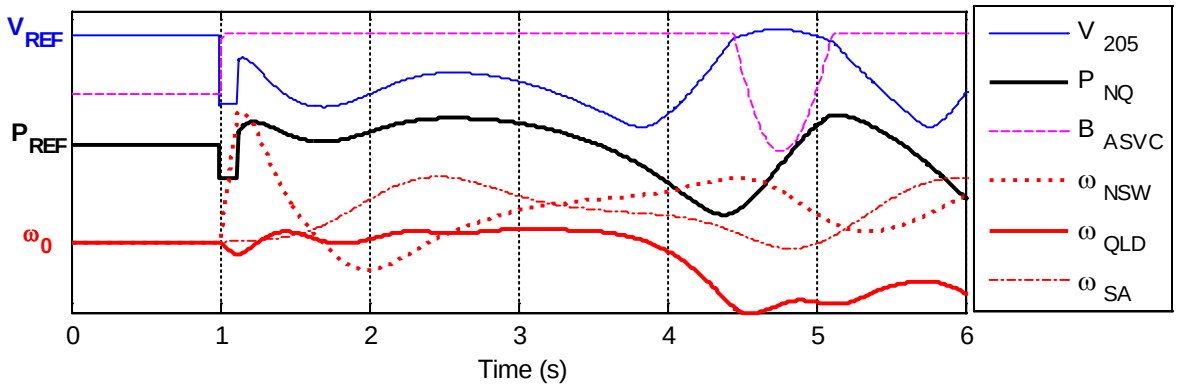

Figure 9-16. Time responses of (i) the bus 205 voltage (V_{205}), (ii) the power flow in circuit #2 from bus 206 to 205 (P_{NQ}), (iii) the susceptance at bus 205 (B_{ASVC}); and (iv) rotor speeds of generators connected to buses 201 (ω_{NSW}), 401 (ω_{QLD}) and 503 (ω_{SA})

Transient instability is manifest when the QLD machines decelerate below the speed of the remaining system. Since the NSW machines accelerate during the fault, and are faster with respect to the QLD machines when the system loses synchronism the equivalent SIME response becomes unstable on a forward-swing. The prognosis is the same for all scenarios where the NSW to QLD transfer is greater than 500MW. For QNI transfers in this range the EBSIME algorithm is able to produce SIME margins for limit prediction.

9.5.1.3. *Dominant Modal Response of Case 1*

It is instructive to examine the dominant modal response of case 1. For 500MW transfer, the three-phase fault is cleared after 10ms. Figure 9-17 shows the rotor speed responses for all of the generators in the system for this scenario. By t=8s, the oscillations in rotor speed caused by the fault are significantly reduced and the oscillations of all but the least damped mode have decayed significantly. Figure 9-18 shows the small oscillations in COI rotor speed from t=8 to 14s. The oscillations experienced by each group of machines have an approximate frequency of 0.36Hz (2.26 rad/s), estimated by measuring the peak-to-peak period of the each of the group oscillations. This is the frequency of one of three inter-area modes of the system [12].

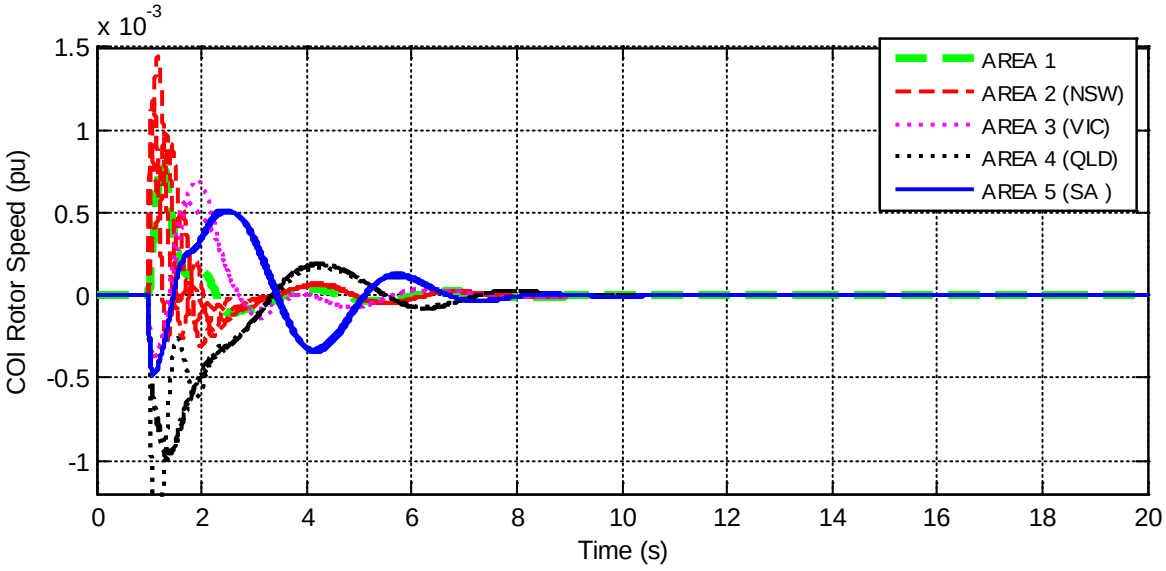

Figure 9-17. Generator COI speed responses for case 1: 500MW transfer, CT=10ms

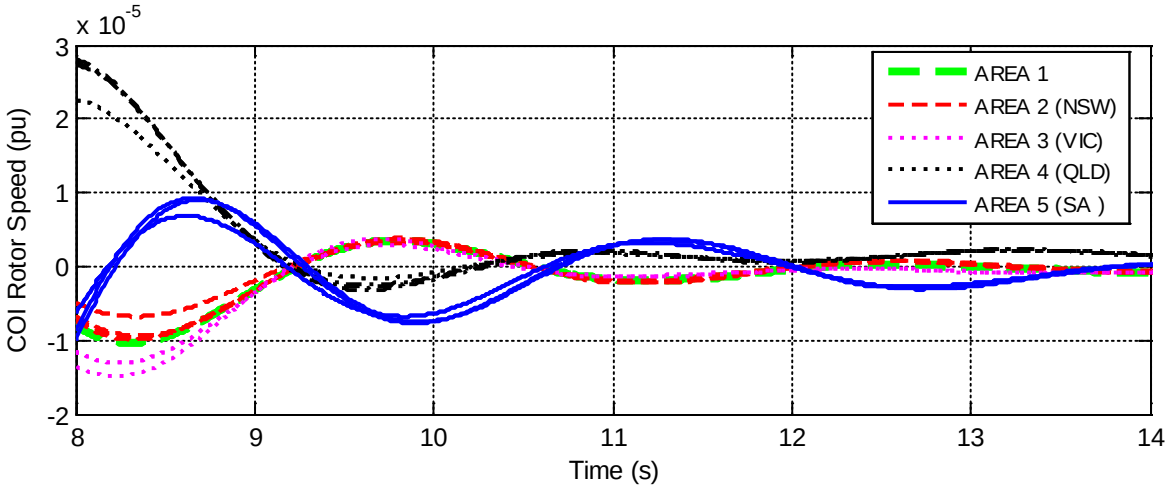

Figure 9-18. Small signal COI speed responses for case 1: 500MW, CT=10ms

Figure 9-19 shows the phasor representation of the COI rotor speeds of the SA, NSW and VIC machines from t=8s with respect to the QLD machines. The SA machines lead the speed of the QLD machines by 100°; the NSW and VIC machines lag behind the speed of the QLD machines by 94°. The SA machines are almost in anti-phase with the NSW and VIC machines with a phase difference of 166°. The magnitude of the oscillations of the SA machines is three times larger than those in the remaining system. This mode is associated with the break-away of the SA machines for the marginally unstable scenario investigated in section 9.5.1.1, case 1 with 500MW transfer.

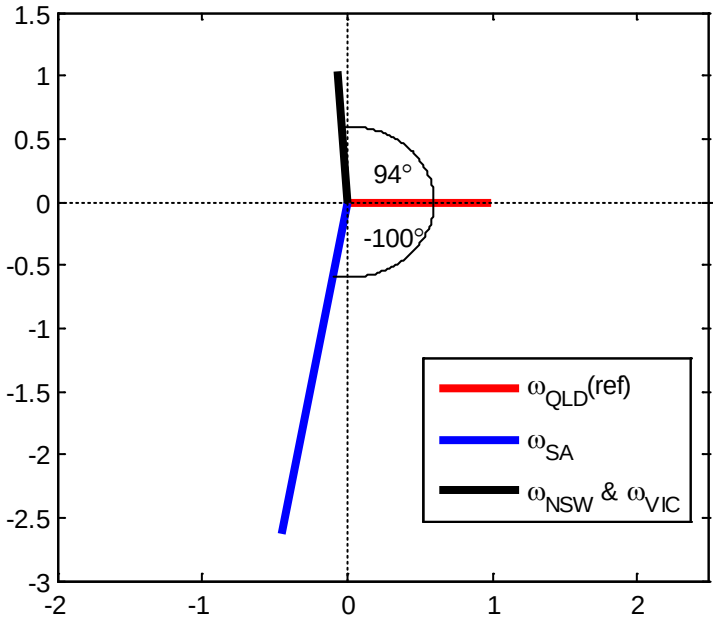

Figure 9-19. Phasor diagram of the generator speeds (i.e. mode shape) for case 1 scenario with CT=10ms, normalized with respect to the QLD machines for the dominant mode.

For transfers greater than 500MW the mode shape is similar to Figure 9-19. For the marginally unstable scenario described in section 9.5.1.2 with 647MW transfer, the QLD machines separate from the remainder of the system.

9.5.2. Case 5: Forward-Swing Instability: Transfers from VIC to SA - Fault at 3A

In case 5, the system operation is constrained by forward-swing instability for all transfers. For all transfers, when the fault is applied the VIC machines accelerate. In case 5, loss of synchronism is either caused by the VIC machines accelerating ahead of the system, or by the SA machines decelerating with respect to the system, including the VIC machines. In either case the loss of synchronism can be interpreted as being due to insufficient deceleration area under the OMIB power angle curve during the forward-swing. Thus for case 5 measurable forward-swing stable or unstable margins can potentially be estimated, and used to accelerate the EBSIME TSL search, for all levels of power transfer.

In section 9.4 a non-monotonic relationship is observed between the CCT and the VSI transfer for case 5. This is due to the different ways that the system machines separate when synchronism is lost depending on the power transfer. There are three different ways that the system machines may separate and cause instability on the forward-swing. They are described in the following sections. Even though the system may lose synchronism in multiple ways depending on the transfer level, section 9.3.4 demonstrates that for case 5 the EBSIME algorithm is able to successfully find the PTL, with a search time that is faster than the plain binary search.

9.5.2.1. *Case 5: VIC to SA Transfers Between 0MW and 450MW: Incorrect Diagnosis of Instability by the SIME ESC*

For all transfers between 0MW and 450MW instability is detected on the forward-swing according to the unstable SIME ESC. However, as shown in the following example, this may be invalid because synchronism is restored on the subsequent swing. Figure 9-20 shows the critical time responses of a case 5 scenario where 300MW (P_{REF}) is transferred over the VSI from VIC to SA. In this scenario a three-phase fault is applied at point 3A in Figure 9-2, and cleared after 180ms.

When the fault is applied at t= 1s:

- Power transfer from VIC to SA (P_{VS}) falls to zero.
- Acceleration of the VIC machines, thus $\omega_{VIC}(t) > \omega_{SA}(t)$ and $\delta_{VIC}(t)$ advances with respect to $\delta_{SA}(t)$.
- The SVC at the centre of the VSI (B_{SSVC} at bus 509) saturates at its capacitive limit causing the SVC voltage (V_{509}) to decrease.

At t=1.188s, when the fault is cleared:

- V_{509} increases but remains well below V_{REF} causing the SVC to remain at its capacitive limit.
- The VIC machines start to decelerate (ω_{VIC} decreases) since $P_{VS} > P_{REF}$.
- P_{VS} falls with decreasing V_{509}.

At t=1.5s P_{VS} is less than P_{REF} again. This causes:

- the VIC machines to resume accelerating, ω_{VIC} rises, and δ_{VIC} continues to increase.
- V_{509} begins to increase due to reduced loading at the interconnection.

It is of interest that the COI angle for δ_{VIC} rises to 180° before the system stabilizes. The SIME ESC would have indicated instability in the vicinity of 1.7s when P_{VS} reaches a minimum and the machine speeds ω_{VIC} and ω_{SA} equalize. The rotor angle and speed responses for all machines, in Figure 9-21 and Figure 9-22, show that the system is transiently stable.

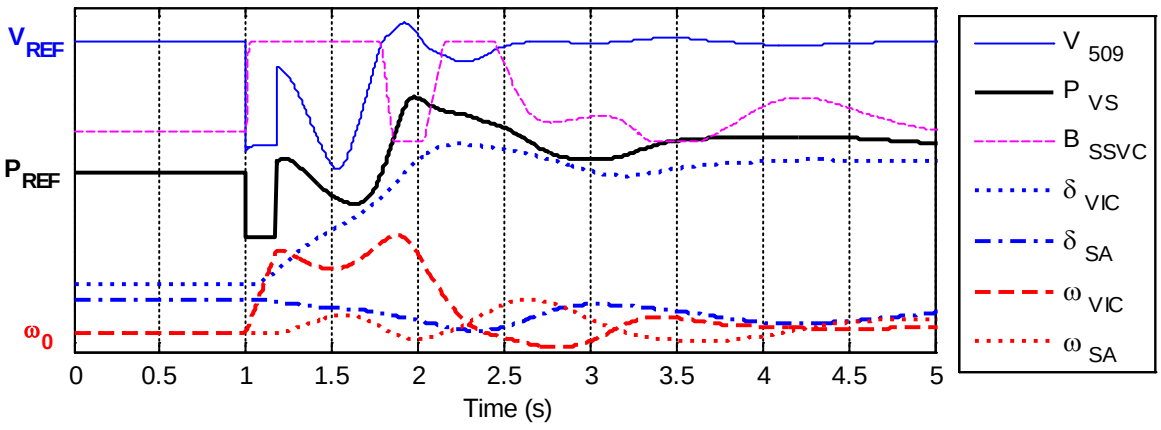

Figure 9-20. Case 5: 300MW VIC to SA: Time responses of (i) bus 509 voltage (V_{509}), (ii) power flow in circuit #2 from bus 509 to 507 (P_{VS}), (iii) SVC susceptance at bus 509 (B_{SSVC}), (iv) rotor angles of the machines connected to buses 301 (δ_{VIC}) and 501 (δ_{SA}), (v) the speeds of the generators at bus 301 (ω_{VIC}) and 501 (ω_{SA}).

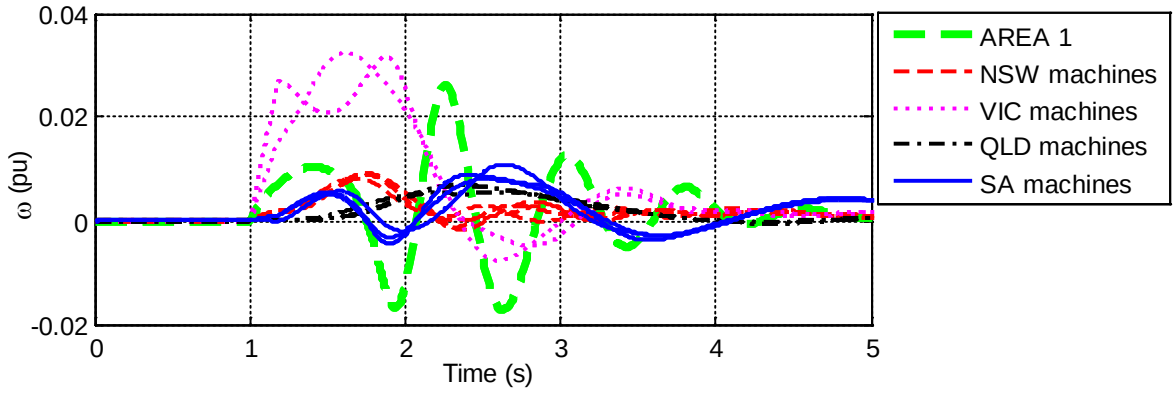

Figure 9-21. Case 5: 300MW VIC to SA, CT = 180ms: COI speeds of the system machines

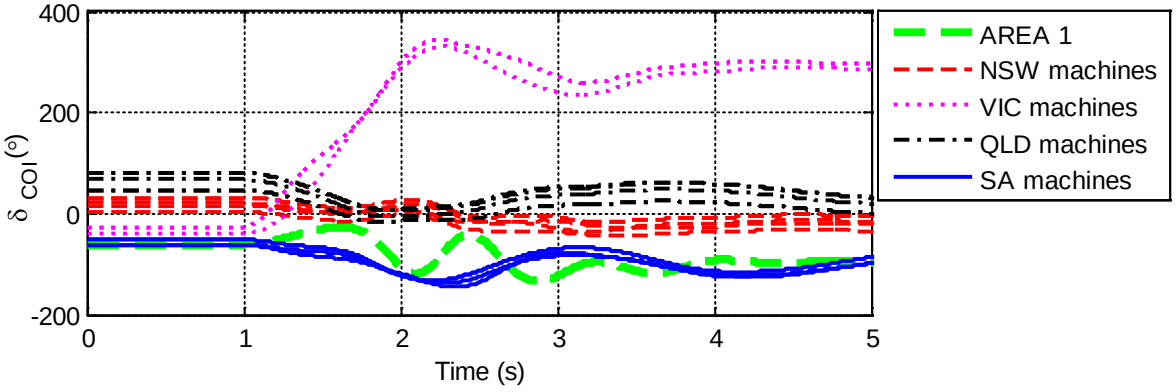

Figure 9-22. Case 5: 300MW VIC to SA, CT = 180ms: COI rotor angles of the system machines

9.5.2.2. *Case 5: Forward-Swing Instability: Transfers from VIC to SA between 450MW and 600MW*

For transfers between 450MW and 600MW loss of synchronism happens on the forward-swing when the system separates into three groups: the VIC machines, the SA machines and the remaining system. Figure 9-23 shows the time responses for a scenario where 500MW power is transferred over the VSI from VIC. The rotor speed and angle responses are shown in Figure 9-24 and Figure 9-25. A three-phase fault is applied after a 1s run-in period and cleared after 160ms such that the scenario is marginally unstable. In the steady-state, the voltage at the SVC at bus 509 (V_{509}) is at the set point level (V_{REF}), and all machines operate at synchronous speed (ω_0).

When the fault is applied at t=1s:

- Power transfer over the VSI (P_{VS}) falls to 0MW.
- The voltage at the mid-point of the VSI decreases, causing the SVC at bus 509 $\left(B_{SSVC}\right)$ to saturate.
- The VIC machines accelerate ahead of the remaining system. This causes the rotor angle of the VIC machines to increase. The speeds of the other machines are less perturbed by the fault.

The fault is cleared at t=1.16s causing:

- P_{VS} to rise above P_{REF} due to the advanced angle of the VIC machines;
- This causes the SA machines to accelerate and ω_{SA} increases.
- The VIC machines respond in anti-phase to the SA machines and decelerate, ω_{VIC} decreases.

At t=1.5s:

- The SVC remains saturated
- V_{509} reaches its nadir, then increases.
- The SA machines start to decelerate, and ω_{SA} and ω_{VIC} increases slightly.
- The rise in V_{509} allows P_{VS} to increase again.

From t=1.9s to 2.2s:

- V_{509} and P_{VS} each rise above V_{REF} and P_{REF} respectively.
- This allows the SVC to briefly resume regulation.
- This causes ω_{SA} to rise, and ω_{VIC} to fall.
- Yet, before ω_{SA} or ω_{VIC} can return to ω_o the SVC saturates again, causing the interconnector voltage and power flow to decrease.
- The speeds of the SA and VIC machines again begin to diverge.
- The SVC cannot inject sufficient reactive power to resynchronize the VIC and SA machines.

After t=2.2s, ω_{VIC} is predominantly above ω_o, thus the angles of the VIC machines increase with respect to the remaining system. Conversely ω_{SA} is less than ω_o, so the angles of the SA machines fall below those of the remaining system. In this scenario the SIME ESC diagnoses instability at around t=1.75s.

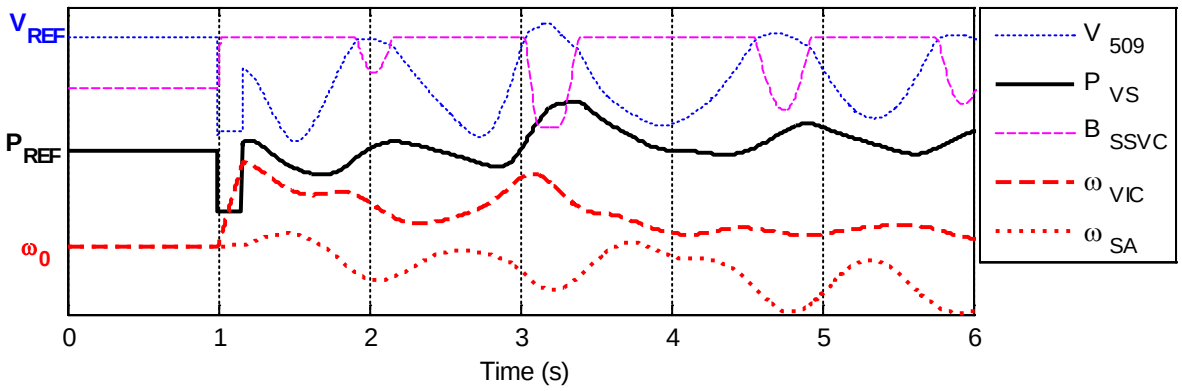

Figure 9-23. Case 5: 500MW VIC to SA: Time responses of (i) bus 509 voltage (V_{509}), (ii) power flow in the circuit at point 3A from bus 315 to 509 (P_{VS}), (iii) the SVC susceptance at bus 509 (B_{SSVC}); and (iv) speed of the machines at buses 301 (ω_{VIC}) and 501 ω_{SA}.

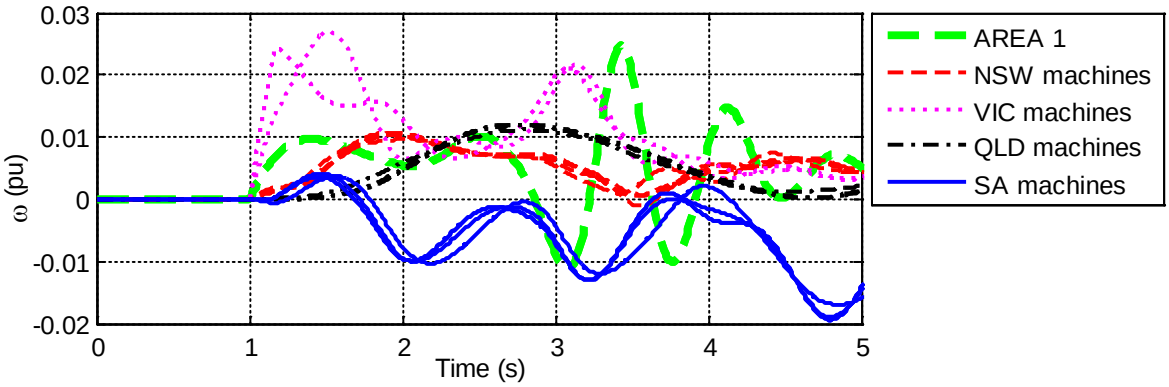

Figure 9-24. Case 5: 500MW VIC to SA: Speed responses of the machines, CT = 160ms

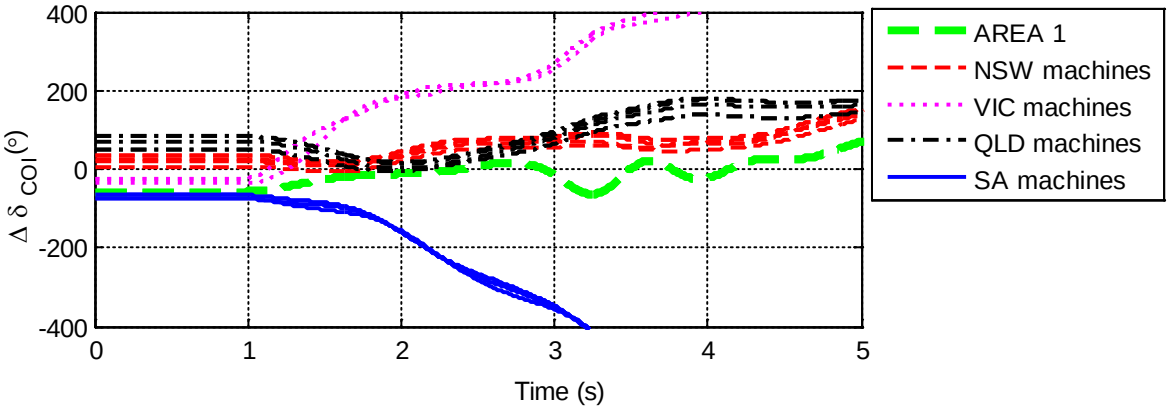

Figure 9-25. Case5: 500MW VIC to SA: COI rotor angles of the machines, CT = 160ms

9.5.2.3. *Case 5: Forward-Swing Instability: Transfers VIC to SA Greater than 600MW*

For transfers above 600MW loss of synchronism happens when the SA machines decelerate with respect to the rest of the system. Significantly, after the VIC machines

accelerate relative to the rest of the system, during the fault they regain synchronism with machines in the northern states on the forward-swing after fault clearance. This is demonstrated in Figure 9-26 and Figure 9-27 which show the rotor angle and speed responses for the marginally unstable scenario where 650MW is transferred from VIC to SA. The three-phase fault applied at point 3A in Figure 9-2 is cleared time after 140ms.

Recall that the load scaling method is used to adjust the power transfer on the VSI. To increase the transfer to a high level, such as 650MW, the load in SA is increased and the load in VIC is reduced by the same amount. The lower demand in VIC reduces stress on the VIC machines and correspondingly increases the stress on the SA machines, which causes the SA machines to decelerate. The system is constrained by forward-swing instability because the VIC machines accelerate relative to the remaining system during the fault. Then when instability happens the speed and angles of the VIC machines remain higher than the SA machines.

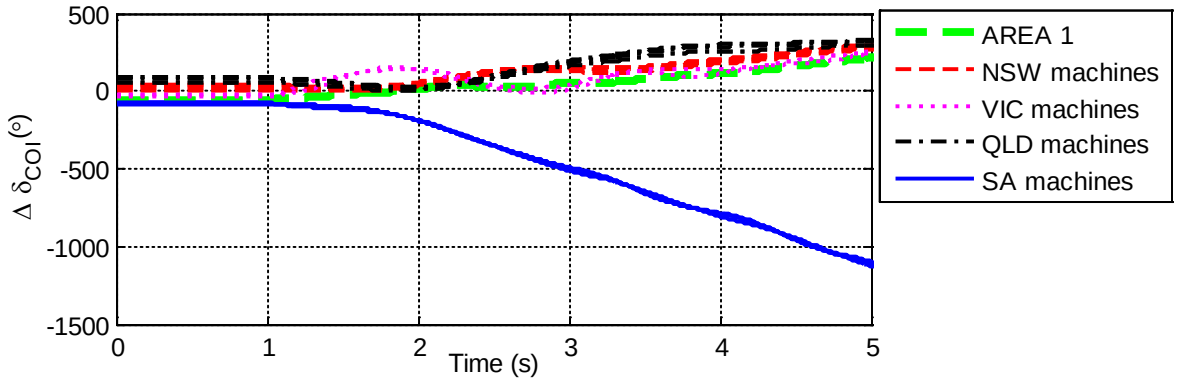

Figure 9-26. Case 5: 650MW transfer VIC to SA: COI rotor angles of the system machines, CT = 140ms

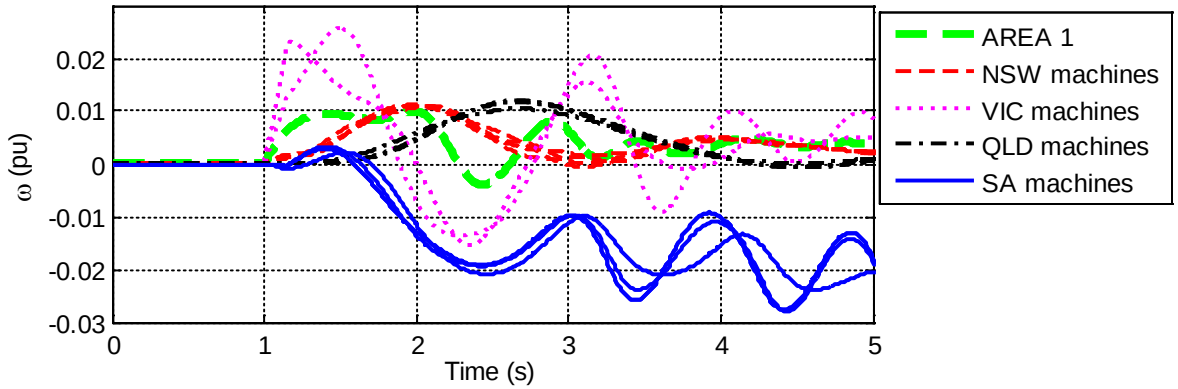

Figure 9-27. Case 5: 650MW transfer VIC to SA: rotor speed of the system machines, CT = 140ms

9.6. Chapter Conclusion

The performance of the EBSIME algorithm for TSA is demonstrated on the AU14GEN system. Power transfer limit (PTL) searches are conducted for the 8 cases in Table 9-2. One CCT search is performed on case 1. In four of the cases (1, 4, 5 and 8) the fault is applied at the sending-end of an interconnector, and the receiving-end in the other four cases (2, 3, 6 and 7). A detailed analysis and investigation of instability mechanisms is performed in this chapter for the cases where a sending-end fault is applied. Detailed analysis of the receiving-end faults is deferred to Chapter 10.

For a sending-end fault, the system operation tends to be constrained by forward-swing instability. These cases are used to demonstrate the performance of the EBSIME algorithm as the SIME forward-swing margins are used in the limit prediction phase of the FSL search. At best the EBSIME algorithm performs 51% faster than the plain binary search; and at worst 10% slower. The time-saving advantages of the algorithm are due to the FSL search phase. Significantly, the searches demonstrate that according to the ESC a forward-swing unstable scenario may be multi-swing stable. Conversely, scenarios that are forward-swing stable according to the ESC may be transiently unstable on a subsequent swing. The reliability and robustness of the EBSIME algorithm is due to the use of bisection to redirect the search when the limit prediction steps diverge; and conducting the residual binary search phase at its conclusion.

Table 9-14 lists the mechanisms leading to transient instability for each of the investigated cases that feature a fault applied at the sending-end of an interconnector. The observations largely agree with the results of the investigations on the two-machine system in Chapter 5, particularly for high power transfers. That is, the relationship between CCT and power transfer is monotonic, and the CCT is inversely proportional to the power transfer over the interconnector. Furthermore the system tends be constrained by forward-swing instability.

An exception is case 5, where the CCT does not change monotonically with respect to power transfer; rather the variation is piecewise linear. This is found to be associated with different ways that the system machines separate and lose synchronism, depending on the power flow. The other exception is case 1 for low QNI transfers. Even though the fault is applied on the QNI, system separation actually occurs on the highly stressed VSI: SA loses synchronism with the rest of the system. In this scenario instability occurs on the back-swing.

Conversely, at higher QNI transfers instability is due to the QLD machines losing synchronism and the system operation is subject to forward-swing stability. In Chapter 5, when a receiving-end fault is applied to the two machine system similar traits to cases 1 and 5 are observed. This similar behaviour is investigated in more detail in Chapter 10.

The investigations also highlight that:

- A scenario may be transiently stable, but the voltage response may be unacceptable. Voltage stability performance must also be considered.
- Dominant inter-area modes may cause machines far from the fault location to lose synchronism. The SIME responses for such scenarios tend to be constrained by back-swing instability, and provide limited information for the SIME limit-prediction search phase.

Chapter 10 TSA for Receiving-End Faults on the AU14GEN System

This chapter explores the cases where a three-phase fault is applied at the receiving-ends of the major interconnectors in the simplified 14-generator model of the South-East Australian power system (AU14GEN). In each case the fault is applied to either the Queensland to New South Wales interconnector (QNI), or the Victoria to South Australia interconnector (VSI). This produces a non-monotonic relationship between the critical clearing time (CCT) and the interconnector transfer. At high transfers the system operation tends to be constrained by the back-swing mechanism of transient instability. When back-swing instability is a concern there is no advantage to the EBSIME algorithm.

The forward- and back-swing mechanisms of instability result in significantly different CCTs for the sending- and receiving-end faults. This asymmetry in the CCTs for the two fault locations for variation in power transfer is explored on the AUG14GEN system. There are similarities to the results in Chapter 5 where the asymmetry in CCTs is investigated on the 9-bus two-machine power system.

10.1. Sensitivity of CCT to Power Transfer For a Receiving-End Fault

Table 10-1 and Table 10-2 list the variation in CCT for the cases where a three-phase fault is applied at the receiving ends of the major interconnectors with respect to variation in the interconnector transfer. In each case the CCT changes non-monotonically with power transfer. First, but counter-intuitively, the CCT increases with increasing transfer, reaching an apex and then it decreases as the interconnector power transfer is increased further. Table 10-1 shows that in case 2 the apex occurs at 300MW and in case 3 it happens at 600MW. Table 10-2 shows that in cases 6 & 7 the apex happens at 300MW and 100MW respectively.

TABLE 10-1. RECEIVING-END FAULT: RELATIONSHIP BETWEEN QNI TRANSFER AND OTHER NETWORK DATA

Case	Direction of Transfer	Fault Location	Property	QNI Power Transfer (MW)			
				0	**300**	**600**	**900**
2	NSW to QLD	4A	CCT(ms)	216	245	245	104
			Steady-state transfer from bus 413 to 410 Via 4A in Figure 9-2 (MW)	0	147.5	289.4	422.8
			Voltage angle drop over line (°)	0.1	3.7	7.7	12.3
3	QLD to NSW	2A	CCT(ms)	141	149	153	0*
			Steady-state transfer from bus 205 to 206 Via 2A in Figure 9-2 (MW)	-184	-40.5	102.5	245.7
			Voltage angle drop over line (°)	7.4	1.7	4.0	10.3
*QNI 900MW transfer is too unstable for a receiving-end 3-phase fault at point 2A in Figure 9-2.							

TABLE 10-2. RECEIVING-END FAULT: RELATIONSHIP BETWEEN VSI TRANSFER AND OTHER NETWORK DATA

Case	Direction of Transfer	Fault Location	Property	VSI Power Transfer (MW)				
				0	100	300	500	700
6	VIC to SA	5A	CCT (ms)	141	173	225	167	0*
			Steady-state transfer from bus 509 to 507 Via point 5A in Figure 9-2. (MW)	-78.8	-33.6	55.6	139.8	217.5
			Voltage angle drop over line (°)	10.0	4.3	6.8	17.7	30.3
7	SA to VIC	3A	CCT (ms)	83	85	75	50	N/A*
			Steady-state transfer from bus 305 to 307 Via point 3A in Figure 9-2. (MW)	639.6	620.3	583.1	548.9	N/A
			Voltage angle drop over line (°)	1.6	1.5	1.4	1.4	N/A
*VSI 700MW transfer is too unstable for a receiving-end 3-phase fault at points 5A & 3A in Figure 9-2								

In case 2, the receiving-end fault is applied to point 4A in Figure 9-2 at the Queensland (QLD) end of the QNI. In case 3, the receiving-end fault is applied to point 2A at the New South Wales (NSW) end of the QNI. The impedance of the circuit at point 2A is 4 times larger than that of the circuit at point 4A. The higher impedance of the circuit at point 2A causes the CCTs in case 3 to be significantly lower than those in case 2.

Similar reasoning applies to cases 6 and 7 where in case 6 the impedance of the faulted circuit (5A) is three times smaller than that of the faulted circuit (3A) in case 7. The higher voltage and impedance of the circuit at point 3A causes the CCTs in case 7 to be much shorter than in case 6.

Table 10-1 and Table 10-2 describe how the steady-state power transfer and voltage-angle-drop over the faulted circuits change when the interconnector transfer is increased. In case 2, the power transfer over the circuit at point 4A increases in proportion to the transfer over the QNI parallel transmission lines. In case 3, when the QNI transfer is increased from 0MW to 900MW, the steady-state transfer over the circuit at point 2A also increases. Similarly, in case 6, the power transfer over the circuit at point 5A increases in proportion to transfer over the parallel transmission lines that form the VSI. The steady-state power transfer over the circuit at point 5A is proportional to the voltage angle drop over the circuit.

In case 7, there is instead an inverse relationship between the steady-state transfer on the faulted circuit at point 3A, with respect to the VSI transfer. When the VSI transfer from SA to VIC is increased from 0MW to 500MW, the steady-state transfer on the circuit 3A from bus 305 to 307 decreases. The inverse relationship is due to the distribution of load in the Victorian region. As the power imported into SA increases the amount of power that needs to be sent from the east-side to the west-side of VIC is reduced.

10.2. Mechanism of Transient Instability for a Receiving-End Fault

Table 10-3 summarizes the main mechanisms causing transient instability in the cases 2, 3, 6 & 7 on the AU14GEN system. In each case there are at least two different mechanisms of instability depending on the power transfer on the interconnector of interest. At low transfers, the system tends to be constrained by forward-swing instability. At high transfers, it is constrained by back-swing instability.

Consideration of Table 10-1, Table 10-2 and Table 10-3 shows that:

- The CCT is proportional to interconnector transfer when the system operation is constrained by forward-swing instability.
- The CCT is inversely proportional to the interconnector transfer when operation is constrained by back-swing instability.
- This is similar to the findings in Chapter 5 where a three-phase fault applied to the receiving-end of the 9-bus two machine power system. The observations from the two machine system and could be used to explain the findings on the AU14GEN system.
- On the two machine system at low power transfers, the system is constrained by forward-swing instability as the available deceleration area is smaller than the available acceleration area, on the P_{aOMIB} - δ_{OMIB} curve of the post-fault network. Increasing the transfer over the interconnector increases the available deceleration area, and decreases the available acceleration area. Consequently, the CCT increases as the interconnector transfer increases; the CCT is proportional to the increasing deceleration area.
- At high transfers the available deceleration area on the P_{aOMIB} - δ_{OMIB} curve is larger than the available acceleration area, thus the system operation is constrained by back-swing instability. This causes the CCT to be proportional to the available acceleration area. When the power transfer is increased the CCT decreases, because the available acceleration area also reduces.

- In case 3 there is an operating condition which occurs in the transition between the forward- and back-swing mechanisms of instability. For QNI transfers near to 600MW the system has a propensity to split into three groups due to the shape of the dominant electro-mechanical mode of the system. This differs from the concept that is used by the EBSIME and original SIME algorithms that instability is caused by the irrevocable separation of the system machines into just two aggregate groups. It would be of interest to consider the impact that system separation into more than 2 groups would have on the EBSIME algorithm. However, this is beyond the scope of the thesis.

Case 6 is used to demonstrate the mechanisms of transient instability that happen for a fault applied at the receiving-end of an interconnector. The system behaviour is similar for cases 2, 3 & 7, although alternative generators and SVCs are responsible for the loss of synchronism, as described in Table 10-3.

TABLE 10-3. MECHANISMS OF TRANSIENT INSTABILITY FOR THE CASES 2, 3, 6 & 7

Case	Fault Location	Direction Of transfer	Transfer Range	Cause of loss of synchronism
2	4A, near to bus 410	NSW to QLD (South to North flow)	<300MW	QLD machines accelerate with respect to the remaining system (forward-swing instability)
			≥300MW	QLD machines decelerate with respect to the remaining system (back-swing instability)
3	2A, near to bus 206	QLD to NSW (North to South flow)	≤600MW	SA machines decelerate with respect to the remaining system (forward-swing instability)
			Near 600MW	Three groups. QLD machines accelerate; SA & VIC machines rapidly decelerate; NSW machines experience minor deceleration.
			>600MW	QLD machines accelerate with respect to the remaining system (back-swing instability)
6	5A, Near to bus 507	VIC to SA (North to South flow)	≤300MW	SA machines accelerate with respect to the remaining system (forward-swing instability)
			>300MW	SA machines decelerate with respect to the remaining system (back-swing instability)
7	3A, near to bus 509	SA to VIC (South to North flow)	≤300MW	VIC and SA machines accelerate with respect to the remaining system (forward-swing instability)
			>300MW	SA machines accelerate with respect to the remaining system (back-swing instability)

10.2.1. Case 6 Forward-Swing Instability: 300MW from VIC to SA – Fault at 5A

Figure 10-1 shows the time responses of key variables for a marginally unstable scenario from case 6, where 300MW is transferred over the VSI from VIC to SA. The receiving-end three-phase fault is applied near to bus 507 in SA, after a 1s run-in period and cleared after 235ms.

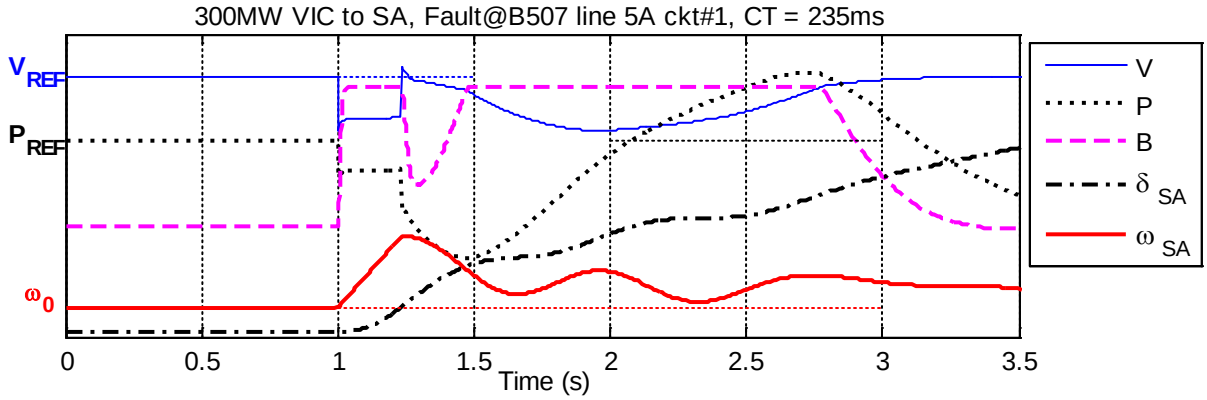

Figure 10-1. Time responses of (i) the bus 509 voltage (V), (ii) the power flow in circuit #2 from bus 315 to 509 (P), (iii) the susceptance of the SVC at bus 509 (B); (iv) the rotor angle (δ_{SA}) and (v) rotor speed (ω_{SA}) of the NPS_5 machine connected to bus 501.

The system begins in the steady-state when the power transfer (P) over the VSI is $P_{REF} = 300MW$, the voltage at the SVC at bus 509 (V) is at the set point level $V_{REF} = 1.03pu$, and all system machines operate at synchronous speed (ω_0).

Application of the three-phase fault at bus 507 causes:

- P to drop from 300MW to 180 MW
- the SA machines to accelerate above synchronous speed ($\omega_{SA} > \omega_0$), and the angle of the SA machines (δ_{SA}) to advance.
- V instantaneously drops to 0.67 pu before slightly increasing to 0.75 pu as the SVC saturates at its capacitive limit.

After the fault is cleared:

- P drops to 20MW and continues to decrease due to the advance of the SA machine angles with respect to those in the rest of the system
- the SA machines generally decelerate, although they experience oscillations induced by local modes.

- V spikes above V_{REF} to a peak of 1.091 pu immediately following fault clearance.
- The SVC susceptance (B) returns within the operating limit in the attempt to restore V to its set point

At t=1.47s:

- P reaches a minimum of -190MW and then starts increasing.
- The SVC has insufficient capacity to restore voltage to its set-point. It therefore saturates at its capacitive limit and the voltage decreases.
- δ_{SA} continues to rise as ω_{SA} remain above ω_0.

At t=2.08s:

- P reaches P_{REF} and continues to increase. Thus there is a net positive generation in SA which causes the continued increase in δ_{SA}.
- This causes δ_{SA} to resume acceleration at t=2.3s, before the SA machines can reach synchronous speed.

The system loses synchronism at t=2.78s when the SA machines diverge from the COI by 180°. Loss of synchronism is caused by the SA machines accelerating ahead of the rest of the system on the forward-swing, since δ_{SA} continually rises during and after application of the fault.

10.2.2. Case 6 Back-swing Instability: 500MW from VIC to SA – Fault at 5A

Figure 10-2 shows the time responses of key variables for a marginally unstable scenario from case 6 where 500MW is transferred from VIC to SA. The fault is applied near to bus 507 after a 1s run-in period, and cleared after 177ms.

The system begins in the steady-state when the VSI power transfer (P) is $P_{REF} = 500MW$, the voltage at the South-East SVC at bus 509 (V) is at the set point level of 1.03 pu (V_{REF}) and all system machines operate at ω_0.

Application of the three-phase fault at bus 507 causes:

- the SA machines to accelerate
- the South-East SVC to saturate
- the power transfer to fall from 500MW to 188MW
- V to fall to 0.7pu, before instantaneously recovering to 0.75 pu.

After the fault is cleared:

- The SA machines start to decelerate.
- Due to the advance in the SA machine angles with respect to the remaining system machines, P swings to a low of -151MW at t=1.69s.
- The reduced power flow on the VSI causes V to increase above V_{REF}. The AVR of the South-East SVC acts to reduce B in order to restore the SVC voltage to its reference.

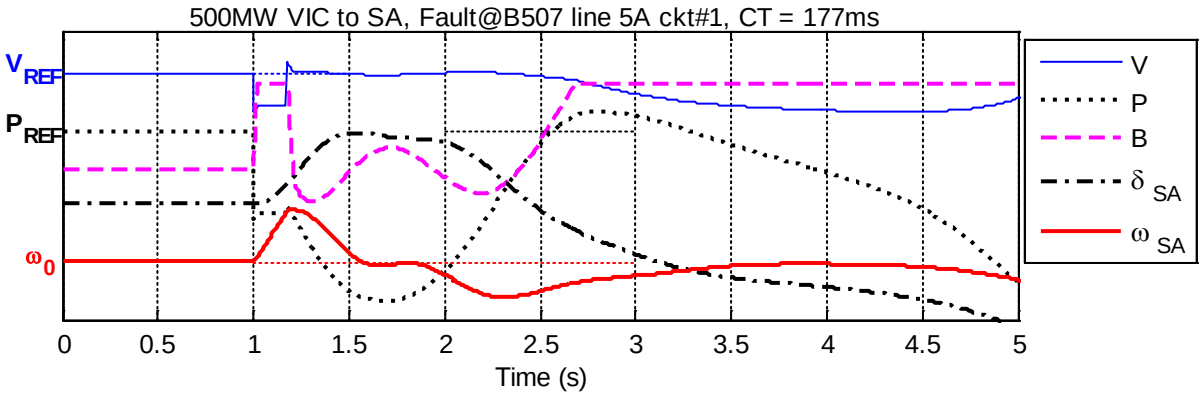

Figure 10-2. Time responses of (i) the bus 509 voltage (V), (ii) the power flow in circuit #2 from bus 315 to 509 (P), (iii) the susceptance of the SVC at bus 509 (B); and (iv) the rotor angle (δ_{SA}) and (v) speed (ω_{SA}) of the NPS_5 machines connected to bus 501.

During the first swing, after the fault:

- the rotors of the SA machines decelerate to synchronous speed and then continue to decelerate.

Once the SA machines slow below synchronous speed, after t=1.7s:

- δ_{SA} decreases slowly
- P begins to increase
- As P increases, the SVC maintains V to V_{REF} by adjusting B.

However, at t = 2.70s:

- the SVC reaches its capacitive limit and the SVC voltage falls below V_{REF}.

At t=3.9s:

- ω_{SA} reaches a local maximum which is marginally less than synchronous speed during the back-swing of δ_{SA}.
- Since $P < P_{REF}$, there is a net deficit of generation in SA, and the SA machines continue to slow down.

– Consequently, synchronism is lost as $\omega_{SA} < \omega_0$ and the SA machines decelerate with respect to the rest of the system. Transient instability is associated with the loss of voltage control caused by the limited capacity to supply reactive power from the South-East SVC at bus 509.

10.3. The EBSIME Search Algorithm Applied to a Receiving-End Fault

The EBSIME algorithm is applied to case 6 to search for the PTL, where the circuit breakers on circuit 5A are configured to open 120ms after the fault is applied. The PTL is found to be 587MW. The search commences between the search bounds of 0MW and 750MW. A search tolerance of 5MW is used. The search traversal is summarized in Table 10-4.

In the first scenario, where power transfer is 750MW, the system operation is constrained by back-swing instability for the reasons outlined in section 10.2.2. Although the scenario is transiently unstable it is diagnosed by the SIME ESC to be forward-swing stable. As the search initialization conditions cannot be met, the SIME component for the search is ineffective. As such, the EBSIME PTL search is the exactly same as a binary search. The same limitations are encountered when the search algorithm is applied to cases 2, 3 & 7, and case 5 which was discussed in Chapter 9. In each of these cases the first search scenario is constrained by back-swing transient instability.

TABLE 10-4. EBSIME PTL SEARCH FOR CASE 6, WHERE THE APPLIED FAULT IS CLEARED AFTER 120MS

k	Power Transfer (MW)	Stable (S) or Unstable (U)	Search bounds (MW)	TSIM (sim-s)
1	750	U	[0, 750]	2.93
2	375	S	[375, 750]	10.00
3	563	S	[563, 750]	10.00
4	657	S	[563, 657]	3.40
5	610	S	[563, 610]	3.87
6	587	S	[587, 610]	10.00
7	599	U	[587, 599]	4.27
8	593	U	[587, 593]	4.82
9	590	U	[587, 590]	6.09
Total Simulated Time				55.64

10.4. The Effect of SVCs on Transient Stability

In cases 1 and 2, where faults are applied at either end of the QNI, the voltage sag is lowest at bus 205. In cases 5 and 9, where faults are applied on the VSI, the voltage sag is the lowest at bus 509. For the investigated cases, it is generally noted that the voltage sag is most significant near the SVC on the middle of the interconnector where the fault is applied. This behaviour is demonstrated in the discussions on cases 1 and 5 in section 9.5. The significant voltage sag at these locations is caused by the SVCs at buses 205 and 509 saturating at their capacitive limits for long periods in response to the applied faults.

This indicates that to improve transient stability it may be beneficial to increase the capacity of the SVC nearest to the impacted interconnector. Case 1 is different due to the significant participation of SA machines in the dominant inter-area modes, as noted in section 9.5.1.3. Thus for Case 1 it may be more effective to increase the capacity of the South-East SVC at bus 509.

Table 10-5 compares the CCTs for cases 5 and 6 when the capacity of the SVC at bus 509 is doubled. In case 5, and for transfers up to 300MW in case 6, the CCT is relatively insensitive to the increase in SVC capacity. However in case 6, for the transfers greater than 300MW, doubling the reactive capacity of the SVC causes a noticeable increase in the CCT. Thus, for the cases that are constrained by forward-swing instability increasing the SVC capacity has negligible effect on the CCT. For the scenarios constrained by back-swing instability increasing the SVC capacity significantly increases the CCT.

These findings are similar to the behaviour observed on the four-machine system in Chapter 7 and the two-machine 9-bus system in Chapter 5. Section 5.3 observes that in a scenario constrained by forward-swing instability, the system operation is limited by the available deceleration area under the OMIB power-angle curve. Increasing the SVC capacity has negligible effect on the OMIB deceleration power, and consequently little effect on the CCT. Similar results are observed on the AU14GEN system, which uses sixth order machine modelling, AVR excitation, power system stabilizers and SVC controls.

Section 5.4 shows that when the system operation is constrained by back-swing instability, the available acceleration area from the OMIB power-angle curve constrains the system operation and is proportional to the CCT. Increasing the SVC capacity increases the magnitude of OMIB acceleration power, and consequently the CCT is higher. This is similar to the results observed in case 6 on the AU14GEN system.

TABLE 10-5. COMPARISON CCTS WHEN THE REACTIVE CAPACITY OF THE SVC AT BUS 509 IS INCREASED

Case	Direction of Transfer	Fault Location	SVC Capacity at bus 509	Power Transfer (MW)				
				0	100	300	500	700
				CCT (ms)				
5	VIC to SA	3A	Base condition B1 (±160 MVar)	157	161	163	149	125
			±320 MVar	159	163	165	153	135
6		5A	±160 MVar	141	173	225	167*	0*
			±320 MVar	141	173	223	177*	63*
All scenarios in this table are constrained by forward-swing mechanism of instability unless they are marked with an (*); in which case the scenario is constrained by back-swing instability.								

10.5. Asymmetry in the CCT for Variation in the Power Transfer

This section investigates the differences between the CCTs for a fault applied at either the sending- or receiving-end of an interconnector on the AU14GEN system, and how this asymmetry is influenced by the interconnector power transfer. This investigation is based on section 5.5.3 where it is observed that the ratio $\left(CCT_S : CCT_R\right)^2$ is less than 1 and decreases linearly with respect to increasing power transfer on the two machine power system. This indicates that the disparity between the CCTs is larger when the power transfer is increased. The investigation assumes that the system operation is constrained by back-swing instability when a fault is applied at the receiving-end, and constrained by forward-swing instability where a fault is applied at the sending-end.

Table 10-6 lists the CCTs of the relevant scenarios from cases 1, 2, 3 and 4 on the AU14GEN system, from Table 9-2, that exhibit these same characteristics. Figure 10-3 shows the corresponding relationship of $\left(CCT_S : CCT_R\right)^2$ to power transfer for these cases. The results in Figure 10-3 shows that the $\left(CCT_S : CCT_R\right)^2$ decreases when the QNI transfer is increased between cases 1 and 2, and between cases 3 and 4. $\left(CCT_S : CCT_R\right)^2$ for cases 3 and 4 decreases with an approximately linear relationship to the transfers from 700MW to 800MW, as was observed on the two machine system in section 5.5.3.

TABLE 10-6. COMPARISON OF CCTS FOR VARIATION OF TRANSFER ON THE QNI

Power Transfer	Case	Fault Location (S) Sending-End (R)-Receiving-End	Power Transfer (MW)				
			600	650	700	750	800
NSW to QLD (QNI)	1	S	110	104	63	-	-
	2	R	245	235	218	-	-
QLD to NSW (QNI)	3	R	-	153	125	102	85
	4	S	-	85	67	40	0
In this table in all scenarios where a sending-end fault (S) is applied they are subject to forward-swing instability. All scenarios where a receiving-end fault (R) is applied are subject to back-swing instability.							

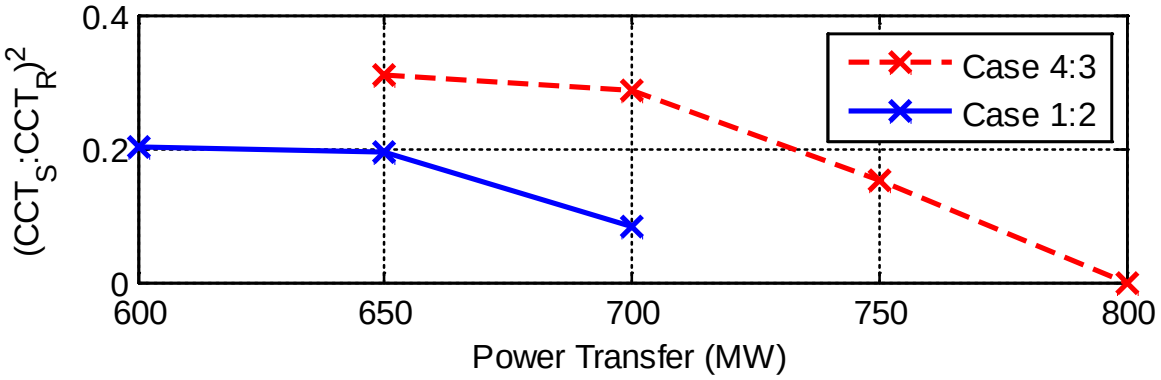

Figure 10-3. The squared ratio of $CCT_S : CCT_R$ as a function of power transfer.

10.6. Similarities in Results on the Two Machine and the AU14GEN Systems

The cases studied on the AU14GEN system in Chapters 9 and 10 show two different categories of behaviour for the relationship between interconnector power transfer and the CCT.

For the sending-end fault cases 1, 4, 5 and 8 on the AU14GEN system:

- Table 9-14 indicates that system operation tends to be constrained by the transient instability on the forward-swing.
- In each of these cases a three-phase fault is applied to the sending-end of the investigated interconnector.

- The forward-swing instability constraint means that the EBSIME algorithm can potentially be used to accelerate a TSL search using the FSL prediction steps for these cases.
- Aside from case 5, there is an inverse proportional relationship between the CCT and the interconnector transfer.
- In case 1 the system operation is constrained by forward-swing transient instability for transfers higher than 500MW. For transfers below 500MW the system operation is constrained by back-swing transient instability. This behaviour is due to the shape of the dominant mode and the associated propensity for the system to separate at the VSI when a fault is applied on the QNI (see section 9.5.1.3).

In case 5 there is a non-monotonic relationship between the CCT and power transfer. For transfers below 450MW, the CCT and power transfer are proportional. For transfers above 450MW the CCT and power transfer are inverse proportional. This is due to the different mechanisms that cause transient instability in the two different regions of operation.

For the receiving-end fault cases 2, 3, 6 and 7 on the AU14GEN system:

- There is a non-monotonic relationship between CCT and interconnector transfer.
- At the lower transfers the CCT is proportional to the interconnector transfer, and the system operation is constrained by forward-swing transient instability.
- At higher transfers the CCT is inversely proportional to interconnector transfer, and the system operation is constrained by back-swing transient instability.
- These results are similar to the observations from the nine-bus two machine power system investigated in Chapter 5. The length of the two-machine system has been selected to represent the physical characteristics of the major corridors on the SE Australian system. The similarities between the two different power systems can therefore be applied to explain the behaviour observed on the AU14GEN system.

On the two machine system, the fault location influences the CCT ands the mechanism of instability. The CCT is proportional to either the available acceleration or deceleration area –whichever is smaller- formed by the P_{aOMIB} - δ_{OMIB} curve for the post-fault network.

For a sending-end fault on the two-machine system:

- There is a monotonic inverse proportional relationship between the CCT and interconnector transfer.
- System operation is constrained by forward-swing transient instability as the

available deceleration area for the post-fault P_{aOMIB} - δ_{OMIB} curve is smaller than the available acceleration area.

For a receiving-end fault on the two-machine system:

- There are two different mechanisms of transient instability, and therefore the CCT varies non-monotonically with respect to the power transfer.
- At low transfers, the system is constrained by forward-swing instability as the available deceleration area is smaller than the available acceleration area, on the P_{aOMIB} - δ_{OMIB} curve of the post-fault network.
- Increasing the power transfer over the effected interconnectors increases the available deceleration area, and decreases the available acceleration area.
- Although it seems counter-intuitive, the CCT increases as power transfer over the interconnector increases; the CCT is proportional to the increasing deceleration area.
- At high transfers the available deceleration area is larger than the available acceleration area, thus the system operation is constrained by back-swing instability.
- Under this circumstance the CCT is proportional to the available acceleration area - both parameters decrease when the power transfer increases.

On the AU14GEN system, doubling the capacity of the critical SVCs on the faulted interconnector causes negligible improvement to the transient stability limits. On the two-machine system the finding is similar. This is because the post-fault available deceleration area which constrains the system operation does not vary much when the SVC support is connected. In fact, increasing the SVC capacity marginally decreases the available deceleration area.

10.7. Chapter Conclusion

This chapter investigates the transient instability of the cases on the AU14GEN system in Table 9-2 where a three-phase fault is applied at the receiving-end of either the Queensland to New South Wales interconnector (QNI), or the Victoria to South Australia interconnector (VSI). These cases demonstrate how the EBSIME algorithm robustly determines the TSLs, even when the back-swing mechanism of instability is encountered.

The motivation of the investigations in Chapters 4 and 5 on the two-machine nine-bus system is to explain the transient stability analysis on the AU14GEN system. A key outcome of this chapter is that there are a number of similarities between the results on the AU14GEN system to the results on the investigations in Chapters 4 and 5. This suggests that there is potential for similar transient stability phenomena on larger power system models to be explained by the two machine 9-bus power system model.

The outcomes of Chapter 10 are summarized in the following points.

Receiving-End Fault: Non-Monotonic Relationship between the CCT and Power transfer

- There is a non-monotonic relationship between the interconnector power transfer and the CCT. At low transfers, the CCT is proportional to the interconnector power flow, and the system operation tends to be constrained by transient-instability on the forward-swing. At high transfers the CCT is inversely proportional to the power flow, and the system operation is constrained by back-swing instability.

Explanation of the Non-Monotonic Relationship

- In Chapter 5 it is found that the CCT is proportional to the constraining acceleration areas defined by the OMIB acceleration power-angle characteristic of the post-fault network.
- At low power transfers the system operation is constrained by the available OMIB deceleration area, which is proportional to the interconnector power flow. This explains the proportional relationship between the CCT and interconnector flow for low transfers.
- At high transfers, the system operation is constrained by the available OMIB acceleration area which is inversely proportional to the interconnector flow. This explains the inverse proportional relationship between the CCT and interconnector flow for the higher transfers.

The Effect of SVC capacity on the CCT

- From Table 10-5 increasing the SVC capacity tends to improve the CCT for receiving-end faults providing the system is subject to back-swing instability. Otherwise the change in CCT is slight.

Chapter 11 Conclusions

The South-East (SE) Australian interconnected power system is susceptible to transient instability due to its narrow transmission corridors and large inter-regional power transfers. To determine the transient stability limits (TSL) of the system the Australian Energy Market Operator (AEMO) perform studies offline due to the computationally intensive calculations that are involved. Faster algorithms are needed to facilitate and improve the reliability of the online dynamic security analysis (DSA).

Methods that preserve full modeling detail in the analysis is desirable due to the importance of generator control systems and their associated limits for the stable operation of the SE Australian system [10]. Static var compensators (SVCs) are also critical to maintaining the transient stability of the SE Australian power system. Of particular importance for system operation, beyond knowing if the system is currently in a secure state, is the knowledge of how "close" the system is to its TSL in the event of critical contingencies.

AEMO's online DSA presently lacks the tools to estimate the distance of the current system operating point to the TSLs in terms of controllable system parameters. Control decisions are determined off-line using trial and error methods that involve the computationally intensive repetition of many similar studies and a significant engineering task of assessing the results. Tools that systematically and efficiently assess the sensitivity of TSLs to the factors which influence them are needed [10] [9]. This could help power system operators to accurately determine transfer limits, and to identify strategies to maximize the transfer capability of the system.

The Single Machine Equivalent (SIME) method has many attractive properties for TSL searching. It:

- employs early stop criteria (ESC) that enables fast detection of forward-swing stability and instability,
- calculates transient stability margins that can estimate a TSL and accelerate the limit search, and
- does not require or make any simplifications to the detailed model of the power system being investigated.

However, the SIME method is dependent on the heuristic tuning of the algorithm parameters not only to the particular system being investigated but also 1) the current operating condition, 2) power transfer, 3) the location and 4) the type of fault within the system.

This thesis proposes the Enhanced Binary SIME (EBSIME) algorithm, an improved approach to the SIME method, to provide a fast, robust and systematic approach to searching for TSL. It does not need to be tuned, therefore ensuring accurate and robust determination of the limit.

The novel contribution of the thesis is presented in three parts:

1) The theory for the EBSIME algorithm is presented and demonstrated on a nine-bus two-machine power system – it provides insights that can explain similar results observed on the 14-generator model of the South East Australian power system (AU14GEN).
2) The design and implementation of the EBSIME algorithm for TSL searching as a modular plug-in for PSS®E is presented. In particular, the algorithm does not need to modify the core PSS®E TSA simulation software.
3) The performance of the EBSIME algorithm for TSL searching is benchmarked on the AU14GEN model and the search results are discussed. A meaningful comparison between the performance of the 2-machine and the AU14GEN systems is made.

11.1. SIME TSA of a Two Machine System

In Chapters 4 and 5, the SIME method is applied to a two machine power system to demonstrate from first principles how the one machine infinite bus (OMIB) response of a fully-detailed multi-machine system is derived, without any model simplifications. Closed-form parameterized solutions are deduced for the two machine system, and then used in the SIME derivation. This perspective of the SIME algorithm has not been considered before.

The OMIB responses are used to demonstrate the application of the SIME early stop criteria (ESC) and the SIME margins, to explain the different observed mechanisms of transient instability and their influence on the TSLs. The kinetic energy exchanged between the two machines in response to a contingency is proportional to the acceleration and decelerations areas of the OMIB power versus angle (P_{aOMIB} - δ_{OMIB}) curve. Figure 11-1, reproduced from Figure 5-9, reveals how the instability mechanism is different for a sending- and receiving-end fault.

When a three-phase fault is applied at the sending-end of the interconnector:

- Generator 1 at the sending-end of the two-machine system, accelerates ahead of generator 2 at the receiving-end. Thus $P_{aOMIB} > 0$ and δ_{OMIB} increases. In Figure 5-9 the P_{aOMIB} - δ_{OMIB} curve transitions from points A-A'-B' during the fault.

- After fault clearance generator 1 decelerates but remains above synchronous speed; the P_{aOMIB} - δ_{OMIB} curve transitions from B'-D.
- The available deceleration area (between B'-D and the δ_{OMIB} axis) is smaller than the acceleration area (between A-B-B' and the δ_{OMIB} axis).
- Transient instability occurs during the forward-swing at point D, when generator 1 experiences insufficient deceleration to equalize with the speed of generator 2.

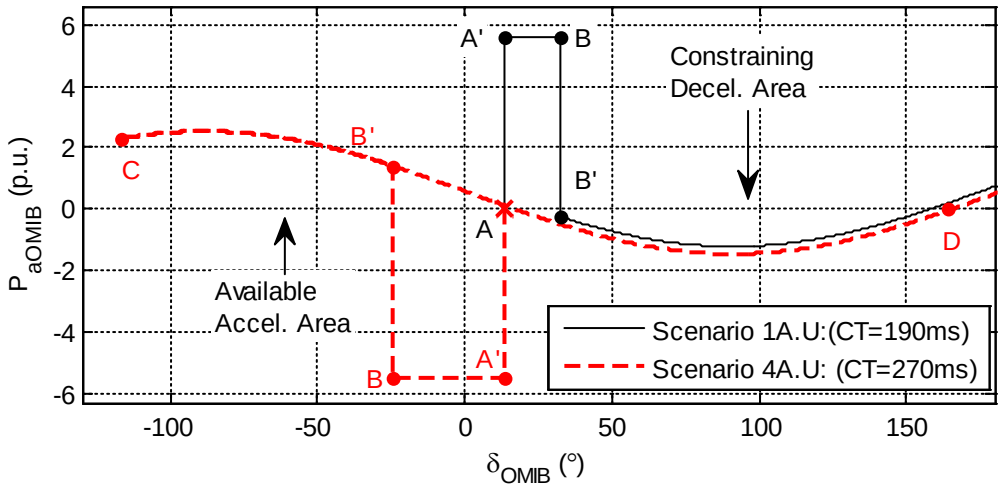

Figure 11-1. $P_{aOMIB} - \delta_{OMIB}$ *curves for the unstable scenarios 1A.U (sending-end fault) and 4A.U (receiving-end fault) on the 9-bus two-machine system.*

When a three-phase fault is applied at the receiving-end of the interconnector:

- During the fault, $P_{aOMIB} < 0$ and δ_{OMIB} decreases since generator 2 at the receiving-end experiences a larger acceleration than generator 1. In the forward-swing the P_{aOMIB} - δ_{OMIB} curve transitions from A-A'-B-B'.
- After fault clearance, δ_{OMIB} continues on the forward-swing from point B' to C. At C it changes direction, increasing during the back-swing from points C-B'-A-D.
- The available deceleration area is smaller than the reacceleration area (between A-B'-C and the δ_{OMIB} axis).
- Transient instability occurs during the back-swing at point D, when generator 2 experiences insufficient deceleration to equalize with the speed of generator 1.

The different mechanisms of transient instability cause an asymmetric variation in the critical fault clearing time (CCT) for a sending-end versus a receiving-end fault for the variation of some network parameters. For example:

Increase of interconnector SVC capacity:

- The CCT monotonically increases for a receiving-end fault;
- The CCT monotonically decreases for a sending-end fault.

Increase of power transfer:

- The CCT monotonically decreases for a sending-end fault.
- For a receiving-end fault:
  a) For low transfers the CCT increases monotonically;
  b) For higher transfers above a threshold the CCT decreases monotonically.

In Chapters 4 and 5, the different nature of the variation in CCT with variation in some network parameters at the different fault locations is found to be due to the asymmetry in the constraining acceleration/ deceleration areas for the two fault locations.

11.2. Design & Implementation of the EBSIME Algorithm

The EBSIME algorithm makes a number of improvements to the original SIME algorithm for TSL searching, that remove the need to tune the SIME algorithm to the investigated system, operating condition and fault location. The EBSIME algorithm, described in Chapters 6 to 8, makes the following improvements:

- Centre of inertia (COI) based criteria are used to identify the two machine groups (MG) which are used to calculate the SIME responses and margins;
- The MG are defined from the first unstable search scenario. The same MG is used in the SIME calculations for the rest of the search;
- Pairs of SIME margins are used to linearly predict the TSL thereby accelerating the search. This is possible since the same MG is used to calculate all SIME margins;
- The SIME margins calculated during a EBSIME search can be used for transient stability sensitivity analysis;
- When limit prediction fails to converge to the limit, bisection of the current search bounds is used to redirect the search towards the TSL.

The software tool developed during this work has been designed and implemented to integrate and execute the EBSIME algorithm with the PSS®E TDS software, without requiring access to, or modification of, the PSS®E source code. The AUSIME tool can be considered as a PSS®E “plug-in” module. The software implementation is composed

of an inner search loop implemented as a Fortran 95 PSS®E user-defined model; and an outer loop written using the Python scripting language to supervise the full limit search.

The AUSIME software features:

- Flexible text-based inputs of search instruction;
- Text-based output reports on the transient stability limits, search timing, traversal and other results;
- OMIB, COI and original time responses are saved to relatively compact binary files that can be converted to a MATLAB readable format for detailed analysis and graphical display of results. This feature is important for algorithm development.
- A modular architecture that allows the AUSIME software to be readily extended to included alternative search algorithms, and to use tried and trusted open source tools;
- The use of dynamically allocatable storage facilitates the analysis of power systems of widely differing sizes, and enables efficient handling of the potentially large volumes of data involved.

11.3. Application to the IEEE Simplified South East Australian System

The EBSIME algorithm for TSL searching is demonstrated on the IEEE 14-generator model of the SE Australian power system (AU14GEN) in Chapters 9 and 10. Faults on the major regional interconnectors, when the system operates under medium and heavy load, are investigated. Interconnector power flow from the north to south direction on the AU14GEN system, and vice versa, are considered. The critical contingency occurs for power flows from the south to north, when a fault is applied near to the South Australian end of the transmission circuits between Victoria and South Australia. The performance of the EBSIME algorithm is benchmarked against the results of the binary search. An independent version of the SIME algorithm for TSL searching could not be implemented within the AUSIME framework because:

- the University of Liège's original SIME software source code is confidential; and
- the original SIME algorithm requires tuning to each investigated power system model.

Similar to the findings on the two-machine power system, on the AU14GEN system a sending-end fault tends to cause the system operation to be constrained by forward-swing transient instability. Since the forward-swing margins can be calculated and applied in the limit prediction phase of the EBSIME search, a set of cases featuring a sending-end fault applied to the major interconnectors are used to assess the performance of the EBSIME algorithm. These cases demonstrate the time saving

advantages of the EBSIME algorithm, and the algorithm robustness for locating the correct limit. At best the EBSIME algorithm is found to be 30% faster than the plain binary search. In the worst case the search is 10% longer than the plain binary search. The success of the algorithm is independent of the search tolerance margin, and the proximity of the predicted forward-swing limit to the actual limit.

In the other cases, where a three-phase fault is applied at the receiving-end of the major interconnectors, there is a non-monotonic relationship between the power transfer and the CCT. The relationship between the CCT and interconnector power transfer characteristic can be categorized into two parts:

1) At low transfers, the CCT is proportional to the interconnector transfer, and the system operation is constrained by the forward-swing mechanism of instability.
2) At high transfers, the CCT is inverse proportional to the interconnector power transfer, and the system operation is constrained by transient instability on the back-swing.

This is similar to the findings in Chapter 5 on the two-machine power system model where analogously a contingency is applied to the receiving-end of the 440km line for a range of transfers. By extension, the results from the AU14GEN system can be explained by the following key points:

- The constraining acceleration area, calculated from the P_{aOMIB} - δ_{OMIB} curve of the post-fault network, is proportional to the CCT.
- At low transfers, the system operation is constrained by the available OMIB deceleration area which is proportional to the interconnector power flow. Therefore the CCT is proportional to the interconnector transfer.
- At high transfers, the system operation is constrained by the available OMIB acceleration area which is inverse proportional to the interconnector flow. Therefore the CCT is inverse proportional to the interconnector flow.

Other notable observations from the studies on the AU14GEN model are:

- Voltage instability constraints must also be considered;
- The mode-shape of the dominant inter-area modes may cause regional groups of machines, far from the fault location, to lose synchronism. In such cases the system tends to be constrained by back-swing instability. Therefore, the EBSIME algorithm is unable to locate a suitable scenario to calculate any SIME margins. Thus EBSIME search proceeds in binary search mode.
- Increasing the reactive output capacity of an SVC at an intermediate point on a long transmission line tends to improve the CCT for a receiving-end fault, although the SVC has little effect on the CCT for a sending-end fault.

11.4. General Conclusions

The novel contribution of the thesis is the EBSIME algorithm, which provides a fast and robust approach to TSL searching on a fully-detailed multi-machine power system. It does not require any model simplifications or tuning. It enhances the original SIME algorithm for limit searching by using bisection of the search bounds to guide the search whenever the SIME steps diverge.

Some important applications for the EBSIME software are perceived within the Australian power industry, therefore it has been implemented as a plug-in to the main PSS®E simulation engine which clearly demonstrates that the method does not require modification of the core PSS®E TSA tools. The EBSIME software uses a modular software architecture which facilitates alternative search methods for research and comparison purposes.

The EBSIME algorithm can apply the accelerating limit prediction steps to operating conditions that are constrained by forward-swing instability. It is shown that a severe fault applied at the sending-end of a long transmission line tends to cause instability on the forward power swing. A fault applied at the receiving-end of a transmission line tends cause transient instability to occur on the back-swing. When the system is subject to back-swing instability the EBSIME search is the same as the binary search.

Search results on the AU14GEN model show that the algorithm can locate the TSL up to 30% faster than a binary search, and at worst a few simulation seconds longer. Other forms of stability such as voltage stability may be more constraining than the TSL. Therefore an accurate determination of the CCT or PTL must also consider these other forms of stability.

The SIME margins generated as a by-product of the EBSIME search can be applied for transient stability sensitivity analysis. The sensitivity information that the EBSIME algorithm provides can potentially be used to operate existing electrical transmission infrastructure closer to the TSLs with the same reliability to which we are accustomed, thereby extending the transfer capability of the system. This could have significant economic and environmental impacts by delaying investments in new infrastructure, effectively saving many millions of dollars.

11.5. Future Work

More work is required before the EBSIME search algorithm can be applied commercially. In the thesis the EBSIME algorithm is investigated on a two-machine power network, a four-machine two-area network, and the AU14GEN power system. These systems provide useful insights into the mechanisms leading to transient instability due to the influence of fault location or inter-area modes. The three networks exhibit similar relationships between the CCT and power transfer for similar operating conditions. It will be beneficial to observe how the EBSIME algorithm performs on a realistic model of the SE Australian power system, and to observe if there are similarities to the results on the smaller networks.

The source code to automate the PTL search remains to be completed. However, it is more complex to implement as additional factors must be considered and a new load-flow solution must be calculated and solved for each search iteration. For a given network, there are numerous ways to achieve a given change in the power transfer over an interconnection. A design for the PTL search and associated input files is suggested in Chapter 8.

For the PTL searches that are performed on three power systems the interconnector transfer is adjusted by load scaling. The results reveal useful insights into the mechanisms of instability associated with the assessed operating conditions, and demonstrate the reliability of the EBSIME algorithm for locating PTLs. Alternative dispatch methods for achieving the desired power transfer would reveal further useful insights into the algorithm’s performance.

This thesis considers single contingency events that comprise the application of a single fault to one circuit which is later cleared by de-energizing the circuit. The influence of a generator trip on transient stability is not considered. A loss of generation/load event may give rise to frequency stability as well as transient stability. There is no inherent limitation of the EBSIME algorithm that would prevent its application to a loss of generation/ load event. There are acknowledged implications for such events, and the consequences on the SIME calculations need to be carefully considered.

Appendices

Appendix A Interpretation of the Power-Angle Curve Area

The equal area criterion is explained in numerous power systems textbooks. This theory is based on the analysis of a One Machine Infinite Bus (OMIB) system. Although the equal area criterion (EAC) cannot be applied to multi-machine systems with detailed representation of synchronous machines, it provides foundational insight into the key concepts and principles of transient stability.

A.1. Overview

In the context of the OMIB, the kinetic energy that is absorbed by the rotor from the turbine during the fault, ΔKE, is the difference between KE_0 and KE_c, which are the kinetic energies of the system at steady-state and when the fault is cleared respectively. To expand:

$$KE_0 = \frac{1}{2} J \omega_0^2 \tag{A.1}$$

$$KEc = \frac{1}{2} J \omega_c^2 \tag{A.2}$$

$$\begin{aligned} \Delta KE &= KE_c - KE_0 \\ &= \frac{1}{2} J \left(\omega_c^2 - \omega_0^2 \right) \end{aligned} \tag{A.3}$$

where ω_c is the rotor angular velocity at the point of fault clearance,

ω_0 is the rotor angular velocity at synchronous speed and

J is the moment of inertia of the generator.

It is commonly claimed that the acceleration and deceleration areas of the power-angle curve (see Figure A-1) represent the changes in kinetic energy that are exchanged between the rotor and the system in the event of a disturbance. An example of this assumption is in [21] which states:

"We shall now show that the [acceleration] area A1 represents the kinetic energy injected into the system during the fault".

Analysis in [21] shows that the acceleration area

$$A1 = \frac{1}{2} J \omega_{cl}^2 \tag{A.4}$$

where ω_{cl} is the perturbation in the rotor angular velocity from synchronous speed when the fault is cleared. The claim is made that this is equal to the kinetic energy injected into the system due to the fault.

However, by its definition

$$\omega_{cl} = \omega_c - \omega_0 \tag{A.5}$$

$$\therefore \frac{1}{2} J \omega_{cl}^2 = \frac{1}{2} J \left(\omega_c - \omega_0 \right)^2 \tag{A.6}$$

Applying (A.4) and (A.3), note that

$$\begin{aligned} \Delta KE - A1 &= \frac{1}{2} J \left(\omega_c^2 - \omega_0^2 \right) - \frac{1}{2} J \left(\omega_c - \omega_0 \right)^2 \\ &= \frac{1}{2} J \left(\omega_c^2 - \omega_0^2 - \left(\omega_c - \omega_0 \right)^2 \right) \\ &= J \omega_0 \left(\omega_c - \omega_0 \right) > 0 \end{aligned} \tag{A.7}$$

From (A.1) and (A.2) it is evident that contrary to the claim in [21], $\frac{1}{2}J\omega_{cl}^2$ is not equal to the change in kinetic energy, ΔKE in (A.3) since $\omega_c^2 - \omega_0^2 \neq (\omega_c - \omega_0)^2$. Equation (A.7) shows that $\Delta KE > A1$ by the amount $J\omega_0(\omega_c - \omega_0)$.

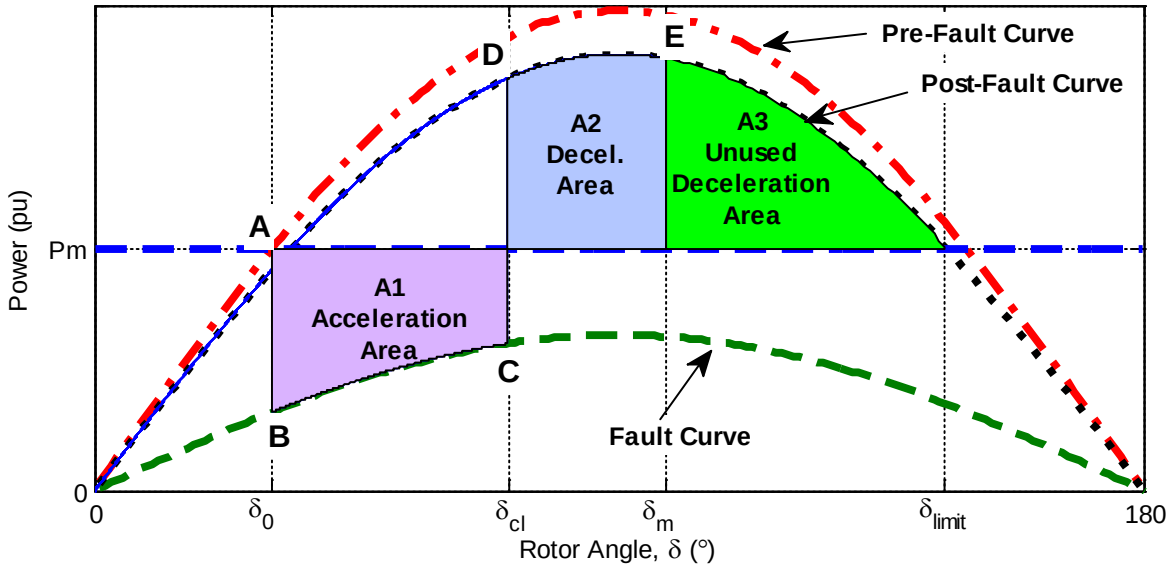

Figure A-1. Generator electrical output power versus rotor angle for a transiently stable disturbance. At A the system is in equilibrium, from B-C a fault is applied, from D-E the fault is cleared.

Kundur's Power System Stability and Control [13] is another textbook where a similar claim is made. In section 13.1 on page 832 Kundur writes:

"The energy gained [during the acceleration] is $E1 = \int_{\delta_0}^{\delta_1}(P_m - P_e)\,d\delta = \text{area } A1$. The energy lost during deceleration is … $E2 = \int_{\delta_1}^{\delta_m}(P_e - P_m)\,d\delta = area\ A_2$."

Here δ_0, δ_m and δ_{cl} are the initial, maximum, and fault clearance rotor angles respectively.

P_m is the input mechanical power;

P_e is the electrical power transferred from the generator.

According to the interpretation in [13], the acceleration area in the power-angle and power-time domain should be equal, or at least be linearly proportional, and similarly for the deceleration area. To test the claim that the acceleration area is equal to the kinetic energy gained by the rotor during the disturbance various faults are simulated based on the second order synchronous machine swing equations. Numerical integration is used to calculate the areas in both the power-angle and power-time domains. It was

consistently found that the areas, calculated with respect to power-time and power-angle, are not linearly related. The purpose of Appendix A is to illustrate that the commonly held interpretation that the 'acceleration area' A1 is proportional to the change in kinetic energy of the rotor during the acceleration phase of a disturbance is invalid.

A.2. Background

The swing equation, which describes the motion of the synchronous machine rotor, can be derived from first principles according to Newton's second law of motion. The variables used in the derivation are described in Table A-1.

TABLE A-1. SYMBOL DEFINITIONS FOR DERIVATION OF THE SWING EQUATION

Symbol	Definition	Units of Measurement
J	Rotor inertia	$N \cdot m \cdot s^2$
T_m	Mechanical torque	$N \cdot m$
T_e	Electrical Torque	$N \cdot m$
δ	Rotor angular position relative to synchronously rotating reference	Radians (rad)
ω	Rotor angular velocity	rad/s
ω_0	Synchronous speed	rad/s
(s)	Standard International Units (SI)	-
(p)	Per unit (pu)	-

$$\frac{d\delta^{(s)}}{dt} = \omega^{(s)} - \omega_0 \tag{A.8}$$

$$J^{(s)} \frac{d\omega^{(s)}}{dt} = T_m^{(s)} - T_e^{(s)} \tag{A.9}$$

$$J^{(s)}\omega^{(s)} \frac{d\omega^{(s)}}{dt} = T_m^{(s)}\omega^{(s)} - T_e^{(s)}\omega^{(s)} = P_m^{(s)} - P_e^{(s)} \tag{A.10}$$

Define:
$$\omega^{(p)} = \frac{\omega^{(s)}}{\omega_0} \tag{A.11}$$

Then
$$\frac{d\delta^{(s)}}{dt} = \left(\omega^{(p)} - 1\right)\omega_0 \tag{A.12}$$

and
$$J\omega^{(p)}\omega_0^2\frac{d\omega^{(p)}}{dt} = P_m^{(s)} - P_e^{(s)} \quad \text{(A.13)}$$

$$\frac{J\omega^{(p)}\omega_0^2\frac{d\omega^{(p)}}{dt}}{MBASE} = \frac{P_m^{(s)} - P_e^{(s)}}{MBASE} \quad \text{(A.14)}$$

H is the machine inertia constant, which represents kinetic energy stored in the rotor at synchronous speed; in per unit of the machine MVA rating (MBASE MVA).

$$H^{(p)} = \frac{1}{2}\frac{J^{(s)}\omega_0^2}{MBASE}\left|\frac{Joules}{Joules/s}\right| \quad \text{(A.15)}$$

This leads to the swing equation in per-unit form:

$$2H^{(p)}\omega^{(p)}\frac{d\omega^{(p)}}{dt} = P_m^{(p)} - P_e^{(p)} \quad \text{(A.16)}$$

The equal area criterion is derived from (A.16).

The deviation in rotor speed from synchronous speed is usually small in realistic power systems. It is therefore common to assume that $\omega(p) \approx 1$ and therefore (A.16) becomes:

$$2H^{(p)}\frac{d\omega(p)}{dt} = P_m^{(p)} - P_e^{(p)} \quad \text{(A.17)}$$

From (A.12):
$$\frac{d\omega^{(p)}}{dt} = \frac{1}{\omega_0}\frac{d^2\delta}{dt^2} \quad \text{(A.18)}$$

Multiplying both sides by:

$$\frac{d\delta}{dt}\frac{d\omega^{(p)}}{dt} = \frac{1}{\omega_0}\frac{d\delta}{dt}\frac{d^2\delta}{dt^2} \quad \text{(A.19)}$$

From (A.17):
$$\frac{d\omega^{(p)}}{dt} = \frac{P_m^{(p)} - P_e^{(p)}}{2H^{(p)}} \quad \text{(A.20)}$$

From (A.19) and (A.20):

$$\frac{P_m^{(p)} - P_e^{(p)}}{2H^{(p)}}\frac{d\delta}{dt} = \frac{1}{\omega_0}\frac{d\delta}{dt}\frac{d^2\delta}{dt^2} \quad \text{(A.21)}$$

$$\left[P_m^{(p)} - P_e^{(p)}\right]\frac{d\delta}{dt} = \frac{2H^{(p)}}{\omega_0}\frac{d\delta}{dt}\frac{d^2\delta}{dt^2} \quad \text{(A.22)}$$

By the chain derivative rule:

$$\frac{d}{dt}\left[\frac{d\delta}{dt}\right]^2 = 2\frac{d\delta}{dt}\frac{d^2\delta}{dt^2} \quad \text{(A.23)}$$

From (A.22) and (A.23):

$$\left[P_m^{(p)} - P_e^{(p)}\right]\frac{d\delta}{dt} = \frac{H^{(p)}}{\omega_0}\frac{d\delta}{dt}\left[\frac{d\delta}{dt}\right]^2 \quad \text{(A.24)}$$

Multiplying both sides of equation (A.24) by dt and then integrating both sides with respect to $d\delta$:

$$\int_{\delta_0}^{\delta} P_m^{(p)} - P_e^{(p)} d\delta = \frac{H^{(p)}}{\omega_0} \int_{\delta_0}^{\delta} \left[\frac{d\delta}{dt} \right]^2 d\delta \tag{A.25}$$

which leads to:

$$\int_{\delta_0}^{\delta} P_m^{(p)} - P_e^{(p)} d\delta = \frac{H^{(p)}}{\omega_0} \left[\frac{d\delta}{dt} \right]^2 \Bigg|_{\delta_0}^{\delta} \tag{A.26}$$

If, following the removal of the disturbances, the rotor speed is able to return to synchronous speed then the SMIB system will remain stable. This happens when $\frac{d\delta}{dt} = 0$ which is assumed to occur when $\delta = \delta_m$ from (A.26). Thus

$$\int_{\delta_0}^{\delta_m} P_m^{(p)} - P_e^{(p)} d\delta = 0 \tag{A.27}$$

$$\int_{\delta_0}^{\delta_{clr}} P_m^{(p)} - P_e^{(p)} d\delta + \int_{\delta_{clr}}^{\delta_m} P_m^{(p)} - P_e^{(p)} d\delta = 0 \tag{A.28}$$

where δ_{clr} is the rotor angle at which the disturbance is cleared.

$$\int_{\delta_0}^{\delta_{clr}} P_m^{(p)} - P_e^{(p)} d\delta = \int_{\delta_{clr}}^{\delta_m} P_e^{(p)} - P_m^{(p)} d\delta \tag{A.29}$$

The acceleration area is: $A1 = \int_{\delta_0}^{\delta_{clr}} \left(P_m^{(p)} - P_e^{(p)} \right) d\delta$ (A.30)

and the deceleration area is: $A2 = \int_{\delta_{clr}}^{\delta_m} \left(P_e^{(p)} - P_m^{(p)} \right) d\delta$ (A.31)

Thus, stability requires that the unused deceleration area, A3, is at least zero such that it is possible for A1 = A2 as per the equal area criterion. The above argument is completely independent of any notion of kinetic energy. That is, the areas A1, A2 and A3 are not necessarily related to kinetic energy. The equal area criterion is derived quite independently of any notion of kinetic energy. There is no need to attribute a physical interpretation to the areas for the equal area criterion to be a useful tool for determining system stability.

A.3. Interpreting the Areas

The equal area criterion is a valid criterion for determining whether a lossless OMIB system, in which a classical model is used to represent the machine, is able to maintain stability following a disturbance. As mentioned earlier, a common interpretation of the acceleration and deceleration areas of the equal area criterion is that they represent respectively (i) the increase in kinetic energy of the rotor during the period from when the fault is applied to when it is cleared and (ii) the corresponding reduction in kinetic energy during the period from when the fault is cleared until the machine returns to

synchronous speed. Conservation of energy in a lossless system requires that the kinetic energy absorbed by the rotor during the acceleration phase be returned to the system during the deceleration phase. However, this is not to say that the areas A1 and A2 in the equal area criterion do represent kinetic energy.

A.4. Change in Kinetic Energy and Acceleration Areas in the Time Domain

In this section the equation for change in kinetic energy, ΔKE, absorbed by a OMIB system during application of 3-phase fault, is derived as a function of the rotor angular speed in per-units. By considering the acceleration and deceleration areas formed in the time domain ΔKE is also derived. These areas are ΔKE, distinct from the acceleration and deceleration areas formed by acceleration power-angle curve, as in Figure A-1. Then

$$KE^{(s)} = \frac{1}{2} J^{(s)} \omega^{(s)2} \tag{A.32}$$

$$\begin{aligned} \Delta KE^{(s)} &= \frac{1}{2} J^{(s)} \omega^{(s)2} \Big|_{\omega_0}^{\omega_{\max}^{(s)}} \\ &= \frac{1}{2} J^{(s)} \omega_{\max}^{(s)2} - \frac{1}{2} J^{(s)} \omega_0^2 \\ &= \frac{1}{2} J^{(s)} \left(\omega_{\max}^{(s)2} - \omega_0^2 \right) \end{aligned} \tag{A.33}$$

From (A.15)

$$J^{(s)} = \frac{2 \times MBASE \times H^{(p)}}{\omega_0^2} \tag{A.34}$$

Substituting (A.34) into (A.33) the change in kinetic energy is:

$$\begin{aligned} \Delta KE^{(s)} &= \frac{1}{2} \times \frac{2 \times MBASE \times H^{(p)}}{\omega_0^2} \left(\omega_{\max}^{(s)2} - \omega_0^2 \right) \\ &= MBASE \times H^{(p)} \left(\omega_{\max}^{(p)2} - 1 \right) \end{aligned} \tag{A.35}$$

$$\Delta KE^{(p)} = H^{(p)} \left(\omega_{\max}^{(p)2} - 1 \right) \tag{A.36}$$

$$T1 = \int_{t_0}^{t_{clr}} P_m - P_e dt \tag{A.37}$$

During a 3 phase fault $P_e = 0$:

$$\begin{aligned} \therefore T1 &= \int_{t_0}^{t_{clr}} P_m dt \\ &= P_m \left(t_{clr} - t_0 \right) \end{aligned} \tag{A.38}$$

From (A.16)

$$\begin{aligned} P_m^{(p)} &= 2H^{(p)}\omega^{(p)}\frac{d\omega^{(p)}}{dt} \\ \therefore T1 &= \int_0^{t_{clr}} 2H^{(p)}\omega^{(p)}\frac{d\omega^{(p)}}{dt}dt \\ &= \int_{\omega_{t=0}}^{\omega_{clr}} 2H^{(p)}\omega^{(p)}d\omega^{(p)} \\ &= \int_{\omega\approx 1}^{\omega_{\max}} 2H^{(p)}\omega^{(p)}d\omega^{(p)} \\ &= H^{(p)}\omega^{(p)2}\Big|_1^{\omega_{\max}} \\ &= H^{(p)}\left(\omega_{\max}^{(p)2}-1\right) \end{aligned} \quad (A.39)$$

which is the increase in rotor kinetic energy, as determined in (A.36). Similarly, between fault clearance and the end of the forward-swing, when $t = t_{eq}$:

$$\begin{aligned} T2 &= \int_{t_{clr}}^{t_{eq}} P_a dt \\ &= -\int_{t_{clr}}^{t_{eq}} 2H^{(p)}\omega^{(p)}\frac{d\omega^{(p)}}{dt}dt \\ &= -\int_{\omega_{\max}^{(p)}}^{1} 2H^{(p)}\omega^{(p)}d\omega^{(p)} \\ &= H^{(p)}\left(\omega_{\max}^{(p)2}-1\right) \end{aligned} \quad (A.40)$$

where $P_a = P_e - P_m = \frac{E_b V_t}{X}\sin\delta - P_m$ (A.41).

A.5. Analysis: Change in Kinetic Energy and the Acceleration Power Area

In this section the OMIB system shown in Figure A-2 is used to numerically verify the equivalent of areas A1 and A2, and T2 and T3, where the generator is represented by a classical machine model. The classical machine is based on the following assumptions [13]:

- Mechanical power input is constant
- Machine losses, saturation and saliency are neglected
- Field flux linkages are assumed to remain constant in the short period following a disturbance. As a result the machine can be represented as a constant voltage behind the transient reactance.

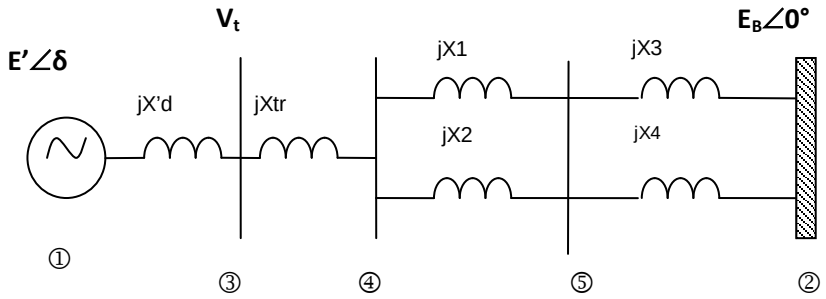

Figure A-2. OMIB system: A simple power system

The OMIB system represents a single generator delivering power to a large system. The large system is represented by an infinite bus - an ideal voltage source that maintains constant magnitude, phase and frequency. The parameter values for the system are listed in Table A-2. The following stable TDS scenario was simulated in MATLAB®.

TABLE A-2. OMIB SYSTEM PARAMETERS

Symbol	Description	Value
X'_d	Transient reactance behind the generator terminal	0.3 pu
H	Machine Inertia constant	3.0 pu-s
V_t	Generator terminal voltage, manual excitation	1.0 pu
X_{tr}	Transformer impedance	0.1 pu
X_1, X_2, X_3, X_4	Transmission Line Impedance	0.1 pu
E_B	Slack Bus Voltage	1.0 ∠0° pu
f_0	System Frequency	50 Hz

In this example, after a 1s run-in period a 3 phase fault is applied near to node 4, on circuit #1, between buses 4 & 5. It is cleared 125ms later by simultaneously opening the circuit breakers at both ends of the fault circuit.

Figure A-3 shows a) rotor angle, b) velocity and c) acceleration power, as a function of time, for a 3 phase fault that is applied at the generator stator terminal. The fault is applied at $t = t_0 = 1s$, and cleared at $t = t_{clr}$ when the corresponding rotor angle is $\delta = \delta_{clr} = 51.3°$. After fault clearance the OMIB system decelerates and returns to synchronous speed $\omega = 1pu$ at $t = t_{eq}$. At this time the maximum rotor angle δ_{eq} is reached. T1 and T2, the acceleration and deceleration areas in the time-domain - calculated using the trapezoidal method - are shown in Figure A-3c). As per equation (A.39) T1 is the kinetic energy absorbed by the generator rotor during the fault; T2 is the kinetic energy the rotor returns to the system when the machine returns to synchronous speed at the end of the forward-swing. As expected from the EAC, T1=T2.

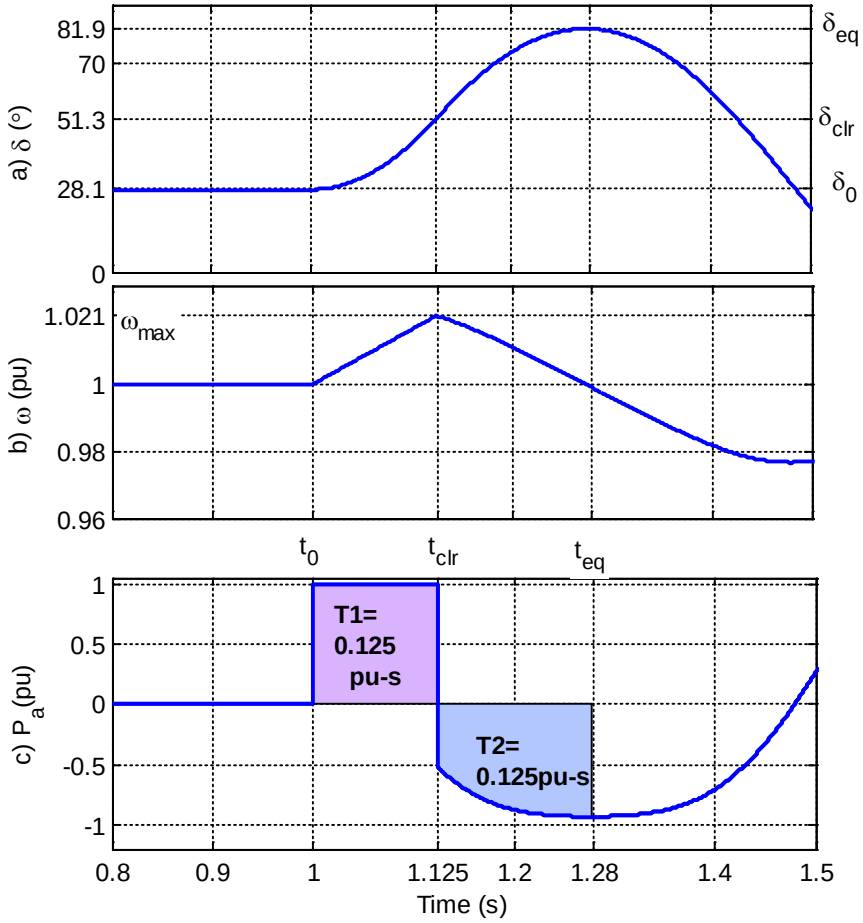

Figure A-3. a) Rotor angle, b) velocity and c) acceleration power time responses of the OMIB system for a 3 phase fault applied near to node 4 on circuit #1 at t=1s, and is cleared after 125ms.

Figure A-4 shows the corresponding OMIB acceleration-power angle curve. The acceleration and deceleration areas A1 and A2 shown in the figure were calculated from the TDS, using the trapezoidal method. As expected from the EAC A1=A2. Comparison of Figure A-3 and Figure A-4 shows that $T1 \neq A1$ and $T2 \neq A2$, emphasizing that acceleration and deceleration power-angle areas defined by the EAC are not kinetic energy.

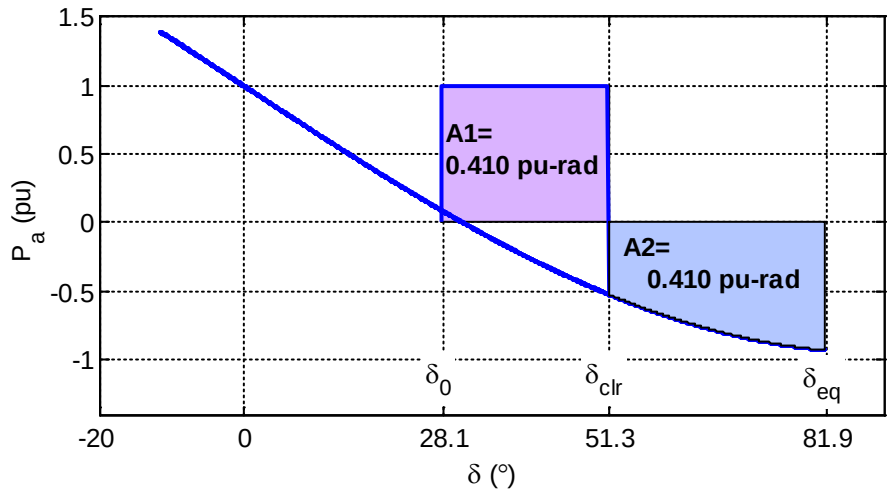

Figure A-4. OMIB acceleration power-angle response, where a 3 phase fault applied near to node 4 on circuit #1 at t=1s, and is cleared after 125ms.

A.6. Conclusion

The EAC provides foundational insight into the key concepts and principles of transient stability. Based on the EAC is commonly claimed that the acceleration and deceleration areas of the power-angle curve represent the changes in kinetic energy that are exchanged between the rotor and the system in the event of a disturbance. Appendix A illustrates that this commonly held interpretation is invalid.

This is demonstrated analytically by deriving the generator dynamic swing equations, and then the EAC from Newton's first principles. The closed form equations show that the acceleration and deceleration areas, A1 and A2, formed by the acceleration-power angle curve are proportional to, but not the same as equivalent areas formed in the acceleration power-time domain T1 and T2. This is also demonstrated numerically from the TDS of a stable scenario on an undamped OMIB power system.

Appendix B The Single Machine Equivalent (SIME) Equations

When the two sorted critical machines groups are known, the centre of inertia (COI) responses of each group is calculated. The respective COI angle responses for the two groups are:

$$\delta_{1COI}(t) = \frac{1}{M_1}\sum_{i\in G1} M_i\delta_i(t) \qquad \text{and} \qquad \delta_{2COI}(t) = \frac{1}{M_2}\sum_{j\in G2} M_j\delta_j(t) \tag{B.1}$$

Similarly the COI speed responses of the two groups are

$$\omega_1(t) = \frac{1}{M_1}\sum_{i\in G1} M_i\omega_i(t) \quad \text{and} \quad \omega_2(t) = \frac{1}{M_2}\sum_{j\in G2} M_j\omega_j(t) \tag{B.2}$$

where
$$M_1 = \sum_{i\in G1} M_i \quad \text{and} \quad M_2 = \sum_{j\in G2} M_j \tag{B.3}$$

By rearranging (B.1) and taking the second derivative, the swing equation is deduced

$$M_1\ddot{\delta}_{1COI}(t) = \sum_{i\in G1} M_i\ddot{\delta}_i(t) = \sum_{i\in G1}\left(P_{mi}(t) - P_{ei}(t)\right) \tag{B.4}.$$

Similarly for machine group 2

$$M_2\ddot{\delta}_{2COI}(t) = \sum_{j\in G2} M_j\ddot{\delta}_j(t) = \sum_{j\in G2}\left(P_{mj}(t) - P_{ej}(t)\right) \tag{B.5}$$

where
$$P_{e_1COI}(t) = \sum_{i\in G1} P_{ei}(t) \qquad \text{and} \qquad P_{e_2COI}(t) = \sum_{j\in G2} P_{ej}(t) \tag{B.6}$$

and similarly
$$P_{m_1COI}(t) = \sum_{i\in G1} P_{mi}(t) \quad \text{and} \quad P_{m_2COI}(t) = \sum_{j\in G2} P_{mj}(t) \tag{B.7}.$$

Equations (B.1) to (B.7) show that for the transformation from the full system responses to the COI responses does not require any changes to the system model. The COI responses for a multi-machine system are obtained by various linear combinations of the system responses. The transformation of the two COI responses to the SIME (or OMIB) representation is described by the following equations

$$\delta_{OMIB}(t) = \delta_{1COI}(t) - \delta_{2COI}(t) \tag{B.8}$$

$$\omega_{OMIB}(t) = \omega_{1COI}(t) - \omega_{2COI}(t) \tag{B.9}$$

$$P_{mOMIB}(t) = M_{OMIB}\left(\frac{1}{M_1}\sum_{i\in G1} P_{mi}(t) - \frac{1}{M_2}\sum_{j\in G2} P_{mj}(t)\right) \tag{B.10}$$

$$P_{eOMIB}(t) = M_{OMIB}\left(\frac{1}{M_1}\sum_{i\in G1} P_{ei}(t) - \frac{1}{M_2}\sum_{j\in G2} P_{ej}(t)\right) \tag{B.11}$$

$$M_{OMIB} = \frac{M_1 M_2}{M_1 + M_2} \tag{B.12}$$

$$M_k = 2H_k \tag{B.13}$$

where H_k is the inertia constant of machine *k*.

Appendix C The IEEE 2-Area 4 Machine Test System with SVC

The single line diagram for the IEEE 2 area 4-machine test system is shown in Figure C-1. In this system the total length of the parallel 230kV transmission lines between the two areas is 440km. A SVC is connected at the middle of the system at node 8. The SVC capacity is adjusted depending on the study being made as described in the main text. The SVC model is shown in Figure C-5. In a number of studies, including the base-line study, the SVC is omitted. The generators in this system are represented with a sixth order machine model, and the governors and automatic voltage regulators fitted to the four machines are represented. The generator, SVC model and network parameters of the system are provided in Table C-1, and are consistent with those as specified in [13, 91].

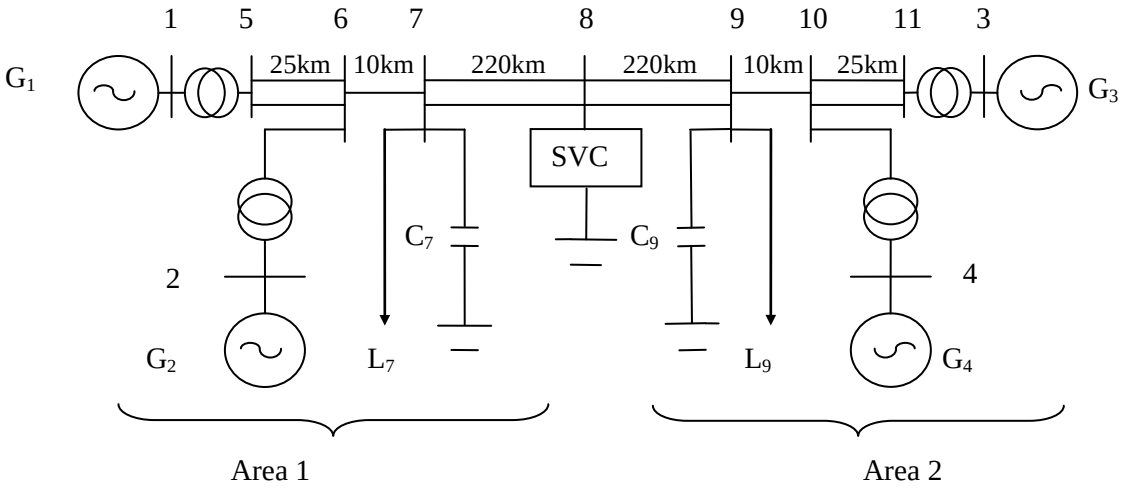

Figure C-1. The IEEE two-area four-machine power system [13, 91] with SVC included at bus 8 of the area interconnection.

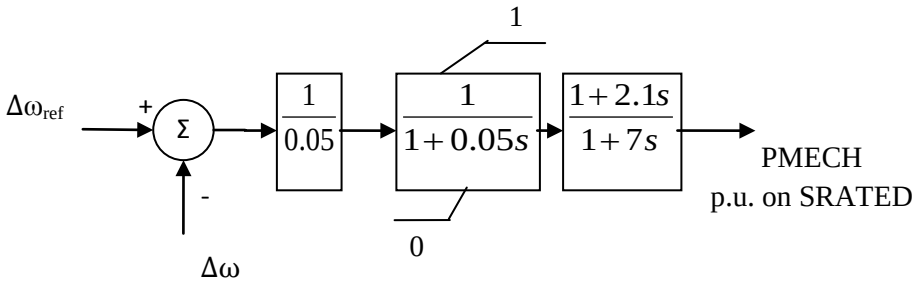

Figure C-2. Governor

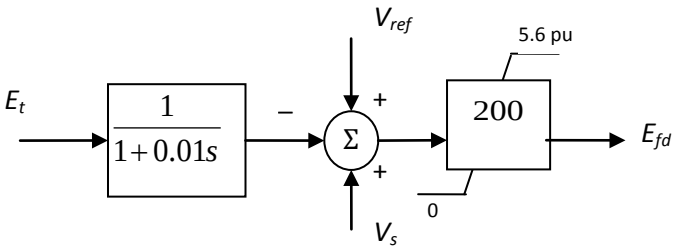

Figure C-3. Automatic voltage regulator (AVR)

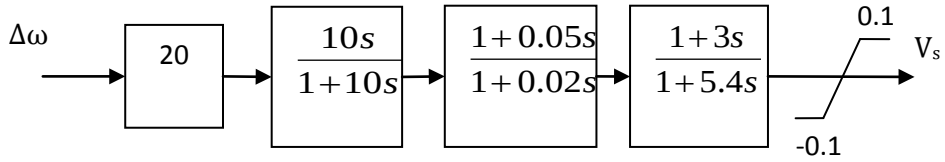

Figure C-4. Power system stabilizer

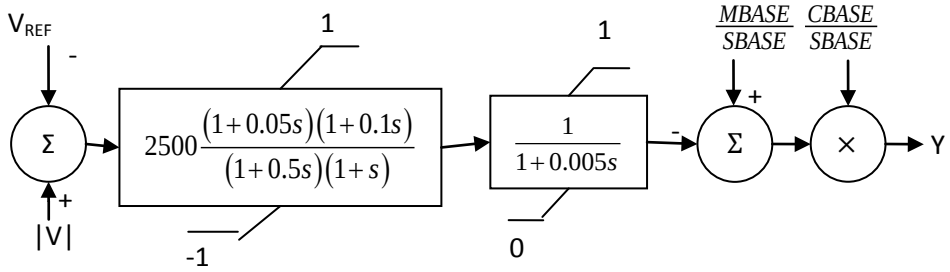

Figure C-5. Static var compensator (SVC)

TABLE C-1. FOUR MACHINE SYSTEM PARAMETERS [13]

Generator Parameters (in p.u. on S_{RATED})			
X_d = 1.8	X_q=1.7	X_l=0.2	X'_d=0.3
X'_q=0.55	X''_d=0.25	X''_q=0.25	R_a=0.0025
T'_{d0}=8.0s	T'_{q0} = 0.4 s	T''_{d0}=0.03 s	T''_{q0}=0.05 s
H = 6.5 (for generators in Area 1) H = 6.175 (for generators in Area 2)			K_D = 0 ψ_{TI} = *0.9*
S_{rated} = 900mva		V_{RATED} = 20kV	f_{SYSTEM}= 50Hz
Step-Up Transformer Parameters			
X = j0.15 pu	S_{RATED} = 900MVA	V_{RATED} = 20/230 kV	Off-Nominal Ratio = 1.0
Transmission Lines			
V_{RATED} =230kV	*r* = 0.0001 pu/km	x_L= 0.001 pu/km	b_C = 0.00175 pu/km
S_{BASE}=100MVA		V_{BASE}=230kV	
Base-Line Generator Operating Condition			
G1	P=700MW	Q=185 MVAr	Et=1.03∠20.2°
G2	P=700MW	Q=235 MVAr	Et=1.01∠10.5°
G3	P=719MW	Q=176 MVAr	Et=1.03∠-6.8°
G4	P=700MW	Q=202 MVAr	Et=1.01∠-17°
Base-line System Load			
For all Power Transfers	Q_{L7}=100MVAr	Q_{C7}=200 MVAr	Q_{L9}=100 MVAr	Q_{C9}=350 MVAr
PT = 0 MW	P_{L7}=1367 MW	P_{L9}=1367 MW	
PT = 200MW	P_{L7}=1167 MW	P_{L9}=1567 MW	
PT = 400MW	P_{L7}=967 MW	P_{L9}=1767 MW	
SVC Parameters (SBASE = 100MVA)			
MBASE – the SVC reactor MVar base(i.e. 400MVar)			
CBASE – the total capacity of the SVC reactor (i.e. 200MVar)			
Y is the susceptance output of the SVC on SBASE			

Notes:

The ratings of the four generators are identical

In the base-line configuration of the system the SVC is omitted

In this system the system frequency of 50Hz is used, instead of 60Hz as per the original system [13]

Appendix D Derivation of the Simplified Two Machine Equivalent System

The two machine system in Figure D-1 is derived from the IEEE two-area four-machine power system in Figure C-1. The two machine system is derived by merging respectively generators 1 and 2, and generators 3 and 4 from the original system. Merging the generators requires the calculation of an equivalent generator inertia constant given by:

$$H_{equivalent} = \frac{1}{SBASE} \sum_{i \in N} H_i \cdot MBASE_i \tag{D.1}$$

where i is the generator number and N is the set of generators in a given area. The equivalent transient reactance, $X_d^{'}$, of a merged set of generators is the parallel transient reactance of each generator in the set. Similarly, the equivalent transformer reactance, X_{tr}, is calculated by parallel combination of the transformer reactances connected to the merged generators. The 25km transmission lines between nodes 5 to 6 from the original 4 machine system, are replaced by a 10km line between nodes 5 and 6. Similarly the 25km lines between nodes 10 and 11 are replaced by a 10km line between nodes 8 and 9. All other parameters are unchanged in the two machine system model.

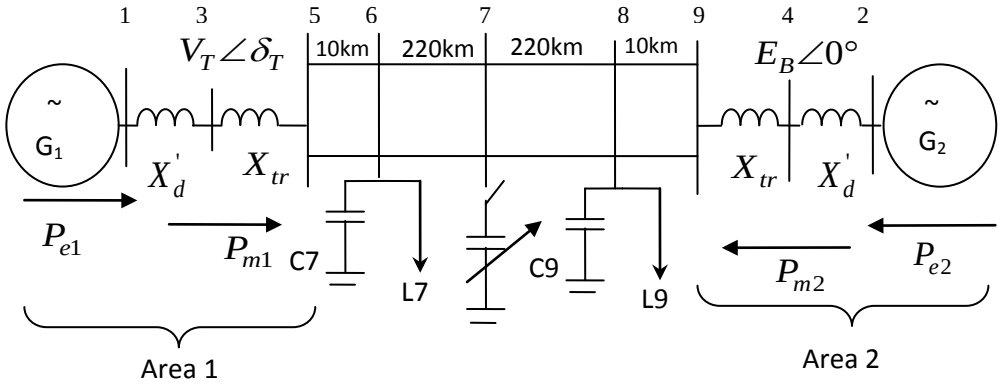

Figure D-1. The 9-bus two-machine power system model

Table D-1 and Table D-2 describe the parameters which are translated from the four machine system to the two machine system.

TABLE D-1. TRANSLATED GENERATOR AND TRANSFORMER PARAMETERS VALUES ON THE IEEE FOUR-MACHINE SYSTEM

Parameter	Units	Value	Description
X'_d	Per Unit	0.3 p.u. on 900MVA base	Transient reactance
X_{tr}	Per Unit	0.15 p.u. on 900MVA base	Transformer Reactance
H_1, H_2	Per Unit	6.5 on 900MVA base	Generator 1 & 2 Inertia
H_3, H_4	Per Unit	6.175 pu on 900MVA base	Generator 3 & 4 Inertia

TABLE D-2. EQUIVALENT GENERATOR AND TRANSFORMER PARAMETERS VALUES ON THE SIMPLIFIED TWO MACHINE SYSTEM MODEL

Parameter	Units	Value	Description
X'_d	Per Unit	0.15 p.u. on 1800MVA base	Transient reactance
X_{tr}	Per Unit	0.075 p.u. on 1800MVA base	Transformer Reactance
H_{1eq}	Per Unit	117 p.u. on 1800 MVA base	Area 1 Equivalent Generator Inertia
H_{2eq}	Per Unit	111.15 pu on 1800 MVA base	Area 2 Equivalent Generator Inertia

Appendix E AUSIME Configuration File Keywords

The software developed in this research (AUSIME) is a flexible and reliable automation tool that is able to accurately locate transient stability limits (TSL) with the Enhanced-Binary SIME (EBSIME) algorithm. The AUSIME software integrates the EBSIME algorithm with the PSS®E TDS software thereby ensuring reliable search results. The AUSIME software is designed with the modular software architecture shown in Figure 8-1 that is composed of two loops - an outer supervisory loop and an inner search loop.

The outer supervisory loop provides the interface between the user and the AUSIME software, and fully automates the TSL search using the EBSIME algorithm. It supervises consecutive search iterations executed by the inner loop. It tracks changes in key parameters as the search progresses, and provides an interface between the inner loop dynamic simulations. The inner loop is implemented as a PSS®E user-defined model. The decision-making calculations for the EBSIME algorithm are implemented within the inner-loop.

The AUSIME software is designed to receive as input a flexible text-based configuration file with instructions to automate a complete TSL search (refer to section 8.4.1.1). The keywords required for this file are described in Table E-1. Some fields are optional and have a default value assigned. Other fields are compulsory and must have a value specified by the user. The main instruction file specifies the location of a fault definition text file- discussed in section 8.4.1.2, which describes the details of the investigated contingency for a TSL search. The meaning of the keywords required by the fault definition text file are described in Table E-2.

Communication between the inner-loop and outer supervisory loop is facilitated by *inner-loop* and *outer-loop* configuration text files. The *inner–loop* configuration file is the input to the inner search loop and is generated by the outer supervisory loop. The *outer-loop* configuration file is the input to the outer supervisory loop and is generated from the inner search loop. Both configuration files contain similar information and are described in Table E-3 to Table E-5. Table E-6 lists the values and meanings of the constant parameters that may be reference in the inner- and outer-loop configuration files.

In all text files the instructions are listed as comma-separated keyword and parameter records, with one record per line. Examples of each type of text-file are provided in Appendix F, in the context of an example EBSIME search.

TABLE E-1. KEYWORDS FOR THE SEARCH INSTRUCTION INPUT FILE

Keyword	Type	Default value	Description
SearchMode	STRING	Field must be specified	The search method 'BINARY' – for binary search 'EBSIME' – for EBSIME search 'LINEAR' – for linear search
TSVTYPE	STRING	Field must be specified	Transient Stability search variable 'CCT' for critical clearing time search 'PTL' for power transfer limit search
TSVUNITS	STRING	Field must be specified	Units used to specify the initial upper and lower search bounds; 's' or 'ms' for a CCT search; 'W' or 'MW' for a PTL search
CASEID	STRING	Field must be specified	A string identifier describing the search (alphanumeric and underscore characters allowed only)
SAVEFOLDER	STRING	Field must be specified	The location of the output folder, relative to the execution directory
GenerateReport	INTEGER	1	If '1' - generate text files to report the search traversal, and search simulation times. If '0' – no reports are generated (Also refer to DEBUGLVL in Table E-4
RecordOMIB	INTEGER	1	If '1' – generate OMIB response to binary files for all scenarios If '0' – no OMIB responses generated
RecordMG	INTEGER	1	If '1' –record machine group information in text file format & binary file. If '0' –machine group information written to binary file only.
TSV_TOL	REAL	Field must be specified	The search tolerance
SEARCHBOUND_UP	REAL	Field must be specified	The initial upper search bound. Magnitude specified according to TSVUNITS in this table.
SEARCHBOUND_LO	REAL	0.0	The initial lower search bound. Magnitude specified according to TSVUNITS in this table. It is assumed that at the system operation at the lower bound is transiently stable.
TRUN	REAL	10.0	The maximum length of the TDS simulation period; in seconds

Keyword	Type	Default value	Description
T_INTERVAL	REAL	0.0001s	The time-step size, in seconds for the TDS recorded to binary file. Must be a multiple of PSSE_SIM_TIMESTEP in Table E-2.
DEBUGLEVEL	INTEGER	0	The level of reporting for debugging and research purposes. See 'DEBUGLVL' described in Table E-6.
BYPASS_NEXT_MG	INTEGER	1	If '1' the MG specified by MGFILE_NM, or otherwise the MG defined from scenario 1, is used for the entire EBSIME search. If '0' a new MG is determined at every unstable search scenario (for research only).
MG_FILENM	STRING	No. Default: Blank String	For research only. The machine group used for a search may be pre-specified. The location of a binary file containing machine group information.
BYPASS_STOP _CRITERIA	INTEGER	0	'1' - All TDS will run for TRUN seconds, and COI and ESC criteria will be ignored. '0' – All applicable stop criteria will be applied. Cannot be used for the EBSIME search. (For research only.)
MAX_ITER_ SEARCH	INTEGER	30	The maximum TDS that can be processed in the search before search is aborted
LoadFlowFile	STRING	Field must be specified	The location and name of the base-case load flow file (or files)
FaultDefFile	STRING	Field must be specified	The location and name of a text file describing contingency-related parameters
DispatchFile	STRING	If omitted, this field is ignored.	Only used by PTL search. The location and name of dispatch text file.
ChannelOUT	STRING	If omitted, this field is ignored.	The location and name of a PSS/E™ response file containing instructions for the activity CHAN, to record simulation variables that are monitored during TDS runs.

Keyword	Type	Default value	Description
FORTRAN_CODE _FOLDER	STRING	Field must be specified	The location of the inner loop object files.
ApplyESC	STRING	IFS	Specifies when the SIME ESC is applied. 'NONE' –ESC is not applied. 'FS_ONLY' –ESC is only applied during the forward-swing limit prediction phase 'IFS' – ESC is applied during the search initialization and FSL phase.
RecordCOI	INTEGER	1	If '0' COI responses are not recorded; if '1' COI search responses are written to a set of binary output files.
RedirectSearch:	STRING	No Default: FIRST	If search diverges happens the next search step will be determined by bisection: 'FIRST-SWING' – using the forward-swing search bounds (which are based on ESC assessment) 'MULTI-SWING'- using multi-swing search bounds (which are based on COI assessment)
NDIV_LIMIT	INTEGER	3	Search divergence threshold. When the EBSIME search diverges this many times it will revert to a binary search at the next search iteration.

TABLE E-2. KEYWORDS AND DEFINITIONS IN THE FAULT DEFINITION TEXT FILE

Keyword	Type	Description
TFAULT	REAL	RUN_IN_PERIOD. Each TDS will operate in the steady-state until t=TFAULT (in seconds) when the fault is applied.
TCLR	REAL	The time when the fault will be cleared. Must be greater than TFAULT. Must be specified for a PTL search.
NLOG_NORMAL	INTEGER	In the run-in period, the frequency with which PSS®E channel data is recorded to the PSS®E progress report file. i.e. If NLOG_DETAIL=100, data is recorded every 100 time-steps.
NCHAN_NORMAL	INTEGER	In the run-in period, the frequency with which PSS®E channel data is recorded to the binary response file. i.e. If NLOG_DETAIL=100, data is recorded every time-step.
NLOG_DETAIL	INTEGER	NLOG_DETAIL determines the frequency with which PSS®E channel data is recorded to the PSS®E progress report file during the fault. i.e. If NLOG_DETAIL=1, data is recorded every time-step. The intent is that from t=TFAULT to t= TFAULT + 2s the TDS is calculated with finer resolution.
NCHAN_DETAIL	INTEGER	Determines the frequency with which PSS®E channel data is recorded to the binary response file during the fault. i.e. If NLOG_DETAIL=1, data is recorded every time-steps. This corresponds to the time-range from t=TFAULT to t= TFAULT + 2s.
FROMBUS	INTEGER	Bus number at the sending-end of the faulted feeder, with respect to the direction of power transfer. The bus at which fault is applied is listed in IBUS below
TOBUS	INTEGER	Bus number at the remote end of the faulted feeder, with respect to the direction of power transfer
IBUS	INTEGER	Bus near to the applied fault - must be the same as either FROMBUS or TOBUS
CKTID	INTEGER	Circuit number of the faulted feeder
MAX_ITER_LF	INTEGER	Maximum number of iterations for solving the load-flow solution (via Newton Raphson method)
ACCEL_FACTOR	REAL	Acceleration factor for solving the load-flow solution
PSSE_SIM_TIMESTEP	REAL	Size of the TDS time-step.

Keyword	Type	Description
TIME_CONSTANT_BUS_FREQ	REAL	Time constant for load-flow bus-frequency calculations
LOADFLOW_tol	REAL	Load flow solution tolerance (in MW)
System_Frequency	REAL	The system frequency (in Hz)
BASEKV	REAL	Base voltage used to calculate the per unit fault admittance
YREAL	REAL	Real component of fault admittance in MVA
YREACTIVE	REAL	Reactive component of fault admittance in MVA
PSSE_REPORT_OUTPUT	STRING	Name and location of the PSS/E output report file. SimplifiedAustralianSystem_DOCU.TXT
DynamicsData	STRING	Name and location of the PSS/E system dynamics data

TABLE E-3. COMMON KEYWORDS USED BY THE INNER AND OUTER LOOP CONFIGURATION FILES

KEYWORD	Value	Description of Value
ISEARCH	Integer	For the inner-loop configuration search file: ISEARCH is the index, k, of the current search scenario. Immediately after the inner loop configuration file is read, the time domain simulation (TDS) for scenario k will be simulated. For the outer-loop configuration search file: ISEARCH is the index, k+1, for next search scenario.
SEARCHMODE	Integer	Instruction code to describe the search type and phase for the specified scenario. (Refer to Table E-5 for values.
TSVNAME	String	The search variable (SV) name. 'PT' for a PTL search 'CT' for a CCT search
TSV	Real number	The value of the search variable for the specified scenario.
TSVUNITS	String	The units for the TSV. 'MW' if SVNAME == 'PT' 'ms' if SVNAME == 'CT'.
TFAULT	Real	Fault application time (run-in period) for the specified scenario. Must be > 0.
TCLR	Real	Time at which fault is cleared for the specified scenario. Must be > TFAULT.
TRUN	Real	Maximum integration time for the TDS of the specified scenario, although the TDS may terminate sooner if the ESC assessment criteria may be applied (see field APPLY_ESC and BYPASS_STOP_CRITERIA).
BINARY_LO_FIRST	Real	Lower Search Bound prior to TDS of the specified scenario. This search bound is used during the initialization and forward-swing limit (FSL) search phase only. It is implied that the scenario described by this field has been assessed and classified as forward-swing (FS) stable by the Early Stop Criteria (ESC).
BINARY_UP_FIRST	Real	Upper Search Bound prior to TDS of the specified scenario. This bound is used during the initialization and FSL search phase only. It is implied that the scenario described by this field has been assessed and classified as FS unstable by the ESC.

KEYWORD	Value	Description of Value
BINARY_LO_MULTI	Real	Lower Search Bound prior to TDS of the specified scenario. This bound is used during the binary search phase. It is implied that the scenario described by this field has been assessed and classified as stable by the Centre of Inertia (COI) stability assessment criteria.
BINARY_UP_MULTI	Real	Upper Search Bound prior to TDS of the specified scenario. This search bound is used during the binary search phase. The scenario described by this field has been assessed and classified as unstable by the COI stability assessment criteria.
TSIM_CUML	Real	Cumulated search time in simulation seconds (sim-s) prior to executing the TDS for the specified scenario.
TWALL_CUML	Real	Cumulated search time with respect to GPS wall clock time prior to executing the TDS for the specified scenario.
TSV_TOL	Real	Search tolerance. TSV_TOL>0.
APPLY_ESC	Integer	Instruction code that describes whether ESC will be applied to the specified scenario. See Table E-6 for valid values of this keyword. This field is for research only.
BYPASS_STOP _CRITERIA	0 or 1	If '0' the TDS of the specified scenario will halt, at the time indicated to stop, by the ESC or COI criteria – whichever criteria is satisfied first. If '1' the TDS of the specified scenario will ignore the ESC and COI assessment criteria and run until t=TRUN.
ISMGDEFINED	0 or 1	If '0', the MG will be determined after simulation of the specified scenario. If '1', the MG for scenario k is read from the binary file described by 'MG_FILENM' (i.e it implies the MG has already been defined by scenario 1). For the EBSIME algorithm, ISMGDEFINED is '0' for scenario 1, and '1' for other search scenarios.
MG_FILENM	String	Location of the binary file that describes the MG. Typically, for the EBSIME algorithm, this file is generated after the TDS and SIME assessment of scenario 1.
LOOP	0 or 1	'0' for output configuration file '1' for input configuration file
CONFIGFILE_OUT	String	Only required by the input configuration file. Name of the output configuration file that will be generated after TDS of the specified scenario.
REDIRECTSEARCH	Integer	Instruction code to indicate how the search will if search diverges (Refer to corresponding field and values in Table E-4)

KEYWORD	Value	Description of Value
NDIV_COUNT	Integer	The number of times that the FSL has diverged, prior to assessment of the specified scenario. Must be ≥0.
NDIV_LIMIT	Integer	Number of times the FSL search may diverge before reverting to binary search. Must be >0.

TABLE E-4. CONFIGURATION FILE KEYWORDS FOR REPORT FILES

KEYWORD	Value	Description of Value
CASEID	String	An identifier for the search case, used in generated report file names.
LOG_FILENM	String	Name of log file to print debug statements
ERROR_FILENM	String	Filename, in the local directory, where error messages are reported
ISRECORDMG	0 or 1	If '0', new MG definitions are not written to a text file If '1', new MG definitions are written to a text file specified by MG_FILENM_TXT
ISRECORDTSIM	0 or 1	If '0', search time report is not generated If '1', search times are written to the file specified by TSI_FILENM_TXT
ISRECORDSIMEINFO	0 or 1	If '0', search information is not generated If '1', search information is generated to the file specified by SIMEINFO_FILENM_TXT
ISRECORDOMIB	0 or 1	If '0', OMIB responses are not recorded If '1', OMIB responses are recorded to file specified by OMIB_FILENM_SAV
ISRECORDCOI	0 or 1	If '0', COI responses are not recorded If '1', COI responses are recorded to file specified by COI_FILENM_SAV
MG_FILENM_TXT	String	Name of the text version of the MG definition file. Required if ISRECORDMG=1
TSIM_FILENM_TXT	String	Filename of the TSIM report text file. Required if ISRECORDTSIM=1
SIMEINFO_FILENM_TXT	String	Filename of the search report Required if ISRECORDSIMEINFO=1
GENVAR_FILENM_SAV	String	Name of the binary file for the current scenario where the full set of time response variables are saved
OMIB_FILENM_SAV	String	Name of the binary file where OMIB responses for the scenario are saved. Required if ISRECORDOMIB=1
COI_FILENM_SAV	String	Name of the binary file where COI responses for the scenario are saved. Required if ISRECORDCOI=1
SAVEFOLDER	String	Folder where all files associated with inner loop are saved.
DEBUGLVL	Integer	Indicates the level of detail required for debugging. See Table E-6.

TABLE E-5. SIME-RELATED KEYWORDS FOR THE INNER AND OUTER LOOP CONFIGURATION FILES

KEYWORD	Value	Description of Value
MARGINGRADE_SAV*	Integer	Instruction code describing the estimated measure for scenario (k-1). If a SIME margin is defined: '1' MARGIN_SAV is a unstable margin '2' MARGIN_SAV is a stable margin Or if the SIME margin is undefined: '-1' scenario (k-1) is too unstable '-2' scenario (k-1) is too stable
MARGIN_SAV*	Real	The SIME margin of scenario (k-1), if it is defined.
ISESCAPPLIED_SAV*	0 or 1	'0' if ESC is not applied for scenario (k-1) '1' if ESC is applied for scenario (k-1)
ISUNSTABLE_SAV*	Integer	'0' if the scenario (k-1) is stable '1' if the scenario (k-1) is unstable
ISEARCH_PREV**	Integer	ISEARCH for the scenario prior to (k-1) with a defined SIME margin
TSV_PREV**	Real	TSV for the scenario prior to (k-1) with a defined SIME margin, that was used in the limit prediction calculation
GENVAR_PREV_FILENM**	String	Name for the binary file where generator time responses are saved; for the scenario prior to (k-1) with a defined SIME margin
TCLR_PREV**	Real	Fault clearing time; for the scenario prior to (k-1) with a defined SIME margin
TFAULT_PREV**	Real	Time at which fault is cleared; for the scenario prior to (k-1) with a defined SIME margin
MARGINGRADE_PREV**	Integer	Instruction code to describe the margin of the *previous* scenario with a defined SIME margin: '1' for a unstable margin '2' for a stable margin
MARGIN_PREV**	Real	The SIME margin of the previous scenario with a defined SIME margin
*These fields will only be generated for ISEARCH>1		
**These fields will only be generated for ISEARCH>2		

TABLE E-6. INSTRUCTION CODE VALUES

KEY WORD	Name of Constant	Integer Value	Interpretation
SEARCH MODE	INITIAL	11	EBSIME search initialization phase
	FIRSTSWING	22	FSL prediction phase
	CONFIRM_ MULTISWING_STABLE	33	End of FSL prediction phase
	MULTISWING	44	Locating search bounds for the binary-search phase
	ENDOFSEARCH	88	Search is complete
	BINARYSEARCH	55	Binary search
	LINEARSEARCH	99	Linear search
REDIRECT SEARCH	RedirectSearch_FIRST	66	If search diverges from FSL, redirect by bisection of SIME_LO and SIME_UP - the forward-swing bounds (used by the EBSIME search)
	RedirectSearch_MULTI	55	If search diverges from FSL, redirect by bisection of BINARY_LO and BINARY_UP - the multi-swing stability bounds. This option is used for research only.
APPLY_ESC	ESC_NoApply	0	Do not apply the ESC during the search . This option is used for research only.
	ESC_FirstSwingOnly	1	Apply the ESC to the limit prediction phase only (for research only)
	ESC_InitialAndFirstSwing	2	Apply the ESC to the initial and limit prediction phases only (used by the EBSIME search)
DEBUGLVL	DEBUG_ALL_TRACES	>4	Generate search reports, Report to the PSS/E console; Report trace statements to log file Report inner loop errors
	DEBUG_LOG	3	Generate search reports, Report trace statements to log file Report inner loop errors
	DEBUG_REPORTS_ONLY	2	Generate search reports, Report inner loop errors
	DEBUG_ERRORS_ONLY	1	Report inner loop errors only
	DEBUG_NONE	0	Do not report anything

Appendix F Application of the AUSIME Tool and Associated Files

This section provides examples of the input and output files, discussed in Chapter 8, that are generated by the AUSIME transient stability limit (TSL) search tool when an Enhanced Binary SIME (EBSIME) search for the CCT is automated. The case investigated is based on case 1 in Chapter 9, on the AU14GEN model. Section F.1 explains the relationship between the search traversal and the AUSIME output report files. Section F.2 provides an example of a main search instruction file for a CCT search. Section F.3 provides examples of some of the inner-loop and outer-loop configuration files that are generated for the CCT search. Section F.4 provides an example of a PSS®E dynamic response command file that is generated for one of the search scenarios. Section F.5 describes an example of how to execute an automated CCT search. Section F.6 provides an example of how to apply the tools for the converting the binary files, generated by AUSIME TSL tool, into the MATLAB® format.

F.1. Example:The AUSIME Report files

In case 1 from Chapter 9, a critical clearing time (CCT) search is performed on the AU14GEN power system where 500MW is transferred from Victoria (VIC) to South Australia (SA) and a three-phase fault is applied near to the VIC end of the VIC to SA interconnector (VSI). Refer to section 9.3.1 for a description of the CCT search traversal using the EBSIME method. Figure F-1, Figure F-2 and Figure F-3 show the corresponding search reports that are generated by the AUSIME TSL Search tool. They are respectively (i) a summary of the search trajectory; (ii) the "wall-clock" time and "simulation-time" for each iteration of the search and the cumulative values of the time and (iii) the machine groups used in the search.

Table F-1 explains the abbreviations that are used in the search traversal report in Figure F-1 the syntax of the report is described in section 8.3.5.1. Each search iteration is described by one line record in Figure F-1. The scenarios are listed in the order of the traversal.

The first line record reveals that scenario 1:

- Assesses the system operation where the applied fault is cleared after 500ms
- is in initialization phase
- is transiently unstable according to the centre of inertia (COI) stability criteria
- does not have a defined SIME margin
- has the respective upper and lower search bounds of 500ms and 0ms

Fields n(k-1) and SV(k-1) are not applicable (N/A) as there is no previous scenario.The MG for the search is defined from scenario k=1 and is explained in the Machine Group Report in Figure F-3. The corresponding MOMIB is listed, and it is the same across all scenarios.

The second line record reveals that scenario 2:

- Assesses system operation for fault clearing time of 250ms
- is also in the initialization phase
- is transiently unstable as determined by the SIME unstable early stop criteria (ESC)
- has an unstable SIME margin of -0.19303590 pu-rad.
- updates the respective upper and lower search bounds to 250ms and 0ms

The third line record for scenario 3 tells that scenario 3:

- Assesses system operation for fault clearing time of 125ms
- is forward-swing limit (FSL) prediction phase
- is transiently unstable as determined by the SIME stable ESC
- has an stable SIME margin of 0.04845975 pu-rad.
- FSL prediction using the margins and CTs of scenarios 2 & 3 determines the next SV to be 150ms
- The upper and lower search bounds are updated to 250ms and 125ms.

Iterations 4 to 6 are similar. Search divergence is recorded on the line record following for scenario 7, by the text 'Redirecting Search'. This is because the predicted next SV is on the upper search bound - 153ms for scenario 7. The divergent SV is mentioned on the same line that search redirection is reported, inside the brackets. The SV for scenario 8 is 202ms, which is the bisection of the scenario 7 search bounds. Search divergence is also reported from scenarios 9 & 10.

In the line record following scenario 10, it is reported that the search divergence threshold is reached, and the algorithm switches to a plain binary search at the 11^{th} search step. SIME margins and the previous (k-1) scenario data are no longer recorded since limit prediction is not required. MOMIB value is reported as the OMIB response may continue to be recorded to binary file.

The 'COI' stability method indicates that transient stability of scenarios 11 to 14 are assessed using the COI stability criteria. The line records for scenario 11 to 14 are continuations of previous search scenarios 4 to 7, to narrow the search bounds for the binary search. This procedure is sufficient to end the search at scenario 14 where the search tolerance of 2ms is reached. The CCT of 150ms is reported in the final line.

```
SV TOL:   2.00000000
============================================================
Scen  n(k-1)     n(k)        SV      SV    Search  TSA   NextSV   Stab.  Search      MOMIB
No.  (pu-rad)   (pu-rad)    (k-1)   (k)   Phase         (CT,ms)  Method Bound (ms) (pu on
                            (ms)    (ms)                                LO    HI   (MBASE)
=============================================================================================
1   N/A          N/A          N/A    500   INITIAL 2-U   250     COI       0   500  224.73
2   N/A         -0.19303590     0    250   INITIAL U     125     ESC       0   250  224.73
3  -0.19303590   0.04845975   250    125   FSL     S     150     ESC     125   250  224.73
4   0.04845975   0.00231033   125    150   FSL     S     151     ESC     150   250  224.73
5   0.00231033   0.00124902   150    151   FSL     S     152     ESC     151   250  224.73
6   0.00124902   0.00054818   151    152   FSL     S     153     ESC     152   250  224.73
7   0.00054818   0.00016695   152    153   FSL     S     153     ESC     153   250  224.73
              ***Redirecting Search *** (153.00)
8   0.00016695  -0.10042851   153    202   FSL     U     153     ESC     153   202  224.73
9  -0.10042851  -0.05186964   202    178   FSL     U     166     ESC     153   178  224.73
              ***Redirecting Search *** (152.00)
10 -0.05186964  -0.02907663   178    166   FSL     U     ---     ESC     153   178  224.73
              ***Redirecting Search *** (151.00).
***Search has reached divergence limit. Search will continue as binary search.***
11  N/A          N/A          N/A    153   BINARY  U     ---     COI       0   153  224.73
12  N/A          N/A          N/A    152   BINARY  U     ---     COI       0   152  224.73
13  N/A          N/A          N/A    151   BINARY  U     ---     COI       0   151  224.73
14  N/A          N/A          N/A    150   BINARY  S     ---     COI     150   153  224.73
                  ***MULTI-SWING LIMIT IS FOUND at CT =   150.000ms***
```

Figure F-1. The search traversal report generated by AUSIME for the CCT search

TABLE F-1. DESCRIPTION OF ABBREVIATIONS USED IN THE SEARCH TRAVERSAL REPORT

Abbreviation	Description
Scen. No. (k)	Scenario number
n(k)	SIME margin for current scenario k
n(k-1)	SIME margin for previous scenario k-1
SV(k)	Search Variable for scenario k
SV(k-1)	Search Variable for scenario k-1
TSA	Transient Stability Assessment (Stable or Unstable)
S	Stable
U	Unstable
2-S	Too Stable for a defined stable SIME margin
2-U	Too Unstable for a defined unstable SIME margin
M-U	Multi-swing unstable, as determined by the COI stability criteria
N/A	Not Applicable
FSL	Forward-swing Limit Search Phase
MOMIB	OMIB inertia used to calculate the OMIB responses for scenario k. It is the same for all scenarios in the EBSIME search. (In the SIME method MOMIB may vary - this field was provided for research purposes.)

Scen. No.	TWALL(s)	TWALL(s) Cumulative	TSIM(s)	TSIM (s) Cumulative	Stab. Method	CT(ms)	Stable? (S/U)
1	1.28	1.28	1.45	1.45	COI	500.00	U
2	1.05	2.34	1.31	2.76	ESC	250.00	U
3	1.33	3.67	1.51	4.27	ESC	125.00	S
4	1.88	5.58	1.8	6.07	ESC	150.00	S
5	1.95	7.55	1.83	7.9	ESC	151.00	S
6	2.00	9.53	1.87	9.77	ESC	152.00	S
7	2.12	11.7	1.91	11.68	ESC	153.00	S
8	1.24	12.92	1.43	13.11	ESC	202.00	U
9	1.44	14.41	1.52	14.63	ESC	178.00	U
10	1.56	16.27	1.6	16.23	ESC	166.00	U
11	0.38	16.65	0.24	16.47	COI	153.00	U
12	0.59	17.24	0.34	16.81	COI	152.00	U
13	0.86	18.10	0.5	17.31	COI	151.00	U
14	10.38	28.48	8.2	25.51	COI	150.00	S

MULTI-SWING LIMIT IS FOUND at CT = 150.000ms

Figure F-2. The search timing report generated by AUSIME for the CCT search

```
----Machine Group Definition---------
 Number of Online Machines:62
 Number of Machines in Group 1:  55
 Number of Machines in Group 2:  7

 Group 1 Machines (PSSE MACHID):
1,       5,     6,     7,   13,    14,    15,    16,    17,    18,
19      20,    21,    22,   23,    24,    25,    26,    27,    28,
29,     30,    31,    32,   33,    44,    45,    46,    49,    50,
51,     52,    53,    54,   55,    56,    57,    58,    59,    60,
61,     62,    63,    64,   65,    67,    68,    69,    70,    71,
72,     73,    74,    75,   76
Group 2 Machines (PSSE MACHID):
36,     37,    38,    39,    40,    41,    42

Group 1 Machines (BUSID):
101,   101,   101,   101,   201,   201,   201,   201,   201,   201,
202,   202,   202,   202,   202,   203,   203,   203,   203,   204,
204,   204,   204,   204,   204,   302,   302,   302,   401,   401,
401,   401,   402,   402,   402,   403,   403,   403,   403,   404,
404,   404,   404,   404,   404,   501,   501,   502,   502,   502,
502,   503,   503,   503,   503
Group 2 Machines (BUSID):
301,   301,   301,   301,   301,   301,   301

//note: in this case multiple generating units are connected to the same bus
```

Figure F-3. The machine group report generated by AUSIME for the CCT search

F.2. Example:The Main Search Instruction File

Figure F-4 and Figure F-5 show the user-supplied instructions to the AUSIME TSL Search tool, that would be used to execute the EBSIME PTL search for PTL search. The user-supplied channel output text file which is mentioned in Figure F-4 is provided in Figure F-6.

```
SearchMode, EBSIME              //The EBSIME search method will be used
SVTYPE, CCT                     //Critical Clearing time search
CASEID, VS_B305_500MW_3A        //used to name files created for the CCT search
SAVEFOLDER, ./CCT_B305/         //The output directory for search files

ApplyESC, IFS                   //Apply the SIME ESC during the initial and FSL search phase
GenerateReport, 1               //Generate text files to report search traversal and search
                                //simulation times
RecordOMIB,     1               // Record OMIB responses to binary files
RecordMG, 1                     //Record machine group information to text and binary file
RecordCOI, 1                    // Record COI responses to binary files
SVUNITS, ms                     //In this file power transfer is specified in ms
SEARCHBOUND_UP, 500.0           //The upper search bound is 500 ms
SEARCHBOUND_LO, 0.0             //The lower search bound is 0 ms
TRUN, 10.0                      //Maximum TDS simulation time is 10 s.
SV_TOL, 2.0                     //Search tolerance is 2ms
DEBUGLEVEL, 2
LoadFlowFile, .\PSSEFILES\LF_Case01_VS500.raw   //load flow //instructions
FaultDefFile,  FaultLOC_B305_3A_LF.txt          //Fault specification

ChannelOUT,ChanOut_AUS.txt      //Instruction file for PSS®E activity CHAN

NDIV_LIMIT, 3   //If the search diverges thrice it will revert to binary search.

FORTRAN_CODE_FOLDER,..\InnerLoop\FortranCode

//Details for this file format are provided in Table E-1 and Table E-6.
```

Figure F-4. The main search instruction file for the example CCT search

```
NLOG_DETAIL, 100        //From t = tfault + 2s, data is recorded to the PSS®E channel
                        //file every 100th time-step
NCHAN_DETAIL, 1         //From t = tfault + 2s, data is recorded to binary response
                            file
                        //at every time step
NLOG_NORMAL, 1000       //During the run-in period, data is recorded to PSS®E
                        //channel file at every 1000th time step.
NCHAN_NORMAL, 10        //During the run-in period, data is recorded to binary
                            response
                        //file at every 10th time step.

FROMBUS, 305            //Bus 305 is at the sending-end of the faulted feeder
TOBUS, 307              //Bus 3 is at the receiving-end of the faulted feeder
CKTID, "2"              //The fault is applied on circuit #2, between bus 305 and 307
IBUS, 305               //The fault is applied near to bus 305

MAX_ITER_LF, 1000       //A maximum of 1000 iterations is allowed for solving the
                        //load-flow solution

ACCEL_FACTOR, 0.1       //Acceleration factor for solving the load-flow solution
PSSE_SIM_TIMESTEP, 0.001        //Size of the TDS time-step.
TIME_CONSTANT_BUS_FREQ, 0.02    //Time constant for load-flow bus-frequency
LOADFLOW_tol, 0.01          //Load flow solution tolerance 0.01 MW
System_Frequency, 50        //System Frequency 50 Hz
BASEKV, 0.00                //Base voltage to calculate the per unit fault
                            //admittance
YREAL, 0.00                 //Real component of fault admittance in MVA
YREACTIVE, -0.20000E+10     //Reactive component of fault admittance in MVA
tfault,1                    //The run-in period. The fault is applied at t=1s.
PSSE_REPORT_OUTPUT,                 //The PSS®E report file
SimplifiedAustralianSystem_DOCU.TXT
DynamicsData, .\PSSEFILES\AU14GEN.dyr       //The PSS®E system
                                            // dynamics data file

//Details of the file format are provided in Table E-2.
```

Figure F-5. The user-supplied fault definition file for a PTL search for Case 5 in Chapter 9

```
CHAN
, , ,
1
101,1 ,DEL.HPS_1    //the rotor angles are recorded for the
201,1 ,DEL.BPS_2    //#1 generators at buses 101, 201, 301,401 & 501
301,1 ,DEL.LPS_3
401,1 ,DEL.TPS_4
501,1 ,DEL.NPS_5

2
101,1 ,P.HPS_1    //the power outputs are recorded for the #1
201,1 ,P.BPS_2    //generators at buses 101, 201, 301,401 & 501
301,1 ,P.LPS_3
401,1 ,P.TPS_4
501,1 ,P.NPS_5

7
101,1 ,W.HPS_1    //the rotor speeds are recorded for the #1
201,1 ,W.BPS_2    //generators at buses 101, 201, 301,401 & 501
301,1 ,W.LPS_3
401,1 ,W.TPS_4
501,1 ,W.NPS_5

10
101,1 ,VS.HPS_1    //the PSS output signals are recorded for the #1
201,1 ,VS.BPS_2    //generators at buses 101, 201, 301,401 & 501
301,1 ,VS.LPS_3
401,1 ,VS.TPS_4
501,1 ,VS.NPS_5

19
4,Y.PSVC          //The susceptance for the five SVC's in
5,Y.SSVC          //the system are recorded.
1,Y.ASVC
2,Y.RSVC
3,Y.BSVC

16                      //The real and reactive power flow is
413,410,1,P.B413_B410_1  //recorded for lines #1 between:
'Q.B413_B410_1'          //buses 413 and 410
206,205,1,P.B206_B205_1
'Q.B206_B205_1'          //buses 205 and 206
305,307,1,P.B305_B307_1
'Q.B305_B307_1'          //buses 305 and 307
509,507,1,P.B509_B507_1
'Q.B509_B507_1'          //buses 509 and 507


//This is the text file ChanOut_Aus.txt described by field 'ChannelOUT' in Figure F-4. Also
refer to Table E-1.
```

Figure F-6. The user-supplied input channel output text file

F.3. Example:The Inner- and Outer-Loop Configuration Files

Figure F-7 shows the inner-loop configuration file generated by the outer supervisory loop for the first search scenario (k=1). Figure F-8 and Figure F-9 shows the outer-loop configuration file generated by the inner search loop after the TDS for scenario 1 is executed.

```
//This file is called  AUSIME_INNERLOOP_CONFIG_VS_B305_500MW_3A_IT1_IN.txt"
ISEARCH, 1                          //First search scenario
SearchMode, 11                      //Search in Initialization phase
SVNAME, CT                          //Critical Clearing time (CCT) search
SV, 500.000                         //Clearing time (CT) for this scenario is 500ms
SVUNITS, ms                         //SV is specified in ms
CASEID, VS_B305_500MW_3A            //Identifier used for generated scenario 1 files
LOG_FILENM, LOG_FILE.txt            //Name of the output log file (to assist debugging)
ERROR_FILENM, ERR_FILE.txt          //Name of the output error file (to assist debugging)
ApplyESC, 2                         //SIME ESC is applied in initial and FSL search phases
IsMGDefined_prev, 0                 //The MG has not been defined for the search yet.
IsRecordTSIM, 1                     //Record search timing information
IsRecordSIMEInfo, 1                 //Record search traversal information
IsRecordOMIB, 1                     //Write OMIB time response to binary file
IsRecordCOI, 1                      //Write COI time response to binary file
IsRecordMG, 1                       //Record MG to text and binary files
SAVEFOLDER, ./CCT_B305/             //Output directory
TSV_TOL, 2.0000000                  //Search tolerance is 5ms
MAX_ITER, 40                        //Maximum allowed search scenarios is 40
TSIM_CUML, 0.0000000                //Search simulation time so far is 0s
TWALL_CUML, 0.0000000               // Search simulation time so far, in GPS time, is 0s
BINARY_UP, 500.0000000              //Initial upper search bound (COI assessment)
BINARY_LO, 0.0000000                //Initial lower search bound (COI assessment)
SIME_UP, 500.0000000                //Initial upper search bound (ESC assessment)
SIME_LO, 0.0000000                  //Initial lower search bound (ESC assessment)
TRUN, 10.0000000                    //Maximum simulation time for TDS
TCLR, 1.50000000                    //The fault is cleared at t=1.5s.
TFAULT, 1.0000000                   //The fault is applied at t=1s.
RedirectSearch, 66                  //If search diverges redirect by bisection of SIME_LO and
                                    UP
DEBUGLVL, 2                         //Generate search reports & report inner loop errors only
LOOP,1                              //Inner loop configuration file
//Location of the outer loop configuration file generated after scenario 1:
ConfigFile_OUT, ./CCT_B305/
AUSIME_INNERLOOP_CONFIG_VS_B305_500MW_3A_IT1_OUT.txt
* See Table E-3 and Table E-4 for description of inner loop configuration file format
```

Figure F-7. Inner-loop configuration file for scenario 1 generated by the outer supervisory loop

```
//This file is called "AUSIME_INNERLOOP_CONFIG_VS_B305_500MW_3A_IT1_OUT.txt"

ISEARCH, 2                          //Search scenario k =2
SearchMode, 11                      //Initial search phase
SVNAME, CT                          // CCT search
SV, 250.000000000                   //Clearing time for this scenario is 250ms
SVUNITS, ms                         //SV is specified in ms
TFAULT, 1.000000000                 //The fault is applied at t=1s.
TCLR, 1.2500000000                  //The fault is cleared at t=1.25s.
TRUN, 10.000000000                  //Maximum simulation time for the TDS
CASEID, VS_B305_500MW_3A            //Identifier used in the filename for all generated
                                    files
LOG_FILENM, LOG_FILE.txt            //Name of the output log file (to assist debugging)
ERROR_FILENM, ERR_FILE.txt          //Name of the output error file (to assist
                                    debugging)
IsRecordTSIM, 1                     //Record search timing information
IsRecordSIMEInfo, 1                 //Record search traversal information
IsRecordOMIB, 1                     //Write OMIB time response to binary file
IsRecordCOI, 1                      //Write COI time response to binary file
IsRecordMG, 1                       //Record MG to text and binary files
SAVEFOLDER, ./CCT_B305/                 //Generated report and binary
                                        //response files are saved to this
                                        location
MG_FILENM, ./CCT_B305/                          //Address of binary file
VS_B305_500MW_3A_MACH_GRP.BIN                   //containing MG
                                                //information
TSIM_FILENM_TXT,./CCT_B305/                     //Address of search
VS_B305_500MW_3A_SEARCHTIME.TXT                 //timing report file
SIMEINFO_FILENM_TXT, ./CCT_B305/                //Address of search
VS_B305_500MW_3A_SIMEINFO.TXT                   //traversal report file
MG_FILENM_TXT, ./CCT_B305/                      //Address of text file
VS_B305_500MW_3A_MACHGRP.TXT                    //containing MG
                                                //information
TSIM_CUML, 1.449011683          //Scenario 1 took 1.45 sim-s to identify transient
                                instability
TWALL_CUML, 3.421999991         //Scenario 1 took 3.42 s in GPS time
DEBUGLVL, 2                     //Generate search reports & report inner loop
                                errors only
BYPASS_STOP_CRITERIA, 0         //Stop simulation when SIME ESC is identified
ApplyESC, 2                     //SIME ESC is applied in initial and FSL search phases

RedirectSearch, 66              //If search diverges from FSL, redirect by bisection of
                                //SIME_LO and SIME_UP
TSV_TOL, 2.000000000            //Search tolerance is 2ms
MAX_ITER, 40                    //Maximum allowed search scenarios is 40
BINARY_UP, 500.000000000        //Initial upper search bound (COI assessment)
BINARY_LO, 0.000000000          //Initial lower search bound (COI assessment)
SIME_UP, 500.000000000          //Initial upper search bound (ESC assessment)
SIME_LO, 0.000000000            //Initial lower search bound (ESC assessment)
```

Figure F-8. Part 1 of 2 of the outer-loop configuration file generated by the inner search loop for scenario 1

```
MarginGrade_sav, -1          //Scenario 1 is unstable and does not have a defined SIME
                             //margin
GENVAR_FILENM_SAV, ./CCT_B305/
VS_B305_500MW_3A_CT_500ms_IT1_GENVAR1.BIN   //Binary response file where full
                                            set of time response variables
                                            are saved for scenario 1.
OMIB_FILENM_SAV,./CCT_B305/                 //Binary response file containing
VS_B305_500MW_3A_CT_500ms_IT1_OMIB.BIN      //OMIB time responses for
                                            scenario 1

COI_FILENM_SAV,/CCT_B305/                   //Binary response file containing
VS_B305_500MW_3A_CT_500ms_IT1_COI.BIN       //COI time responses for
                                            scenario 1
IsESCApplied_sav,      0     //The SIME ESC was not applied for
                             scenario 1
IsUnstable_sav,      1       //Scenario 1 is transiently unstable.

GENVAR_PREV_FILENM,                         //Binary response file where full
./CCT_B305/                                 set of
VS_B305_500MW_3A_CT_500ms_IT1_GENVAR1.BIN   //time response variables are
                                            saved for
                                            //the previous scenario.

NDIV_COUNT, 0          //Search has diverged from the FSL 0 times
NDIV_LIMIT, 3          //If search diverges from FSL 3 times, the search will revert
                       //to a binary search
LOOP,0           //This is an outer loop configuration file.

                 (See Table E-3 to Table E-5 for description of file format)
```

Figure F-9. Part 2 of 2 of the outer-loop configuration file generated by the inner search loop for scenario 1

F.4. Example: PSS®E Command File Generated by the Outer Supervisory Loop

Figure F-10, Figure F-11, Figure F-12 and Figure F-13 show the PSS®E command file that is generated by the outer supervisory loop to execute the TDS for the first search scenario. The figures include comments identifying the python functions that are used to generate each section of the file as per section 8.4.5.4.

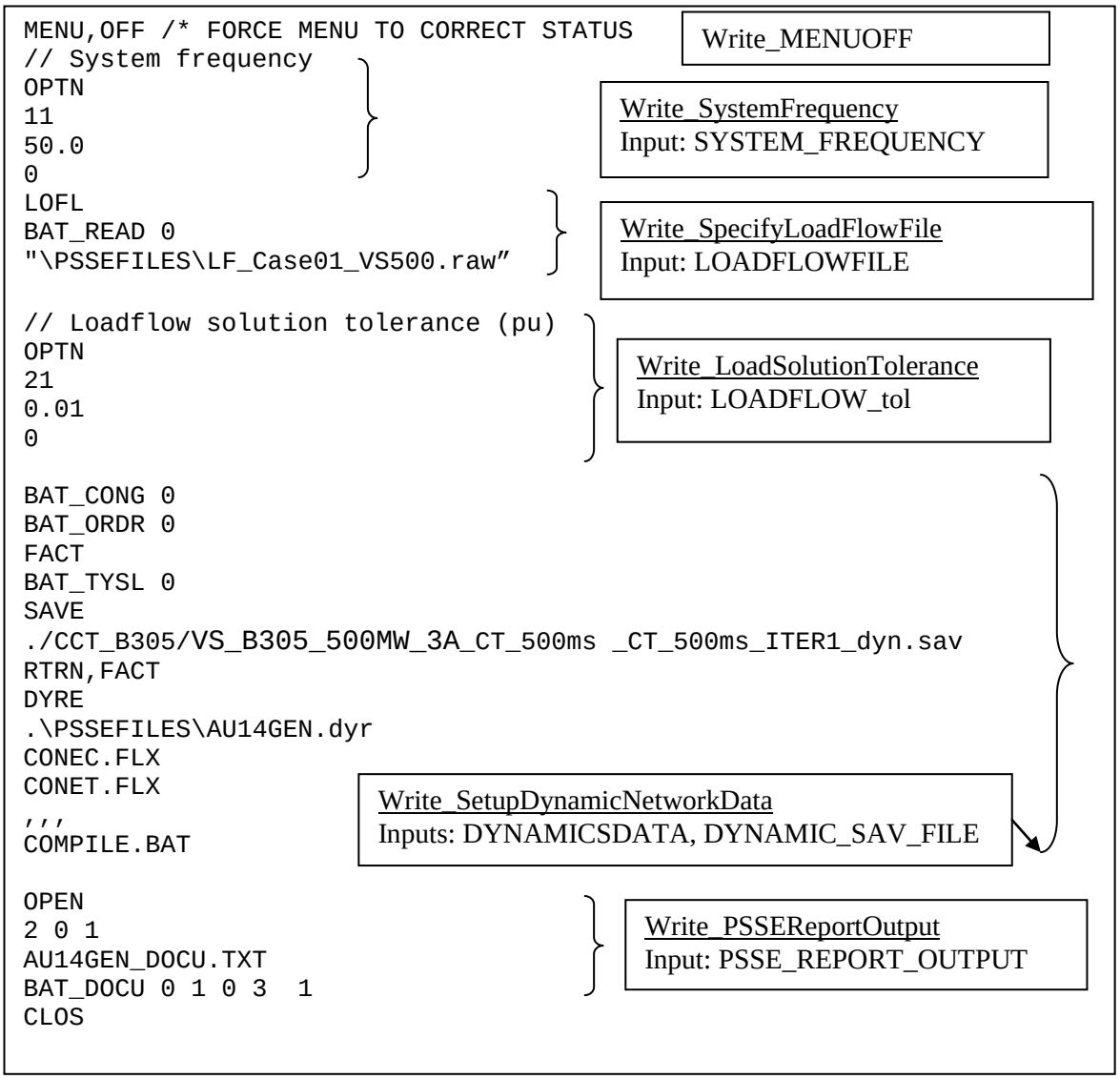

Figure F-10. Part 1 of 4 of the PSS®E response file generated for scenario 1 by the outer supervisory loop. The python functions responsible for generating each section are noted in the comments.

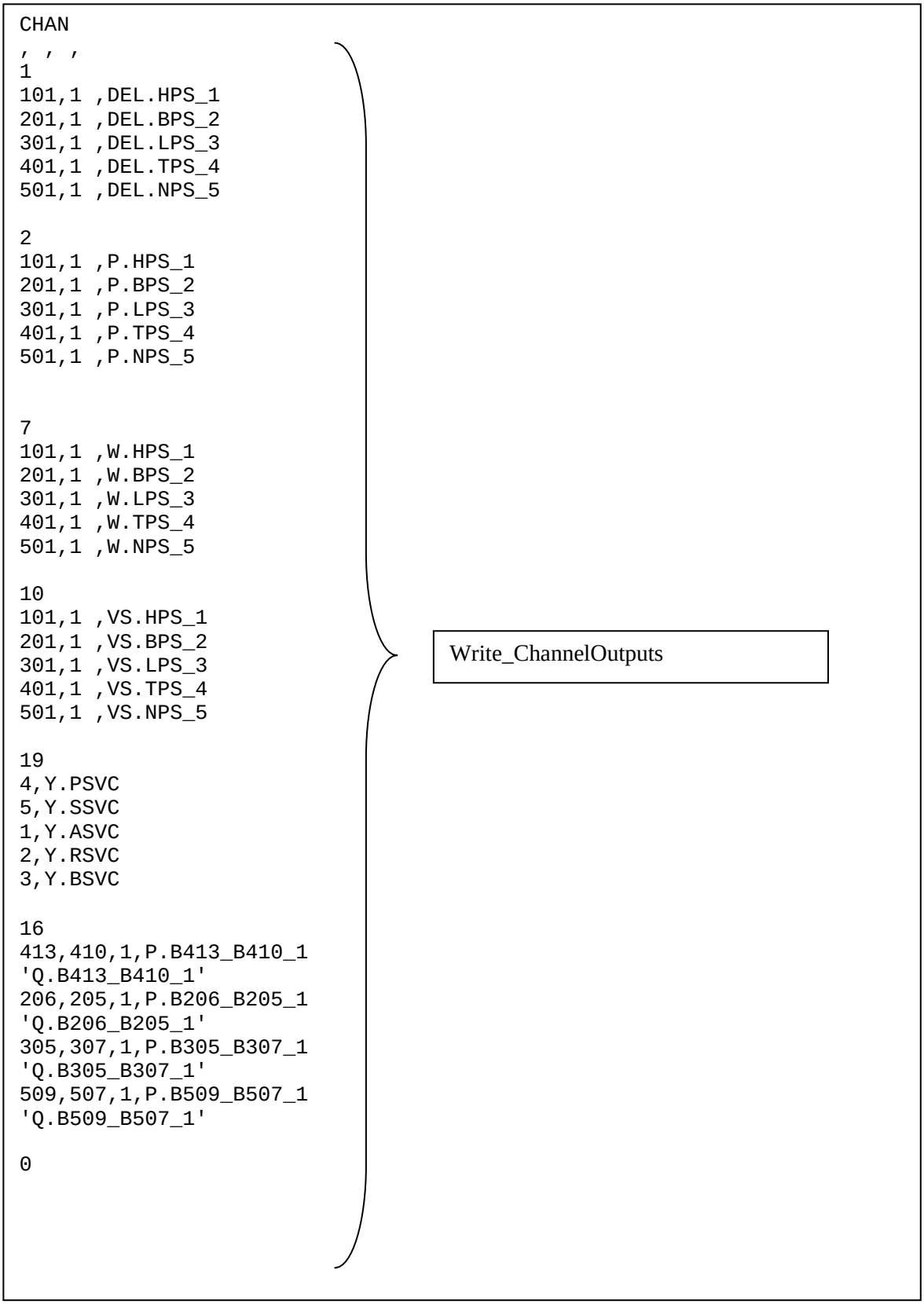

Figure F-11. Part 2 of 4 of the PSS®E response file generated for scenario 1 by the outer-supervisory loop

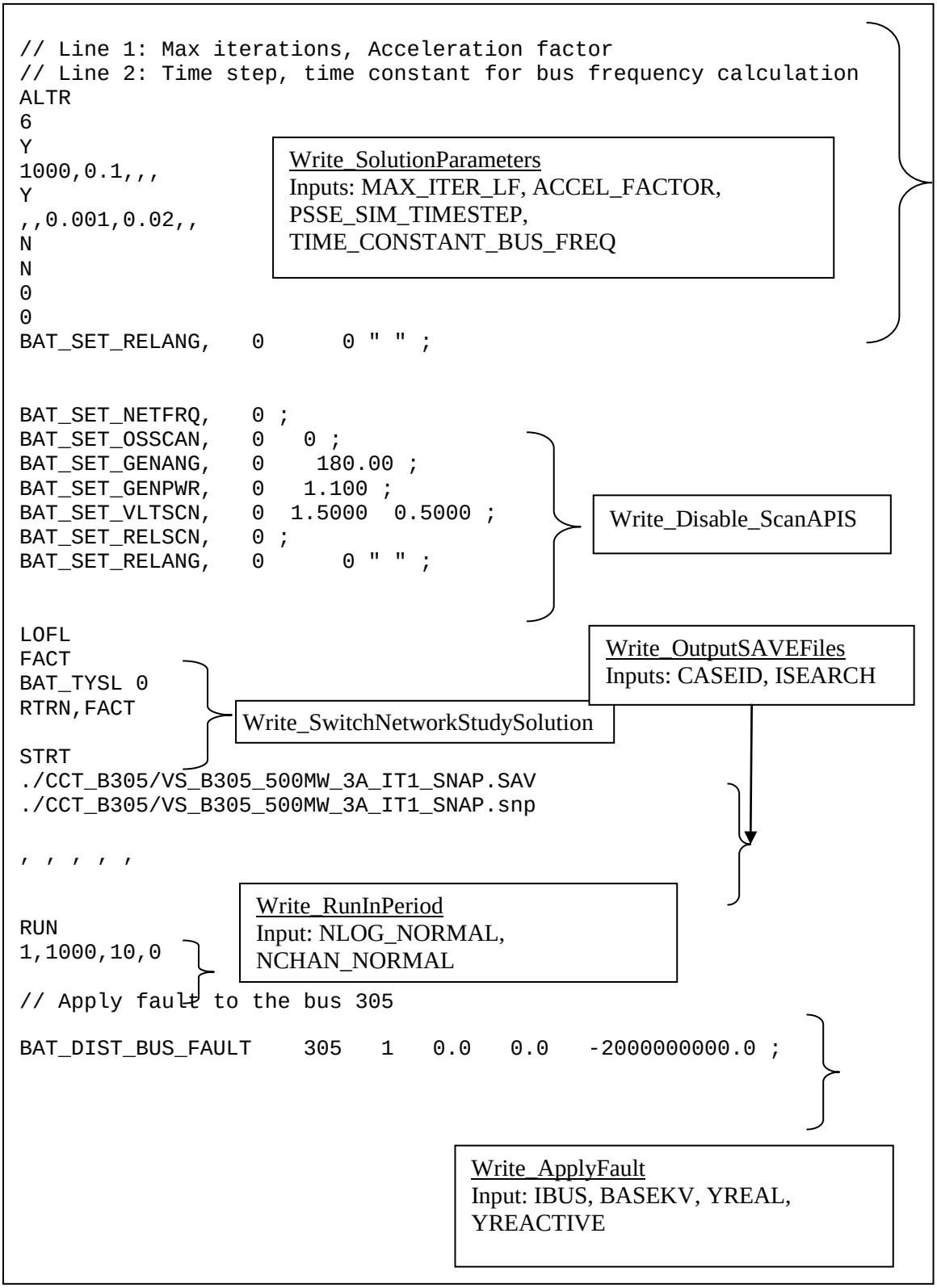

Figure F-12. Part 3 of 4 of the PSS®E response file generated for scenario 1 by the outer-supervisory loop

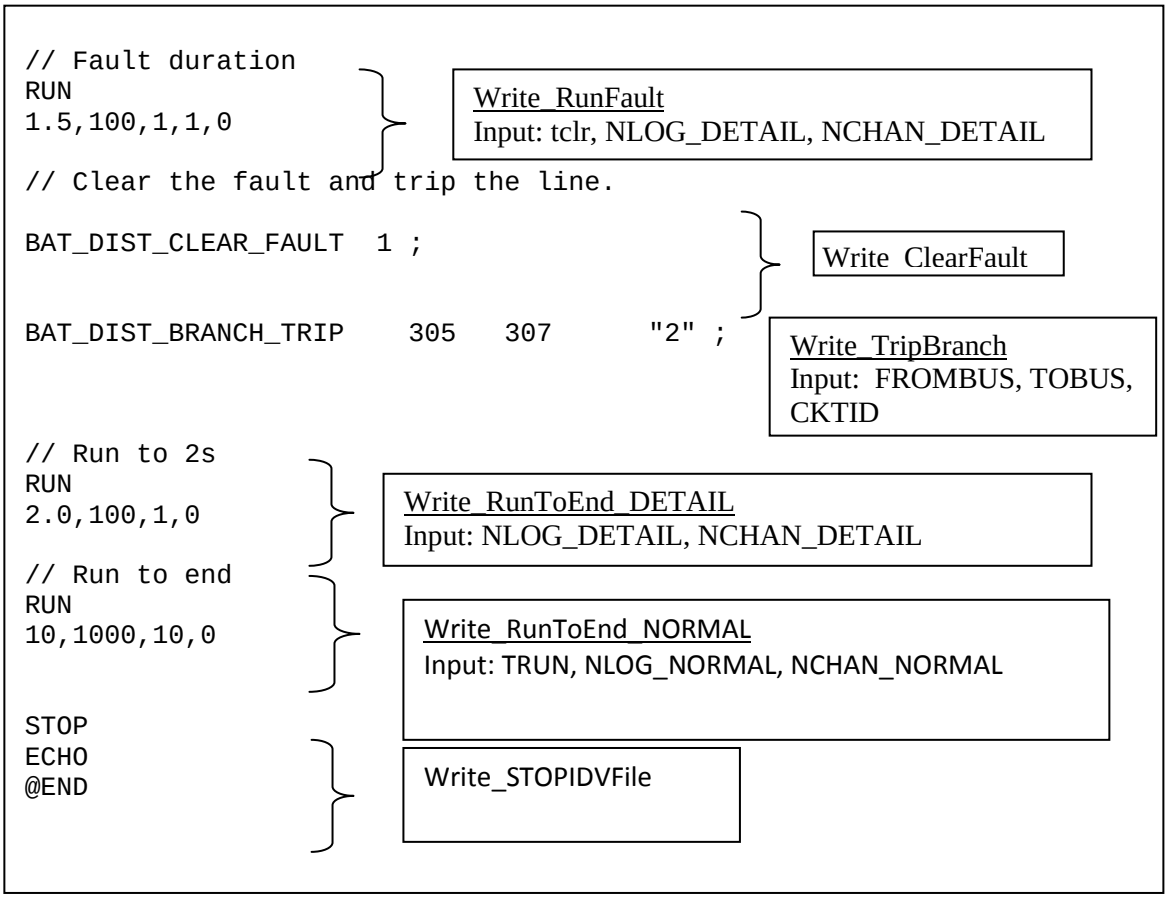

Figure F-13. Part 4 of 4 of the PSS®E response file generated for scenario 1 by the outer-supervisory loop

F.5. Executing the EBSIME TSL search

The AUSIME TSL search tool is designed to run a fully automated TSL by executing a single command called from the DOS command prompt as described in section 8.4.3. To do so the AUSIME user-defined model must be linked to PSS®E from the desired working directory, as described in section F.5.1. At the time of writing the thesis only the CCT search has been automated in the outer supervisory loop, the PTL search example has been performed manually. A high level example of the instructions to run an automated a CCT search with the EBSIME method is provided in section F.5.2.

To replicate these results the user must have Lahey-Fujitsu Intel® Fortran 95 compiler (at least version 10.1) and the PSS®E simulation engine (at least version 30) installed on the operating system.

F.5.1. Compiling and Linking the AUSIME User Defined Inner Loop model Using PSS®E™

The AUSIME TSL search tool must be declared in the PSS®E dynamics data file (.dyr) and compiled and linked to operate in the intended working directory. The syntax to declare the AUSIME user-defined model within PSS®E dynamics data file (.dyr) is:

```
BUSID 'USRMDL' IM 'model name' IC IT NI NC NS NV data list/
```

Each field and its assigned value for the AUSIME tool, is described in Chapter 8. As such the AUSIME model is declared by appending the following record to the dynamics data file: `0 'USRMDL' 0 'AUSIME' 8 0 0 0 0 0 /`
The AUSIME declares its own data-structures quite separately from the PSS®E data structures. Thus the AUSIME model does not use any of the PSS®E constants or variable arrays.

The DOS commands shown in Figure F-14 to compile and link the AUSIME PSS®E model are generated by the outer-search loop. In line 1, the response file 'INIT_V30.IDV 'is called to initialize the AUSIME model for use with the simplified South Australian power system model. INIT_V30.IDV is shown in Figure F-15. The base-case load flow '`LF_Case01_IA_VS500.raw`' and the dynamics data file 'SimplifiedAustralianSystem.dyr' are referenced and must be present in the working directory. Line 4 and 17, the respective paths of the load flow and dynamic data files, must be adjusted for use with alternative power system network models.

TABLE F-2. SUMMARY OF THE FIELDS USED TO DECLARE THE AUSIME USER DEFINED MODEL

Field	Definition	Value for the AUSIME model
BusID	The identifier of the bus at which a dynamic equipment model is to be placed	0
IM	The identifier of the machine that is influenced by the user defined model	0
Model name	The name of the user defined model	'AUSIME'
IC	User model type code	8 (denotes the model other than a device related model)
IT	When IC = 8, IT describes whether the user model is IT=1: a current injection model IT=2: a metering model IT=0: neither of the above listed models	0 (denotes that the model does not interact with the network)
NI	The number of circuit identifiers used by the model	0
NC	The number of constant parameters used by the model	0
NS	The number of state variables used by the model.	0
NV	The number of algebraic variables used by the model.	0
Data list	A list of NI circuit identifiers, followed by NC constant parameters	-

```
CALL pssds4 -gnikool off -inpdev INIT_V30.IDV>text.txt
del dsusr.*
Call compile.bat
call cload4
..\InnerLoop\FortranCode\comon4.obj
..\InnerLoop\FortranCode\KindModule.obj
..\InnerLoop\ConstantModule.obj
..\InnerLoop\errorcodemodule.obj
..\InnerLoop\decode_M.obj
..\InnerLoop\Sort_AUSIME.obj
..\InnerLoop\FileInfoModule.obj
..\InnerLoop\ErrorModule.obj
..\InnerLoop\GenParamModule.obj
..\InnerLoop\GenVarmodule.obj
..\InnerLoop\MachineGroupingModule.obj
..\InnerLoop\SearchInfomodule.obj
..\InnerLoop\ConfigFileModule.obj
..\InnerLoop\OMIBModule.obj
..\InnerLoop\checkstability.obj
..\InnerLoop\AUSIME_InitialiseModule.obj
..\InnerLoop\ProcessTimeStepModule.obj
..\InnerLoop\FinaliseSimulationModule.obj
..\InnerLoop\ausime.obj
..\InnerLoop\J4SAVE.obj
..\InnerLoop\FDUMP.obj
..\InnerLoop\XERHLT.obj
..\InnerLoop\XERCNT.obj
..\InnerLoop\I1MACH.obj
..\InnerLoop\xgetua.obj
..\InnerLoop\XERSVE.obj
..\InnerLoop\XERPRN.obj
..\InnerLoop\XERMSG.obj
..\InnerLoop\xsetua.obj
..\InnerLoop\DP1VLU.obj
..\InnerLoop\DPCOEF.obj
..\InnerLoop\DPOLFT.obj
..\InnerLoop\FinaliseSimulation_INIT_Module.obj
..\InnerLoop\FinaliseSimulation_FIRSTSWING_Module.obj
```

Figure F-14. Batch file 'CompileLinkAUSIME.bat' with instructions to compile and link the inner loop model by the Python function RunLinkPSSE from the PSSEWrapperModule

```
MENU,OFF      /* FORCE MENU TO CORRECT STATUS
LOFL
BAT_READ 0
"LF_Case01_IA_VS500.raw"   // line 4
OPTN
21
0.010000
0
BAT_CONG 0
BAT_ORDR 0
FACT
BAT_TYSL 0
SAVE
Case01_VS500_dyn.sav
RTRN,FACT
DYRE
SimplifiedAustralianSystem.dyr    // line 17
CONEC.FLX
CONET.FLX
,,,
COMPILE.BAT

STOP
ECHO
@END
```

Figure F-15. The INIT_V30.IDV response file, to initialize of the AUSIME inner loop model with PSS®E

F.5.2. Example:Instructions for Executing the Automated CCT search

This section describes the steps required to run the case CCT search using the AUSIME TSL Search tool. The main search instruction text file for this CCT search is shown in Figure F-4. Consider the folder structure shown in Figure F-16.

```
C:\Automated_CCT_Search
├──InnerLoop
├──OuterLoop
├──PSSEFILES
└──WorkingDir_B305
    └──CCT_B305
```

Figure F-16. Example directory structure for the automated CCT search

Prior to executing the search the working directory
"C:\Automated_CCT_Search\WorkingDir_B305" contains:

- the main instruction text file (CCT_B410_4A_EBSIME.txt of Figure F-4)
- the fault definition file (FaultLOC_B410_4A_LF.txt of (Figure F-5) and
- Instruction file for PSS®E activity CHAN (ChanOut_AUS.txt of Figure F-6). The dynamic response file 'INIT_V30.IDV' to initialize the AUSIME tool into the working directory.

The directory "C:\Automated_CCT_Search\InnerLoop" contains the source code and object files for the PSS®E user-defined model for the AUSIME inner-loop.

"C:\Automated_CCT_Search\OuterLoop" contains the python source code and object files for the AUSIME outer supervisory loop.

"C:\Automated_CCT_Search\PSSEFILES" contains:

- the load flow file (LF_Case01_QN900.raw) and
- the dynamic file (SimplifiedAustralianSystem_rev1.dyr)

The search is run by executing the series commands shown in Figure F-17 from the DOS command prompt. As indicated in the main instruction file, the report and time response files are created in:
"C:\Automated_CCT_Search\WorkingDir_B305\CCT_B305".

Lines 1 and 2 are only required the first time the AUSIME tool is executed from the working directory. Line 1 runs the batch file in Figure F-14 to compile and link the AUSIME software with PSS®E. Line 2 enables the python modules to be imported into the working directory. The files 'Error.txt' and 'Log.txt' are text files that are either created or overwritten when the search is executed.

```
C:\Automated_CCT_Search\WorkingDir_B305>
call CompileLinkAUSIME.bat                                    //line 1
set PYTHONPATH=PYTHONPATH;..\outerloop\pythoncode\             //line 2
python AUSIMEDriver.py CCT_B410_4A_EBSIME.txt Error.txt       //line 3
Log.txt
```

Figure F-17. Commands to run the automated EBSIME CCT search from the DOS command prompt

F.6. Application of the Binary Response to MATLAB® conversion tools

This section demonstrates how the MATLAB® conversion tools provided with the AUSIME software can be applied to generate MATLAB® m-files from the binary response files. Figure F-18 shows a batch file with calls to the three executable conversion tools described in section 8.3.6.6 that are used to translate the binary response files into the MATLAB® m-file format. The calls are made from the output directory "C:\Automated_CCT_Search\WorkingDir_B305\ CCT_B305" as in Figure F-16. It is assumed that the executable files 'generatemfile_genvars.exe', 'generatemfile_COI.exe' and 'generatemfile_OMIB.exe' have also been placed in this directory.

In Figure F-3 it is reported that 62 out of 83 machines are online. The call to generatemfile_genvars.exe generates 83 files in the sub-directory: "./MATLAB/". For each created file, the file name is 'Example _G<i>', where i= 1 to 83. The identity of the corresponding machine is contained within the generated m-file (refer to Table 8-6). The call to generatemfile_COI.exe generates a file called 'Example_COI' containing the COI response in the same directory. Similarly, the call to generatemfile_OMIB.exe generates a file called 'Example_OMIB' in the same directory.

Figure F-19 shows an example of a MATLAB script that uses the generator variable, COI and OMIB information generated from the MATLAB conversion tool. The graphs plotted by this script are shown in Figure F-20 and Figure F-21.

```
call generatemfile_genvars
VS_500MW_B305_3A_CT_178_ms_IT11_GENVAR1.BIN
.\MATLAB\   Example GeneratorParams.bin

call generatemfile_COI VS_500MW_B305_3A_CT_178_ms_IT11_COI.BIN
.\MATLAB\Example

call generatemfile_OMIB VS_500MW_B305_3A_CT_178_ms_IT11_OMIB.BIN
.\MATLAB\Example
```

Figure F-18. Commands to convert PSS®E channel data generated by AUSIME into m-files containing the generator variables, and the COI and OMIB responses, by the MATLAB conversion tool.

```
% Load responses for selected generators from each region in the
AU14GEN system
G1 = Example_G1; %Slack bus
G13 = Example_G13; %A NSW machine
G36 = Example_G36; %A VIC machine
G53 = Example_G53; %A QLD machine
G67 = Example_G67; %A SA machine
COI = Example_COI; % Load  the COI response
OMIB = Example_OMIB; % Load  the OMIB response

%Plot the rotor speed response with respect to centre of inertia
figure(1), hold on, grid on, box on
plot(G1 .t, G1 .omega-COI.omega,'b:','displayname', 'Slack' )
plot(G13.t, G13.omega-COI.omega,'r','displayname','NSW')
plot(G36.t, G36.omega-COI.omega,'b--','linewidth',1, ...
'displayname','VIC')
plot(G53.t, G53.omega-COI.omega,'r-' ,'linewidth',2, ...
'displayname','QLD')
plot(G67.t, G67.omega-COI.omega,'b--','linewidth',2, ...
'displayname','SA')
legend show; xlabel ('Time (s)');ylabel ('\omega_{dev}(pu)')

%Plot the OMIB Acceleration Power Vs Rotor Angle Curve
figure(2), hold on, grid on, box on
plot(OMIB.delta, OMIB.Pa,'b' ,'linewidth',2)
xlabel ('\delta_{OMIB} (\circ)'); ylabel ('Pa_{OMIB} (pu)')
```

Figure F-19. A MATLAB script demonstrating how to plot the responses generated by the MATLAB conversion tools

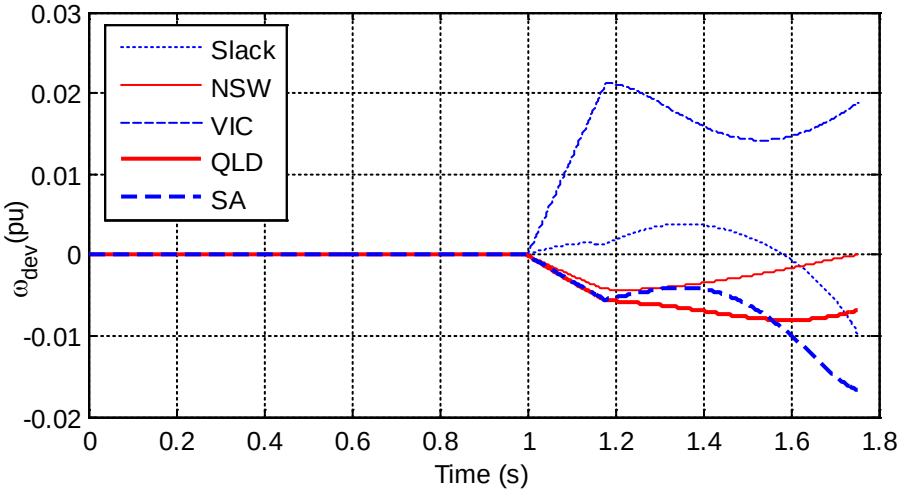

Figure F-20. Plot of the generator speed responses from the AU14GEN generators for case 1, scenario 11, where the fault is cleared after CT =178ms .

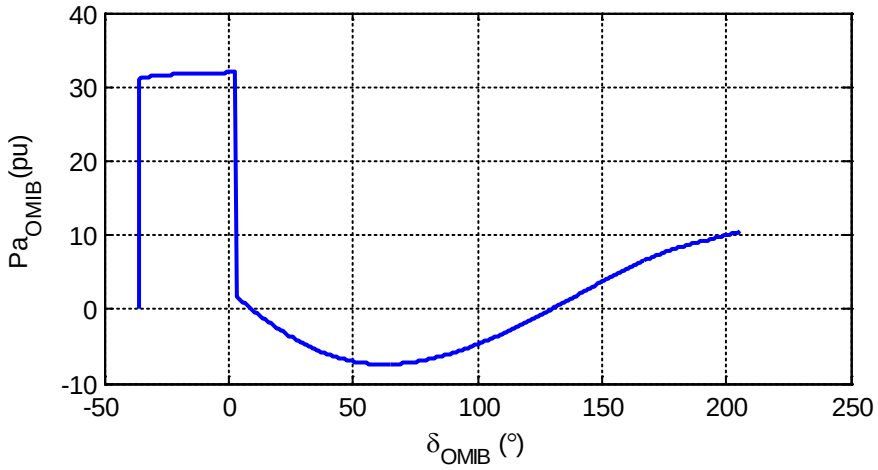

Figure F-21. OMIB Acceleration power-angle curve for case 1, scenario 11, where the fault is cleared CT =178ms

Appendix G Alternative Machine Groups

This appendix describes an alternative search traversal and timing using the Enhanced Binary SIME (EBSIME) for the critical fault clearing time (CCT discussed in section 9.3.1, for case 1 from Table 9-2 on the IEEE simplified 14-generator model of the South-East Australian power system (AU14GEN). This search uses a corrected arrangement for the two groups of machines (MG) used to calculate the SIME responses, and margins. The corrected MG is determined by running the first search scenario for an additional 1s after the SIME ESC has classified the initial search scenario as forward-swing unstable. The Victorian machines LPS_3 and YPS_3 form one MG, and the remaining system machines form the other MG. This MG is a correction of the MG applied in the EBSIME search described in section 9.3.1. This alternative search traversal is described in Table G-1. The search tolerance of 2ms is applied for the CCT search.

The EBSIME search initialization occurs from search iterations 1 to 4. The SIME limit prediction phase occurs from iterations 5 to 9, where the forward-swing limit (FSL) is identified at step 9, when the distance between the FSL search bounds falls below the search tolerance. The influence of the corrected MG is:

1) The search converges to a higher FSL of 158ms, compared to 153ms, in the search in section 9.3.1, and
2) No search redirection is required as the FSL search phase converges to the limit. The FSL search phase with the corrected MG is completed in 19.16 sim-s. In contrast, in section 9.3.1 the FSL search phase takes 16.2 sim-s.

In Table G-1 the residual binary takes another 32 sim-s to locate the TSL, after exiting the SIME limit prediction phase. Since the scenarios near the FSL were all transiently unstable, the remaining search required the simulation of three transiently stable scenarios which significantly slowed down the search.

In conclusion, correcting the MG to reflect the actual system separation, may not result in a faster EBSIME search. Furthermore the EBSIME search traversal is sensitive to the MG used in the SIME calculations.

TABLE G-1. EBSIME CCT SEARCH CASE 1: VIC TO SA: FAULT AT LINE 3A, PT = 500MW FOR ALTERNATIVE CORRECTED MACHINE GROUPING

k	η(k-1) (rad-pu)	η(k) (rad-p u)	CT (ms)	Search bounds (ms)	Predicted CCT (ms)	TSA Criteria	Stable (S)/ Unstable (U)	TSIM (sim-s)
1	-	-	500	[0,500]	-	COI	U	2.4
2	-	-	250	[0,250]	-	COI	U	1.52
3		-	125	[125,250]	-	ESC	S	1.57
4		-0.090262	188	[125,188]	-	ESC	U	1.36
5	-0.090262	0.035041	157	[157,188]	166	ESC	S	2
6	0.035041	-0.045692	166	[157,166]	161	ESC	U	1.7
7	-0.045692	-0.016658	161	[157,161]	158	ESC	U	2.14
8	-0.016658	0.034794	158	[158,161]	160	ESC	S	2.05
9	0.034794	-0.008990	160	[158,160]	-	ESC	U	2.42
FSL identified. Revert to binary search to confirm transient stability limit.								
10	-	-	158	[0,158]	-	COI	U	2
11	-	-	157	[0,157]	-	COI	U	0.02
12	-	-	125	[125,157]	-	COI	S	8.43
13	-	-	141	[141,157]	-	COI	S	10
14	-	-	149	[149,157]	-	COI	S	10
15	-	-	153	[149,153]	-	COI	U	2.15
16	-	-	151	[149,151]	-	COI	U	2.33
Total TSIM								52.1

Appendix H Published Papers

This appendix contains preprints of three published conference papers which summarize some of the main points in the thesis.

H.1. Statement of Authorship

Statement of Authorship

Title of Paper	Transient Stability Sensitivity Analysis of a Simplified Power System
Publication Status	☑ Published ☐ Accepted for Publication ☐ Submitted for Publication ☐ Unpublished and Unsubmitted work written in manuscript style
Publication Details	H.M. Tan, R. Zivanovic, "Transient Stability Sensitivity Analysis Of A Simplified Power System", Australian Universities Power Engineering Conference, Perth, Australia, 2007.

Principal Author

Name of Principal Author (Candidate)	Hui-Min Tan
Contribution to the Paper	Wrote and benchmarked the simulation model in MATLAB, generated and interpreted the data, wrote manuscript and acted as corresponding author.
Overall percentage (%)	90%
Certification:	This paper reports on original research I conducted during the period of my Higher Degree by Research candidature and is not subject to any obligations or contractual agreements with a third party that would constrain its inclusion in this thesis. I am the primary author of this paper.
Signature	Date: 17/11/2015

Co-Author Contributions

By signing the Statement of Authorship, each author certifies that:

i. the candidate's stated contribution to the publication is accurate (as detailed above);

ii. permission is granted for the candidate in include the publication in the thesis; and

iii. the sum of all co-author contributions is equal to 100% less the candidate's stated contribution.

Name of Co-Author	Rastko Zivanovic
Contribution to the Paper	Supervised research progress and helped in manuscript evaluation.
Signature	Date: 18/11/15

Statement of Authorship

Title of Paper	Integrating the SIME Method with Standard Time Domain Simulation Software to Search for Transient Stability Limits
Publication Status	☑ Published ☐ Accepted for Publication ☐ Submitted for Publication ☐ Unpublished and Unsubmitted work written in manuscript style
Publication Details	H.M. Tan, D.Vowles, R. Zivanovic, "Integrating the SIME Method with Standard Time Domain Simulation Software to Search for Transient Stability Limits", Australian Universities Power Engineering Conference, Sydney, Australia, 2008.

Principal Author

Name of Principal Author (Candidate)	Hui-Min Tan
Contribution to the Paper	Designed the Enhanced Binary-SIME limit searching algorithm, generated, analysed and benchmarked the simulation data, wrote manuscript and acted as corresponding author.
Overall percentage (%)	80%
Certification:	This paper reports on original research I conducted during the period of my Higher Degree by Research candidature and is not subject to any obligations or contractual agreements with a third party that would constrain its inclusion in this thesis. I am the primary author of this paper.
Signature	Date: 17/11/2015

Co-Author Contributions

By signing the Statement of Authorship, each author certifies that:

i. the candidate's stated contribution to the publication is accurate (as detailed above);

ii. permission is granted for the candidate in include the publication in the thesis; and

iii. the sum of all co-author contributions is equal to 100% less the candidate's stated contribution.

Name of Co-Author	Rastko Zivanovic
Contribution to the Paper	Supervised development of the algorithm, helped in manuscript evaluation.
Signature	Date: 18/11/15

Name of Co-Author	David Vowles
Contribution to the Paper	Assisted with design development of the novel Enhanced Binary-SIME limit searching algorithm, interpretation and benchmarking the data, and manuscript evaluation
Signature	Date: 24/11/15

Statement of Authorship

Title of Paper	Implementation of the Enhanced Binary-SIME method for Finding Transient Stability Limits with PSS®E
Publication Status	☑ Published ☐ Accepted for Publication ☐ Submitted for Publication ☐ Unpublished and Unsubmitted work written in manuscript style
Publication Details	H.M. Tan, D. Vowles, R. Zivanovic, "Implementation of the Enhanced Binary-SIME method for Finding Transient Stability Limits with PSS®E", IEEE PowerTech Conference, Bucharest, Romania, 2009.

Principal Author

Name of Principal Author (Candidate)	Hui-Min Tan
Contribution to the Paper	Implemented the Enhanced Binary-SIME limit searching algorithm using the PSS/E® software, generated, analysed and benchmarked the simulation data, wrote manuscript and acted as corresponding author.
Overall percentage (%)	80%
Certification:	This paper reports on original research I conducted during the period of my Higher Degree by Research candidature and is not subject to any obligations or contractual agreements with a third party that would constrain its inclusion in this thesis. I am the primary author of this paper.
Signature	Date: 17/11/2015

Co-Author Contributions

By signing the Statement of Authorship, each author certifies that:

i. the candidate's stated contribution to the publication is accurate (as detailed above);

ii. permission is granted for the candidate in include the publication in the thesis; and

iii. the sum of all co-author contributions is equal to 100% less the candidate's stated contribution.

Name of Co-Author	Rastko Zivanovic
Contribution to the Paper	Supervised development of the software, helped in manuscript evaluation.
Signature	Date: 18/11/15

Name of Co-Author	David Vowles
Contribution to the Paper	Assisted with the software design, data analysis and benchmarking, and review of manuscript.
Signature	Date: 24/11/15.

TRANSIENT STABILITY SENSITIVITY ANALYSIS OF A SIMPLIFIED POWER SYSTEM

Hui-Min Tan and Rastko Zivanovic

The University of Adelaide

School of Electrical & Electronic Engineering

North Terrace Campus

Adelaide, 5005, Australia

Abstract

There are many limits in power system operation however transient stability poses some of the most stringent limitations. Typical measures to assess transient stability, such as critical fault clearing time, provide some indication of whether or not a power system will remain stable after a large disturbance. However, these measures do not give any further insight into how system parameters should be regulated to ensure adequate system security. This paper explores the sensitivity of (a) power transfer-limits and (b) transient stability margins to variations in a number of system parameters for a single machine infinite bus system. Several alternative stability margins are considered.

Index Terms—Electric power systems, transient stability assessment, sensitivity analysis

I. INTRODUCTION

Existing power system networks are large complex structures with a large number of interconnections. Power systems are exposed to various contingencies which may lead to steady-state, transient or dynamic system instability. A system disturbance, such as a transmission line fault, may cause a loss of synchronism between machines in the system leading to transient instability. The operation of many power systems is restricted by transient stability limits. Typical measures used to assess transient stability, such as critical fault clearing time, provide some indication for whether or not a power system will remain stable after a large disturbance. However, these measures do not give any further insight into how system parameters, such as interconnector-transfer levels, generator outputs or system load should be regulated to ensure adequate system security. For system operators, knowledge of the sensitivity of operating limits to controllable system parameters will reduce their dependence on trial and error analysis and will augment operator experience [1]. Such information could enable existing power systems to operate closer to limits, increasing power transfer capacity and potentially defer expensive investments in infrastructure.

Based on simplified and idealized models this paper explores the sensitivity of:

(i) Power transfer-limits (Plimit) to variations of the parameters listed in Table 1; and

(ii) a number of alternative measures of transient stability margin to variation in initial generator power output (Pm) and also to the parameters listed in Table 1.

The paper discusses:

(i) Advantages and disadvantages of the transient stability margins, as revealed in this investigation; and

(ii) the relative importance of the factors in Table 1 in determining the transfer limit of the system.

TABLE 1 THE SYSTEM PARAMETERS THAT ARE INVESTIGATED BY SENSITIVITY ANALYSIS

Line impedance (X)	Fault type
Machine impedance (X'd)	Fault location
Infinite bus voltage (EB)	Fault clearance method
Generator terminal voltage (Vt)	Idealized automatic voltage regulator (AVR)
Fault clearing time (tc)	Idealized Static Var Compensator (SVC)
Machine inertia (H)	

II. TRANSIENT STABILITY ASSESSMENT

In this paper the equal area criterion and time domain simulations are used to assess the transient stability of a lossless single machine infinite bus (SMIB) system. The reduced network admittance matrix is used to represent the network for the purpose of interfacing with the controllable current sources representing the machines and other dynamic devices in the system. These concepts are explained in the following sections.

A. SMIB System

The system under investigation is shown in Figure 1 where the generator is represented by a classical machine model. The classical machine is based on the following assumptions [2, 3]:

a) Mechanical power input is constant
b) Machine losses, saturation and saliency are neglected
c) Field flux linkages are assumed to remain constant in the short period following a disturbance. As a result the machine can be represented as a constant voltage behind the transient reactance.

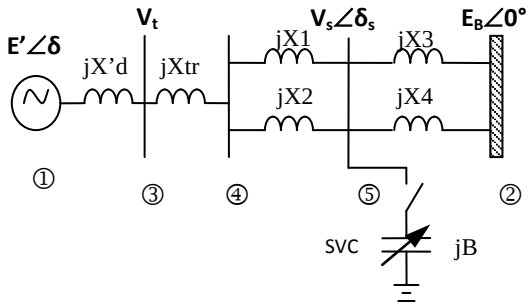

Figure 1 SMIB system: A simplified power system

The SMIB system represents a single generator delivering power to a large system. The large system is represented by an infinite bus - an ideal voltage source that maintains constant magnitude, phase and frequency. Parameter values for this system are listed in Tables 2 and 3. In transient stability studies the rotor dynamics for the machine are described by the swing equation [2]:

$$2H\omega\frac{d\omega}{dt} = P_m - P_e \;,\; \frac{d\delta}{dt} = \omega_{syn}(\omega - 1) \qquad (1)$$

where H is the machine inertia constant,
$\omega_{syn} = 2\pi f_0$ where f_0 is the nominal system frequency,
ω is the per-unit angular velocity of the rotor,
δ is the rotor angle (in radians),
P_m is the per-unit mechanical power supplied by the prime mover (minus mechanical losses) and
P_e is the per-unit electrical power output from the generator.

B. Reduced Admittance Matrix Representation of the network

The system of Figure 1 can be represented by the nodal network equations, partitioned so as to separate buses connected to current sources from passive nodes:

$$\begin{bmatrix} Y_{TT} & Y_{TN} \\ Y_{NT} & Y_{NN} \end{bmatrix}\begin{bmatrix} V_T \\ V_N \end{bmatrix} = \begin{bmatrix} I_T \\ 0 \end{bmatrix} \qquad (2)$$

where, for a system with a total of n nodes and n_i nodes to which current sources are connected,
V_T is the n_i vector of voltages at buses to which current sources are connected,
V_N is the (n - n_i) vector of voltages at the remaining buses, and
I_T is the n_i vector of injected currents.
From equation (2) the following relationships can be deduced:

$$\begin{aligned} V_N &= -(Y_{NN})^{-1}Y_{NT}V_T \\ I_T &= (Y_{TT} - Y_{TN}(Y_{NN})^{-1}Y_{NT})V_T \\ &= \hat{Y}_{TT}V_T \end{aligned} \qquad (3)$$

where $\hat{Y}_{TT}$ is the reduced network admittance matrix.
The electrical power output of the ith current source (e.g. machine, infinite bus or SVC) is then:

$$p_{ei} = \mathrm{Re}[V_{Ti}I_{Ti}^{*}] \quad i = 1, 2, \ldots n_i \qquad (4)$$

In the event of a transient disturbance the network topology changes as the result of the application of the fault and the network switching operations required to clear the fault. Thus, three network states are identified for which different nodal admittances apply: $\hat{Y}_{TT(pre)}$, $\hat{Y}_{TT(fault)}$ and $\hat{Y}_{TT(post)}$. For a lossless SMIB system in which the machine is connected to node 1 and the infinite bus is connected to node 2, the generator power output is (4):

$$P_{e1} = \hat{b}_{12}E'E_B\sin\delta \qquad (5)$$

where E' is the internal generator voltage and the transfer susceptance $\hat{b}_{12} = \mathrm{Im}[\hat{Y}_{TT}(1,2)]$ changes depending on the network state.

C. Equal Area Criterion for Stability

The equal area criterion is used to determine if a SMIB system is stable following a disturbance, without solving the system state-equations (1). Stability is established by using the power-angle curve to determine if the kinetic energy absorbed by the rotor during the fault can be transferred to the system following fault clearance, so as to return the rotor to synchronous speed.

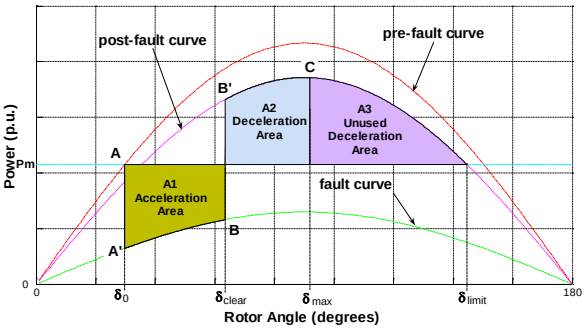

Figure 2 A power-angle curve demonstrating the Equal Area Criterion

Figure 2 describes the power-angle response for a disturbed SMIB system. After the fault is applied (A→A') the net torque is positive and the rotor accelerates and the rotor angle increases (A'→B'), until the fault is cleared at $\delta = \delta_{clear}$ (B→B'). After fault clearance the net torque is negative which causes the rotor to decelerate, although the rotor angle will continue to increase to the maximum value δ_{max} (B'→C) at which time the rotor speed again returns to synchronous. It can be shown that the point C occurs when the deceleration area A2 is equal to the acceleration area A1. Stability requires that $P(\delta_{max}) \geq P_m$ or equivalently $\delta_{max} \leq \delta_{limit}$.

The clearing angle is dependent on the fault clearing time, t_c. For a three phase fault δ_c is given by:

$$\delta_c = \frac{\omega_{syn}P_m}{4H}t_c^{\,2} + \delta_0 \,. \qquad (6)$$

In general, if the fault clearing time is delayed the clearing angle will rise, causing an increase in both the acceleration and deceleration areas and in δ_{max}. The critical fault clearing time, denoted t_{crit}, is the longest fault duration allowable for stability for a given fault type and location. The clearing angle corresponding to t_{crit} is termed the critical clearing angle, δ_{crit}.

D. Time Domain Responses

Some time domain responses, of the SMIB system in Figure 1, are examined as the initial steady-state power transfer (P_m) is increased from a stable to critically stable and finally to an unstable level. The system is analysed with the parameters in Table 2. It has a power transfer limit of Plimit = 1.024 p.u.

TABLE 2 BASE PARAMETERS

X'_d = 0.3 p.u.	H = 3.0 p.u.-s	X_{tr} = 0.1 p.u.
V_t = 1.0 p.u.	t_c = 0.18 s	f_0 = 50 Hz
3 phase fault	Fault Location (node): 4	
Manual Excitation	E_B = 1.0 ∠0° p.u	
X_1 = X2 = X3 = X4 = 0.1 p.u.		
Fault clearance: Disconnect X1		

As the initial steady-state level of power transfer increases, the initial value of E' must be increased as shown in Figure 3 in order to maintain the generator terminal voltage V_t fixed at its nominal set point value of 1.0 pu. At a given transfer level, the internal machine voltage E' is assumed to be constant preceding, during and following a disturbance.

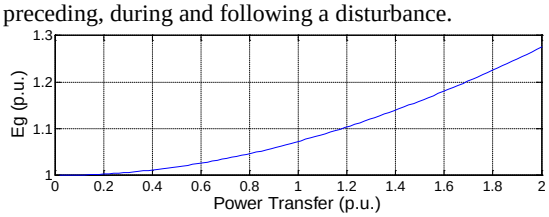

Figure 3 The internal machine voltage versus the power transfer level

Figure 4 shows the responses of the rotor-angle, rotor-speed and electrical power output from the generator for power transfers of 80% (stable), 100% (critically stable) and 120% (unstable) of the transfer-limit.

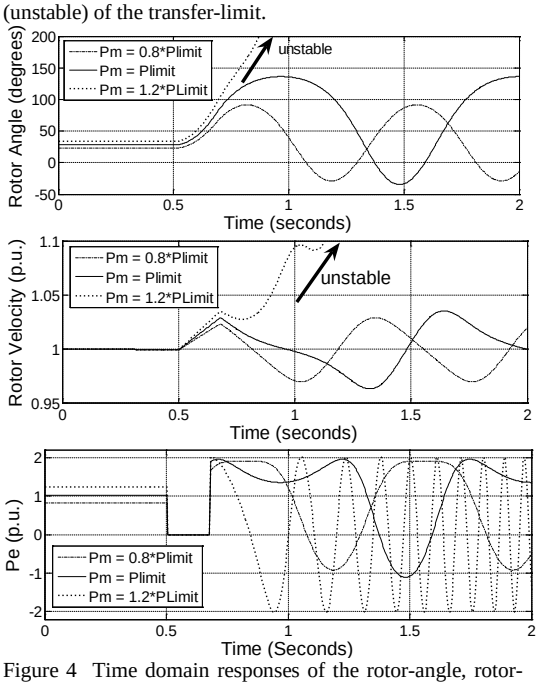

Figure 4 Time domain responses of the rotor-angle, rotor-speed and electrical power output of the generator

III. STABILITY MARGIN MEASURES

This section provides a discussion of each of the stability margins considered for sensitivity analysis in this paper. The variation of each margin with respect to changes in power transfer level is plotted for the SMIB system of Figure 1, with the base parameters specified in Table 2.

A. Critical Clearing Time, K_{time}

The critical clearing time margin is defined as [4]:

$$K_{time} = t_{crit} - t_{act} / t_{crit} \quad (7)$$

where t_{crit} and t_{act} are the critical and actual clearing times, respectively.

t_{crit} may be calculated by a step-by-step simulation until δ_{crit} is reached. Figure 5 shows the sensitivity of K_{time} to power-transfer for the base case. The K_{time} criterion is able to provide useful information for both stable and unstable operating points. The sensitivity of K_{time} to the power transfer level appears to vary in an approximately linear manner if the system is stable.

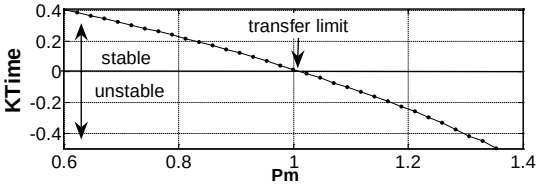

Figure 5 The sensitivity of Ktime to power transfer

B. Unused Deceleration Area, K_{area}

The unused deceleration area margin is defined as [4]:

$$K_{area} = \frac{Unused \quad deceleration \quad area}{Total \quad available \quad deceleration \quad area}$$

If the system is unstable K_{area} = 0. (8).

From Figure 2 the unused deceleration area is A3, and the total available deceleration area is A2 + A3. Figure 6 shows the sensitivity of the K_{area} criterion to the power transfer level. The K_{area} margin can provide information on how close a stable system is to the power transfer limit. As the power transfer limit is approached K_{area} becomes more sensitive. Since K_{area} is a non-linear function of Pm, extrapolation to estimate the transfer-limit is not straight-forward.

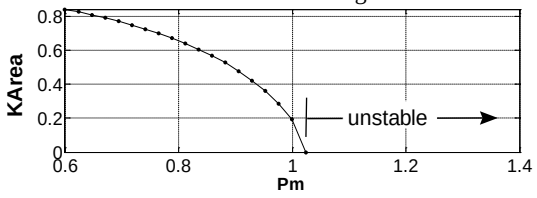

Figure 6 The sensitivity of K_{area} to power transfer

C. Wu's Stability Margin, K_{wu}

For a transiently stable system, where the rotor angle exceeds 90°, K_{wu} is defined as the deceleration power at the maximum rotor angle [5]. K_{wu} is simple to compute. For its defined region of application it is simply the deceleration power at the maximum swing angle. A disadvantage to K_{wu} is that it provides information for a reduced range of power transfer. The non-linear sensitivity of K_{wu} to the power transfer level means it is difficult to extrapolate data to determine the transfer limit. Figure 7 shows the sensitivity of K_{wu} to the power transfer level.

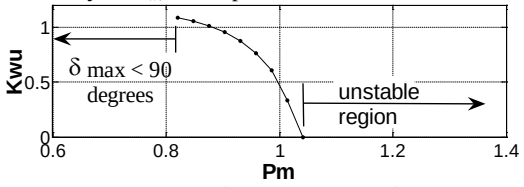

Figure 7 The sensitivity of K_{wu} to power transfer

D. Deficit Energy Margin, $K_{deficit}$

For an unstable system the deficit energy margin is defined as:

$$K_{deficit} = AccelerationArea - DecelerationArea$$

and for a stable system it is:

$$K_{deficit} = -(Unused\ Deceleration\ Area) \quad (9)$$

The acceleration area is A1 as described in Figure 2. The $K_{deficit}$ margin is applicable in both the stable and

unstable regions of operation. The $K_{deficit}$ criterion appears to vary linearly with power transfer as shown in Figure 8.

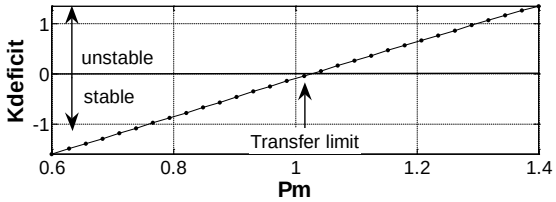

Figure 8 The sensitivity of $K_{deficit}$ to power transfer

E. Sensitivity Studies of the SMIB System

The margin measures described in section 3 are used to investigate the sensitivity of the power transfer limit to the parameters and factors described in Table 3. The results of the sensitivity studies are presented in the order of the system parameters and factors that are described in Table 3.

TABLE 3 PARAMETER VALUES AND OTHER FACTORS INVESTIGATED IN THE SENSITIVITY ANALYSIS

Machine and System Parameters			
$X=X_1=X_2=X_3=X_4$: 0.1 to 0.5 p.u.			
X'_d:	0.2 to 0.5 p.u.	t_c:	0.05 to 0.3 s
E_B:	0.9 to 1.1 p.u.	H:	2.0 to 8.0 p.u.-s
Vt:	0.9 to 1.1 p.u.		
Fault type and location			
Fault type: 3 Phase Fault Line to ground Double line to ground		Fault clearance: X1 disconnected X1 and X3 disconnected No lines switched	
Fault location (node): 4, 5			
Manual Excitation or AVR			
SVC connected or disconnected			

The following method is used to relate system parameters to power transfer and transfer-limits:

1. For a given system calculate the stability margin for a range of P_m values.
2. Plot the stability margin as a function of P_m.
3. Use this plot to deduce the power-transfer limit.
4. Repeat steps 1 – 3, varying the target parameter.
5. Plot P_{limit} as a function of the target parameter.

F. Sensitivity to Machine and System Parameters

The sensitivity results for the machine and system parameters are shown in Figures 9 and 10. From Figure 9a) and 10a) a higher transmission line impedance decreases the transfer limit. As line impedance increases the stability margin also becomes less sensitive to power transfer. The machine impedance, shown in Figure 9b), has a similar effect on the system stability.

Figure 9c) shows that the transfer limit is relatively insensitive to the infinite bus voltage, and a higher value of E_B yields a lower transfer limit.

Increasing the generator terminal voltage, raises the power transfer limit. From Figure 9d) the transfer limit increases by about 0.3 p.u. due to a 0.2 p.u. increase in V_t. It is evident that the generator terminal voltage set point has a significant influence on the transfer capability and transient stability of the system.

Figures 9e) and 10b) show that reducing the fault clearing time significantly increases the power transfer limit. Figure 10c) reveals that larger machine inertia will allow higher transfer capability.

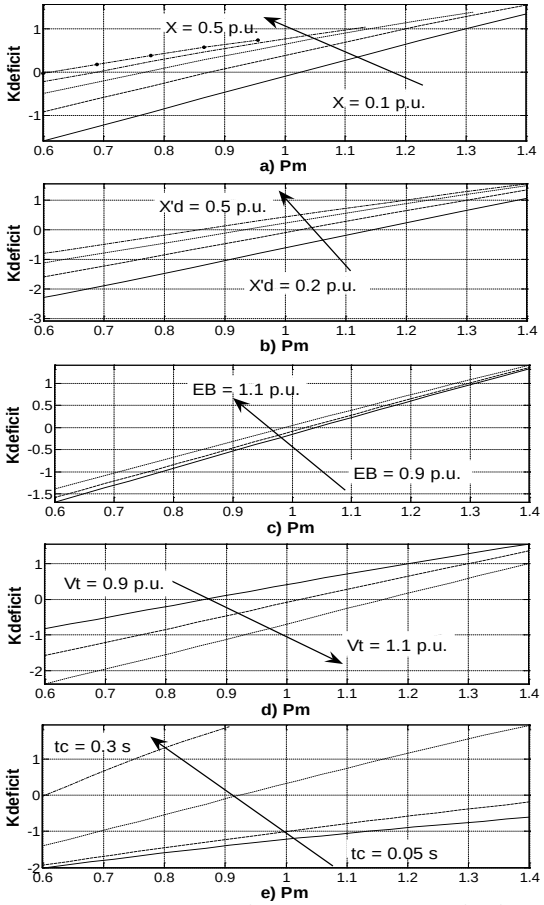

Figure 9 The sensitivity of $K_{deficit}$ to power transfer for variations in a) transmission line impedance, b) machine impedance, c) infinite bus voltage, d) generator terminal voltage, and e) fault clearing time.

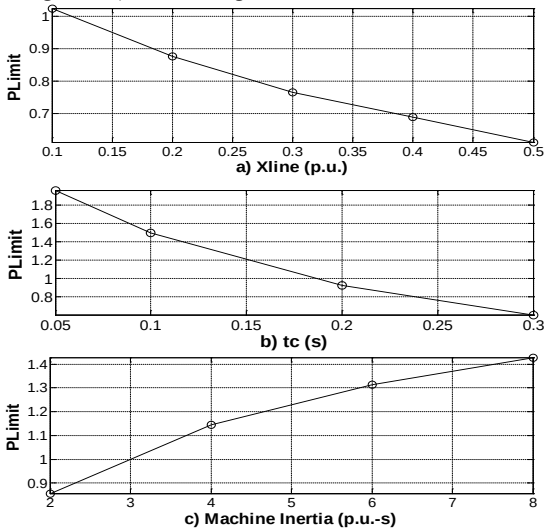

Figure 10 The sensitivity of PLimit to: a) line impedance, b) fault clearing time and c) machine inertia.

G. Sensitivity to Fault Type and Location

The effects of the fault type and location on the transfer-limit are shown in Figure 11a). This figure shows that the 3 phase fault is significantly more onerous than a 2 phase-ground fault, which is the next most severe type of fault. In the investigation of fault type, the fault at node 4 is represented by the appropriate connection of per-unit positive (Z1),

negative (Z2) and zero (Z0) sequence impedances Z1 = Z2 = j0.08, and Z0 = j0.0732, and the fault at node 5 by Z1 = Z2 = j0.045, and Z0 = j0.0868. For both cases X = 0.1 p.u and the SVC is disconnected.

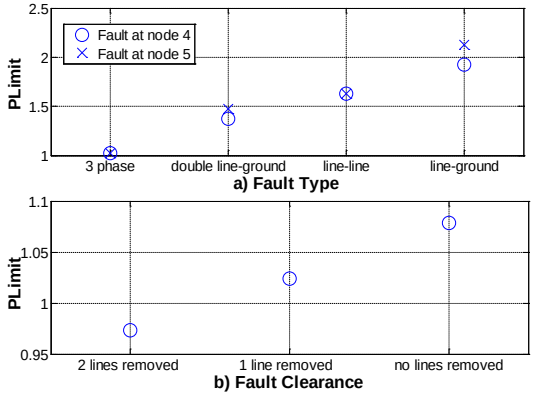

Figure 11 The sensitivity of PLimit to: a) the fault type where the fault location is varied and b) the post-fault network.

For system planning purposes it may be too pessimistic to require stable operation in the event of a 3 phase fault, which is expected to occur extremely rarely [6]. For unbalanced faults moving the fault location away from the machine terminals tends to reduce the transfer impedance between the machine and infinite bus during the fault. This reduces the acceleration area, thus enhancing stability. It is interesting to note that for a line-to-line fault that occurs at nodes 4 and 5 the transfer limits are the same. This is because the equivalent fault transfer impedances for a line-to-line fault at node 4, and node 5, are virtually identical.

By partitioning the interconnecting line between the machine and infinite bus it is only necessary to disconnect a segment of the interconnector when clearing a line fault. Thus the post-fault transfer impedance is lower, which increases the deceleration area and thereby stability. The variation of the transfer capability with respect to the means of fault clearance is reflected in Figure 11b).

H. Sensitivity to AVR

Typically, modern machines are equipped with high gain, fast acting AVRs which act to automatically regulate the terminal voltage of the machine, and rapidly increase field flux linkages during fault conditions. To accurately represent the performance of a machine equipped with an AVR it is necessary to model the field dynamics of the machine and the dynamic performance of the AVR. However, for conceptual purposes an idealized AVR is represented in which the machine terminal voltage is held fixed at its set point before, during and following the fault by varying the machine internal voltage E' without restriction.

Figure 12 compares the power-angle characteristics of a system with (i) the idealized AVR and (ii) manual excitation. The idealized AVR increases the available deceleration area which implies an increase in the transfer capability of the system. It should be noted that a practical AVR will cause a smaller increase in the transfer limit.

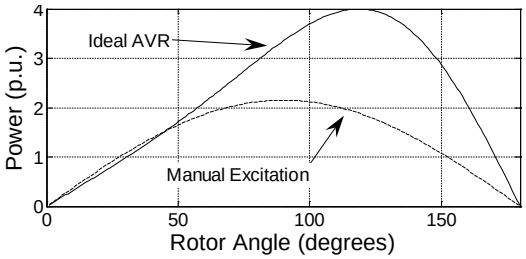

Figure 12 The effect of an ideal AVR on the power-angle curve of the base system

I. Sensitivity to SVC

1) Modelling of Idealized SVC

An idealized SVC is modelled as a current source that is constrained by the requirements $V_S = V_{ref}$ and $P_s = 0$. It injects reactive power, without restriction, to maintain the voltage V_s, in Figure 1, fixed at its specified set point before, during and after a fault is applied. For a lossless SMIB system with SVC connected at node 5, the generator power output is (4):

$$Pe1 = \hat{b}_{12} E' E_B \sin\delta + \hat{b}_{13} V_S E' \sin(\delta - \delta_S) \quad (10).$$

The transfer susceptance between the generator and SVC, $\hat{b}_{13} = \mathrm{Im}[\hat{Y}_{TT}(1,3)]$, changes according to the network state.

2) Effect of Idealized SVC on Transfer Limit

Figure 13 shows the effect of connecting an idealized SVC at node 5 on the power-angle curve, where the line impedance X = 0.5 p.u. and V_{ref} = 1.05 p.u. It demonstrates that the SVC increases the available deceleration area and thereby the transfer limit.

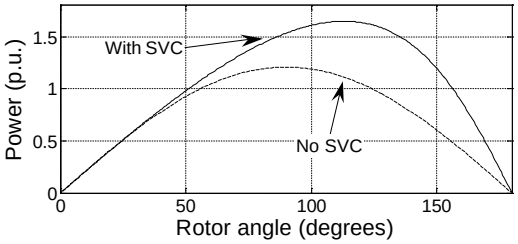

Figure 13 The effect of the idealized SVC on the power-angle curve

IV. CONCLUSION

This paper employs simple and idealized models to explore the sensitivity of the transient-stability of a SMIB system to a variety of factors. The equal area criterion is used as a basis for stability analysis and for the several transient-stability margin criteria which are considered. A motivation for examining various margin criteria is to obtain insight into whether it may be feasible to use them for a variety of purposes including controller design and accelerating the search for transfer-limits in practical systems.

V. REFERENCES

[1] Pavella, Mania, 'Power System Transient Stability Assessment - Traditional vs Modern Methods', Control Engineering Practice, Volume 6, Issue 10, October 1998, pp. 1233-1246.

[2] P. Kundur, 1994, Power System Stability and Control, McGraw-Hill, USA.

[3] Y.C. Choo, M.A. Kashem, M Negnevitsky, 'Transient Stability Assessment of a Small Power System Subjected to Large Disturbances', paper presented at

AUPEC 2006, 10 – 13 December, Melbourne, Victoria, Australia.
[4] J. Machowski, J. Bialek, J. Bumby, 1997, Power System Dynamics and Stability, John Wiley & Sons, England.
[5] Z.Q. Wu, Y.N. Wang, H.H. Chen, W.W. Tang, L.Q. Pan, 'Transient Stability Sensitivity Analysis', Electric Power Components and Systems, Volume 33, Issue 3 December 2004, pages 247 – 261.
[6] Australian Energy Market Commission, "National Electricity Rules", Version 15, 16/8/07

H.3. Integrating SIME with the TDS Software Paper

This paper entitled "Integrating the SIME Method with Standard Time Domain Simulation Software to Search for Transient Stability Limits" was presented at the Australian Universities Power Engineering Conference in Sydney, Australia, in December 2008.

Integrating the SIME Method with Standard Time Domain Simulation Software to Search for Transient Stability Limits

H.M. Tan and R. Zivanovic
The University of Adelaide
School of Electrical & Electronic Engineering
North Terrace Campus
Adelaide, 5005, Australia

***Abstract*- The Single Machine infinite bus Equivalent (SIME) method provides a means of estimating transient stability margins and for accelerating the search for transient stability limits for multi-machine power systems. This paper presents the SIME algorithm, with particular focus on how it may be integrated with a standard time domain simulation program to search for stability limits. Novel enhancements aimed at increasing the robustness of the SIME algorithm are proposed. The enhanced algorithm is applied to search for the critical clearing time (CCT). The binary-search method is compared with the hybrid Binary-SIME method in the search for CCTs.**

I. INTRODUCTION

The Single Machine Infinite bus Equivalent (SIME) method [1] provides a robust and flexible approach to estimating transient stability margins and predicting transient stability limits for multi-machine power systems. It combines the merits of time-domain methods and the Equal Area Criterion (EAC) [2]. The key feature of SIME is that it employs fully detailed device and controller models in its analysis and does not make any simplifying assumptions. The SIME method is based on the derivation of the response of an equivalent One Machine Infinite Bus (OMIB) system from the transient responses of all the machines in a fully detailed model of a multi-machine system. Determination of stability margins is based on an analysis of the responses of the OMIB system. The SIME method does not require the determination of the parameters of the equivalent OMIB system, apart from its equivalent inertia constant. Thus, SIME has the ability to accurately analyse arbitrarily complex power system models. SIME has the capability to identify both first-swing and multi-swing stability limits. A benefit of SIME for limit searching is that it is peripheral to the time-domain simulation (TDS) software and therefore has the potential to be integrated with commonly used commercial transient stability packages without requiring access to, or modification of, the TDS source code. The limit and margin information it provides also make it useful to applications such as sensitivity analysis and control.

This paper gives a systematic review and proposes a potential enhancement of the standard SIME algorithm. In the proposed improvement a binary-search procedure is incorporated to efficiently and robustly identify suitable starting scenarios for the SIME procedure. Furthermore, a method of detecting the failure of the SIME procedure to converge to the transient stability limit and of then switching to a binary-search procedure to complete the limit search is proposed. The SIME based algorithm is applied to search for critical clearing times (CCT) and power transfer limits (PTL). Particular emphasis is placed on integrating the method with a standard TDS program. A comparison between the performance of the binary-search and the enhanced Binary-SIME methods is made.

II. THE BINARY-SEARCH METHOD

A binary-search for the transient stability limit involves assessing the stability of a fully detailed multi-machine system model at the selected upper and lower search bounds. The initial bounds on the binary-search for the CCT are selected by the user (e.g. in Fig. 1 the initially selected search bounds are 0ms and 500ms). It is assumed that the system is stable at the lower bound and unstable at the upper bound. Thus the CCT exists in between these bounds. If this is not the case then the search will fail and appropriate corrective action is required (i.e. the upper bound must be increased if it is found to be stable or a new system scenario will need to be selected if the lower bound is unstable). The binary-search proceeds iteratively. TDS is used to determine the stability of the system at the midpoint of the current search bounds. Unstable scenarios are detected by running the TDS until the maximum angular deviation between any 2 system machines exceeds 360°. Stable scenarios are simulated for a full integration period (i.e. 10 seconds). If the current test point is stable then it becomes the new lower bound and the previous upper bound is retained for the next iteration of the search. Conversely if the current test point is unstable it becomes the new upper bound and the lower bound is retained. This process continues until the difference between the search bounds is within the search tolerance. In this paper the binary-search pursues the limit to a tolerance of 2ms. The limit is the last identified lower bound.

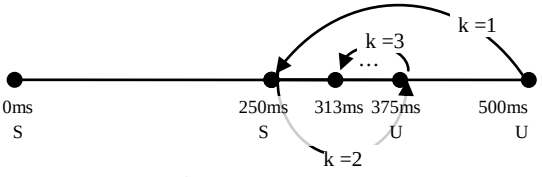

Figure 1. An example of the binary-search iteration procedure. S indicates 'stable', and U indicates 'unstable' cases. The indices indicate the search iteration number.

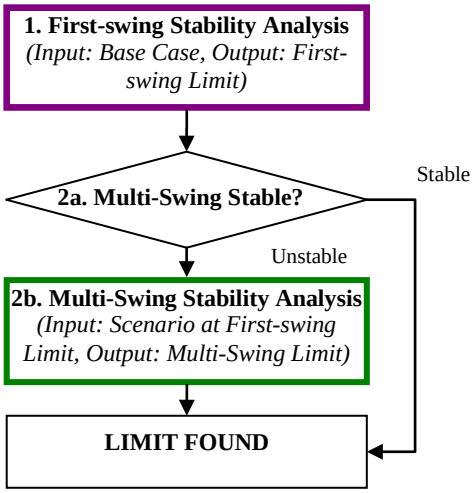

Figure 2. Overview of the Binary-SIME limit search algorithm.

Table 1. Definitions of Abbreviations in the SIME flow chart of Fig 3

Abbreviation	Meaning
OMIB	One Machine Infinite Bus
PT	Power Transfer
CT	Clearing Time
PTL	Power Transfer Limit
CCT	Critical Clearing Time
MG	Machine Group information
k	Search iteration number
Scenario	System model + disturbance
TDS	Time domain simulation
δ	Matrix of machine rotor angles
w	Matrix of machine rotor velocities
M	Matrix of machine inertia constants
t	Time vector
Pe	Matrix of machine electrical power outputs
Pm	Matrix of machine mechanical power inputs
δ_OMIB	OMIB rotor angle vector
Pa_OMIB	OMIB accelerating power vector
η	Stability margin

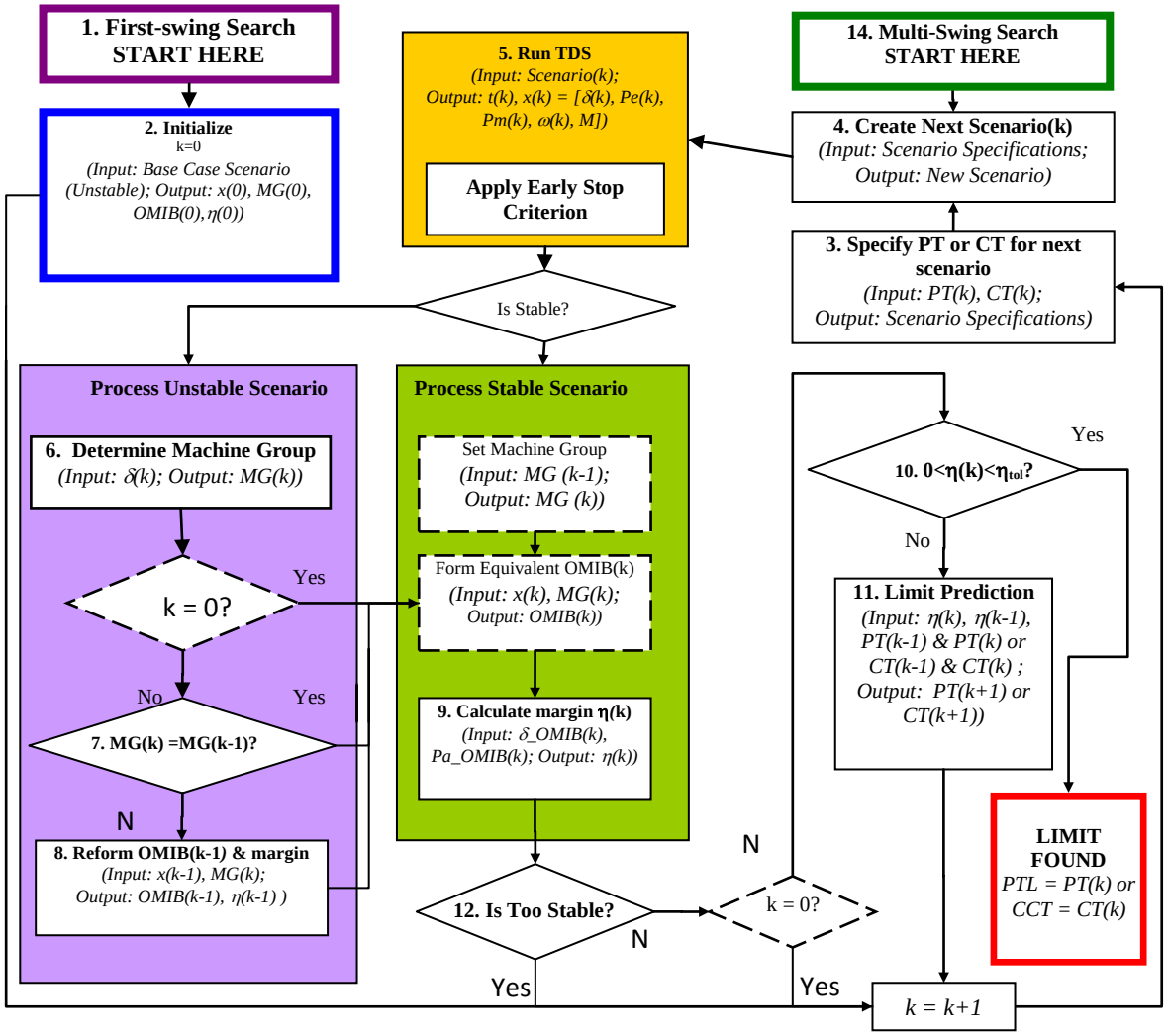

Figure 3. Core elements of the Binary-SIME limit search algorithm. The boxes in dashed lines are specific to the multi-swing search only. Symbols and abbreviations are outlined in Table 1.

III. THE BINARY-SIME SEARCH

1. Overview (Fig. 2)

The Binary-SIME search for transient stability limits combines the best features of the SIME and binary-search methods. A significant advantage of the SIME method is its capacity to reduce the total search simulation time. This is achieved by applying first-swing early stop criteria for transient stability assessment, as described later, and by using the approximately linear relationship between the SIME stability margins and the CCT or PTL to achieve faster convergence to the limit. The binary-search component ensures the success of the limit search by selecting a suitable search starting point and intervening when the SIME search fails to converge.

The two principle stages to the Binary-SIME approach are the first-swing stability limit search (Fig. 2. step 1) and the conditional multi-swing stability limit search (Fig. 2 step 2b). The latter is required if TDS reveals that the system is multi-swing unstable at the first-swing stability limit (Fig. 2 step 2a). This paper focuses on the first-swing stability limit search. The procedure to perform a multi-swing limit search [1, 3] is reflected in Figs. 2 and 3.

2. Problem Definition

In the following sections the Binary-SIME method is demonstrated by application to the following example. In the system shown in Fig. 4 [2, 4] 400MW of power is transferred from area 1 to area 2. A 3 phase fault is applied to the node 7 end of the #1 circuit between nodes 7 and 8. The fault is cleared by de-energizing the circuit. Governors are not represented in the example. The objective is to determine the CCT for this case using the Binary-SIME search. The methodology can be extended to a search for the PTL. The test system parameters are given in the Appendix.

3. First-swing Stability Analysis (Fig. 2, 3)

The details of the first-swing stability limit search, in step 1 of Fig. 2, are given in the Binary-SIME search algorithm flow chart in Fig. 3. The search begins at step 1 of Fig. 3.

A. Initialization block (Fig. 3, 5)

The first-swing limit search is initialized by selecting a starting scenario with the necessary characteristics for the Binary-SIME search to proceed. Initialization occurs in Fig. 3 step 2 with details of the procedure given in Fig. 5. Binary-search steps are used to determine the starting scenario. For the example an initial clearing time (CT) of 500ms is chosen; it is assumed that the system is stable with a CT of 0ms. The latter assumption is expected to be correct in the vast majority of cases – however, if it is incorrect the algorithm will still succeed in identifying the fact that the system is inherently unstable.

A.1) Starting the Initialization Procedure (Fig. 5)

Initialization commences by loading the first scenario with the CT at the upper bound (Step 2.A). A criterion of the starting scenario is that it must be unstable (Step 2.C). A TDS (Step 2.B) is conducted and instability is detected by using the same criterion as is used by the binary-search. If the first scenario is stable then the CT is doubled (Fig. 5. step 2.D) and the TDS and stability test is repeated.

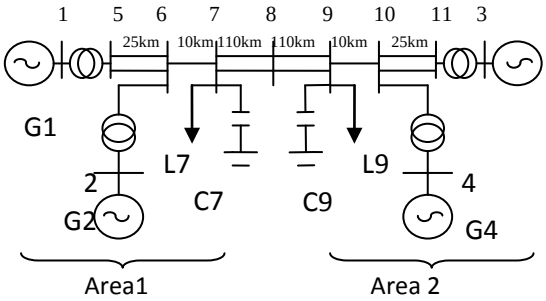

Figure 4. The 2-Area 4-machine test system.

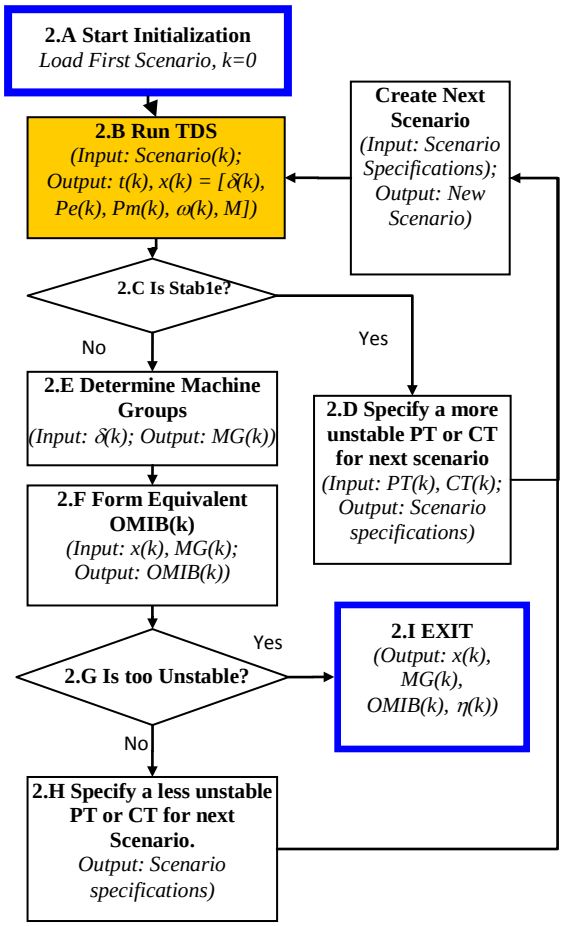

Figure 5. Flow chart of the initialization phase

A.2) Determining the Machine Groups (Fig. 5 step 2.E)

The SIME approach to transient stability assessment is based upon the proposition that loss of synchronism is caused by the irrevocable angular separation of a system into two machine groups (MGs) [1]. The MGs are determined from an unstable TDS at the instant when instability is identified. The steps to organise the system machines into these groups are [3]:

1. Sort the machine rotor angles into descending order;
2. Calculate the separation between adjacent angles in the ordered list;

3. Identify the maximum separation;
4. Split the system machines into 2 groups – the machines with angles above the maximum separation, and the machines below. This is demonstrated in Fig. 6.

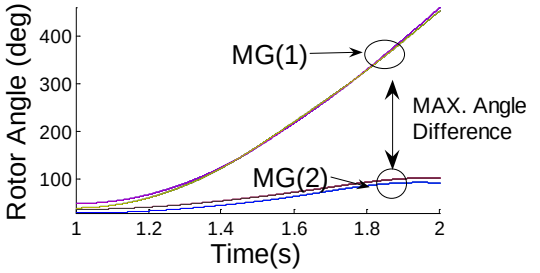

Figure 6. The machine groups are determined from the machine angle responses of an unstable scenario.

A.3) Forming the Equivalent OMIB responses (Fig. 5)

Once the MGs have been identified the responses of the OMIB are calculated by the Center of Angle (COA) equations described in [1, 3] (step 2.F). For assessment of the starting scenario the OMIB responses of interest are the electrical (P_e), mechanical (P_m) and acceleration (P_a) powers, where $P_a(t) = P_m(t) - P_e(t)$.

A.4) Selecting the initial search scenario (Fig. 5)

It is possible for an unstable scenario to be too unstable for use in the limit search (step 2.G). This occurs when the OMIB acceleration power does not become negative before the end of the first-swing, indicating that there is no capacity for the system balance to be restored after the fault. Fig. 7 shows that the CT of 500ms in the example is too unstable. A binary-search step is used to obtain the CT of (0 + 500)/2 = 250ms for the next scenario (step 2.H). However, TDS shows this scenario is stable and is thus unsuitable. The next scenario selected has a CT of (250 + 500)/2 = 375ms. Fig. 7 shows that the acceleration power of this unstable scenario drops below zero and is thus an acceptable starting point. The OMIB transformations of the machine angle (δ), speed deviation (ω) and P_e for the starting scenario are shown in Fig. 8.

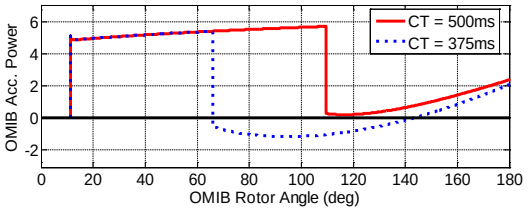

Figure 7. First-swing OMIB Acceleration-Power angle response of the test system.

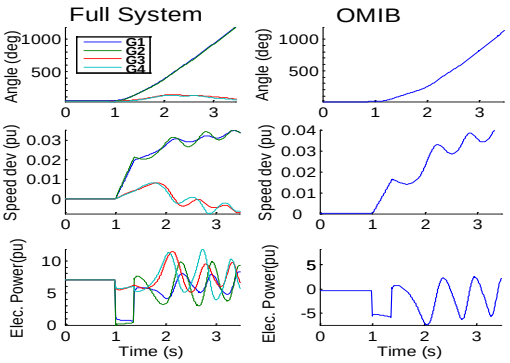

Figure 8. Full system and equivalent OMIB responses for rotor angle, speed deviation and electrical power, where the CT is 375ms

A.5) Calculate the first-swing unstable margin (Fig. 5)

The first-swing transient stability of a power system can be determined by assessing the OMIB acceleration-power angle curve (step 2.I), as shown in Fig. 9. By the EAC if the total deceleration area (A_{dec}) is less than the acceleration area (A_{acc}) then the system is unstable. Thus the unstable margin is defined as:

$$\eta_{uA} = -(A_{acc} - A_{dec}) = \int_{\delta_0}^{\delta_{lim}} P_a d\delta \quad (1)$$

where δ_0 and δ_{lim} are the respective OMIB rotor angles at steady state and the rotor angle limit (Fig. 9).

It is noteworthy that this interpretation of the unstable margin differs from the kinetic energy-based approaches of [1, 3] where it is assumed that the deficit deceleration area is also equal to

$$\eta_{uKE} = -\frac{1}{2} M \omega_{lim}^2 \quad (2).$$

Here M is the OMIB inertia coefficient [1, 3] and ω_{lim} is the OMIB generator speed when $\delta = \delta_{lim}$. However, analysis of (1) and (2) in the case of a lossless system reveals the following relationship

$$\eta_{uA} = \int_{\delta_0}^{\delta_{lim}} P_a d\delta = -\frac{1}{2\omega_0} M \omega_{lim}^2 = \frac{\eta_{uKE}}{\omega_0} \quad (3)$$

where $\omega_0 = 2\pi f_0$ and f_0 is the nominal system frequency. It should also be noted that (2) does not represent the kinetic energy or the change in kinetic energy of the rotor.

A.6) Normalization of margins

To make the calculated margin independent of the system capacity the margin is normalized by dividing it by the OMIB machine inertia constant, M [1].

B. Iterative Search Procedure (Fig. 3)

B.1) Calculating the second CT or PT (Fig. 3 step 3)

Following initialization, the binary-search is employed to calculate the next value of the search variable. For the example the next scenario has a CT of (375 + 250)/2 = 313ms.

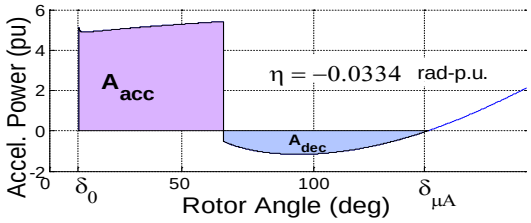

Figure 9. The power angle curve at a CT of 375ms. The acceleration and deceleration areas are shown.

B.2) Running the TDS with first-swing (in)stability early stop criteria (Fig. 3 steps 4-5)

For each successive search scenario a load flow and TDS are required. As mentioned in section II the TDS of an unstable scenario is stopped as soon as the angular difference between any two machines exceeds 360°. However by applying the SIME early stop criterion for instability even further reductions in simulation time can be gained. This early stop criterion requires the incorporation of the SIME method with the TDS software to calculate the equivalent OMIB response at each time step of the TDS. The criterion [1, 3] is that first-swing instability occurs when the OMIB responses $P_a(t_u) = 0$, $dP_a(t_u)/dt > 0$, and $\omega(t) > 0$ for $t > t_0$, where t_u is the time when the system loses synchronism and t_0 is the fault application time.

The criterion for the early determination of first-swing stability [1, 3] is that at the time t_r when the OMIB rotor-speed $\omega(t_r)=0$ the accelerating power must be negative (i.e. $P_a(t_r) < 0$). This assumes $\omega(t) > 0$ for $t_0<t<t_r$.

In the example the early stop instability criterion is applied to the scenario with a CT of 313ms. The case is unstable at a simulation time of 0.57s after the applied fault. This is less than the simulation time required by the binary-search method which runs until 1.27s after the applied fault.

B.3) First-swing Assessment of an Unstable Scenario (Fig. 3 steps 6-9)

The MGs are determined for the current unstable scenario using the algorithm in III.3.A.2. It is required that the MGs for successive unstable scenarios are identical (step 9). This is because the stability margins obtained from different machine groupings are unrelated and cannot be reliably combined to estimate the CCT or PTL. In the example the MGs do not change at any of the search steps. Loss of synchronism occurs between the areas 1 and 2 for the fault that has been considered. In the event that the MGs do change then the stability margin is recomputed for the previous (i.e. more unstable) scenario using the MGs of the current scenario (step 8). The unstable margin is (re)calculated as described in Section III.3.A.5 (step 9).

B.4) Determining convergence to the limit (Fig. 3 step 10)

The convergence test for the current scenario is $0<\eta(k)<\eta_{tol}$.

On some occasions the search may stall due to convergence failure. In such situations the next CT is determined by a binary-search step. Otherwise the next CT can be determined by linear prediction based on stability margins.

B.5) Limit Prediction (Fig. 3 step 11)

The CCT or PTL is predicted by linear inter(extra)polation using $\eta(k)$ and $\eta(k-1)$. The relationship of the first-swing margin to CT or PT is approximately linear. For the example, using the margins for the CTs of 313ms and 375ms the estimated CCT is 286ms, as demonstrated in Fig. 10.

B.6) First-swing Assessment of a Stable Scenario (Fig. 3)

Performing steps 3 to 5 of Fig. 3 the scenario with CT

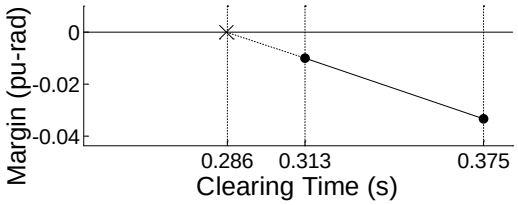

Figure 10. The margins for CTs 313ms and 375ms are used to predict the CCT.

at 286ms proves to be first-swing stable. Referring to Fig. 11 the stable margin is defined as:

$$\eta_s = \text{Unused deceleration area} = \int_{\delta r}^{\delta_{lim}} P_a d\delta \quad (4)$$

where δ_r is the OMIB return angle when the system has returned to synchronism and δ_{lim} is the estimated rotor-angle limit.

This corresponds to the area outlined in Fig. 11. It is not possible to calculate this area by using actual data; rather the unused deceleration area is approximated with a quadratic function [5]. It is possible for a scenario to be too stable, thus producing an unreliable margin measure (Fig. 3, step 12). In such circumstances the scenario should be aborted and a binary-search step applied to search for the next CT.

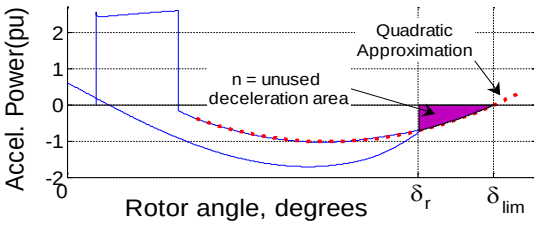

Figure 11. The OMIB power angle response for a stable case where CT = 286ms.

B.7) Determining the First-swing Stability Limit (Fig. 3)

The first-swing limit can be identified by iteratively repeating steps 3 to 11 of Fig. 3. In the example the CCT is found to be 290ms and TDS confirms it is multi-swing stable.

IV. RESULTS

The information that was calculated during the search in the example is summarized in Table 2, where k is the scenario number. The convergence of the two search methods is shown in Fig. 12. The benefits of the early stop criteria are evident – the simulation time for Binary-SIME limit search is 30.5 sec. which is about 15 seconds less than for the binary-search.

Table 2. Summary of the Binary-SIME CCT search for the example system.

k	CT (ms)	η(k-1) (rad-pu)	η(k) (rad-pu)	CCT(k) (ms)	TSIM (s)	Comment
1	500	-	-	-	1.99	Too unstable; binary step.
2	250	-	-	-	10.00	Initial step must be unstable; binary step.
3	375	-	-0.0334	-	2.21	1st SIME step
4	313	-0.0334	-0.0102	0.2857	1.88	2nd SIME step
5	286	-0.0102	0.0035	0.2928	2.13	3rd SIME step
6	292	0.0035	-0.0020	0.2898	2.32	4th SIME step
7	290	-0.0020	0.0006	0.2904	10.00	5th SIME step
				Total simulation time	30.52	

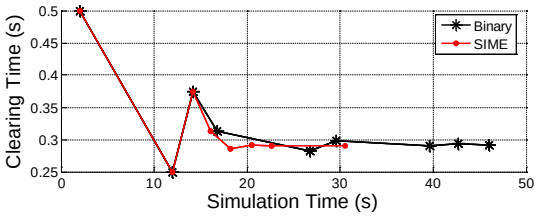

Figure 12. Convergence to the CCT by the binary-search and binary-SIME methods.

The multi-machine and OMIB time responses for the example at the CCT of 290 ms are shown in Fig. 13.

Table 3 provides a comparison of the simulation time and the CCT between the two search methods for a range of operating conditions and for scenarios with and without governors. It should be noted that the 0MW power transfer case, without governors, is 2nd-swing unstable. Thus the true CCT of 270ms which is determined by the binary-search is 7ms less than the first-swing stability limit of 277 ms determined by the binary-SIME search.

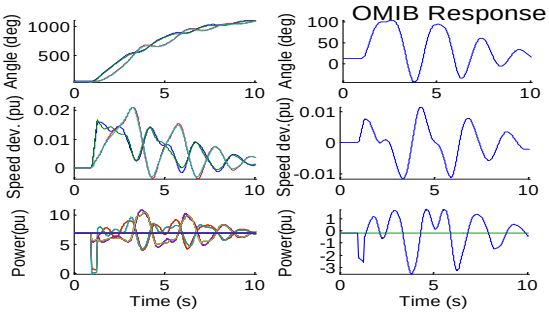

Figure 13. The multi-machine and OMIB system responses for the base case at the CCT of 290ms

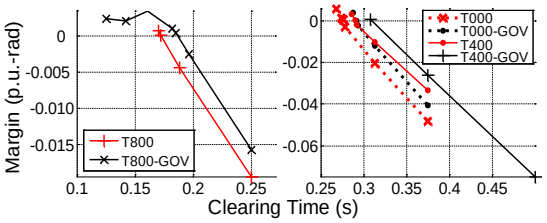

Figure 14. The margin versus clearing time characteristics

Fig. 14 displays the relationship between the margins and CTs as calculated during the Binary-SIME limit search. The approximately linear nature of the characteristics makes them suitable for linear prediction of the limit. For the investigated cases it is evident that the unstable margins will provide a reliable linear limit prediction. However, the stable margins show observable inconsistencies. The inconsistent stable margins indicate scenarios in the algorithm where the search stalled, and the binary method was required to obtain the next CT. Despite the extra iterations required Table 3 indicates a lesser simulation time for the Binary-SIME search.

Table 3. The total simulation time and CCT for the system under various operating conditions

Power Transfer (MW)	Governor Status	First-swing Limit Binary-SIME search		Standard Binary-search	
		TSIM (s)	CCT (ms)	TSIM (s)	CCT (ms)
0	OFF	(32.27)	(277)	44.59	270
	ON	30.56	292	53.25	292
400	OFF	30.52	290	46.05	290
	ON	15.54	308	61.09	308
800	OFF	19.48	172	60.72	171
	ON	23.2	185	68.14	185

Governors adjust the mechanical shaft power to restore the generator to synchronous speed. This effectively reduces the amount of acceleration and deceleration energies exchanged between system machines in the event of a disturbance. This is reflected in the higher CCTs when the governors are included in the test system.

V. CONCLUSION

The SIME method provides an approach to assessing transient stability margins for fully detailed multi-machine power systems. An equivalent OMIB system response is derived from the transient responses of all machines in the detailed system model. By applying the EAC to the equivalent system responses the transient stability margins and early stop criteria are defined. The stability margins exhibit an approximately linear relationship to the clearing time and to power transfer levels [6]. By linear inter(extra)polation of the stability margins from successive cases, the stability limit is estimated in an iterative process. First-swing early stop criteria are employed to minimize simulation times. If instability occurs during the first-swing then the simulation time required to identify the stability limit can be significantly less than that required if a binary-search algorithm is employed. The limit search and early stop criteria can be extended to multi-swing limits [1] although it is not explored in this paper.

This paper proposes incorporating binary-search steps within the basic SIME algorithm to enhance the

robustness and reliability of the limit search. Binary-search steps are used to initialize the search by selecting a suitable start scenario. It is also used to redirect the search, when convergence failure is detected. The algorithm is formulated in a way that allows relatively straight-forward incorporation into a standard TDS program.

A valuable by-product of the Binary-SIME limit search is the stability margin information. The margin data can be applied to sensitivity analysis to determine the relationship of the transient stability limits to various system parameters and factors [6]. The stable margins are estimated by quadratic extrapolation and are therefore prone to inaccuracy. However, others have investigated possible improvements [5]. In this paper some scenarios are classified as too unstable for margin calculation, however [1, 3] provide an alternative margin measure in these scenarios. These potential enhancements will be considered for inclusion in the Binary-SIME algorithm.

APPENDIX - EXAMPLE SYSTEM

The example is based on the system described in [2, 4]. Each generator includes an automatic voltage regulator and power system stabilizer. System loads are voltage dependent with the real and reactive parts having constant current and constant impedance characteristics respectively.

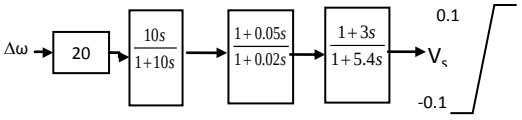

Figure A.1 Power System Stabilizer

TABLE A.1 SYSTEM PARAMETERS [2]

GENERATOR PARAMETERS (in p.u. on S_{RATED})			
X_d = 1.8	X_q=1.7	X_l=0.2	X'_d=0.3
X'_q=0.55	X''_d=0.25	X''_q=0.25	R_a=0.0025
T'_{d0}=8.0s	T''_{q0} = 0.05 s	T''_{d0}=0.03 s	T''_{q0}=0.05 s

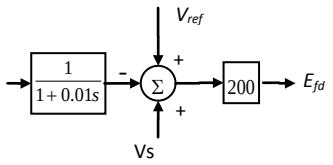

Figure A.2 Automatic Voltage Regulator

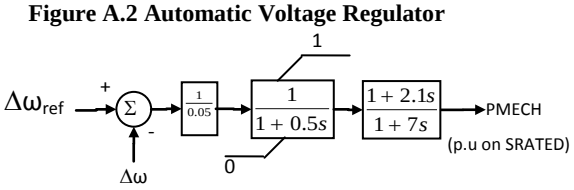

Figure A.3 Governor

H = 6.5 (for generators in Area 1) H = 6.175 (for generators in Area 2)				K_D = 0 ψ_{TI} = *0.9*
S_{RATED} = 900MVA		V_{RATED} = 20kV		f_{SYSTEM}= 50Hz
STEP-UP TRANSFORMER PARAMETERS				
X = j0.15 pu	P_{RATED} = 900MVA	V_{RATED} = 20/230 kV		Off-Nominal Ratio = 1.0
TRANSMISSION LINES				
V_{RATED} =230kV	*r* = 0.0001 pu/km		x_L= 0.001 pu/km	b_C = 0.00175 pu/km
S_{BASE}=100MVA		V_{BASE}=230kV		
GENERATOR LOAD				
G1	P=700MW		Q=185 MVAr	Et=1.03∠20.2°
G2	P=700MW		Q=235 MVAr	Et=1.01∠10.5°
G3	P=719MW		Q=176 MVAr	Et=1.03∠-6.8°
G4	P=700MW		Q=202 MVAr	Et=1.01∠-17°
SYSTEM LOAD				
For all Power Transfers	Q_{L7}=100M VAr	Q_{C7}=200 MVAr	Q_{L9}=100 MVAr	Q_{C9}=350 MVAr
PT = 0 MW	P_{L7}=1367 MW		P_{L9}=1367 MW	
PT = 400MW	P_{L7}=1167 MW		P_{L9}=1567 MW	
PT = 800MW	P_{L7}=967 MW		P_{L9}=1767 MW	

REFERENCES

[1] M. Pavella, D. Ernst, D. Ruiz-Vega, 2000, Transient Stability of Power Systems: A Unified Approach to Assessment and Control, Kluwer Academic Publishers, USA, pp 33 – 134.

[2] P. Kundur, 1994, *Power System Stability and Control*, McGraw-Hill, USA; Chapters 12 & 13.

[3] Y. Zhang, L. Wehenkel, P. Rousseaux and M. Pavella. "SIME: A hybrid approach to fast transient stability assessment and contingency selection" electrical power & energy systems, Vol. 19, No. 3, pp. 195- 208, 1997.

[4] M. Klein, G.J. Rogers, P. Kundur, "A fundamental study of inter-area oscillations in power systems", IEEE Transactions on Power Systems, Vol. 6, No. 3, August 1991.

[5] W. Fujii, J. Wakisaka, S. Iwamoto, "Transient Stability Analysis Based on Dynamic Single Machine Equivalent", 39th North American Power Symposium, 2007.

[6] H.M. Tan, R. Zivanovic, "Transient Stability Sensitivity Analysis Of A Simplified Power System", Australian Universities Power Engineering Conference, 2007.

H.4. Enhanced BSIME Algorithm Implementation Paper

This paper entitled “Implementation of the Enhanced Binary-SIME method for Finding Transient Stability Limits with PSS®E” was presented at the IEEE PowerTech Conference in 2009, Bucharest, Romania.

Implementation of the Enhanced Binary-SIME method for Finding Transient Stability Limits with PSS®E

H.M. Tan, *Student Member, IEEE*, D.J. Vowles, *Member, IEEE* and R. Zivanovic, *Member, IEEE*

***Abstract*-- The Enhanced Binary-Single Machine Infinite bus Equivalent (Binary-SIME) method is an enhancement of the SIME method. It provides a robust and flexible approach to searching for the transient stability limits (TSLs) in a fully detailed model of a multi-machine power system. This paper describes the modular implementation of the Binary-SIME method with the PSS®E time domain simulation package. Extension to incorporate alternative search approaches is facilitated by the modular architecture. The Binary-SIME search implementation is applied to the IEEE simplified model of the Australian power system to search for power transfer limits (PTLs) and critical clearing times (CCTs). The Binary-SIME method is compared with the binary search method in the search for TSLs.**

***Index Terms*—Power System Transient Stability, Reliability, Security Assessment, Simulation Software**

I. Nomenclature

CT –Clearing Time
CCT – Critical Clearing Time
ESC – Early Stop Criterion
k - search iteration number
η - SIME stability margin
MG – Machine Group
OMIB – One Machine Infinite Bus
PTL – Power Transfer Limit
SIME – Single Machine Equivalent
SI - SIME Search Iteration start
SE - SIME Search iteration Exit
t - the i^{th} time domain simulation step
TDS – Time Domain Simulation
TSL – Transient Stability Limit

II. Introduction

The SIME method [1] is based on the derivation of the response of an equivalent One Machine Infinite Bus (OMIB) system from the transient responses of all the machines in a fully detailed model of a multi-machine system. This approach enables the determination of transient stability margins which can be used to predict the forward-swing transient stability limit. The OMIB response also enables the use of early stop criteria (ESC) which allows early identification of forward-swing (in)stability. Prediction of the TSL based on the margin information, together with the application of the ESC, enables accelerated computation of the TSL.

The Binary-SIME search technique [2] enhances the robustness of the basic SIME algorithm by switching to a binary search step whenever the SIME limit prediction cannot be applied. This occurs during search initialization, or where the SIME limit prediction fails to converge, or if a system scenario is too (un)stable for the SIME margin to be calculated.

The enhanced Binary-SIME method for limit searching is peripheral to the TDS software and does not require access to, or modification of, the TDS source code. The modular implementation of the Binary-SIME algorithm with the Siemens PSS®E software [3] is depicted in Fig. 1. The proposed implementation is designed such that alternative limit search methods can be readily incorporated. Besides producing TSLs the Binary-SIME method provides transient-stability margin information which may be useful for sensitivity analysis and control.

In III the implementation of the enhanced Binary-SIME algorithm is described. In IV and V the methodology to search for the forward-swing and multi-swing TSL is explained. The Binary-SIME and binary search algorithms are applied to search for TSLs on the IEEE simplified South East (SE) Australian Power System model [4] which is described in VI. Results of the investigation are discussed in VII.

III. Implementation of the Binary-SIME software

The Binary-SIME implementation is composed of an outer loop to produce the next search scenario (Fig. 1) and an inner loop to execute the Binary-SIME algorithm for each scenario (Fig. 2). The search is automated using PSS®E automation facilities [3]. The outer loop of the search is implemented in Python [3, 5], and the inner loop is implemented as a PSS®E user-defined model using the Fortran 95 language [3, 6]. The model is compiled and linked into the PSS®/E software. Fortran 95 modules are used to implement the inner loop of the algorithm. This allows variations in the algorithm, such as alternative ESC, to be implemented and explored in a straight forward manner. Dynamically allocatable storage is used to facilitate efficient handling of the large volumes of data and for analyzing power systems of widely differing sizes. The current software implementation has been designed with both research and production use in mind.

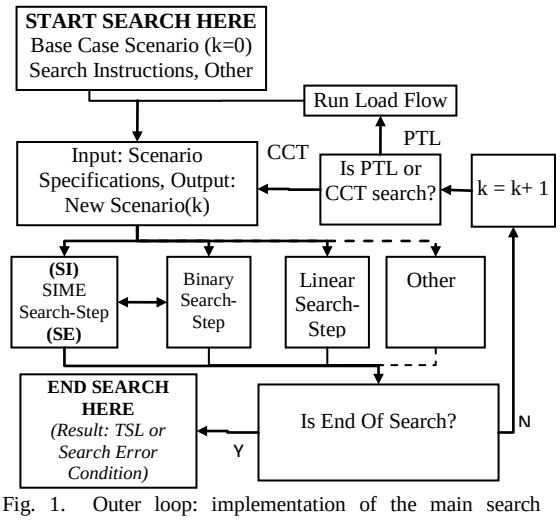

Fig. 1. Outer loop: implementation of the main search traversal

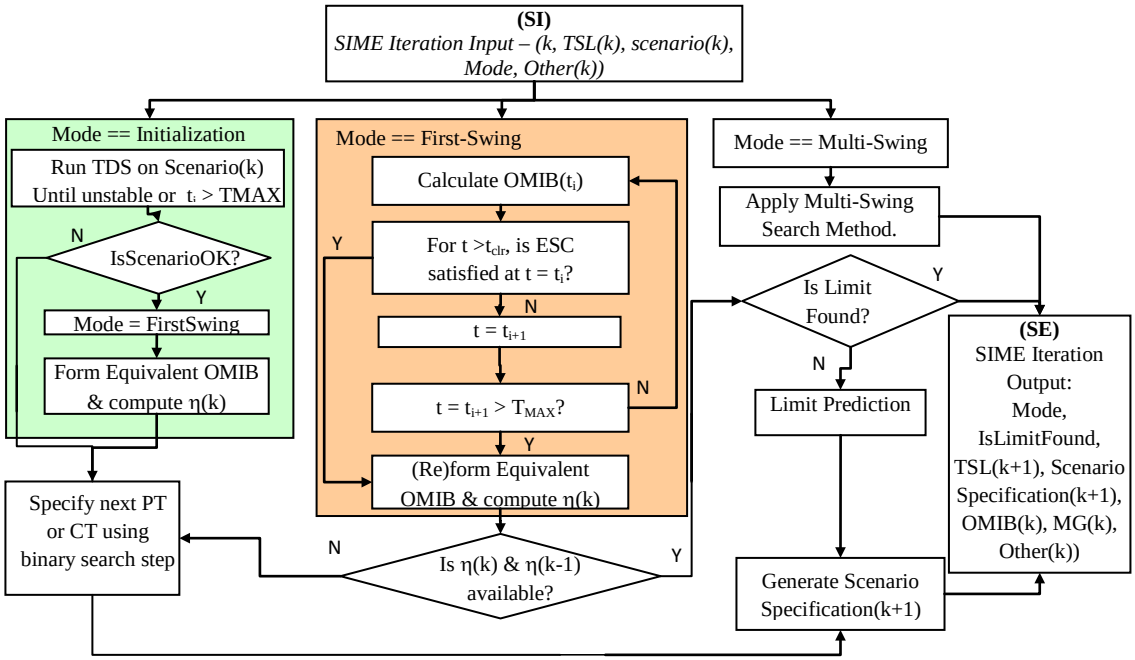

Fig. 2. Inner Loop: implementation of the Binary-SIME search iteration algorithm

Facilities include:

- flexible text based configuration of a TSL search
- comprehensive TSL search summaries

- options to save all generator, OMIB and Centre of Inertia [7] (COI) data into compact binary files. These can be easily translated for viewing with MATLAB® [8]
- enable/ disable use of the SIME ESC during the search.
- record the wall-clock execution time and simulated time, for each search scenario individually and cumulatively.
- options to select the level and detail of diagnostic and error reporting
- options to redirect search traversal based on forward- or multi-swing search boundaries
- options to specify machine groups (see IV.B.) for SIME OMIB calculations

IV. SEARCH FOR THE FORWARD-SWING LIMIT

As described in [2] and Fig. 2. the purpose of the initialization and first-swing phases of the Binary-SIME search is to locate the forward-swing stability limit. The implementation of these phases is described in the following sections.

A. Stability Assessment – Stopping Criteria

For all scenarios the rotor-angles of all machines with respect to the COI angle is examined at each time step of the TDS. If the rotor angle of any machine deviates by more than 180° from the COI angle then the system is declared unstable. Stable scenarios are simulated for a full integration period (i.e. 10 seconds in this paper). During the initialization and first-swing phases of the Binary-SIME search the SIME forward-swing ESC may be applied to terminate the simulation earlier. The ESC identifies forward-swing stability. The ESC are based on the application of the Equal Area Criterion to the OMIB accelerating-power – rotor-ange response in the period immediately following the application of the fault and whilst the rotor-speed is above synchronous speed (i.e. the forward swing) [1,2,9].

B. Machine grouping

To apply SIME assessment and calculate the OMIB responses the system must be divided into two machine groups (MGs). The MGs can be determined from the first unstable scenario [2]. In the enhanced-SIME implementation there is an option to update the MGs whenever an unstable scenario is encountered during the search. However, results of TSLs on the simplified Australian system and from [9] indicate that the MGs should be determined from a very unstable first scenario and should not be modified during the course of the search.

C. SIME Margins

The SIME margins, η, are determined from the forward-swing analysis of the OMIB power-angle response. As soon as two scenarios with valid margins (by the same MG) have been identified the SIME limit prediction can be applied.

1) Unstable margin

The unstable margin is calculated by applying the trapezoidal method to calculate the difference between the acceleration and deceleration areas of the OMIB power-angle curve[1, 2].

2) Stable Margin

Unlike the unstable margin, the stable margin cannot be calculated directly from the OMIB response. The path of the power angle curve must be extrapolated from the forward-swing return angle, δ_r, to the angle of instability, δ_{lim}, where the OMIB acceleration power (P_a) is zero (Fig. 3). A linear least squares (LLS) estimation algorithm is applied to fit a quadratic function to the OMIB power-angle response spanning from the clearing angle, δ_{clr} to δ_r [10]. An initial investigation indicates that about 400 points, equally spaced on the rotor-angle axis, yields a quadratic function which is sufficiently accurate and usually insensitive to relatively small deviations in the power-angle curve. This is the number of data points used in the paper, although it is configurable in the software. If the estimated curve does not intersect the rotor angle axis (at $P_a = 0$, for $\delta > \delta_r$), then the scenario is classified as to "too stable" for the purpose of margin calculation.

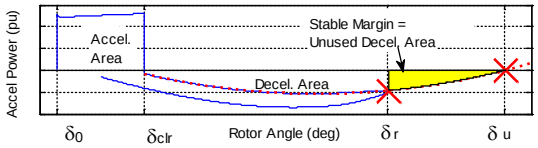

Fig.3. The power angle curve for a stable scenario. It shows the projected path of the curve to instability, and subsequent stable margin.

C. Search Bounds

In the binary-SIME algorithm there are two sets of search bounds – one set of bounds applies to multi-swing stability and the other to forward-swing stability. The algorithm ensures that the forward-swing bounds are always on or within the multi-swing bounds. If the COI stopping criterion is applied to a given scenario, then in the ensuing assessment, both sets of search bounds are updated. If the ESC criterion is applied then only the forward-swing search bounds are updated.

D. Convergence to the Forward-Swing Limit

The forward-swing limit is found if either one of the following conditions is satisfied:

d) $0<\eta(k)<\eta_{tol}$. [2], where $\eta(k)$ is the SIME margin of the current scenario and η_{tol} is the search margin tolerance

e) The difference between the updated forward-swing search bounds is within the binary search tolerance. This condition is important in case the selected η_{tol} is unrealistically low.

E. Detecting Failure To Converge And Redirecting The Search

Failure of Binary-SIME search convergence is detected by the following conditions:

a) If, before the TSL is found, the reduction in the SIME margin between successive scenarios is less than a user defined threshold of η_{slow} then the convergence rate is deemed to be too slow: i.e. convergence failure occurs if $|\eta(k)-\eta(k-1)|<\eta_{slow}$. In these studies $\eta_{slow}=\eta_{tol}$.

b) the predicted TSL is outside of the forward-swing search bounds.

If condition a) occurs then the next search step is redirected to the bisection of the forward-swing bounds. In the event of condition b) the next search step is determined by bisecting the multi-swing bounds, and the forward-swing bounds are reset to the multi-swing bounds. Following condition b) the COI stop criterion must be applied to update the multi-swing bounds to guard against a circular search traversal. It is possible that following search redirection a previously assessed scenario may be repeated. Such circumstances are recognized by the outer search loop; previous margin information can be reused without re-simulating the scenario; and snapshots of previous simulations can be recovered and continued from their last time point. If failure to converge occurs more than once then the algorithm will be completed using a binary search.

V. MULTI-SWING PHASE

When the forward-swing limit is identified it must be assessed for multi-swing stability using the COI stability criterion. If the forward-swing limit is also multi-swing stable then the search is complete and the limit is found. Otherwise, the forward-swing limit becomes the upper search bound and the search must continue in multi-swing mode (see Fig. 2.).

As mentioned above, PSS®E provides the ability to recall previous simulations and to continue running them from the last simulation point. Where it is beneficial, this facility is employed in the multi-swing search phase.

The multi-swing search phase proceeds by applying the COI stability criterion to determine the multi-swing stability of scenarios which were previously assessed for forward-swing stability by the ESC. The scenarios are examined for multi-swing stability in order from the least to most stable, as originally determined by the ESC. If a previous scenario is determined to be multi-swing unstable then it replaces the upper binary search bound, otherwise it replaces the lower binary search bound. Once a multi-swing stable scenario is identified, or if all previous simulations have been examined, then the multi-swing search continues with a binary search until the TSL is found.

VI. THE SIMPLIFIED MODEL OF THE SE AUSTRALIAN SYSTEM

The IEEE simplified model of the South-East (SE) Australian power system [4] is used to investigate the Binary-SIME search algorithm. It is a 50 Hz system that consists of 14 multi-machine power stations and represents a relatively weak longitudinal system as compared to the more tightly meshed networks found in much of Europe and the USA. As shown in the geographical layout in Fig. 4 the system comprises four weakly interconnected areas. Hence there are three inter-area modes of oscillation, as well as ten local-area Each of the 14 power stations comprises between 2 to 12 identical generating units. The generator models are detailed 5th or 6th order machine models and are fitted with detailed excitation system models (including Power System Stabilizers which are necessary for system stability). The model also incorporates six Static Var Compensators, with realistic controls including current-droop compensation and susceptance limits. In the investigated cases three phase faults are applied to various lines on the South Australia (SA) to Victoria (VIC) interconnection. Fig. 5 depicts the SA and VIC components of the system in detail.

VII. RESULTS

In this section the enhanced Binary-SIME method is applied to search for TSLs on the simplified SE Australian power system model. The results provide a comparison of the performance of the Binary-SIME algorithm with respect to the standard binary-search. They also reveal some limitations of the SIME technique and thus the necessity of reverting to binary search steps to ensure that the correct TSL is found. In the following examples all references to search time refer to the simulated time (SIM) and not the computation time. The simulated time is used since it is independent of the computing hardware and transient stability program used.

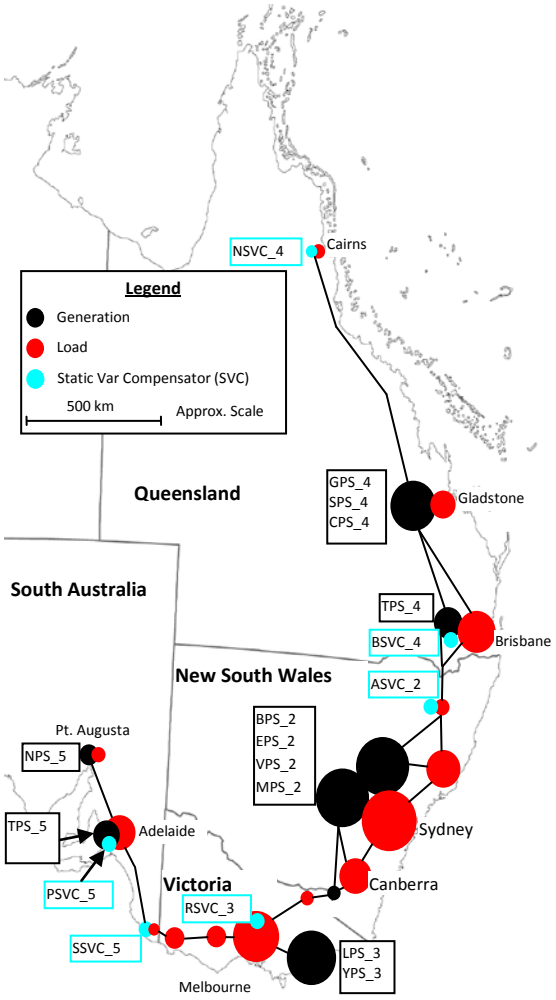

Fig. 4. A geographical representation of the simplified S-E Australian Power System. Relative magnitudes of loads and generation are indicated by the areas of the respective symbols.

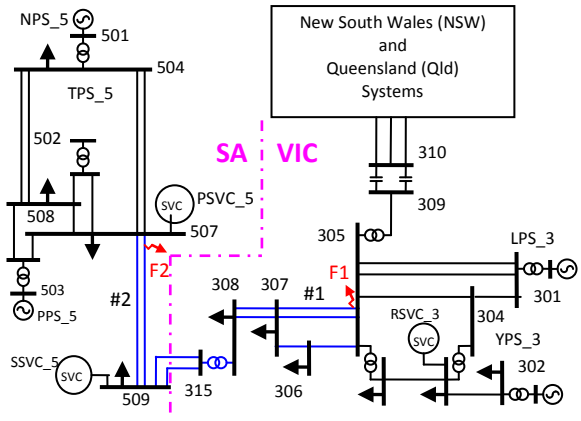

Fig. 5. The one line diagram of the SA & VIC regions of the power system. The elements of the VIC-SA interconnector are shown in blue.

A. Case 1.

In this case the power transfer from Victoria to South Australia is 500 MW over the VIC-SA interconnection. A three-phase fault (F1 in Fig. 5) is applied near to the bus 305 end of transmission circuit #1 connecting bus 305 to bus 307. The fault is cleared by simultaneously tripping the circuit breakers at each end of the faulted line. Table 1 summarizes the results of a binary search for the CCT. The search tolerance is 2 ms.

TABLE 1. SUMMARY OF BINARY SEARCH FOR CCT FOR 500MW POWER TRANSFER FROM VIC-SA, FAULT APPLIED AT BUS 305

k	CT (ms)	Stable/ Unstable	M-S Search bounds (ms)	SIM Time (s)
1	500	U	[0, 500]	1.50
2	250	U	[0, 250]	1.52
3	125	S	[125, 500]	10.00
4	188	U	[125, 188]	1.69
5	157	U	[125, 157]	2.02
6	141	S	[141, 157]	10.00
7	**CCT = 149**	**S**	**[141, 149]**	**10.00**
8	153	U	[149, 153]	2.15
9	151	U	[149, 151]	2.33
Total Simulated Time (s)				41.20

A CCT search using the binary-SIME algorithm is also applied to this case, where a margin tolerance of 0.0002 rad-p.u., and search bound tolerance of 2ms are used. The search is summarized in Table 2.

TABLE 2. SUMMARY OF THE BINARY-SIME SEARCH FOR CCT FOR 500MW POWER TRANSFER FROM VIC-SA, FAULT APPLIED AT BUS 305

k	η(k-1) (rad-pu)	η(k) (rad-pu)	CT (ms)	F-S search bounds (ms)	M-S search bounds (ms)	SIM Time (s)
1	-	-	500	[0, 500]	[0, 500]	1.5
2	-	-0.19304	250	[0, 250]	[0, 500]	1.31
3	-0.19304	0.048460	125	[125, 250]	[0, 500]	1.51
4	0.048460	0.002310	150	[150, 250]	[0, 500]	1.80
5	0.002310	0.001250	151	[151, 250]	[0, 500]	1.83
6	0.001250	0.000548	152	[152, 250]	[0, 500]	1.87
7	0.000548	0.000167	153	[153, 250]	[0, 500]	1.91
8	-	-	153	-	[0, 153]	0.24
9	-	-	152	-	[0, 152]	0.34
10	-	-	151	-	[0, 151]	0.50
11	-	-	**150**	-	**[150, 151]**	**8.20**
Total Simulated Search time (s)						**28.42**

The Binary-SIME search commences in the initial search phase (see Fig. 2) between the binary search bounds of [0, 500] ms. In the first search iteration a scenario with a clearing time of 500ms is assessed. Transient instability is identified by the COI stop criteria at t=1.432s (see Fig. 6). At this time, the largest angle separation occurs between the LPS_3 generators at bus B301 and the rest of the system. This separation defines the MGs which are used for the rest of the Binary-SIME search. It is interesting to note that the system actually separates into 3 sections – SA, VIC and the rest of the system. This seems to differ from the SIME assumption that loss of synchronism is caused by the separation between two groups of machines [1].

Furthermore, it is observed from Fig. 6 that the two VIC stations, LPS_3 & YPS_3 separate together from the remainder of the system, although at the time when the machine groups are identified (i.e. t = 1.432 s) the YPS_3 machine is grouped with the remainder of the system rather than with LPS_3. This apparent inconsistency in machine grouping requires further investigation.

Since, during this first iteration, the system does not commence decelerating before synchronism is lost a stability margin cannot be determined.

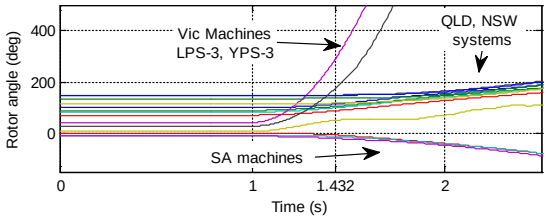

Fig. 6. Rotor Angle responses of the test system where PT is 500MW from VIC-SA, and CT is 500ms.

Bisection is used to determine the CT of 250 ms in the second iteration. It is identified as forward-swing unstable, at t = 1.31s by application of the ESC to the OMIB response. An unstable margin is determined for this scenario, thus the Binary-SIME search can commence the first-swing phase at the next step. The CT of 125 ms of the first scenario of first-swing phase (at k = 3) is determined by a binary step. By the ESC the scenario is determined to be forward-swing stable at t = 1.51s. It provides an estimated stable margin of 0.04846 rad-pu. Since the stability margin is greater than the search tolerance the CT of the next search step is estimated from the margins of iterations 2 and 3 by interpolation to be 150ms. The process of determining forward-swing stability or instability by the ESC, calculating the SIME margin, and predicting the CCT at the next step continues for iterations 4 to 7 inclusive. At scenario 7 the calculated margin is stable and less than the search tolerance, thus the forward-swing limit is found at a CT of 153ms. The simulation for this scenario is continued, in step 8, to determine if the forward-swing limit is also multi-swing stable. The COI stop criterion determines that it is not. Thus, the multi-swing phase of the search commences with the multi-swing search bounds of [0, 153] ms.

The multi-swing search phase (see V.) commences in step 9. The simulation of the step 6 scenario (i.e. the least stable of steps 4 to 6 according to the ESC) is continued and is found to be multi-swing unstable. Similarly, in step 10 the simulation of the scenario in step 5 is continued and is found to be multi-swing unstable. Finally, in step 11, the simulation of the step 4 scenario is continued and is found to be multi-swing stable. Since the difference between the CT in steps 10 (151 ms, unstable) & 11 (150 ms, stable) is less than the binary search tolerance of 2 ms, the CCT is found to be 150 ms in step 11.

Here, the SIME limit prediction technique provides a good CCT estimate and fast convergence to the limit. The cumulative simulation time of the binary search is 41.2 s which is about 30% higher than the 28.42s total simulation time of the Binary-SIME (BSIME) search. The convergence of the two methods are compared in Fig. 7. Note that the simulation times reported are slightly skewed because the simulation is run for 1 s before applying the disturbance.

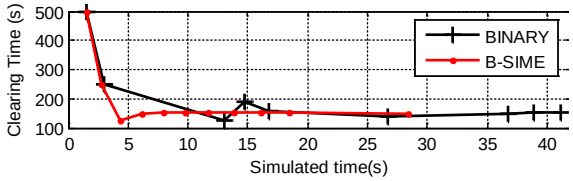

Fig. 7. A comparison of the Binary-SIME and binary searches for Case 1.

B. Case 2

The system operating conditions are the same as in Case 1. In Case 2 the objective is to determine the CCT for a 3-phase fault applied at the bus 507 end of the #1 transmission circuit between buses 507 & 509 (i.e. fault F2 in Fig. 5). The fault is cleared by simultaneously tripping the circuit breakers at each end of the line. The results of a binary search for the CCT of 167 ms in this case are summarized in Table 3.

TABLE 3. SUMMARY OF THE BINARY SEARCH FOR CCT FOR 500MW POWER TRANSFER FROM VIC-SA, FAULT APPLIED AT BUS 507

k	CT (s)	Stable/ Unstable	M-S Search bounds (ms)	SIM Time (s)
1	500	U	[0, 500]	3.45
2	250	U	[0, 250]	10.00
3	125	S	[125, 500]	3.28
4	188	U	[125, 188]	10.00
5	157	U	[125, 157]	3.60
6	173	U	[125, 173]	10.00
7	165	S	[165, 173]	3.88
8	169	U	[165, 169]	10.00
9	CCT = 167	S	[167, 169]	3.45
Total Simulated Time				55.79

The results of the Binary-SIME search for the CCT for this case are summarized in Table 4.

TABLE 4. SUMMARY OF THE BINARY SEARCH FOR CCT FOR 500MW POWER TRANSFER FROM VIC-SA, FAULT APPLIED AT BUS 507

K	η(k-1) (rad-pu)	η(k) (rad-pu)	CT (ms)	F-S search bounds (ms)	M-S search bounds (ms)	SIM Time (s)
1	-	-	500	[0, 500]	[0, 500]	1.57
2	-	-0.00662	250	[0, 250]	[0, 500]	1.71
3	-0.00662	0.00267	125	[125, 250]	[0, 500]	1.57
4	0.00267	0.00365	161	[161, 250]	[0, 500]	1.62
	Predicted CCT: *28 ms* - Redirection using binary search bounds					
5	0.00365	-0.00662	250	[0, 250]	[0, 250]	1.74
6	-0.00662	0.00382	193	[193, 250]	[0, 250]	1.82
7	0.00382	-0.00357	214	[193, 214]	[0, 250]	1.71
8	-0.00357	-0.00312	204	[193, 204]	[0, 250]	1.72
	Predicted CCT: *135 ms* - Redirection using binary search bounds					
9	-	-	125	-	[125, 250]	8.43
10	-	-	188	-	[125, 188]	3.28
11	-	-	157	-	[157, 188]	10.00
12	-	-	173	-	[125,173]	3.60
13	-	-	165	-	[165, 173]	10.00
14	-	-	169	-	[165, 169]	3.88
15			**167**		**[167, 169]**	**10.00**
Total Simulated Search time						62.56

In this example the presence of back-swing instability causes the SIME component of the search to fail. Eventually the binary search is employed to ensure that the search converges to the limit.

The search commences with the clearing time, at the upper binary search bound, of 500ms. By COI assessment it is determined to be unstable at t = 1.57 s. At this point two of the SA machines, NPS_5 and TPS_5, are identified as one MG, with the remaining machines forming the other MG. However, Fig. 8 indicates that in this scenario eventually all three SA machines lose synchronism with the remainder of the system.

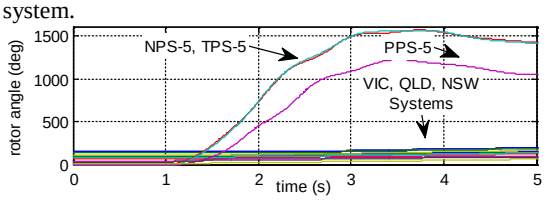

Fig. 8. The machine rotor angle responses of the full system for Case 02.

The second scenario with a CT of 250 ms, determined by bisection, is assessed as unstable by the ESC. The SIME unstable margin is determined for this scenario and the search is able to proceed to the first-swing phase. The CT in the third scenario is determined by a binary step using the forward-swing bounds to be 125 ms. It provides a stable margin, which is outside the search tolerance. Thus, interpolation of the stable margin at the current step and unstable margin of the previous step is used to estimate the CCT to be 161 ms.

The first-swing search phase proceeds with the same process described in Case 1. However, at k = 4 the CCT is estimated to be 28ms, which is outside the forward-swing bounds. Thus the Binary-SIME search must be redirected. The forward-swing bounds are reset to the multi-swing bounds of [0, 250] ms. The scenario with CT = 250ms is confirmed in the 5th step to be unstable using the COI stop criterion. The margin at 250 ms clearing time is used with the margin of the previous scenario (k = 4, CT = 161ms) to estimate the CCT of 193 ms at the next search step (k = 6). At step 6, the scenario with CT = 193 ms is assessed by the ESC to be forward-swing stable. However, this scenario is, in fact, unstable. This is where the SIME method begins to misdirect the limit search.

Fig. 9 shows the OMIB responses of the rotor-angle, rotor-speed and accelerating power for the scenario with CT = 193 ms. It is apparent that application of the ESC shows the system is forward-swing stable at t = t_A = 1.65 s. However, at t = t_D = 3.6 s the rotor-speed reaches a local maximum which is sub-synchronous and at the same time the accelerating power is decreasing.

Consequently, the OMIB system decelerates uncontrollably and synchronism is lost. Thus, although the OMIB system for this scenario correctly reveals that the system is unstable, the ESC which is based only on analysis of the forward-swing incorrectly predicts that the system is stable.

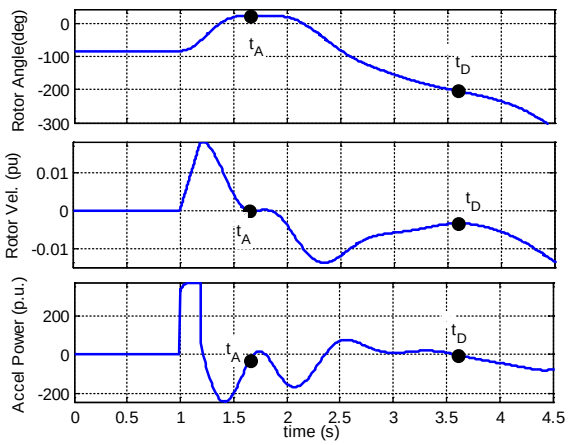

Fig. 9. The OMIB rotor angle, velocity and acceleration power responses where the fault clearing time is 193ms.

It is instructive to examine responses of variables in the detailed system model to explain the reason for the occurrence of instability in the back-swing. Fig. 10 shows the responses of (i) the bus 509 voltage (V); (ii) the power flow in the #2 circuit from bus 509 to 507 (P); (iii) the susceptance of the SVC SSVC_5 which is connected to bus 509 (B); and (iv) the rotor-speed of the TPS_5 machine which is connected to bus 502 (W).

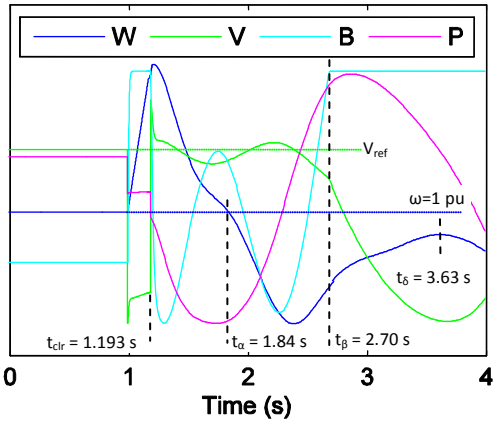

Fig 10. Time responses of: (i) the bus 509 voltage (V); (ii) the power flow in the #2 circuit from bus 509 to 507; (iii) the susceptance of the SVC SSVC_5 connected to bus 509 (B); the rotor-speed of the TPS_5 machine.

In the period immediately following the clearance of the fault the power flow from VIC to SA falls below its pre-disturbance level due to the advance in the rotor-angles of the SA machines with respect to those in the remainder of the system which occurs during the fault.

Due to the reduced power flow on the VIC to SA interconnector (P) the voltage at bus 509 (V) tends to increase above the SSVC_5 voltage set-point. The SVC AVR therefore acts to reduce the SVC susceptance (B). During the first swing following the fault, the rotors of the SA machines decelerate, slow to synchronous speed ($t\alpha$ = 1.84 s for the TPS_5 machine) and thence continue to decelerate. Once the rotor speeds of the SA machines slow below synchronous, the power flow from VIC to SA begins to increase. As the power transfer increases the bus 509 voltage tends to decrease. The SVC responds to this voltage decrease by increasing the SVC susceptance. However, at time $t\beta$ = 2.70s the SVC reaches its capacitive limit. As the interconnector power flow continues to increase the voltage at bus 509 continues to decline. The declining voltage is associated with a reduction in the interconnector power transfer which means that the rotor-speeds of the SA machines are unable to accelerate to synchronous speed. (The TPS_5 machine reaches a maximum rotor-speed of 0.997 pu at $t\delta$ = 3.64s during the back-swing). The net generation deficit in SA means that its machines continue to decelerate and as a result synchronism is lost.

Instability is associated with the loss of voltage control by the SVC at bus 509. This loss of control necessarily occurs after the SA machines first decelerate to synchronous speed following the clearance of the fault. If, at the time when the SA machines first return to synchronous speed following fault clearance, the net power consumption of SA is positive then according to the forward-swing early stop criteria the system is stable – which yields an incorrect diagnosis of stability in this case.

Steps k = 7 and 8 continue the search for the forward-swing limit with failure to converge eventually being identified at scenario 8, where the predicted CCT of 135ms is outside of the forward-swing search bounds. As this is the second time that convergence failure has

been detected, the Binary-SIME algorithm switches to the binary search mode to complete the search.

Fig. 11. shows a comparison of the performances of the binary-SIME and the binary search methods.

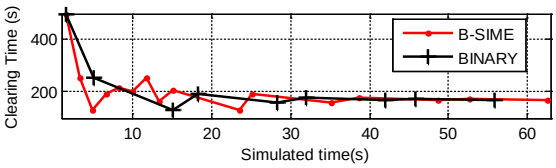

Fig. 11. Performance of the binary-SIME and binary searches for Case 2.

Due to the failure of the ESC to identify instability in the back-swing and the associated convergence failures during the forward-swing limit-search the search time of the Binary-SIME method (62.6s) was slightly greater than that required by the binary-search method (55.8s). However, the ability of the Binary-SIME search to identify the convergence failures and switch to a binary search mode means that the method does correctly identify the CCT. Furthermore, the extra search time, as compared to a binary-search, is minimized because snapshots of previous simulations in the search are recovered and continued.

C. Case 3

In this case the objective is to search for the power transfer limit from VIC to SA. A three phase fault is applied at the bus 507 end of #1 transmission circuit between buses 507 and 509 (i.e. fault F2 in Fig. 5.). The fault is cleared by disconnecting the faulted circuit in 120ms. The Binary-SIME and binary search algorithms were applied to search for the power transfer limit. A summary of the binary search, run to a resolution of 5MW, is listed in Table 5. (It should be noted that when the simulations are run for an integration period of 20s, the actual PTL is revealed to be 571MW because in the case with a power transfer of 572 MW, instability occurs at approximately t = 11s.)

TABLE 5. SUMMARY OF THE BINARY AND BINARY-SIME SEARCHES FOR PTL FOR CT = 120MS, FAULT APPLIED AT BUS 507

k	PT (MW)	Stable/ Unstable	M-S Search bounds (MW)	SIM Time (s)
1	650	U	[0, 650]	1.79
2	325	S	[325, 650]	10.00
3	488	S	[488, 650]	10.00
4	569	S	[569, 650]	10.00
5	610	U	[569, 610]	3.55
6	590	U	[569, 590]	3.85
7	580	U	[569, 580]	4.26
8	575	U	[569, 575]	4.87
9	**572**	**S**	**[572, 575]**	**10.00**
Total Simulated Time				59.78

As with Case 2 the system is limited by back-swing instability which means the SIME component for the binary-SIME search is relatively ineffective. In this case incorrect diagnosis of stability by the forward-swing early stop criterion is evident from the first search scenario.

The first search scenario of the Binary-SIME algorithm commences at a power transfer level of 650MW. By the COI stop criterion the system is identified to be unstable at t = 1.79s. From this point the SA machines NPS_5 and TPS_5 were identified in one MG with the machines of the remainder of the system in the other group, as in Case 2. Having identified the MGs the OMIB response is calculated for the scenario. As part of assessing the SIME margin the ESC conditions are checked for consistency. However, OMIB acceleration power and rotor velocity responses reveal, in Fig. 12, the scenario is forward-swing stable. The ESC classification contradicts the COI assessment. This is a possible indication that the scenario is back-swing unstable. In view of this information, the Binary-SIME algorithm switches immediately to a binary search to complete the PTL search, thereby avoiding needless deviations. Therefore, the trajectories of the Binary and Binary-SIME searches are identical in this case.

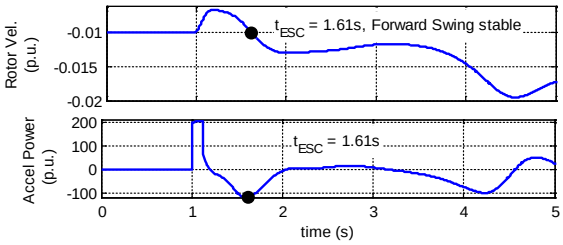

Fig. 12. The OMIB acceleration power-angle response for power transfer of 650MW from VIC. to SA. This response indicates that Case 3 is back-swing unstable.

VIII. CONCLUSION

The implementation of the enhanced Binary-SIME algorithm, to search for TSLs, using the PSS®E software, is described. The implemented TSL searching software provides useful facilities to perform subsidiary investigations from the information generated during a search, for both research and production purposes.

The Binary-SIME algorithm takes advantage of the SIME ESC and limit prediction, to accelerate the search; and switches to binary steps, when the SIME limit prediction fails. It is applied to search for CCTs and PTLs on the IEEE simplified model of the SE Australian Power System. When compared to the binary search method, the results indicate the significant savings in the simulated search time that can be achieved. However, they also reveal limitations of the SIME limit prediction and ESC, particularly in the presence of back-swing instability phenomena due to the limited capacity of SVCs on some interconnectors. In these cases the binary-SIME method does locate the TSL despite the failure of the SIME component of the algorithm. Therefore the binary-SIME method is shown to be more robust than the SIME algorithm, for the cases examined. In such cases, little or no extra time is required by the binary-SIME algorithm as compared to the plain binary search.

The investigation has revealed that enhancements to the ESC are required to identify the occurrence of back-swing instability. It is unclear without further investigation if margin information from forward- and back-swing instability can be utilized for limit prediction within the same search.

The technique for identifying machine groups requires further investigation because there are indications in the cases investigated that some machines may be assigned to an incorrect group. In particular, it may be more appropriate to run the simulation used to identify machine groups for longer than required to detect

instability according to the COI angle divergence criterion.

Further investigation of the binary-SIME algorithm including the development of additional enhancements. will be pursued. Such developments will be tested by searching for TSLs in the IEEE Simplified Model of the SE Australian power system, as well as other system models.

IX. REFERENCES

[1] M. Pavella, D. Ernst, D. Ruiz-Vega, 2000, Transient Stability of Power Systems: A Unified Approach to Assessment and Control, Kluwer Academic Publishers, USA.

[2] H.M. Tan, R. Zivanovic, "Integrating the SIME Method with Standard Time Domain Simulation Software to Search for Transient Stability Limits", Australian Universities Power Engineering Conference, Sydney, Australia, 2008.

[3] PSS®E Power System Simulator for Engineering, Version 30.2, Siemens Power Transmission & Distribution, Inc., Schenectady, NY, Nov. 2005.

[4] M. Gibbard, D. Vowles, "Simplified 14-Generator Model of the South East Australian Power System", The School of Electrical & Electronic Engineering, The University of Adelaide, May 2008
http://psdyn.ece.wisc.edu/IEEE_benchmarks

[5] "Python Programming Language -- Official Website", © 1990-2008, Python Software Foundation, http://www.python.org/.

[6] M. Metcalf, J. Reid, M. Cohen, "Fortran 95/2003 Explained", Oxford University Press, 2004.

[7] Z. Lan, D.Q. Gan, L.B. Shi, Y.X. Ni and T.S Bi, "Dynamic COI-tracking concept for the control of generators in multi-machine power systems", Euro. Trans. Electr. Power 2008; John Wiley & Sons, Vol 18, pp 50–64, February 2007

[8] MATLAB ®, The MathWorks Inc., © 1994 – 2009, http://www.mathworks.com.au/.

[9] Y. Zhang, L. Wehenkel, P. Rousseaux and M. Pavella. "SIME: A hybrid approach to fast transient stability assessment and contingency selection", Electrical Power & Energy Systems, Vol. 19, No. 3, pp. 195- 208, 1997

[10] "SLATEC Common Mathematical Library", Version 4.1, July 1993, http://www.netlib.org/slatec/

[11] Australian Government, Geoscience Australia, *Maps of Australia – Geoscience Australia*, http://www.ga.gov.au/map, viewed 5 March 2009.

X. ACKNOWLEDGEMENT

The authors gratefully acknowledge the work of our colleague Dr. Mike Gibbard in developing the simplified model of the SE Australian power system used in the paper.

Bibliography

[1] M. Pavella, D. Ernst and D. Ruiz-Vega, Transient Stability of Power Systems: A Unified Approach to Assessment and Control. Boston/ Dordrecht/ London: Kluwer Academic Publishers, 2000.

[2] P. Kundur, J. Paserba, V. Ajjarapu, G. Andersson, A. Bose, C. Canizares, N. Hatziargyriou, D. Hill, A. Stankovic, C. Taylor, T. Van Cutsem and V. Vittal, "Definition and classification of power system stability IEEE/CIGRE joint task force on stability terms and definitions", IEEE *Transactions on Power Systems,* vol. 19, pp. 1387-1401, 2004.

[3] *Review of On-Line Dynamic Security Assessment Tools and Techniques*, CIGRE Technical Brochure prepared by Work Group 601.C4, 2007.

[4] P. Pourbeik, D. Vowles and M. Gibbard, *Small-signal stability, control and dynamic performance of power systems.* Adelaide: The University of Adelaide Press, 2015.

[5] D.J. Sobajic, J. Bucciero and M. Terbrueggen, *Interconnected Power System Dynamics Tutorial.* Third ed. Palo Alto, California: Electric Power Research Institute, 1998.

[6] National Electricity Rules Version 60," Australian Energy Market Commission, 2014. Available at: http://www.aemc.gov.au/Electricity/National-Electricity-Rules/Current-Rules.html

[7] K. Morison, L. Wang, F. Howell, J. Viikinsalo and A. Martin, "Implementation of Online Dynamic Security Assessment at Southern Company," in *Real-Time Stability Assessment in Modern Power System Control Centers*. Edited by S. C. Savulescu, Hoboken, New Jersey: John Wiley & Sons, 2009.

[8] S. J. Boroczky and E. Gentle, "Real-time transient security assessment in Australia at NEMMCO," in *Power Systems Conference and Exposition, 2009. PSCE '09. IEEE/PES*, 2009, pp. 1-6.

[9] S.C. Savulescu, Ed., *Real-Time Stability Asessment in Modern Power System Control Centres* (IEEE Press Series on Power Engineering Hoboken, New Jersey: John Wiley & Sons Inc., 2009.

[10] S. J. Boroczky, "Real-Time Transient Security Assessment in Australia At NEMMCO," in *Real-Time Stability Assessment in Modern Power System Control Centers*. Edited by S. C. Savulescu, Hoboken, New Jersey: John Wiley & Sons, 2009.

[11] Siemens Power Technologies International, "PSS®E". Version 30.3, 2008.

[12] M. Gibbard and D. Vowles, Simplified 14-Generator Model of the South East Australian Power System. The School of Electrical & Electronic Engineering, The University of Adelaide, Australia, 2008. Available at: http://www.eleceng.adelaide.edu.au/groups/PCON/PowerSystems/IEEE/BenchmarkData/index.html. Accessed:7 Jan 2011

[13] P. Kundur, *Power system stability and control.* New York: McGraw-Hill, 1994.

[14] B. Bonvini, S. Massucco, A. Morini and T. Siewierski, "A comparative analysis of power system transient stability assessment by direct and hybrid methods," in *Electrotechnical Conference, 1996. MELECON '96., 8th Mediterranean*, 1996, pp. 1575-1579 vol.3.

[15] J. Astic, A. Bihain and M. Jerosolimski, "The mixed Adams-BDF variable step size algorithm to simulate transient and long term phenomena in power systems", IEEE *Transactions on Power Systems,* vol. 9, pp. 929-935, 1994.

[16] S.C. Savulescu, "Online Security Assessment for the Brazilian System," in *Real-Time Stability Assessment in Modern Power System Control Centers*. Edited by S. C. Savulescu, Hoboken, New Jersey: John Wiley & Sons, 2009.

[17] V. Jalili-Marandi and V. Dinavahi, "Large-scale transient stability simulation on graphics processing units," in *Power & Energy Society General Meeting, 2009. PES '09. IEEE*, 2009, pp. 1-6.

[18] V. Jalili-Marandi and V. Dinavahi, "SIMD-Based Large-Scale Transient Stability Simulation on the Graphics Processing Unit", IEEE *Transactions on Power Systems,* vol. 25, pp. 1589-1599, 2010.

[19] H.M. Tan and R. Zivanovic, "Transient stability sensitivity analysis of a simplified power system," in *Australasian Universities Power Engineering Conference,* 2007, pp. 1-7.

[20] J. Grainger and W. Stevenson, *Power System Analysis.* New York: McGraw-Hill, 1994.

[21] P.W. Sauer and M.A. Pai, *Power System Dynamics and Stability.* Upper Saddle River, N.J: Prentice Hall, 1998.

[22] J. Machowski, J.W. Bialek, J.R. Bumby and F. Knovel, *Power System Dynamics and Stability.* Chichester; New York: John Wiley, 1997.

[23] S. Bhat, M. Glavic, M. Pavella, T.S. Bhatti and D. Kothari, "A transient stability tool combining the SIME method with MATLAB and SIMULINK," *International Journal of Electrical Engineering Education,* vol. 43, no. 2, pp. 119-133, 2006.

[24] M. Pavella, "Generalized one-machine equivalents in transient stability studies," *Power Engineering Review, IEEE,* vol. 18, pp. 50-52, 1998.

[25] M. Pavella, "Power system transient stability assessment - traditional vs modern methods," *Control Engineering Practice,* vol. 6, pp. 1233-1246, 1998.

[26] A.D. Lotufo, M.L. Lopes and C.R. Minussi, "Sensitivity analysis by neural networks applied to power systems transient stability," *Electric Power Systems Research,* vol. 77, pp. 730-738, 2007.

[27] H.D. Chiang and L. Fekih-Ahmed, "On the direct method for transient stability analysis of power system structure preserving models," in*, ISCAS '92 Proceedings, 1992 IEEE International Symposium on Circuits and Systems*, 1992, pp. 2545-2548 vol.5.

[28] G.A. Maria, C. Tang and J. Kim, "Hybrid transient stability analysis [power systems]", IEEE *Transactions on Power Systems,* vol. 5, pp. 384-393, 1990.

[29] A.A. Fouad and S.E. Stanton, "Transient Stability of a Multi-Machine Power System Part I: Investigation of System Trajectories*", IEEE Transactions on Power Apparatus and Systems,* vol. PAS-100, pp. 3408-3416, 1981.

[30] A.A. Fouad and S.E. Stanton, "Transient Stability of a Multi-Machine Power System. Part II: Critical Transient Energy", *IEEE Transactions on Power Apparatus and Systems,* vol. PAS-100, pp. 3417-3424, 1981.

[31] D.Z. Fang, T.S. Chung, Z. Yao and S. Wennan, "Transient stability limit conditions analysis using a corrected transient energy function approach", *IEEE Transactions on Power Systems,* vol. 15, pp. 804-810, 2000.

[32] E. Vaahedi, Y. Mansour, A.Y. Chang, B.R. Corns and E.K. Tse, "Enhanced Second Kick methods for on-line dynamic security assessment*", IEEE Transactions on Power Systems,* vol. 11, pp. 1976-1982, 1996.

[33] A. Rahimi, "Generalized equal-area criterion: a method for on-line transient stability analysis," in *Conference Proceedings., IEEE International Conference on Systems, Man and Cybernetics*, 1990, pp. 684-688.

[34] Y. Xue, T. Van Custem and M. Ribbens-Pavella, "Extended equal area criterion justifications, generalizations, applications", *IEEE Transactions on Power Systems,* vol. 4, pp. 44-52, 1989.

[35] M.A. El-Kady, C.K. Tang, V.F. Carvalho, A.A. Fouad and V. Vittal, "Dynamic Security Assessment Utilizing the Transient Energy Function Method", IEEE *Transactions on Power Systems,* vol. 1, pp. 284-291, 1986.

[36] Y. Xue, T. Van Cutsem and M. Ribbens-Pavella, "Real-time analytic sensitivity method for transient security assessment and preventive control," *Generation, Transmission and Distribution, IEE Proceedings C,* vol. 135, pp. 107-117, 1988.

[37] M.H. Haque, "Equal-area criterion: an extension for multimachine power systems," *Generation, Transmission and Distribution, IEE Proceedings,* vol. 141, pp. 191-197, 1994.

[38] M.H. Haque, "Further developments of the equal-area criterion for multimachine power systems," *Electric Power Systems Research,* vol. 33, pp. 175-183, 1995.

[39] M.H. Haque and A.H. Rahim, "Determination of first swing stability limit of multimachine power systems through Taylor series expansions," *Generation, Transmission and Distribution, IEE Proceedings C,* vol. 136, pp. 373-380, 1989.

[40] Y. Xue, L. Wehenkel, R. Belhomme, P. Rousseaux, M. Pavella, E. Euxibie, B. Heilbronn and J.F. Lesigne, "Extended equal area criterion revisited [EHV power systems]", IEEE *Transactions on Power Systems,* vol. 7, pp. 1012-1022, 1992.

[41] V. Vittal, S. Rajagopal, A.A. Fouad, M.A. El-Kady, E. Vaahedi and V.F. Carvalho, "Transient stability analysis of stressed power systems using the energy function method", IEEE *Transactions on Power Systems,* vol. 3, pp. 239-244, 1988.

[42] A.A. Fouad, V. Vittal and O. Tae Kyoo, "Critical Energy for Direct Transient Stability Assessment of a Multimachine Power System", *IEEE Transactions on Power Apparatus and Systems,* vol. PAS-103, pp. 2199-2206, 1984.

[43] Y. Mansour, E. Vaahedi, A.Y. Chang, B.R. Corns, B.W. Garrett, K. Demaree, T. Athay and K. Cheung, "BC Hydro's on-line transient stability assessment (TSA) model development, analysis and post-processing", IEEE *Transactions on Power Systems,* vol. 10, pp. 241-253, 1995.

[44] T. Athay, R. Podmore and S. Virmani, "A Practical Method for the Direct Analysis of Transient Stability", *IEEE Transactions on Power Apparatus and Systems,* vol. PAS-98, pp. 573-584, 1979.

[45] N. Kakimoto, Y. Ohnogi, H. Matsuda and H. Shibuya, "Transient Stability Analysis of Large-Scale Power System by Lyapunov's Direct Method", *IEEE Transactions on Power Apparatus and Systems,* vol. PAS-103, pp. 160-167, 1984.

[46] H.D. Chiang and C.C. Chu, "Theoretical foundation of the BCU method for direct stability analysis of network-reduction power system. Models with small transfer conductances", *IEEE Transactions on Circuits and Systems I: Fundamental Theory and Applications,* vol. 42, pp. 252-265, 1995.

[47] J. Tong, H.D. Chiang and T. P. Conneen, "A sensitivity-based BCU method for fast derivation of stability limits in electric power systems", *IEEE Transactions on Power Systems,* vol. 8, pp. 1418-1428, 1993.

[48] I. Luna-Lopez, J. M. Canedo and A. Loukianov, "Dynamical method for CUEP detection in power system transient stability assessment," in *IEEE Power Engineering Society Winter Meeting,* 2002, pp. 189-194 vol.1.

[49] C.W. Liu and J. S. Thorp, "A novel method to compute the closest unstable equilibrium point for transient stability region estimate in power systems", *IEEE Transactions on Circuits and Systems I: Fundamental Theory and Applications,* vol. 44, pp. 630-635, 1997.

[50] R.T. Treinen, V. Vittal and W. Kliemann, "An improved technique to determine the controlling unstable equilibrium point in a power system", *IEEE Transactions on Circuits and Systems I: Fundamental Theory and Applications,* vol. 43, pp. 313-323, 1996.

[51] A.R. Bergen and D.J. Hill, "A Structure Preserving Model for Power System Stability Analysis", *IEEE Transactions on Power Apparatus and Systems,* vol. PAS-100, pp. 25-35, 1981.

[52] I.A. Hiskens and D.J. Hill, "Energy functions, transient stability and voltage behaviour in power systems with nonlinear loads", *IEEE Transactions on Power Systems,* vol. 4, pp. 1525-1533, 1989.

[53] N. Narasimhamurthi and M. Musavi, "A generalized energy function for transient stability analysis of power systems*", IEEE Transactions on Circuits and Systems,* vol. 31, pp. 637-645, 1984.

[54] N. Tsolas, A. Arapostathis and P. Varaiya, "A structure preserving energy function for power system transient stability analysis*", IEEE Transactions on Circuits and Systems,* vol. 32, pp. 1041-1049, 1985.

[55] U. Gabrijel and R. Mihalic, "Transient stability assessment of power systems with phase shifting transformers," in *The IEEE Region 8 EUROCON 2003. Computer as a Tool*, 2003, pp. 235-239 vol.2.

[56] R. Mihalic and U. Gabrijel, "A structure-preserving energy function for a static series synchronous compensator", *IEEE Transactions on Power Systems,* vol. 19, pp. 1501-1507, 2004.

[57] V. Azbe, U. Gabrijel, D. Povh and R. Mihalic, "The Energy Function of a General Multimachine System With a Unified Power Flow Controller", *IEEE Transactions on Power Systems,* vol. 20, pp. 1478-1485, 2005.

[58] M. Ribbens-Pavella and F.J. Evans, "Direct methods for studying dynamics of large-scale electric power systems--A survey," *Automatica,* vol. 21, pp. 1-21, 1985.

[59] D.J. Hill and I.M. Mareels, "Stability theory for differential/algebraic systems with application to power systems", *IEEE Transactions on Circuits and Systems,* vol. 37, pp. 1416-1423, 1990.

[60] Y. Zou, M.H. Yin and H.D. Chiang, "Theoretical foundation of the controlling UEP method for direct transient-stability analysis of network-preserving power system models", *IEEE Transactions on Circuits and Systems I: Fundamental Theory and Applications,* vol. 50, pp. 1324-1336, 2003.

[61] D. Ernst, D. Ruiz-Vega, M. Pavella, P.M. Hirsch and D. Sobajic, "A unified approach to transient stability contingency filtering, ranking and assessment", *IEEE Transactions on Power Systems,* vol. 16, pp. 435-443, 2001.

[62] D. Ruiz-Vega, M. Glavic and D. Ernst, "Transient stability emergency control combining open-loop and closed-loop techniques," in *, IEEE Power Engineering Society General Meeting, 2003*, p. 2059 Vol. 4.

[63] EUROSTAG ®, 2009.

[64] A. Bihain, D. Cirio, M. Fiorina, R. Lopez, D. Lucarella, S. Massucco, D. R. Vega, C. Vournas, T. Van Cutsem and L. Wehenkel, "OMASES: a dynamic security assessment tool for the new market environment," in *IEEE Bologna Power Tech Conference Proceedings, 2003*, p. 8 pp. Vol.3.

[65] D. Cirio, D. Lucarella, G. Vimercati, S. Massucco, A. Morini, F. Silvestro, D. Ernst, M. Pavella and L. Wehenkel, "Application of an Advanced Transient Stability Assessment and Control Method to a Realistic Power System," presented at the 15th Power System Control Centres (PSCC) Workshop, Session 20, 2005.

[66] T. Van Cutsem, J. Kabouris, G. Christoforidis and C. D. Vournas, "Application of real-time voltage security assessment to the Hellenic interconnected system," *Generation, Transmission and Distribution, IEE Proceedings-,* vol. 152, pp. 123-131, 2005.

[67] B. Lee, S.H. Kwon, J. Lee, H.K. Nam, J.B. Choo and D.H. Jeon, "Fast contingency screening for online transient stability monitoring and assessment of the KEPCO system," *Generation, Transmission and Distribution, IEE Proceedings,* vol. 150, pp. 399-404, 2003.

[68] J. Lee, B. Lee, S.H. Kwon, H.K. Nam, J.B. Choo and K. Yi, "Fast contingency screening for on-line transient stability monitoring of the KEPCO system", in *Power Engineering Society Summer Meeting, 2001. IEEE*, 2001, pp. 314-319 vol.1.

[69] L. Mariotto, H. Pinheiro, G.C. Junior and M.R. Muraro, "An Analytical Tool for Computing Transient Stability Margins of Power Systems with Large Amount of Wind Power", in *International Conference on Clean Electrical Power, 2007 (ICCEP '07),* pp. 747-753.

[70] Z.Q. Wu, "Single Machine Equal Area Criterion for Multimachine System Stability Assessment Based on Time Domain Simulation," *IEEE Power Engineering Review,* vol. 21, pp. 51-52, 2001.

[71] Z.Q. Wu, Y.N. Wang, H.H. Chen, W.W. Tang and L.Q. Pan, "Transient Stability Sensitivity Analysis," *Electric Power Components and Systems,* vol. 33, pp. 247 - 261, 2005.

[72] H.D. Chiang, F.F. Wu and P.P. Varaiya, "A BCU method for direct analysis of power system transient stability", *IEEE Transactions on Power Systems,* vol. 9, pp. 1194-1208, 1994.

[73] Y. Tada, A. Kurita, Z. Yicheng, K. Koyanagi, H.D. Chiang and Z. Yan, "BCU-guided time-domain method for energy margin calculation to improve BCU-DSA system," in *Transmission and Distribution Conference and Exhibition 2002: Asia Pacific. IEEE/PES*, pp. 366-371 vol.1.

[74] G.C. Ejebe, C. Jing, J.G. Waight, V. Vittal, G. Pieper, F. Jamshidian, D. Sobajic and P.M. Hirsch, "Transient Energy Based Screening and Monitoring for Stability Limits," in *IEEE PES Summer Meeting Panel Session on Transient Stability Limit Search*, Berlin, Germany, 1997, pp. 1-10.

[75] "SLATEC Common Mathematical Library". Version 4.1, 1993. Available at: http://www.netlib.org/slatec/

[76] R.J. Marceau, M. Sirandi, S. Soumare and X.D. Do, "Signal Energy Search Strategies for Transient Stability Transfer Limit Determination," in *IEEE PES Summer Meeting Panel Session on Transient Stability Limit Search*, Berlin, Germany, 1997, pp. 1-9.

[77] R.J. Marceau, F.D. Galiana, R. Mailhot, F. Denomme and D.T. McGillis, "Fourier methods for estimating power system stability limits", IEEE *Transactions on Power Systems,* vol. 9, pp. 764-771, 1994.

[78] R.J. Marceau and S. Soumare, "A unified approach for estimating transient and long-term stability transfer limits", IEEE *Transactions on Power Systems,* vol. 14, pp. 693-701, 1999.

[79] B. Carlson, P. Crilly and J. Rutledge, *Communication Systems: An Introduction to Signals and Noise in Electrical Communication.* 4th ed. Dubuque, Iowa: McGraw-Hill, 2002.

[80] E. Kreyzig, *Advanced Engineering Mathematics.* 8 ed. New York: John Wiley & Sons, 1999.

[81] M.J. Jin, K.W. Chan, S.W. Mei, N. Mo and Q. Lo, "A parallel transient stability limit search method for online transient stability assessment," in *International Conference on Power System Technology, 2004. PowerCon 2004*, pp. 1474-1478 Vol.2.

[82] I.A. Hiskens and M.A. Pai, "Trajectory sensitivity analysis of hybrid systems", IEEE Transactions on Circuits and Systems I: Fundamental Theory and Applications, vol. 47, pp. 204-220, 2000.

[83] M.J. Laufenberg and M.A. Pai, "A new approach to dynamic security assessment using trajectory sensitivities", IEEE *Transactions on Power Systems,* vol. 13, pp. 953-958, 1998.

[84] I.A. Hiskens, "Iterative computation of marginally stable trajectories," *International Journal of Robust and Nonlinear Control,* vol. 14, pp. 911-924, 2004.

[85] I.A. Hiskens and M.A. Pai, "Sensitivity analysis of power system trajectories: recent results," in *Proceedings of the IEEE International Symposium on Circuits and Systems, 1998 (ISCAS '98)*, pp. 439-443 vol.3.

[86] I.A. Hiskens and M. Akke, "Analysis of the Nordel power grid disturbance of January 1, 1997 using trajectory sensitivities", IEEE *Transactions on Power Systems,* vol. 14, pp. 987-994, 1999.

[87] I.A. Hiskens and M.A. Pai, "Power system applications of trajectory sensitivities," in *Power Engineering Society Winter Meeting, 2002. IEEE*, 2002, pp. 1200-1205 vol.2.

[88] I.A. Hiskens and J. Alseddiqui, "Sensitivity, Approximation and Uncertainty in Power System Dynamic Simulation", IEEE *Transactions on Power Systems,* vol. 21, pp. 1808-1820, 2006.

[89] I.A. Hiskens, "Trajectory approximation near the stability boundary," in *Proceedings of 2010 IEEE International Symposium on Circuits and Systems (ISCAS)* , pp. 533-536.

[90] D.Z. Fang and Y.F. Qin, "A new trajectory sensitivity approach for computations of critical parameters," *Electric Power Systems Research,* vol. 77, pp. 303-307, 2007.

[91] M. Klein, G.J. Rogers and P. Kundur, "A fundamental study of inter-area oscillations in power systems", IEEE *Transactions on Power Systems,* vol. 6, pp. 914-921.

[92] C.L. Wadhwa, *Electrical Power Systems.* 2nd ed. New York: J. Wiley, 1991.

[93] H.M. Tan, D.J. Vowles and R. Zivanovic, "Implementation of the Enhanced Binary-SIME method for finding transient stability limits with PSS®E ," in *IEEE Bucharest PowerTech Conference, 2009,* pp. 1-8.

[94] Y. Zhang, L. Wehenkel, P. Rousseaux and M. Pavella, "SIME: A hybrid approach to fast transient stability assessment and contingency selection," *Electrical Power & Energy Systems,* vol. 19, pp. 195-205, 1997.

[95] The University of Liege, Montefiere Institute, Department of Electrical Engineering and Computer Science, "SIME software". Version, 2000.

[96] M. Yin, C.Y. Chung, K.P. Wong, Y. Xue and Y. Zou, "An Improved Iterative Method for Assessment of Multi-Swing Transient Stability Limit", *IEEE Transactions on Power Systems,* vol. PP, pp. 1-8, 2011.

[97] H.M. Tan and R. Zivanovic, "Integrating the SIME method with standard time domain simulation software to search for transient stability limits," in *Power Engineering Conference, 2008 (AUPEC '08), Australasian Universities*, pp. 1-7.

[98] W. Fujii, J. Wakisaka and S. Iwamoto, "Transient Stability Analysis Based on Dynamic Single Machine Equivalent," in *Power Symposium, 2007. NAPS '07. 39th North American*, pp. 217-222.

[99] The MathWorks Inc., "MATLAB ". Version 7.6.0.324 (R2008a), Natick, Massachusetts, 2008.

[100] Python Programming Language -- Official Website. Python Software Foundation, 1990-2008. Available at: http://www.python.org/.

[101] M. Metcalf, J. Reid and M. Cohen, *Fortran 95/2003 Explained.* Oxford University Press, 2004.

[102] PSS®E Version 30.3 Program Application Guide: Volume II. Siemens Power Technologies International, 2008.

[103] "Potential Sites For Emergency Control Systems (ECS) in the NEM", prepared by the Australian Energy Market Operator (AEMO), 2013.

[104] "NEM – Market Event Report – High FCAS Prices in South Australia – October and November 2015", prepared by AEMO, 2015.

[105] "Update to Renewable Energy Integration in South Australia – A Joint AEMO and ElectraNet Report", prepared by AEMO and ElectraNET, February 2016.

[106] D.Vowles; "Rotor Angle Small Signal Stability", presented at *A Residential School in Electrical Power Engineering* (Brisbane, 2004). Electric Energy Society of Australia (EESA).